Volume 33, Number 1 September 2024
ISSN:1521-1398 PRINT,1572-9206 ONLINE

Journal of Computational Analysis and Applications

EUDOXUS PRESS,LLC

Journal of Computational Analysis and Applications
ISSNno.'s:1521-1398 PRINT,1572-9206 ONLINE

SCOPE OF THE JOURNAL

An international publication of Eudoxus Press, LLC
(published biannually) www.eudoxuspress.com.

Editor in Chief: George Anastassiou
Department of Mathematical Sciences,
University of Memphis, Memphis, TN 38152-3240, U.S.A
ganastss@memphis.edu, ganastss2@gmail.com
http://web0.msci.memphis.edu/~ganastss/jocaaa/

The main purpose of "J.Computational Analysis and Applications" is to publish high quality research articles from all subareas of Computational Mathematical Analysis and its many potential applications and connections to other areas of Mathematical Sciences. Any paper whose approach and proofs are computational,using methods from Mathematical Analysis in the broadest sense is suitable and welcome for consideration in our journal, except from Applied Numerical Analysis articles. Also plain word articles without formulas and proofs are excluded. The list of possibly connected mathematical areas with this publication includes, but is not restricted to: Applied Analysis, Applied Functional Analysis, Approximation Theory, Asymptotic Analysis, Difference Equations, Differential Equations, Partial Differential Equations, Fourier Analysis, Fractals, Fuzzy Sets, Harmonic Analysis, Inequalities, Integral Equations, Measure Theory, Moment Theory, Neural Networks, Numerical Functional Analysis, Potential Theory, Probability Theory, Real and Complex Analysis, Signal Analysis, Special Functions, Splines, Stochastic Analysis, Stochastic Processes, Summability, Tomography, Wavelets, any combination of the above, e.t.c.

"J.Computational Analysis and Applications" is a peer-reviewed Journal. See the instructions for preparation and submission **of articles to JOCAAA.**

Journal of Computational Analysis and Applications(JoCAAA) is published by **EUDOXUS PRESS,LLC**,1424 Beaver Trail Drive,Cordova,TN38016,USA,anastassioug@yahoo.com http://www.eudoxuspress.com. **Annual Subscription Prices**:For USA and Canada,Institutional:Print $600, Electronic OPEN ACCESS. Individual:Print $300. For any other part of the world add $150 more(handling and postages) to the above prices for Print. No credit card payments.

JoCAAA is reviewed and abstracted by Elsevier-Scopus, available also via EBSCO publishing and EBSCO.

Editorial Board

Associate Editors of Journal of Computational Analysis and Applications

George Cybenko
Thayer School of Engineering
Dartmouth College
8000 Cummings Hall,
Hanover, NH 03755-8000
603-646-3843 (X 3546 Secr.)
e-mail:george.cybenko@dartmouth.edu
Approximation Theory and Neural Networks

Sever S. Dragomir
School of Computer Science and Mathematics, Victoria University,
PO Box 14428,
Melbourne City,
MC 8001, AUSTRALIA
Tel. +61 3 9688 4437
Fax +61 3 9688 4050
e-mail: sever.dragomir@vu.edu.au
Inequalities, Functional Analysis, Numerical Analysis, Approximations, Information Theory, Stochastics.

Oktay Duman
TOBB University of Economics and Technology,
Department of Mathematics, TR-06530, Ankara, Turkey,
e-mail: oduman@etu.edu.tr
Classical Approximation Theory, Summability Theory, Statistical Convergence and its Applications

J .A. Goldstein
Department of Mathematical Sciences
The University of Memphis
Memphis, TN 38152
901-678-3130
e-mail: jgoldste@memphis.edu
Partial Differential Equations, Semigroups of Operators

H. H. Gonska
Department of Mathematics
University of Duisburg
Duisburg, D-47048
Germany
011-49-203-379-3542
e-mail: heiner.gonska@uni-due.de
Approximation Theory, Computer Aided Geometric Design

John R. Graef
Department of Mathematics
University of Tennessee at Chattanooga
Chattanooga, TN 37304 USA
e-mail: John-Graef@utc.edu
Ordinary and functional differential equations, difference equations, impulsive systems, differential inclusions, dynamic equations on time scales, control theory and their applications

Weimin Han
Department of Mathematics
University of Iowa
Iowa City, IA 52242-1419
319-335-0770
e-mail: whan@math.uiowa.edu
Numerical analysis, Finite element method, Numerical PDE, Variational inequalities, Computational mechanics

Tian-Xiao He
Department of Mathematics and Computer Science
P.O. Box 2900, Illinois Wesleyan University
Bloomington, IL 61702-2900, USA
Tel (309)556-3089
Fax (309)556-3864
e-mail: the@iwu.edu
Approximations, Wavelet, Integration Theory, Numerical Analysis, Analytic Combinatorics

Margareta Heilmann
Faculty of Mathematics and Natural Sciences, University of Wuppertal
Gaußstraße 20
D-42119 Wuppertal, Germany,
heilmann@math.uni-wuppertal.de
Approximation Theory (Positive Linear Operators)

Xing-Biao Hu
Institute of Computational Mathematics
AMSS, Chinese Academy of Sciences
Beijing, 100190, CHINA
e-mail: hxb@lsec.cc.ac.cn
Computational Mathematics

Jong Kyu Kim
Department of Mathematics
Kyungnam University
Masan Kyungnam,631-701,Korea
Tel 82-(55)-249-2211
Fax 82-(55)-243-8609

tel: +30(210) 772 1722
Fax +30(210) 772 1775
e-mail: papanico@math.ntua.gr
Partial Differential Equations, Probability

Choonkil Park
Department of Mathematics
Hanyang University
Seoul 133-791
S. Korea,
e-mail: baak@hanyang.ac.kr
Functional Equations

Svetlozar (Zari) Rachev,
Professor of Finance, College of Business, and Director of Quantitative Finance Program,
Department of Applied Mathematics & Statistics
Stonybrook University
312 Harriman Hall, Stony Brook, NY 11794-3775
tel: +1-631-632-1998,
svetlozar.rachev@stonybrook.edu

Alexander G. Ramm
Mathematics Department
Kansas State University
Manhattan, KS 66506-2602
e-mail: ramm@math.ksu.edu
Inverse and Ill-posed Problems, Scattering Theory, Operator Theory, Theoretical Numerical Analysis, Wave Propagation, Signal Processing and Tomography

Tomasz Rychlik
Polish Academy of Sciences
Instytut Matematyczny PAN
00-956 Warszawa, skr. poczt. 21
ul. Śniadeckich 8
Poland
e-mail: trychlik@impan.pl
Mathematical Statistics, Probabilistic Inequalities

Boris Shekhtman
Department of Mathematics
University of South Florida
Tampa, FL 33620, USA
Tel 813-974-9710
e-mail: shekhtma@usf.edu
Approximation Theory, Banach spaces, Classical Analysis

T. E. Simos
Department of Computer Science and Technology
Faculty of Sciences and Technology
University of Peloponnese
GR-221 00 Tripolis, Greece
Postal Address:
26 Menelaou St.
Anfithea - Paleon Faliron
GR-175 64 Athens, Greece
e-mail: tsimos@mail.ariadne-t.gr
Numerical Analysis

Jagdev Singh
JECRC University, Jaipur, India
jagdevsinghrathore@gmail.com
Fractional Calculus, Mathematical Modelling, Special Functions, Numerical Methods

H. M. Srivastava
Department of Mathematics and Statistics
University of Victoria
Victoria, British Columbia V8W 3R4
Canada
tel.250-472-5313; office,250-477-6960 home, fax 250-721-8962
e-mail: harimsri@math.uvic.ca
Real and Complex Analysis, Fractional Calculus and Appl., Integral Equations and Transforms, Higher Transcendental Functions and Appl.,q-Series and q-Polynomials, Analytic Number Th.

I. P. Stavroulakis
Department of Mathematics
University of Ioannina
451-10 Ioannina, Greece
e-mail: ipstav@cc.uoi.gr
Differential Equations
Phone +3-065-109-8283

Jessada Tariboon
Department of Mathematics
King Mongut’s University of Technology N. Bangkok
1518 Pracharat 1 Rd., Wongsawang, Bangsue, Bangkok, Thailand 10800
e-mail: jessada.t@sci.kmutnb.ac.th
Time scales
Differential/Difference Equations, Fractional Differential Equations

Manfred Tasche
Department of Mathematics
University of Rostock

D-18051 Rostock, Germany
manfred.tasche@mathematik.uni-rostock.de
Numerical Fourier Analysis, Fourier Analysis, Harmonic Analysis, Signal Analysis, Spectral Methods, Wavelets, Splines, Approximation Theory

Juan J. Trujillo
University of La Laguna
Departamento de Analisis Matematico
C/Astr.Fco.Sanchez s/n
38271. LaLaguna. Tenerife.
SPAIN
Tel/Fax 34-922-318209
e-mail: Juan.Trujillo@ull.es
Fractional: Differential Equations-Operators-Fourier Transforms, Special functions, Approximations, and Applications

Xiao-Jun Yang
State Key Laboratory for Geomechanics and Deep Underground Engineering, China
University of Mining and Technology, Xuzhou 221116, China
Local Fractional Calculus and Applications, Fractional Calculus and Applications, General Fractional Calculus and Applications, Variable-order Calculus and Applications, Viscoelasticity and Computational methods for Mathematical Physics.dyangxiaojun@163.com

Xiang Ming Yu
Department of Mathematical Sciences
Southwest Missouri State University
Springfield, MO 65804-0094
417-836-5931
e-mail: xmy944f@missouristate.edu
Classical Approximation Theory, Wavelets

Richard A. Zalik
Department of Mathematics
Auburn University
Auburn University, AL 36849-5310
USA.
Tel 334-844-6557 office
Fax 334-844-6555
e-mail: zalik@auburn.edu
Approximation Theory, Chebychev Systems, Wavelet Theory

Ahmed I. Zayed
Department of Mathematical Sciences
DePaul University
2320 N. Kenmore Ave.
Chicago, IL 60614-3250
773-325-7808
e-mail: azayed@condor.depaul.edu
Shannon sampling theory, Harmonic analysis and wavelets, Special functions and orthogonal polynomials, Integral transforms

Ding-Xuan Zhou
Department Of Mathematics
City University of Hong Kong
83 Tat Chee Avenue
Kowloon, Hong Kong
852-2788 9708,Fax:852-2788 8561
e-mail: mazhou@cityu.edu.hk
Approximation Theory, Spline functions, Wavelets

Xin-long Zhou
Fachbereich Mathematik, Fachgebiet Informatik
Gerhard-Mercator-Universitat Duisburg
Lotharstr.65, D-47048 Duisburg, Germany
e-mail:Xzhou@informatik.uni-duisburg.de
Fourier Analysis, Computer-Aided Geometric Design, Computational Complexity, Multivariate Approximation Theory, Approximation and Interpolation Theory

Instructions to Contributors
Journal of Computational Analysis and Applications

An international publication of Eudoxus Press, LLC, of TN.

Editor in Chief: George Anastassiou

Department of Mathematical Sciences
University of Memphis
Memphis, TN 38152-3240, U.S.A.

1. Manuscripts files in Latex and PDF and in English, should be submitted via email to the Editor-in-Chief:

Prof.George A. Anastassiou
Department of Mathematical Sciences
The University of Memphis
Memphis,TN 38152, USA.
Tel. 901.678.3144
e-mail: ganastss@memphis.edu

Authors may want to recommend an associate editor the most related to the submission to possibly handle it.

Also authors may want to submit a list of six possible referees, to be used in case we cannot find related referees by ourselves.

2. Manuscripts should be typed using any of TEX,LaTEX,AMS-TEX,or AMS-LaTEX and according to EUDOXUS PRESS, LLC. LATEX STYLE FILE. (Click HERE to save a copy of the style file.)They should be carefully prepared in all respects. Submitted articles should be brightly typed (not dot-matrix), double spaced, in ten point type size and in 8(1/2)x11 inch area per page. Manuscripts should have generous margins on all sides and should not exceed 24 pages.

3. Submission is a representation that the manuscript has not been published previously in this or any other similar form and is not currently under consideration for publication elsewhere. A statement transferring from the authors(or their employers,if they hold the copyright) to Eudoxus Press, LLC, will be required before the manuscript can be accepted for publication.The Editor-in-Chief will supply the necessary forms for this transfer.Such a written transfer of copyright,which previously was assumed to be implicit in the act of submitting a manuscript,is necessary under the U.S.Copyright Law in order for the publisher to carry through the dissemination of research results and reviews as widely and effective as possible.

4. The paper starts with the title of the article, author's name(s) (no titles or degrees), author's affiliation(s) and e-mail addresses. The affiliation should comprise the department, institution (usually university or company), city, state (and/or nation) and mail code.

The following items, 5 and 6, should be on page no. 1 of the paper.

5. An abstract is to be provided, preferably no longer than 150 words.

6. A list of 5 key words is to be provided directly below the abstract. Key words should express the precise content of the manuscript, as they are used for indexing purposes.

The main body of the paper should begin on page no. 1, if possible.

7. All sections should be numbered with Arabic numerals (such as: 1. INTRODUCTION) .
Subsections should be identified with section and subsection numbers (such as 6.1. Second-Value Subheading).
If applicable, an independent single-number system (one for each category) should be used to label all theorems, lemmas, propositions, corollaries, definitions, remarks, examples, etc. The label (such as Lemma 7) should be typed with paragraph indentation, followed by a period and the lemma itself.

8. Mathematical notation must be typeset. Equations should be numbered consecutively with Arabic numerals in parentheses placed flush right, and should be thusly referred to in the text [such as Eqs.(2) and (5)]. The running title must be placed at the top of even numbered pages and the first author's name, et al., must be placed at the top of the odd numbed pages.

9. Illustrations (photographs, drawings, diagrams, and charts) are to be numbered in one consecutive series of Arabic numerals. The captions for illustrations should be typed double space. All illustrations, charts, tables, etc., must be embedded in the body of the manuscript in proper, final, print position. In particular, manuscript, source, and PDF file version must be at camera ready stage for publication or they cannot be considered.

Tables are to be numbered (with Roman numerals) and referred to by number in the text. Center the title above the table, and type explanatory footnotes (indicated by superscript lowercase letters) below the table.

10. List references alphabetically at the end of the paper and number them consecutively. Each must be cited in the text by the appropriate Arabic numeral in square brackets on the baseline.
References should include (in the following order):
initials of first and middle name, last name of author(s)
title of article,

name of publication, volume number, inclusive pages, and year of publication.

Authors should follow these examples:

Journal Article

1. H.H.Gonska,Degree of simultaneous approximation of bivariate functions by Gordon operators, (journal name in italics) *J. Approx. Theory*, 62,170-191(1990).

Book

2. G.G.Lorentz, (title of book in italics) *Bernstein Polynomials* (2nd ed.), Chelsea,New York,1986.

Contribution to a Book

3. M.K.Khan, Approximation properties of beta operators,in(title of book in italics) *Progress in Approximation Theory* (P.Nevai and A.Pinkus,eds.), Academic Press, New York,1991,pp.483-495.

11. All acknowledgements (including those for a grant and financial support) should occur in one paragraph that directly precedes the References section.

12. Footnotes should be avoided. When their use is absolutely necessary, footnotes should be numbered consecutively using Arabic numerals and should be typed at the bottom of the page to which they refer. Place a line above the footnote, so that it is set off from the text. Use the appropriate superscript numeral for citation in the text.

13. After each revision is made please again submit via email Latex and PDF files of the revised manuscript, including the final one.

14. Effective 1 Nov. 2009 for current journal page charges, contact the Editor in Chief. Upon acceptance of the paper an invoice will be sent to the contact author. The fee payment will be due one month from the invoice date. The article will proceed to publication only after the fee is paid. The charges are to be sent, by money order or certified check, in US dollars, payable to Eudoxus Press, LLC, to the address shown on the Eudoxus homepage.

No galleys will be sent and the contact author will receive one (1) electronic copy of the journal issue in which the article appears.

15. This journal will consider for publication only papers that contain proofs for their listed results.

Analysing the conduction of heat in porous medium via Caputo fractional operator with Sumudu transform

Lalit Mohan[a,b], Amit Prakash[a,*]

[a]National Institute of Technology Kurukshetra, Kurukshetra 136119, Haryana, India,
[b] Department of Applied Science, Government Polytechnic Dhamlawas, Rewari-123401, India.
Corresponding author:amitmath@nitkkr.ac.in(A. Prakash)

Abstract. In this article, we analyse the fractional Cattaneo heat equation for studying the conduction of heat in porous medium. This equation is also used in studying extended irreversible thermodynamics, material, plasma, cosmological model, computational biology, and diffusion theory in crystalline solids. The Sumudu adomian decomposition technique, which is combination of Sumudu transform and a numerical technique, is applied for getting numerical solution. The existence and uniqueness is analysed by using the fixed point theorem and the highest error of the designed technique is also analysed. Finally, the accuracy of the designed numerical method is presented by solving two examples and the findings are compared with the existing method.

Keywords: Fractional Cattaneo heat equation (FCHE), Caputo derivative, Sumudu transform, Existence and Uniqueness Analysis, Error Analysis.

1 Introduction

The Fractional calculus (FC) has developed into a vital tool for modelling and solving the events in engineering and sciences. It is utilised in many different scientific fields. Additionally, because of its ability to be remembered and passed on, it is quite useful in replicating and understanding natural occurrences. The fractional Caputo derivative [1] is one of the best fractional derivatives available in the literature. Various fractional mathematical models were explored and examined by numerous researchers, like the fractional diffusion-wave equation studied in [2], the fractional Brain tumour model [3], Whitham–Broer–Kaup equation with fractional order is presented in [4], the problem of oil spill is analysed in [5], the existence and

uniqueness for fractional Cauchy reaction diffusion equations is analysed in [6], the time fractional wave equations is studied in [7], the 2019-nCOV outbreaks is studied in [8], the COVID-19 model is analysed through singular and non-singular fractional operators in [9], the fractional hosta parasitoid population dynamical model is studied in [10], the fractional model for population dynamics of two interacting species is studied in [11], the fractional Riccati differential equation is studied in [12], the Coupled Schrodinger-KdV equation is analysed with Caputo-Katugampola Type Memory in [13], the SIR model is studied via Morgan-Voyce series in [14], the singularly perturbed Volterra integro-differential equations with delay is solved in [15] and the generalized equal width wave equation is investigated in [16].

There are many numerical techniques available in the literature for solving fractional order differential equations such as; the generalized Adams-Bashforth-Moultan method [17], the optimal control technique [18], the Taylor series expansion method [19], the Haar wavelet method [20], the homotopy perturbation Sumudu transform method [21] and the sine-gordon expansion method [22].

The fractional diffusion models have been used to define anomalous diffusion in a variety of ways [23,24,25,26]. As a result, anticipating heat transport behaviour has caught scientists' attention. The heat conduction model based of Fouriera's law is sufficient for the majority of applications. However, this model violates the rules of physics since the thermal disturbances propagate at an infinite pace [27,28,29]. For instance, fractional order derivatives describe the Fick's laws of fractional order, which are available. This method is used to produce the Cattaneo equation, which is used to explain fractional order diffusion models and heat and mass transport [30]. The law of heat condition was given by Fourier [31], first time in 1822. Even though it was simply a hypothesis law, it gave the two centuries of thermal conduction study that followed a framework and made it possible to characterise heat transport routes. Fourier's law was updated by Cattaneo [32] in 1948 by include the idea of relaxation time. Using Oldroyd's upper convected derivative [33] and modifying the rule given by the Cattaneo in 2009, Christov [34] created an equation with a only one parameter of temperature.

We consider the following fractional Cattaneo heat equation (FCHE)

$$ {}_0^cD_t^\alpha u(x,y,t) + \beta u_t(x,y,t) - \Delta u(x,y,t) = f(x,y,t), \quad (x,y,t) \in \Omega \times (0,T] \tag{1} $$

with

$$ u(x,y,0) = g(x,y), \frac{\partial u(x,y,0)}{\partial t} = \varphi(x,y), (x,y) \in \Omega \tag{2} $$

where $u(x,y,t)$ is the heat distribution function, β is a constant, $f(x,y,t)$ is the given source term, Ω is bounded domain , ${}_0^cD_t^\alpha$ is the Caputo fractional operator of order α with $1 < \alpha \leq 2, g(x,y)$, and $\varphi(x,y)$ are given smooth functions.
The main aim of this research is to examine the FCHE with Caputo fractional operator. The Sumudu adomian decomposition technique (SADT) is used to get numerical solution. The existence and uniqueness is analysed by using the fixed point theorem, also the maximum error of the SADT is investigated. The uniqueness of this study is that it provides an accurate prediction regarding the method of conduction of heat for addressing thermo-elastic issues in porous medium. The main achievement of this work is to design a very effective technique for solution of FCHE that allows for the detailed investigation of the heat conduction process in porous media. This study's findings will be useful for studying extended irreversible thermodynamics, material, plasma, cosmological model, computational biology, and diffusion theory in crystalline solids.

2 Basic definitions of Fractional Calculus

Def. 2.1. [1]The Caputo derivative of $y(t)$ is given by

$$ \mathrm{D}^\alpha y(t) = I^{m-\alpha} D^m y(t) = \frac{1}{\Gamma(m-\alpha)} \int_0^t (t-f)^{m-\alpha-1} y^m(f) df $$

where $m-1 < \alpha \leq m$.
Def. 2.2. [35] The Sumudu transform (ST) of a given function $y(t)$ is defined as

$$ ST[y(t)] = \int_0^\infty e^{-t} y(vt) dt, v \in (-t_1, t_2) \, . $$

Def. 2.3. [35] The ST of the Caputo fractional order derivative is given by

$$ST\left[D_t^{\alpha}y(t)\right] = v^{-\alpha}ST[y(t)] - \sum_{k=0}^{m-1} v^{(-\alpha+k)}y^{(k)}(0)$$

Theorem 2.1. [1] If ${}_0^cD_t^{\alpha}y(t) = e(t)$, then its unique solution is defined as

$$y(t) = \frac{1}{\Gamma(\alpha)}\int_0^t (t-f)^{\alpha-1}e(f)df$$

where $0 < \alpha \leq 1$.

3 Existence and Uniqueness Analysis of the FCHE

The FCHE is given by equation (1) can be written in the form

$${}_0^cD_t^{\alpha} = \psi(x, y, t, u), \tag{3}$$

where $\psi(x, y, t, u) = \Delta u(x, y, t) - \beta u_t(x, y, t) + f(x, y, t)$.
Equation (3) can be converted into the Voltera type integral equation using theorem (2.1):

$$u(x, y, t) - u(x, y, 0) = \frac{1}{\Gamma(\alpha)}\int_0^t (t-s)^{\alpha-1}\psi(x, y, s, u)ds. \tag{4}$$

Next, we have to prove that $\psi(x, y, t, u)$ satisfy Lipschitz condition.
Theorem 3.1. [3] The function $\psi(x, y, t, u)$ in the given Voltera equation satisfies both the contraction if $0 < \eta \leq 1$, where $\eta = \delta^2 - \beta\mu$ and the Lipschitz condition.
Proof: Let $u(x, y, t)$ is bounded. So, we have

$$\begin{aligned}\|\psi(x, y, t, u) - \psi(x, y, t, \rho)\| &= ||u_{xx}(x, y, t) - \beta u_t(x, y, t) \\ &\quad + f(x, y, t) - \rho_{xx}(x, y, t) \\ &\quad + \beta\rho_t(x, y, t) - f(x, y, t)|| \\ &= \|(u_{xx} - \rho_{xx}) - \beta(u_t - \rho_t)\|, \\ &\leq \delta^2\|(u - \rho)\| - \beta\mu\|(u - \rho)\|\end{aligned}$$

$$\|\psi(x,y,t,u) - \psi(x,y,t,\rho)\| \leq (\delta^2 - \beta\mu)\|(u-\rho)\| \tag{5}$$

Letting $\eta = (\delta^2 - \beta\mu)$, then

$$\|\psi(x,y,t,u) - \psi(x,y,t,\rho)\| \leq \eta\|(u-\rho)\|$$

Thus, $\psi(x,y,t,u)$ satisfies Lipschitz and contraction condition if $0 < \eta \leq 1$. So, the iterative formula for the existence of above condition is represented as

$$u_{n+1}(x,y,t) = \frac{1}{\Gamma(\alpha)}\int_0^t (t-s)^{\alpha-1}\psi(x,y,s,u_n)ds, \tag{6}$$

with initial condition as $u(x,y,0) = u(x,y,t_0)$.
The two consecutive terms are differ by

$$\begin{aligned}\psi_n(x,y,t) &= u_n(x,y,t) - u_{n+1}(x,y,t)\\ &= \frac{1}{\Gamma(\alpha)}\int_0^t (t-s)^{\alpha-1}\{\psi(x,y,s,u_{n-1}) - \psi(x,y,t,u_{n-2})\}ds\end{aligned} \tag{7}$$

It can be observed that

$$u_n(x,y,t) = \sum_{i=0}^{n}\psi_i(x,y,t) \tag{8}$$

so, from equation (7), we have

$$\|\psi_n(x,y,t)\| = \|u_n(x,y,t) - u_{n-1}(x,y,t)\|. \tag{9}$$

Using Triangular inequality, equation (6) becomes

$$\|\psi_n(x,y,t)\| \leq \frac{1}{\Gamma(\alpha)}\eta\|\int_0^t (t-s)^{\alpha-1}\psi_{n-1}(x,y,s)ds\|. \tag{10}$$

Theorem 3.2. [3] The solution of the equation (3) exist if there exists a t_0 which satisfy

$$\frac{1}{\Gamma(\alpha)}\eta t_0^{\alpha} \leq 1.$$

Proof: Let $u(x,y,t)$ is be bounded and Lipschitz function then using equation (10), we get

$$\|\psi_n(x,y,t)\| \leq \|u_n(x,y,t)\| \left[\frac{1}{\Gamma(\alpha)}\eta.t^{\alpha}\right]^n. \tag{11}$$

Thus, it is established that the given solution exists and is continuous.

$$u(x,y,t) - u(x,y,0) = u_n(x,y,t) - \gamma_n(x,y,t), \tag{12}$$

here, we consider that

$$\begin{aligned}
\|\gamma_n(x,y,t)\| &= \|\frac{1}{\Gamma(\alpha)}\int_0^t (t-s)^{\alpha-1}\{\psi(x,y,s,u_n) - \psi(x,y,t,u_{n-1})\}ds\|, \\
&\leq \frac{1}{\Gamma(\alpha)}\|\int_0^t (t-s)^{\alpha-1}\{\psi(x,y,s,u_n) - \psi(x,y,t,u_{n-1})\}ds\|, \\
&\leq \frac{1}{\Gamma(\alpha)}\eta\|u_n(x,y,t) - u_{n-1}(x,y,t)t\|.
\end{aligned}$$

In the same way at t_0, we have

$$\|\gamma_n(x,y,t)\| \leq \left[\frac{1}{\Gamma(\alpha)}t_0^{\alpha}\right]^{n+1} \eta^{n+1}M. \tag{13}$$

As $n \to \infty$, we can clearly see that $\|\gamma_n(x,u,t)\| \to 0$.

Theorem 3.3. [3] The FCHE will have a unique solution if the following condition holds

$$\left(1 - \frac{1}{\Gamma(\alpha)}\eta t^{\alpha}\right) > 0.$$

Proof: Let $w(x,y,t)$ is another solution of (3), then

$$\begin{aligned}
\|u(x,y,t) - w(x,y,t)\| = \|\frac{1}{\Gamma(\alpha)}\int_0^t (t-s)^{\alpha-1}(\psi(x,y,s,u) \\
- \psi(x,y,t,w))ds\|,
\end{aligned}$$

$$\|u(x,y,t) - w(x,y,t)\| \leq \frac{1}{\Gamma(\alpha)}\eta\|u(x,y,t) - w(x,y,t)\| \tag{14}$$

Now, on simplifying (14), we have

$$\|u(x,y,t)-w(x,y,t)\|\left(1-\frac{1}{\Gamma(\alpha)}\eta t^{\alpha}\right)\leq 0$$

hence, if

$$\left(1-\frac{1}{\Gamma(\alpha)}\eta t^{\alpha}\right)>0. \tag{15}$$

then, $u(x,y,t)=w(x,y,t)$.
Hence, the FCHE possess a unique solution.

4 Application of the designed technique to the FCHE

In this part of the article, we apply the proposed technique to the FCHE and we consider the following FCHE

$${}_0^cD_0^{\alpha}u(x,y,t)+\beta u_t(x,y,t)-\Delta u(x,y,t)=f(x,y,t) \tag{16}$$

where $(x,y,t)\in\Omega(0,T], 1<\alpha\leq 2$, with

$$u(x,y,0)=g(x,y),\ \frac{\partial u(x,y,0)}{\partial t}=\phi(x,y),(x,y)\in\Omega. \tag{17}$$

Now, we apply ST on equation (16), we have

$$ST\left[{}_0^cD_t^{\alpha}u(x,y,t)\right]=ST[\Delta u(x,y,t)-\beta u_t(x,y,t)+f(x,y,t)].$$

From definition (2.3) and equation (17), we have

$$\frac{1}{v^{\alpha}}ST[u(x,y,t)]-\frac{1}{v^{\alpha}}u(x,y,0)-\frac{1}{v^{\alpha-1}}\frac{\partial u(x,y,\theta)}{\partial t}=ST[\Delta u(x,y,t)-\beta u_t(x,y,t)+f(x,y,t)]$$

$$\frac{1}{v^{\alpha}}ST[u(x,y,t)]=\frac{1}{v^{\alpha}}u(x,y,0)+\frac{1}{v^{\alpha-1}}\frac{\partial u(x,y,\theta)}{\partial t}+ST[\Delta u(x,y,t)-\beta u_t(x,y,t)+f(x,y,t)]$$

$$ST[u(x,y,t)] = g(x,y) + v\varphi(x,y) + v^{\alpha}ST[\Delta u(x,y,t) - \beta u_t(x,y,t) + f(x,y,t)].$$

Applying ST inverse on above equation, we have

$$u(x,y,t) = g(x,y) + t\varphi(x,y,t) + ST^{-1}\Big\{v^{\alpha}[ST\Delta u(x,y,t) - \beta u_t(x,y,t) + f(x,y,t)]\Big\}. \tag{18}$$

Applying the Adomian decomposition method to equation (18), so we take

$$u(x,y,t) = \sum_{n=0}^{\infty} p^n u(x,y,t).$$

Hence, we get

$$\sum_{n=0}^{\infty} p^n u(x,y,t) = g(x,y) + t\varphi(x,y) + ST^{-1}\Big\{v^{\alpha}ST\Big[\sum_{n=0}^{\infty} p^n \Delta u_n(x,y,t) - \beta\sum_{n=0}^{\infty} p^n (u_n)_t(x,y,t) + f(x,y,t)\Big]\Big\}. \tag{19}$$

Comparing the coefficient of like powers of p of equation (19), we have

$$u_0(x,y,t) = g(x,y) + t\varphi(x,y), \tag{20}$$

$$u_1(x,y,t) = ST^{-1}\{v^{\alpha}ST[\Delta u_0(x,y,t) - \beta(u_0)_t(x,y,t) + f(x,y,t)]\}, \tag{21}$$

$$u_2(x,y,t) = ST^{-1}\{v^{\alpha}ST[\Delta u_1(x,y,t) - \beta(u_1)_t(x,y,t) + f(x,y,t)]\}, \tag{22}$$

$$u_n(x,y,t) = ST^{-1}(v^{\alpha}ST[\Delta u_{n-1}(x,y,t) - \beta(u_{n-1})_t(x,y,t) + f(x,y,t)]), \tag{23}$$

The final solution is given by

$$u(x,y,t) = \lim_{k\to\infty} \sum_{n=0}^{k} u_n(x,y,t). \tag{24}$$

5 Error Analysis of the SADT

The maximum error of the SADT is examined in this section.
Theorem 5.1. [3] If $\exists, 0 < \epsilon < 1$ such that $\|u_{n+1}(x,y,t)\| \leq \epsilon\|u_n(x,y,t)\|$, for all n and if the series $\sum_{n=0}^{r} u_n(x,y,t)$ is the approximate solution $u(x,y,t)$, then the maximum error is given by

$$\|u(x,y,t) - \sum_{n=0}^{r} u_n(x,y,t)\| \leq \frac{\epsilon^{r+1}}{(1-\epsilon)}\|u_0(x,y,t)\|.$$

Proof: We have

$$\begin{aligned}
\|u(x,y,t) - \sum_{n=0}^{r} u_n(x,y,t)\| &= \|\sum_{n=r+1}^{\infty} u_n(x,y,t)\| \\
&\leq \sum_{n=r+1}^{\infty} \|u_n(x,y,t)\| \\
&\leq \sum_{n=r+1}^{\infty} \epsilon^m \|u_0(x,y,t)\| \\
&\leq (\epsilon)^{r+1}[1 + (\epsilon)^1 + (\epsilon)^2 + \cdots]\|u_0(x,y,t)\| \\
&\leq \frac{\epsilon^{r+1}}{1-\epsilon}\|u_0(x,y,t)\|.
\end{aligned}$$

Hence proved.

6 Numerical Simulation

Two examples of the FCHE have been solve in this section to validate the designed technique
Application 6.1. Consider FCHE given in the article [36]

$${}_0^c D_t^{\alpha} u(x,y,t) + u_t(x,y,t) - \Delta u(x,y,t) = \left(\frac{6t^{3-\alpha}}{\Gamma(4-\alpha)} - 2t^3 + 3t^2\right) e^{x+y} \tag{25}$$

$(x, y, t) \in \Omega \times (0, T]$, and the analytical solution of equation (25) at $\alpha = 2$ is $u(x, y, t) = t^3 e^{x+y}$.

Solution. Here $\beta = 1$, $f(x, y, t) = \left(\frac{6t^{3-\alpha}}{\Gamma(4-\alpha)} - 2t^3 + 3t^2\right) e^{x+y}$, and from the analytical solution we can find the initial conditions. Now, we apply SADT to equation (25) so, we get

$u_0(x, y, t) = 0,$

$u_1(x, y, t) = e^{x+y}\left[6\frac{t^3}{\Gamma(4)} - 2\frac{t^{\alpha+3}}{\Gamma(\alpha+4)} + 3\frac{t^{\alpha+2}}{\Gamma(\alpha+3)}\right],$

$$u_2(x, y, t) = e^{x+y}\left[6\frac{t^3}{\Gamma(4)} - \frac{3}{2}\frac{t^{\alpha+3}}{\Gamma(\alpha+4)} + \frac{9}{4}\frac{t^{\alpha+2}}{\Gamma(\alpha+3)} - 4\frac{t^{2\alpha+3}}{\Gamma(2\alpha+4)}\right.$$

$$\left. + \frac{3(\alpha+2)}{(\alpha+3)}\frac{t^{2\alpha+1}}{\Gamma(2\alpha+2)} + \frac{(9\alpha+24)}{(\alpha+3)}\frac{t^{2\alpha+2}}{\Gamma(2\alpha+3)}\right],$$

$$u_3(x, y, t) = e^{x+y}\left[6\frac{t^3}{\Gamma(4)} - 42\frac{t^{\alpha+3}}{\Gamma(\alpha+4)} + 6\frac{t^{\alpha+2}}{\Gamma(\alpha+3)} - 3\frac{t^{2\alpha+3}}{\Gamma(2\alpha+4)}\right.$$

$$-8\frac{t^{3\alpha+3}}{\Gamma(3\alpha+4)} + \frac{(9\alpha+18)}{(4\alpha+12)}\frac{t^{2\alpha+1}}{\Gamma(2\alpha+2)} + \frac{(21\alpha+15)}{(2\alpha+8)}\frac{t^{2\alpha+2}}{\Gamma(2\alpha+3)}$$

$$+\left(\frac{18\alpha+48}{\alpha+3} + \frac{8\alpha+12}{2\alpha+4}\right)\frac{t^{3\alpha+2}}{\Gamma(3\alpha+3)} - \frac{3(2\alpha+1)(\alpha+2)}{(2\alpha+2)(\alpha+3)}\frac{t^{3\alpha}}{\Gamma(3\alpha+1)}$$

$$\left. + \left(\frac{(6\alpha+12)}{(\alpha+3)} - \frac{(9\alpha+24)(2\alpha+2)}{(\alpha+3)(2\alpha+3)}\right)\frac{t^{3\alpha+1}}{\Gamma(3\alpha+2)}\right].$$

The final solution is given by

$$\mathrm{u}(x, y, t) = u_0(x, y, t) + u_1(x, y, t) + u_2(x, y, t) + u_3(x, y, t) + \ldots \tag{26}$$

Table 1. Maximum absolute error for $(x, y) \in [0.01, 0.1]$ and distinct value of t and α for Ex. 6.1.

t	$\alpha = 2$	$\alpha = 1.95$
0.01	$1.901724e^{-06}$	$2.023245e^{-06}$
0.02	$2.115769e^{-05}$	$2.279847e^{-05}$
0.03	9.413964^{-05}	$2.023245e^{-04}$
0.04	$2.856856e^{-04}$	$3.085486e^{-04}$
0.05	$7.015689e^{-04}$	$7.553783e^{-04}$
0.06	$1.505322e^{-03}$	$1.613395e^{-03}$
0.07	$2.939414e^{-03}$	$3.132917e^{-03}$
0.08	$5.350787e^{-03}$	$5.667438e^{-03}$
0.09	$9.220735e^{-03}$	$9.701331e^{-03}$
0.10	$1.519915e^{-02}$	$1.519915e^{-02}$

Table 2. The Comparative analysis of maximum absolute error for the SADT and existing methods for distinct value of t and α, for Ex. 6.1.

t	$\alpha = 1.45$		$\alpha = 1.65$	
Methods	**SADT**	**RBF PU Method [36]**	**SADT**	**RBF PU Method [36]**
1/40	$1.2520e^{-04}$	$1.4587e^{-04}$	$7.6894e^{-04}$	$1.9204e^{-04}$
1/80	$1.0872e^{-05}$	$5.0793e^{-05}$	$6.3571e^{-06}$	$7.6507e^{-05}$
1/160	$1.0045e^{-06}$	$1.7519e^{-05}$	$5.7788e^{-07}$	$3.0822e^{-05}$
1/320	$9.6980e^{-08}$	$6.1028e^{-06}$	$5.6512e^{-08}$	$1.2305e^{-05}$
1/640	$9.7131e^{-09}$	$2.1131e^{-06}$	$5.8764e^{-09}$	$4.8922e^{-06}$
1/1280	$1.0060e^{-09}$	$7.2381e^{-07}$	$6.4297e^{-10}$	$1.9304e^{-06}$

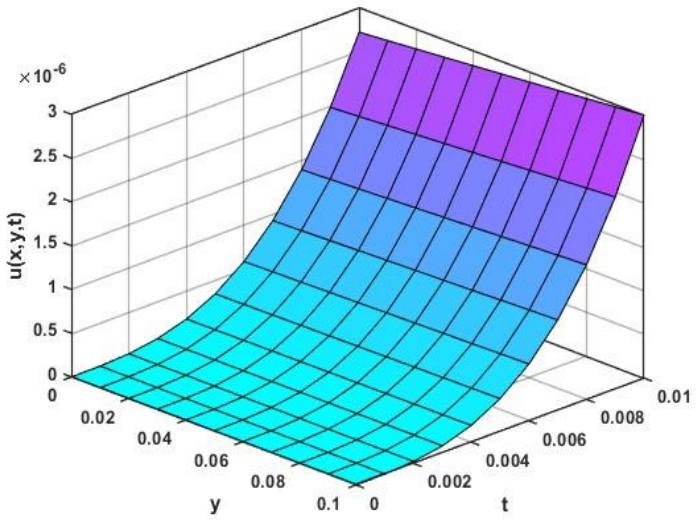

Fig. 1. Approximate solution $u(x, y, t)$ at $x = 0.1$ and α=2, for Ex. 6.1.

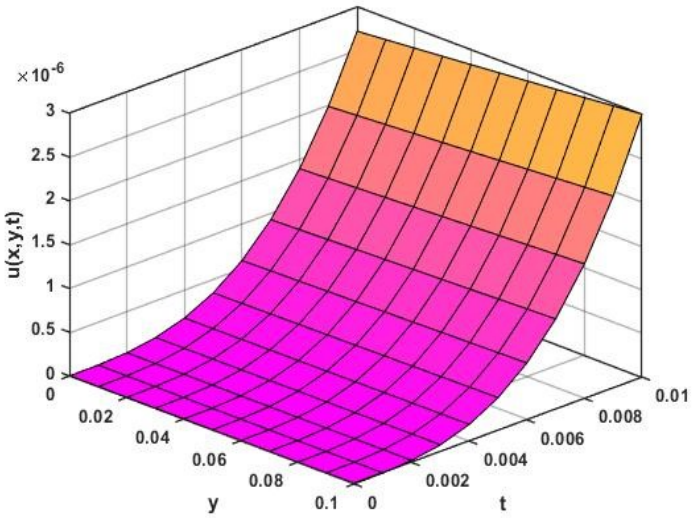

Fig. 2. Analytical solution $u(x, y, t)$ at $x = 0.1$ and α=2, for Ex. 6.1.

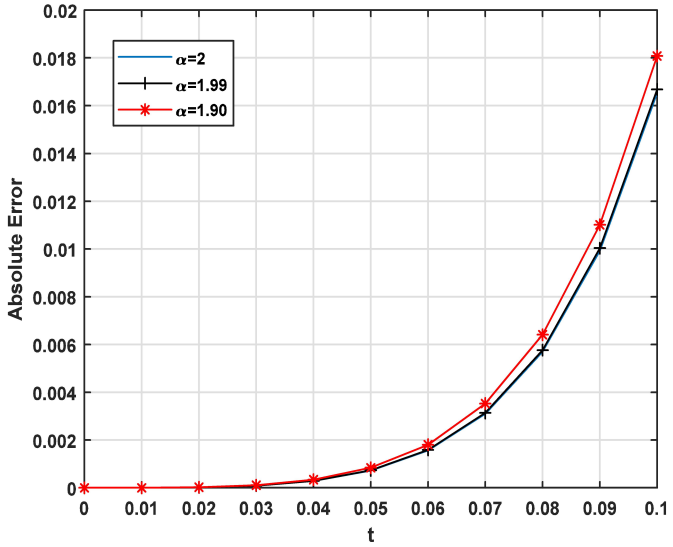

Fig. 3. Absolute error of SADT at $x = 0.1$ and distinct value of α, for Ex. 6.1.

Application 6.2. Consider another form of FCHE given in the article [36]

$$ {}_0^cD_t^\alpha u(x,y,t)+u_t(x,y,t) - \Delta u(x,y,t) = (\frac{6t^2}{\Gamma(4-\alpha)} + (2+\alpha)t^{1+\alpha} + 2\pi^2 t^{2+\alpha})\sin(\pi x)\sin(\pi y) \tag{27} $$

Where $(x,y,t) \in \Omega \times (0,T]$, and the analytical solution of (27) is $u(x,y,t) = \sin(\pi x)\sin(\pi y)t^{\alpha+2}$.

Solution. Here $f(x,y,t) = \left(\frac{6t^2}{\Gamma(4-\alpha)} + (2+\alpha)t^{1+\alpha} + 2\pi^2 t^{2+\alpha}\right)$ $\sin(\pi x)\sin(\pi y)$, $\beta = 1$, and from the analytical solution we can find the initial conditions. Now, we apply the proposed technique, SADT, to equation (27) so, we get

$u_0(x,y,t) = 0$,

$$ u_1(x,y,t) = \left[\frac{12}{\Gamma(4-\alpha)}\frac{t^{\alpha+2}}{\Gamma(\alpha+3)} + (2+\alpha)\Gamma(\alpha+2)\frac{t^{2\alpha+1}}{\Gamma(2\alpha+2)} + 2\pi^2\Gamma(\alpha+2)\frac{t^{2\alpha+2}}{\Gamma(2\alpha+3)}\right]\sin(\pi x)\sin(\pi y) $$

$$ u_2(x,y,t) = \left[\left(\frac{-24}{\Gamma(4-\alpha)} + 2\pi^2\Gamma(\alpha+3)\right) \times \frac{t^{2\alpha+2}}{\Gamma(2\alpha+3)} + \frac{t^{3\alpha}}{\Gamma(3\alpha+1)} \times \frac{(\alpha+2)(2\alpha+1)\Gamma(\alpha+2)}{(2\alpha+2)} + \left((2+\alpha)\Gamma(\alpha+2) - \frac{12(\alpha+2)}{(\alpha+3)\Gamma(4-\alpha)}\right) \times \frac{t^{2\alpha+1}}{\Gamma(2\alpha+2)} + \left(\frac{-2\pi^2\Gamma(2\alpha+2)\Gamma(\alpha+3)}{(2\alpha+3)} - 2(2+\alpha)\Gamma(\alpha+2)\right) \times \frac{t^{3\alpha+1}}{\Gamma(3\alpha+2)} - 4\pi^2\Gamma(\alpha+3)\frac{t^{3\alpha+2}}{\Gamma(3\alpha+3)} + \frac{12}{\Gamma(4-\alpha)}\frac{t^{\alpha+2}}{\Gamma(\alpha+3)}\right] \times \sin(\pi x)\sin(\pi y), $$

$$ u_3(x,y,t) = \left[\left(\frac{-2\pi^2(2\alpha+2)\Gamma(\alpha+3)}{(2\alpha+3)} - \frac{24\pi^2(\alpha+2)}{(\alpha+3)\Gamma(4-\alpha)} - \frac{24(2\alpha+2)}{(2\alpha+3)\Gamma(4-\alpha)} + 2\pi^2(2+\alpha)\frac{\Gamma(\alpha+2)}{\Gamma(2)}\right) \times \frac{t^{3\alpha+1}}{\Gamma(3\alpha+2)} + \left(\frac{-24}{\Gamma(4-\alpha)} + \right. \right. $$

$$2\pi^2\Gamma(\alpha+3))\frac{t^{2\alpha+2}}{\Gamma(2\alpha+3)}+\left(-\frac{12(\alpha+2)(2\alpha+1)}{(\alpha+3)\Gamma(4-\alpha)(2\alpha+2)}+\right.$$

$$\left.\frac{(\alpha+2)(2\alpha+1)\Gamma(\alpha+2)}{(2\alpha+2)}\right)+\frac{t^{3\alpha}}{\Gamma(3\alpha+1)}\left(\frac{48\pi^2}{\Gamma(4-\alpha)}-4\pi^2\Gamma(\alpha+3)\right)$$

$$\frac{t^{3\alpha+2}}{\Gamma(3\alpha+3)}+\frac{t^{4\alpha}}{\Gamma(4\alpha+1)}\left(\frac{2\pi^2(2\alpha+1)(\alpha+2)\Gamma(\alpha+2)}{(2\alpha+2)}\right.$$

$$\left.-\frac{2\pi^2\Gamma(\alpha+3)(2\alpha+2)(3\alpha+1)}{\Gamma(3\alpha+2)(2\alpha+3)}-\frac{2\Gamma(\alpha+2)(\alpha+2)(3\alpha+1)}{(3\alpha+2)}\right)+$$

$$\left((2+\alpha)\Gamma(\alpha+2)+\frac{12(\alpha+2)}{(\alpha+3)\Gamma(4-\alpha)}\right)\frac{t^{2\alpha+1}}{\Gamma(2\alpha+2)}+\frac{12}{\Gamma(4-\alpha)}\frac{t^{\alpha+2}}{\Gamma(\alpha+3)}$$

$$+8\pi^4\Gamma(\alpha+2)\frac{t^{4\alpha+2}}{\Gamma(4\alpha+3)}+\left(\frac{-4\pi^4(2\alpha+2)\Gamma(\alpha+3)}{(2\alpha+3)}-\frac{4\pi^2\Gamma(2\alpha+3)(3\alpha+2)}{(3\alpha+3)}\right.$$

$$\left.+4\pi^2(2+\alpha)\frac{\Gamma(\alpha+2)}{\Gamma(2)}\right)\frac{t^{4\alpha+1}}{\Gamma(4\alpha+2)}\Big]\times\sin(\pi x)\sin(\pi y)$$

The final solution is given by

$$\mathrm{u}(x,y,t)=u_0(x,y,t)+u_1(x,y,t)+u_2(x,y,t)+u_3(x,y,t)+\ldots \tag{28}$$

Table 3. Maximum absolute error for $(x,y)\in[0.01,0.1]$ and distinct value of t and α for Ex. 6.2.

t	$\alpha=2$	$\alpha=1.95$
0.01	$2.745706e^{-07}$	$5.304699e^{-07}$
0.02	$4.393655e^{-06}$	$7.142152e^{-06}$
0.03	2.224556^{-05}	$3.269201e^{-05}$
0.04	$7.031549e^{-05}$	$9.620824e^{-05}$
0.05	$1.716896e^{-04}$	$2.222602e^{-04}$
0.06	$3.560595e^{-04}$	$4.405737e^{-04}$
0.07	$6.597259e^{-04}$	$7.857576e^{-04}$
0.08	$1.125603e^{-03}$	$1.297095e^{-03}$
0.09	$1.803226e^{-03}$	$2.018378e^{-03}$
0.10	$2.748749e^{-03}$	$2.997764e^{-03}$

Table 4. The Comparative analysis of maximum absolute error for the SADT and existing methods for distinct value of t and α, for Ex. 6.2.

t	$\alpha = 1.45$		$\alpha = 1.65$	
Methods	**SADT**	**RBF PU Method [36]**	**SADT**	**RBF PU Method [36]**
1/40	$1.6721e^{-07}$	$1.9018e^{-04}$	$8.6385e^{-08}$	$8.5648e^{-04}$
1/80	$1.9760e^{-08}$	$5.7019e^{-05}$	$6.1827e^{-09}$	$73.9328e^{-04}$
1/160	$2.2424e^{-09}$	$1.7025e^{-05}$	$4.3288e^{-10}$	$1.7791e^{-04}$
1/320	$2.4825e^{-10}$	$4.9817e^{-06}$	$3.0108e^{-11}$	$8.1217e^{-05}$
1/640	$2.7049e^{-11}$	$1.4812e^{-06}$	$2.0899e^{-12}$	$3.6646e^{-05}$
1/1280	$2.9160e^{-12}$	$4.3706e^{-07}$	$1.4497e^{-13}$	$1.6309e^{-05}$

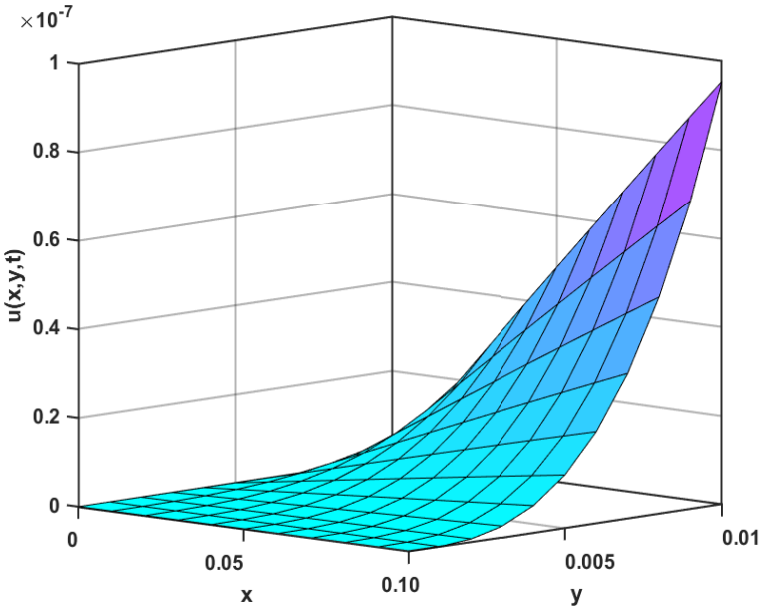

Fig. 4. Approximate solution $u(x, y, t)$ at $t = 0.1$ and α=2, for Ex. 6.2.

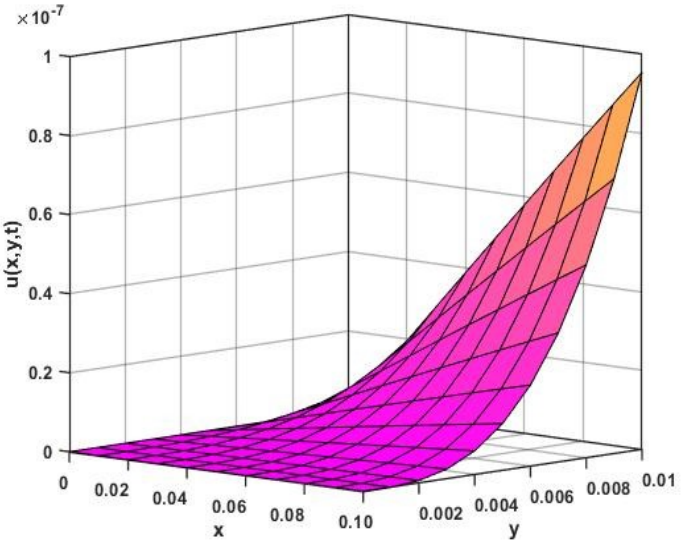

Fig. 5. Analytical solution $u(x, y, t)$ at $t = 0.1$, for Ex. 6.2.

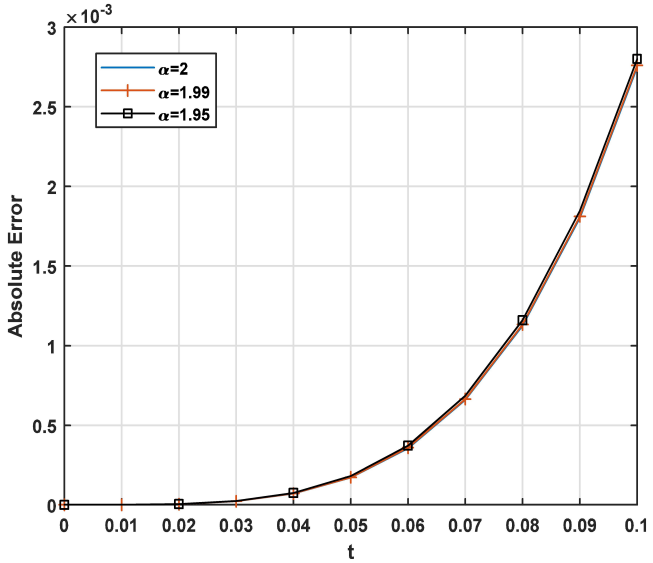

Fig. 6. Absolute error of SADT at x=0.1 and distinct value of α, for Ex. 6.2.

7 Simulation results and discussion

This article uses SADT to solve two FCHE examples. For Ex. 6.1 and Ex. 6.2, the maximum absolute errors are found for distinct value of α and t. The results are shown in tables 1 and 3, for Ex. 6.1 and Ex. 6.2. It is evident that the SADT has relatively small maximum absolute errors. The current techniques for Ex. 6.1 and Ex. 6.2 are compared with the maximum absolute errors of the SADT in Tables 2 and 4. The results show that the SADT is more accurate than the existing techniques,with a maximum absolute errors that is lower than the RBF-PU approach.
The exact solution and the approximate solution by the SADT are represented by graphs at $y = 0.1$ and distinct value of x, t, α in Fig. $(1) - (2)$ for Ex. 6.1 and in Fig. $(4) - (5)$ for Ex. 6.2. Figure 3 illustrates the absolute, whereas Fig. 6 illustrates the absolute for Ex. 6.2. It is evident that the precise answer and the numerical solution are almost identical in nature. Therefore, it is evident from the figures and tables that the suggested method, SADT, is a very effective and efficient method for solving the fractional models.

8 Conclusions

In this article, we investigate the FCHE for analysing the conduction of heat in porous medium via Caputo fractional order operator. The existence and uniqueness is analysed by using the fixed point theorem and the highest errors of the designed method, SADT, is also analysed. Two different cases are solved, and the proposed approach, SADT, yields more accurate results than the existing methods; also, the maximum absolute errors for SADT are smaller than those of the existing method. This research will be beneficial for handling the issues of thermo-elastic in porous media since it provides an accurate forecast about the heat conduction and a mathematical explanation of how it works. Hence, we can conclude that the SADT is a highly efficient technique that can be used to find the solution of non-linear fractional order models arising in real life phenomena.

References

1. Z. Odibat, Approximations of fractional integrals and Caputo fractional derivatives, Applied Mathematics and Computation, 178(2), 527-533 (2006).
2. L. Mohan, A. Prakash A, Stability and numerical analysis of fractional BBM-Burger equation and fractional diffusion-wave equation with Caputo derivative. Optical and Quantum Electronics, 1-25 (2024). https://doi.org/10.1007/s11082-023-05608-9.
3. A. Prakash, L. Mohan, Application of Caputo fractional operator to analyse the fractional model of Brain Tumour via modified technique. International Journal of Applied and Computational Mathematics, 9, 1-33 (2023). DOI :10.1007/s40819-023-01591-7
4. A. Prakash, V. Verma, D. Baleanu, Two novel methods for fractional nonlinear Whitham–Broer–Kaup equations arising in Shallow water. Int. J. Appl. Comput. Math 9, 39, 1-16, (2023). https://doi.org/10.1007/s40819-023-01497-4.
5. L. Mohan, A. Prakash, An efficient technique for solving fractional diffusion equation arising in oil pollution via Natural transform. Waves in Random and Complex Media, 2273323, 1-24 (2023). https://doi.org/10.1080/17455030.2023.227332.
6. S. Kumar, A. Kumar, S. Abbas, A modified analytical approach with existence and uniqueness for fractional Cauchy reaction–diffusion equations. Advances in Difference Equations, 28, 1-19 (2020).
7. M. Jleli, S. Kumar, R. Kumar, B. Samet, Analytical approach for time fractional wave equations in the sense of Yang-Abdel-Aty-Cattani via the homotopy perturbation transform method. Alexandria Engineering Journal, 59(5), 2859-2863 (2020).
8. M.A. Khan, S. Ullah, S. Kumar, A robust study on 2019-nCOV outbreaks through non-singular derivative. The European Physical Journal Plus, 136, 168, 1-20 (2021).
9. S. Kumar, R.P. Chauhan, S. Momani, S. Hadid, Numerical investigations on COVID-19 model through singular and non-singular fractional operators. Numerical Methods for Partial Differential Equations, 1-27 (2020). https://doi.org/10.1002/num.22707.
10. S. Kumar, A. Kumar, B. Samet, H. Dutta, A study on fractional host–parasitoid population dynamical model to describe insect species. Numerical Methods for Partial Differential Equations, 37 (2), 1673-169 (2021).
11. S. Kumar, S. Ghosh, R. Kumar, M. Jleli, A fractional model for population dynamics of two interacting species by using spectral and Hermite wavelets methods. Numerical Methods for Partial Differential Equations. 37 (2), 1652-1672 (2021).
12. J. Singh, A. Gupta, D. Kumar, Computational Analysis of the Fractional Riccati Differential Equation with Prabhakar-type Memory. Mathematics. 2, 11(3):644. (2023). https://doi.org/10.3390/math11030644.
13. J. Singh, A. Gupta, D. Baleanu, Fractional Dynamics and Analysis of Coupled Schrodinger-KdV Equation With Caputo-Katugampola Type Memory. Journal of Computational and Nonlinear Dynamics. 18(9) (2023). https://doi.org/10.1115/1.4062391.
14. O. İlhan, G. Şahin, A numerical approach for an epidemic SIR model via Morgan-Voyce series. International Journal of Mathematics and Computer in Engineering. 1(2), 229–242 (2024).
15. F. Erdogan, A second order numerical method for singularly perturbed Volterra integro-differential equations with delay. International Journal of Mathematics and Computer in Engineering. 2(1), 85-96 (2024).
16. M. Nasir, S. Jabeen, F. Afzal, A. Zafar, Solving the generalized equal width wave equation via sextic-spline collocation technique. International Journal of Mathematics and Computer in Engineering. 2(1), 123-138 (2023).

17. C. Baishya, S. J. Achar, P. Veeresha, D. Kumar, Dynamical analysis of fractional yellow fever virus model with efficient numerical approach, Journal of Computational Analysis and Applications, 140(2023).
18. M. A. Rao, A. Venkatesh, SEAIQHRDP mathematical model Analysis for the transmission dynamics of COVID-19 in India, Journal of Computational Analysis and Applications, 31(1) (2023).
19. S. Dubey, S. Chakraverty, M. Kundu, Approximate solutions of space and time fractional telegraph equations using Taylor series expansion method, Journal of Computational Analysis and Applications, 48 (2023).
20. S. Kumar, R. Kumar, R. P. Agarwal, B. Samet, A study of fractional Lotka-Volterra population model using Haar wavelet and Adams-Bashforth-Moulton methods, Mathematical Methods in the Applied Sciences, 43(8), 5564-5578 (2020).
21. A. Goswami, J. Singh, D. Kumar, An efficient analytical approach for fractional equal width equations describing hydro-magnetic waves in cold plasma, Physica A: Statistical Mechanics and its Applications, 524, 563-575 (2019).
22. H.M. Baskonus, H. Bulut, T.A. Sulaiman, New complex hyperbolic structures to the lonngren-wave equation by using sine-gordon expansion method, Applied Mathematics and Nonlinear Sciences, 4(1), 129-138, (2019).
23. Ghanbari, Ghodsieh, Razzaghi, Mohsen, Numerical solutions for fractional optimal control problems by using generalised fractional-order Chebyshev wavelets, International Journal of Systems Science, 53, 1-15 (2021).
24. R. Metzler, J. Klafter, The restaurant at the end of the random walk: recent developments in the description of anomalous transport by fractional dynamics, Journal of Physics A: Mathematical and General, 37(31), R161 (2004).
25. E.K. Lenzi, L.C. Malacarne, R.S. Mendes, I.T. Pedron, Anomalous diffusion, nonlinear fractional Fokker–Planck equation and solutions, Physica A: Statistical Mechanics and its Applications, 319, 245-252 (2003).
26. R. Metzler, J. Klafter, The random walk's guide to anomalous diffusion: a fractional dynamics approach, Physics reports, 339(1), 1-77 (2000).
27. J. Crank, The mathematics of diffusion, Oxford university press, (1979).
28. S.M. Zubair, M.A. Chaudhry, Heat conduction in a semi-infinite solid due to time-dependent laser source, International Journal of Heat and Mass Transfer, 39(14), 3067-3074 (1996).
29. T.T. Lam, Thermal propagation in solids due to surface laser pulsation and oscillation, International journal of thermal sciences, 49(9), 1639-1648 (2010).
30. B.F. Blackwell, Temperature profile in semi-infinite body with exponential source and convective boundary condition, ASME Journal of Heat and Mass Transfer, (1990).
31. L. Wang, X. Zhou, X. Wei, Heat conduction: mathematical models and analytical solution, Springer Science and Business Media, (2007).
32. J.B.J. Fourier, G. Darboux, Théorie analytique de la chaleur, Paris: Didot, 504 (1822).
33. C. Cattaneo, Sulla conduzione del calore, Atti Sem. Mat. Fis. Univ. Modena, 3, 83-101 (1948).
34. C.I. Christov, On frame indifferent formulation of the Maxwell–Cattaneo model of finite-speed heat conduction, Mechanics Research Communications, 36(4), 481-486 (2009).
35. G. Watugala, Sumudu transform: a new integral transform to solve differential equations and control engineering problems, Integrated Education, 24(1), 35-43 (1993).

36. O. Nikan O, Z. Avazzadeh, J.T. Machado, Numerical approach for modeling fractional heat conduction in porous medium with the generalized Cattaneo model, Applied Mathematical Modelling, 100, 107-124 (2021).

Generalization of Hermite-Hadamard inequality for differentiable convex and quasi-convex function

Bhavin M. Rachhadiya[1,*], Twinkle R. Singh[2]

December 28, 2023

[1], [2] Department of Mathematics, Sardar vallabhbhai National Institute of Technology, India
*Corresponding author: bhavinrachhadiya289@gmail.com

Received

Abstract

In this paper, the generalization of Simpson's identity has been derived. This generalized identity has been used to obtain new Hermite-Hadamard inequalities for differentiable convex and quasi-convex functions. Also, the validation of the derived inequalities has been established using suitable examples.

2020 Mathematics Subject Classification. 26A33, 26A51, 26D10.
Key words and phrases. Hermite-Hadamard inequality, quasi-convex function, convex function.

1 Introduction

The theory of inequality has many applications in mathematics, physical sciences and engineering fields. It includes the study of various inequalities such as Holder's inequality, Jensen' inequality, Azuma's inequality, Boole's inequality, Hermite-Hadamard inequality and many more well known inequalities. Hermite-Hadamard inequality is one of the most famous inequality in mathematics. It was derived independently by Charles Hermite and Jacques Hadamard. It is involved with the convexity of function. In 1998, Dragomir and Agarwal[6] derived the inequality associated with the right hand side of Hermite-Hadamard inequality for differentiable convex function. Later on this estimate was improved by Pearce and Pecaric[21]. Kirmaci[17] discovered the inequality linked with the left hand side of Hermite-Hadamard inequality. By using the work of Dragomir et al. and Kirmaci many researcher have derived the inequalities associated with left side and right side of Hermite-Hadamard inequality. The Hermite-Hadamard integral inequality for convex functions is used in Kirmaci's work to present a number of inequalities for differentiable convex functions. Kirmaci's work employs the Hermite-Hadamard integral inequality holding for convex functions to describe a few inequalities for differentiable convex functions. Additionally, certain applications to unique real number means were offered, and some midway formula error estimates were discovered. Later, the inequality related to right hand side of Hermite-Hadamard inequality for quasi-convex function was discovered by D. A Ion.[15]

Before discussing the the main findings of the paper, some prilimianary concepts that are useful for the better understanding of the research. We begin with the Hermite-Hadamard inequality.

$$\varrho\left(\frac{y_1+z_1}{2}\right) \leq \frac{1}{z_1-y_1}\int_{y_1}^{z_1}\varrho(s)ds \leq \frac{\varrho(y_1)+\varrho(z_1)}{2}. \tag{1}$$

Next, we define convex and quasi convex function.

Definition 1. *A function $\varrho : \mathcal{I} \to \mathbb{R}$ is said to be convex if*

$$\varrho(y_1\varkappa + (1-\varkappa)z_1) \leq \varkappa\varrho(y_1) + (1-\varkappa)\varrho(z_1),$$

for all $y_1, z_1 \in \mathcal{I}$ and $0 < \varkappa < 1$.

Definition 2. *A function $\varrho : \mathcal{I} \to \mathbb{R}$ is said to be quasi-convex if*

$$\varrho(y_1\varkappa + (1-\varkappa)z_1) \leq max\{\varrho(y_1), \varrho(z_1)\},$$

for all $y_1, z_1 \in \mathcal{I}$ and $0 < \varkappa < 1$.

In [20](page 3 , Lemma 1), Alomari et al. has derived the following identity.

Lemma 1. *Let $L[y_1, z_1]$ denote the class of all Lebesgue integrable functions on $[y_1, z_1]$. Let $\varrho : [y_1, z_1] \to \mathbb{R}$ be a differentiable function on (y_1, z_1) with $y_1 < z_1$. If $\varrho' \in L[y_1, z_1]$, then*

$$\begin{aligned}&\left(\frac{z_1 - y_1}{3}\right)\left[\frac{\varrho(y_1) + \varrho(z_1)}{2} + 2f\left(\frac{y_1 + z_1}{2}\right)\right] - \int_{y_1}^{z_1} \varrho(s)ds \\ &= \int_0^1 \left[\left(\varkappa - \frac{1}{3}\right)\varrho'\left(\varkappa\left(\frac{y_1 + z_1}{2}\right) + (1-\varkappa)y_1\right) + \left(\varkappa - \frac{2}{3}\right)\varrho'\left(\varkappa z_1 + (1-\varkappa)\left(\frac{y_1 + z_1}{2}\right)\right)\right]d\varkappa.\end{aligned} \tag{2}$$

2 Main Results

In this section, we generalize the identity obtained by Alomari et al.[20]. Also, with the help of this generalized identity, several Hermite-Hadamard-type inequalities have been derived. Also, the validity of derived inequalities has been derived.

Theorem 1. *Let $\varrho : [y_1, z_1] \to \mathbb{R}$ be a differentiable function on (y_1, z_1) with $y_1 < z_1$. If $\varrho' \in L[y_1, z_1]$, then the following equality holds:*

$$\begin{aligned}&\frac{2(z_1 - y_1)\varrho(x)}{3} + \frac{(x - y_1)\varrho(y_1)}{3} + \frac{(z_1 - x)\varrho(z_1)}{3} - \int_{y_1}^{z_1} \varrho(s)ds \\ &= (x - y_1)^2 \int_0^1 \left(\varkappa - \frac{1}{3}\right)\varrho'(\varkappa x + (1-\varkappa)y_1)d\varkappa + (z_1 - x)^2 \int_0^1 \left(\varkappa - \frac{2}{3}\right)\varrho'(\varkappa z_1 + (1-\varkappa)x)d\varkappa.\end{aligned} \tag{3}$$

Proof. By applying integration by parts two times,

$$\begin{aligned}I_1 &= \int_0^1 \left(\varkappa - \frac{1}{3}\right)\varrho'(\varkappa x + (1-\varkappa)y_1)d\varkappa \\ &= \left(\varkappa - \frac{1}{3}\right)\frac{\varrho(\varkappa x + (1-\varkappa)y_1)}{x - y_1}\Bigg|_0^1 - \frac{1}{(x - y_1)}\int_0^1 \varrho(\varkappa x + (1-\varkappa)y_1)d\varkappa \\ &= \frac{2\varrho(x)}{3(x - y_1)} + \frac{\varrho(y_1)}{3(x - y_1)} - \frac{1}{(x - y_1)}\int_0^1 \varrho(\varkappa x + (1-\varkappa)y_1)d\varkappa.\end{aligned} \tag{4}$$

Making use of change of the variable $s = \varkappa x + (1-\varkappa)y_1$ and multiplying by $(x - y_1)^2$ both sides, we have

$$(x - y_1)^2 I_1 = \frac{2}{3}(x - y_1)\varrho(x) + \frac{1}{3}(x - y_1)\varrho(y_1) - \int_{y_1}^{x} \varrho(s)ds. \tag{5}$$

Similarly,

$$(x - z_1)^2 I_2 = \frac{2}{3}(z_1 - x)\varrho(x) + \frac{1}{3}(z_1 - x)\varrho(z_1) - \int_{x}^{z_1} \varrho(s)ds. \tag{6}$$

By adding (5) and (6) we have required identity. □

Remark 1. *By setting $x = \frac{y_1 + z_1}{2}$ in Theorem1, the identity (3) becomes the identity (2)*

Next, the certain estimates associated with RHS of (3) are given.

Theorem 2. *Let $\varrho : [y_1, z_1] \to \mathbb{R}$ be a differentiable function on (y_1, z_1) with $y_1 < z_1$. If $|\varrho'|$ is convex on $[y_1, z_1]$, then the following inequality holds:*

$$\left|\frac{2(z_1-y_1)\varrho(x)}{3}+\frac{(x-y_1)\varrho(y_1)}{3}+\frac{(z_1-x)\varrho(z_1)}{3}-\int_{y_1}^{z_1}\varrho(s)ds\right| \leq (x-y_1)^2\left(\frac{29|\varrho'(x)|}{162}+\frac{8|\varrho'(y_1)|}{81}\right)+(z_1-x)^2\left(\frac{8|\varrho'(z_1)|}{81}+\frac{29|\varrho'(x)|}{162}\right). \tag{7}$$

Proof. Using Theorem 1 and the convexity of $|\varrho'|$, we have

$$\begin{aligned}
&\left|\frac{2(z_1-y_1)\varrho(x)}{3}+\frac{(x-y_1)\varrho(y_1)}{3}+\frac{(z_1-x)\varrho(z_1)}{3}-\int_{y_1}^{z_1}\varrho(s)ds\right| \\
&\leq (x-y_1)^2\int_0^1|\varkappa-\frac{1}{3}||\varrho'(\varkappa x+(1-\varkappa)y_1)|d\varkappa+(z_1-x)^2\int_0^1|\varkappa-\frac{2}{3}||\varrho'(\varkappa z_1+(1-\varkappa)x)|d\varkappa. \\
&\leq (x-y_1)^2\int_0^1|\varkappa-\frac{1}{3}|\big(\varkappa|\varrho'(x)|+(1-\varkappa)|\varrho'(y_1)|\big)d\varkappa \\
&\qquad+(z_1-x)^2\int_0^1|\varkappa-\frac{2}{3}|\big(\varkappa|\varrho'(z_1)|+(1-\varkappa)|\varrho'(x)|d\varkappa \\
&=(x-y_1)^2\left[|\varrho'(x)|\int_0^1\varkappa|\varkappa-\frac{1}{3}|d\varkappa+|\varrho'(y_1)|\int_0^1(1-\varkappa)|\varkappa-\frac{1}{3}|d\varkappa\right] \\
&\qquad+(z_1-x)^2\left[|\varrho'(z_1)|\int_0^1\varkappa|\varkappa-\frac{2}{3}|d\varkappa+|\varrho'(x)|\int_0^1(1-\varkappa)|\varkappa-\frac{2}{3}|d\varkappa\right] \\
&=(x-y_1)^2\left(\frac{29|\varrho'(x)|}{162}+\frac{8|\varrho'(y_1)|}{81}\right)+(z_1-x)^2\left(\frac{8|\varrho'(z_1)|}{81}+\frac{29|\varrho'(x)|}{162}\right).
\end{aligned}$$

This completes the proof.

□

Example 1. *Let the function f be defined as $f(x)=x^6$. Then the function f is convex on $[1,2]$. We have*

$$\left|\frac{2(z_1-y_1)\varrho(x)}{3}+\frac{(x-y_1)\varrho(y_1)}{3}+\frac{(z_1-x)\varrho(z_1)}{3}-\int_{y_1}^{z_1}\varrho(s)ds\right|=\left|\frac{2x^6}{3}+\frac{2}{15}+\frac{508}{21}\right| \tag{8}$$

and

$$\begin{aligned}
&(x-y_1)^2\left(\frac{29|\varrho'(x)|}{162}+\frac{8|\varrho'(y_1)|}{81}\right)+(z_1-x)^2\left(\frac{8|\varrho'(z_1)|}{81}+\frac{29|\varrho'(x)|}{162}\right) \\
&=(x-1)^2\left(\frac{16}{27}+\frac{29|x|^5}{27}\right)+(2-x)^2(\frac{512}{27}+\frac{29|x|^5}{27}).
\end{aligned} \tag{9}$$

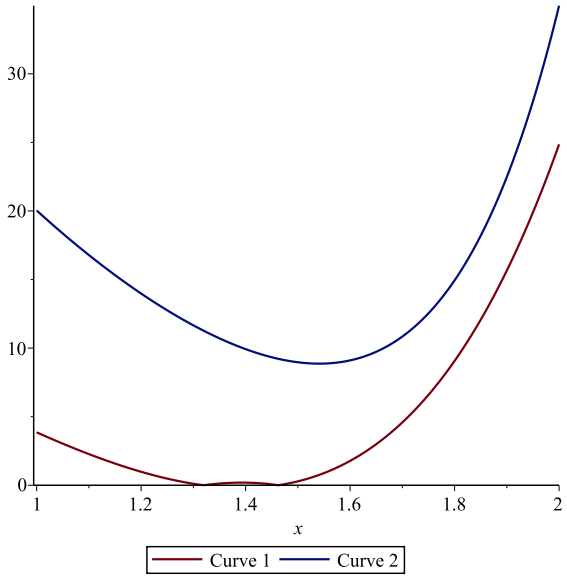

Figure 1:

Here Curve 1 and Curve 2 represents the expression (8) and (9) respectively. Figure 1 depicts that the Curve 1 is below Curve 2. Hence, it also refers to our calculation where the value of the expression (8) is less than the expression (9). This validates the inequality (7).

Theorem 3. *Let $\varrho : [y_1, z_1] \to \mathbb{R}$ be a differentiable function on (y_1, z_1) with $y_1 < z_1$. If $|\varrho'|^q$ is convex on $[y_1, z_1]$, then the following inequality holds:*

$$\left|\frac{2(z_1-y_1)\varrho(x)}{3}+\frac{(x-y_1)\varrho(y_1)}{3}+\frac{(z_1-x)\varrho(z_1)}{3}-\int_{y_1}^{z_1}\varrho(s)ds\right|$$
$$\leq \left(\frac{2^{p+1}+1}{(3p+3)3^p}\right)^{\frac{1}{p}}\frac{1}{2^{\frac{1}{q}}}\left[(x-y_1)^2\left(|\varrho'(y_1)|^q+|\varrho'(x)|^q\right)^{\frac{1}{q}}+(z_1-x)^2\left(|\varrho'(x)|^q+|\varrho'(z_1)|^q\right)^{\frac{1}{q}}\right]. \quad (10)$$

Proof. Using Theorem 1, Holder's inequality and the convexity of $|\varrho'|^q$, we have

$$\left|\frac{2(z_1-y_1)\varrho(x)}{3}+\frac{(x-y_1)\varrho(y_1)}{3}+\frac{(z_1-x)\varrho(z_1)}{3}-\int_{y_1}^{z_1}\varrho(s)ds\right|$$
$$\leq (x-y_1)^2\int_0^1\left|\varkappa-\frac{1}{3}\right||\varrho'(\varkappa x+(1-\varkappa)y_1)|d\varkappa+(z_1-x)^2\int_0^1\left|\varkappa-\frac{2}{3}\right||\varrho'(\varkappa z_1+(1-\varkappa)x)|d\varkappa.$$
$$\leq (x-y_1)^2\left(\int_0^1\left|\varkappa-\frac{1}{3}\right|^p d\varkappa\right)^{\frac{1}{p}}\left(\int_0^1|\varrho'(\varkappa x+(1-\varkappa)y_1)|^q d\varkappa\right)^{\frac{1}{q}}$$
$$+(z_1-x)^2\left(\int_0^1\left|\varkappa-\frac{2}{3}\right|^p\right)^{\frac{1}{p}}\left(\int_0^1|\varrho'(\varkappa z_1+(1-\varkappa)x)|^q d\varkappa\right)^{\frac{1}{q}}$$
$$\leq (x-y_1)^2\left(\frac{2^{p+1}}{(3p+3)3^p}\right)^{\frac{1}{p}}\left(\int_0^1\left(\varkappa|\varrho'(x)|^q+(1-\varkappa)|\varrho'(y_1)|^q\right)d\varkappa\right)^{\frac{1}{q}}$$
$$+(z_1-x)^2\left(\frac{2^{p+1}+1}{(3p+3)3^p}\right)^{\frac{1}{p}}\left(\int_0^1\left(\varkappa|\varrho'(z_1)|^q+(1-\varkappa)|\varrho'(x)|^q d\varkappa\right)\right)^{\frac{1}{q}}$$
$$=\left(\frac{2^{p+1}+1}{(3p+3)3^p}\right)^{\frac{1}{p}}\frac{1}{2^{\frac{1}{q}}}\left[(x-y_1)^2\left(|\varrho'(y_1)|^q+|\varrho'(x)|^q\right)^{\frac{1}{q}}+(z_1-x)^2\left(|\varrho'(x)|^q+|\varrho'(z_1)|^q\right)^{\frac{1}{q}}\right].$$

This completes the proof. □

Example 2. *Let the function f be defined as $f(x) = x^4$. Then the function f is convex on $[0,1]$. We have*

$$\left|\frac{2(z_1-y_1)\varrho(x)}{3}+\frac{(x-y_1)\varrho(y_1)}{3}+\frac{(z_1-x)\varrho(z_1)}{3}-\int_{y_1}^{z_1}\varrho(s)ds\right| = \left|\frac{2x^4}{3}+\frac{2}{15}-\frac{x}{3}\right| \tag{11}$$

and

$$\leq \left(\frac{2^{p+1}+1}{(3p+3)3^p}\right)^{\frac{1}{p}} \frac{1}{2^{\frac{1}{q}}}\left[(x-y_1)^2\left(|\varrho'(y_1)|^q+|\varrho'(x)|^q\right)^{\frac{1}{q}}+(z_1-x)^2\left(|\varrho'(x)|^q+|\varrho'(z_1)|^q\right)^{\frac{1}{q}}\right]$$
$$= \frac{17^{\frac{1}{3}}2^{\frac{2}{3}}3^{\frac{2}{3}}}{9}(|x|^5+(|x|^{\frac{9}{2}}+1)^{\frac{2}{3}}x^2-2((|x|^5+(|x|^{\frac{9}{2}}+1)^{\frac{2}{3}})x+(|x|^5+(|x|^{\frac{9}{2}}+1)^{\frac{2}{3}}). \tag{12}$$

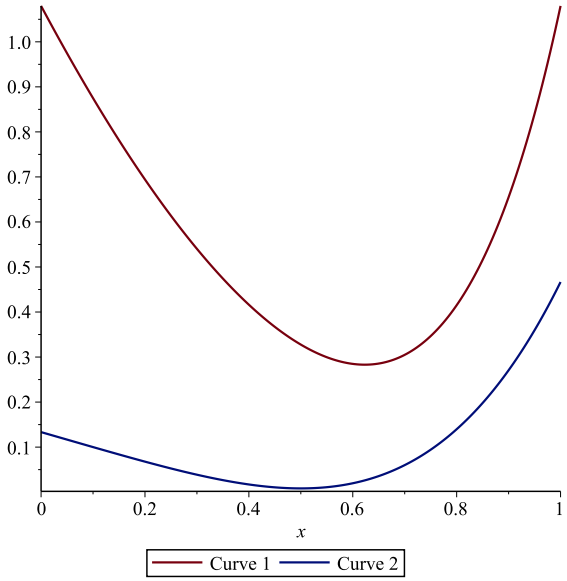

Figure 2:

Here Curve 1 and Curve 2 represents the expression (11) and (12) respectively. Figure 2 depicts that the Curve 1 is below Curve 2. Hence, it also refers to our calculation where the value of the expression (11) is less than the expression (12). This validates the inequality (10).

Theorem 4. *Let $\varrho : [y_1, z_1] \to \mathbb{R}$ be a differentiable function on (y_1, z_1) with $y_1 < z_1$. If $|\varrho'|^q$ is convex on $[y_1, z_1]$, then the following inequality holds:*

$$\left|\frac{2(z_1-y_1)\varrho(x)}{3}+\frac{(x-y_1)\varrho(y_1)}{3}+\frac{(z_1-x)\varrho(z_1)}{3}-\int_{y_1}^{z_1}\varrho(s)ds\right|$$
$$\leq \left(\frac{5}{18}\right)^{\frac{1}{p}}\left[(x-y_1)^2\left(\frac{8|\varrho'(y_1)|^q}{81}+\frac{29|\varrho'(x)|^q}{162}\right)^{\frac{1}{q}}+(z_1-x)^2\left(8\frac{|\varrho'(x)|^q}{81}+\frac{29|\varrho'(z_1)|^q}{162}\right)^{\frac{1}{q}}\right]. \tag{13}$$

Proof. Using Theorem 1, Power-mean inequality and the convexity of $|\varrho'|^q$, we have

$$\begin{aligned}
&\left|\frac{2(z_1-y_1)\varrho(x)}{3}+\frac{(x-y_1)\varrho(y_1)}{3}+\frac{(z_1-x)\varrho(z_1)}{3}-\int_{y_1}^{z_1}\varrho(s)ds\right| \\
&\leq (x-y_1)^2\int_0^1\left|\varkappa-\frac{1}{3}\right||\varrho'(\varkappa x+(1-\varkappa)y_1)|d\varkappa+(z_1-x)^2\int_0^1\left|\varkappa-\frac{2}{3}\right||\varrho'(\varkappa z_1+(1-\varkappa)x)|d\varkappa. \\
&\leq (x-y_1)^2\left(\int_0^1\left|\varkappa-\frac{1}{3}\right|d\varkappa\right)^{\frac{1}{p}}\times\left(\int_0^1\left|\varkappa-\frac{1}{3}\right||\varrho'(\varkappa x+(1-\varkappa)y_1)|^q d\varkappa\right)^{\frac{1}{q}} \\
&+(z_1-x)^2\left(\int_0^1\left|\varkappa-\frac{2}{3}\right|d\varkappa\right)^{\frac{1}{p}}\times\left(\int_0^1\left|\varkappa-\frac{2}{3}\right||\varrho'(\varkappa z_1+(1-\varkappa)x)|^q d\varkappa\right)^{\frac{1}{q}} \\
&\leq (x-y_1)^2\left(\frac{5}{18}\right)^{\frac{1}{p}}\left(\int_0^1\left|\varkappa-\frac{1}{3}\right|\left(\varkappa|\varrho'(x)|^q+(1-\varkappa)|\varrho'(y_1)|^q\right)d\varkappa\right)^{\frac{1}{q}} \\
&\quad+(z_1-x)^2\left(\frac{5}{18}\right)^{\frac{1}{p}}\left(\int_0^1\left|\varkappa-\frac{2}{3}\right||\left(\varkappa|\varrho'(z_1)|^q+(1-\varkappa)|\varrho'(x)|^q d\varkappa\right)^{\frac{1}{p}}d\varkappa \\
&=(x-y_1)^2\left(\frac{5}{18}\right)^{\frac{1}{p}}\left(\int_0^1\varkappa\left|\varkappa-\frac{1}{3}\right||\varrho'(x)|^q d\varkappa+\int_0^1(1-\varkappa)\left|\varkappa-\frac{1}{3}\right||\varrho'(y_1)|^q d\varkappa\right)^{\frac{1}{q}} \\
&\quad+(z_1-x)^2\left(\frac{1}{3}\right)^{\frac{1}{p}}\left(\int_0^1\varkappa\left|\varkappa-\frac{2}{3}\right||\varrho'(z_1)|^q d\varkappa+\int_0^1(1-\varkappa)\left|\varkappa-\frac{2}{3}\right||\varrho'(x)|^q d\varkappa\right)^{\frac{1}{q}} \\
&=\left(\frac{5}{18}\right)^{\frac{1}{p}}\left[(x-y_1)^2\left(\frac{8|\varrho'(y_1)|^q}{81}+\frac{29|\varrho'(x)|^q}{162}\right)^{\frac{1}{q}}+(z_1-x)^2\left(8\frac{|\varrho'(x)|^q}{81}+\frac{29|\varrho'(z_1)|^q}{162}\right)^{\frac{1}{q}}\right].
\end{aligned}$$

This completes the proof. □

Example 3. *Let the function f be defined as $f(x)=x^3$. Then the function f is convex on $[0,1]$. We have*

$$\left|\frac{2(z_1-y_1)\varrho(x)}{3}+\frac{(x-y_1)\varrho(y_1)}{3}+\frac{(z_1-x)\varrho(z_1)}{3}-\int_{y_1}^{z_1}\varrho(s)ds\right|=\left|\frac{4x^3}{3}-\frac{2x}{3}\right| \tag{14}$$

and

$$\begin{aligned}
&\left(\frac{5}{18}\right)^{\frac{1}{p}}\left[(x-y_1)^2\left(\frac{8|\varrho'(y_1)|^q}{81}+\frac{29|\varrho'(x)|^q}{162}\right)^{\frac{1}{q}}+(z_1-x)^2\left(8\frac{|\varrho'(x)|^q}{81}+\frac{29|\varrho'(z_1)|^q}{162}\right)^{\frac{1}{q}}\right] \\
&=\frac{5^{\frac{1}{4}}3^{\frac{1}{2}}}{27}(x+1)^2(29|x|^{\frac{8}{3}}+16)^{\frac{3}{4}}
\end{aligned} \tag{15}$$

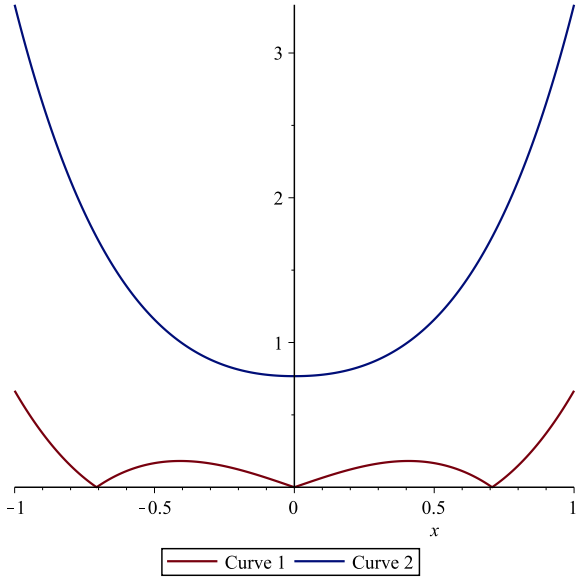

Figure 3:

Here Curve 1 and Curve 2 represents the expression (14) and (15) respectively. Figure 3 depicts that the Curve 1 is below Curve 2. Hence, it also refers to our calculation where the value of the expression (14) is less than the expression (15). This validates the inequality (13).

Theorem 5. *Let $\varrho : [y_1, z_1] \to \mathbb{R}$ be a differentiable function on (y_1, z_1) with $y_1 < z_1$. If $|\varrho'|$ is quasi-convex on $[y_1, z_1]$, then the following inequality holds:*

$$\left|\frac{2(z_1-y_1)\varrho(x)}{3}+\frac{(x-y_1)\varrho(y_1)}{3}+\frac{(z_1-x)\varrho(z_1)}{3}-\int_{y_1}^{z_1}\varrho(s)ds\right|$$
$$\leq \frac{5(x-y_1)^2}{18}max\{|\varrho'(x)|,|\varrho'(y_1)|\}+\frac{5(z_1-x)^2}{18}max\{|\varrho'(z_1),|\varrho'(x)|\}. \tag{16}$$

Proof. Using Theorem 1 and the quasi-convexity of $|\varrho'|$, we have

$$\left|\frac{2(z_1-y_1)\varrho(x)}{3}+\frac{(x-y_1)\varrho(y_1)}{3}+\frac{(z_1-x)\varrho(z_1)}{3}-\int_{y_1}^{z_1}\varrho(s)ds\right|$$
$$\leq (x-y_1)^2\int_0^1\left|\varkappa-\frac{1}{3}\right||\varrho'(\varkappa x+(1-\varkappa)y_1)|d\varkappa+(z_1-x)^2\int_0^1\left|\varkappa-\frac{2}{3}\right||\varrho'(\varkappa z_1+(1-\varkappa)x)|d\varkappa.$$
$$\leq (x-y_1)^2\int_0^1\left|\varkappa-\frac{1}{3}\right|max\{|\varrho'(x)|,|\varrho'(y_1)|\}d\varkappa+(z_1-x)^2\int_0^1\left|\varkappa-\frac{2}{3}\right|max\{|\varrho'(z_1),|\varrho'(x)|\}d\varkappa$$
$$=\frac{5(x-y_1)^2}{18}max\{|\varrho'(x)|,|\varrho'(y_1)|\}+\frac{5(z_1-x)^2}{18}max\{|\varrho'(z_1),|\varrho'(x)|\}$$

This completes the proof. □

Example 4. *Let the function f be defined as $f(x) = x^5$. Then the function f is convex on $[-3, 5]$. We have*

$$\left|\frac{2(z_1-y_1)\varrho(x)}{3}+\frac{(x-y_1)\varrho(y_1)}{3}+\frac{(z_1-x)\varrho(z_1)}{3}-\int_{y_1}^{z_1}\varrho(s)ds\right|=|\frac{16x^5}{3}-\frac{3368x}{3}+\frac{7448}{3}| \tag{17}$$

and

$$\frac{5(x-y_1)^2}{18}max\{|\varrho'(x)|,|\varrho'(y_1)|\}+\frac{5(z_1-x)^2}{18}max\{|\varrho'(z_1),|\varrho'(x)|\}$$
$$=\frac{5(x+3)^2max\{405,5x^4\}}{18}+\frac{5(5-x)^2max\{3125,5x^4\}}{18}. \tag{18}$$

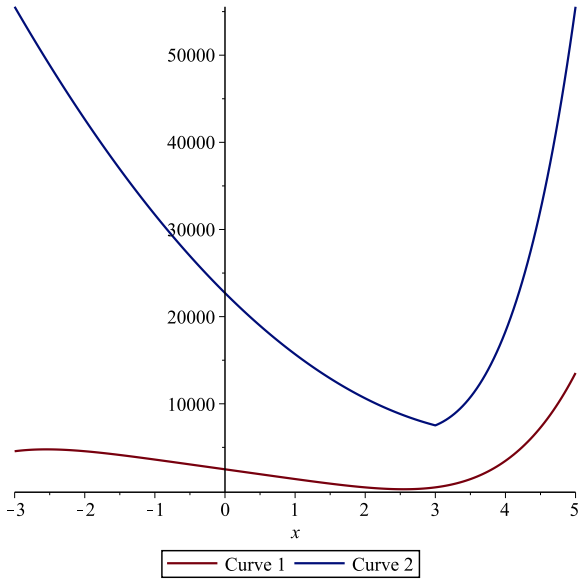

Figure 4:

Here Curve 1 and Curve 2 represents the expression (17) and (18) respectively. Figure 4 depicts that the Curve 1 is below Curve 2. Hence, it also refers to our calculation where the value of the expression (17) is less than the expression (18). This validates the inequality (16).

Theorem 6. *Let $\varrho : [y_1, z_1] \to \mathbb{R}$ be a differentiable function on (y_1, z_1) with $y_1 < z_1$. If $|\varrho'|^q$ is quasi-convex on $[y_1, z_1]$, then the following inequality holds:*

$$\begin{aligned}
&\left|\frac{2(z_1-y_1)\varrho(x)}{3}+\frac{(x-y_1)\varrho(y_1)}{3}+\frac{(z_1-x)\varrho(z_1)}{3}-\int_{y_1}^{z_1}\varrho(s)ds\right| \\
&\leq (x-y_1)^2\left(\frac{2^{p+1}+1}{(3p+1)3^p}\right)^{\frac{1}{p}}\left(max\{|\varrho'(x)|^q,|\varrho'(y_1)|^q\}\right)^{\frac{1}{q}} \\
&\quad+(z_1-x)^2\left(\frac{2^{p+1}+1}{(3p+1)3^p}\right)^{\frac{1}{p}}\left(max\{|\varrho'(z_1)|^q,|\varrho'(x)|^q\}\right)^{\frac{1}{q}}. \qquad (19)
\end{aligned}$$

Proof. Using Theorem 1, Holder's inequality and the quasi-convexity of $|\varrho'|^q$, we have

$$\begin{aligned}
&\left|\frac{2(z_1-y_1)\varrho(x)}{3}+\frac{(x-y_1)\varrho(y_1)}{3}+\frac{(z_1-x)\varrho(z_1)}{3}-\int_{y_1}^{z_1}\varrho(s)ds\right| \\
&\leq (x-y_1)^2\int_0^1\left|\varkappa-\frac{1}{3}\right||\varrho'(\varkappa x+(1-\varkappa)y_1)|d\varkappa+(z_1-x)^2\int_0^1\left|\varkappa-\frac{2}{3}\right||\varrho'(\varkappa z_1+(1-\varkappa)x)|d\varkappa. \\
&\leq (x-y_1)^2\left(\int_0^1\left|\varkappa-\frac{1}{3}\right|^p d\varkappa\right)^{\frac{1}{p}}\left(\int_0^1|\varrho'(\varkappa x+(1-\varkappa)y_1)|^q d\varkappa\right)^{\frac{1}{q}} \\
&\quad+(z_1-x)^2\left(\int_0^1\left|\varkappa-\frac{2}{3}\right|^p d\varkappa\right)^{\frac{1}{p}}\left(\int_0^1|\varrho'(\varkappa z_1+(1-\varkappa)x)|^q d\varkappa\right)^{\frac{1}{q}} \\
&\leq (x-y_1)^2\left(\frac{2^{p+1}+1}{(3p+1)3^p}\right)^{\frac{1}{p}}\left(max\{|\varrho'(x)|^q,|\varrho'(y_1)|^q\}\right)^{\frac{1}{q}} \\
&\quad+(z_1-x)^2\left(\frac{2^{p+1}+1}{(3p+1)3^p}\right)^{\frac{1}{p}}\left(max\{|\varrho'(z_1)|^q,|\varrho'(x)|^q\}\right)^{\frac{1}{q}}. \qquad (20)
\end{aligned}$$

This completes the proof. □

Example 5. *Let the function f be defined as $f(x) = x^7$. Then the function f is convex on $[-2, 1]$. We have*

$$\left|\frac{2(z_1 - y_1)\varrho(x)}{3} + \frac{(x - y_1)\varrho(y_1)}{3} + \frac{(z_1 - x)\varrho(z_1)}{3} - \int_{y_1}^{z_1} \varrho(s)ds\right| = |2x^7 - 43x - \frac{425}{8}| \tag{21}$$

and

$$\begin{aligned}(x - y_1)^2\left(\frac{2^{p+1}+1}{(3p+1)3^p}\right)^{\frac{1}{p}}\left(max\{|\varrho'(x)|^q, |\varrho'(y_1)|^q\}\right)^{\frac{1}{q}} \\ + (z_1 - x)^2\left(\frac{2^{p+1}+1}{(3p+1)3^p}\right)^{\frac{1}{p}}\left(max\{|\varrho'(z_1)|^q, |\varrho'(x)|^q\}\right)^{\frac{1}{q}} \\ = \frac{1}{3}(x+2)^2(max\{200704, 49x^12\})^{\frac{1}{2}} + \frac{1}{3}(1-x)^2(max\{49, 49x^12\})^{\frac{1}{2}}.\end{aligned} \tag{22}$$

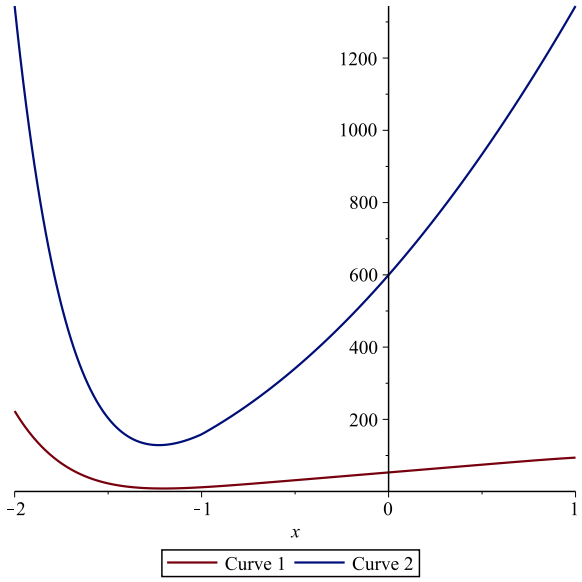

Figure 5:

Here Curve 1 and Curve 2 represents the expression (21) and (22) respectively. Figure 5 depicts that the Curve 5 is below Curve 2. Hence, it also refers to our calculation where the value of the expression (21) is less than the expression (22). This validates the inequality (19).

Theorem 7. *Let $\varrho : [y_1, z_1] \to \mathbb{R}$ be a differentiable function on (y_1, z_1) with $y_1 < z_1$. If $|\varrho'|^q$ is quasi-convex on $[y_1, z_1]$, then the following inequality holds:*

$$\begin{aligned}&\left|\frac{2(z_1 - y_1)\varrho(x)}{3} + \frac{(x - y_1)\varrho(y_1)}{3} + \frac{(z_1 - x)\varrho(z_1)}{3} - \int_{y_1}^{z_1} \varrho(s)ds\right| \\ &\leq \frac{5(x - y_1)^2}{18}\left(max\{|\varrho'(x)|^q, |\varrho'(y_1)|^q\}\right)^{\frac{1}{q}} + \frac{5(z_1 - x)^2}{18}\left(max\{|\varrho'(z_1)|^q, |\varrho'(x)|^q\}\right)^{\frac{1}{q}}.\end{aligned} \tag{23}$$

Proof. Using Theorem 1, Power-mean inequality and the quasi-convexity of $|\varrho'|^q$, we have

$$\begin{aligned}
&\left|\frac{2(z_1-y_1)\varrho(x)}{3}+\frac{(x-y_1)\varrho(y_1)}{3}+\frac{(z_1-x)\varrho(z_1)}{3}-\int_{y_1}^{z_1}\varrho(s)ds\right| \\
&\leq (x-y_1)^2\int_0^1\left|\varkappa-\frac{1}{3}\right||\varrho'(\varkappa x+(1-\varkappa)y_1)|d\varkappa+(z_1-x)^2\int_0^1\left|\varkappa-\frac{2}{3}\right||\varrho'(\varkappa z_1+(1-\varkappa)x)|d\varkappa. \\
&\leq (x-y_1)^2\left(\int_0^1\left|\varkappa-\frac{1}{3}\right|d\varkappa\right)^{\frac{1}{p}}\times\left(\int_0^1\left|\varkappa-\frac{1}{3}\right||\varrho'(\varkappa x+(1-\varkappa)y_1)|^q d\varkappa\right)^{\frac{1}{q}} \\
&\qquad+(z_1-x)^2\left(\int_0^1\left|\varkappa-\frac{2}{3}\right|d\varkappa\right)^{\frac{1}{p}}\times\left(\int_0^1|\left|\varkappa-\frac{2}{3}\right|\varrho'(\varkappa z_1+(1-\varkappa)x)|^q d\varkappa\right)^{\frac{1}{q}} \\
&\leq (x-y_1)^2\left(\frac{5}{18}\right)^{\frac{1}{p}}\left(\int_0^1\left|\varkappa-\frac{1}{3}\right|(max\{|\varrho'(x)|^q,|\varrho'(y_1)|^q\}d\varkappa\right)^{\frac{1}{q}} \\
&\quad+(z_1-x)^2\left(\frac{5}{18}\right)^{\frac{1}{p}}\left(\int_0^1\left|\varkappa-\frac{2}{3}\right|(max\{|\varrho'(z_1)|^q,|\varrho'(x)|^q\}d\varkappa\right)^{\frac{1}{q}} \\
&=(x-y_1)^2\left(\frac{5}{18}\right)^{\frac{1}{p}}\left(\frac{5}{18}\right)^{\frac{1}{q}}\left(max\{|\varrho'(x)|^q,|\varrho'(y_1)|^q\}\right)^{\frac{1}{q}} \\
&\quad+(z_1-x)^2\left(\frac{5}{18}\right)^{\frac{1}{p}}\left(\frac{5}{18}\right)^{\frac{1}{q}}\left(max\{|\varrho'(z_1)|^q,|\varrho'(x)|^q\}\right)^{\frac{1}{q}} \\
&=\frac{5(x-y_1)^2}{18}\left(max\{|\varrho'(x)|^q,|\varrho'(y_1)|^q\}\right)^{\frac{1}{q}}+\frac{5(z_1-x)^2}{18}\left(max\{|\varrho'(z_1)|^q,|\varrho'(x)|^q\}\right)^{\frac{1}{q}}. \qquad (24)
\end{aligned}$$

This completes the proof. □

Example 6. *Let the function f be defined as $f(x)=x^3$. Then the function f is convex on $[-8,-2]$. We have*

$$\left|\frac{2(z_1-y_1)\varrho(x)}{3}+\frac{(x-y_1)\varrho(y_1)}{3}+\frac{(z_1-x)\varrho(z_1)}{3}-\int_{y_1}^{z_1}\varrho(s)ds\right|=|4x^3-168x-340| \qquad (25)$$

and

$$\begin{aligned}
&\frac{5(x-y_1)^2}{18}\left(max\{|\varrho'(x)|^q,|\varrho'(y_1)|^q\}\right)^{\frac{1}{q}}+\frac{5(z_1-x)^2}{18}\left(max\{|\varrho'(z_1)|^q,|\varrho'(x)|^q\}\right)^{\frac{1}{q}} \\
&=\frac{5^{\frac{4}{5}}(65)^{\frac{1}{5}}}{54}\left((x+8)^2max\{384(2^{\frac{1}{2}})(3^{\frac{1}{4}}),3^{\frac{5}{4}}|x|^{\frac{5}{2}}\}^{\frac{4}{5}}+(2+x)^2max\{12,3^{\frac{5}{4}|x|^{\frac{5}{2}}}\}\right). \qquad (26)
\end{aligned}$$

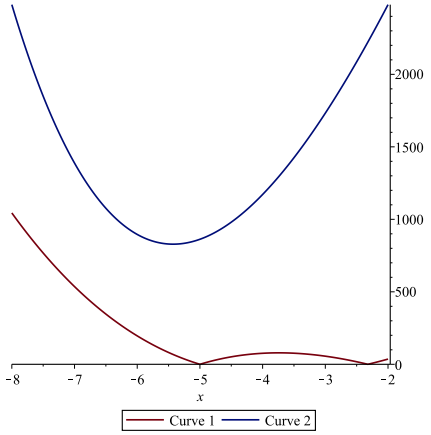

Figure 6:

Here Curve 1 and Curve 2 represents the expression (25) and (26) respectively. Figure 6 depicts that the Curve 1 is below Curve 2. Hence, it also refers to our calculation where the value of the expression (25) is less than the expression (26). This validates the inequality (23).

References

[1] L. Ciurdariu, (2012) A note concerning several Hermite-Hadamard inequalities for different types of convex functions. Int. J. Math. Anal.,33-36, 1623-1639.

[2] Alomari, M., Darus, M., & Dragomir, S.S. (2009). New inequalities of Hermite-Hadamard type for functions whose second derivatives absolute value are quasi-convex. RGMIA Res. Rep. Coll., 12(Supplement), Article 17.

[3] Sarikaya, M., Set, E., & Ozdemir, M. (2013). On New Inequalities of Simpson's Type for Functions Whose Second Derivatives Absolute Values are Convex. Journal of Applied Mathematics, Statistics and Informatics, 9(1), 37-45.

[4] Sarikaya, M. On the some generalization of inequalities associated with Bullen, Simpson, Midpoint and Trapezoid type. Retrieved from https://www.researchgate.net/publication/358884784.

[5] Lei, H., Hu, G., Nie, J., & Du, T. (2020). Generalized Simpson-type inequalities considering first derivatives through the k-Fractional Integrals. IAENG Int. J. Appl. Math., 50(3), 1-8.

[6] Dragomir, S.S., & Agarwal, R.P. (1998). Two inequalities for differentiable mappings and applications to special means of real numbers and to trapezoidal formula. Appl. Math. Lett., 11(5), 91-95.

[7] Sarikaya, M.Z., & Bardak, S. (2019). Generalized Simpson type integral inequalities. Konuralp Journal of Mathematics, 7(1), 186-191.

[8] Sarikaya, M.Z., Set, E.,& Ozdemir, M.E. (2013). On new inequalities of Simpson's type for functions whose second derivatives absolute values are convex. J. of Appl. Math., Statistics and Informatics, 9(1).

[9] Cakmak, M. (2019). On some Bullen-type inequalities via conformable fractional integrals. Journal of Scientific Perspectives, 3(4), 285-298.

[10] Pecaric, J., Proschan, F., & Tong, Y.L. (1991). Convex functions, partial ordering and statistical applications. Academic Press, New York.

[11] H. Hudzik, and L. Maligranda, (1994). *Some remarks on s-convex functions,* Ae. Ma. **4**8, 100–111.

[12] S. S. Dragomir, (2002) *On some new inequalities of Hermite-Hadamard type for m –convex functions,* Tamkang Journal of Mathematics, **33**, 45–56.

[13] S.Dragomir and S.Fitzpatrick, (1999). The Hadamard's inequality for s-convex functions in the second sense, *Demonstr. Math.* **32**, 687–696.

[14] G. Toader,(1985) Some generalizations of the convexity, *Proceedings of the Colloquium on Approximation and Optimization*, **1984**, 329-338.

[15] Ion, D. A. (2007). Some estimates on the Hermite-Hadamard inequality through quasi-convex functions. Annals of the University of Craiova-Mathematics and Computer Science Series, 34, 82-87.

[16] E Godunova and V Levin, (1985). Neravenstva dlja funkcii sirokogo klassa, soderzascego vypuklye, monotonnye i nekotorye drugie vidy funkii. vycislitel. mat. i. Fiz. Mezvuzov. Sb. Nauc. Trudov, MGPI, Moskva, 166:138–142.

[17] Kirmaci, U. S. (2004). Inequalities for differentiable mappings and applications to special means of real numbers and to midpoint formula. Applied mathematics and computation, 147(1), 137-146.

[18] S. Dragomir, J. Pecaric and L. Persson, (1995). Some inequalities of Hadamard type Soochow *J. Math.* **21**, 335-341.

[19] Iscan, (2014). Hermite-Hadamard type inequalities for harmonically convex functions. Hacet. J. Math. Stats., 43(6),935-942.

[20] Alomari, M., Darus, M., Dragomir, S.S.: New inequalities of simpson's type for s-convex functions with applications. Res. Rep. Collect. 12(4) (2009)

[21] C. Pearce, J. Pecaric and V. Simic, Stolarsky means and Hadamard's inequality. J. Math. Anal. Appl. 1998, 220, 99–109.

A Note On Nielsen-Type Integrals, Logarithmic Integrals And Higher Harmonic Sums

Bhawna Gupta [a*], M. I. Qureshi[b], M. S. Baboo[a]

December 27, 2023

[a] Department of Mathematics, School of Basic Sciences and Research, Sharda University, Greater Noida, Uttar Pradesh, 201306, India.
***Corresponding Author**
E-Mail: 2022302257.bhawna@dr.sharda.ac.in
E-Mail: mesub007@gmail.com
[b]Department of Applied Sciences and Humanities, Faculty of Engineering and Technology, Jamia Millia Islamia (A Central University), New Delhi -110025, India.
E-Mail: miqureshi_delhi@yahoo.co.in

Abstract

Due to the great success of hypergeometric functions, we provide the analytical solutions of certain definite logarithmic integrals and Nielsen-type integrals in terms of multi-variable Kampé de Fériet functions with suitable convergence conditions and higher harmonic sums by using series rearrangement technique and incomplete Gamma function.
Further we also obtain the solution of other related logarithmic integrals in terms of generalized hypergeometric functions and Kummer's confluent hypergeometric functions by using series rearrangement technique.
The results presented in the paper and comparable outcomes are hoped to be supplied by the use of computer-aid programs, for example, Mathematica.

Key Words and Phrases. Polylogarithm functions; Harmonic sums; Finite Mellin transforms; Nielsen-type integrals.
2020 Mathematics Subject Classification. 33B15, 33B30, 33C20, 33C99.

1. Introduction, definitions and known results

Here and elsewhere, we use the following standard notations, let $\mathbb{R}$ and $\mathbb{C}$ denote the sets of real and complex numbers, respectively. Also let

$$\mathbb{N}_0 = \mathbb{N} \cup \{0\} \quad , \qquad \mathbb{N} = \{1, 2, 3, \dots\} = \mathbb{N}_0 \backslash \{0\} \quad ,$$
$$\mathbb{Z}_0^- = \{0, -1, -2, \dots\} = \mathbb{Z}^- \cup \{0\} \quad , \qquad \mathbb{Z}^- = \{-1, -2, -3, \dots\},$$

and $\mathbb{Z} = \mathbb{Z}_0^- \cup \mathbb{N}$ being the sets of integers.

The incomplete gamma function is denoted by $\gamma(z, \alpha)$ ([23, p.127, Question (2)], see also [13, p. 15, Question. (10)]) and is defined by :

$$\gamma(z, \alpha) := \int_0^\alpha e^{-t} t^{z-1} \mathrm{d}t \qquad ; (\Re(z) > 0,\ |arg(\alpha)| < \pi),$$
$$= \frac{\alpha^z}{z} {}_1F_1 \left[\begin{matrix} z; \\ z+1; \end{matrix} \quad -\alpha \right]. \tag{1.1}$$

The polylogarithm function (also known as Jonquière's function) ([27, pp.197–198], see also [14] and [15]) $\mathrm{Li}_s(z)$, is defined for any complex s and z;

$$\mathrm{Li}_s(z) = F(z,s) = \mathrm{PolyLog}[s,z] := \sum_{n=1}^{\infty} \frac{z^n}{n^s} = \sum_{n=0}^{\infty} \frac{z^{n+1}}{(n+1)^s}; \qquad s \neq 1,$$

$$\Big(|z|<1, s \in \mathbb{C}\backslash\{1\}; |z|=1, z \neq 1, \Re(s) > 0; z = 1, \Re(s) > 1\Big).$$

The polylogarithm integrals ([3, p.79, Equation (14)], see also [11, p.1232, Equation (1.1)]) are given by:

$$\mathrm{Li}_n(x) := S_{n-1,1}(x) = \frac{(-1)^{n-1}}{(n-2)!} \int_0^1 \frac{1}{z} [\ell n(z)]^{n-2} \ell n(1-zx) dz,$$

$$\Big(n \in \mathbb{N}\backslash\{1\} \ ; \ x \in \mathbb{C}\Big).$$

The Nielsen-integrals ([3, p. 77, Equation (4)], see also [10, p. 647, Equation (1)], [11, p.1232, Equation (1.3)] and [18]) are given by:

$$S_{n,p}(x) := \frac{(-1)^{n+p-1}}{(n-1)!p!} \int_0^1 \frac{1}{z} [\ell n(z)]^{n-1} [\ell n(1-zx)]^p dz,$$

$$\Big(n,p \in \mathbb{N} \ ; \ x \in \mathbb{C}\Big).$$

Generalized Nielsen-integrals ([3, p. 80, Equation (18)], see also [12], [24]) are given by:

$$S_{n,p,q}(x) := \frac{(-1)^{n+p+q-1}}{(n-1)!p!q!} \int_0^1 \frac{1}{z} [\ell n(z)]^{n-1} [\ell n(1-zx)]^p [\ell n(1+zx)]^q dz, \tag{1.2}$$

$$\Big(\ p,n \in \mathbb{N} \ ; \ x \in \mathbb{C} \ ; \ q \in \mathbb{N}_0\Big).$$

2. Development of finite Mellin transform and harmonic sums

The Development of finite Mellin transform and harmonic sums is in the continuation of ([20, p.1, Equations (1), (3) and (3') and pp.4-5, Equations (6) and (7)], see also [7], [21]).

One-sided or unilateral Laplace transform is defined by:

$$L[f(t);z] = \int_0^{\infty} e^{-tz} f(t) dt = \phi(z), \tag{2.1}$$

then by the substitution $t = -\ell n(x)$, the one-sided Laplace transform (2.1) is converted into a finite Mellin transforms, given by (2.2):

$$M[f(-\ell n(x));z] = \phi(z) = \int_0^1 x^{z-1} f(-\ell n(x)) dx, \tag{2.2}$$

provided that the integrals (2.1) and (2.2) exist subject to suitable convergence condition on real part of complex parameter z.

The infinite Mellin transform is defined by:

$$M[g(x);z] = \int_0^{\infty} x^{z-1} g(x) dx = \psi(z), \tag{2.3}$$

provided that above integral exist.

This integral transform is closely connected to the theory of Dirichlet series, and is often used in number theory, mathematical statistics and the theory of asymptotic expansions, it is closely related to the Laplace transform and the Fourier transform, and the theory of the Gamma function and allied special functions. Also the Mellin transform is extremely useful for certain applications including solving Laplace equation in polar coordinates, as well as for estimating integrals.
The substitution $x = e^{-t}$ transforms (2.3) into two-sided Laplace transforms (2.4) or into the sum of two, one-sided Laplace transforms (2.5), therefore

$$\psi(z) = \int_{-\infty}^{+\infty} e^{-tz} g(e^{-t}) dt, \tag{2.4}$$

$$= \int_0^{\infty} e^{-tz} g(e^{-t}) dt + \int_0^{\infty} e^{-t(-z)} g(e^{t}) dt. \tag{2.5}$$

In the literature one often defines the transform shifted over "one" as in [34, p.2042, Equation (30)]. One may consider the Mellin-transformation ([4, p.1, Equation (2)], see also [16, p. 159]) for the function $f(z)$, in the form:

$$M\{f(z); N\} = \int_0^1 z^{N-1} f(z) dz,$$

provided that the above integral exists. Here N denotes the integer moment-index, (which is even or odd positive integers depending on the quantity being studied).
The Mellin transform of just a power of $\ell n(1-z)$ can be replaced immediately using the formula, ([3, p.89, Equation (84)], [34, pp.2042–2043, Equations (35) and (36)]):

$$\int_0^1 z^m \ell n^p (1-z) dz = \frac{(-1)^p p!}{(m+1)} S_{\underbrace{1,...,1}_{p}}(m+1), \tag{2.6}$$

in which the S-function has p indices that are all 1.
[7, p137, Equation (1) and p. 312, Equation (1)] see also [20], [21]

$$\int_0^{\infty} e^{-\alpha x} x^{s-1} \mathrm{d}x = \frac{\Gamma(s)}{\alpha^s} \qquad ; (\Re(\alpha) > 0, \Re(s) > 0). \tag{2.7}$$

Using suitable substitution in equation (2.7) and further adjustment of parameters, we can derive the following integral:

$$\int_0^1 z^m \ell n^p (z) dz = \frac{(-1)^p \Gamma(p+1)}{(m+1)^{p+1}}, \tag{2.8}$$

$$(\Re(m) > -1, \Re(p) > -1).$$

The functions emerging in perturbation calculations in massless Quantum Field Theories belong to the class discussed by Nielsen [18] and their Mellin-convolutions. By explicit calculation we will show that the Mellin-transforms of such functions can be represented by linear combinations of the finite harmonic sums (see [3, p.77, Equation (3)], [4, p.1, Equation (4)]).

$$S_{k_1,...,k_m}(N) = \sum_{n_1=1}^{N} \frac{(sign(k_1))^{n_1}}{n_1^{|k_1|}} \sum_{n_2=1}^{n_1} \frac{(sign(k_2))^{n_2}}{n_2^{|k_2|}} ... \sum_{n_m=1}^{n_{m-1}} \frac{(sign(k_m))^{n_m}}{n_m^{|k_m|}}; \; N \in \mathbb{N}, \forall \ell, k_\ell \neq 0.$$

The notation that is used for the various functions and series in this paper is closely related to how useful it can be for a computer program. This notation stays as closely as possible to existing ones. The harmonic series [34, p.2037, Equations (1) and (2)] is defined by:

$$S_m(n) = \sum_{i=1}^{n} \frac{1}{i^m},$$

$$S_{-m}(n)=\sum_{i=1}^{n}\frac{(-1)^i}{i^m},$$

in which $m>0$. The general single harmonic sums $S_{\pm k}(N),\ k>0$ [4, p. 3, Equations (14), (15), (16) and (17)] are obtained by :

$$S_k(N)=\frac{(-1)^{k-1}}{(k-1)!}\int_0^1[\ell n(x)]^{k-1}\left(\frac{x^N-1}{x-1}\right)dx,$$

$$S_{-k}(N)=\frac{(-1)^{k-1}}{(k-1)!}\int_0^1[\ell n(x)]^{k-1}\left(\frac{(-x)^N-1}{x+1}\right)dx,$$

$$\sum_{k=1}^{N}\frac{x^k}{k^\ell}=\frac{(-1)^{\ell-1}}{(\ell-1)!}\int_0^x[\ell n(z)]^{\ell-1}\left(\frac{z^N-1}{z-1}\right)dz,$$

$$\sum_{k=1}^{N}\frac{(-x)^k}{k^\ell}=\frac{(-1)^{\ell-1}}{(\ell-1)!}\int_0^x[\ell n(z)]^{\ell-1}\left(\frac{(-z)^N-1}{z+1}\right)dz.$$

One can define higher harmonic series [34, pp.2037–2038, Equations (3), (4) and (5)] given by:

$$S_{m,j_1,...,j_p}(n)=\sum_{i=1}^{n}\frac{1}{i^m}S_{j_1,...,j_p}(i),$$

$$S_{-m,j_1,...,j_p}(n)=\sum_{i=1}^{n}\frac{(-1)^i}{i^m}S_{j_1,...,j_p}(i),$$

with the same conditions on m. The m and the j_i, $(1\le i\le p)$ are referred to as the indices of the harmonic series. Hence

$$S_{1,-5,3}(n)=\sum_{i=1}^{n}\frac{1}{i}\sum_{j=1}^{i}\frac{(-1)^j}{j^5}\sum_{k=1}^{j}\frac{1}{k^3}.$$

For numerical computations one may use the recursion relations [4, p.22, Equations (163) and (164)] for complex values of N, in terms of products of single harmonic sums only

$$S_{\underbrace{-1,...,-1}_{k}}(N)=\frac{1}{k}\sum_{\ell=1}^{k}S_{(-1)^\ell|\ell|}(N)S_{\underbrace{-1,...,-1}_{k-\ell}}(N),$$

$$S_{\underbrace{1,...,1}_{k}}(N)=\frac{1}{k}\sum_{\ell=1}^{k}S_\ell(N)S_{\underbrace{1,...,1}_{k-\ell}}(N).$$

The finite harmonic sums are connected by various algebraic relations. We will only consider the multiple harmonic sums into a single sum: [4, p.19, Equation (126)] see also [34, p. 2056, Equation (92)]

$$S_{1,1}(N)=\frac{1}{2}\left[S_1^2(N)+S_2(N)\right].$$

[4, p.20, Equation (144)] see also [34, p. 2056, Equation (93)]

$$S_{1,1,1}(N)=\frac{1}{6}S_1^3(N)+\frac{1}{2}S_1(N)S_2(N)+\frac{1}{3}S_3(N).$$

[4, p.21, Equation (156)] see also [34, p. 2056, Equation (94)]

$$S_{1,1,1,1}(N)=\frac{1}{4}S_4(N)+\frac{1}{8}S_2^2(N)+\frac{1}{3}S_3(N)S_1(N)+\frac{1}{4}S_2(N)S_1^2(N)+\frac{1}{24}S_1^4(N).$$

The multi-variable extension of Kampé de Fériet double hypergeometric function [28, p. 454] see also [9], [31, pp.65-66], [32, p. 1127, Eq. (4.1)] is given in the form:

$$F_{\ell:m_1;m_2;\ldots;m_n}^{p:q_1;q_2;\ldots;q_n}\left[\begin{array}{ll}(a_p):(b_{q_1}^{(1)});\ldots;(b_{q_n}^{(n)}); & \\ & x_1,\ldots,x_n \\ (\alpha_\ell):(\beta_{m_1}^{(1)});\ldots;(\beta_{m_n}^{(n)}); & \end{array}\right]$$

$$=\sum_{s_1,\ldots,s_n=0}^{\infty}\Lambda(s_1,\ldots,s_n)\frac{{x_1}^{s_1}}{s_1!}\ldots\frac{{x_n}^{s_n}}{s_n!}\ , \tag{2.9}$$

where

$$\Lambda(s_1,\ldots,s_n)=\frac{\prod_{j=1}^{p}(a_j)_{s_1+\ldots+s_n}\prod_{j=1}^{q_1}(b_j^{(1)})_{s_1}\ldots\prod_{j=1}^{q_n}(b_j^{(n)})_{s_n}}{\prod_{j=1}^{\ell}(\alpha_j)_{s_1+\ldots+s_n}\prod_{j=1}^{m_1}(\beta_j^{(1)})_{s_1}\ldots\prod_{j=1}^{m_n}(\beta_j^{(n)})_{s_n}}\ ,$$

and, for convergence of the multiple hypergeometric series in (2.9),

$$\text{When}\qquad 1+\ell+m_k-p-q_k>0,\qquad k=1,\ldots,n$$

then $|x_1|<\infty,...,|x_n|<\infty$.

$$\text{When}\qquad 1+\ell+m_k-p-q_k=0,\qquad k=1,\ldots,n;\quad p>\ell$$

then $\quad |x_1|^{\frac{1}{p-\ell}}+\ldots+|x_n|^{\frac{1}{p-\ell}}<1.$

$$\text{When}\qquad 1+\ell+m_k-p-q_k=0,\qquad k=1,\ldots,n;\quad p\leqq\ell$$

then $\quad max\{|x_1|,\ldots,|x_n|\}<1.$

For absolutely and conditionally convergence of above multiple series (2.9), the readers and researchers can refer a beautiful paper of Hai *et al.* [8, pp.113-114, Theorums 4, 5 and 6], when $x_1,x_2,...,x_n\in\{-1,1\}$. Niukkanen [19] discovers several possible applications of such multiple hypergeometric functions (2.9).

For positive integers $m_1,m_2,m_3,\ldots,m_r$ $(r\geq 1)$, the following multiple series identity [31, p.102, Equation (16)], holds true:

$$\sum_{n=0}^{\infty}\left(\sum_{k_1=0}^{\infty}\sum_{k_2=0}^{\infty}\ldots\sum_{k_r=0}^{\infty}\Phi(k_1,k_2,\ldots,k_r;n)\right)$$

$$=\sum_{n=0}^{\infty}\left(\sum_{k_1,k_2,\ldots,k_r=0}^{k_1m_1+k_2m_2+\ldots+k_rm_r\leq n}\Phi(k_1,k_2,\ldots,k_r;n-m_1k_1-m_2k_2-\ldots-m_rk_r)\right), \tag{2.10}$$

provided that the above multiple series are absolutely convergent.

The paper considers Kampé de Fériet and related (generalized) hypergeometric functions at special (constants) arguments implied by Mellin transforms of special ordinary harmonic Polylogarithm. Some of the integrals are related to Mellin transforms of Nielsen integrals.

The present article is motivated by the work of the researchers: Blümlein *et.al* [4], [5], Kölbig *et.al* [10], [11], [12], Nielsen [18], Qureshi-Baboo [22], Remiddi *et.al* [24] and Vermaseren [34], see also sharma *et.al* [25], [26] and Tyagi *et.al* [33].

- In sections 3 and 4, we provide the analytical solution of the logarithmic integral: $\int_0^1 z^m(\ell n[1-z])^k(\ell n[1+z])^\ell \mathrm{d}z$ in terms of multi-variable Kampé de Fériet function and higher harmonic sums.

- In section 5, we also yield the solution of Nielsen-type integrals and related integrals: $\int_0^1 \frac{1}{z}[\ell n(z)]^{n-1}[\ell n(1-zx)]^p[\ell n(1+zx)]^q dz$ in terms of multi-variable Kampé de Fériet function with suitable convergence conditions.
- In section 6, we evaluate special integrals: $\int_{-1}^0 \frac{(\ell n[1+z])^m}{z^n}\mathrm{d}z$, $\int_0^1 \frac{(\ell n[1+z])^p m}{z^n}\mathrm{d}z$ in terms of generalized hypergeometric functions using series rearrangement technique.
- In section 7, we obtain the solution of the general integral: $\int_a^b \frac{(\ell n[1+z])^c}{z^d}\mathrm{d}z$ in terms of Kummer's confluent hypergeometric function using incomplete Gamma function

3. Evaluation of $\int_0^1 z^m(\ell n[1-z])^k(\ell n[1+z])^\ell \mathrm{d}z$ in terms of multi-variable Kampé de Fériet function ; where $k,\ell \in \mathbb{N}$ and $m \in \mathbb{C}$

Theorem 3.1. *The following result holds true:*

$$L_1 = \int_0^1 z^m(\ell n[1-z])^k(\ell n[1+z])^\ell dz = \frac{(-1)^k}{(1+m+k+\ell)}\times$$

$$\times F^{1:2;...;2;2;...;2}_{1:1;...;1;1;...;1}\left[\begin{array}{l} 1+m+k+\ell : \overbrace{1,1;\ldots;1,1}^{k};\overbrace{1,1;...;1,1}^{\ell}; \\ \\ 2+m+k+\ell : \underbrace{2\ ;\ ...\ ;\ 2}_{k};\underbrace{2\ ;\ ...\ ;\ 2}_{\ell}; \end{array} \quad \underbrace{1,...,1}_{k},\underbrace{-1,...,-1}_{\ell} \right], \tag{3.1}$$

where $\Re(m+k+\ell) \neq -1,-2,-3,..... .$

Remark: In view of the theorem of Hải *et al.*[8, pp 113–114, Theorem 4, Equations (3.1), (3.2) and (3.3)], the right hand side (i.e. multiple hypergeometric series) of equation (3.1) is absolutely convergent since arguments $\in \{-1,1\}$.

Proof: Since

$$\ell n(1+z) = -\sum_{q=1}^{\infty}\frac{(-1)^q z^q}{q}\ ; \qquad -1 < z \leq 1,$$

$$\ell n(1-z) = -\sum_{p=1}^{\infty}\frac{z^p}{p}\ ; \qquad -1 \leq z < 1.$$

Therefore

$$L_1 = \int_0^1 z^m(\ell n[1-z])^k(\ell n[1+z])^\ell \mathrm{d}z$$

$$= \int_0^1 z^m \left(-\sum_{p_1=1}^{\infty}\frac{z^{p_1}}{p_1}\right)\left(-\sum_{p_2=1}^{\infty}\frac{z^{p_2}}{p_2}\right)...\left(-\sum_{p_k=1}^{\infty}\frac{z^{p_k}}{p_k}\right)\left(-\sum_{q_1=1}^{\infty}\frac{(-1)^{q_1}z^{q_1}}{q_1}\right)\left(-\sum_{q_2=1}^{\infty}\frac{(-1)^{q_2}z^{q_2}}{q_2}\right)....\left(-\sum_{q_\ell=1}^{\infty}\frac{(-1)^{q_\ell}z^{q_\ell}}{q_\ell}\right)\mathrm{d}z$$

$$= (-1)^{k+\ell}\sum_{p_1=1}^{\infty}\sum_{p_2=1}^{\infty}...\sum_{p_k=1}^{\infty}\frac{1}{p_1p_2...p_k}\sum_{q_1=1}^{\infty}\sum_{q_2=1}^{\infty}...\sum_{q_\ell=1}^{\infty}\frac{(-1)^{q_1+q_2+...+q_\ell}}{q_1q_2...q_\ell}\int_0^1 z^{m+p_1+p_2...+p_k+q_1+q_2+...+q_\ell}\mathrm{d}z$$

$$= (-1)^{k+\ell}\sum_{p_1=1}^{\infty}\sum_{p_2=1}^{\infty}...\sum_{p_k=1}^{\infty}\frac{1}{p_1p_2...p_k}\sum_{q_1=1}^{\infty}\sum_{q_2=1}^{\infty}...\sum_{q_\ell=1}^{\infty}\frac{(-1)^{q_1+q_2+...+q_\ell}}{q_1q_2...q_\ell}\times$$

$$\times\frac{1}{(1+m+p_1+p_2...+p_k+q_1+q_2+...+q_\ell)}$$

$$=(-1)^k\sum_{p_1=0}^{\infty}\sum_{p_2=0}^{\infty}...\sum_{p_k=0}^{\infty}\frac{1}{(1+p_1)(1+p_2)...(1+p_k)}\sum_{q_1=0}^{\infty}\sum_{q_2=0}^{\infty}...\sum_{q_\ell=0}^{\infty}\frac{(-1)^{q_1+q_2+...+q_\ell}}{(1+q_1)(1+q_2)...(1+q_\ell)}\times$$

$$\times\frac{1}{\{(1+m+k+\ell)+(p_1+p_2+...+p_k+q_1+q_2+...+q_\ell)\}}$$

$$=\frac{(-1)^k}{(1+m+k+\ell)}\sum_{p_1=0}^{\infty}\sum_{p_2=0}^{\infty}...\sum_{p_k=0}^{\infty}\sum_{q_1=0}^{\infty}\sum_{q_2=0}^{\infty}...\sum_{q_\ell=0}^{\infty}\frac{(1)_{p_1}(1)_{p_2}...(1)_{p_k}}{(2)_{p_1}(2)_{p_2}....(2)_{p_k}}\frac{(1)_{q_1}(1)_{q_2}...(1)_{q_\ell}}{(2)_{q_1}(2)_{q_2}....(2)_{q_\ell}}\times$$

$$\times\frac{(1+m+k+\ell)_{p_1+p_2+...+p_k+q_1+q_2+...+q_\ell}}{(2+m+k+\ell)_{p_1+p_2+...+p_k+q_1+q_2+...+q_\ell}}(1)^{p_1+p_2+...+p_k}(-1)^{q_1+q_2+...+q_\ell}$$

$$=\frac{(-1)^k}{(1+m+k+\ell)}\sum_{p_1=0}^{\infty}\sum_{p_2=0}^{\infty}...\sum_{p_k=0}^{\infty}\sum_{q_1=0}^{\infty}\sum_{q_2=0}^{\infty}...\sum_{q_\ell=0}^{\infty}\frac{(1)_{p_1}(1)_{p_2}...(1)_{p_k}}{(2)_{p_1}(2)_{p_2}....(2)_{p_k}}\frac{(1)_{q_1}(1)_{q_2}...(1)_{q_\ell}}{(2)_{q_1}(2)_{q_2}....(2)_{q_\ell}}\times$$

$$\times\frac{(1)_{p_1}(1)_{p_2}...(1)_{p_k}}{p_1!p_2!....p_k!}\frac{(1)_{q_1}(1)_{q_2}...(1)_{q_\ell}}{q_1!q_2!....q_\ell!}\times$$

$$\times\frac{(1+m+k+\ell)_{p_1+p_2+...+p_k+q_1+q_2+...+q_\ell}}{(2+m+k+\ell)_{p_1+p_2+...+p_k+q_1+q_2+...+q_\ell}}(1)^{p_1+p_2+...+p_k}(-1)^{q_1+q_2+...+q_\ell}.$$

Now applying the definition (2.9) of multi-variable extension of Kampé de Fériet function, we obtain the right hand side of the integral L_1.

4. Evaluation of $\int_0^1 z^m(\ell n[1-z])^k(\ell n[1+z])^\ell \mathbf{d}z$ in terms of harmonic sums; where k,ℓ and $m\in\mathbb{N}$

Theorem 4.1. *The following results hold true:*
Case I: When $\ell\geq 2$, *then*

$$L_2=\int_0^1 z^m(\ell n[1-z])^k(\ell n[1+z])^\ell dz$$

$$=(-1)^k k!\sum_{q_1=0}^{\infty}\left(\sum_{q_2,q_3,...q_\ell=0}^{q_2+q_3+...+q_\ell\leq q_1}(-1)^{q_1}\frac{S_{\underbrace{1,...,1}_{k}}(1+m+\ell+q_1)}{(1+q_1-q_2-q_3-...-q_\ell)(1+q_2)...(1+q_\ell)(1+m+\ell+q_1)}\right). \tag{4.1}$$

Case II: When $\ell=1$, *then*

$$L_3=\int_0^1 z^m(\ell n[1-z])^k(\ell n[1+z])dz$$

$$=(-1)^k k!\sum_{q=0}^{\infty}\left(\frac{(-1)^q}{(1+q)(2+m+q)}S_{\underbrace{1,...,1}_{k}}(2+m+q)\right).$$

Proof of case I: Since $\ell n(1+z) = -\sum_{q=1}^{\infty} \frac{(-1)^q\ z^q}{q}; \qquad -1 < z \leq 1$, therefore

$$L_2 = \int_0^1 z^m (\ell n[1-z])^k (\ell n[1+z])^\ell \mathrm{d}z$$

$$= (-1)^\ell \sum_{q_1=1}^{\infty} \sum_{q_2=1}^{\infty} ... \sum_{q_\ell=1}^{\infty} \frac{(-1)^{q_1+q_2+...+q_\ell}}{q_1 q_2 ... q_\ell} \int_0^1 z^{m+q_1+q_2+...+q_\ell} (\ell n[1-z])^k \mathrm{d}z.$$

Now using the integral (2.6), we have

$$L_2 = (-1)^\ell \sum_{q_1=1}^{\infty} \sum_{q_2=1}^{\infty} ... \sum_{q_\ell=1}^{\infty} \frac{(-1)^{q_1+q_2+...+q_\ell}}{q_1 q_2 ... q_\ell} \times$$

$$\times \frac{(-1)^k\ k!}{(1+m+q_1+q_2+...+q_\ell)} S_{\underbrace{1,...,1}_{k}} (1+m+q_1+q_2+...+q_\ell).$$

Now replacing q_1 by $1+q_1$, q_2 by $1+q_2$, q_3 by $1+q_3$, ... and q_ℓ by $1+q_\ell$, we obtain

$$L_2 = (-1)^{\ell+k} k! \sum_{q_1=0}^{\infty} \left(\sum_{q_2=0}^{\infty} ... \sum_{q_\ell=0}^{\infty} \frac{(-1)^{\ell+q_1+q_2+...+q_\ell}}{(1+q_1)(1+q_2)...(1+q_\ell)(1+m+\ell+q_1+q_2+...+q_\ell)} \times \right.$$

$$\left. \times S_{\underbrace{1,...,1}_{k}} (1+m+\ell+q_1+q_2+...+q_\ell) \right).$$

Now replacing q_1 by $q_1 - q_2 - q_3 - ... - q_\ell$ and applying multiple series identity (2.10), we get the right hand side of assertion (4.1). Similarly we can derive case second when $\ell = 1$.

Some deductions of case I:

(i): When $k = 1$ and $\ell \geq 2$, then

$$\int_0^1 z^m (\ell n[1-z])(\ell n[1+z])^\ell \mathrm{d}z$$

$$= \sum_{q_1=0}^{\infty} \left(\sum_{q_2,q_3,...q_\ell=0}^{q_2+q_3+...+q_\ell \leq q_1} (-1)^{1+q_1} \frac{S_1(1+m+\ell+q_1)}{(1+q_1-q_2-q_3-...-q_\ell)(1+q_2)...(1+q_\ell)(1+m+\ell+q_1)} \right).$$

(ii): When $k = 2$ and $\ell \geq 2$ and applying the harmonic series relation (2.6), we have

$$\int_0^1 z^m (\ell n[1-z])^2 (\ell n[1+z])^\ell \mathrm{d}z$$

$$= \sum_{q_1=0}^{\infty} \left(\sum_{q_2,q_3,...q_\ell=0}^{q_2+q_3+...+q_\ell \leq q_1} (-1)^{q_1} \frac{\{S_1^2(1+m+\ell+q_1) + S_2(1+m+\ell+q_1)\}}{(1+q_1-q_2-q_3-...-q_\ell)(1+q_2)...(1+q_\ell)(1+m+\ell+q_1)} \right).$$

(iii): When $k = 3$ and $\ell \geq 2$ and applying the harmonic series relation (2.7), we get

$$\int_0^1 z^m (\ell n[1-z])^3 (\ell n[1+z])^\ell \mathrm{d}z$$

$$= \sum_{q_1=0}^{\infty} \left(\sum_{q_2,q_3,...q_\ell=0}^{q_2+q_3+...+q_\ell \leq q_1} (-1)^{1+q_1} \frac{\{S_1^3(\beta) + 3S_1(\beta) S_2(\beta) + 2S_3(\beta)\}}{(1+q_1-q_2-q_3-...-q_\ell)(1+q_2)...(1+q_\ell)(1+m+\ell+q_1)} \right),$$

where $\beta = 1 + m + \ell + q_1$.
(iv): When $k = 4$ and $\ell \geq 2$ and applying the harmonic series relation (2.8), we obtain

$$\int_0^1 z^m (\ell n[1-z])^4 (\ell n[1+z])^\ell \mathrm{d}z$$

$$= \sum_{q_1=0}^{\infty} \left(\sum_{q_2,q_3,\ldots q_\ell=0}^{q_2+q_3+\ldots+q_\ell \leq q_1} \frac{(-1)^{q_1} \{6S_4(\beta) + 3S_2^2(\beta) + 8S_3(\beta) S_1(\beta) + 6S_2(\beta) S_1^2(\beta) + S_1^4(\beta)\}}{(1+q_1-q_2-q_3-\ldots-q_\ell)(1+q_2)\ldots(1+q_\ell)(1+m+\ell+q_1)} \right),$$

where $\beta = 1 + m + \ell + q_1$.

Some deductions of case II:
(a): When $k = 1$ and $\ell = 1$, then

$$\int_0^1 z^m (\ell n[1-z])(\ell n[1+z])\mathrm{d}z = \sum_{q=0}^{\infty} \left(\frac{(-1)^{1+q}}{(1+q)(2+m+q)} S_1(2+m+q) \right).$$

(b): When $k = 2$ and $\ell = 1$, then

$$\int_0^1 z^m (\ell n[1-z])^2 (\ell n[1+z])\mathrm{d}z = \sum_{q=0}^{\infty} \left(\frac{(-1)^q \{S_1^2(2+m+q) + S_2(2+m+q)\}}{(1+q)(2+m+q)} \right).$$

(c): When $k = 3$ and $\ell = 1$, then

$$\int_0^1 z^m (\ell n[1-z])^3 (\ell n[1+z])\mathrm{d}z$$

$$= \sum_{q=0}^{\infty} \left(\frac{(-1)^{1+q}}{(1+q)(2+m+q)} \{S_1^3(\lambda) + 3S_1(\lambda) S_2(\lambda) + 2S_3(\lambda)\} \right),$$

where $\lambda = 2 + m + q$.
(d): When $k = 4$ and $\ell = 1$, then

$$\int_0^1 z^m (\ell n[1-z])^4 (\ell n[1+z])\mathrm{d}z$$

$$= \sum_{q=0}^{\infty} \left(\frac{(-1)^q}{(1+q)(2+m+q)} \{6S_4(\lambda) + 3S_2^2(\lambda) + 8S_3(\lambda) S_1(\lambda) + 6S_2(\lambda) S_1^2(\lambda) + S_1^4(\lambda)\} \right),$$

where $\lambda = 2 + m + q$.

5. Evaluation of Nielsen-type integrals and related integrals in terms of multi-variable Kampé de Fériet function; where $n, p \in \mathbb{N}$ and $q \in \mathbb{N}_0$

Theorem 5.1. *The following result for Nielsen-type integrals holds true:*

$$S_{n,p,q}(x) = \frac{(-1)^{n+p+q-1}}{(n-1)!p!q!} \int_0^1 \frac{1}{z} [\ell n(z)]^{n-1} [\ell n(1-zx)]^p [\ell n(1+zx)]^q dz$$

$$= \frac{(-1)^q x^{p+q}}{(p+q)^n p!q!} \times$$

$$\times F_{n:1;...;1;1;...;1}^{n:2;...;2;2;...;2}\left[\begin{array}{lll} \overbrace{p+q,\ldots,p+q}^{n} & : & \overbrace{1,1;\ldots;1,1;}^{p}\overbrace{1,1;...;1,1;}^{q} \\ \underbrace{1+p+q,\ldots,1+p+q}_{n}: & \underbrace{2\ ;\ ...\ ;\ 2}_{p};\underbrace{2\ ;\ ...\ ;\ 2}_{q}; & \underbrace{x,...,x}_{p},\underbrace{-x,...,-x}_{q} \end{array}\right], \qquad (5.1)$$

$$\Big(|x|\leq 1\ ;\quad n,p\in\mathbb{N}\ ;\quad q\in\mathbb{N}_0\Big).$$

Note: $S_{n,p,0}(x)\equiv S_{n,p}(x)\quad ;\quad S_{n-1,1}(x)\equiv \mathrm{Li}_n(x)$
and Kölbig integrals[10, p.647, Equation (2)]:

$$\int_0^1 z^{-1}[\ell n(z)]^{n-1}[\ell n(1-z)]^p dz=(-1)^{n+p-1}(n-1)!p!S_{n,p}(1).$$

Proof
Since

$$\ell n(1-z)=-\sum_{r=1}^{\infty}\frac{z^r}{r}\ ; \qquad -1\leq z<1,$$

$$\ell n(1+z)=-\sum_{s=1}^{\infty}\frac{(-1)^s z^s}{s}\ ; \qquad -1<z\leq 1.$$

Therefore

$$S_{n,p,q}(x)=\frac{(-1)^{n+p+q-1}}{(n-1)!p!q!}\int_0^1\frac{1}{z}[\ell n(z)]^{n-1}[\ell n(1-zx)]^p[\ell n(1+zx)]^q dz$$

$$=\frac{(-1)^{n+p+q-1}}{(n-1)!p!q!}\int_0^1\frac{1}{z}[\ell n(z)]^{n-1}\left(-\sum_{r_1=1}^{\infty}\frac{z^{r_1}x^{r_1}}{r_1}\right)...\left(-\sum_{r_p=1}^{\infty}\frac{z^{r_p}x^{r_p}}{r_p}\right)\left(-\sum_{s_1=1}^{\infty}\frac{(-1)^{s_1}z^{s_1}x^{s_1}}{s_1}\right)...\left(-\sum_{s_q=1}^{\infty}\frac{(-1)^{s_q}z^{s_q}x^{s_q}}{s_q}\right)dz \qquad (5.2)$$

$$=\frac{(-1)^{n-1}}{(n-1)!p!q!}\sum_{r_1=1}^{\infty}...\sum_{r_p=1}^{\infty}\frac{x^{r_1+...+r_p}}{(r_1)...(r_p)}\sum_{s_1=1}^{\infty}...\sum_{s_q=1}^{\infty}\frac{(-1)^{s_1+...+s_q}x^{s_1+...+s_q}}{(s_1)...(s_q)}\times$$

$$\times\int_0^1 z^{r_1+...+r_p+s_1+...+s_q-1}[\ell n(z)]^{n-1}dz$$

Now using the result (2.8), we get

$$S_{n,p,q}(x)=\frac{1}{p!q!}\sum_{r_1=1}^{\infty}...\sum_{r_p=1}^{\infty}\sum_{s_1=1}^{\infty}...\sum_{s_q=1}^{\infty}\frac{(-1)^{s_1+...+s_q}x^{r_1+...+r_p+s_1+...+s_q}}{(r_1+...+r_p+s_1+...+s_q)^n(s_1)...(s_q)(r_1)...(r_p)}.$$

Now replacing r_1 by $1+r_1$, r_2 by $1+r_2$, ..., r_p by $1+r_p$, and s_1 by $1+s_1, s_2$ by $1+s_2$, ..., s_q by $1+s_q$, we obtain

$$S_{n,p,q}(x)=\frac{1}{p!q!}\sum_{r_1=0}^{\infty}...\sum_{r_p=0}^{\infty}\sum_{s_1=0}^{\infty}...\sum_{s_q=0}^{\infty}\frac{(-1)^{q+s_1+...+s_q}x^{p+q+r_1+...+r_p+s_1+...+s_q}}{\{(p+q)+(r_1+...+r_p+s_1+...+s_q)\}^n}\times$$

$$\times\frac{(1)_{r_1}(1)_{r_2}...(1)_{r_p}(1)_{s_1}(1)_{s_2}...(1)_{s_q}}{(2)_{r_1}(2)_{r_2}...(2)_{r_p}(2)_{s_1}(2)_{s_2}...(2)_{s_q}}.$$

Now applying the definition (2.9) of multi-variable extension of Kampé de Fériet function, we get the required result (5.1).

6. Evaluation of $\int_{-1}^{0} \frac{(\ell n[1+z])^m}{z^n}\mathrm{d}z$, $\int_{0}^{1} \frac{(\ell n[1+z])^m}{z^n}\mathrm{d}z$ in terms of generalized hypergeometric functions; where $m, n \in \mathbb{N}$

Theorem 6.1. *The following results hold true:*
When $m \geq n$, then

$$L_4 = \int_{-1}^{0} \frac{(\ell n[1+z])^m}{z^n}\,dz = (-1)^{m-n} m! \;\; {}_{m+2}F_{m+1}\left[\begin{matrix} \overbrace{1,1,\ldots,1}^{m+1}, n; \\ \underbrace{2,2,\ldots,2}_{m+1}; \end{matrix} \; 1\right], \tag{6.1}$$

When $m \geq 2$, then

$$L_5 = \int_{0}^{1} (\ell n[1+z])^m dz = (-1)^{m+1} m! + 2(\ell n[2])^m \;\; {}_2F_0\left[\begin{matrix} -m, 1; \\ -; \end{matrix} \; (\ell n[2])^{-1}\right], \tag{6.2}$$

When $m \geq n \geq 2$, then

$$L_6 = \int_{0}^{1} \frac{(\ell n[1+z])^m}{z^n}\,dz = \frac{(m)!}{(n-1)^{m+1}} \;\; {}_{m+1}F_m\left[\begin{matrix} \overbrace{n-1, n-1, \ldots, n-1}^{m+1}; \\ \underbrace{n, n, \ldots, n}_{m}; \end{matrix} \; 1\right] -$$

$$- \sum_{k=0}^{m} \frac{k!\binom{m}{k}(\ell n[2])^{m-k}}{2^{n-1}(n-1)^{k+1}} \;\; {}_{k+1}F_k\left[\begin{matrix} \overbrace{n-1, n-1, \ldots, n-1}^{k+1}; \\ \underbrace{n, n, \ldots, n}_{k}; \end{matrix} \; \frac{1}{2}\right]. \tag{6.3}$$

Independent proof of the integral (6.1):
The integral (6.1) can be solved by substituting $1 + z = e^{-t}$ and using the result (2.7) of Laplace transforms.
Independent proof of the integral (6.2):

$$\text{Suppose} \qquad L_5 = \int_{0}^{1} (\ell n[1+z])^m \mathrm{d}z.$$

Put $1 + z = e^t$, then we have

$$L_5 = \int_{0}^{\ell n[2]} t^m e^t \mathrm{d}t.$$

Now integrating by parts, we get

$$L_5 = \left[\binom{m}{0}(-1)^0 t^m e^t + \binom{m}{1}(-1)^1 t^{m-1} e^t + \binom{m}{2}(-1)^2 t^{m-2} e^t 2! + \binom{m}{3}(-1)^3 t^{m-3} e^t 3! + \ldots \right.$$

$$\left. + \binom{m}{m-1}(-1)^{m-1} t e^t (m-1)! + \binom{m}{m}(-1)^m e^t m! \right]_0^{\ell n[2]}$$

$$L_5 = (-1)^{m+1} m! + 2\sum_{k=0}^{m} \binom{m}{k} (\ell n[2])^{m-k} (-1)^k k!$$

$$\text{or} \quad L_5 = (-1)^{m+1}m! + 2(\ell n[2])^m \ {}_2F_0\left[\begin{array}{ll} -m, 1; & \\ -; & (\ell n[2])^{-1}\end{array}\right].$$

Independent proof of the integral (6.3):

$$\text{Suppose} \qquad L_6 = \int_0^1 \frac{(\ell n[1+z])^m}{z^n}\mathrm{d}z$$

Now substitute $1+z=e^t$, then we have

$$L_6 = \int_0^{\ell n[2]} \frac{t^m e^t}{(e^t-1)^n}\mathrm{d}t = \int_0^{\ell n[2]} t^m e^{-t(n-1)}(1-e^{-t})^{-n}\mathrm{d}t = \sum_{r=0}^{\infty}\frac{(n)_r}{r!}\int_0^{\ell n[2]} t^m e^{-t(n+r-1)}\mathrm{d}t$$

Further, integrate by parts with $\alpha = n+r-1$, we get

$$L_6 = \sum_{r=0}^{\infty}\frac{(n)_r}{r!}\left[-\binom{m}{0}\frac{t^m e^{-\alpha t}}{(\alpha)} - \binom{m}{1}\frac{t^{m-1}e^{-\alpha t}}{(\alpha)^2} - \binom{m}{2}\frac{t^{m-2}e^{-\alpha t}2!}{(\alpha)^3} - \binom{m}{3}\frac{t^{m-3}e^{-\alpha t}3!}{(\alpha)^4} - \cdots \right.$$

$$\left. - \binom{m}{m-1}\frac{te^{-\alpha t}(m-1)!}{(\alpha)^m} - \binom{m}{m}\frac{e^{-\alpha t}m!}{(\alpha)^{m+1}}\right]_0^{\ell n[2]}$$

$$= -\sum_{r=0}^{\infty}\frac{(n)_r}{r!}\binom{m}{0}\frac{t^m e^{-\alpha t}}{(\alpha)} - \sum_{r=0}^{\infty}\frac{(n)_r}{r!}\binom{m}{1}\frac{t^{m-1}e^{-\alpha t}}{(\alpha)^2} - \sum_{r=0}^{\infty}\frac{(n)_r}{r!}\binom{m}{2}\frac{t^{m-2}e^{-\alpha t}2!}{(\alpha)^3} - \cdots$$

$$- \sum_{r=0}^{\infty}\frac{(n)_r}{r!}\binom{m}{m-1}\frac{\ell n[2](m-1)!}{2^\alpha(\alpha)^m} - \sum_{r=0}^{\infty}\frac{(n)_r}{r!}\frac{(m)!}{2^\alpha(\alpha)^{m+1}} + \sum_{r=0}^{\infty}\frac{(n)_r}{r!}\frac{(m)!}{(\alpha)^{m+1}}$$

$$= \sum_{r=0}^{\infty}\frac{(n)_r}{r!}\frac{(m)!}{(n+r-1)^{m+1}} - \sum_{r=0}^{\infty}\frac{(n)_r}{r!}\left[\sum_{k=0}^{m}\frac{k!\binom{m}{k}(\ell n[2])^{m-k}}{2^{n+r-1}(n+r-1)^{k+1}}\right]$$

$$= \sum_{r=0}^{\infty}\frac{\{(n-1)_r\}^{m+1}}{(n-1)^{m+1}r!}\frac{(m)!}{\{(n)_r\}^m} - \sum_{k=0}^{m}\frac{k!\binom{m}{k}(\ell n[2])^{m-k}}{2^{n-1}}\sum_{r=0}^{\infty}\frac{(n)_r}{2^r(n+r-1)^{k+1}r!}.$$

Now using the well-known definition of generalized hypergeometric function ${}_pF_q$, we obtain the desired result.

7. Evaluation of $\int_a^b \frac{(\ell n[1+z])^c}{z^d}\mathrm{d}z$ in terms of Kummer's confluent hypergeometric functions; where $b>a>0$, $\Re(d)>1$, $\Re(c+1)>0$

Theorem 7.1. *The following general result holds true:*

$$L_7 = \int_a^b \frac{(\ell n[1+z])^c}{z^d}dz = \sum_{r=0}^{\infty}\frac{(d)_r}{r!}\left\{\frac{(\ell n[1+b])^{c+1}}{c+1}{}_1F_1\left[\begin{array}{ll} c+1; & \\ c+2; & -(d+r-1)\ell n[1+b]\end{array}\right] - \right.$$

$$\left. - \frac{(\ell n[1+a])^{c+1}}{c+1}{}_1F_1\left[\begin{array}{ll} c+1; & \\ c+2; & -(d+r-1)\ell n[1+a]\end{array}\right]\right\}, \qquad (7.1)$$

where $\Re(c+1)>0$ *and* $\Re(d)>1$.

Independent proof of the integral (7.1):

$$\text{Suppose} \qquad L_7 = \int_a^b \frac{(\ell n[1+z])^c}{z^d}\mathrm{d}z$$

Now substitute $1+z=e^t$, then we have

$$L_7 = \int_{\ell n[1+a]}^{\ell n[1+b]} t^c e^{-t(d-1)}(1-e^{-t})^{-d}\mathrm{d}t = \sum_{r=0}^{\infty}\frac{(d)_r}{r!}\int_{\ell n[1+a]}^{\ell n[1+b]} t^c e^{-t(d+r-1)}\mathrm{d}t.$$

Further put $t(d+r-1)=x$, we get

$$L_7 = \sum_{r=0}^{\infty}\frac{(d)_r}{r!(d+r-1)^{c+1}}\int_{(d+r-1)\ell n[1+a]}^{(d+r-1)\ell n[1+b]} e^{-x}x^c\mathrm{d}x$$

$$L_7 = \sum_{r=0}^{\infty}\frac{(d)_r}{r!(d+r-1)^{c+1}}\left\{\int_0^{(d+r-1)\ell n[1+b]} e^{-x}x^c\mathrm{d}x - \int_0^{(d+r-1)\ell n[1+a]} e^{-x}x^c\mathrm{d}x\right\}.$$

Now using the definition of incomplete Gamma function, we obtain

$$L_7 = \sum_{r=0}^{\infty}\frac{(d)_r}{r!(d+r-1)^{c+1}}\left\{\gamma(c+1,(d+r-1)\ell n[1+b]) - \gamma(c+1,(d+r-1)\ell n[1+a])\right\}.$$

Now expressing incomplete Gamma in terms of hypergeometric notation (1.1), we get the right hand side of equation (7.1) which is always convergent, in view of convergence conditions of hypergeometric function ${}_pF_q(z)$ when $p=q$ then $|z|<\infty$.

8. Concluding remarks and Future scope

In this paper we have obtained some results involving hypergeometric functions and harmonic sums. We conclude our present investigation by observing that several other theorems of the similar types integrals related with other mathematical functions, different from the following integrals, are obtained in an analogous manner:

$$\int_a^b \frac{(\ell n[1+z])^c}{z^d}\mathrm{d}z;$$

$$\int_{-a}^{-b} \frac{(\ell n[1-z])^c}{z^d}\mathrm{d}z = \frac{1}{(-1)^{d+1}}\int_a^b \frac{(\ell n[1+z])^c}{z^d}\mathrm{d}z;$$

$$\int_0^1 z^m(\ell n[1-z])^k(\ell n[1+z])^\ell \mathrm{d}z = (-1)^m\int_{-1}^0 z^m(\ell n[1+z])^k(\ell n[1-z])^\ell \mathrm{d}z$$

and generalized Nielsen integrals with special cases.
Moreover the results derived in this paper are quite significant and are expected to be beneficial for the researchers in the field of applied mathematics, mathematical sciences and other branches of science and engineering. The interested readers and researchers can consult an appendix (Section 7 on Mellin Transforms) of the beautiful paper by "Blümlein and Kurth" [4, pp.27-39] for the Mellin integrals, which are different from the present paper.

Conflicts of interests: The authors declare that there are no conflicts of interests.

Acknowledgments: The authors want to express their thanks to referees, for a very valuable remark.

References

[1] Appell, P. and Kampé de Fériet, J. (1926). *Fonctions Hypergéométriques et Hypersphérique Polynômes d'Hermité*, Gauthiers Villars, Paris.

[2] Baboo, M. S. (2017). *Exact Solutions of Outstanding Problems and Novel Proofs Through Hypergeometric Approach*, Ph.D. Thesis, Jamia Millia Islamia, A Central University, New Delhi (India), August 2017.

[3] Blümlein, J. (2000). Analytic continuation of Mellin transforms up to two-loop order. *Comput. Physics Commun.*, 133(1), 76–104.

[4] Blümlein, J. and Kurth, S. (1999). Harmonic Sums and Mellin transforms up to two-loop order. `arXiv:hep-ph/9810241v2,31Aug2000`, *Phys.Rev.*, D-60, 014–018.

[5] Blümlein, J., Saragnese, M. and Schneider, C. (2021). Hypergeometric Structures in Feynman Integrals. `arXiv:2111.15501v1[math-ph]`

[6] Bradley, D. M. (2001) Representations of Catalan's constant, Research gate, `https://www.researchgate.net/publication/2325473RepresentationsofCatalan'sConstant/citations`

[7] Erdélyi, A., Magnus, W., Oberhettinger, F. and Tricomi, F. G. (1954). *Tables of Integral Transforms,* Vol. I, McGraw -Hill Book Company, New York, Toronto and London.

[8] Hải, N. T., Marichev O. I. and Srivastava, H. M. (1992). A note on the convergence of certain families of multiple hypergeometric series, *J. Math. Anal. Appl.* **164**(1), 104–115. `https://doi.org/10.1016/0022-247X(92)90147-6`

[9] Karlsson, P. W. (1973). Reduction of certain generalized Kampé de Fériet function, *Math. Scand.,* 32, 265–268.

[10] Kölbig, K. S. (1982). Closed expressions for $\int_0^1 t^{-1}[\ell n(t)]^{n-1}[\ell n(1-t)]^p dt$, *Math. Comput.,* 39(160), 647–654.

[11] Kölbig, K. S. (1986). Nielsen's generalized polylogarithms, *Siam J. Math. Anal.,* 17(5), 1232–1258.

[12] Kölbig, K. S., Mignaco, J. A. and Remiddi, E. (1970). On Nielsen's generalized polylogarithms and their numarical calculations, *BIT,* 10, 38–74.

[13] Lebedev, N. N. (1965). *Special Functions and Their Applications*,(Translated by R. A. Silverman) Prentice-Hall, Englewood Cliffs, New Jersey.

[14] Lewin, L. (1958). *Dilogarithms and Associated Functions*, Macdonald, London.

[15] Lewin, L. (1981). *Polylogarithms and Associated Functions*, Elsevier, North Holland, New York and London.

[16] Mellin, HJ. (1902). Über den Zusammenhang Zwischen den Linearen Differential- und Differenzengleichungen. *Acta Mathematica*, 25, 139–164. doi:10.1007/bf02419024

[17] Meyer, J. L. (2007). A Generalization of an integral of Ramanujan, *Ramanujan J.*, 14, 79–88.

[18] Nielsen, E. (1909). Der Eulersche Dilogarithmus und seine Verallgemeinerungen, Nova Acta Leopold., Vol. XC, Nr. 3, Halle, 123–211.

[19] Niukkanen, A. W. (1983). Generalized hypergeometric series ${}^N F(x_1, ..., x_N)$ arising in physical and quantum chemical applications *J. Phys. A*, 16, 1813–1825.

[20] Oberhettinger, F. (1974). *Tables of Mellin Transforms*, Springer-Verlag, Berlin.

[21] Oberhettinger, F. and Badii, L. (1973). *Tables of Laplace Transforms*, Springer-Verlag, Berlin.

[22] Qureshi, M. I. and Baboo, M. S. (2018). Power series and hypergeometric representations associated with positive integral powers of logarithm function, *South Asian Journal of Mathematics*, 8(3), 144–150.

[23] Rainville, E. D. (1971). *Special Functions*, The Macmillan Company, New York, 1960 ; Reprinted by Chelsea Publ. Co., Bronx, New York.

[24] Remiddi, E. and Vermaseren, J. A. M. (2000). Harmonic Polylogarithms, *Int. J. Mod. Phys*, $A-15$, 725–754.

[25] Sharma, R., Singh, J., Kumar, D. and Singh, Y. (2022). An application of incomplete I-Functions with two variables to solve the nonlinear differential equations using S-Function, *Journal of Computational analysis and Applications*, 31, 80-95.

[26] Sharma, R., Singh, J., Kumar, D. and Singh, Y. (2022). Certain Unied Integrals Associated with Product of the General Class of Polynomials and Incomplete I-Functions, *International Journal of Applied and Computational Mathematics*, 8–7.

[27] Srivastava, H. M. and Choi, J.(2012). *Zeta and q-Zeta Functions and Associated Series and Integrals,* Elsevier Science Publishers, Amsterdam, London and New York.

[28] Srivastava, H. M. and Daoust, M. C. (1969). Certain generalized Neumann expansions associated with the Kampé de Fériet function, *Nederl. Akad. Wetensch. Pros. Ser. A 72= Indag. Math.*, 31, 449–457.

[29] Srivastava, H. M. and Daoust, M. C. (1972). A note on the convergence of Kampé de Fériet's double hypergeometric series, *Math. Nachr.*, 53, 151–159.https://doi.org/10.1002/mana.19720530114

[30] Srivastava, H. M. and Karlsson, P. W. (1985). *Multiple Gaussian Hypergeometric Series*, Halsted Press (Ellis Horwood Limited, Chichester, U.K.), John Wiley and Sons, New York, Chichester, Brisbane and Toronto.

[31] Srivastava, H. M. and Manocha, H. L. (1984). *A Treatise on Generating Functions*, Halsted Press (Ellis Horwood Limited, Chichester), John Wiley and Sons, New York, Chichester, Brisbane and Toronto.

[32] Srivastava, H. M. and Panda, R. (1975). Some analytic or asymptotic confluent expansions for functions of several variables, *Math. Comput.*, (29), 1115–1128.

[33] Tyagi, S., Jain, M. and Singh, J. (2022) Large Deflection of a Circular Plate with Incomplete Aleph Functions Under Non-uniform Load, *International Journal of Applied and Computational Mathematics*, 8:267.

[34] Vermaseren, J. A. M.; Harmonic sums, Mellin transforms and Integrals, arXiv:hep-ph/9806280v1~5june1998, *Int. J. Mod. Phys.* A-14: (1999), 2037–2076.

Solution of Integral Equations of Fredholm Kind Involving Incomplete ℵ-Function, Generalized Extended Mittag-Leffler Function and S-Function

Devendra Kumar[1] **and Rishi Dassani**[2,3,*]

[1]Department of Mathematics, University of Rajasthan,
Jaipur-302004, Rajasthan, India

Email: devendra.maths@gmail.com

[2]Department of Mathematics, University of Rajasthan,
Jaipur-302004, Rajasthan, India

[3]Kanoria PG Mahila Mahavidyalaya, Jaipur-302004, Rajasthan, India

Email: rishidassani25@yahoo.com

[*]Corresponding author

ABSTRACT

The main objective of this paper is to solve Fredholm integral equations (IEs) that involve S-function, generalized extended Mittag-Leffler function (GEMLF), and incomplete ℵ-function as the kernel. These types of integral equations appear frequently in applied mathematics, particularly in mathematical physics, engineering, and finance. To solve these integral equations, we employ two powerful mathematical tools, namely fractional calculus (FC) and integral transforms. Specifically, we use the Weyl operator and Mellin transform to solve the integral equation associated with S-functions, GEMLF, and incomplete ℵ-functions. These techniques allow us to express the solution in a closed form, which is essential for practical applications. Moreover, we present several special cases of the solutions obtained, which provide additional insights into the behavior of the solutions. These results are significant for the study of integral equations, as they can be used to derive several known results. Furthermore, the techniques used in this study can be applied to other integral equations that involve different types of functions.

Keywords: Integral equations of Fredholm kind, S- function, generalized extended Mittag-Leffler function, incomplete ℵ- functions, Mellin inversion theorem, Weyl fractional integral operator, Mellin transform.

1. Introduction and Preliminaries

Integral equation is an essential tool in solving problems related to science and engineering. The equations are highly versatile and are used in a diverse range of fields. In the problems related to heat and mass transfer, these equations are used to model and predict the behavior of thermal and fluid systems, such as the flow of fluids through pipes and the transfer of heat in buildings. In scattering theory, these equations are used to study how particles or waves interact with each other and with their environment. In the kinetic theory of gases, they are used to describe the behavior of gases on a microscopic level, including the motion and collisions of individual gas molecules. In integral geometry, these equations are used to study how geometric shapes interact with each

Key words: Integral equations of Fredholm kind, S- function, generalized extended Mittag-Leffler function, incomplete ℵ- functions, Mellin inversion theorem, Weyl fractional operator, Mellin transform.

other and with their surroundings. In construction science, they are used to understand how materials behave under different conditions, to optimize the design and construction of buildings and other structures. Many researchers have done notable work in these fields [3–5,22,26–32,35,36].

Among the different types of integral equations, the Fredholm integral equation is particularly significant in the study of special functions. Incomplete special functions have a unique role in distribution theory, mathematical modeling, probability theory, and other fields. Its properties and applications have been extensively studied by many authors [1,6,9–12,16,17,20,33,34].

A specific area of focus for mathematicians has been the study of Fredholm integral equations involving incomplete hypergeometric functions, incomplete I-functions, incomplete H-functions, and incomplete $\overline{H}$-functions as kernels. Singh *et. al.* [37] have done very novel work on applications of the fractional differential equations associated with integral operators involving $\aleph$-function in the kernel. Motivated by the work mentioned above, we have now turned our attention to investigating the Fredholm integral equation that involves the multiplication of incomplete $\aleph$-functions, GEMLF, and $\mathcal{S}$-function as the kernel. This research will advance our understanding of the properties and applications of these functions and their role in solving complex problems in various fields.

Definition 1: L. Euler [24] investigated the Gamma function as the extension of the factorial operation given below:

$$\Gamma(n+1) = n!. \tag{1.1}$$

The Gamma function is defined by a convergent improper integral as:

$$\Gamma(\theta) = \begin{cases} \int_0^\infty e^{-t} t^{\theta-1} dt, & (\Re(\theta) > 0) \\ \\ \frac{\Gamma(\theta+\omega)}{(\theta)_\omega}, & (\theta \in \mathbb{C} \setminus \mathbb{Z}_0^-; \omega \in \mathbb{N}_0). \end{cases} \tag{1.2}$$

where $(\theta)_\omega$ is the Pochhammer symbol [2] and is defined as:

$$(\theta)_\omega = \frac{\Gamma(\theta+\omega)}{\Gamma(\theta)} = \begin{cases} 1, & (\omega = 0; \theta \in \mathbb{C} \setminus \{0\}) \\ \theta(\theta+1)\dots(\theta+k-1), & (\omega = k \in \mathbb{N}; \theta \in \mathbb{C}). \end{cases} \tag{1.3}$$

Definition 2: The incomplete gamma function [13] is widely applicable in various fields, including physics and medical sciences. The properties of the real incomplete gamma functions are commonly used in complex analysis.
The upper and lower incomplete gamma functions are defined as:

$$\gamma(u,x) = \int_0^x v^{u-1} e^{-v} dv \quad (\Re(u) > 0; x \geq 0), \tag{1.4}$$

and

$$\Gamma(u,x) = \int_x^\infty v^{u-1} e^{-v} dv \quad (x \geq 0; \Re(u) > 0), \tag{1.5}$$

where

$$\gamma(u,x) + \Gamma(u,x) = \Gamma(u) \quad (\Re(u) > 0). \tag{1.6}$$

Definition 3: Sdland *et. al.* [23] have introduced a new concept called the ℵ-function. This function has recently been expanded upon by Bansal *et. al.* [19], who have introduced the incomplete ℵ-function. This new function is a generalization of the original ℵ-function, which leads to further advancements in mathematical theory and applications.

$$
\begin{aligned}
{}^{(\Gamma)}\aleph_{P_i,Q_i,\delta_i;R}^{M,N}[z] &= {}^{(\Gamma)}\aleph_{P_i,Q_i,\delta_i,R}^{M,N}\left[z\left|\begin{array}{c}(\mathfrak{b}_1,\mathfrak{B}_1,x),(\mathfrak{b}_j,\mathfrak{B}_j)_{2,N},[\delta_i(\mathfrak{b}_{ji},\mathfrak{B}_{ji})]_{N+1,P_i}\\ \\ (\mathfrak{a}_j,\mathfrak{A}_j)_{1,M},[\delta_i(\mathfrak{a}_{ji},\mathfrak{A}_{ji})]_{M+1,Q_i}\end{array}\right.\right] \qquad (1.7)\\
&= \frac{1}{2\pi i}\int_{\mathcal{L}}\Phi(\nu,x)z^{-\nu}d\nu,
\end{aligned}
$$

where $z\neq 0$ and

$$
\Phi(\nu,x)=\frac{\Gamma(1-\mathfrak{b}_1-\mathfrak{B}_1\nu,x)\prod_{j=1}^{M}\Gamma(\mathfrak{a}_j+\mathfrak{A}_j\nu)\prod_{j=2}^{N}\Gamma(1-\mathfrak{b}_j-\mathfrak{B}_j\nu)}{\sum_{i=1}^{R}\delta_i\left[\prod_{j=M+1}^{Q_i}\Gamma(1-\mathfrak{a}_{ji}-\mathfrak{A}_{ji}\nu)\prod_{j=N+1}^{P_i}\Gamma(\mathfrak{b}_{ji}+\mathfrak{B}_{ji}\nu)\right]}. \qquad (1.8)
$$

$$
\begin{aligned}
{}^{(\gamma)}\aleph_{P_i,Q_i,\delta_i;R}^{M,N}[z] &= {}^{(\gamma)}\aleph_{P_i,Q_i,\delta_i,R}^{M,N}\left[z\left|\begin{array}{c}(\mathfrak{b}_1,\mathfrak{B}_1,x),(\mathfrak{b}_j,\mathfrak{B}_j)_{2,N},[\delta_i(\mathfrak{b}_{ji},\mathfrak{B}_{ji})]_{N+1,P_i}\\ \\ (\mathfrak{a}_j,\mathfrak{A}_j)_{1,M},[\delta_i(\mathfrak{a}_{ji},\mathfrak{A}_{ji})]_{M+1,Q_i}\end{array}\right.\right] \qquad (1.9)\\
&= \frac{1}{2\pi i}\int_{\mathcal{L}}\Psi(\nu,x)z^{-\nu}d\nu,
\end{aligned}
$$

where where $z\neq 0$ and

$$
\Psi(\nu,x)=\frac{\gamma(1-\mathfrak{b}_1-\mathfrak{B}_1\nu,x)\prod_{j=1}^{M}\Gamma(\mathfrak{a}_j+\mathfrak{A}_j\nu)\prod_{j=2}^{N}\Gamma(1-\mathfrak{b}_j-\mathfrak{B}_j\nu)}{\sum_{i=1}^{R}\delta_i\left[\prod_{j=M+1}^{Q_i}\Gamma(1-\mathfrak{a}_{ji}-\mathfrak{A}_{ji}\nu)\prod_{j=N+1}^{P_i}\Gamma(\mathfrak{b}_{ji}+\mathfrak{B}_{ji}\nu)\right]}. \qquad (1.10)
$$

The both incomplete ℵ-functions $\left({}^{(\Gamma)}\aleph_{P_i,Q_i,\delta_i;R}^{M,N}[z] \text{ and } {}^{(\gamma)}\aleph_{P_i,Q_i,\delta_i;R}^{M,N}[z]\right)$ given by Eq. (1.7) and Eq. (1.9) exist for all $x\geq 0$ with the following conditions:

- The contour $\mathcal{L}$ extends from $C-\iota\infty$ to $C+\iota\infty$ on the complex plane, $C\in\Re$.
- Poles of $\Gamma(1-\mathfrak{b}_j-\mathfrak{B}_j\zeta)$, $j=\overline{2,N}$ never match exactly with the poles of $\Gamma(\mathfrak{a}_j+\mathfrak{A}_j\zeta)$, $j=\overline{1,M}$.
- The parameters M,N,P_i,Q_i are non negative integers that satisfy $0\leq N\leq P_i$, $0\leq M\leq Q_i$ and $i=\overline{1,R}$.
- Parameters $\mathfrak{B}_{\mathfrak{j}},\mathfrak{A}_{\mathfrak{j}},\mathfrak{B}_{\mathfrak{ji}},\mathfrak{A}_{\mathfrak{ji}}$ are positive real numbers and $\mathfrak{b}_{\mathfrak{j}},\mathfrak{a}_{\mathfrak{j}},\mathfrak{b}_{\mathfrak{ji}},\mathfrak{a}_{\mathfrak{ji}}$ are complex numbers.
- All the poles of $\Phi(\zeta,y)$ and $\Psi(\zeta,y)$ are supposed to be simple, and the null product is considered as unity.
- $$
\mathfrak{F}_i\geq 0,\quad |\arg(z)|<\frac{\pi}{2}\mathfrak{F}_i\quad\text{and}\quad\Re(\mathfrak{G}_i)+1<0,\quad i=\overline{1,R}, \qquad (1.11)
$$

where

$$\mathfrak{F}_i = \sum_{j=1}^{N} \mathfrak{B}_j + \sum_{j=1}^{M} \mathfrak{A}_j - \left(\sum_{j=N+1}^{P_i} \mathfrak{B}_{ji} + \sum_{j=M+1}^{Q_i} \mathfrak{A}_{ji} \right), \tag{1.12}$$

$$\mathfrak{G}_i = \sum_{j=1}^{M} \mathfrak{a}_j - \sum_{j=1}^{N} \mathfrak{b}_j + \left(\sum_{j=M+1}^{Q_i} \mathfrak{B}_{ji} - \sum_{j=N+1}^{P_i} \mathfrak{A}_{ji} \right) + \frac{1}{2}\left(P_i - Q_i\right). \tag{1.13}$$

Definition 4: GEMLF is defined by Bansal *et al.* [18] as:

$$E_{\mu,\lambda}^{\phi;\rho}\Big(y;\xi,\psi,\omega\Big) = \sum_{m=0}^{\infty} \frac{\mathbf{B}_{\xi}^{\psi,\omega}(\phi+m,\rho-\phi)}{\mathbf{B}(\phi,\rho-\phi)} \frac{(\rho)_m}{\Gamma(\mu m+\lambda)} \frac{y^m}{(m)!}, \tag{1.14}$$

$$(\xi \geq 0, \Re(\rho) > \Re(\phi) > 0, \Re(\mu) > 0, \Re(\lambda) > 0).$$

Here $\mathbf{B}_{p}^{\psi,\omega}(\alpha,\beta)$ is generalized beta function [8].

Definition 5: The $\mathcal{S}$-function [7] is defined as follows:

$$\mathcal{S}_{(p,q)}^{\sigma,\eta,\epsilon,\tau,\kappa}\Big[g_1,g_2,\ldots,g_p;h_1,h_2,\ldots,h_q;y\Big] = \sum_{n=0}^{\infty} \frac{(g_1)_n (g_2)_n \ldots (g_p)_n (\epsilon)_{n\tau,\kappa}}{(h_1)_n (h_2)_n \ldots (h_q)_n \Gamma_\kappa(n\sigma+\eta)} \frac{y^n}{n!}, \tag{1.15}$$

where the κ-Pochhammer symbol [25] is defined as:

$$(\epsilon)_{n,\kappa} = \begin{cases} \frac{\Gamma_\kappa(\kappa n+\epsilon)}{\Gamma_\kappa(\epsilon)}, & \left(\kappa \in \Re, \epsilon \in \frac{\mathbb{C}}{\{0\}}\right) \\ \\ \epsilon(\epsilon+\kappa)\ldots(\epsilon+(n-1)\kappa), & (n \in \mathbb{N}, \epsilon \in \mathbb{C}). \end{cases} \tag{1.16}$$

Definition 6: The Mellin transforms of incomplete $\aleph$-functions are investigated by Bansal *et. al.* [19] in following manner:

$$\mathfrak{M}\left\{ {}^{(\Gamma)}\aleph_{P_i,Q_i,\delta_i;R}^{M,N}\left[kz^{\mu} \,\middle|\, \begin{matrix} (\mathfrak{b}_1,\mathfrak{B}_1,x),(\mathfrak{b}_j,\mathfrak{B}_j)_{2,N},[\delta_i(\mathfrak{b}_{ji},\mathfrak{B}_{ji})]_{N+1,P_i} \\ (\mathfrak{a}_j,\mathfrak{A}_j)_{1,M},[\delta_i(\mathfrak{a}_{ji},\mathfrak{A}_{ji})]_{M+1,Q_i} \end{matrix} \right];\mathfrak{p} \right\} = \frac{k^{-\mathfrak{p}/\mu}}{\mu}\Phi\left(\frac{\mathfrak{p}}{\mu},x\right), \tag{1.17}$$

and

$$\mathfrak{M}\left\{ {}^{(\gamma)}\aleph_{P_i,Q_i,\delta_i;R}^{M,N}\left[kz^{\mu} \,\middle|\, \begin{matrix} (\mathfrak{b}_1,\mathfrak{B}_1,x),(\mathfrak{b}_j,\mathfrak{B}_j)_{2,N},[\delta_i(\mathfrak{b}_{ji},\mathfrak{B}_{ji})]_{N+1,P_i} \\ (\mathfrak{a}_j,\mathfrak{A}_j)_{1,M},[\delta_i(\mathfrak{a}_{ji},\mathfrak{A}_{ji})]_{M+1,Q_i} \end{matrix} \right];\mathfrak{p} \right\} = \frac{k^{-\mathfrak{p}/\mu}}{\mu}\Psi\left(\frac{\mathfrak{p}}{\mu},x\right), \tag{1.18}$$

where Φ and Ψ are defined by Eq.(1.8) and Eq. (1.10) respectively.

Definition 7: The Weyl fractional integral operator of order β [14] is defined as:

$$\mathcal{W}^{-\beta}\{\mathfrak{F}(\mathfrak{z})\} = \frac{1}{\Gamma(\beta)}\int_{\mathfrak{z}}^{\infty}(\mathfrak{t}-\mathfrak{z})^{\beta-1}\mathfrak{F}(\mathfrak{z})d\mathfrak{t}, \qquad (\Re(\beta)>0, \mathfrak{F}\in\mathcal{A}), \tag{1.19}$$

here $\mathcal{A}$ indicates the space of all functions $\mathfrak{F}$ defined on $\mathbb{R}=[0,\infty)$ [15].

2. Solution of Integral Equation of Fredholm Kind Involving Incomplete ℵ-function, GEMLF and $\mathcal{S}$-Function

In this section, we will be applying the Mellin transform method as well as the Weyl fractional integral operator to solve the Fredholm integral equation which involves incomplete ℵ-function, GEMLF, and $\mathcal{S}$-function. By utilizing these mathematical techniques, we aim to provide a comprehensive and precise solution to the problem.

Lemma 1. Let

(i) The parameters M, N, P_i, Q_i are non negative integers that satisfy $0 \leq N \leq P_i$, $0 \leq M \leq Q_i$ and $i = \overline{1, R}$.

(ii) $\Re(\alpha - s) > 0; \quad \Re(\mathfrak{G}_i) + 1 < 0 \quad (i = \overline{1, R})$ where $\mathfrak{G}_i$ is given by Eq. (1.13).

(iii) $x \geq 0$, $\beta > 0$ and $\alpha \in \mathbb{C}$.

(iv) $|\arg(C)| < \frac{\pi}{2}\mathfrak{F}_i$ where $\mathfrak{F}_i$ is given by Eq. (1.12).

Then,

$$W^{s-\alpha}\left\{u^{-\alpha}E_{\mu,\lambda}^{\phi;\rho}\Big(u;\xi,\psi,\omega\Big)\mathcal{S}_{(p,q)}^{\sigma,\eta,\epsilon,\tau,\kappa}\Big[g_1,g_2,\ldots,g_p;h_1,h_2,\ldots,h_q;u\Big]\right.$$

$$\left.\times\,{}^{(\Gamma)}\aleph_{P_i,Q_i,\delta_i,R}^{M,N}\left[C\left(\frac{y}{u}\right)^{\beta}\,\middle|\,\begin{matrix}(\mathfrak{b}_1,\mathfrak{B}_1,x),(\mathfrak{b}_j,\mathfrak{B}_j)_{2,N},[\delta_i(\mathfrak{b}_{ji},\mathfrak{B}_{ji})]_{N+1,P_i}\\ (\mathfrak{a}_j,\mathfrak{A}_j)_{1,M},[\delta_i(\mathfrak{a}_{ji},\mathfrak{A}_{ji})]_{M+1,Q_i}\end{matrix}\right]\right\}$$

$$=u^{-s}\sum_{m=0}^{\infty}\sum_{n=0}^{\infty}\frac{\mathbf{B}_{\xi}^{\psi,\omega}(\phi+m,\rho-\phi)}{\mathbf{B}(\phi,\rho-\phi)}\frac{(\rho)_m}{\Gamma(\mu m+\lambda)}\frac{(g_1)_n(g_2)_n\ldots(g_p)_n(\epsilon)_{n\tau,\kappa}}{(h_1)_n(h_2)_n\ldots(h_q)_n\Gamma_{\kappa}(n\sigma+\eta)}\frac{u^{m+n}}{m!n!}$$

$$\times\,{}^{(\Gamma)}\aleph_{P_i+1,Q_i+1,\delta_i,R}^{M,N+1}\left[C\left(\frac{y}{u}\right)^{\beta}\,\middle|\,\begin{matrix}(\mathfrak{b}_1,\mathfrak{B}_1,x),(1-s+m+n,\beta),(\mathfrak{b}_j,\mathfrak{B}_j)_{2,N},[\delta_i(\mathfrak{b}_{ji},\mathfrak{B}_{ji})]_{N+1,P_i}\\ (\mathfrak{a}_j,\mathfrak{A}_j)_{1,M},[\delta_i(\mathfrak{a}_{ji},\mathfrak{A}_{ji})]_{M+1,Q_i},(1-\alpha+m+n,\beta)\end{matrix}\right]. \tag{2.1}$$

Proof. To attain the desired result, we commence our process by expressing the incomplete ℵ-function in terms of the Mellin Barne contour integral. Afterward, we proceed to expand the GEMLF and $\mathcal{S}$-function in series form and then change the order of integral and summation. At last, we apply the Weyl operator, interpret the result using the definition of the incomplete ℵ-function, and get the desired result. □

Lemma 2. Let

(i) The parameters M, N, P_i, Q_i are non negative integers that satisfy $0 \leq N \leq P_i$, $0 \leq M \leq Q_i$ and $i = \overline{1, R}$.

(ii) $\Re(\alpha - s) > 0; \quad \Re(\mathfrak{G}_i) + 1 < 0 \quad (i = \overline{1, R})$ where $\mathfrak{G}_i$ is given by Eq. (1.13).

(iii) $x \geq 0$, $\beta > 0$ and $\alpha \in \mathbb{C}$.

(iv) $|\arg(C)| < \frac{\pi}{2}\mathfrak{F}_i$ where $\mathfrak{F}_i$ is given by Eq. (1.12).

Then,

$$W^{s-\alpha}\Bigg\{u^{-\alpha}E_{\mu,\lambda}^{\phi;\rho}\Big(u;\xi,\psi,\omega\Big)\mathcal{S}_{(p,q)}^{\sigma,\eta,\epsilon,\tau,\kappa}\Big[g,g_2,\ldots,g_p;h_1,h_2,\ldots,h_q;u\Big]$$

$$\times {}^{(\gamma)}\aleph_{P_i,Q_i,\delta_i,R}^{M,N}\left[C\left(\frac{y}{u}\right)^{\beta}\middle|\begin{array}{c}(\mathfrak{b}_1,\mathfrak{B}_1,x),(\mathfrak{b}_j,\mathfrak{B}_j)_{2,N},[\delta_i(\mathfrak{b}_{ji},\mathfrak{B}_{ji})]_{N+1,P_i}\\ (\mathfrak{a}_j,\mathfrak{A}_j)_{1,M},[\delta_i(\mathfrak{a}_{ji},\mathfrak{A}_{ji})]_{M+1,Q_i}\end{array}\right]\Bigg\}$$

$$= u^{-s}\sum_{m=0}^{\infty}\sum_{n=0}^{\infty}\frac{\mathbf{B}_{\xi}^{\psi,\omega}(\phi+m,\rho-\phi)}{\mathbf{B}(\phi,\rho-\phi)}\frac{(\rho)_m}{\Gamma(\mu m+\lambda)}\frac{(g_1)_n(g_2)_n\ldots(g_p)_n(\epsilon)_{n\tau,\kappa}}{(h_1)_n(h_2)_n\ldots(h_q)_n\Gamma_{\kappa}(n\sigma+\eta)}\frac{u^{m+n}}{m!n!}$$

$$\times {}^{(\gamma)}\aleph_{P_i+1,Q_i+1,\delta_i,R}^{M,N+1}\left[C\left(\frac{y}{u}\right)^{\beta}\middle|\begin{array}{c}(\mathfrak{b}_1,\mathfrak{B}_1,x),(1-s+m+n,\beta),(\mathfrak{b}_j,\mathfrak{B}_j)_{2,N},[\delta_i(\mathfrak{b}_{ji},\mathfrak{B}_{ji})]_{N+1,P_i}\\ (\mathfrak{a}_j,\mathfrak{A}_j)_{1,M},[\delta_i(\mathfrak{a}_{ji},\mathfrak{A}_{ji})]_{M+1,Q_i},(1-\alpha+m+n,\beta)\end{array}\right]. \tag{2.2}$$

Proof. To attain the desired result, we commence our process by expressing the incomplete $\aleph$-function in terms of the Mellin Barne contour integral. Afterward, we proceed to expand the GEMLF and $\mathcal{S}$-function in series form and then change the order of integral and summation. At last, we apply the Weyl operator, interpret the result using the definition of the incomplete $\aleph$-function, and get the desired result. □

Theorem 2.1 *Let*

(i) The parameters M, N, P_i, Q_i are non negative integers that satisfy $0 \leq N \leq P_i$, $0 \leq M \leq Q_i$ and $i = \overline{1,R}$

(ii) $\Re(\alpha - s) > 0; \quad \Re(\mathfrak{G}_i) + 1 < 0 \quad (i = \overline{1,R})$ where $\mathfrak{G}_i$ is given by (1.13)

(iii) $x \geq 0$, $\beta > 0$ and $\alpha \in \mathbb{C}$

Then, the relation given below holds :

$$\int_0^\infty u^{-s}\sum_{m=0}^{\infty}\sum_{n=0}^{\infty}\frac{\boldsymbol{B}_{\xi}^{\psi,\omega}(\phi+m,\rho-\phi)}{\boldsymbol{B}(\phi,\rho-\phi)}\frac{(\rho)_m}{\Gamma(\mu m+\lambda)}\frac{(g_1)_n(g_2)_n\dots(g_p)_n(\epsilon)_{n\tau,\kappa}}{(h_1)_n(h_2)_n\dots(h_q)_n\Gamma_\kappa(n\sigma+\eta)}\frac{u^{m+n}}{m!n!}$$

$$\times\,{}^{(\Gamma)}\aleph_{P_i+1,Q_i+1,\delta_i,R}^{M,N+1}\left[C\left(\frac{y}{u}\right)^{\beta}\middle|\begin{matrix}(\mathfrak{b}_1,\mathfrak{B}_1,x),(1-s+m+n,\beta),(\mathfrak{b}_j,\mathfrak{B}_j)_{2,N},[\delta_i(\mathfrak{b}_{ji},\mathfrak{B}_{ji})]_{N+1,P_i}\\(\mathfrak{a}_j,\mathfrak{A}_j)_{1,M},[\delta_i(\mathfrak{a}_{ji},\mathfrak{A}_{ji})]_{M+1,Q_i},(1-\alpha+m+n,\beta)\end{matrix}\right]g(u)du$$

$$=\int_0^\infty u^{-\alpha}E_{\mu,\lambda}^{\phi;\rho}\Big(u;\xi,\psi,\omega\Big)\mathcal{S}_{(p,q)}^{\sigma,\eta,\epsilon,\tau,\kappa}\Big[g_1,g_2,\dots,g_p;h_1,h_2,\dots,h_q;u\Big]$$

$$\times\,{}^{(\Gamma)}\aleph_{P_i,Q_i,\delta_i,R}^{M,N}\left[C\left(\frac{y}{u}\right)^{\beta}\middle|\begin{matrix}(\mathfrak{b}_1,\mathfrak{B}_1,x),(\mathfrak{b}_j,\mathfrak{B}_j)_{2,N},[\delta_i(\mathfrak{b}_{ji},\mathfrak{B}_{ji})]_{N+1,P_i}\\(\mathfrak{a}_j,\mathfrak{A}_j)_{1,M},[\delta_i(\mathfrak{a}_{ji},\mathfrak{A}_{ji})]_{M+1,Q_i}\end{matrix}\right]D^{s-\alpha}\{g(u)\}du, \tag{2.3}$$

provided that $\mathfrak{F}\in\mathcal{A}$ *and* $y>0$.

Proof. Let $\mathbb{I}$ refers to the left-hand side of Eq. (2.3), then

$$\mathbb{I}=\int_0^\infty u^{-s}\sum_{m=0}^{\infty}\sum_{n=0}^{\infty}\frac{\mathbf{B}_{\xi}^{\psi,\omega}(\phi+m,\rho-\phi)}{\mathbf{B}(\phi,\rho-\phi)}\frac{(\rho)_m}{\Gamma(\mu m+\lambda)}\frac{(g_1)_n(g_2)_n\dots(g_p)_n(\epsilon)_{n\tau,\kappa}}{(h_1)_n(h_2)_n\dots(h_q)_n\Gamma_\kappa(n\sigma+\eta)}\frac{u^{m+n}}{m!n!}$$

$$\times\,{}^{(\Gamma)}\aleph_{P_i+1,Q_i+1,\delta_i,R}^{M,N+1}\left[C\left(\frac{y}{u}\right)^{\beta}\middle|\begin{matrix}(\mathfrak{b}_1,\mathfrak{B}_1,x),(1-s+m+n,\beta),(\mathfrak{b}_j,\mathfrak{B}_j)_{2,N},[\delta_i(\mathfrak{b}_{ji},\mathfrak{B}_{ji})]_{N+1,P_i}\\(\mathfrak{a}_j,\mathfrak{A}_j)_{1,M},[\delta_i(\mathfrak{a}_{ji},\mathfrak{A}_{ji})]_{M+1,Q_i},(1-\alpha+m+n,\beta)\end{matrix}\right]g(u)du$$

$$=\int_0^\infty g(u)W^{s-\alpha}\left\{u^{-\alpha}E_{\mu,\lambda}^{\phi;\rho}\Big(u;\xi,\psi,\omega\Big)\mathcal{S}_{(p,q)}^{\sigma,\eta,\epsilon,\tau,\kappa}\Big[g_1,g_2,\dots,g_p;h_1,h_2,\dots,h_q;u\Big]\right.$$

$$\left.\times\,{}^{(\Gamma)}\aleph_{P_i,Q_i,\delta_i,R}^{M,N}\left[C\left(\frac{y}{u}\right)^{\beta}\middle|\begin{matrix}(\mathfrak{b}_1,\mathfrak{B}_1,x),(\mathfrak{b}_j,\mathfrak{B}_j)_{2,N},[\delta_i(\mathfrak{b}_{ji},\mathfrak{B}_{ji})]_{N+1,P_i}\\(\mathfrak{a}_j,\mathfrak{A}_j)_{1,M},[\delta_i(\mathfrak{a}_{ji},\mathfrak{A}_{ji})]_{M+1,Q_i}\end{matrix}\right]\right\}du. \qquad \text{(using Eq. (2.1))}$$

Using Eq. (1.19) and changing the order of integration, we obtain

$$\mathbb{I}=\int_0^\infty t^{-\alpha}E_{\mu,\lambda}^{\phi;\rho}\Big(t;\xi,\psi,\omega\Big)\mathcal{S}_{(p,q)}^{\sigma,\eta,\epsilon,\tau,\kappa}\Big[g_1,g_2,\dots,g_p;h_1,h_2,\dots,h_q;t\Big]$$

$$\times\,{}^{(\Gamma)}\aleph_{P_i,Q_i,\delta_i,R}^{M,N}\left[C\left(\frac{y}{t}\right)^{\beta}\middle|\begin{matrix}(\mathfrak{b}_1,\mathfrak{B}_1,x),(\mathfrak{b}_j,\mathfrak{B}_j)_{2,N},[\delta_i(\mathfrak{b}_{ji},\mathfrak{B}_{ji})]_{N+1,P_i}\\(\mathfrak{a}_j,\mathfrak{A}_j)_{1,M},[\delta_i(\mathfrak{a}_{ji},\mathfrak{A}_{ji})]_{M+1,Q_i}\end{matrix}\right]\left(\int_0^t\frac{(t-u)^{\alpha-s-1}}{\Gamma(\alpha-s)}g(u)du\right)dt.$$

Afterward, by utilizing Riemann-Liouville's fractional derivative [14], we get

$$\mathbb{I}=\int_0^\infty t^{-\alpha}E_{\mu,\lambda}^{\phi;\rho}\Big(t;\xi,\psi,\omega\Big)\mathcal{S}_{(p,q)}^{\sigma,\eta,\epsilon,\tau,\kappa}\Big[g_1,g_2,\ldots,g_p;h_1,h_2,\ldots,h_q;t\Big]$$

$$\times\,{}^{(\Gamma)}\aleph_{P_i,Q_i,\delta_i,R}^{M,N}\left[C\left(\frac{y}{t}\right)^{\beta}\,\middle|\,\begin{matrix}(\mathfrak{b}_1,\mathfrak{B}_1,x),(\mathfrak{b}_j,\mathfrak{B}_j)_{2,N},[\delta_i(\mathfrak{b}_{ji},\mathfrak{B}_{ji})]_{N+1,P_i}\\(\mathfrak{a}_j,\mathfrak{A}_j)_{1,M},[\delta_i(\mathfrak{a}_{ji},\mathfrak{A}_{ji})]_{M+1,Q_i}\end{matrix}\right]D^{s-\alpha}\{g(t)\}dt,$$

which is the right-hand side of Eq. (2.3). □

Theorem 2.2 *Let*

(i) The parameters M,N,P_i,Q_i are non negative integers that satisfy $0\le N\le P_i$, $0\le M\le Q_i$ and $i=\overline{1,R}$.

(ii) $\Re(\alpha-s)>0;\quad \Re(\mathfrak{G}_i)+1<0\quad (i=\overline{1,R})$ where $\mathfrak{G}_i$ is given by (1.13).

(iii) $x\ge 0$, $\beta>0$ and $\alpha\in\mathbb{C}$.

Then, the relation given below holds :

$$\int_0^\infty u^{-s}\sum_{m=0}^{\infty}\sum_{n=0}^{\infty}\frac{\boldsymbol{B}_{\xi}^{\psi,\omega}(\phi+m,\rho-\phi)}{\boldsymbol{B}(\phi,\rho-\phi)}\frac{(\rho)_m}{\Gamma(\mu m+\lambda)}\frac{(g_1)_n(g_2)_n\ldots(g_p)_n(\epsilon)_{n\tau,\kappa}}{(h_1)_n(h_2)_n\ldots(h_q)_n\Gamma_\kappa(n\sigma+\eta)}\frac{u^{m+n}}{m!n!}$$

$$\times\,{}^{(\gamma)}\aleph_{P_i+1,Q_i+1,\delta_i,R}^{M,N+1}\left[C\left(\frac{y}{u}\right)^{\beta}\,\middle|\,\begin{matrix}(\mathfrak{b}_1,\mathfrak{B}_1,x),(1-s+m+n,\beta),(\mathfrak{b}_j,\mathfrak{B}_j)_{2,N},[\delta_i(\mathfrak{b}_{ji},\mathfrak{B}_{ji})]_{N+1,P_i}\\(\mathfrak{a}_j,\mathfrak{A}_j)_{1,M},[\delta_i(\mathfrak{a}_{ji},\mathfrak{A}_{ji})]_{M+1,Q_i},(1-\alpha+m+n,\beta)\end{matrix}\right]g(u)du$$

$$=\int_0^\infty u^{-\alpha}E_{\mu,\lambda}^{\phi;\rho}\Big(u;\xi,\psi,\omega\Big)\mathcal{S}_{(p,q)}^{\sigma,\eta,\epsilon,\tau,\kappa}\Big[g_1,g_2,\ldots,g_p;h_1,h_2,\ldots,h_q;u\Big]$$

$$\times\,{}^{(\gamma)}\aleph_{P_i,Q_i,\delta_i,R}^{M,N}\left[C\left(\frac{y}{u}\right)^{\beta}\,\middle|\,\begin{matrix}(\mathfrak{b}_1,\mathfrak{B}_1,x),(\mathfrak{b}_j,\mathfrak{B}_j)_{2,N},[\delta_i(\mathfrak{b}_{ji},\mathfrak{B}_{ji})]_{N+1,P_i}\\(\mathfrak{a}_j,\mathfrak{A}_j)_{1,M},[\delta_i(\mathfrak{a}_{ji},\mathfrak{A}_{ji})]_{M+1,Q_i}\end{matrix}\right]D^{s-\alpha}\{g(u)\}du, \tag{2.4}$$

provided that $\mathfrak{F}\in\mathcal{A}$ and $y>0$.

Proof. The proof of this theorem follows a similar process to that of Theorem 2.1. □

3. Conclusions

Our research yields significant implications across a wide range of fields. Our methodology involves the solution of an integral equation of Fredholm kind, which includes S-function, generalized extended Mittag-Leffler function (GEMLF), and incomplete $\aleph$-function in the kernel. Specifically, we have discovered that a vast array of results as derived by authors [12, 21, 34, 35], can be obtained by setting specific values for different parameters of the S-function, generalized extended Mittag-Leffler function (GEMLF), and incomplete $\aleph$-function. As a result, the outcomes presented in this

article have the potential to contribute to numerous advancements in science and engineering by providing valuable insights into the behavior of special functions relevant to these fields.

Acknowledgments

The first author acknowledges the financial support received from UGC, New Delhi, India through the UGC-BSR Research Start-Up Research Grant (No.F.30-516/2020(BSR)).

References

[1] A. Erdiyi, An integral equation involving Legendre functions. J. Soc. Ind. Appl. Math. 1964, 12, 1530.

[2] A. Erdlyi *et al.*, Higher Transcendental Functions. Vol. I. McGraw-Hill, New York. 1953.

[3] A. Koshev, V. Kuzina, Solution of Integral Equations Arising in Mathematical Problems of Construction Science, using the Bogolyubov Krylov method. IOP Conf. Ser. Mater. Sci. Eng. 2019, 603, 15.

[4] A.G. Ramm, Solution of Some Integral Equations Arising in Integral Geometry. Appl. Math. Lett. 1991, 4, 7781.

[5] A.G. Ramm, Integral Equations Arising in the Open System Theory. In Theory and Applications of Some New Classes of Integral Equations. Springer, New York, NY, USA. 1980.

[6] A.M. Mathai, R.K. Saxena, The H-Function with Applications in Statistics Other Disciplines. Wiley Eastern, New Delhi & Wiley Halsted, New York, NY, USA. 1978.

[7] D.L. Suthar and Teklay Hailay, Euler-Type Integral Operator Involving $\mathcal{S}$. Abstract and Applied Analysis. 2020, 7. 10.1155/2020/8267638.

[8] E. zergin, M.A. zarslan, A. Altin, Extension of gamma, beta and hypergeometric functions. J. Comput. Appl. Math. 2011, 235, 46014610.

[9] E.R. Love, Some integral equations involving hypergeometric functions. Proc. Edinb. Math. Soc. 1967, 15, 169198.

[10] E.R. Love, T.R. Prabhakar, N.K. Kashyap, A confluent hypergeometric integral equation. Glasg. Math. J. 1982, 23, 3140.

[11] H.M. Srivastava, R.K. Saxena, R.K. Parmar,; Some Families of the Incomplete H-functions and the Incomplete H-functions and Associated Integral Transforms and Operators of Fractional Calculus with Applications. Russ. J. Math. Phys. 2018, 25, 116138.

[12] H.M. Srivastava, R.K. Raina, On certain methods of solving a class of integral equation of Fredholm type. J. Austral. Math. Soc. (Ser. A). 1992, 52, 110.

[13] K.B. Oldham, J.C. Myland, J. Spanier, The Incomplete Gamma Functions. In: An Atlas of Functions. Springer, New York, NY. 2008. $https://doi.org/10.1007/978-0-387-48807-3\_46$.

[14] K.S. Miller, B. Ross, An Introduction to the Fractional Calculus and Fractional Differential Equations. New York: John Wiley & Sons, INC. 1993.

[15] M.J. Lighthill, Introduction to Fourier Analysis and Generalized Functions. Cambridge Monographs on Mechanics and Applied Mathematics. Cambridge University Press: Cambridge, UK, London, UK, New York, NY, USA. 1958.

[16] M.K. Bansal, D. Kumar, I. Khan, J. Singh, K.S. Nisar, Certain Unified Integrals Associated with Product of M-Series and Incomplete H-functions. Mathematics. 2019, 7, 1191.

[17] M.K. Bansal, J. Choi, A Note on Pathway Fractional Integral Formulas Associated with the Incomplete H-functions. Int. J. Appl. Comput. Math. 2019, 5, 133.

[18] M.K. Bansal, N. Jolly, R. Jain, D. Kumar, An integral operator involving generalized Mittag-Leffler function and associated fractional calculus results. J. Anal. 2019, 27(3), 727740.

[19] M.K. Bansal, D. Kumar, K.S. Nisar, J. Singh, Certain fractional calculus and integral transform results of incomplete ℵ-functions with applications. Math. Meth. Appl. Sci. 2020, 43, 56025614.

[20] M.K. Bansal, D. Kumar, On the integral operators pertaining to a family of incomplete I-functions. AIMS-Math. 2020, 5, 12471259.

[21] M.K. Bansal, D. Kumar, J. Singh, K.S. Nisar, On the Solutions of a Class of Integral Equations Pertaining to Incomplete H-Function and Incomplete $\overline{H}$-Function. Mathematics. 2020, 8, 819. https://doi.org/10.3390/math8050819

[22] M.M. Doroftei, S. Trean, Higher-order hyperbolic equations involving a finite set of derivations. Balk. J. Geom. Appl. 2012, 17, 2233.

[23] N. Sdland ,B. Baumann, TF Nannenmacher, Open problem: who knows about the ℵ-function Appl Anal. 1998, 1(4):401-402.

[24] P. J. Davis, Leonhard Euler's Integral: A Historical Profile of the Gamma Function. American Mathematical Monthly. 1959, 66 (10): 849869. doi:10.2307/2309786.

[25] R. Daz and E. Pariguan, On hypergeometric functions and Pochhammer k-symbol, Divulgaciones Matematicas. 2007, vol. 15, no. 2, pp. 179192.

[26] R. Sharma, J. Singh, D. Kumar, Y. Singh, An Application of Incomplete I-Functions with Two Variables to Solve the Nonlinear Differential Equations Using S-Function. Journal of Computational Analysis and Applications. 2022, 31. 80-95.

[27] S. Hu, M. Khavanin, W. Zhuang, Integral equations arising in the kinetic theory of gases. Appl. Anal. 1989, 34, 261266.

[28] S.R. Manam, Multiple integral equations arising in the theory of water waves. Appl. Math. Lett. 2011, 24, 13691373.

[29] S.T. McDaniel, P.R. Krauss, Expansion of integral equations arising in scattering theory. J. Acoust. Soc. Am. 1991, 89, 1113.

[30] S. Trean, On the Kernel of a Polynomial of Scalar Derivations. Mathematics. 2020, 8, 515.

[31] S. Trean, Gradient Structures Associated with a Polynomial Differential Equation. Mathematics. 2020, 8, 535.

[32] S. Trean, C Vrsan, Weak small controls and approximations associated with controllable affine control systems. J. Differ. Equ. 2013, 255, 18671882.

[33] T.R. Prabhakar, A class of integral equations with Gauss functions in the kernels. Math. Nachr. 1972, 52, 7183.

[34] T.R. Prabhakar, N.K. Kashyap, A new class of hypergeometric integral equations. Indian J. Pure Appl. Math. 1980, 11, 9297.

[35] V.B.L. Chaurasia, D. Kumar, On the Solutions of Integral Equations of Fredholm type with Special Functions. Tamsui Oxf. J. Inf. Math. Sci. 2012, 28, 4961.

[36] Y. Ioannou, M.M. Fyrillas, C. Doumanidis, Approximate solution to Fredholm integral equations using linear regression and applications to heat and mass transfer. Eng. Anal. Bound. Elem. 2012, 36, 12781283.

[37] Y. Singh, V. Gill, J. Singh, M. Jain, D. Kumar, Progress in Fractional Differentiation and Applications On the Fractional Differential Equations Associated with Integral Operator Involving Aleph Function in the Kernel. Progress in Fractional Differentiation and Applications. 2023, 9. 665-679, DOI:10.18576/pfda/090410.

Investigation of Casson Fluid Flow Past an Enlarging Surface with Thermal Radiation and Heat Source/sink in the presence of Buoyancy Effects

Abhishek Neemawat and Jagdev Singh
Department of Mathematics, JECRC University, Jaipur, India

December 23, 2023

Corresponding Author :jagdevsinghrathore@gmail.com (J.Singh)

Abstract: This study considers in depth the flow of the boundary layer of an incompressible, viscous, and steady Casson fluid through an expanding surface when thermal radiation, heat source, Soret, and Dufour effects are present. Using suitable similarity transformations, the governing non-linear partial differential equations are converted into coupled ordinary differential equations and then estimated using the MATLAB software bvp4c using a shooting process. Variable values of the parameters employed in the current inquiry are offered, together with solutions for the parameters of momentum, temperature, concentration, coefficient of local skin friction, and local Nusselt number. It is observed that the Casson fluid parameter improves fluid velocity and decreases the temperature. Also, it is found that thermal radiation and the presence of a heat source/sink increase the temperature of the fluid. We compared the present investigation with previously published papers and found them harmonious.

Keywords: Casson fluid; Heat source/sink, Thermal radiation; Enlarging sheet; Soret and Dufour effects.

1 Introduction

A few examples of industries where the viscous non-Newtonian fluid in the boundary layer province caused by an expanding flat plate has extensive technical applications include the cooling and drying of paper, aerodynamic extrusion, production of glass fibres, wire drawing, glass blowing, polymer and metal processing industries, and hot rolling.
Nadeem et al. [1] investigated the influences of thermal radiation on a Jeffery fluid's boundary layer along a planar sheet that was expanding exponentially.

They discovered that local skin friction is a declining function of the local suction parameter, and the heat transfer rate is a reducing function of the suction parameter and Eckert number while a rising function of the Prandtl number and radiation parameter. Hiemenz [2] was most likely the first to investigate 2D stagnation flow to transform the NS equations to non-linear ODEs. Crane [3] conducted ground-breaking research on constant boundary layers caused by a linearly expanding sheet. Similarity solutions are also permitted for the flow brought on by stretching sheets, which is significant in extrusion issues. Wang [4] found similar solutions for the axisymmetric situation. The most common fluid model nowadays is the Casson fluid, described as a fluid that thins under shear and has infinite viscosity at zero shear rates. Fredrickson [5] discovered the Casson fluid's continuous flow property in a pipe. Boyd et al. [6] analyzed the oscillatory blood flow while accounting for Casson fluid. They discovered that Casson and Carreau-Yasuda flow display remarkable changes in the steady flow compared to equivalent Newtonian-type flows. Casson fluids are non-Newtonian in nature. The constitutive equation for Casson fluid includes shear stress since it acts like elastic materials like tomato sauce, jelly, soup, honey, and concentrated fruit liquids. Another example of a Casson fluid is human blood. Later on, the MHD flow of a non-Newtonian fluid caused by an exponentially contracting surface was discovered by Nadeem et al. [7]. They found that the issue in the provided situation becomes a Newtonian scenario if the fluid parameter approaches infinity. Casson fluid flow analysis due to a permeable contracting surface with viscous dissipation was explored by Qasim and Nooren [8]. Bhattacharyya et al. [9] created the critical solution of the magnetohydrodynamic porous flow of a Casson fluid along an enlarging sheet. This investigation found that the partial slip strongly affects the velocity. A drop in the mass suction parameter is shown for the Casson fluid flow as the boundary slip parameter is raised. Nandy [10] provided a solution for the MHD Casson fluid flow approaching a stagnation point toward a stretched plate in the presence of a partial slip. To analyse how radiation influenced the fluid mass and heat transfer assessment of a Casson fluid along an unevenly stretched sheet. Swati [11] used the suction and blowing effects. She found that the fluid velocity initially falls when the unsteadiness parameter is raised. Additionally, it is discovered that as the Casson parameter increases, the fluid temperature rises, the fluid velocity field is suppressed, and thermal radiation improves the thermal diffusivity of the fluid, taken into consideration. Peri et al. [12] investigated the dual solutions of Casson fluid flow over a stretching or shrinking sheet. They demonstrated that the Dufour number enhances the velocity and temperature throughout the boundary layer. The concentration boundary layer thickness is enhanced by an increase in the Soret number. The shrinking ratio reduces the velocity of the fluid but enhances the concentration. The skin friction, heat and mass transfer rates increase with the Casson parameter. Many more researchers [13-16] did pioneer work in analytic solutions of ODEs and PDEs and mathematical modeling. Sushila et al. [17] analyzed a hybrid analytical model for thin film in fluid dynamics for non-Newtonian fluids. They found that the homotopy perturbation Elzaki transform method leads over the Elzaki decomposition method

since the non-linear problems are solved without utilizing Adomian polynomials. Moreover, Singh et al.[18] discovered computational analysis of Fractional Lienard's equation with exponential Memory.

The current paper aims to investigate the Casson fluid flow across a stretched sheet. The modified similarity equation's numerical solution is achieved for the stretching sheet. Plots are provided and analyzed in detail for the emerging physical parameters incorporated in the suggested problem.

2 Mathematical construction of the problem

Nakamura and Sawada [19] provided a definition of the rheological equation of Casson fluid flow as given under:

$$\tau_{ij} = \begin{cases} \left(\mu_B + \frac{1}{\sqrt{2\pi}}\tau_y\right) 2e_{ij}, & \pi > \pi_c \\ \left(\mu_B + \frac{1}{\sqrt{2\pi_c}}\tau_y\right) 2e_{ij}, & \pi < \pi_c \end{cases}, \tag{1}$$

where μ_B is used for the Casson fluid's plastic dynamic viscosity, τ_y is taken as the yield stress, π is considered as deformation rate, and it is $\pi = e_{ij}e_{ij}$, where the component of the deformation at $(i,j)^{th}$ position is e_{ij}. τ_c expresses the critical value of π.

Consider 2D steady and incompressible Casson fluid flow near the stagnation point on a permeable enlarging plane surface. The direction of the plane surface is along the X, and the Y axis is taken normal to the surface. The axial velocity components in the above directions are u and v, respectively. The sheet is stretched by applying two equal pressures in the x direction immediately to produce the flow. The plane surface is extended with a linear velocity of the form $u_w(x) = cx$ while preserving the origin fixed, where c is a constant and it is taken as $c > 0$ for an expanding surface, for shrinking sheet $c < 0$ and $c = 0$ for a static surface.

Under the aforementioned assumptions, for this Casson fluid flow, the stable boundary layer equations for incompressible stagnation-point flow are given as follows:

Equation of Continuity:

$$\frac{\partial u}{\partial x} + \frac{\partial u}{\partial y} = 0, \tag{2}$$

Equation of Momentum:

$$u\frac{\partial u}{\partial x} + v\frac{\partial u}{\partial y} = u_e\frac{du_e}{dx} + \nu\left(1 + \frac{1}{\beta}\right)\frac{\partial^2 u}{\partial y^2} + g\beta_T\left(T - T_\infty\right), \tag{3}$$

Equation of Energy:

$$u\frac{\partial T}{\partial x}+v\frac{\partial T}{\partial y}=\alpha_m\frac{\partial^2 T}{\partial y^2}+\frac{D_m K_T}{C_s C_p}\frac{\partial^2 C}{\partial y^2}-\frac{1}{\rho C_p}\frac{\partial q_r}{\partial y}+\frac{Q_0}{\rho C_p}\left(T-T_\infty\right), \tag{4}$$

Equation of Concentration:

$$u\frac{\partial C}{\partial x}+v\frac{\partial C}{\partial y}=D_m\frac{\partial^2 C}{\partial y^2}+\frac{D_m K_T}{T_m}\frac{\partial^2 T}{\partial y^2}-K_0\left(C-C_\infty\right), \tag{5}$$

The following are the borderline circumstances for equations (2) to (5):

$$\left.\begin{array}{l} u=xc,\ \ v=0,\ T-T_\infty=xb,\ C-C_\infty=xd,\ \ when\ y=0,\\ u\to xa,\ \ T\to T_\infty,\ \ C\to C_\infty,\ \ as\ y\to\infty. \end{array}\right\}. \tag{6}$$

where $u_w\left(x\right)=cx$ is the fluid velocity at the wall and c is a constant, $u_e\left(x\right)=ax$ is the ambient fluid velocity where a is a constant, $\beta=\mu_B\sqrt{2\pi_c}/\tau_y$ symbolizes the Casson fluid parameter, β_T is used for the coefficient of thermal expansion, T expresses the fluid temperature, T_w represents the temperature of the sheet, T_∞ is constant, and it is considered as uniform ambient temperature, g is taken as gravitational acceleration, α_m expresses the effective thermal diffusivity, the mean temperature of fluid is T_m, the effective solutal diffusivity is D_m, K_T is used for the ratio of thermal diffusion, C_p is taken as the specific heat at constant pressure, and C_s is the concentration susceptibility.
The stream function ψ is defined as

$$u=\frac{\partial\psi}{\partial y},\qquad v=-\frac{\partial\psi}{\partial x},$$

where $\psi=\sqrt{a\nu}xf\left(\eta\right)$, dimensionless stream function is $f\left(\eta\right)$ and similarity variable is $\eta=y\sqrt{\frac{a}{\nu}}$. Solving this, we get the values of velocity components in both directions are given by

$$\begin{aligned} u&=xaf'\left(\eta\right),\\ v&=-\sqrt{a\nu}f\left(\eta\right). \end{aligned} \tag{7}$$

The Casson fluid temperature and concentration are taken as

$$\theta\left(\eta\right)=\frac{T-T_\infty}{\Delta T}\ \ and\ \ \phi\left(\eta\right)=\frac{C-C_\infty}{\Delta C}, \tag{8}$$

where $\theta\left(\eta\right)$ and $\phi\left(\eta\right)$ are dimensionless temperature and concentration respectively. Equations (2) to (5) become the subsequent two-point boundary value problem when equations (7) and (8) are used:

$$\left(1+\beta^{-1}\right)f'''+ff''-f'^2+\lambda\theta=-1, \tag{9}$$

$$Pr^{-1}\left(1+\frac{4}{3}R\right)\theta''+f\theta'-f'\theta+D_f\phi''+Q\theta=0, \tag{10}$$

$$Sc^{-1}\phi''+f\phi'-f'\phi+Sr\theta''-K\phi=0, \tag{11}$$

The transformed borderline circumstances are:

$$\left.\begin{array}{l} f=0,\ \ f'=\frac{c}{a},\ \ \theta=1,\ \ \phi=1 \quad at\ \ \eta=0, \\ f'\to 1,\ \ \theta\to 0,\ \ \phi\to 0 \quad as \quad \eta\to\infty \end{array}\right\}. \tag{12}$$

where prime ($'$) indicates differentiation with respect to similarity variable η. The non-dimensional parameters used in this article are as follows: $\lambda=\frac{g\beta_T b}{a^2}$ (Buoyancy parameter), $\Pr=\frac{\nu}{\alpha_m}$ (Prandtl number), $Sc=\frac{\nu}{D_m}$ (Schmidt number), $D_f=\frac{D_m K_T(C_w-C_\infty)}{C_s C_p \nu(T_w-T_\infty)}$ (Dufour parameter), $Sr=\frac{D_m K_T(T_w-T_\infty)}{T_m \nu(C_w-C_\infty)}$ (Soret parameter), $R=\frac{4\sigma^* T_\infty^3}{\rho C_p k^* \alpha_m}$ (Radiation parameter), $Q=\frac{Q_0}{a\rho C_p}$ (Heat source/sink parameter) and $K=\frac{K_0}{a}$ (Chemical reaction parameter).

Significant physical entities of a particular flow field, temperature field, and concentration are presented graphically and tabularly in terms of skin friction, local Sherwood number, and Nusselt number, considering engineering and practical value and uses. These are the three measures of attention in the present study.
The surface shearing stress is shown by τ_w and calculated using

$$\tau_w=\left(\mu_B+\frac{\tau_y}{\sqrt{2\pi_c}}\right)\left(\frac{\partial u}{\partial y}\right)_{y=0}=\left(\mu_B+\frac{\tau_y}{\sqrt{2\pi_c}}\right)\sqrt{\frac{a^3}{\nu}}xf''(0), \tag{13}$$

The term for the local skin-friction coefficient is C_f, and its definition is

$$C_f=\frac{\tau_w}{\rho u_e x^2}, \tag{14}$$

Using equation (13) in equation (14), we get

$$Re_x^{1/2}C_f=\left(1+\beta^{-1}\right)f''(0). \tag{15}$$

The formula for the wall's rate of heat transmission is

$$q_w=-k\left(\frac{\partial T}{\partial y}\right)_{y=0}+(q_r)_{y=0}=-k(T_w-T_\infty)\sqrt{\frac{a}{\nu}}\theta'(0)-\frac{16\sigma^* T_\infty^3}{3k^*}(T_w-T_\infty)\sqrt{\frac{a}{\nu}}\theta'(0), \tag{16}$$

The local Nusselt number, represented by the symbol Nu_x, is defined as

$$Nu_x=\frac{xq_w}{k(T_w-T_\infty)}, \tag{17}$$

Using equations (16) and (17), the local Nusselt number can be expressed as follows

$$\frac{Nu_x}{Re_x^{1/2}} = -\left(1+\frac{4}{3}R\right)\theta'(0). \tag{18}$$

q_m stands for the mass flow at the wall and is defined as

$$q_m = -D_s\left(\frac{\partial C}{\partial y}\right)_{y=0} = -\left(C_w - C_\infty\right)D_s\sqrt{\frac{a}{\nu}}\phi'(0), \tag{19}$$

The local Sherwood number is denoted by Sh_x and is defined as

$$Sh_x = \frac{xq_m}{D_s\left(C_w - C_\infty\right)}, \tag{20}$$

Using equations (19) and (20), the Sherwood number can be expressed as follows

$$\frac{Sh_x}{Re_x^{1/2}} = -\phi'(0). \tag{21}$$

Here $Re_x = \frac{xu_e}{\nu}$ is taken as the local Reynolds number.

3 Influence of diverse restrictions on the flow

The given system of coupled ODEs from (9) to (11) with borderline circumstances given in equation (12) was solved using the MATLAB coding package named bvp4c ODEs solver. This portion of the text discusses the effects or influences of several physical non-dimensional parameters on the profiles of energy, momentum, concentration, skin friction, and rate of change of heat transfer. To authorize the outcomes of our numerical method, the values of $\left(1+\beta^{-1}\right)f''(0)$ were compared with values obtained by the researchers Peri [12], Bhattacharyya [20], and Ishak et al. [21] and they are found in very good agreement. Figures in the form of line graphs from 2 to 10 are used to display the distribution of axial velocity, temperature, and concentration. The following is a summary of the findings.

The comparison of the current results to those that have been published is shown in table 1. It is found to an excellent reliability between the present and published results. It also confirms the validity of the method used in the present paper. It can be shown from this table that when stretching parameter values increase, the local skin friction coefficient decreases.

Table 2 contains tabular values of $-\theta'(0)$ for various stretching/shrinking parameter values corresponding to specific fixed values of the other considered parameters. The data show that heat transport reduces as the stretching parameter values increase.

Figure 1 shows that for some fixed values of the stretching parameter, fluid velocity increases as the Casson parameter increases. Also, as the stretching parameter rises, fluid velocity rises in figure 2.

The energy profiles are shown in figures 3 to 7. It is examined that Casson fluid temperature increases as the radiation parameter and heat source parameter increase. Also, temperature decreases for increasing values of the stretching parameter, Prandtl number, and Casson parameter.
Figures 8 and 9 show the concentration distribution of the Casson fluid flow. We noticed that the fluid concentration falls when the stretching parameter and Schmidt number are increased for some fixed values of other parameters.
The effects of temperature and mass distribution on the stretching sheet parameter are depicted in figures 4 and 8. The stretching parameter affects the temperature and mass distributions in the opposite direction. We discovered that the temperature and mass distributions reduce as the stretching parameter increases. This is due to the stretching parameter's direct relationship with the heated fluid's heat transfer coefficient. The amount of convective energy transferred is inversely correlated with the thermal resistance of the warm fluid. As the stretching parameter rises, the warm fluid convection resistance falls, lowering the surface temperature.

4 Conclusion

This paper studies the flow of Casson fluid past an enlarging surface with thermal radiation and heat source/sink in the presence of Buoyancy effects. The Soret and Dufour effects on a Casson fluid are investigated about a stagnation point on a stretching sheet. The momentum, temperature, and concentration equations are written as a system of ordinary differential equations using a suitable similarity transformation and then solved numerically using a code-named MATLAB bvp4c solver. It is found that heat transport reduces as the stretching parameter increases. Also, fluid velocity rises with the Casson and stretching parameters. For the temperature of the fluid, it is seen that it increases with radiation parameter and decreases with increasing Prandtl number and stretching parameter values.
Here are some future scope suggestions for the paper entitled "Investigation of Casson fluid flow past an enlarging surface with thermal radiation and heat source/sink in the presence of buoyancy effects":
1. Examine other non-Newtonian fluid models, apart from Casson fluid, to comprehend how variations in fluid rheology impact the flow properties.
2. Examine the effects of adding nanoparticles to the Casson fluid to produce Casson-based nanofluids. Examine how heat sources, sinks, and thermal radiation affect these nanofluid systems.
3. To capture flow patterns and heat transfer characteristics that are more realistic, expand the current work to three-dimensional simulations. This might offer a more realistic depiction of the actual mechanism.
4. Examine how the system under study affects the environment, considering energy efficiency, sustainability, and possible uses in eco-friendly technologies.

Table 1: Assessment of $\left(1+\frac{1}{\beta}\right) f''(0)$ with Peri [12], Bhattacharyya [20], and Ishak et al. [21] for $\lambda = \Pr = D_f = 0 = Sc = Sr$ and $\beta = 10^8$

c/a	**Present study**	**Peri [12]**	**Bhattacharyya [20]**	**Ishak et al. [21]**
-0.25	1.40224031	1.4022408	1.4022405	1.402241
-0.50	1.49566920	1.4956698	1.4956697	1.495670
-0.75	1.48929749	1.4892982	1.4892981	1.489298
-1.00	1.32881613	1.3288169	1.3288169	1.328817
-1.15	1.08223159	1.0822312	1.0822316	1.082231
-1.20	0.93247562	0.9324734	0.9324728	0.932474
-1.2465	0.58428232	0.5842817	0.5842915	0.584295
0.0	1.23258722	-	-	-
0.2	1.05112962	-	-	-
0.4	0.83407188	-	-	-
0.6	0.58483595	-	-	-
0.8	0.30609469	-	-	-

Table 2: $-\theta'(0)$ for various values of $\beta = 3.5$, $\lambda = 0.01$, $D_f = Sr = Sc = 0.1, \Pr = 0.72, K = Q = R = 0.2$

c/a	$-\theta'(0)$
0.0	1.4034650
0.2	1.19728995
0.4	0.95082859
0.6	0.66793854
0.8	0.35163572
-0.25	1.59653352
-0.5	1.70350740
-0.75	1.69804589
-1.00	1.520163541
-1.15	1.248976011
-1.20	1.08891235
-1.2465	0.81579824

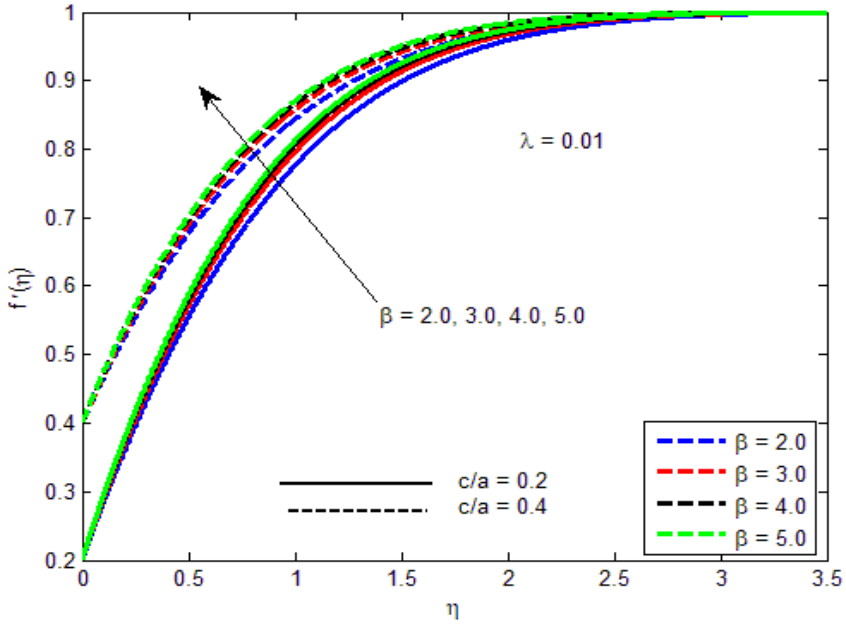

Figure 1: $f'(\eta)$ for unlike facts of β

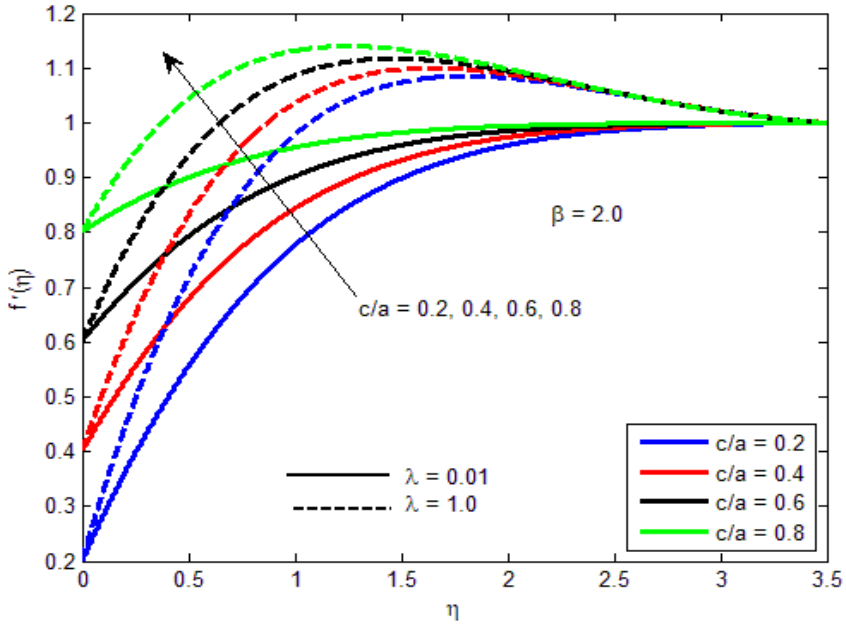

Figure 2: $f'(\eta)$ for unlike facts of c/a

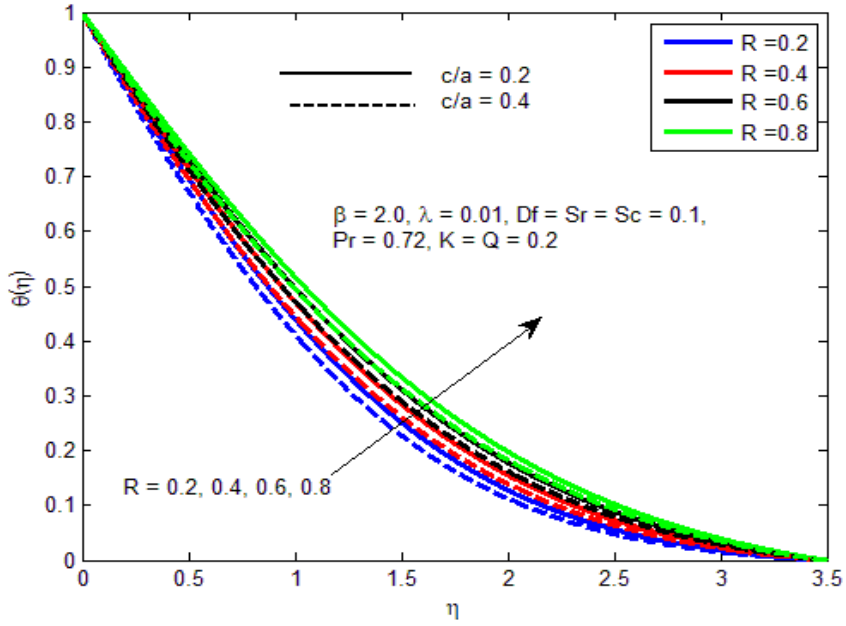

Figure 3: $\theta(\eta)$ for unlike facts of R

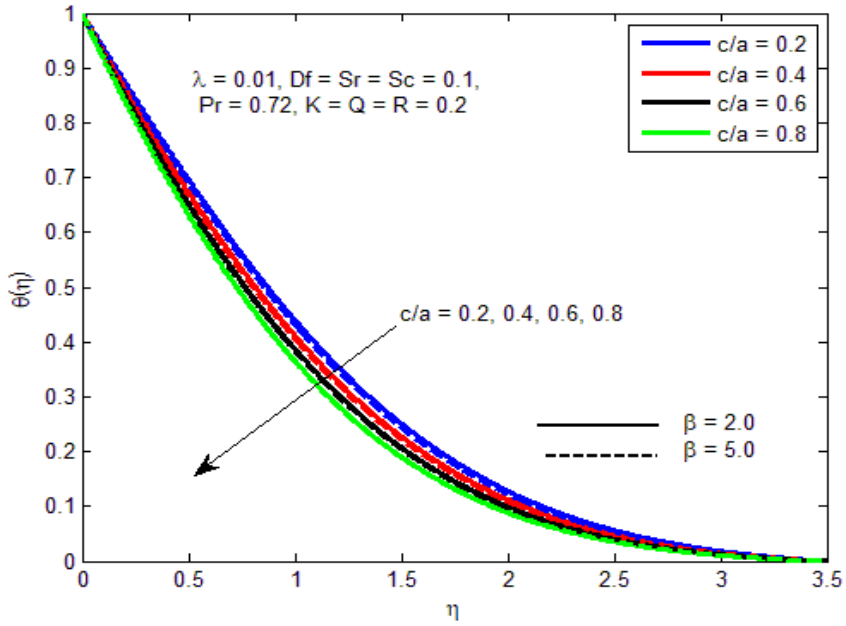

Figure 4: $\theta(\eta)$ for unlike facts of c/a

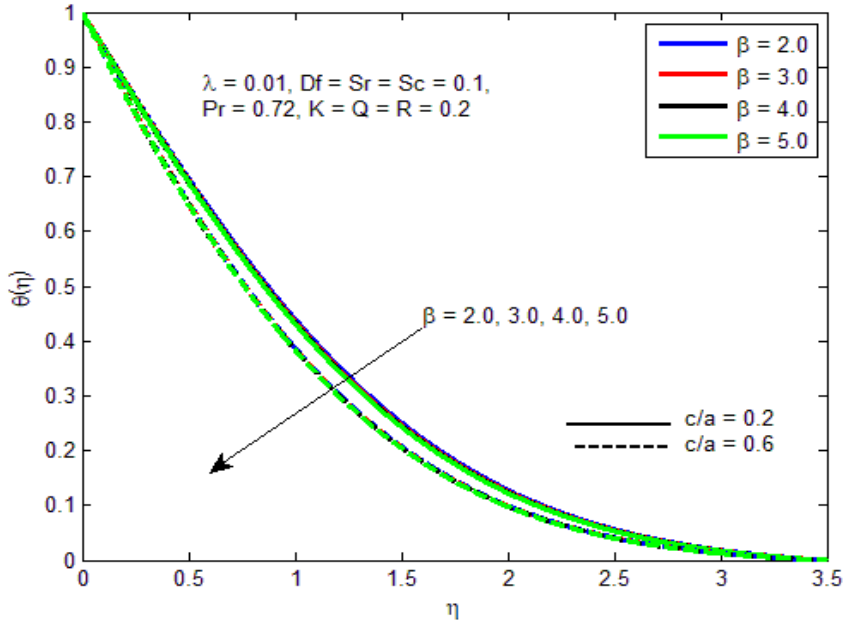

Figure 5: $\theta(\eta)$ for unlike facts of β

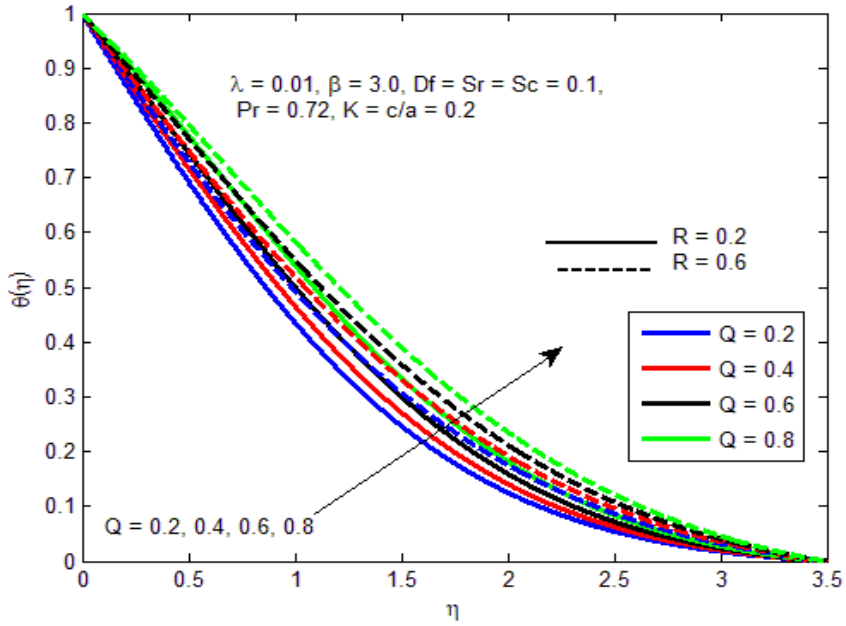

Figure 6: $\theta(\eta)$ for unlike facts of Q

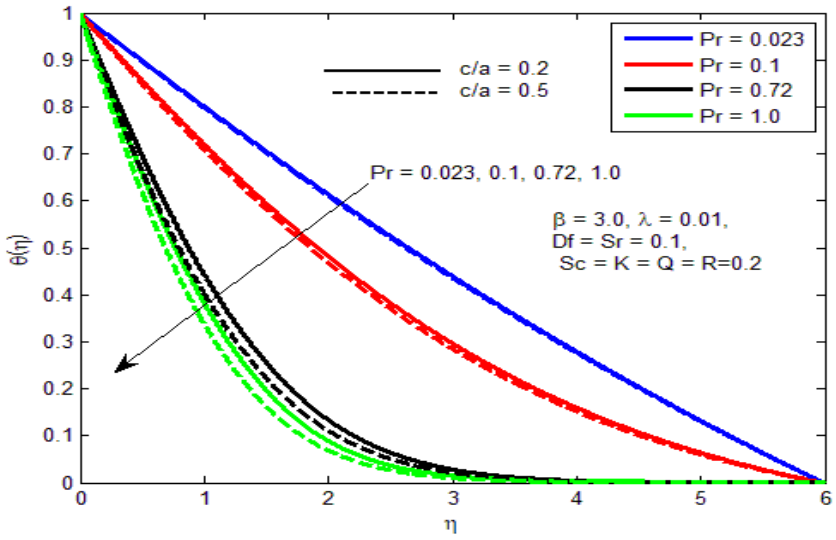

Figure 7: $\theta(\eta)$ for unlike facts of Pr

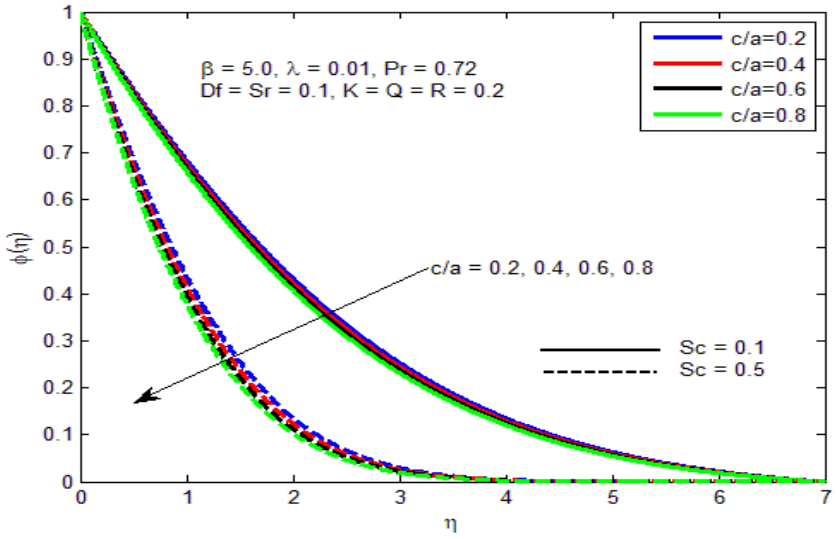

Figure 8: $\phi(\eta)$ for unlike facts of c/a

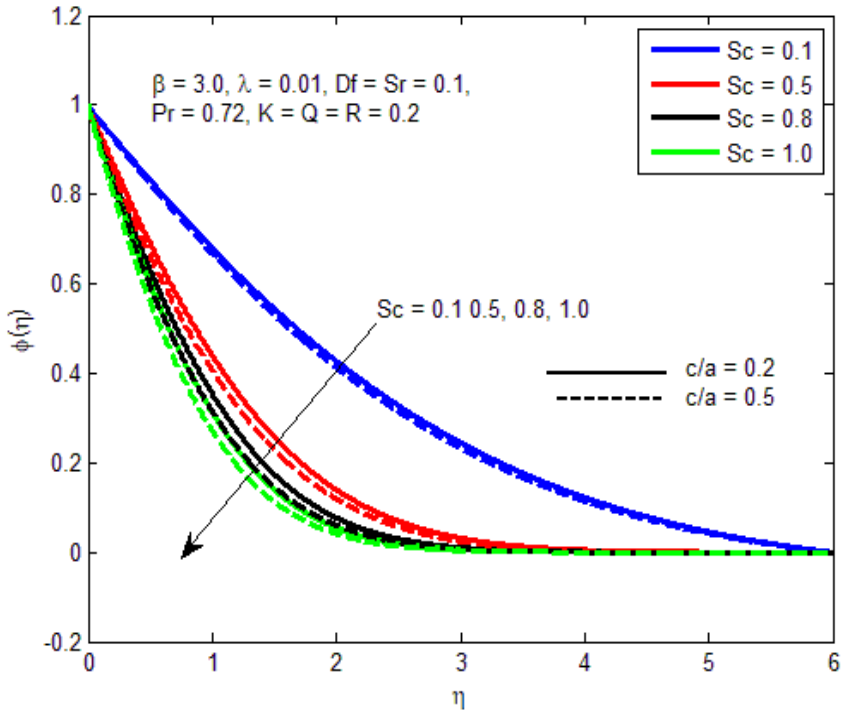

Figure 9: $\phi(\eta)$ for unlike facts of Sc

5 References

[1] Nadeem S., Zaheer S., and Fang T., Effects of thermal radiation on the boundary layer flow of a Jeffery fluid over an exponentially stretching surface, Num. Algor., 2011, 57, 187-205.
[2] Hiemenz K., Die Grenzschicht an einem in den gleichformingen Flussigkeitsstrom eingetauchten graden Kreiszylinder, Dinglers Polytech. J., 1911, 326, 321–324.
[3] Crane L. J., Flow past a stretching plate, Z. Angew. Math. Phys., 1970, 21, 645–647.
[4] Wang C. Y., The three-dimensional flow due to a stretching flat surface, Phys. Fluids, 1984, 27, 1915–1917.
[5] Fredrickson A. G., Principles and applications of Rheology, Prentice-Hall, Englewood Cliffs, N. J., 1964.
[6] Boyd J., Buick J. M., and Green S., Analysis of the Casson and Carreau-Yasuda non-Newtonian blood models in steady and oscillatory flow using the lattice Boltzmann method, Phys. Fluids, 2007, 19, 093103.
[7] Nadeem S., Rizwan U. H., and Lee C., MHD flow of a Casson fluid over an exponentially shrinking sheet, Scientia Iranica B., 2012, 19, 1550-1553.
[8] Qasim M., and Noreen S., Heat transfer in the boundary layer flow of a

Casson fluid over a permeable shrinking sheet with viscous dissipation, Eur. Phys. J. Plus, 2014, 7, 129.
[9] Bhattacharya K., Vajravelu K., and Hayat T., Slip effect on parametric space and the solution for the boundary layer flow of Casson fluid over a non-porous stretching/shrinking sheet, Int. J. Fluid Mech. Research, 2013, 40, 482-493.
[10] Nandy S. K., Analytical solution of MHD stagnation-point flow and heat transfer of Casson fluid over a stretching sheet with partial slip, ISRN Thermodynamics, 2013, Article ID 108264, 9 pages.
[11] Mukhopadhyay S., Effect of thermal radiation on Casson fluid flow and heat transfer over unsteady stretching surface subject to suction/blowing, Chin. Phys. B., 2013, 22, 1-7.
[12] Peri K., Shaw S., and Sibanda P., Dual solutions of Casson fluid flow over a stretching or shrinking sheet, Sadhana, 2014, 39, Part 6, 1573–1583.
[13] Kumar D., Dubey V. P., Dubey S., Singh J. and Alshehri A. M., Computational analysis of local fractional partial differential equations in Realm of fractal calculus, Chaos, Solitons and Fractals 167, 2023, 113009.
[14] Dubey V. P., Singh J., Alshehri A. M., Dubey S. and Kumar D., Analysis and fractal dynamics of some local fractional partial differential equations occurring in physical sciences, J. Comput. Nonlinear Dynam. 18(3), 2023, 1-23.
[15] Dubey V. P., Singh J., Alshehri A. M., Dubey S. and Kumar D., Analysis of Cauchy problems and diffusion equations associated with the Hilfer-Prabhakar fractional derivative via Kharrat-Toma transform, Fractal and Fractional, 2023, 7(5)413, 1-16, https://doi.org/10.3390/fractalfract7050413.
[16] Dubey V. P., Singh J., Alshehri A. M., Dubey S., and Kumar D., Forecasting the behavior of fractional order Bloch equations appearing in NMR flow via a hybrid computational technique, Chaos Solitons Fract., 2022, 164, 112691.
[17] Sushila, Singh J., Kumar D. and Baleanu D., A hybrid analytical algorithm for thin film problem occurring in non-Newtonian fluid mechanics, Ain Shams Engineering Journal, 2021, 12 (2), 2297-2302.
[18] Singh J., Alshehri A. M., Sushila and Kumar D., Computational analysis of fractional Lienard's equation with exponential memory, Journal of Computational and Nonlinear Dynamics, ASME (The American Society of Mechanical Engineers), 2023, 18(4), 041004, https://doi.org/10.1115/1.4056858.
[19] Nakamura M. and Sawada T., Numerical study on the flow of a non-Newtonian fluid through an axisymmetric stenosis, J. Biomech. Eng., 1988, 110, 137–143.
[20] Bhattacharyya K., Dual solutions in boundary layer stagnation-point flow and mass transfer with chemical reaction past a stretching/shrinking sheet, Int. Commun. Heat Mass Transf., 2011, 38, 917–922.
[21] Ishak A., Lok Y. Y. and Pop I., Stagnation-point flow over a shrinking sheet in a micropolar fluid, Chem. Eng. Comm., 2010, 197, 1417–1427.

Neural network based fractional order sliding mode tracking control of nonholonomic mobile robots

Naveen Kumar[a,b], Km Shelly Chaudhary[a,*]

[a]National Institute of Technology Kurukshetra, Kurukshetra 136119, Haryana, India,
[b] Mahatma Jyotiba Phule Rohilkhand University Bareilly, Bareilly 243006, Uttar Pradesh, India,
[*]Meerut College Meerut, Meerut 250002, Uttar Pradesh, India
Corresponding author:shelly_62000004@nitkkr.ac.in(KS.Chaudhary)

Abstract. In this study, the position tracking control problem of a nonholonomic mobile robots with system uncertainties and external disturbances is examined. In the design approach, a fractional-order sliding surface is presented that offers asymptotic stability of the system states towards their equilibrium points. A fractional order sliding mode controller is developed based on the presented sliding surface in order to handle system uncertainties and external disturbances in a robust manner. A radial basis function neural network is used to approximate the nonlinearities of the dynamic structure. The weighted matrices of neural networks are updated in an online mode. The controller's adaptive bound portion is used to manage neural network reconstruction error and provide upper bounds on disturbances and uncertainty. Using the Lyapunov technique and Barbalat's Lemma, the asymptotic stability of the control system is evaluated. Moreover, a numerical simulation study is carried out to illustrate the effectiveness of the proposed control approach by comparing the results with the existing control approaches.

Keywords: Nonholonomic mobile robots, Fractional order sliding surface; Sliding mode control; Neural networks

1 Introduction

Because of their wide applications in the field of medical profession, industries, military operations, and many other areas [1,2,3], trajectory tracking control of nonholonomic mobile robots has become a very intriguing study area in recent years. Nonholonomic mobile robots are the mechatronic structures that are extremely nonlinear, coupled, and time-varying. Because of these nonlinearities, uncertainties, and external disruptions, there are several practical

challenges in managing them. To address these challenges, various classical control schemes such as Model-based controllers, PID controllers, Back-stepping based controllers, Sliding mode controllers, Adaptive controllers, etc. [4,5,6] have been presented in the literature to control these systems.

Among these, sliding mode controllers (SMC) [7] are the most commonly used controllers because of their inherent capacity to resist uncertainty and external disturbances. The intrinsic adaptability attribute of the sliding mode control scheme is that when the system is operated on the sliding manifold, it functions independently of the system dynamics. In sliding mode controller, a sliding syrface is utilized to assure the convergence of tracking errors toward zero. For superior controller performance, linear and nonlinear sliding surfaces are now utilized in SMCs. Using linear sliding surface, Linear sliding mode controllers [8] (LSMC) have been presented in the study. LSMC investigates the asymptotic convergence of the trajectory tracking error even when the finite-time trajectory tracking error cannot be solved by these controllers. Terminal sliding mode controllers (TSMC) [9] have been presented in the literary texts to solve this issue. In TSMC, a non-linear sliding manifold is employed instead of a linear sliding manifold. These controllers guarantee tracking error convergence in a finite amount of time, but occasionally they pose singularity problems that result in unboundedly high control input values. The Non-singular Terminal Sliding Mode Controller (NTSMC) [10], which restricts the non-linear sliding manifold's parameters, has been proposed as a modified controller to handle this problem. The singularity problem is solved in NTSMC, although it has a slow convergence rate at the equilibrium point due to the presence of the term $e^{r/s}, r > s$ in the sliding manifold, resulting in a reduction in the convergence rate's magnitude away from the equilibrium.

For the enhanced and precise performance of controllers, different combinations of sliding mode controllers with Fractional Calculus [11,12,13] have been presented in the literature. Because of their greater order convergence speed, fractional-order controllers outperform integer-order controllers [14,15,16]. The study on integrating the fractional-order derivative [17] with SMC begins with applying the fractional order derivative to LSMC , which is known as the

fractional-order sliding mode controller (FoSMC) [18]. These controllers give superior tracking performance as compared to simple sliding mode controllers. The reason for this is that the fractional-order system's mathematical solution has a faster order convergence speed than the integer-order system. As fractional order sliding mode controllers are very efficient controller but the presence of uncertainties and disturbances in the dynamic structure of the manipulator causes many real-time difficulties. So, the employment of intelligent approaches such as neural networks [19,20,21] and fuzzy logics [22,23] improves the controller's suitability for real-world deployments. In the article [24], the design of a fractional-order sliding mode controller with a time-varying sliding surface is presented for trajectory tracking problem of robot manipulators. In this paper authors prove asymptotic convergence of tracking errors towards their system states. Authors of the article [25] present a fractional adaptation law for sliding mode control scheme for multi-input multi-output nonlinear dynamic system. In the article [26] authors present a coupled fractional-order sliding mode control scheme using obstacle avoidance for the control of a four-wheeled steerable mobile robot. A new fractional-order global sliding mode control scheme for nonholonomic mobile robot systems under external disturbances is presented in article [27]. While many studies have been conducted on the position tracking problem of dynamic systems under the influence of external disturbances and system uncertainties, relatively few of these studies combine intelligent techniques with the advantageous features of fractional-order sliding mode controllers for the control of nonholonomic mobile robots. So, the novelty of the presented work lies on the combination of fractional order sliding surface and the presented contoller that enhances the performance of the dynamical system in a robust manner.

In this paper to enhance the performance of the controller, a neural network based fractional-order sliding mode controller is presented for the position control problem of nonholonomic mobile robots under the influence of uncertainties and disturbances. The radial basis function neural network (RBFNN) is utlized in the developed controller to resemble the nonlinearity of the dynamic structure, and the exponential reaching rule is utilized when the system is independent of its general dynamics. The designed controller's adaptive

compensator part handles the neural networks reconstruction error and upper bounds on disturbances. The Lyapunov stability criterion and Barbalat's lemma are used to examine the asymptotic convergence of tracking errors towards their equilibrium states. Moreover, simulation studies are performed to validate the proposed controller's performance in a comparative manner
The main contribution of the presented work is as follows:

1. A new combination of fractional order sliding surface with neural network based fractional order sliding mode controller is presented.
2. The position tracking problem for nonholonomic mobile manipulators under the influence of system uncertainties and external disturbances is discussed.
3. The stability and asymptotic convergence of tracking errors is examined using Lyapunov stability criterion and Barbalat's lemma.
4. Simulation studies are used to compare the performance of the proposed controller to that of existing controllers.

The remaining part of the paper is divided as follows. Sections 2 offer a dynamic model for a nonholonomic mobile robot. Section 3 presents the controller design, while section 4 contains the stability analysis. Section 5 offers a simulation study, and section 6 concludes the article.

2 Dynamics of nonholonomic mobile robots

The dynamics equation for 3-dof nonholonomic mobile robots with generalized cordinates $q = [x, y, \theta]^T$ satisfies the Euler-Lagrange equation is given by:

$$M(q)\ddot{q} + V_m(q, \dot{q})\dot{q} + F(\dot{q}) + T_d = B(q)\tau + A^T(q)\lambda \qquad (1)$$

where $M(q) \in R^{3\times3}$ be inertial matrix, $V(q, \dot{q}) \in R^{3\times3}$ be centripetal-coriolis matrix, $F(\dot{q}) \in R^{3\times1}$ be friction vector, $T_d \in R^{3\times1}$ be unknown bounded disturbance, $B(q) \in R^{3\times2}$ be input transformation matrix, $\tau \in R^{3\times1}$ be control input, $A^T(q) \in R^{3\times1}$ be constraint associated matrix and $\lambda \in R$ be Langranges multiplier.

With $M(q) = \begin{bmatrix} m & 0 & m_1 \\ 0 & m & -m_2 \\ m_1 & -m_2 & I \end{bmatrix}, V_m(q,\dot{q}) = \begin{bmatrix} 0\,0 & -m_2\dot{\theta} \\ 0\,0 & m_1\dot{\theta} \\ 0\,0 & 0 \end{bmatrix}, A^T(q) = \begin{bmatrix} -\sin\theta \\ \cos\theta \\ 0 \end{bmatrix}, B(q) = \begin{bmatrix} \cos\theta/r & \cos\theta/r \\ \sin\theta/r & \sin\theta/r \\ b/r & -b/r \end{bmatrix}, m_1 = mh\sin\theta, m_2 = mh\cos\theta$ where m is total mass of nonholonomic mobile base, I is moment of inertia of mobile base.

Let the mobile robot system is subject to the following nonholonomic kinematic constraint.

$$A(q)\dot{q} = 0 \tag{2}$$

These constraints are limitations on the dynamic equation of mobile robots to the manifold $\Im_B$ as $\Im_B = \{(q,\dot{q})|B(q)\dot{q} = 0\}$. From equation (2), we can get the full rank matrix $P(q) \in R^{3\times 2}$ as:

$$P^T(q)A^T(q) = 0 \tag{3}$$

From constraints given in equations (2) and (3), we have a new vector $\dot{v} \in R^2$ satisfies the following condition

$$\dot{q} = P(q)\dot{v} \tag{4}$$

Differentiating equation (4), we have

$$\ddot{q} = P(q)\ddot{v} + \dot{P}(q)\dot{v} \tag{5}$$

Putting equation (4) and (5) in equation (1) and multiplying the obtained equation by P^T we get

$$\bar{M}_f\ddot{v} + \bar{V}_f\dot{v} + \bar{F}_f + \bar{\tau}_{fd} = P^T\tau \tag{6}$$

where $\bar{M}_f = P^TM(q)P, \bar{V}_f = P^TM(q)\dot{P} + P^TV_m(q,\dot{q})P, \bar{F}_f = P^TF(\dot{q})$, $\bar{\tau}_{fd} = P^TT_d$.

Let the dynamics equation (6) of nonholonomic mobile robots satisfy the following properties and assumptions.

Property 1 The Inertial matrix $\bar{M}_f$ is symmetric, bounded positive-definite and invertible,.

Property 2 The term $A = (\dot{\bar{M}}_f - 2\bar{V}_f)$ satisfies skew-symmetric property *i.e.* $x^TAx = 0 \quad \forall x \in R^n$.

Assumption 1 $\bar{F}_f \leq a_1 + a_2\|\dot{v}\|$ for arbitrary positive constants a_1, a_2 .
Assumption 2 $\|\bar{\tau}_{fd}\| \leq a_3$ for arbitrary positive constant a_3.
Assumption 3 If $v = [y, \theta]^T \in R^2$ is uniformally bounded and continuous, then all the jacobian matrices are also uniformally bounded and continuous.

3 Controller Structure

3.1 Fractional-order sliding surface

The proposed fractional-order sliding surface is given as

$$S(t) = D^{\alpha+1}\eta(t) + \dot{\eta}(t) + \lambda\eta(t) \tag{7}$$

where $\alpha \in (0, 1)$, $\eta(t) = v_d(t) - v(t)$ denotes position tracking error, $v_d(t) \in R^2$ denotes desired trajectory, $\lambda = diag[\lambda_1, \lambda_2] \in R^{2\times2}$ with $\lambda_1, \lambda_2 > 0$, and $S(t) = [S_1(t), S_2(t)]^T \in R^2$ be sliding variable. The j^{th} element of the proposed sliding surface is written as

$$S_j(t) = D^{\alpha+1}\eta_j(t) + \dot{\eta}_j(t) + \lambda\eta_j(t) \tag{8}$$

where $j = 1, 2$
On differentiating equation (8), we have

$$\dot{S}_j(t) = D^{\alpha+2}\eta_j(t) + \ddot{\eta}_j(t) + \lambda\dot{\eta}_j(t) \tag{9}$$

The reduced dynamics equation for nonholonomic mobile robots in terms of sliding variable $S(t) \in R^2$ can be written as

$$\bar{M}_f\dot{S} = -\bar{V}_f S - P^T\tau + f(y) + \bar{\tau}_{fd} + \bar{F}_f(\dot{v}) \tag{10}$$

where, $f(y) = \bar{M}_f[D^{\alpha+2}\eta(t) + \ddot{v}_d + \lambda\dot{\eta}(t)] + \bar{V}_f(v, \dot{v})[\dot{v}_d + D^{\alpha+1}\eta(t) + \lambda\eta(t)]$ be non-linear dynamics part comprises of two factors as $f(y) = \hat{f}(y) + \bar{f}(y)$ in which $\hat{f}(y)$ is known dynamic part of the system and $\bar{f}(y)$ is uncertain part of the dynamic system. For approximating this non-linear function $f(y)$, radial basis function neural networks (RBFNN) has been utilized. The input vector y during approximation of non-linear function $f(y)$ by RBFNN is choosen as $y = [\eta^T, \dot{\eta}^T, D^{\alpha+1}\eta^T, D^{\alpha+2}\eta^T]^T$.

3.2 RBFNN

Due to the adaptive nature of RBFNN [28], it is utilized to reproduce the non-linear part of the manipulator's dynamics. Let the function approximation on a simply connected compact set of the continuous function $f(y)$ be

$$f(y) = W^T \xi(y) + \epsilon(y) \tag{11}$$

where, $W \in R^{N \times b}$ demonstrates weight matrix, it will update online in an adaptive manner, $\xi(\cdot)$: $R \rightarrow R^N$ denotes predefine basis array, $\epsilon(y)$: $R \rightarrow R^b$ denotes reconstruction error, N denotes the no. of nodes used in the structure of neural-networks. So, we have $\|\epsilon(y)\|<\epsilon_N$ for some $\epsilon_N>0$.
For larger values of N, $\epsilon(y)$ may be reduced to very small value.
In the structure of RBFNN, the Gaussian function $\xi(y)$ [29], has been used which is given as

$$\xi_i(y) = exp(\frac{-\|y - c_i\|^2}{\sigma_i^2}), \quad i = 1, 2...N. \tag{12}$$

Putting the value of function $f(y)$ from (11) into (10). then, the reduced error dynamical equation be given by

$$\bar{M}_f \dot{S} = -\bar{V}_f S - P^T \tau + W^T \xi(y) + \epsilon(y) + \bar{\tau}_{fd} + \bar{F}_f(\dot{v}) \tag{13}$$

3.3 Adaptive bound

From assumptions 1,2 and the upper bound ϵ_N, we have

$$\|\bar{\tau}_{fd} + \bar{F}_f(\dot{v}) + \epsilon(y)\| \leq a_1 + a_2\|\dot{v}\| + a_3 + \epsilon_N \tag{14}$$

As an adaptive bound, define $\mu = a_1 + a_2\|\dot{v}\| + a_3 + \epsilon_N$

$$\mu = \begin{bmatrix} 1 & \|\dot{v}\| & 1 & 1 \end{bmatrix} \begin{bmatrix} a_1 & a_2 & a_3 & \epsilon_N \end{bmatrix}^T = H^T(\|\dot{v}\|)\phi \tag{15}$$

where $H \in R^m$ is known vector function and $\phi \in R^m$ be the parameter vector.
To compensate the influence of friction, reconstruction error, and disturbances, the adaptive compensator is chosen as

$$\chi = \frac{\hat{\mu}^2 S}{\hat{\mu}\|S\| + \delta} \tag{16}$$

where $\dot{\delta} = -\beta\delta$, $\delta(0) > 0$, $\beta > 0$ and $\hat{\mu} = H^T\hat{\phi}$.
The control input law is offered as follows to reach the reference trajectory

$$P^T\tau = \hat{W}^T\xi(y) + K_1S + K_2sign(S) + \chi \tag{17}$$

with K_1, K_2 as gain matrices and $\tau = [\tau_1, \tau_2]^T \in R^2$
Using equation (17), the reduced dynamics equation in form of sliding variable $S(t)$ can be given as

$$\bar{M}_f\dot{S} = -\bar{V}_fS + \tilde{W}^T\xi(y) - K_1S - K_2sign(S) + \epsilon(y) + \bar{\tau}_{fd} + \bar{F}_f(\dot{v}) - \chi \tag{18}$$

where $\tilde{W} = W - \hat{W}$

4 Stability analysis

4.1 Asymptotical convergence of tracking error and boundedness of signals

If we select the update laws for varying parameters as:

$$\dot{\hat{W}} = \Lambda_w\xi(y)S^T \tag{19}$$

$$\dot{\hat{\phi}} = \Lambda_\phi H\|S\| \tag{20}$$

where $\Lambda_w = \Lambda_w^T \in R^{N\times N}$ and $\Lambda_\phi = \Lambda_\phi^T \in R^{m\times m}$ are positive-definite matrices. Then, the trajectory tracking error asymptotically converges to zero along with the boundedness of signals.
Proof: Let the Lyapunov function be

$$L = \frac{1}{2}S^T\bar{M}_fS + \frac{1}{2}tr(\tilde{W}^T\Lambda_w^{-1}\tilde{W}) + \frac{1}{2}tr(\tilde{\phi}^T\Lambda_\phi^{-1}\tilde{\phi}) + \frac{\delta}{\beta} \tag{21}$$

where $\tilde{W} = W - \hat{W}$ and $\tilde{\phi} = \phi - \hat{\phi}$.
Differentiating equation (21), we get

$$\dot{L} = \frac{1}{2}S^T\dot{\bar{M}}_fS + S^T\bar{M}_f\dot{S} + tr(\tilde{W}^T\Lambda_w^{-1}\dot{\tilde{W}}) + tr(\tilde{\phi}^T\Lambda_\phi^{-1}\dot{\tilde{\phi}}) + \frac{\dot{\delta}}{\beta} \tag{22}$$

Putting equation (18) into equation (22) with $\dot{\tilde{W}} = -\dot{\hat{W}}, \dot{\tilde{\phi}} = -\dot{\hat{\phi}}$, and $\dot{\delta} = -\beta\delta$, we get

$$\dot{L} = \frac{1}{2}S^T(\dot{\bar{M}}_f - 2\bar{V}_f)S + S^T\tilde{W}^T\xi(y) - S^T(K_1S + K_2 sign(S)) + S^T(\bar{F}_f (\dot{v}) + \epsilon(y) + \bar{\tau}_{fd}) - \frac{\hat{\mu}^2 S}{\hat{\mu}\|S\| + \delta}) - tr(\tilde{W}^T\Lambda_w^{-1}\dot{\hat{W}}) - tr(\tilde{\phi}^T\Lambda_\phi^{-1}\dot{\hat{\phi}}) - \delta \tag{23}$$

From equations (19), (20), and property 2, equation (23) can be written as

$$\dot{L} = - S^T(K_1S + K_2 sign(S)) + S^T(\bar{F}_f(\dot{v}) + \epsilon(y) + \bar{\tau}_{fd}) - \frac{\hat{\mu}^2\|S\|^2}{\hat{\mu}\|S\| + \delta} - \tilde{\phi}^T H\|S\| - \delta \tag{24}$$

Using adaptive bound μ, we get

$$S^T(\bar{F}_f(\dot{v}) + \epsilon(y) + \bar{\tau}_{fd}) \leq H^T(\hat{\phi} + \tilde{\phi})\|S\| \tag{25}$$

From (25), we have equation (24) as

$$\dot{L} \leq -S^T K_1 S - S^T K_2 sign(S) - \frac{(H^T\hat{\phi})^2\|S\|^2}{H^T\hat{\phi}\|S\| + \delta} + (H^T\hat{\phi})\|S\| - \delta \tag{26}$$

$$\dot{L} \leq -S^T K_1 S - \frac{\delta(H^T\hat{\phi})\|S\|}{H^T\hat{\phi}\|S\| + \delta} - \delta = -S^T K_1 S - \frac{\delta^2}{H^T\hat{\phi}\|S\| + \delta} \tag{27}$$

$$\dot{L} \leq -S^T K_1 S \leq -K_{min}\|S\|^2 \tag{28}$$

where K_{min} be the min. eigenvalue of matrix K_1.
So, it is concluded that $L_1(S(0), \tilde{W}, \tilde{\phi})$ and $L_1(S(t), \tilde{W}, \tilde{\phi})$ are both bounded functions with $L_1(S(t), \tilde{W}, \tilde{\phi})$ as non-increasing function . Thus, it has been shown that $S(t)$, $\tilde{W}$, and $\tilde{\phi}$ are all bounded. As $S(t)$ is function of location and velocity tracking error, so bounded value of $S(t)$ leads to the boundedness of these tracking errors.
Differentiating equation (28), we have $\ddot{L} \leq -2S^T K_1\dot{S}$. As $S(t)$ and

$\dot{S}(t)$ (Equation (18)) are both bounded implies $\ddot{L}_1$ is also bounded, that means $\dot{L}_1$ is uniformly continuous. Using to Barbalat's lemma, the position tracking errors approaches to zero in an asymptotic manner.

5 Simulation

To show the effecient performance of the designed controller, a simulation study is carried out on a nonholonomic mobile robot. The dynamic structure and parameters used in this study for position tracking problem of nonholonomic mobile robot is given in [30]. The non-holonomic constraint applied on mobile robot system is considered as: $-\dot{x}\sin(\theta) + \dot{y}\cos(\theta) = 0$. The simulation study on nonholonomic mobile robot is carried out using Matlab. ODE45 Matlab solver is utilized to solve ordinary differential equation. For calculating fractional order derivative, definition of Grunwald-Letnikov(GL) derivative [31] has been used.
To show the effectiveness and robustness of the proposed control scheme, the performance of the proposed control scheme is compared with the existing controller given in article [32], proposed controller by taking adaptive compensator is equal to zero and with desired trajectory. Figures 1-6 show how well the suggested control technique for a nonholonomic mobile robot system works. Figures 1 and 2 compare the location and velocity tracking errors of the proposed controller. These data demonstrate that the trajectory tracking errors for the proposed control method converge rapidly when compared to the existing controller. The location tracking performance is displayed in Figures 3 and 4. In the second case *i.e.* proposed controller with $\Delta = 0$, due to the presence of the disturbances and reconstruction error, there is some fluctuations during the tracking of reference trajectory but the performance of the proposed controller is very smooth that shows the robustness of the proposed controll approach. These Figures shows that the dynamic system tracks the desired trajectory very efficiently for the proposed case as compare to the other two cases. In Figures 5 and 6, velocity tracking performance is given that shows in the initial phase, the velocity of the mobile robot system fluctuates but after a very small duration, it

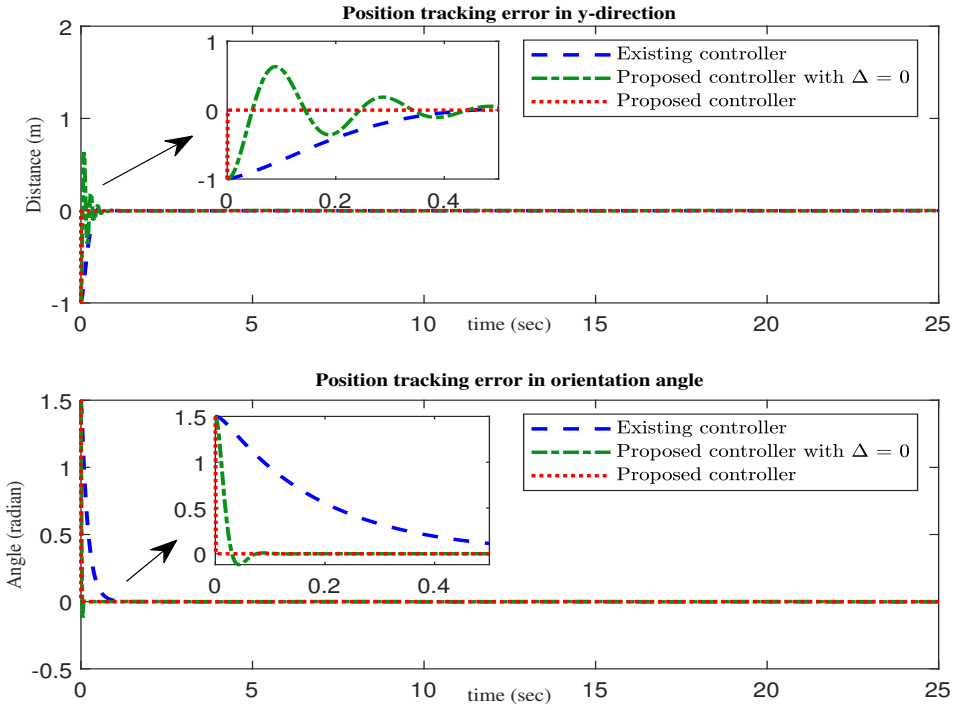

Fig. 1. Position tracking errors

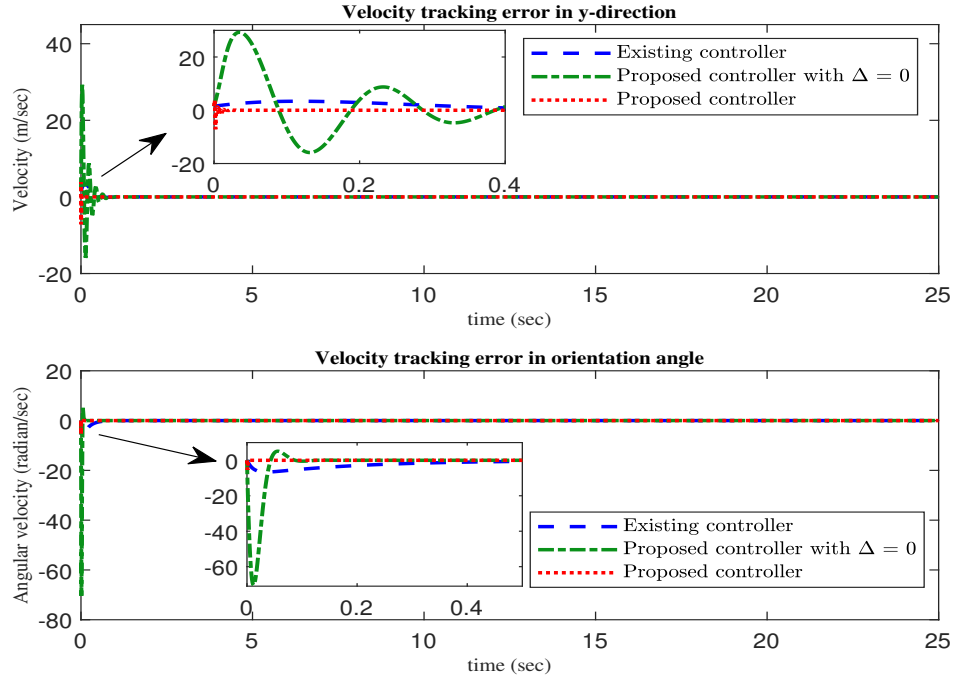

Fig. 2. Velocity tracking errors

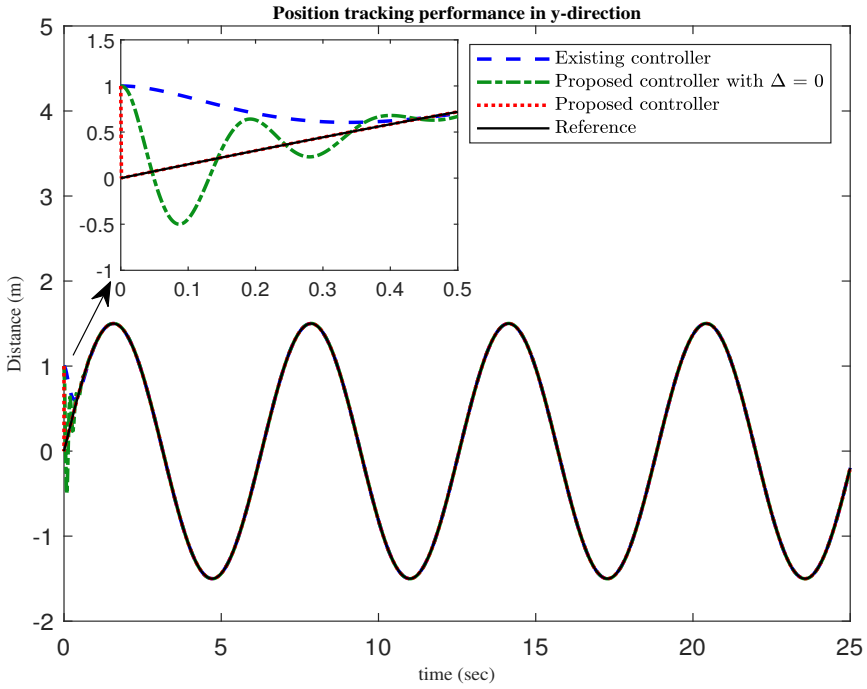

Fig. 3. Position tracking performance in y-direction

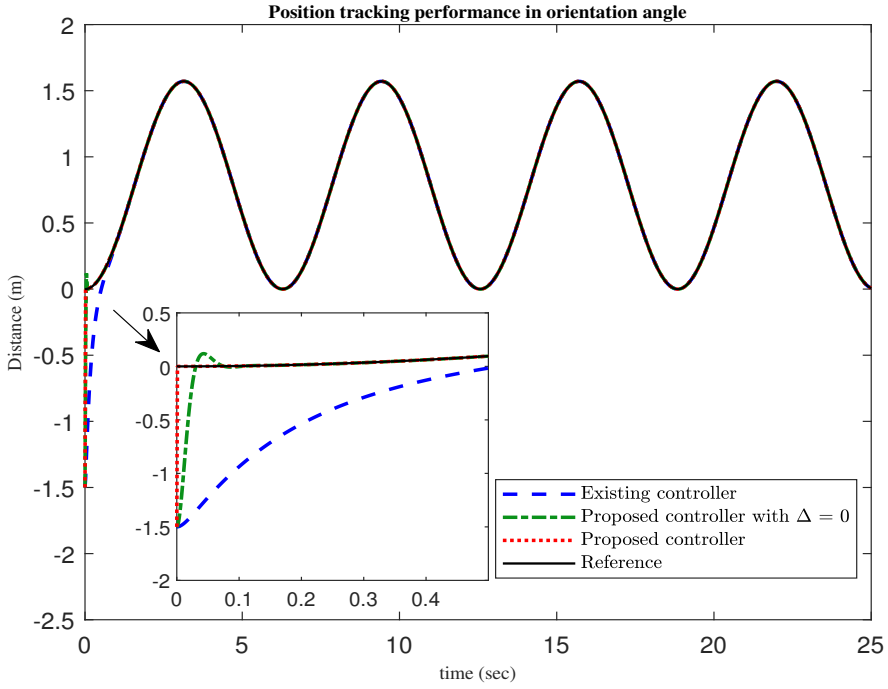

Fig. 4. Position tracking performance of orientation angle

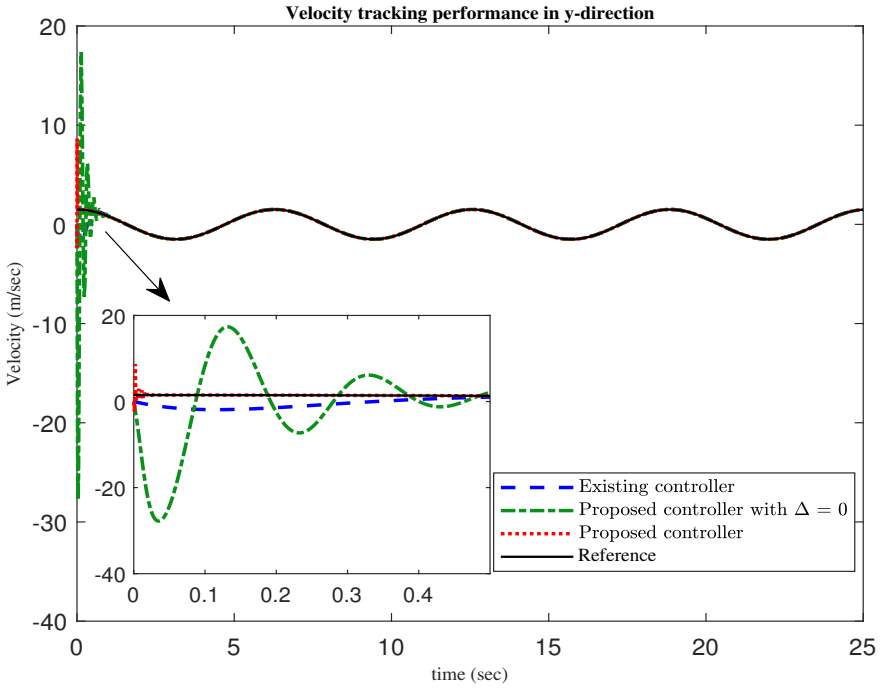

Fig. 5. Velocity tracking performance in y-direction

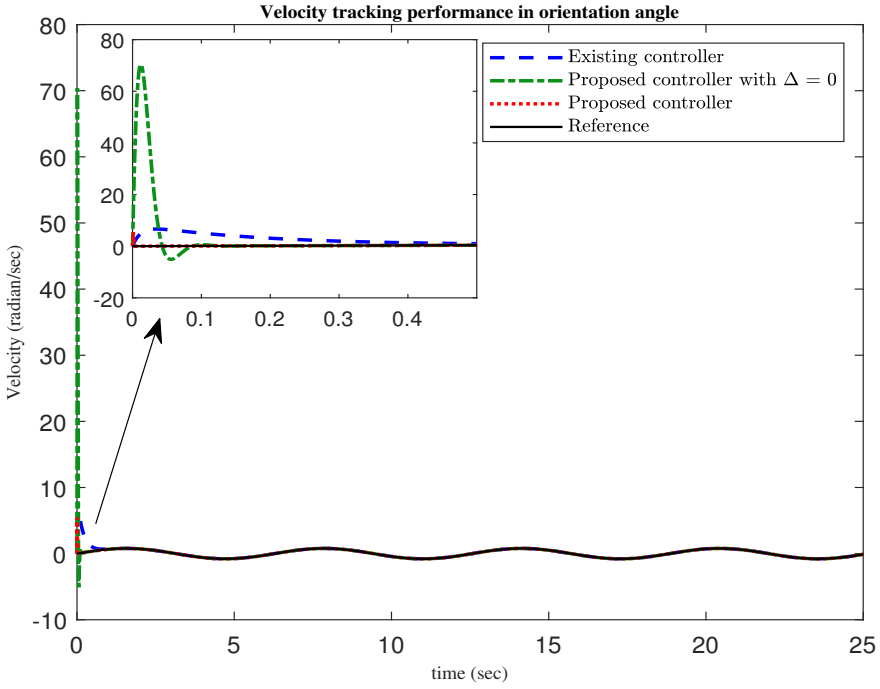

Fig. 6. Velocity tracking performance of orientation angle

tracks the reference velocity very smoothly for the proposed approach while for other two cases, the trajectory achieve after some time. From these figures, We get to the conclusion that the proposed controller precisely and quickly tracks the reference trajectory in a robust manner.
Further to compare the performance of controllers statistically, L^2 norm error analysis is presented in tabular form by comparing these parameters with existing controllers. Formula used for L^2 norm is given as

$$L^2[\eta] = \sqrt{\frac{1}{t_f - t_0} \int_{t_0}^{t_f} \|\eta(t)\|^2 dt} \tag{29}$$

Table 1. L^2-norm of position tracking error

Controllers	$L^2[\eta_1]$	$L^2[\eta_2]$
Existing controller [32]	0.1548	0.2180
Proposed controller with $\Delta = 0$	0.0997	0.0696
Proposed Controller	0.0100	0.0150

A lower value of $L^2[\eta]$ shows a lower tracking error, which demonstrates the effectiveness of the control strategy.

6 Conclusions

In this article, a neural network based fractional-order sliding mode controller is designed for the trajectory tracking problem of nonholonomic mobile robots. In the designed controller, RBFNN is used for approximation of the nonlinear part of dynamic structure, and an exponential reaching law is adopted. An adaptive compensator makes up for reconstruction error and disturbance upper limits. In order to analyze the convergence of tracking errors asymptotically, the Lyapunov stability criterion and Barbalat's lemma are used. To show the effectiveness and robustness of the presented controller, a simulation study is carried out in a comparative manner. It can be evident from the simulated data and statistical analysis that the efficiency of the proposed controller is enhanced. Further this control

approach can be implemented to another dynamical systems such as mobile manipulator systems, cart-pendulum systems, constrained reconfigurable dynamical systems ect.

References

1. X. Wu, Y. Wang, X. Dang, Robust adaptive sliding-mode control of condenser-cleaning mobile manipulator using fuzzy wavelet neural network, Fuzzy Sets and Systems 235 (2014) 62-82, doi:10.1016/j.fss.2013.07.009
2. H. Xie, J. Zheng, R. Chai, H.T. Nguyen, Robust tracking control of a differential drive wheeled mobile robot using fast nonsingular terminal sliding mode, Computers and Electrical Engineering 96 (2021) 107488. doi:10.1016/j.compeleceng.2021.107488
3. W. Dong, W. Huo,Tracking control of wheeled mobile robots with unknown dynamics, Proceedings 1999 IEEE International Conference on Robotics and Automation 4 (1999) 2645-2650. doi:10.1109/ROBOT.1999.773997
4. N. Chen, F. Song, G. Li, X. Sun, C. Ai, An adaptive sliding mode backstepping control for the mobile manipulator with nonholonomic constraints, Communications in Nonlinear Science and Numerical Simulation 18 (10) (2013) 2885-2899. doi:10.1016/j.cnsns.2013.02.002
5. M. Begnini, D.W. Bertol, N.A. Martins, A robust adaptive fuzzy variable structure tracking control for the wheeled mobile robot: Simulation and experimental results, Control Engineering Practice 64 (2017) 27-43. doi:10.1016/j.conengprac.2017.04.006
6. K.S. Chaudhary, N. Kumar, Fractional order fast terminal sliding mode control scheme for tracking control of robot manipulators. ISA transactions. 2023 Nov 1;142:57-69. doi:10.1016/j.isatra.2023.08.008
7. M. Defoort, T. Floquet, A. Kokosy, W. Perruquetti, Sliding-mode formation control for cooperative autonomous mobile robots, IEEE Transactions on Industrial Electronics 55 (11) (2008). doi:10.1109/TIE.2008.2002717
8. Gambhire, S. J., Kishore, D. R., Londhe, P. S., Pawar, S. N.: Review of sliding mode based control techniques for control system applications. International Journal of dynamics and control, 9, 363-378 (2021). doi:10.1007/s40435-020-00638-7
9. L. Zuo, R. Cui, W. Yan, Terminal sliding mode-based cooperative tracking control for non-linear dynamic systems, Transactions of the Institute of Measurement and Control 39 (7) (2017) 1081-1087. doi:10.1177/01423312166292
10. M.H. Korayem, R. Shiri, S.R. Nekoo, Z. Fazilati, Non-singular terminal sliding mode control design for wheeled mobile manipulator, Industrial Robot: An International Journal 44 (4) (2017) 501-511. doi:10.1108/IR-10-2016-0263
11. J. Singh, A. Gupta, D. Kumar, Computational Analysis of the Fractional Riccati Differential Equation with Prabhakar-type Memory. Mathematics. 2023 Jan 27;11(3):644. https://doi.org/10.3390/math11030644
12. J. Singh, A. Gupta, D. Baleanu, Fractional Dynamics and Analysis of Coupled Schrödinger-KdV Equation With Caputo-Katugampola Type Memory. Journal of Computational and Nonlinear Dynamics. 2023 Sep 1;18(9). https://doi.org/10.1115/1.4062391

13. J. Singh, Babu R, V.P. Dubey, D. Kumar, A homotopy based computational scheme for local fractional Helmholtz and Laplace equations. Journal of Computational Analysis and Applications. 2023 Jan 1;31(1).
14. J. Singh, R. Agrawal, K.S. Nisar. A new forecasting behavior of fractional model of atmospheric dynamics of carbon dioxide gas. Partial Differential Equations in Applied Mathematics. 2023 Nov 28:100595. https://doi.org/10.1016/j.padiff.2023.100595
15. V.P. Dubey, J. Singh, S. Dubey, D. Kumar. Analysis of Cauchy Problems and Diffusion Equations Associated with the Hilfer–Prabhakar Fractional Derivative via Kharrat–Toma Transform. Fractal and Fractional. 2023 May 20;7(5):413. https://doi.org/10.3390/fractalfract7050413
16. L. Mohan, A. Prakash, Stability and numerical analysis of fractional BBM-Burger equation and fractional diffusion-wave equation with Caputo derivative. Optical and Quantum Electronics 2024; 1-25. https://doi.org/10.1007/s11082-023-05608-9
17. A. Prakash, L. Mohan, Application of Caputo fractional operator to analyse the fractional model of Brain Tumour via modified technique, International Journal of Applied and Computational Mathematics 9, 1-33 (2023). 10.1007/s40819-023-01591-7
18. Y. Xie, X. Zhang, W. Meng, S. Zheng, L. Jiang, J. Meng, S. Wang, Coupled fractional-order sliding mode control and obstacle avoidance of a four-wheeled steerable mobile robot, ISA transactions 108 (2021) 282-294. doi:10.1016/j.isatra.2020.08.025
19. Lewis, F. W., Jagannathan, S., Yesildirak, A.: Neural network control of robot manipulators and non-linear systems. CRC press (1998).
20. Yin, F. C., Ji, Q. Z., Wen, C. W.: An adaptive terminal sliding mode control of stone-carving robotic manipulators based on radial basis function neural network. Applied Intelligence, 1-18 (2022). doi:10.1007/s10489-022-03445-z
21. Sonker, S., Devi, N.: Approximation of Signals by $E_l^1 E_l^1$ Product Summability Means of Fourier–Laguerre Expansion (2023). 10.1007/978-981-19-9906-2_5
22. Gao, Y., Er, M. J., Yang, S.: Adaptive control of robot manipulators using fuzzy neural networks. IEEE Transactions on Industrial Electronics, 48(6), 1274-1278 (2001). doi:10.1109/41.969410
23. Sonker, S., Moond, P.: Rate of Convergence of parametrically generalized bivariate Baskakov-Stancu operators (2023). 10.2298/FIL2327197S
24. Eray, O., Tokat, S.: The design of a fractional-order sliding mode controller with a time-varying sliding surface. Transactions of the Institute of Measurement and Control, 42(16), 3196-3215 (2020). doi:10.1177/01423312209446
25. Efe, M. O., Kasnakoglu, C.: A fractional adaptation law for sliding mode control. International Journal of Adaptive Control and Signal Processing, 22(10), 968-986 (2008). doi:0.1002/acs.1062
26. Xie, Y., Zhang, X., Meng, W., Zheng, S., Jiang, L., Meng, J., Wang, S.: Coupled fractional-order sliding mode control and obstacle avoidance of a four-wheeled steerable mobile robot. ISA transactions, 108, 282-294 (2021). https://doi.org/10.1016/j.isatra.2020.08.025
27. Labbadi, M., Boubaker, S., Djemai, M., Mekni, S. K., Bekrar, A.: Fixed-time fractional-order global sliding mode control for nonholonomic mobile robot systems under external disturbances. Fractal and Fractional, 6(4), 177 (2022). https://doi.org/10.3390/fractalfract6040177
28. Park, J., Sandberg, I. W.: Universal approximation using radial-basis-function networks. Neural computation, 3(2), 246-257 (1991). doi:10.1162/neco.1991.3.2.246

29. Feng, G., Chak, C. K.: Robot tracking in task space using neural networks. In Proceedings of 1994 IEEE International Conference on Neural Networks (ICNN'94) (Vol. 5, pp. 2854-2858). IEEE (1994). doi:10.1109/ICNN.1994.374684
30. Xie, H., Zheng, J., Sun, Z., Wang, H., Chai, R.: Finite-time tracking control for nonholonomic wheeled mobile robot using adaptive fast nonsingular terminal sliding mode. Nonlinear Dynamics, 110(2), 1437-1453 (2022). https://doi.org/10.1007/s11071-022-07682-2
31. Podlubny, I.: Fractional differential equations, mathematics in science and engineering (1999).
32. Boukattaya, M., Damak, T., & Jallouli, M.: Robust adaptive sliding mode control for mobile manipulators. aa, 2(2), 2 (2017).

Mathematical modeling of transmission dynamics and optimal control strategy for COVID-19 in India

M. Ankamma Rao [1] and A.Venkatesh[2*]

[1,2]Department of Mathematics,
AVVM Sri Pushpam College (Affiliated to Bharathidasan University),
Poondi, Thanjavur(Dt), Tamilnadu, India-613 503.

December 28, 2023

Abstract

Mathematical models are being used to investigate the dynamics of disease dissemination, forecast future trends, and access the most effective preventative measures to minimise the extent of epidemic outbreaks. This study formulates an eight compartmental epidemiological model to analyze the COVID-19 dynamics. The stability analysis of infection-free equilibrium is performed. The parameters are estimated by fitting this model to reported confirmed COVID-19 cases in India for 350 days. Sensitivity analysis is executed to identify the most sensitive parameters in this model. An optimal control analysis for India is implemented by incorporating four controls: 1) Public awareness initiatives using the media and civic society to persuade uninfected people not to interact with infected ones, 2) the effort of vaccinating susceptible individuals by supposing all of the susceptible people who got their vaccination are promptly moved to the recovered class 3) encouraging those who are infected with COVID-19 disease to stay at home or join in quarantine centres, as well as encouraging the severe cases admit in the hospital. The results are demonstrated that employing all four control measures significantly reduced the proportion of COVID-19 infections.

Keywords: : Mathematical model, Stability analysis, Sensitivity analysis, optimal control.
Subject Classification: 92D30, 37N25, 34D20, 49J15.

1 Introduction

The most current and dangerous virus is COVID-19, a new coronavirus that initially emerged in early 2020 and is still uncontrolled. Although the first cases are found on 31 December, 2019, in Wuhan, China, the disease's biological origin has not yet been fully determined. Later, the WHO designated the novel coronavirus disease as COVID-19 [1]. On January 30, 2020, the WHO is declared the outbreak a significant global public concern. The COVID-19 pandemic, which is now the major public health issue confronting the world after the Second World War, has already reached 767,972,961 infected cases and more than 6,950,655 fatalities as of July 12, 2023 [2]. Numerous

*Corresponding author: avenkateshmaths@gmail.com

studies demonstrate that COVID-19 may have been a zoonotic (transmitted from animal to human). The significant increase in COVID-19 cases also highlights the crucial fact that secondary dissemination occurs from person to person through direct contact or via particles of the virus dispersed by an infected person's coughing or sneezing.

Mathematical models are used to analyze the dissemination dynamics of epidemic infections with appropriate structures. Among the various models used in the study of epidemic diseases, compartmental models are widely used for the disease dissemination dynamics by subdividing into several compartments based on the need of the investigation [3]. Nowadays researchers prefer the compartmental models for their controllable and simple nature. An overview of several compartmental models is given in [4]. By applying a classical SIR (Susceptible, Infected, Recovered) model to various lockdown situations, Bagal et al. [5] are provided a complete study on COVID-19 spread in lockdown periods. Anand et al [6] are predicted the COVID-19 dissemination in India using the SIR model by considering isolation and testing parameters. This study also analyses the effects of lockdown before and after an rising the COVID-19 cases. At the beginning of the pandemic, the data shown that some infected populations, who has not show any symptoms have capable to spread COVID-19. These individuals are corresponding to the asymptomatic class. The asymptomatic individuals become symptomatic on an average period of three [7]. Similarly, a mathematical model [8] containing 22 compartments was introduced which related to susceptible, exposed, asymptomatic, pre-symptomatic, mildly symptomatic, severely symptomatic, detected, undetected, hospitalized, critical, recovered, dead compartments, etc. These extended models are accurate in defining the process of reality but they could not find perfect values for unknown parameters [9]. In recent years, the researchers are adopted various mathematical modeling approaches using real incidence datasets (especially in the case of COVID-19) with different parameters of the outbreak throughout the world. The concept of optimal control [10], transmissible illnesses must be controlled by giving appropriate dosages at the proper times for preventative measures. In contrast, mathematical modelling of transmissible illnesses has shown that the combination of vaccination, isolation, hospitalisation, and awareness campaigns are required to completely eradicate transmissible illnesses. The implementation of non-pharmaceutical intervention techniques can be a crucial factor in lowering the prevalence of infected populations. Investigating the dissemination of COVID-19 using the theory of optimum control techniques, Silva et al [11] are demonstrated that the diseases require optimal doses to be controlled. Mondal et al [12] are examined the COVID-19 disease dissemination dynamics employing vaccination as a control factor.

Dupey et al. [32] devised an effective computer technique called the Sumudu residual power series method for solving fractional Bloch equations arising in NMR flow. Alshehri et al [33] apply the local fractional natural homotopy perturbation technique to solve specific local fractional partial differential equations with fractal beginning conditions that arise in the physical sciences within the fractal domain. Dupey et al. have constructed a mathematical model for hepatitis E that incorporates a fractional derivative to describe the viral dynamics. Dupey et al. [34] are constructed a model to analyzed using a combination of semi-analytical techniques, including homotopy polynomial equations as well as the Sumudu transform method. Dupey et al.[35] investigated a fractional order model of the phytoplankton-toxic phytoplankton-zooplankton system using the Caputo fractional derivative. They employed three computational methods to investigate this model: the residual power series method, the homotopy perturbation Sumudu transform method, and the homotopy analysis Sumudu transform method. Dupey et al. [36] have created a fractional model that describes the changes in atmospheric CO_2 content. They explored this model using a combination of a semi-analytical homotopy scheme, Sumudu transform, and homotopy polynomials. Devendra et al. [37] devised a hybrid local frac-

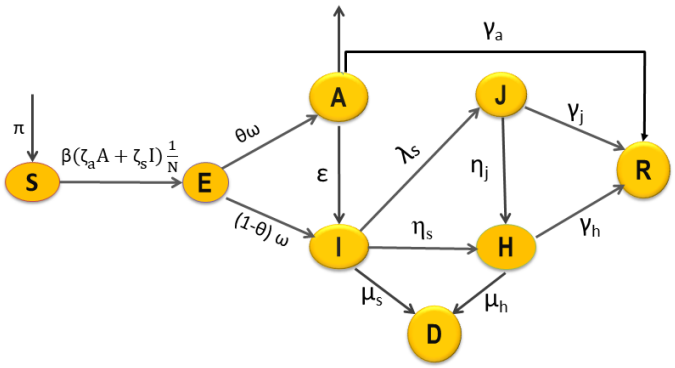

Figure 1: Flow chart of SEAIJHRD model.

tional method for solving certain local fractional partial differential equations. Fractal models can be effectively represented by local fractional derivatives in partial differential equations.

In this study, we are developed a deterministic mathematical model with eight compartments to analyse the COVID-19 dissemination dynamics in India. This model extends to optimal control approach incorporating three distinct control strategies to lower the COVID-19 dissemination. The rest of the article structured as follows: a full explanation of the model formulation is provided in Section.2 The stability analysis of the infection equilibrium is performed and the fundamental reproduction number is determined in Section.3. The model calibration, sensitivity analysis, and effect of parameters on infected classes are performed in Section.4. The optimal control technique with four distinct controls and their numerical simulations are discussed in Section.5. The final section 6 ends with conclusion.

2 Model formulation

In this study we formulate a deterministic mathematical model with eight compartments to analyze the dissemination dynamics of COVID-19. The total population N(t) in this model divided into Susceptible population $(S(t))$, Exposed population $(E(t))$, Asymptomatic infected population (A(t)), Symptomatic infected population $(I(t))$, isolated population $(J(t))$, Hospitalized population $(H(t))$, Recovered population $(R(t))$ and Deceased population $(D(t))$. Then
N (t) = S (t) + E (t) + A (t) + I(t) + J (t) + H (t) + R (t)+D(t).

Dynamics of susceptible population S(t): A susceptible population are those who is at risk of becoming infected by a virus after moving closed with the infected person. This population increased by a constant inflow rate π and diminished by a natural mortality rate μ. In this case $\beta\zeta_a$ and $\beta\zeta_s$ denote the dissemination coefficients of susceptible to asymptomatic and symptomatic populations where ζ_a and ζ_s adjustment factors for

asymptomatic infected and symptomatic infected populations. So the susceptible population decreases at the rates $\beta\zeta_a$ and $\beta\zeta_s$ respectively. The rate of change of susceptible population can be expressed as
$\frac{dS}{dt} = \pi - \beta(\zeta_a A + \zeta_s I)\frac{S}{N} - \mu S.$
Dynamics of exposed population E(t): It is the group of people who have been exposed to COVID-19 but have not yet exhibited any symptoms. As a result of the susceptible individuals exposure to infection, this population grows. At a rate of ω, a portion θ of the exposed population moves to the asymptomatic population (A) and the remaining portion $(1-\theta)$ moves to the symptomatic infected population (I). So the exposed population decreases at rate ω and also it reduces by μ. Hence the rate of change of exposed population is represented as
$\frac{dE}{dt} = \beta(\zeta_a A + \zeta_s I)\frac{S}{N} - (\omega + \mu)E.$
Dynamics of asymptomatic infected population A(t): Asymptomatic infected individuals are those who exposed to the virus but does not shows any symptoms. Since the exposed population transition to the asymptomatic population at the rate ω by a constant proportion θ, this population grows at a portion $\theta\omega$. Since some individuals of the asymptomatic population are recovered themselves at rate γ_a while others become symptomatic at rate ϵ by exhibiting symptoms, this population reduces at rates γ_a and ϵ. This population also diminishes by natural death rate μ. So the rate of change of asymptomatic population is defined by
$\frac{dA}{dt} = \theta\omega E - (\epsilon + \gamma_a + \mu)A.$
Dynamics of symptomatic infected population I(t): Symptomatic infected individuals are those who exposed to COVID-19 virus and are able to spread the disease are considered to be symptomatic. This population grows at the rate $(1-\theta)$ because the constant portion $(1-\theta)\omega$ of exposed population exhibits symptomatic at rate ω. Due to some of this population being isolation at a rate λ_s of and some other population being hospitalised at a rate η_s because of severe illness, this symptomatic population decreases by λ_s and η_s rates. Since some of asymptomatic populations exhibits symptoms at the rate ϵ, the symptomatic individuals decreases at rate ϵ. Also this population diminishes by both symptomatic individuals death rate μ_s and natural death rate μ. As results the rate of change of symptomatic population is stated as
$\frac{dI}{dt} = (1-\theta)\omega E + \epsilon A - (\lambda_s + \eta_s + \mu_s + \mu)I.$
Dynamics of isolated population J(t): Infected population who are join in isolation centers or placed in self-isolation comprise the isolated population. Since some of symptomatic infected individuals are joined in isolation centers at a rate λ_s, this population increases by the rate λ_s. As some of these isolated individuals recovered at a rate γ_j and some are joined in hospitals at the rate η_j due to severe illness, this population decreases at the rates γ_j and η_j. This population also decreases by natural mortality rate μ. So that, the rate of change in the isolated population can be represented by
$\frac{dJ}{dt} = \lambda_s I - (\eta_j + \gamma_j + \mu)J.$
Dynamics of hospitalization population H(t): The hospitalized individuals are those who have developed COVID-19 clinical symptoms and are admitted to the hospital for treatment. Due to severity of illness some of symptomatic infected population and some of isolation population are hospitalized at the rates η_s and η_j. So that this population enhanced by the rates η_s and η_j. Since some of this population recovered at the rate γ_h while other some of this population died at the rate μ_h, this population decreases by the rates γ_h and μ_h.The rate of natural death μ also diminished their population. Hence the rate of change of hospitalized population can be articulated as
$\frac{dH}{dt} = \eta_s I + \eta_j J - (\gamma_h + \mu_h + \mu)H.$
Dynamics of recovered population R(t): These are the individuals who have cured from the asymptomatic infected, isolated, and hospitalized populations. Since some of

the individuals from asymptomatic infected, isolation, and hospitalized populations are recovered from COVID-19 at the rates γ_a, γ_j and γ_h, this population grows by the rates γ_a, γ_j and γ_h. This population also reduces by natural mortality rate μ. Thus the rate of change of recovered population can be represented as
$\frac{dR}{dt} = \gamma_a A + \gamma_j J + \gamma_h H - \mu R$.
Dynamics of deceased population D(t): These are the individuals who died at severeness of COVID-19 disease. This population increases at the mortality rate μ_s of symptomatic infected individuals and at the mortality rate μ_h of hospitalised individuals. Hence the rate of change of deceased population is defined as
$\frac{dD}{dt} = \mu_s I + \mu_h H$.

Using all of the aforementioned biological hypotheses, we provide a graphical depiction of the proposed model in Figure 1 and then the model is governed by the following eight nonlinear system of differential equations as follows :

$$\begin{aligned}
\frac{dS}{dt} &= \pi - \beta(\zeta_a A + \zeta_s I)\frac{S}{N} - \mu S,\\
\frac{dE}{dt} &= \beta(\zeta_a A + \zeta_s I)\frac{S}{N} - (\omega + \mu)E,\\
\frac{dA}{dt} &= \theta\omega E - (\epsilon + \gamma_a + \mu)A,\\
\frac{dI}{dt} &= (1-\theta)\omega E + \epsilon A - (\lambda_s + \eta_s + \mu_s + \mu)I,\\
\frac{dJ}{dt} &= \lambda_s I - (\eta_j + \gamma_j + \mu)J,\\
\frac{dH}{dt} &= \eta_s I + \eta_j J - (\gamma_h + \mu_h + \mu)H,\\
\frac{dR}{dt} &= \gamma_a A + \gamma_j J + \gamma_h H - \mu R,\\
\frac{dD}{dt} &= \mu_s I + \mu_h H.
\end{aligned} \tag{1}$$

with the primary conditions

$$S(0) \geq 0, E(0) \geq 0, A(0) \geq 0, I(0) \geq 0, J(0) \geq 0, H(0) \geq 0, R(0) \geq 0, \& D(0) \geq 0. \tag{2}$$

The information of the various parameters used in the proposed model are listed in Table 1.

3 SEAIJHRD model analysis

3.1 Positivity and boundedness

Theorem 1. *For $t \geq 0$, all the solutions $(S(t), E(t), A(t), I(t), J(t), H(t), R(t), D(t)) \in \boldsymbol{R}^8_+$ of the system (1) with primary conditions (2) are non-negative and uniformly bounded in the specified region Ω.*

Proof. Let $(S(t), E(t), A(t), I(t), J(t), H(t), R(t), D(t)) \in \mathbf{R}^8_+$ be a solution of system (1) for $t \in [0, t_0]$, where $t_0 \geq 0$.
From the first equation of (1), we get
$\frac{dS}{dt} = \pi - (\zeta_a A + \zeta_s I)\frac{S}{N} - \mu S = \pi - \Phi(t)S$, where $\Phi(t) = \beta(\zeta_a A + \zeta_s I)\frac{1}{N} + \mu$.

Table 1: Complete depiction of model parameters of the SEAIJHRD model.

Parameter	Description	Value	Source
π	Net inflow of susceptible population	varies	-
θ	Proportion of exposed population	0.7	[13, 14]
ω	Conversion rate from exposed to infected population	0.4	[14, 15]
ζ_a,	Adjustment factor for asymptomatic infected population	0.3	[16]
ζ_s	Adjustment factor for symptomatic infected population	0.4	[17]
β	Infection dissemination rate	0.5313	Estimated
ϵ	The transition rate of asymptomatic infected individuals to symptomatic infected individuals	0.0168	[18]
λ_s	Isolation rate from symptomatic infected population	0.0828	[19]
η_s	Hospitalization rate of symptomatic infected population	0.0094	Estimated
η_j	Hospitalization rate of isolated population	0.1125	Estimated
γ_a	Recovery rate of asymptomatic population	0.1302	[20]
γ_j	Recovery rate of isolated population	0.017	[21]
γ_h	Recovery rate of hospitalized population	0.07048	[22]
μ_s	Mortality rate of symptomatic infected population	0.00001945	[23]
μ_h	Mortality rate of hospitalization population	0.00001945	[23]
μ	Natural death rate	0.0000391	[24]

Following integration, we obtain
$S(t) = S_0 \exp\left(-\int_0^t \Phi(s)\,ds\right) + \pi \exp\left(-\int_0^t \Phi(s)\,ds\right) \int_0^t e^{\int_0^s \Phi(u)\,du}\,ds > 0.$
From the second equation of (1), we have
$\frac{dE}{dt} = (\zeta_a A + \zeta_s I)\frac{S}{N} - (\omega+\mu)E \geq -(\omega+\mu)E,$
which leads to $E(t) = E_0 \exp(-\int_0^t (\omega+\mu)\,ds) \geq 0$.
The third equation of (1) gives
$\frac{dA}{dt} = \theta\omega E - (\gamma_a + \epsilon + \mu)A \geq -(\gamma_a+\epsilon+\mu)A,$
which implies to $A(t) = A_0 \exp(-\int_0^t (\gamma_a+\epsilon+\mu)\,ds) \geq 0$.
Similarly we can prove that from remaining equations of (1), $I(t) \geq 0$, $J(t) \geq 0$, $H(t) \geq 0$, $R(t) \geq 0$ and $D(t) \geq 0$.
We now establish the system (1) solutions' boundedness.
consider the total population$N = S + E + A + I + J + H + R + D$.
Taking the differentiation of above equation and using (1), we get $\frac{dN}{dt} = \pi - \mu N$,
which leads to $N(t) = N(0)e^{-\mu t} + \frac{\pi}{\mu}(1 - e^{-\mu t})$.
Hence $N(t) \leq \frac{\pi}{\mu}$ if $N(0) \leq \frac{\pi}{\mu}$.
Consequently if $N(0) > \frac{\pi}{\mu}$ then N(t) approaches to $\frac{\pi}{\mu}$ and the amount of infections in E, A, I, J and H shall be zero as $t \to \infty$.
Therefore $S + E + A + I + J + H + R + D \leq \frac{\pi}{\mu}$.
Hence all solution trajectories (S, E, A, I, J, H, R, D) are uniformly bounded in the region $\Omega = \{(S, E, A, I, J, H, R, D) \in \mathbf{R}_+^8 : S + E + A + I + J + H + R + D \leq \frac{\pi}{\mu}\}$. □

3.2 Infection-free equilibrium and fundamental reproduction number

The first seven equations in system (1) are independent of the final equation, so it can be eliminated. By equating the right-hand side of the system of equations (1) to zero and then using $E = A = I = J = H = 0$, the infection-free equilibrium (E^0) of the

model system (1) is obtained. Therefore $E^0 = (\frac{\pi}{\mu}, 0, 0, 0, 0, 0, 0)$.

One of the most important measures in contagious diseases is the fundamental reproduction number R_0. It is defined as the average number of secondary cases that would be generated by a primary infected individual in an entire susceptible population. The total number of infected cases will rise if $R_0 > 1$, as it would at the beginning of an epidemic. Where $R_0 = 1$, the illness is endemic, and if $R_0 < 1$, the total number of cases will decrease. Through the next generation matrix method [25, 26], we determine the fundamental reproduction number R_0 as follows:

$$\mathcal{F} = \begin{pmatrix} \beta\zeta_a + \beta\zeta_s \\ 0 \\ 0 \end{pmatrix} \text{ and } \mathcal{V} = \begin{pmatrix} (\omega+\mu)E \\ -\theta\omega E + (\epsilon+\gamma_a+\mu)A \\ -(1-\theta)\omega E + \epsilon A - (\lambda_s+\eta_s+\mu_s+\mu) \end{pmatrix}$$

The Jacobian matrices of $\mathcal{F}$ and $\mathcal{V}$ at E^0 are expressed as

$$F = \begin{pmatrix} 0 & \beta\zeta_a & \beta\zeta_s \\ 0 & 0 & 0 \\ 0 & 0 & 0 \end{pmatrix} \text{ \& } V = \begin{pmatrix} \omega+\mu & 0 & 0 \\ -\theta\omega & \epsilon+\gamma_a+\mu & 0 \\ -(1-\theta)\omega & -\epsilon & \lambda_s+\eta_s+\mu_s+\mu \end{pmatrix}.$$

The fundamental reproduction number, the largest eigen value of the matrix FV^{-1} is

$$R_0 = \frac{\theta\omega\beta\zeta_a}{(\epsilon+\gamma_a+\mu)(\omega+\mu)} + \frac{\beta\zeta_s[(\epsilon+\gamma_a+\mu)(1-\theta)\omega+\theta\omega\epsilon]}{(\epsilon+\gamma_a+\mu)(\lambda_s+\eta_s+\mu_s+\mu)(\omega+\mu)}$$

Theorem 2. *If $R_0 < 1$ then the infection-free equilibrium $E^0 = (\frac{\pi}{\mu}, 0, 0, 0, 0, 0, 0)$ is locally asymptotically stable (LAS).*

Proof. The variation matrix corresponding to the system (1) at E^0 is
$J_{(E^0)} =$

$$\begin{pmatrix} -\mu & 0 & -\beta\zeta_a & -\beta\zeta_s & 0 & 0 & 0 \\ 0 & \omega+\mu & \beta\zeta_a & \beta\zeta_s & 0 & 0 & 0 \\ 0 & 0 & -(\epsilon+\gamma_a+\mu) & 0 & 0 & 0 & 0 \\ 0 & \theta\omega & \epsilon & -(\lambda_s+\eta_s+\mu_s+\mu) & 0 & 0 & 0 \\ 0 & (1-\theta)\omega & 0 & \lambda_s & -(\eta_j+\gamma_j+\mu) & 0 & 0 \\ 0 & 0 & 0 & \eta_s & \eta_j & -(\gamma_h+\mu_h+\mu) & 0 \\ 0 & 0 & \gamma_a & 0 & \gamma_j & \gamma_h & -\mu \end{pmatrix}$$

The characteristic equation $\mid J_{E^0} - \lambda I \mid = 0$ is represented by
$(\lambda + (\eta_j+\gamma_j+\mu))(\lambda + (\gamma_h+\mu_h+\mu))(\lambda+\mu)^2(\lambda^3 + a_1\lambda^2 + a_2\lambda + a_3) = 0$,
where $a_1 = (\epsilon+\gamma_a+\mu) + (\lambda_s+\eta_s+\mu_s+\mu) + (\omega+\mu)$,
$a_2 = ((\epsilon+\gamma_a+\mu) + (\lambda_s+\eta_s+\mu_s+\mu))(\omega+\mu) + (\epsilon+\gamma_a+\mu)(\lambda_s+\eta_s+\mu_s+\mu) - (\theta\omega\beta\zeta_a + (1-\theta)\omega\beta\zeta_s)$, and
$a_3 = (\epsilon+\gamma_a+\mu)(\lambda_s+\eta_s+\mu_s+\mu)(\omega+\mu)(1-R_0)$.
There are seven eigenvalues, among that the first four values are $-\mu$, -μ, -$(\eta_j+\gamma_j+\mu)$, -$(\gamma_h+\mu_h+\mu)$ and the remaining three eigen values are cube roots of an equation $(\lambda^3 + a_1\lambda^2 + a_2\lambda + a_3) = 0$.
Routh–Hurwitz Criteria asserts that theE^0 is LAS if $a_1 > 0, a_2 > 0, a_3 > 0$ and $a_1a_2 > a_3$.
Clearly $a_1 > 0$ and $a_2 > 0$.
$a_3 = (\epsilon+\gamma_a+\mu)(\lambda_s+\eta_s+\mu_s+\mu)(\omega+\mu)(1-R_0) > 0$ and
$a_1a_2 - a_3 = (\epsilon+\gamma_a+\mu) + (\lambda_s+\eta_s+\mu_s+\mu) + (\omega+\mu)((\epsilon+\gamma_a+\mu) + (\lambda_s+\eta_s+\mu_s+\mu))(\omega+\mu)$
$+ (\epsilon+\gamma_a+\mu)(\lambda_s+\eta_s+\mu_s+\mu) - (\theta\omega\beta\zeta_a + (1-\theta)\omega\beta\zeta_s) - (\epsilon+\gamma_a+\mu)(\lambda_s+\eta_s+\mu_s+\mu)(\omega+\mu)(1-R_0) > 0$ if $R_0 < 1$.
Hence E^0 is LAS if $R_0 < 1$. □

Theorem 3. *The infection free equilibrium* $E^0 = (\frac{\pi}{\mu}, 0, 0, 0, 0, 0, 0)$ *of system* (1) *is globally asymptotic stable (GAS) if* $R_0 < 1$.

Proof. Based on equation (1), it is evident that S and R represent classes that are free from infection, while E, A, I, J, and H represent classes that are infected. Therefore (1) can be expressed as
$\frac{dX}{dt} = U(X, Y)$,
$\frac{dY}{dt} = V(X, Y)$, $V(X, 0) = 0$,
where $X = (S, R) \in \mathbb{R}^2_+$ denotes the disinfected population and $Y = (E, A, I, J, H) \in \mathbb{R}^5_+$ represents the infected population.
Thus $E^0 = (X^*, 0)$ identified as the infection free equilibrium of system (1).
For the model (1), U(X, Y) and V(X, Y) are described as follows:

$$\text{U(X, Y)} = \begin{pmatrix} \pi - \beta(\zeta_a A + \zeta_s I)\frac{S}{N} - \mu S \\ \gamma_a A + \gamma_j J + \gamma_h H - \mu R \end{pmatrix} \text{ \& V(X, Y)} = \begin{pmatrix} \beta(\zeta_a A + \zeta_s I)\frac{S}{N} - (\omega + \mu)E \\ \theta\omega E - (\epsilon + \gamma_a + \mu)A \\ (1-\theta)\omega E + \epsilon A - (\lambda_s + \eta_s + \mu_s + \mu)I \\ \lambda_s I - (\eta_j + \gamma_j + \mu)J \\ \eta_s I + \eta_j J - (\gamma_h + \mu_h + \mu)H \end{pmatrix}$$

From the expression V(X, Y), easily show that V(X, 0) = 0
To prove that E^0 is GAS, we verify the following two conditions
(I). $\frac{dX}{dt} = U(X, 0)$ where X^* is GAS.
(II). $V(X, Y) = KY - \bar{V}(X, Y)$, $\bar{V}(X, Y) \geq 0$, for $(X, Y) \in \Omega$
where $K = D_Y V(X^*, 0)$ is M- Matrix in the region Ω.
The deterministic model system (1) stated in (I) can be expressed as

$\frac{d}{dt}\begin{pmatrix} S \\ R \end{pmatrix} = \begin{pmatrix} \pi - \mu S \\ -\mu R \end{pmatrix}$,
$\Rightarrow S(t) = \frac{\pi}{\mu} + (S(0) - \frac{\pi}{\mu})e^{-\mu t}$ and $R(t) = R(0)e^{-\mu t}$

As $t \to \infty$, $S(t) = \frac{\pi}{\mu}$ and $R(0) = 0$.

Thus X^* is GAS for $\frac{dX}{dt} = U(X, 0)$ and hence the first condition (I) is satisfied for system (1).

Now the matrices K and $\bar{V}(X, Y)$ of model system (1) can be expressed as K =

$$\begin{pmatrix} -(\omega+\mu) & \beta\zeta_a & \beta\zeta_s & 0 & 0 \\ \theta\omega & -(\epsilon+\gamma_a+\mu_a+\mu) & 0 & 0 & 0 \\ (1-\theta)\omega & \epsilon & -(\lambda_s+\eta_s+\mu_s+\mu) & 0 & 0 \\ 0 & 0 & \lambda_s & -(\eta_j+\gamma_j+\mu) & 0 \\ 0 & 0 & \eta_s & \eta_j & -(\gamma_h+\mu_h+\mu) \end{pmatrix}$$

$$\text{\& } \bar{V}(X, Y) = \begin{pmatrix} \beta(\zeta_a A(1-\frac{S}{N}) + \zeta_s I(1-\frac{S}{N}) \\ 0 \\ 0 \\ 0 \\ 0 \end{pmatrix}.$$

Since all non-diagonal elements of matrix K are non-negative, K is M- matrix and as $S(t) \leq N(t)$, $\bar{V}(X, Y) \geq 0$ for all $(X, Y) \in \Omega$.
Thus the (II) condition is satisfied.
Hence E^0 is GAS for $R_0 < 1$. □

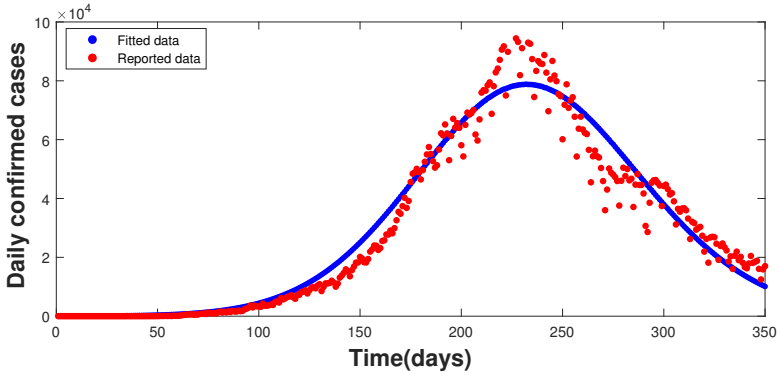

Figure 2: Model fitting based on reported data.

4 Numerical simulation

4.1 Model calibration

In this section, the model (1) fits to confirmed COVID -19 cases for all over India acquired from official site COVID-19 India API (Application Programming Interface) [27] in time period between January 30, 2020, and January 12, 2021. The parameter values β, η_s and η_j are estimated by minimizing the sum of squared error (SSE) method (lsqnonlin function) in MATLAB. We minimize the sum of squared error (SSE) as $SSE = \sum_{t=1}^{n}((Z(t) - \bar{Z(t)})^2$.
where $Z(t)$ denotes the reported COVID-19 confirmed cases while $\bar{Z(t)}$ signifies the model (1) output respectively. The estimated parameter values and other fixed parameter values obtained from the literature are listed in Table 1. Figure 2 illustrates that the model fit with the daily COVID-19 confirmed cases in India. The model solution is represented by red circles, while the reported data is shown by a blue dotted line.

4.2 Sensitivity analysis

Sensitivity analysis performance is very important in detecting the influence of different parameters in the spreading of the coronavirus. This method is very useful for discerning the increase and decrease in the R_0 value with respect to different parameters. A complete report of dengue fever sensitivity is executed in [28]. The sensitivity of parameters defines whether the contagious diseases will spread throughout the population or not. Through sensitive analysis, we analyze the influence of parameters on the model. Whenever parameters are determined, different techniques can be carried out for attaining excellent results. Through the normalized forward sensitivity technique [29] a for R_0, normalized forward sensitivity index of significant parameter p is determined as $\Gamma_p^{R_0} = \frac{\partial R_0}{\partial p} \times \frac{p}{R_0}$.

The parameter on R_0 that has a greater magnitude index is more sensitive. If the sensitivity index is positive, R_0 grows as the parameter p grows. Similarly if the sensitivity index has a negative sign, in which case R_0 falls as p grows. Thus, our sensitivity analysis yields the parameters ζ_a, ζ_s, ω and β have positive effect on R_0 while the parameters θ, λ_s, η_s, γ_a, μ_s and μ are the negative effect on R_0. Among these parameters ζ_a, ω and β are more effective on rise of R_0 whereas λ_s and η_s are more efficient on fall of R_0.

Figure 4(a) indicates the contour Plot of R_0 in relation to virus dissemination rate

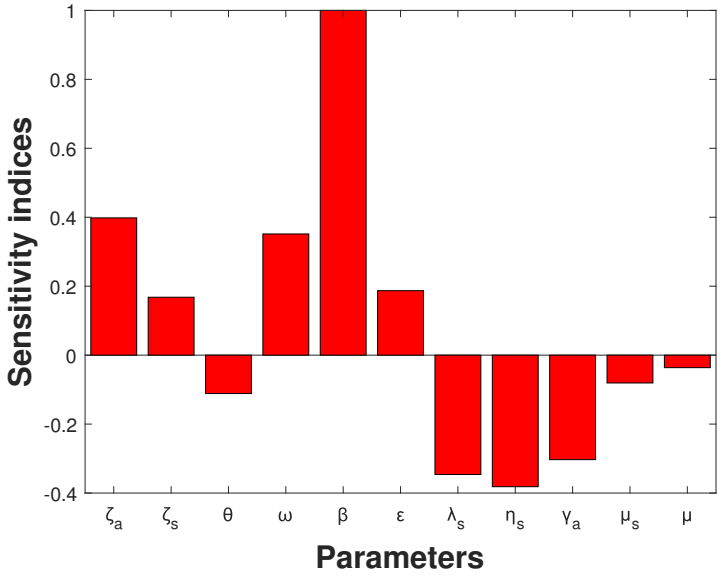

Figure 3: Sensitivity indices of R_0

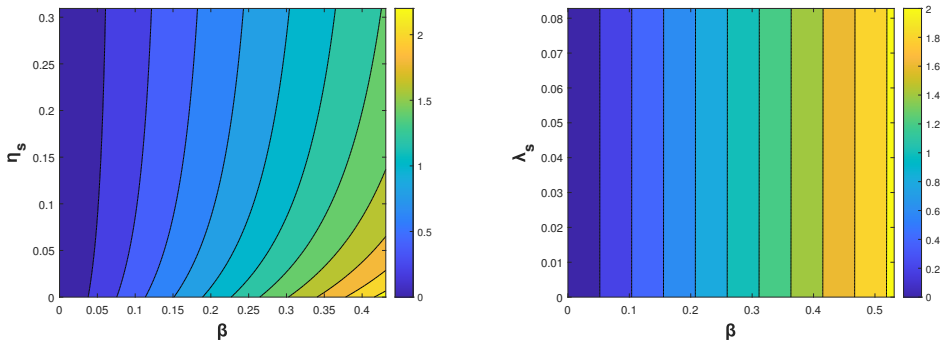

(a) (b)

Figure 4: Contour plots of R_0 with respect to parameters (a)(β, η_s) and (b)(β, λ_s).

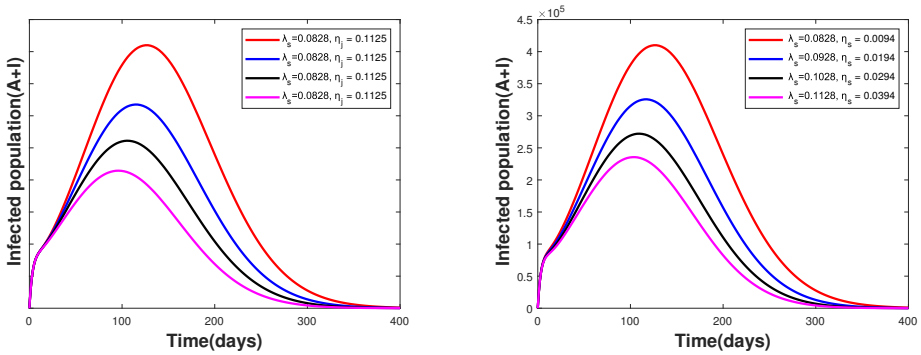

(a) (b)

Figure 5: Variations in infected population with respect to parameters (a) (λ_s, η_j) and (b) (λ_s, η_s).

(β) and hospitalization rate (η_s) from symptomatic infected population. This plot is revealed that whenever the contact rate(β) decreases and the hospitalization rate(η_s) increases, the basic reproduction number decreases. Figure 4(b) indicates the contour Plot of R_0 in relation to virus dissemination rate (β) and quarantine rate (λ_s) from symptomatic infected populations. This plot is demonstrated that whenever the contact rate (β) decreases and quarantine rate (λ_s) increases, the R_0 value decreases so that the spreading of virus decreases.

4.3 COVID-19 Prevalence changes with significant parameters

In this section, we analyse the effect of parameters on infected population. Figure 5 is demonstrated that the infected population reduces when the isolation rate (λ_s) of symptomatic infected population and hospitalization rate (η_j) of isolated population risen. Similarly the disease dissemination will be decreased if both isolation and hospitalization rates of symptomatic infected population increased.

5 Optimal control

5.1 Optimal control model

In the fields of engineering, sciences, and economics, optimal control has major significance. Optimal control is used in detecting parameters that can control definite variables to yield the optimum result. By implementing the most effective intervention measures, we aim to reduce the number of infected, isolated, and hospitalised individuals. The system (1) is extended to optimal control model by including four control variables u, v, w_1 and w_2. The control u involves awareness campaigns in the media and in civil society to encourage people to use face masks, sanitation and keep their distance from infected people to diminish the spread of disease. The second control v represents the effort of vaccinating susceptible individuals by supposing all of the susceptible people who got their vaccination are promptly moved to the recovered class. The last two controls w_1 and w_2 represent encouraging the asymptomatic infected individuals to join isolation and symptomatic infected individuals to join either hospitals or isolated. As a result, w_1 and w_2 are evaluated in comparison to improved medical facilities, such as an increase

in beds, ventilators, mobile isolation centres, etc. Therefore the set of four controls is defined as

$$\mathcal{U} = \{u, v, w_1, w_2 : \text{Lebesgue integral and} \quad 0 \leq u, v, w_1, w_2 \leq 1, \quad t \in [0, T]\}.$$

Taking into account all of the aforementioned presumptions, the formulated optimal control model is

$$\begin{aligned}
\frac{dS}{dt} &= \pi - (1-u(t))\beta(\zeta_a A + \zeta_s I)\frac{S}{N} - \mu S - v(t)S, \\
\frac{dE}{dt} &= (1-u(t))\beta(\zeta_a A + \zeta_s I)\frac{S}{N} - (\omega + \mu)E, \\
\frac{dA}{dt} &= \theta\omega E - (\epsilon + \gamma_a + \mu)A - w_1(t)A, \\
\frac{dI}{dt} &= (1-\theta)\omega E + \epsilon A - (\lambda_s + \eta_s + \mu_s + \mu)I - w_2(t)I, \\
\frac{dJ}{dt} &= w_1(t)A + \lambda_s I - (\eta_j + \gamma_j + \mu)J + \rho w_2(t)I, \\
\frac{dH}{dt} &= \eta_s I + \eta_j J - (\gamma_h + \mu_h + \mu)H + (1-\rho)w_2(t)I, \\
\frac{dR}{dt} &= \gamma_a A + \gamma_j J + \gamma_h H - \mu R + v(t)S, \\
\frac{dD}{dt} &= \mu_s I + \mu_h H.
\end{aligned} \tag{3}$$

For the fixed T, the objective functional is presented by

$$\mathcal{J} = \int_0^T (C_1 A + C_2 I + C_3 J + C_4 H + \frac{1}{2}(C_5 u^2 + C_6 v^2 + C_7 w_1^2 + C_8 w_2^2)\ dt. \tag{4}$$

Here C_1, C_2, C_3, C_4, C_5, C_6, C_7 and C_8 are non negative weight constants.

The objective is to determine the control variables u^*, v^*, w_1^* and w_2^* such that $\mathcal{J}(u^*, v^*, w_1^*, w_2^*) = \min_{u,v,w_1,w_2 \in \mathcal{U}} \mathcal{J}(u, v, w_1, w_2)$.
The Lagrangian of this model (3) is
$\mathcal{L}(S, E, A, I, J, H, R, D, u(t), v(t), w_1(t), w_2(t)) = C_1 A + C_2 I + C_3 J + C_4 H + \frac{1}{2}(C_5 u^2 + C_6 v^2 + C_7 w_1^2 + C_8 w_2^2)$.
For this problem, the Hamiltonian function $\mathcal{H}$ is defined as
$\mathcal{H} = C_1 A + C_2 I + C_3 J + C_4 H + \frac{1}{2}(C_5 u^2 + C_6 v^2 + C_7 w_1^2 + C_8 w_2^2) + \lambda_1 \frac{dS}{dt} + \lambda_2 \frac{dE}{dt} + \lambda_3 \frac{dA}{dt} + \lambda_4 \frac{dI}{dt} + \lambda_5 \frac{dJ}{dt} + \lambda_6 \frac{dH}{dt} + \lambda_7 \frac{dR}{dt} + \lambda_8 \frac{dD}{dt}$.
where λ_i for i = 1,2,3,...8 are the adjoint variables.

Theorem 4. *If the couple (S^*, E^*, A^*, I^*, J^*, H^*, R^*, D^*) is solutions of the system* (3) *that minimizes the objective functional* (4) *with relation to optimal controls $u^*(t)$, $v^*(t)$, w_1^*, $w_2^* \in \mathcal{U}$, then there are adjoint variables λ_i for i =1,2,3,...8 satisfies the*

canonical equations:

$$\begin{aligned}
\lambda_1' &= -\frac{\partial \mathcal{H}}{\partial S} = (\lambda_1-\lambda_2)\beta(1-u)(\zeta_a A+\zeta_s I)\frac{1}{N}+(\lambda_1-\lambda_7)v+\lambda_1\mu,\\
\lambda_2' &= -\frac{\partial \mathcal{H}}{\partial E} = (\lambda_2-\lambda_4)\omega+(\lambda_4-\lambda_3)\theta\omega+\lambda_2\mu,\\
\lambda_3' &= -\frac{\partial \mathcal{H}}{\partial A} = -C_1+(\lambda_1-\lambda_2)\beta(1-u)\frac{\zeta_a S}{N}+(\lambda_3-\lambda_4)\epsilon+(\lambda_3-\lambda_5)w_1+(\lambda_3-\lambda_7)\gamma_a+\lambda_3\mu,\\
\lambda_4' &= -\frac{\partial \mathcal{H}}{\partial I} = -C_2+(\lambda_1-\lambda_2)\beta(1-u)\frac{\zeta_s S}{N}+(\lambda_4-\lambda_5)\lambda_s+(\lambda_4-\lambda_6)(\eta_s+w_2)\\
&\quad +(\lambda_6-\lambda_5)\rho w_2+(\lambda_4-\lambda_7)\mu_s+\lambda_4\mu,\\
\lambda_5' &= -\frac{\partial \mathcal{H}}{\partial J} = -C_3+(\lambda_5-\lambda_6)\eta_j+(\lambda_5-\lambda_7)\gamma_j+\mu\lambda_5,\\
\lambda_6' &= -\frac{\partial \mathcal{H}}{\partial H} = -C_4+(\lambda_6-\lambda_7)\gamma_h+(\lambda_6-\lambda_8)\mu_h+\mu\lambda_6,\\
\lambda_7' &= -\frac{\partial \mathcal{H}}{\partial R} = \mu\lambda_7,\\
\lambda_8' &= -\frac{\partial \mathcal{H}}{\partial D} = 0.
\end{aligned}$$

with the transversality conditions at time T: $\lambda_i(T)=0$*, for all i=1,2,3,...,8. Furthermore the corresponding optimal controls* $u^*(t)$*,* $v^*(t)$*,* $w_1^*(t)$ *and* $w_2^*(t)$ *are given by*
$u^*(t)=\min\{1,\max(0,\frac{1}{NC_5}(\lambda_1-\lambda_2)\beta S(\zeta_a A+\zeta_s I))\}$,
$v^*(t)=\min\{1,\max(0,\frac{1}{C_6}((\lambda_1-\lambda_7)S))\}$,
$w_1^*(t)=\min\{1,\max(0,\frac{1}{C_7}((\lambda_3-\lambda_5)A))\}$, *and*
$w_2^*(t)=\min\{1,\max(0,\frac{1}{C_8}((\lambda_4-\lambda_6)+\rho(\lambda_6-\lambda_5))I)\}$.

Proof. We examine the necessary criteria for the control variables using the maximum principle of Pontryagin for the system (3). To achieve this, for all $t\in[0,T]$, we define the Hamiltonian $\mathcal{H}$ as

$\mathcal{H} = C_1A+C_2I+C_3J+C_4H+\frac{1}{2}(C_5u^2+C_6v^2+C_7w_1^2+C_8w_2^2)+\lambda_1(\pi-(1-u(t))\beta(\zeta_aA+\zeta_sI)\frac{S}{N}-\mu S-v(t)S)+\lambda_2((1-u(t))\beta(\zeta_aA+\zeta_sI)\frac{S}{N}-(\omega+\mu)E)+\lambda_3(\theta\omega E-(\epsilon+\gamma_a+\mu)A-w_1(t)A)+\lambda_4((1-\theta)\omega E+\epsilon A-(\lambda_s+\eta_s+\mu_s+\mu)I-w_2(t)I)+\lambda_5(w_1(t)A+\lambda_sI-(\eta_j+\gamma_j+\mu)J+\rho w_2(t)I)+\lambda_6(\eta_sI+\eta_jJ-(\gamma_h+\mu_h+\mu)H+(1-\rho)w_2(t)I)+\lambda_7(\gamma_aA+\gamma_jJ+\gamma_hH-\mu R+v(t)S)+\lambda_8(\mu_sI+\mu_hH)$.
Because of maximum principle of Pontryagin [30], there are co-states λ_1', λ_2', λ_3',...,λ_8' that satisfying the following canonical equations
$\lambda_1'=-\frac{\partial\mathcal{H}}{\partial S}$, $\lambda_2'=-\frac{\partial\mathcal{H}}{\partial E}$, $\lambda_3'=-\frac{\partial\mathcal{H}}{\partial A}$, $\lambda_4'=-\frac{\partial\mathcal{H}}{\partial I}$,...,+ $\lambda_8'=-\frac{\partial\mathcal{H}}{\partial D}$.
with transversality conditions $\lambda_i(T)=0$, for all i=1,2,3,...,8.
Now we get the optimal controls by using the optimal condition, $\frac{\partial\mathcal{H}}{\partial u}=0$, $\frac{\partial\mathcal{H}}{\partial v}=0$, $\frac{\partial\mathcal{H}}{\partial w_1}=0$ and $\frac{\partial\mathcal{H}}{\partial w_2}=0$.
$\frac{\partial\mathcal{H}}{\partial u}=C_5u+\beta\lambda_1(\zeta_aA+\zeta_sI)\frac{S}{N}-\lambda_2(\zeta_aA+\zeta_sI)\frac{S}{N}=0$.
Then $u=\frac{\beta S(\zeta_aA+\zeta_sI)}{NC_5}(\lambda_1-\lambda_2)$ at $u=u^*$.
$\frac{\partial\mathcal{H}}{\partial v}=C_6v-\lambda_1S+\lambda_7)S=0$.
Then $v=\frac{1}{C_6}(\lambda_1-\lambda_7)S$ at $v=v^*$.
$\frac{\partial\mathcal{H}}{\partial w_1}=C_7w_1-\lambda_3A+\lambda_5A=0$.
Then $w_1=\frac{1}{C_7}(\lambda_3-\lambda_5)A$ at $w_1=w_1^*$.
$\frac{\partial\mathcal{H}}{\partial w_2}=C_8w_2-(\lambda_4-\lambda_6)I-(\lambda_5-\lambda_6)\rho I=0$.
Then $w_2=\frac{1}{C_8}((\lambda_4-\lambda_6)+\rho(\lambda_6-\lambda_5))I$ at $w_1=w_2^*$.
By taking the bounds for u(t), v(t), $w_1(t)$ and $w_2(t)$, we characterize the optimal controls:

$u^*(t) = \min\{1, \max(0, \frac{1}{NC_5}(\lambda_1 - \lambda_2)\beta S(\zeta_a A + \zeta_s I))\}$,
$v^*(t) = \min\{1, \max(0, \frac{1}{C_6}((\lambda_1 - \lambda_7)S))\}$,
$w_1^*(t) = \min\{1, \max(0, \frac{1}{C_7}((\lambda_3 - \lambda_5)A))\}$ and
$w_2^*(t) = \min\{1, \max(0, \frac{1}{C_8}((\lambda_4 - \lambda_6) + \rho(\lambda_6 - \lambda_5))I)\}$. □

5.2 Optimal control model simulation

The model simulation is carried out in MATLAB during the time interval [0,400] using the model parameters listed in Table 1. The optimality system is solved by an iterative method. The extended system (3) is computed by using forward difference approximation [31] and then the adjoint system is calculated by using backward difference approximation. Choose $C_1 = 1$, $C_2 = 1$, $C_3 = 1$, $C_4 = 1$, $C_5 = 40$, $C_6 = 50$, $C_7 = 55$ and $C_8 = 55$ with the initial conditions $S(0) = 1217378052, E(0) = 13000, A(0) = 5, I(0) = 2, J(0) = 1, H(0) = 1$, $R(0) = 0$ and $D(0) = 0$. Figure 6 displays that variations in susceptible, exposed, asymptomatic infected, symptomatic infected, isolated, hospitalized, recovered and deceased populations within and without controls. This Figure is illustrated that the infected populations with controls swiftly decreased in comparison to the populations without controls, whereas the disinfected populations with controls rapidly increased in comparison to the disinfected population without controls. The optimal control variable profiles of u(t), v(t), $w_1(t)$ and $w_2(t)$ are shown in Figure 7. From this Figure, it can be observed that, in comparison to $w_1(t)$ and $w_2(t)$ controls, the controls u(t) and v(t) which related to awareness campaigns and vaccinating of susceptible population must be kept at 1 over a longer period of time. Figure 8 illustrates the variations in control profile related cost for each control increases. This Figure is demonstrated that the time needed to maintain these controls at 1 decreases if the cost of each control variables is risen.

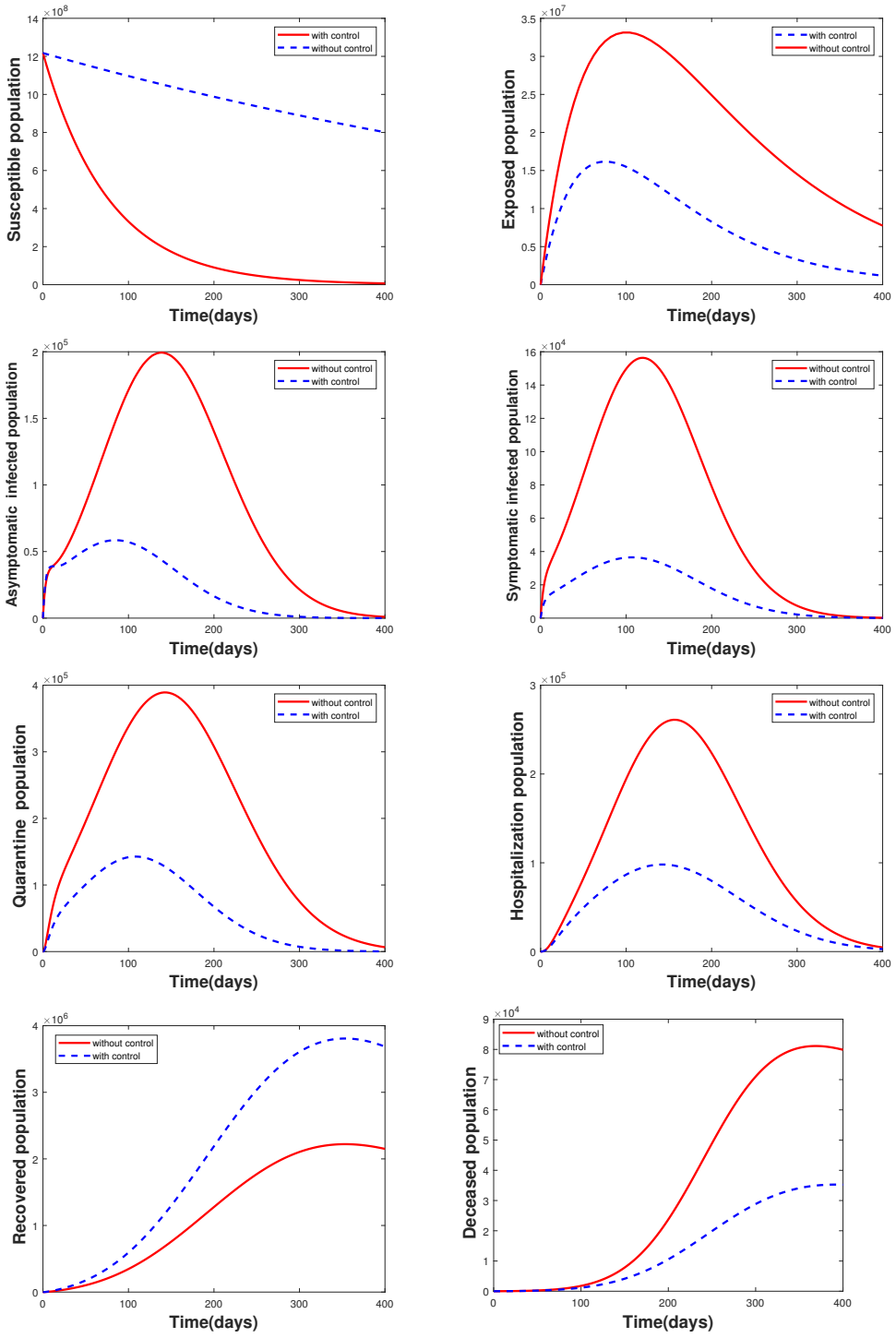

Figure 6: Variations in infected and disinfected populations with and without controls.

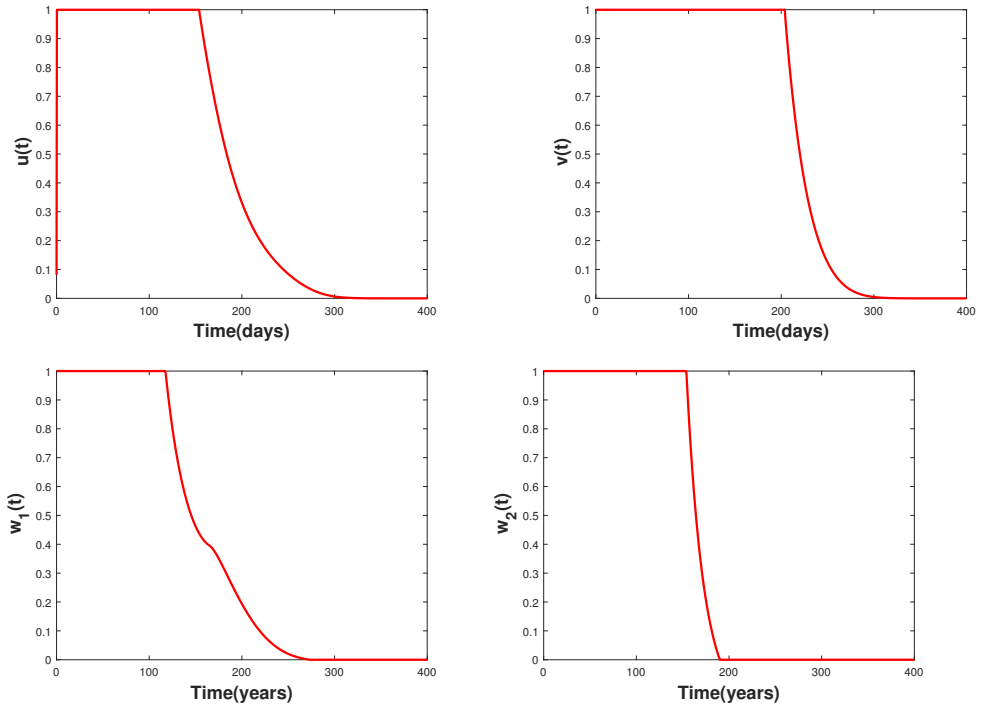

Figure 7: Optimal control variable profiles u(t), v(t), $w_1(t)$ and $w_2(t)$.

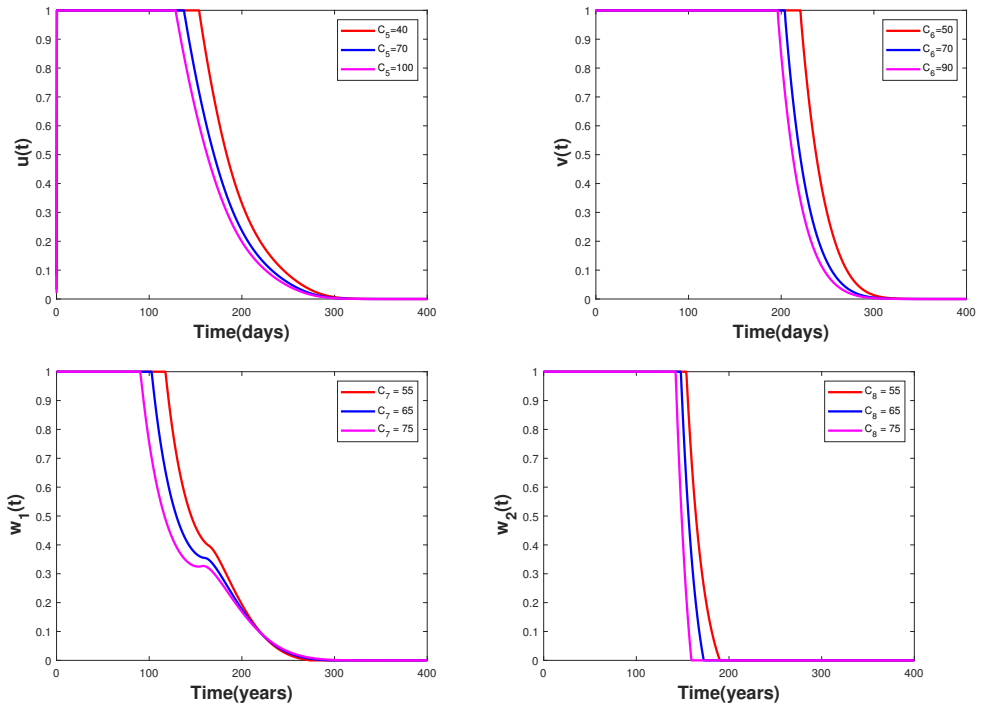

Figure 8: Variations in control variables with respect to relative costs.

6 Conclusion

When precise diagnostic tests or medical facilities were unavailable, compartmental epidemiological models helped us understand how epidemic diseases spread and devise preventative measures. In this paper, SEAIJHRD model was formulated to observe the dissemination dynamics of COVID-19 spread in India. We first established the model's positivity and boundedness, and then, R_0 value was determined to be 1.682. The infection free equilibrium was both LAS and GAS for $R_0 < 1$. By fitting the model to reported COVID-19 data, the infection dissemination rate, hospitalization rates of symptomatic infected and isolated populations were estimated. The sensitive analysis of R_0 determined that both isolation rate (λ_s) and hospitalization rate (η_s) of symptomatic individuals were more effective in reducing R_0. In addition, the proposed model was expanded to an optimal control problem by integrating four controls: 1) awareness programs through media and civil society that the susceptible population do not interact with infected ones 2) vaccination process for susceptible population, and 3) urging the infected population to go into isolation or join hospitals. The combination of four controls had greater impact on reducing the number of infected individuals. Our model concludes that vaccination for susceptible individuals, isolation of the infected population, severe disinfection safeguards using, and social distance maintenance were effective roles in controlling virus spread in a community and may even eradicate the corona virus disease. In future, there will be possible to develop an epidemic model to examine the impact of COVID-19 on HIV/AIDS or TB infected individuals.

References

[1] N. Zhu, D. Zhang, W. Wang, W. Xu, G. Wu, G.F. Gao, W. Tan, China Novel Coronavirus Investigating and Research Team, A Novel Coronavirus from Patients with Pneumonia in China, 2019, N Engl J Med., 382(8), 727-733(2020).

[2] https:// covid19.who.int.

[3] M.L. Danzetta, R. Bruno, F. Sauro, L. Savini, P. Calistri, Rift Valley fever trasmission dynamics described by compartmental models, Prev Vet Med., 134, 197-210(2016).

[4] A. Anirudh, Mathematical modeling and the transmission dynamics in predicting the Covid-19 - What next in combating the pandemic, Infect Dis Model, 5, 366–374(2020).

[5] D.K. Bagal, A. Rath, A. Barua, D. Patnaik, Estimating the parameters of susceptible-infected-recovered model of COVID-19 cases in India during lockdown periods, Chaos, Solitons Fractals, 140, 110154(2020).

[6] N. Anand, A. Sabarinath, S. Geetha, S. Somanath, Predicting the spread of COVID-19 using SIR model augmented to incorporate quarantine and testing, Trans. Indian National Acad. Eng, 5(2), 141–148(2020).

[7] Y. Li, J. Shi, J. Xia, Y. Yuan, L. Gong, X. Yang, H. Gao, C. Wu, Asymptomatic and Symptomatic Patients With Non-severe Coronavirus Disease (COVID-19) Have Similar Clinical Features and Virological Courses: A Retrospective Single Center Study, Frontiers in microbiology, 11, 1570(2020).

[8] E. Armstrong, M. Runge, J. Gerardin, Identifying the measurements required to estimate rates of COVID-19 transmission, infection, and detection, using variational data assimilation, Infect Dis Model, 6, 133-147(2021).

[9] J.T. Wu, K. Leung, G.M. Leung, Nowcasting and forecasting the potential domestic and international spread of the 2019-nCoV outbreak originating in Wuhan, China: a modelling study, Lancet, 395, 689-697(2020).

[10] O. Sharomi, T. Malik , Optimal control in epidemiology, Ann. Oper. Res., 251(1), 55–71(2017).

[11] C.J. Silva, C. Cruz, D.F.M. Torres, A.P. Muñuzuri, W. Abreu, J. Mira, Optimal control of the COVID-19 pandemic: controlled sanitary deconfinement in Portugal, Sci., 11(1), 3451(2021).

[12] J. Mondal, S. Khajanchi, Mathematical modeling and optimal intervention strategies of the COVID-19 outbreak, Nonlinear Dyn, 109(1), 177-202(2022).

[13] N.Fergusonm, Report 9: Impact of non-pharmaceutical interventions (NPIs) to reduce COVID19 mortality and healthcare demand, 2020.

[14] R. Li, S. Pei, B. Chen, Y. Song, T. Zhang, W. Yang, J. Shaman, Substantial undocumented infection facilitates the rapid dissemination of novel coronavirus (SARS-CoV-2), Science, 368, 489–493(2020).

[15] S.A. Lauer, K.H. Grantz, Q. Bi, F.K. Jones, Q. Zheng, N.G. Reich, J. Lessler, The incubation period of coronavirus disease 2019 (COVID-19) from publicly reported confirmed cases: estimation and application, Ann. Internal Med., 172(9), 577–582(2020).

[16] A.B. Gumel, S.Ruan, T. Day, J. Watmough, F. Brauer, P. van den Driessche, J. Wu, B.M. Sahai, Modelling strategies for controlling SARS outbreaks, Proc Biol Sci., 271(1554), 2223-2232(2004).

[17] S.S. Nadim, I. Ghosh, J. Chattopadhyay, Short-term predictions and prevention strategies for COVID-19: A model-based study, Appl. Math Comput., 404, 126251(2021).

[18] K. Sarkar, S. Khajanchi, J.J. Nieto, Modeling and forecasting the COVID-19 pandemic in India, Chaos, Solitons & Fractals, 139, 110049(2020).

[19] S.K. Ghosh, S. Ghosh, A mathematical model for COVID-19 considering waning immunity, vaccination and control measures, 13(1), 3610(2020).

[20] M. Ankamma Rao, A. Venkatesh, SEAIQHRDP mathematical model Analysis for the transmission dynamics of COVID-19 in India, Journal of Computational Analysis & Applications, 31(1), 96-116(2023).

[21] V. Bajiya, S. Bugalia, J. Tripathi, Mathematical modeling of COVID-19: Impact of non-pharmaceutical interventions in India. Chaos, 30, 1063(2020).

[22] S.R. Bandekar, M. Ghosh, Mathematical modeling of COVID-19 in India and Nepal with optimal control and sensitivity analysis. Eur Phys J Plus., 136(10), 1058(2021).

[23] S. Khajanchi, K. Sarkar, J. Mondal, SF. Abdelwahab, Mathematical modeling of the COVID-19 pandemic with intervention strategies, Results Physics, 25, 104285(2021).

[24] Open government data (OGD) platform India or data.gov.in. 2020, data.gov.in/resources/crude-death-rate-india-2011(2020).

[25] O. Diekmann, J.A.P. Heesterbeek, J.A.J. Metz, On the definition and the computation of the basic reproduction ratio R_0 in models for infectious diseases in heterogeneous populations, J. Math. Biol., 28, 365–382(1990).

[26] P.Van den Driessche, J. Watmough, Reproduction numbers and sub-threshold endemic equilibria for compartmental models of disease transmission. Math Biosci, 180, 29-48(2002).

[27] https://data.covid19india.org/

[28] H.S. Rodrigues, M. Teresa, T. Monteiro, F.M. Delfim, Sensitivity Analysis in a Dengue Epidemiological Model, In: Conference Papers in Mathematics, 1-7(2013).

[29] N. Chitnis, J.M. Hyman, J.M. Cushing, Determining important parameters in the spread of malaria through the sensitivity analysis of a mathematical model, Bull Math Biol., 70(5), 1272-1296(2008).

[30] L.S. Pontryagin, Mathematical Theory of Optimal Processes, Routledge, 1987. https://doi.org/10.1201/9780203749319.

[31] J.T. Workman, S. Lenhart, Optimal Control Applied to Biological Models, CRC Press, Boca Raton, 2007(2007).

[32] V.P. Dubey, J. Singh, A.M. Alshehri, S. Dupey, D. kumar, Forecasting the behavior of fractional order Bloch equations appearing in NMR flow via a hybrid computational technique. Chaos, Solitons & Fractals 164, 112691(2022).

[33] V.P. Dubey, J. Singh, A.M. Alshehri, S. Dupey, D. Kumar, Analysis and Fractal Dynamics of Local Fractional Partial Differential Equations Occurring in Physical Sciences. Journal of Computational and Nonlinear Dynamics 18(3), 1-23(2022).

[34] V.P. Dubey, D. Kumar, S. Dupey, A modified computational scheme and convergence analysis for fractional order Hepatitis E virus model, In book: Advanced Numerical Methods for Differential Equations: Applications in Science and Engineering, 279-312 (2021).

[35] V.P. Dubey, J. Singh, A.M. Alshehri, S. Dupey, D. Kumar, Numerical investigation of fractional model of Phytoplankton–Toxic Phytoplankton–Zooplankton system with convergence analysis, Int. J. Biomath. 15(4), 2250006(2022).

[36] V.P. Dubey, D. Kumar, S. Dupey, J. Singh, A computational study of fractional model of atmospheric dynamics of carbon dioxide gas, Chaos, Solitons & Fractals, 142, 110375(2021).

[37] D. Kumar, V.P. Dubey, S. Dupey, J. Singh, A.M. Alshehri, Computational Analysis of Local Fractional Partial Differential Equations in Realm of Fractal Calculus, Chaos, Solitons & Fractals 167, 113009(2023).

Certain Integrals Involving the Incomplete Fox-Wright Functions

Nishant[1,*], Sanjay Bhatter[1], Sapna Meena[1], Kamlesh Jangid[2] and Sunil Dutt Purohit[3,4]

[1]Department of Mathematics, Malaviya National Institute of Technology, Jaipur, India.

nishantjangra1996@gmail.com, sbhatter.maths@mnit.ac.in, sapnabesar1996@gmail.com

[2]Department of Mathematics, Central University of Rajasthan, Ajmer, India.

jangidkamlesh7@gmail.com

[3]Department of HEAS (Mathematics), Rajasthan Technical University, Kota, India.

sunil_a_purohit@yahoo.com

[4]Department of Computer Science and Mathematics, Lebanese American University, Beirut, Lebanon. sunil_a_purohit@yahoo.com

Abstract

Hundreds of special functions have been employed in applied mathematics and computing sciences for many centuries due to their outstanding features and wide range of applications. When considering the relevance of these consequences in the evaluation of generalized integrals, applied physics, and many engineering areas, the illustration of image formulas involving one or more variable special functions is significant under various definite integrals. In this paper, it is devoted to study the various integral identities involving incomplete Fox-Wright functions and Srivastava's polynomials. It is shown that the integrals of the Fox-Wright functions are also the Fox-Wright functions but of greater order. Due to the fact that our results are unified, a substantial number of new results can be constructed as special instances from our leading results. The results obtained in this work are general in nature and very useful in science, engineering and finance.

Keywords: Incomplete Gamma function, Incomplete Fox-Wright-function, Generalized family of polynomials.
MSC 2020: 33B20, 33C60, 33E12.

*Corresponding author

1 Introduction and Preliminaries

Several integral formulas have been established that include variety of special functions and play a major role in certain physical problems [21]. Such functions, in addition, are frequently connected to a variety of issues in various branches of mathematics. Therefore, a notable researcher has produced several integral formulas in turning a particular category of special functions [14], for instance Nisar et al. [9] evaluated unified integrals associated with the Struve function; Suthar et al. [19] evaluated unified integrals associated with the hypergeometric function; Choi et al. [2], Choi et al. [3], Menaria et al. [8], Nisar et al. [9], Suthar and Habenom [20] established certain integrals involving Bessel type functions.

In this study, under certain known integrals, we look at the possibility of having some new integrals that include incomplete Fox-Wright functions as well as family of polynomials. The integral formulas established in the present work are very useful to obtain the transformations of various simpler special functions. The findings from this research are of a generic nature and are extremely beneficial in the fields of engineering, economics, and chemical sciences, digital signals, image processing, finance and ship target recognition by sonar system and radar signals.

For our ends, we begin by looking back on the preceding incomplete Fox-Wright functions (see [18] also), ${}_p\Psi_q^{(\gamma)}$ and ${}_p\Psi_q^{(\Gamma)}$, with both the p numerator and q denominator parameters, introduced by Choi et. al [4]:

$$ {}_p\Psi_q^{(\gamma)}\left[\begin{array}{cc} (\mathfrak{f}_1,\mathfrak{F}_1,x),(\mathfrak{f}_j,\mathfrak{F}_j)_{2,\,p}\,; & \\ (\mathfrak{g}_j,\mathfrak{G}_j)_{1,\,q}\,; & z \end{array}\right]=\sum_{\ell=0}^{\infty}\frac{\gamma(\mathfrak{f}_1+\mathfrak{F}_1\ell,x)\prod_{j=2}^{p}\Gamma(\mathfrak{f}_j+\mathfrak{F}_j\ell)}{\prod_{j=1}^{q}\Gamma(\mathfrak{g}_j+\mathfrak{G}_j\ell)}\frac{z^\ell}{\ell!} \tag{1} $$

and

$$ {}_p\Psi_q^{(\Gamma)}\left[\begin{array}{cc} (\mathfrak{f}_1,\mathfrak{F}_1,x),(\mathfrak{f}_j,\mathfrak{F}_j)_{2,\,p}\,; & \\ (\mathfrak{g}_j,\mathfrak{G}_j)_{1,\,q}\,; & z \end{array}\right]=\sum_{\ell=0}^{\infty}\frac{\Gamma(\mathfrak{f}_1+\mathfrak{F}_1\ell,x)\prod_{j=2}^{p}\Gamma(\mathfrak{f}_j+\mathfrak{F}_j\ell)}{\prod_{j=1}^{q}\Gamma(\mathfrak{g}_j+\mathfrak{G}_j\ell)}\frac{z^\ell}{\ell!}\,, \tag{2} $$

where, $\mathfrak{F}_j,\,\mathfrak{G}_j\in\mathbb{R}^+$, $\mathfrak{f}_j,\,\mathfrak{g}_j\in\mathbb{C}$ and series converges absolutely $\forall z\in\mathbb{C}$ when $\Delta=1+\sum_{j=1}^{q}\mathfrak{G}_j-\sum_{j=1}^{p}\mathfrak{F}_j\;>0$ (see [7, 16]).

The incomplete Fox-Wright functions, ${}_p\Psi_q^{(\gamma)}$ and ${}_p\Psi_q^{(\Gamma)}$ fulfill the decomposition formula given below:

$$ {}_p\Psi_q^{(\gamma)}[z]+\,{}_p\Psi_q^{(\Gamma)}[z]=\,{}_p\Psi_q[z], \tag{3} $$

where, ${}_p\Psi_q[z]$ is Fox-Wright function [22].

Srivastava's polynomials [15] or broader category of polynomials of index $n(n=0,1,2,...)$ are described as follows (see [1, 13] also):

$$ S_n^m[x]=\sum_{s=0}^{[n/m]}\frac{(-n)_{m\,s}}{s!}A_{n,\,s}\,x^s, \tag{4} $$

where $m \in \mathbb{Z}^+$ and $A_{n,\,s}(n,\, s \geq 0)$ are real or complex numbers arbitrary constant. The notations "$[\,.\,]$" and $(-n)_m$, respectively represent greatest integer function and Pochhammer symbol. Numerous well-known polynomials are provided by Srivastava's polynomials as special cases for appropriately specializing the coefficient $A_{n,\,s}$.

The rest of the paper is organized as follows. In section 2 incomplete Fox-Wright function and Srivastava polynomial are combined, and various integrals like: Oberhettinger type integrals, Lavoie type integral, MacRobert type integral and integral defined by Srivastava and Panda have been established. In section 3, we develop the particular instances of the main findings by specializing the parameters. In section 4, the paper is completed by presenting concluding remark of the paper.

2 Main Results

In this part, we use some existing integral identities which shall be helpful to develop new results involving incomplete Fox-Wright functions, ${}_p\Psi_q^{(\gamma)}$ and ${}_p\Psi_q^{(\Gamma)}$.

2.1 Integral defined by Srivastava and Panda

Srivastava and Panda [17] defined and studied the following integral

$$\int_0^\infty u^{\varpi-1}(u+v)^{-\varsigma}\,du = \frac{\Gamma(\varpi)\Gamma(\varsigma-\varpi)}{\Gamma(\varsigma)}v^{\varpi-\varsigma} \tag{5}$$

with $\Re(\varsigma) > \Re(\varpi) > 0$.

Theorem 1. *If* $\Delta,\, \varkappa,\, \varrho,\, \vartheta,\, \Omega > 0$ *and* $\Re(\varsigma) > \Re(\varpi) > 0$, *then*

$$\begin{aligned}
&\int_0^\infty u^{\varpi-1}(u+v)^{-\varsigma}\, S_n^m[u^{\varkappa}(u+v)^{-\varrho}]\,{}_p\Psi_q^{(\Gamma)}[z\,u^{\vartheta}(u+v)^{-\Omega}]du \\
&= v^{\varpi-\varsigma}\sum_{s=0}^{[n/m]}\frac{(-n)_{m\,s}}{s!}A_{n,\,s}\,v^{s(\varkappa-\varrho)}\times \\
&{}_{p+2}\Psi_{q+1}^{(\Gamma)}\left[\begin{matrix}(\mathfrak{f}_1,\mathfrak{F}_1,x),(\varpi+s\varkappa,\vartheta),(\varsigma-\varpi+s(\varrho-\varkappa),\Omega-\vartheta)\,, \\ (\varsigma+s\varrho,\Omega),\end{matrix}\right. \\
&\qquad\qquad\left.\begin{matrix}(\mathfrak{f}_j,\mathfrak{F}_j)_{2,\,p}\,; \\ (\mathfrak{g}_j,\mathfrak{G}_j)_{1,\,q}\,;\end{matrix}\quad zv^{\vartheta-\Omega}\right].
\end{aligned} \tag{6}$$

Proof. To demonstrate the outcome (6), we begin with L.H.S. Let us consider

$$I = \int_0^\infty u^{\varpi-1}(u+v)^{-\varsigma}\, S_n^m[u^{\varkappa}(u+v)^{-\varrho}]\,{}_p\Psi_q^{(\Gamma)}[z\,u^{\vartheta}(u+v)^{-\Omega}]du. \tag{7}$$

Using the definitions (2) and (4) in (7), we obtain

$$
\begin{aligned}
I = \int_0^\infty u^{\varpi-1}(u+v)^{-\varsigma} \sum_{s=0}^{[n/m]} \frac{(-n)_{m\,s}}{s!} A_{n,\,s}\, u^{s\varkappa}(u+v)^{-s\varrho} \\
\times \sum_{\ell=0}^{\infty} \frac{\Gamma(\mathfrak{f}_1+\mathfrak{F}_1\ell, x)\prod_{j=2}^{p}\Gamma(\mathfrak{f}_j+\mathfrak{F}_j\ell)}{\prod_{j=1}^{q}\Gamma(\mathfrak{g}_j+\mathfrak{G}_j\ell)} \frac{z^\ell\, u^{\ell\vartheta}(u+v)^{-\ell\Omega}}{\ell!} du \\
= \sum_{s=0}^{[n/m]} \frac{(-n)_{m\,s}}{s!} A_{n,\,s} \sum_{\ell=0}^{\infty} \frac{\Gamma(\mathfrak{f}_1+\mathfrak{F}_1\ell, x)\prod_{j=2}^{p}\Gamma(\mathfrak{f}_j+\mathfrak{F}_j\ell)}{\prod_{j=1}^{q}\Gamma(\mathfrak{g}_j+\mathfrak{G}_j\ell)\;\ell!} z^\ell \\
\times \int_0^\infty u^{\varpi+s\varkappa+\ell\vartheta-1}(u+v)^{-\varsigma-s\varrho-\ell\Omega} du \\
= \sum_{s=0}^{[n/m]} \frac{(-n)_{m\,s}}{s!} A_{n,\,s} \sum_{\ell=0}^{\infty} \frac{\Gamma(\mathfrak{f}_1+\mathfrak{F}_1\ell, x)\prod_{j=2}^{p}\Gamma(\mathfrak{f}_j+\mathfrak{F}_j\ell)}{\prod_{j=1}^{q}\Gamma(\mathfrak{g}_j+\mathfrak{G}_j\ell)\;\ell!} z^\ell \\
\times \frac{\Gamma(\varpi+s\varkappa+\ell\vartheta)\Gamma(\varsigma+s\varrho+\ell\Omega-\varpi-s\varkappa-\ell\vartheta)}{\Gamma(\varsigma+s\varrho+\ell\Omega)} v^{\varpi-\varsigma+s(\varkappa-\varrho)+\ell(\vartheta-\Omega)}, \text{ (using (5))} \\
= v^{\varpi-\varsigma} \sum_{s=0}^{[n/m]} \frac{(-n)_{m\,s}}{s!} A_{n,\,s}\, v^{s(\varkappa-\varrho)} \sum_{\ell=0}^{\infty} \frac{\Gamma(\mathfrak{f}_1+\mathfrak{F}_1\ell, x)\prod_{j=2}^{p}\Gamma(\mathfrak{f}_j+\mathfrak{F}_j\ell)}{\prod_{j=1}^{q}\Gamma(\mathfrak{g}_j+\mathfrak{G}_j\ell)} \\
\times \frac{\Gamma(\varpi+s\varkappa+\ell\vartheta)\Gamma(\varsigma-\varpi+s(\varrho-\varkappa)+\ell(\Omega-\vartheta))}{\Gamma(\varsigma+s\varrho+\ell\Omega)} \frac{z^\ell\, v^{\ell(\vartheta-\Omega)}}{\ell!}.
\end{aligned}
$$

Next, using (2) we achieved the desired outcome (6). □

The proof of below theorem is similiar to Theorem 1, so it is claim here without proof.

Theorem 2. *If* Δ, $\varkappa$, ϱ, ϑ, $\Omega > 0$ *and* $\Re(\varsigma) > \Re(\varpi) > 0$, *then*

$$
\begin{aligned}
&\int_0^\infty u^{\varpi-1}(u+v)^{-\varsigma}\, S_n^m[u^\varkappa(u+v)^{-\varrho}]\, {}_p\Psi_q^{(\gamma)}[z\,u^\vartheta(u+v)^{-\Omega}] du \\
&= v^{\varpi-\varsigma} \sum_{s=0}^{[n/m]} \frac{(-n)_{m\,s}}{s!} A_{n,\,s}\, v^{s(\varkappa-\varrho)} \times \\
&\quad {}_{p+2}\Psi_{q+1}^{(\gamma)}\left[\begin{matrix} (\mathfrak{f}_1, \mathfrak{F}_1, x), (\varpi+s\varkappa, \vartheta), (\varsigma-\varpi+s(\varrho-\varkappa), \Omega-\vartheta), \\ (\varsigma+s\varrho, \Omega), \end{matrix} \right. \\
&\qquad\qquad \left. \begin{matrix} (\mathfrak{f}_j, \mathfrak{F}_j)_{2,\,p}\,; \\ (\mathfrak{g}_j, \mathfrak{G}_j)_{1,\,q}\,; \end{matrix} \quad zv^{\vartheta-\Omega} \right]. \qquad (8)
\end{aligned}
$$

2.2 Oberhettinger type integral

Oberhettinger [11] gives an integral formula as (see [10] also):

$$\int_0^\infty u^{\varpi-1}\left(u+k+\sqrt{u^2+2ku}\right)^{-\varsigma}du = 2\varsigma k^{-\varsigma}\left(\frac{k}{2}\right)^{\varpi}\frac{\Gamma(2\varpi)\Gamma(\varsigma-\varpi)}{\Gamma(\varpi+\varsigma+1)}, \quad (9)$$

with $\varpi,\varsigma\in\mathbb{C}$ and $0<(\varpi+\overline{\varpi})<(\varsigma+\overline{\varsigma})$.

Theorem 3. *If $\Delta>0$, $\varkappa>0,\vartheta>0$, $\varpi,\varsigma\in\mathbb{C}$ and $0<(\varpi+\overline{\varpi})<(\varsigma+\overline{\varsigma})$, then*

$$\begin{aligned}&\int_0^\infty u^{\varpi-1}(u+k+\sqrt{u^2+2ku})^{-\varsigma}\,S_n^m[u^\varkappa]\,{}_p\Psi_q^{(\Gamma)}[z\,u^\vartheta]du\\ &=2\varsigma(k)^{-\varsigma}(k/2)^{\varpi}\sum_{s=0}^{[n/m]}\frac{(-n)_{m\,s}}{s!}A_{n,\,s}\left(\frac{k}{2}\right)^{s\varkappa}\times\\ &{}_{p+2}\Psi_{q+1}^{(\Gamma)}\left[\begin{matrix}(\mathfrak{f}_1,\mathfrak{F}_1,x),(2\varpi+2s\varkappa,2\vartheta),(\varsigma-\varpi-s\varkappa,-\vartheta),(\mathfrak{f}_j,\mathfrak{F}_j)_{2,\,p}\,;\\ (1+\varpi+\varsigma+s\varkappa,\vartheta),(\mathfrak{g}_j,\mathfrak{G}_j)_{1,\,q}\,;\end{matrix}\quad z\left(\tfrac{k}{2}\right)^{\vartheta}\right].\end{aligned} \quad (10)$$

Proof. To demonstrate the outcome (10), we begin with L.H.S. Let us consider

$$I=\int_0^\infty u^{\varpi-1}(u+k+\sqrt{u^2+2ku})^{-\varsigma}\,S_n^m[u^\varkappa]\,{}_p\Psi_q^{(\Gamma)}[z\,u^\vartheta]du. \quad (11)$$

Using the definitions (2) and (4) in (11), after simplification we obtain

$$\begin{aligned}I&=\sum_{s=0}^{[n/m]}\frac{(-n)_{m\,s}}{s!}A_{n,\,s}\sum_{\ell=0}^{\infty}\frac{\Gamma(\mathfrak{f}_1+\mathfrak{F}_1\ell,x)\prod_{j=2}^{p}\Gamma(\mathfrak{f}_j+\mathfrak{F}_j\ell)}{\prod_{j=1}^{q}\Gamma(\mathfrak{g}_j+\mathfrak{G}_j\ell)\;\ell!}z^\ell\\ &\qquad\times\int_0^\infty u^{\varpi+s\varkappa+\ell\vartheta-1}(u+k+\sqrt{u^2+2ku})^{-\varsigma}du\\ &=\sum_{s=0}^{[n/m]}\frac{(-n)_{m\,s}}{s!}A_{n,\,s}\sum_{\ell=0}^{\infty}\frac{\Gamma(\mathfrak{f}_1+\mathfrak{F}_1\ell,x)\prod_{j=2}^{p}\Gamma(\mathfrak{f}_j+\mathfrak{F}_j\ell)}{\prod_{j=1}^{q}\Gamma(\mathfrak{g}_j+\mathfrak{G}_j\ell)\;\ell!}z^\ell\\ &\qquad\times 2\varsigma k^{-\varsigma}\left(\frac{k}{2}\right)^{\varpi+s\varkappa+\ell\vartheta}\frac{\Gamma(2\varpi+2s\varkappa+2\ell\vartheta)\Gamma(\varsigma-\varpi-s\varkappa-\ell\vartheta)}{\Gamma(1+\varpi+\varsigma+s\varkappa+\ell\vartheta)},\ \text{(using (9))}.\end{aligned}$$

Next, using (2) we achieved the desired outcome (10). □

The proof of below theorem is similiar to Theorem 3, so it is claim here without proof.

Theorem 4. *If* $\Delta > 0,\ \varkappa > 0, \vartheta > 0,\ \varpi, \varsigma \in \mathbb{C}$ *and* $0 < (\varpi + \overline{\varpi}) < (\varsigma + \overline{\varsigma})$, *then*

$$\int_0^\infty u^{\varpi-1}(u+k+\sqrt{u^2+2ku})^{-\varsigma}\, S_n^m[u^\varkappa]\, {}_p\Psi_q^{(\gamma)}[z\,u^\vartheta]du$$
$$= 2\varsigma(k)^{-\varsigma}(k/2)^{\varpi} \sum_{s=0}^{[n/m]} \frac{(-n)_{m\,s}}{s!} A_{n,\,s} \left(\frac{k}{2}\right)^{s\varkappa} \times$$
$${}_{p+2}\Psi_{q+1}^{(\gamma)}\left[\begin{matrix} (\mathfrak{f}_1, \mathfrak{F}_1, x), (2\varpi + 2s\varkappa, 2\vartheta), (\varsigma - \varpi - s\varkappa, -\vartheta), (\mathfrak{f}_j, \mathfrak{F}_j)_{2,\,p}\,; \\ (1+\varpi+\varsigma+s\varkappa, \vartheta), (\mathfrak{g}_j, \mathfrak{G}_j)_{1,\,q}\,; \end{matrix} \quad z\left(\tfrac{k}{2}\right)^{\vartheta}\right]. \tag{12}$$

2.3 Lavoie type integral

Lavoie [5] gives an integral formula as:

$$\int_0^\infty u^{\varpi-1}\left(1-\frac{u}{3}\right)^{2\varpi-1}(1-u)^{2\varsigma-1}\left(1-\frac{u}{4}\right)^{\varsigma-1} du = \left(\frac{2}{3}\right)^{2\varpi}\frac{\Gamma(\varpi)\Gamma(\varsigma)}{\Gamma(\varpi+\varsigma)}, \tag{13}$$

with $\varpi, \varsigma \in \mathbb{C}$ and $\Re(\varpi), \Re(\varsigma) > 0$.

Theorem 5. *If* $\Delta > 0,\ \varkappa > 0, \varrho > 0, \vartheta > 0, \Omega > 0,\ \varpi, \varsigma \in \mathbb{C}$ *and* $\Re(\varpi), \Re(\varsigma) > 0$, *then*

$$\int_0^\infty u^{\varpi-1}\left(1-\frac{u}{3}\right)^{2\varpi-1}(1-u)^{2\varsigma-1}\left(1-\frac{u}{4}\right)^{\varsigma-1}$$
$$\times S_n^m\left[u^\varkappa\left(1-\frac{u}{3}\right)^{2\varkappa}(1-u)^{2\varrho}\left(1-\frac{u}{4}\right)^{\varrho}\right]$$
$$\times\ {}_p\Psi_q^{(\Gamma)}\left[z\,u^\vartheta\left(1-\frac{u}{3}\right)^{2\vartheta}(1-u)^{2\Omega}\left(1-\frac{u}{4}\right)^{\Omega}\right] du$$
$$= \left(\frac{2}{3}\right)^{2\varpi}\sum_{s=0}^{[n/m]}\frac{(-n)_{m\,s}}{s!}A_{n,\,s}\left(\frac{2}{3}\right)^{2s\varkappa}$$
$$\times\ {}_{p+2}\Psi_{q+1}^{(\Gamma)}\left[\begin{matrix} (\mathfrak{f}_1, \mathfrak{F}_1, x), (\varpi + s\varkappa, \vartheta), (\varsigma + s\varrho, \Omega), (\mathfrak{f}_j, \mathfrak{F}_j)_{2,\,p}\,; \\ (\varpi+\varsigma+s(\varkappa+\varrho), \vartheta+\Omega), (\mathfrak{g}_j, \mathfrak{G}_j)_{1,\,q}\,; \end{matrix} \quad z\left(\tfrac{2}{3}\right)^{2\vartheta}\right]. \tag{14}$$

Theorem 6. *If* $\Delta > 0,\ \varkappa > 0, \varrho > 0, \vartheta > 0, \Omega > 0,\ \varpi, \varsigma \in \mathbb{C}$ *and* $\Re(\varpi), \Re(\varsigma) >$

0, *then*

$$\begin{aligned}
&\int_0^\infty u^{\varpi-1}\left(1-\frac{u}{3}\right)^{2\varpi-1}(1-u)^{2\varsigma-1}\left(1-\frac{u}{4}\right)^{\varsigma-1}\\
&\qquad\times S_n^m\left[u^{\varkappa}\left(1-\frac{u}{3}\right)^{2\varkappa}(1-u)^{2\varrho}\left(1-\frac{u}{4}\right)^{\varrho}\right]\\
&\qquad\qquad\times {}_p\Psi_q^{(\gamma)}\left[z\,u^{\vartheta}\left(1-\frac{u}{3}\right)^{2\vartheta}(1-u)^{2\Omega}\left(1-\frac{u}{4}\right)^{\Omega}\right]du\\
&=\left(\frac{2}{3}\right)^{2\varpi}\sum_{s=0}^{[n/m]}\frac{(-n)_{m\,s}}{s!}A_{n,\,s}\left(\frac{2}{3}\right)^{2s\varkappa}\\
&\times {}_{p+2}\Psi_{q+1}^{(\gamma)}\left[\begin{matrix}(\mathfrak{f}_1,\mathfrak{F}_1,x),(\varpi+s\varkappa,\vartheta),(\varsigma+s\varrho,\Omega),(\mathfrak{f}_j,\mathfrak{F}_j)_{2,\,p}\,;\\ (\varpi+\varsigma+s(\varkappa+\varrho),\vartheta+\Omega),(\mathfrak{g}_j,\mathfrak{G}_j)_{1,\,q}\,;\end{matrix}\quad z\,\left(\tfrac{2}{3}\right)^{2\vartheta}\right].
\end{aligned}\tag{15}$$

The proof of above theorems are immediate consequences of definitions (1), (2), (4) and (13), hence they are given without proof here.

2.4 MacRobert type integral

MacRobert [6] gives an integral formula as:

$$\int_0^1 u^{\varpi-1}(1-u)^{\varsigma-1}[au+b(1-u)]^{-\varpi-\varsigma}du=\frac{1}{a^{\varpi}b^{\varsigma}}\frac{\Gamma(\varpi)\Gamma(\varsigma)}{\Gamma(\varpi+\varsigma)}\tag{16}$$

with $\Re(\varpi)$, $\Re(\varsigma)>0$ and $|u|\le 1$.

Theorem 7. *If* $\Delta>0$, $\varkappa>0,\varrho>0,\vartheta>0,\Omega>0$, $\Re(\varpi)$, $\Re(\varsigma)>0$ *and* $|u|\le 1$, *then*

$$\begin{aligned}
&\int_0^1 u^{\varpi-1}(1-u)^{\varsigma-1}[au+b(1-u)]^{-\varpi-\varsigma}\\
&\qquad\times S_n^m\left[u^{\varkappa}(1-u)^{\varrho}[au+b(1-u)]^{-\varkappa-\varrho}\right]\\
&\qquad\times {}_p\Psi_q^{(\Gamma)}\left[z\,u^{\vartheta}(1-u)^{\Omega}[au+b(1-u)]^{-\vartheta-\Omega}\right]du\\
&=\frac{1}{a^{\varpi}\,b^{\varsigma}}\sum_{s=0}^{[n/m]}\frac{(-n)_{m\,s}}{s!}A_{n,\,s}\,\frac{1}{a^{s\varkappa}\,b^{s\varrho}}\\
&\times {}_{p+2}\Psi_{q+1}^{(\Gamma)}\left[\begin{matrix}(\mathfrak{f}_1,\mathfrak{F}_1,x),(\varpi+s\varkappa,\vartheta),(\varsigma+s\varrho,\Omega),(\mathfrak{f}_j,\mathfrak{F}_j)_{2,\,p}\,;\\ (\varpi+\varsigma+s(\varkappa+\varrho),\vartheta+\Omega),(\mathfrak{g}_j,\mathfrak{G}_j)_{1,\,q}\,;\end{matrix}\quad\frac{z}{a^{\vartheta}\,b^{\Omega}}\right].
\end{aligned}\tag{17}$$

Theorem 8. *If* $\Delta>0$, $\varkappa>0,\varrho>0,\vartheta>0,\Omega>0$, $\Re(\varpi)$, $\Re(\varsigma)>0$ *and* $|u|\le 1$,

then

$$\int_0^1 u^{\varpi-1}(1-u)^{\varsigma-1}[au+b(1-u)]^{-\varpi-\varsigma} \times S_n^m\left[u^{\varkappa}(1-u)^{\varrho}[au+b(1-u)]^{-\varkappa-\varrho}\right] \times {}_p\Psi_q^{(\gamma)}\left[z\,u^{\vartheta}(1-u)^{\Omega}[au+b(1-u)]^{-\vartheta-\Omega}\right] du$$
$$= \frac{1}{a^{\varpi}\,b^{\varsigma}} \sum_{s=0}^{[n/m]} \frac{(-n)_{m\,s}}{s!} A_{n,\,s}\, \frac{1}{a^{s\varkappa}\,b^{s\varrho}}$$
$$\times {}_{p+2}\Psi_{q+1}^{(\gamma)}\left[\begin{matrix}(\mathfrak{f}_1,\mathfrak{F}_1,x),(\varpi+s\varkappa,\vartheta),(\varsigma+s\varrho,\Omega),(\mathfrak{f}_j,\mathfrak{F}_j)_{2,\,p}\,; \\ (\varpi+\varsigma+s(\varkappa+\varrho),\vartheta+\Omega)\,,(\mathfrak{g}_j,\mathfrak{G}_j)_{1,\,q}\,;\end{matrix} \quad \frac{z}{a^{\vartheta}\,b^{\Omega}}\right]. \quad (18)$$

The proof of above theorems are immediate consequences of definitions (1), (2), (4) and (16), hence they are given without proof here.

3 Particular Cases

By appropriately specializing the coefficient $A_{n,\,s}$, specific special cases of derived findings can be developed to identify many spectrums of the existing polynomials. Only two special cases are given here and the remaining we kept for interested readers. If we put $m = 2$ and $A_{n,\,s} = (-1)^s$ in the broad category of polynomials (i.e., $S_n^2[x] = x^{n/2}\mathrm{H}_n\left(\frac{1}{2\sqrt{x}}\right)$, where $\mathrm{H}_n(x)$ is Hermite polynomial [1, 15]) of above theorems, then we obtain the following respective corollaries.

Corollary 1. *If* Δ, $\varkappa$, ϱ, ϑ, $\Omega > 0$ *and* $\Re(\varsigma) > \Re(\varpi) > 0$, *then*

$$\int_0^{\infty} u^{\varpi+\frac{n}{2}\varkappa-1}(u+v)^{-\varsigma-\frac{n}{2}\varrho}\,\mathrm{H}_n\left(\frac{1}{2\sqrt{u^{\varkappa}(u+v)^{-\varrho}}}\right) {}_p\Psi_q^{(\Gamma)}[z\,u^{\vartheta}(u+v)^{-\Omega}]du$$
$$= v^{\varpi-\varsigma}\,n! \sum_{s=0}^{[n/2]} \frac{(-1)^s}{s!(n-2s)!}\, v^{s(\varkappa-\varrho)} \times$$
$${}_{p+2}\Psi_{q+1}^{(\Gamma)}\left[\begin{matrix}(\mathfrak{f}_1,\mathfrak{F}_1,x),(\varpi+s\varkappa,\vartheta),(\varsigma-\varpi+s(\varrho-\varkappa),\Omega-\vartheta)\,, \\ (\varsigma+s\varrho,\Omega), \\ (\mathfrak{f}_j,\mathfrak{F}_j)_{2,\,p}\,; \\ (\mathfrak{g}_j,\mathfrak{G}_j)_{1,\,q}\,;\end{matrix} \quad zv^{\vartheta-\Omega}\right]. \quad (19)$$

Corollary 2. *If* $\Delta > 0$, $\varkappa$, ϱ, ϑ, $\Omega > 0$ *and* $\Re(\varsigma) > \Re(\varpi) > 0$, *then*

$$\int_0^\infty u^{\varpi+\frac{n}{2}\varkappa-1}(u+v)^{-\varsigma-\frac{n}{2}\varrho}\,\mathrm{H}_n\left(\frac{1}{2\sqrt{u^{\varkappa}(u+v)^{-\varrho}}}\right)\,{}_p\Psi_q^{(\gamma)}[z\,u^{\vartheta}(u+v)^{-\Omega}]du$$
$$= v^{\varpi-\varsigma}\,n!\sum_{s=0}^{[n/2]}\frac{(-1)^s}{s!(n-2s)!}\,v^{s(\varkappa-\varrho)}\times$$
$${}_{p+2}\Psi_{q+1}^{(\gamma)}\left[\begin{matrix}(\mathfrak{f}_1,\mathfrak{F}_1,x),(\varpi+s\varkappa,\vartheta),(\varsigma-\varpi+s(\varrho-\varkappa),\Omega-\vartheta)\,,\\ (\varsigma+s\varrho,\Omega),\end{matrix}\right.$$
$$\left.\begin{matrix}(\mathfrak{f}_j,\mathfrak{F}_j)_{2,\,p}\,;\\ (\mathfrak{g}_j,\mathfrak{G}_j)_{1,\,q}\,;\end{matrix}\quad zv^{\vartheta-\Omega}\right]. \tag{20}$$

Corollary 3. *If* $\Delta > 0$, $\varkappa > 0, \vartheta > 0$, $\varpi, \varsigma \in \mathbb{C}$ *and* $0 < (\varpi + \overline{\varpi}) < (\varsigma + \overline{\varsigma})$, *then*

$$\int_0^\infty u^{\varpi+\frac{n}{2}\varkappa-1}(u+k+\sqrt{u^2+2ku})^{-\varsigma}\,\mathrm{H}_n\left(\frac{1}{2\sqrt{u^{\varkappa}}}\right)\,{}_p\Psi_q^{(\Gamma)}[z\,u^{\vartheta}]du$$
$$= 2\varsigma(k)^{-\varsigma}(k/2)^{\varpi}\,n!\sum_{s=0}^{[n/2]}\frac{(-1)^s}{s!(n-2s)!}\,\left(\frac{k}{2}\right)^{s\varkappa}\times$$
$${}_{p+2}\Psi_{q+1}^{(\Gamma)}\left[\begin{matrix}(\mathfrak{f}_1,\mathfrak{F}_1,x),(2\varpi+2s\varkappa,2\vartheta),(\varsigma-\varpi-s\varkappa,-\vartheta),(\mathfrak{f}_j,\mathfrak{F}_j)_{2,\,p}\,;\\ (1+\varpi+\varsigma+s\varkappa,\vartheta),(\mathfrak{g}_j,\mathfrak{G}_j)_{1,\,q}\,;\end{matrix}\quad z\left(\tfrac{k}{2}\right)^{\vartheta}\right]. \tag{21}$$

Corollary 4. *If* $\Delta > 0$, $\varkappa > 0, \vartheta > 0$, $\varpi, \varsigma \in \mathbb{C}$ *and* $0 < (\varpi + \overline{\varpi}) < (\varsigma + \overline{\varsigma})$, *then*

$$\int_0^\infty u^{\varpi+\frac{n}{2}\varkappa-1}(u+k+\sqrt{u^2+2ku})^{-\varsigma}\,\mathrm{H}_n\left(\frac{1}{2\sqrt{u^{\varkappa}}}\right)\,{}_p\Psi_q^{(\gamma)}[z\,u^{\vartheta}]du$$
$$= 2\varsigma(k)^{-\varsigma}(k/2)^{\varpi}\,n!\sum_{s=0}^{[n/2]}\frac{(-1)^s}{s!(n-2s)!}\,\left(\frac{k}{2}\right)^{s\varkappa}\times$$
$${}_{p+2}\Psi_{q+1}^{(\gamma)}\left[\begin{matrix}(\mathfrak{f}_1,\mathfrak{F}_1,x),(2\varpi+2s\varkappa,2\vartheta),(\varsigma-\varpi-s\varkappa,-\vartheta),(\mathfrak{f}_j,\mathfrak{F}_j)_{2,\,p}\,;\\ (1+\varpi+\varsigma+s\varkappa,\vartheta),(\mathfrak{g}_j,\mathfrak{G}_j)_{1,\,q}\,;\end{matrix}\quad z\left(\tfrac{k}{2}\right)^{\vartheta}\right]. \tag{22}$$

Corollary 5. *If* $\Delta > 0$, $\varkappa > 0, \varrho > 0, \vartheta > 0, \Omega > 0$, $\varpi, \varsigma \in \mathbb{C}$ *and* $\Re(\varpi), \Re(\varsigma) >$

0, *then*

$$\int_0^\infty u^{\varpi+\frac{n}{2}\varkappa-1}\left(1-\frac{u}{3}\right)^{2(\varpi+\frac{n}{2}\varkappa)-1}(1-u)^{2(\varsigma+\frac{n}{2}\varrho)-1}\left(1-\frac{u}{4}\right)^{\varsigma+\frac{n}{2}\varrho-1}$$
$$\times \mathrm{H}_n\left(\frac{1}{2\sqrt{u^\varkappa\left(1-\frac{u}{3}\right)^{2\varkappa}(1-u)^{2\varrho}\left(1-\frac{u}{4}\right)^{\varrho}}}\right)$$
$$\times {}_p\Psi_q^{(\Gamma)}\left[z\,u^\vartheta\left(1-\frac{u}{3}\right)^{2\vartheta}(1-u)^{2\Omega}\left(1-\frac{u}{4}\right)^{\Omega}\right]du$$
$$=\left(\frac{2}{3}\right)^{2\varpi} n!\sum_{s=0}^{[n/2]}\frac{(-1)^s}{s!(n-2s)!}\left(\frac{2}{3}\right)^{2s\varkappa}$$
$$\times {}_{p+2}\Psi_{q+1}^{(\Gamma)}\left[\begin{matrix}(\mathfrak{f}_1,\mathfrak{F}_1,x),(\varpi+s\varkappa,\vartheta),(\varsigma+s\varrho,\Omega),(\mathfrak{f}_j,\mathfrak{F}_j)_{2,\,p}\,;\\ (\varpi+\varsigma+s(\varkappa+\varrho),\vartheta+\Omega),(\mathfrak{g}_j,\mathfrak{G}_j)_{1,\,q}\,;\end{matrix}\quad z\,\left(\tfrac{2}{3}\right)^{2\vartheta}\right]. \tag{23}$$

Corollary 6. *If* $\Delta>0$, $\varkappa>0,\varrho>0,\vartheta>0,\Omega>0$, $\varpi,\varsigma\in\mathbb{C}$ *and* $\Re(\varpi),\Re(\varsigma)>0$, *then*

$$\int_0^\infty u^{\varpi+\frac{n}{2}\varkappa-1}\left(1-\frac{u}{3}\right)^{2(\varpi+\frac{n}{2}\varkappa)-1}(1-u)^{2(\varsigma+\frac{n}{2}\varrho)-1}\left(1-\frac{u}{4}\right)^{\varsigma+\frac{n}{2}\varrho-1}$$
$$\times \mathrm{H}_n\left(\frac{1}{2\sqrt{u^\varkappa\left(1-\frac{u}{3}\right)^{2\varkappa}(1-u)^{2\varrho}\left(1-\frac{u}{4}\right)^{\varrho}}}\right)$$
$$\times {}_p\Psi_q^{(\gamma)}\left[z\,u^\vartheta\left(1-\frac{u}{3}\right)^{2\vartheta}(1-u)^{2\Omega}\left(1-\frac{u}{4}\right)^{\Omega}\right]du$$
$$=\left(\frac{2}{3}\right)^{2\varpi} n!\sum_{s=0}^{[n/2]}\frac{(-1)^s}{s!(n-2s)!}\left(\frac{2}{3}\right)^{2s\varkappa}$$
$$\times {}_{p+2}\Psi_{q+1}^{(\gamma)}\left[\begin{matrix}(\mathfrak{f}_1,\mathfrak{F}_1,x),(\varpi+s\varkappa,\vartheta),(\varsigma+s\varrho,\Omega),(\mathfrak{f}_j,\mathfrak{F}_j)_{2,\,p}\,;\\ (\varpi+\varsigma+s(\varkappa+\varrho),\vartheta+\Omega),(\mathfrak{g}_j,\mathfrak{G}_j)_{1,\,q}\,;\end{matrix}\quad z\,\left(\tfrac{2}{3}\right)^{2\vartheta}\right]. \tag{24}$$

Corollary 7. *If* $\Delta>0$, $\varkappa>0,\varrho>0,\vartheta>0,\Omega>0$, $\Re(\varpi),\Re(\varsigma)>0$ *and*

$|u| \leq 1$, *then*

$$\int_0^1 u^{\varpi+\frac{n}{2}\varkappa-1}(1-u)^{\varsigma+\frac{n}{2}\varrho-1}[au+b(1-u)]^{-\varpi-\varsigma-\frac{n}{2}(\varkappa+\varrho)} \times \mathrm{H}_n\left(\frac{1}{2\sqrt{u^{\varkappa}(1-u)^{\varrho}[au+b(1-u)]^{-\varkappa-\varrho}}}\right) \times {}_p\Psi_q^{(\Gamma)}\left[z\,u^{\vartheta}(1-u)^{\Omega}[au+b(1-u)]^{-\vartheta-\Omega}\right] du$$

$$= \frac{n!}{a^{\varpi}\,b^{\varsigma}} \sum_{s=0}^{[n/2]} \frac{(-1)^s}{s!(n-2s)!} \frac{1}{a^{s\varkappa}\,b^{s\varrho}} \times {}_{p+2}\Psi_{q+1}^{(\Gamma)}\left[\begin{matrix}(\mathfrak{f}_1,\mathfrak{F}_1,x),(\varpi+s\varkappa,\vartheta),(\varsigma+s\varrho,\Omega),(\mathfrak{f}_j,\mathfrak{F}_j)_{2,\,p}\,; \\ (\varpi+\varsigma+s(\varkappa+\varrho),\vartheta+\Omega)\,,(\mathfrak{g}_j,\mathfrak{G}_j)_{1,\,q}\,;\end{matrix}\quad \frac{z}{a^{\vartheta}\,b^{\Omega}}\right]. \quad (25)$$

Corollary 8. *If* $\Delta > 0$, $\varkappa > 0, \varrho > 0, \vartheta > 0, \Omega > 0$, $\Re(\varpi), \Re(\varsigma) > 0$ *and* $|u| \leq 1$, *then*

$$\int_0^1 u^{\varpi+\frac{n}{2}\varkappa-1}(1-u)^{\varsigma+\frac{n}{2}\varrho-1}[au+b(1-u)]^{-\varpi-\varsigma-\frac{n}{2}(\varkappa+\varrho)} \times \mathrm{H}_n\left(\frac{1}{2\sqrt{u^{\varkappa}(1-u)^{\varrho}[au+b(1-u)]^{-\varkappa-\varrho}}}\right) \times {}_p\Psi_q^{(\gamma)}\left[z\,u^{\vartheta}(1-u)^{\Omega}[au+b(1-u)]^{-\vartheta-\Omega}\right] du$$

$$= \frac{n!}{a^{\varpi}\,b^{\varsigma}} \sum_{s=0}^{[n/2]} \frac{(-1)^s}{s!(n-2s)!} \frac{1}{a^{s\varkappa}\,b^{s\varrho}} \times {}_{p+2}\Psi_{q+1}^{(\gamma)}\left[\begin{matrix}(\mathfrak{f}_1,\mathfrak{F}_1,x),(\varpi+s\varkappa,\vartheta),(\varsigma+s\varrho,\Omega),(\mathfrak{f}_j,\mathfrak{F}_j)_{2,\,p}\,; \\ (\varpi+\varsigma+s(\varkappa+\varrho),\vartheta+\Omega)\,,(\mathfrak{g}_j,\mathfrak{G}_j)_{1,\,q}\,;\end{matrix}\quad \frac{z}{a^{\vartheta}\,b^{\Omega}}\right]. \quad (26)$$

Again, by setting $m = 1$ and $A_{n,\,s} = \dfrac{s!}{(-n)_{m\,s}}$ for $s = r$ and $A_{n,\,s} = 0$ for $s \neq r$ in the general class of polynomials (i.e., $S_n^1[x] = x^r$) of above theorems, then we obtain the following respective corollaries.

Corollary 9. *If* $\Delta > 0$, $\varkappa$, ϱ, ϑ, $\Omega > 0$ *and* $\Re(\varsigma) > \Re(\varpi) > 0$, *then*

$$\int_0^{\infty} u^{\varpi+r\varkappa-1}(u+v)^{-\varsigma-r\varrho}\,{}_p\Psi_q^{(\Gamma)}[z\,u^{\vartheta}(u+v)^{-\Omega}]du = v^{\varpi-\varsigma+r(\varkappa-\varrho)} \times {}_{p+2}\Psi_{q+1}^{(\Gamma)}\left[\begin{matrix}(\mathfrak{f}_1,\mathfrak{F}_1,x),(\varpi+r\varkappa,\vartheta), \\ (\varsigma+r\varrho,\Omega), \\ (\varsigma-\varpi+r(\varrho-\varkappa),\Omega-\vartheta)\,,(\mathfrak{f}_j,\mathfrak{F}_j)_{2,\,p}\,; \\ (\mathfrak{g}_j,\mathfrak{G}_j)_{1,\,q}\,;\end{matrix}\quad zv^{\vartheta-\Omega}\right]. \quad (27)$$

Corollary 10. *If* $\Delta > 0$, $\varkappa$, ϱ, ϑ, $\Omega > 0$ *and* $\Re(\varsigma) > \Re(\varpi) > 0$, *then*

$$\int_0^\infty u^{\varpi+r\varkappa-1}(u+v)^{-\varsigma-r\varrho}\,{}_p\Psi_q^{(\gamma)}[z\,u^{\vartheta}(u+v)^{-\Omega}]du$$
$$= v^{\varpi-\varsigma+r(\varkappa-\varrho)} \times {}_{p+2}\Psi_{q+1}^{(\gamma)}\left[\begin{matrix}(\mathfrak{f}_1,\mathfrak{F}_1,x),(\varpi+r\varkappa,\vartheta),\\ (\varsigma+r\varrho,\Omega),\end{matrix}\right.$$
$$\left.\begin{matrix}(\varsigma-\varpi+r(\varrho-\varkappa),\Omega-\vartheta),(\mathfrak{f}_j,\mathfrak{F}_j)_{2,\,p}\,;\\ (\mathfrak{g}_j,\mathfrak{G}_j)_{1,\,q}\,;\end{matrix}\quad zv^{\vartheta-\Omega}\right]. \tag{28}$$

Corollary 11. *If* $\Delta > 0$, $\varkappa > 0, \vartheta > 0$, $\varpi, \varsigma \in \mathbb{C}$ *and* $0 < (\varpi + \overline{\varpi}) < (\varsigma + \overline{\varsigma})$, *then*

$$\int_0^\infty u^{\varpi+r\varkappa-1}(u+k+\sqrt{u^2+2ku})^{-\varsigma}\,{}_p\Psi_q^{(\Gamma)}[z\,u^{\vartheta}]du$$
$$= 2\varsigma(k)^{-\varsigma}(k/2)^{\varpi+r\varkappa}\times$$
$${}_{p+2}\Psi_{q+1}^{(\Gamma)}\left[\begin{matrix}(\mathfrak{f}_1,\mathfrak{F}_1,x),(2\varpi+2r\varkappa,2\vartheta),(\varsigma-\varpi-r\varkappa,-\vartheta),(\mathfrak{f}_j,\mathfrak{F}_j)_{2,\,p}\,;\\ (1+\varpi+\varsigma+r\varkappa,\vartheta),(\mathfrak{g}_j,\mathfrak{G}_j)_{1,\,q}\,;\end{matrix}\quad z\left(\tfrac{k}{2}\right)^{\vartheta}\right]. \tag{29}$$

Corollary 12. *If* $\Delta > 0$, $\varkappa > 0, \vartheta > 0$, $\varpi, \varsigma \in \mathbb{C}$ *and* $0 < (\varpi + \overline{\varpi}) < (\varsigma + \overline{\varsigma})$, *then*

$$\int_0^\infty u^{\varpi+r\varkappa-1}(u+k+\sqrt{u^2+2ku})^{-\varsigma}\,{}_p\Psi_q^{(\gamma)}[z\,u^{\vartheta}]du$$
$$= 2\varsigma(k)^{-\varsigma}(k/2)^{\varpi+r\varkappa}\times$$
$${}_{p+2}\Psi_{q+1}^{(\gamma)}\left[\begin{matrix}(\mathfrak{f}_1,\mathfrak{F}_1,x),(2\varpi+2r\varkappa,2\vartheta),(\varsigma-\varpi-r\varkappa,-\vartheta),(\mathfrak{f}_j,\mathfrak{F}_j)_{2,\,p}\,;\\ (1+\varpi+\varsigma+r\varkappa,\vartheta),(\mathfrak{g}_j,\mathfrak{G}_j)_{1,\,q}\,;\end{matrix}\quad z\left(\tfrac{k}{2}\right)^{\vartheta}\right]. \tag{30}$$

Corollary 13. *If* $\Delta > 0$, $\varkappa > 0, \varrho > 0, \vartheta > 0, \Omega > 0$, $\varpi, \varsigma \in \mathbb{C}$ *and* $\Re(\varpi), \Re(\varsigma) > 0$, *then*

$$\int_0^\infty u^{\varpi+r\varkappa-1}\left(1-\frac{u}{3}\right)^{2(\varpi+r\varkappa)-1}(1-u)^{2(\varsigma+r\varrho)-1}\left(1-\frac{u}{4}\right)^{\varsigma+r\varrho-1}$$
$$\times\ {}_p\Psi_q^{(\Gamma)}\left[z\,u^{\vartheta}\left(1-\frac{u}{3}\right)^{2\vartheta}(1-u)^{2\Omega}\left(1-\frac{u}{4}\right)^{\Omega}\right]du = \left(\frac{2}{3}\right)^{2(\varpi+r\varkappa)}$$
$$\times\ {}_{p+2}\Psi_{q+1}^{(\Gamma)}\left[\begin{matrix}(\mathfrak{f}_1,\mathfrak{F}_1,x),(\varpi+r\varkappa,\vartheta),(\varsigma+r\varrho,\Omega),(\mathfrak{f}_j,\mathfrak{F}_j)_{2,\,p}\,;\\ (\varpi+\varsigma+r(\varkappa+\varrho),\vartheta+\Omega),(\mathfrak{g}_j,\mathfrak{G}_j)_{1,\,q}\,;\end{matrix}\quad z\left(\tfrac{2}{3}\right)^{2\vartheta}\right]. \tag{31}$$

Corollary 14. *If* $\Delta > 0$, $\varkappa > 0, \varrho > 0, \vartheta > 0, \Omega > 0$, $\varpi, \varsigma \in \mathbb{C}$ *and*

$\Re(\varpi), \Re(\varsigma) > 0$, *then*

$$\int_0^\infty u^{\varpi+r\varkappa-1}\left(1-\frac{u}{3}\right)^{2(\varpi+r\varkappa)-1}(1-u)^{2(\varsigma+r\varrho)-1}\left(1-\frac{u}{4}\right)^{\varsigma+r\varrho-1}$$
$$\times\ {}_p\Psi_q^{(\gamma)}\left[z\,u^{\vartheta}\left(1-\frac{u}{3}\right)^{2\vartheta}(1-u)^{2\Omega}\left(1-\frac{u}{4}\right)^{\Omega}\right]du = \left(\frac{2}{3}\right)^{2(\varpi+r\varkappa)}$$
$$\times\ {}_{p+2}\Psi_{q+1}^{(\gamma)}\left[\begin{matrix}(\mathfrak{f}_1,\mathfrak{F}_1,x),(\varpi+r\varkappa,\vartheta),(\varsigma+r\varrho,\Omega),(\mathfrak{f}_j,\mathfrak{F}_j)_{2,\,p}\,; \\ (\varpi+\varsigma+r(\varkappa+\varrho),\vartheta+\Omega),(\mathfrak{g}_j,\mathfrak{G}_j)_{1,\,q}\,;\end{matrix}\quad z\,\left(\tfrac{2}{3}\right)^{2\vartheta}\right]. \tag{32}$$

Corollary 15. *If* $\Delta > 0$, $\varkappa > 0, \varrho > 0, \vartheta > 0, \Omega > 0$, $\Re(\varpi)$, $\Re(\varsigma) > 0$ *and* $|u| \le 1$, *then*

$$\int_0^1 u^{\varpi+r\varkappa-1}(1-u)^{\varsigma+r\varrho-1}[au+b(1-u)]^{-\varpi-\varsigma-r(\varkappa+\varrho)}$$
$$\times\ {}_p\Psi_q^{(\Gamma)}\left[z\,u^{\vartheta}(1-u)^{\Omega}[au+b(1-u)]^{-\vartheta-\Omega}\right]du = \frac{1}{a^{\varpi+r\varkappa}\,b^{\varsigma+r\varrho}}$$
$$\times\ {}_{p+2}\Psi_{q+1}^{(\Gamma)}\left[\begin{matrix}(\mathfrak{f}_1,\mathfrak{F}_1,x),(\varpi+r\varkappa,\vartheta),(\varsigma+r\varrho,\Omega),(\mathfrak{f}_j,\mathfrak{F}_j)_{2,\,p}\,; \\ (\varpi+\varsigma+r(\varkappa+\varrho),\vartheta+\Omega),(\mathfrak{g}_j,\mathfrak{G}_j)_{1,\,q}\,;\end{matrix}\quad \frac{z}{a^{\vartheta}\,b^{\Omega}}\right]. \tag{33}$$

Corollary 16. *If* $\Delta > 0$, $\varkappa > 0, \varrho > 0, \vartheta > 0, \Omega > 0$, $\Re(\varpi)$, $\Re(\varsigma) > 0$ *and* $|u| \le 1$, *then*

$$\int_0^1 u^{\varpi+r\varkappa-1}(1-u)^{\varsigma+r\varrho-1}[au+b(1-u)]^{-\varpi-\varsigma-r(\varkappa+\varrho)}$$
$$\times\ {}_p\Psi_q^{(\gamma)}\left[z\,u^{\vartheta}(1-u)^{\Omega}[au+b(1-u)]^{-\vartheta-\Omega}\right]du = \frac{1}{a^{\varpi+r\varkappa}\,b^{\varsigma+r\varrho}}$$
$$\times\ {}_{p+2}\Psi_{q+1}^{(\gamma)}\left[\begin{matrix}(\mathfrak{f}_1,\mathfrak{F}_1,x),(\varpi+r\varkappa,\vartheta),(\varsigma+r\varrho,\Omega),(\mathfrak{f}_j,\mathfrak{F}_j)_{2,\,p}\,; \\ (\varpi+\varsigma+r(\varkappa+\varrho),\vartheta+\Omega),(\mathfrak{g}_j,\mathfrak{G}_j)_{1,\,q}\,;\end{matrix}\quad \frac{z}{a^{\vartheta}\,b^{\Omega}}\right]. \tag{34}$$

4 Concluding Remarks

The integral formulas concerning combination of a general polynomial system and incomplete Fox-Wright functions are investigated and the outcomes are described in terms of those other incomplete Fox-Wright functions. When $x = 0$, the incomplete Fox-Wright function mentioned by (2) reduces to the Fox-Wright function ${}_p\Psi_q(\mathfrak{t})$, whose particular cases are known to the number of special functions arising in the mathematical, physical and engineering sciences. In addition, a huge number of recognized polynomials may be obtained as a specific case of general class of polynomials by correctly specialization the factor $A_{n,\,s}$. We conclude by stating that the findings mentioned here appear to be of broad importance and can lead to multiple integrals for a particular class of hypergeometric polynomials as well as other special functions, which we left for interested readers.

Acknowledgements

The authors would like to thank anonymous referees for their useful critical comments and suggestions for improving the research paper.

References

[1] Bhatter, S., Nishant, Suthar, D. L., & Purohit, S. D. (2023). Boros Integral Involving the Product of Family of Polynomials and the Incomplete I-Function. J. Comput. Anal. Appl., 400.

[2] Choi, J., Agarwal, P., Mathur, S., & Purohit, S. D. (2014). Certain new integral formulas involving the generalized Bessel functions. Bull. Korean Math. Soc., 51(4), 995-1003.

[3] Choi, J., Kumar, D., & Purohit, S. D. (2016). Integral formulas involving a product of generalized Bessel functions of the first kind. Kyungpook Math. J., 56(1), 131-136.

[4] Choi, J., Parmar, R. K., & Srivastava, H. M. (2018). The incomplete Lauricella functions of several variables and associated properties and formulas. Kyungpook Math. J., 58(1), 19-35.

[5] Lavoie, J. L., & Trottier, G. (1969). On the sum of certain Appell's series. Ganita, 20(1), 31-32.

[6] MacRobert, T. M. (1961). Beta-function formulae and integrals involving E-functions. Math. Annalen., 142(5), 450-452.

[7] Mathai, A. M., Saxena, R. K., & Haubold, H. J. (2009). The H-function: theory and applications. Springer Science & Business Media.

[8] Menaria, N., Parmar, R. K., Purohit, S. D., & Nisar, K. S. (2017). Certain unified integrals involving product of generalized k-Bessel function and general class of polynomials. Honam Math. J., 39(3), 349-361.

[9] Nisar, K. S., Suthar, D. L., Purohit, S. D., & Aldhalfallah, M. (2017). Some unified integrals associated with the generalized Struve function. Proc. Jangjeon Math. Soc., 20(2), 261-267.

[10] Nisar, K. S., Suthar, D. L., Purohit, S. D., & Amsalu, H. (2020). Unified integrals involving product of multivariable polynomials and generalized Bessel functions. Bol. Soc. Parana. Mat, 38(6), 73-83.

[11] Oberhettinger, F. (1974), Tables of Mellin Transforms, Springer, New York.

[12] Qureshi, M. I., Quraishi, K. A., & Pal, R. (2011). Some definite integrals of Gradshteyn-Ryzhil and other integrals. Glob. J. Sci. Front. Res., 11(4), 75-80.

[13] Sharma, R., Singh, J., Kumar, D., & Singh, Y. (2022). Certain unified integrals associated with product of the general class of polynomials and incomplete I-functions. Int. J. Appl. Comput. Math., 8(1), 7.

[14] Sharma, R., Singh, J., Kumar, D., & Singh, Y. (2023). An application of incomplete I-functions with two variables to solve the nonlinear differential equations using S-function. J. Comput. Anal. Appl., 80.

[15] Srivastava, H.M. & Singh, N.P. (1983). The integration of certain products of the multivariable H-function with a general class of polynomials, Rend. Circ. Mat. Palermo, 32(2), 157-187.

[16] Srivastava, H., & Manocha, H. (1984). Treatise on generating functions. John Wiley & Sons, New York, Chichester, Brisbane and Toronto 605.

[17] Srivastava, H. M., & Panda, R. (1975). Some expansion theorems and generating relations for the H-function of several complex variables. Comment. Math. Univ. St. Paul., 24(2), 119-137.

[18] Srivastava, H. M. (2021). An introductory overview of fractional-calculus operators based upon the Fox-Wright and related higher transcendental functions. J. Adv. Eng. Comput., 5(3), 135-166.

[19] Suthar, D. L., Purohit, S. D., & Agarwal, S. (2017). Class of integrals involving generalized hypergeometric function and Srivastava's polynomials. Int. J. Appl. Comput. Math., 3(1), 1197-1203.

[20] Suthar, D. L., & Habenom, H. (2016). Integrals involving generalized Bessel-Maitland function. J. Sci. Arts, 16(4), 357.

[21] Tyagi, S., Jain, M., & Singh, J. (2022). Large deflection of a circular plate with incomplete aleph functions under non-uniform load. Int. J. Appl. Comput. Math., 8(5), 267.

[22] Wright, E. M. (1935). The asymptotic expansion of the generalized hypergeometric function. J. London Math. Soc., 1(4), 286-293.

Computational analysis of MHD blood flow of SWCNT and MWCNT suspended nanofluid over a non-linear stretching sheet

Santosh Chaudhary[1], Ajay Singh[1] and Devendra Kumar[2,*]
[1]Department of Mathematics, Malaviya National Institute of Technology, Jaipur-302017, India
Email: d11.santosh@yahoo.com, ajaykaswaan21@gmail.com
[2]Department of Mathematics, University of Rajasthan, Jaipur-302004, India
Email: devendra.maths@gmail.com

December 29, 2023

Abstract

In this study, a computational analysis has been made for a steady, incompressible, MHD flow of the SWCNT-blood and the MWCNT-blood nanofluids past a non-linear stretching sheet of variable thickness. Darcy porous medium has been considered for fluid flow. Consequences of homogeneous-heterogeneous chemical reactions on heat and mass transfer along with Joule heating and viscous dissipation have been explored. Appropriate similarity transformations have been applied to convert the governing equations of nanofluid flow into non-linear ordinary differential equations. Galerkin finite element scheme has been used to examine the resulting system with corresponding boundary conditions. Numerical solutions of equations are demonstrated via graphs for various physical parameters, and these graphs have also been analyzed. Comparison of velocity, thermal, and concentration profiles of SWCNT-blood and MWCNT-blood nanofluids has been established. It is concluded that flow profiles of MWCNT-blood nanofluid dominate. Concentration profile declines with homogeneous and heterogeneous reaction parameters whereas increases with the Schimdt number for both nanofluids. Then, a comparison between present and the existing results was made, and they are in good agreement. After that, several physical quantities such as the local Nusselt number, skin friction coefficient, and concentration rate are exhibited in a table.

Keywords: MHD; Carbon nanotubes; Nanofluid; Stretching sheet

Nomenclatures

$A^\star$	Chemical species
$a^\star$	Concentration of chemical species $A^\star$
a_0	Positive constant
A	Ratio parameter
b	Dimensionless constant
B	Small constant
B_0	Magnitude of magnetic field strength
$B^\star$	Chemical species
$b^\star$	Concentration of chemical species $B^\star$
Br	Brinkman number
C_f	Skin friction coefficient
c_s	Heat capacity of the solid surface
C_p	Specific heat at constant pressure
D_A, D_B	Diffusion coefficients
Ec	Eckert number
F, f	Dimensionless stream function
k_1, k_s	Rate constants
$k^\star, k$	Permeability of porous medium
K	Homogeneous parameter
K_s	Heterogeneous parameter
m	Velocity power index parameter
M	Melting parameter
Nu_x	Local Nusselt number
Pr	Prandtl number
Re_m	Magnetic parameter
Re_x	Local Reynolds number
Sc	Schmidt number
T	Temperature of the fluid within the boundary layer
T_w	Melting surface temperature
T_∞	Ambient temperature
T_0	Temperature of the solid surface
u	Velocity component along $x-$axis
U_w	Non linear stretching velocity
U_e	Free stream velocity
U_∞, U_0	Reference velocities
v	Velocity component along $y-$axis
w_1, w_2, w_3	Weight functions
x	Direction parallel to the fluid flow
y	Direction perpendicular to the fluid flow
Greek symbols	
α	Thermal diffusivity
$\alpha^\star$	Wall thickness parameter
δ	Ratio of diffusion coefficients

ρ	Density
σ_e	Electrical conductivity
κ	Thermal conductivity
λ	Latent heat of the nanofluid
ψ	Stream function
μ	Viscosity
ν	Kinematic viscosity
ϑ, Φ, φ	Dimensionless concentration
ϕ	Solid volume fraction
ψ_s	Shape function
Θ, θ	Dimensionless temperature
ξ	Similarity variable
Subscripts	
bf	Base fluid
nf	Nanofluid
CNT	Carbon nanotubes
Superscripts	
$\prime$	Derivative of the function

1 Introduction

The investigation of fluid behavior of the electrically conducting fluid in a magnetic field is known as magnetohydrodynamics (MHD). The investigation of MHD has been fascinating due to its extensive range of applications in various fields and the property of good heat transfer performance. The applications of MHD flow can be seen in petroleum production, turbines, liquid metal blankets, tritium breeding, and astrophysics sensors. Davidson (2001) appraised the MHD flow problems and explored the basics of MHD and its applications in engineering. After that, Bozkaya and Tezer-Sezgin (2007) brought an elemental solution for equations, which includes convection and diffusion. The impacts of thermal radiation on an unsteady flow are illustrated by Turkyilmazoglu (2011). Ellahi (2013) investigated the MHD non-Newtonian fluid flow. An MHD stagnation-point flow over a porous sheet has been examined by Jalilpour et al. (2014). Shehzad et al. (2015) perceived the impacts of convective heat on an MHD nanofluid flow. Numerical analysis of the MHD stagnation-point flow of a micropolar nanofluid using the Runge-Kutta fourth-order has been performed by Rashidi et al. (2016). Chaudhary et al. (2018) also discussed the MHD flow over a stretching sheet under the Newtonian and convective boundary restrictions. Chaudhary and Kanika (2020) scrutinized viscous dissipation and joule heating effects in a Marangoni boundary layer flow of an electrically conducting fluid in a magnetic field. Mehta et al. (2022) explored the MHD stagnation point stream flow past a vertical porous sheet along with heat generation, viscous dissipation, Joule heating, and thermal effect. Recently, Jain et al. (2023) investigated the MHD spinning fluid flow over a rotating disk with Brownian motion and inverse linear angular velocity.

Nowadays, the applications of nanoproducts are seen significantly in industries, while carbon nanotubes (CNTs) are among them. CNTs having high specific surface areas, high

mechanical strength, and a good conductor of electricity have appreciable applications in industries and other areas, for instance, medicine, sensors, delivery of DNA into cells, and composite materials. Initially, CNTs were explored by Lijima (1991). Wen and Ding (2004) tested the aqueous suspension of carbon nanotubes (CNTs) experimentally and found significant results in enhancing thermal conductivity. After that, Ding et al. (2006) examined the heat transfer capabilities of multi-walled CNT nanofluids. Many studies found that the surface friction is inferior for CNTs, which has been experimentally verified by Whiteby and Quirke (2007). Wang et al. (2008) studied the thermal effects on the vibration of CNTs delegating fluid using the Bernoulli-Euler beam model. The authenticity of different types of theoretical beam models is explored by Wang (2010). Khan et al. (2013) discussed the fluid flow and heat transfer in CNTs nanofluid by applying the Navier slip boundary condition. Further, the Marangoni convective MHD flow with viscous dissipation and joule heating is illustrated by Mahanthesh et al. (2017). Recently, Chaudhary and Kanika (2019) have numerically illustrated the SWCNT and MWCNT-based MHD flow.

To increase heat transfer capabilities, many efforts have been made by researchers. For the same, Choi and Eastman (1995) developed the notion of nanofluid. Nanofluid is a fluid composed of nanometer-sized solid nanoparticles and the base fluid. These nanoparticles are generally made of metals, oxides, and carbides such as Cu, Ag, and CuO. In various investigations, it has been spotted that the thermal conductivity of heat transfer fluid is enhanced when solid nanoparticles are added to traditional fluids. Due to the improved heat transfer capabilities, nanofluids have many applications in cancer therapy, microelectronics, and biomedicine. Initially, Zhou and Ni (2008) performed an experimental study to compute the specific heat capacity of nanofluid and indicated that nanoparticles and base fluid remain in equilibrium in the nanofluid system. The steady boundary layer of a nanofluid over a moving flat plate has been investigated analytically by Bachok et al. (2010). Ahmed et al. (2011) paid their attention to the enlargement in heat transfer in a corrugated channel due to nanofluids. They illustrated it for distinct values of the Reynolds number. The unsteady mixed convection flow and heat transfer of nanofluids past a stretching surface have been numerically analyzed by Mahdy (2012). Rashidi et al. (2014) demonstrated the Buoyancy impact on the MHD flow of an incompressible viscous nanofluid, and non-linear governing equations are numerically handled by the shooting technique. The impact of thermal radiation on an MHD nanofluid flow was explored by Sheikholeslami et al. (2015). They also investigated the heat transfer between two parallel plates. Further, Turkyilmazoglu (2016) explored the efficiency of direct absorption solar collectors using nanofluid, and Ghalandari et al. (2019) illustrated the numerical simulation of nanofluid flow. Chaudhary (2022) examined the impact of nanoparticle shape over a moving plate. The effect of thermal radiation, convective boundary condition, and Brownian motion on the electro-magnetohydrodynamic(EMHD) flow of nanofluid with the Darcy-Forchheimer porous medium has been reported by Chaudhary and Chouhan (2023). Jangid et al. (2023) discussed the MHD flow of Williamson nanofluid past a permeable stretching sheet with buoyancy force, thermal radiation, and Joule heating.

The exploration of heat transformation through the boundary layer over a stretching sheet has attracted scientists to study the important concept due to its many practical uses in diverse fields of science and engineering. Some stretching surface applications include

thermal insulation, solar collectors, glass-fiber and paper production, food processing, and plasma studies. Initially, flow along a stretching sheet was reported by Crane (1970). Further, Mahapatra and Gupta (2002) investigated heat transfer in stagnation-point flow due to a stretching sheet stretched in its plane. The hydromagnetic flow of a micropolar fluid past a stretching surface is explored by Kumar (2009), and for solving the system of governing equations, he used the finite element method. Bachok et al. (2010) reported the steady stagnation-point flow numerically along with a linear stretching/shrinking sheet. A dusty fluid flow over a stretching sheet is illustrated by Gireesha et al. (2011) while considering the influence of heat source/sink. Noghrehabadi et al. (2013) discussed the impacts of thermal convective boundary restrictions on boundary layer flow and heat transfer of nanofluids via a stretching sheet. Further, Noor et al. (2015) and Hsiao (2016) paid their attention to the mixed convection stagnation point flow having slip boundaries by taking different stretching sheets. After that, Chaudhary and Choudhary (2018) illustrated a flow problem along with a stretching sheet with thermal radiation. Recently, Kumar et al. (2023) reported the MHD flow of micropolar liquid over a porous stretching sheet along with heat source, thermal radiation, and slip boundary conditions.

The review of the above-mentioned literature concludes that the study of the influence of homogeneous-heterogeneous chemical reaction on heat and mass transfer of an electro-hydrodynamic flow of nanofluid over a non-linear stretching sheet has not been explored yet. The thickness of the sheet is taken to be variable. The effect of Joule heating and viscous dissipation on heat transfer has been considered. The suspension of SWCNT and MWCNT in human blood has been taken into account. The CNTs have been chosen as nanoparticles due to their high thermal conductivity, exceptional corrosion resistance, and mechanical strength. The Galerkin finite element method is employed to numerically solve the system of equations. The consequences of various controlling parameters are shown visually for velocity, thermal, and concentration profiles. The numeric values of the local skin friction coefficient, Nusselt number, and Sherwood number are presented in the table. The accuracy of the results obtained in the present study is verified with already published work.

2 Problem description

Let us take a steady, two-dimensional, electro-hydrodynamic boundary layer flow of viscous, incompressible nanofluid over a porous non-linear stretching sheet with a variable thickness $y = B(x+b)^{\frac{1-m}{2}}$. B is a small constant, b is a non-dimensional constant, and m is a velocity power index. In addition, the flow is affected by viscous dissipation and ohmic heating. A combination of homogeneously distributed nanoparticles SWCNT and MWCNT in the base fluid− human blood is used as a nanofluid. As demonstrated in Fig. 1, a cartesian coordinate system (x, y) is considered in which carbon nanotubes− SWCNT and MWCNT are also shown symbolically. The $x-$axis is taken in the direction of motion of the non-linear stretching surface, and the $y-$axis is vertical. The flow is bounded in the upper half-plane $y > 0$. A magnetic field of constant strength B_0 is supposed to be used orthogonal to the surface. The induced magnetic field is negligible if the magnetic Reynolds number is minimal. The non-linear stretching velocity $U_w = U_0(x+b)^m$ and free

stream velocity $U_e = U_\infty(x+b)^m$ are considered, here U_0 and U_∞ are the reference velocities. Melting surface temperature T_w is taken to be less than the ambient temperature T_∞. The heat produced throughout the irreversible chemical reaction is not taken into account.

The homogeneous cubic autocatalytic reaction is

$$A^\star + 2B^\star \to 3B^\star, \quad rate = k_1 a^\star b^{\star 2} \tag{1}$$

while on the catalyst surface, the heterogeneous reaction of the first order is as

$$A^\star \to B^\star, \quad rate = k_s a^\star \tag{2}$$

here $a^\star$ and $b^\star$ indicate the concentrations of chemical species $A^\star$ and $B^\star$, respectively, while k_1 and k_s are the rate constants. The reaction rate tends to be zero at the external and outer edges of the boundary layer flow. Under these assumptions, the governing equations for the problem are described as

$$\frac{\partial u}{\partial x} + \frac{\partial v}{\partial y} = 0 \tag{3}$$

$$u\frac{\partial u}{\partial x} + v\frac{\partial u}{\partial y} = U_e\frac{dU_e}{dx} + \nu_{nf}\left[\frac{\partial^2 u}{\partial y^2} - \frac{u}{k} - \frac{(\sigma_e)_{nf}B_0^2}{\mu_{nf}}(u - U_e)\right] \tag{4}$$

$$u\frac{\partial T}{\partial x} + v\frac{\partial T}{\partial y} = \frac{1}{(\rho C_p)_{nf}}\left[\kappa_{nf}\frac{\partial^2 T}{\partial y^2} + \mu_{nf}\left(\frac{\partial u}{\partial y}\right)^2 + (\sigma_e)_{nf}B_0^2(u - U_e)^2\right] \tag{5}$$

$$u\frac{\partial a^\star}{\partial x} + v\frac{\partial a^\star}{\partial y} = D_A\frac{\partial^2 a^\star}{\partial y^2} - k_1 a^\star b^{\star 2} \tag{6}$$

$$u\frac{\partial b^\star}{\partial x} + v\frac{\partial b^\star}{\partial y} = D_B\frac{\partial^2 b^\star}{\partial y^2} + k_1 a^\star b^{\star 2} \tag{7}$$

with the boundary conditions

$$\begin{aligned} y = B(x+b)^{(1-m)/2}: \quad & u = U_w(x), \quad v = 0, \quad T = T_w, \\ & \kappa_{nf}\frac{\partial T}{\partial y} = \rho_{nf}\left[\lambda + c_s(T_w - T_0)\right]v, \\ & D_A\frac{\partial a^\star}{\partial y} = k_s a^\star, \quad D_B\frac{\partial b^\star}{\partial y} = -k_s a^\star \\ y \to \infty: \quad & u \to U_e(x), \quad T \to T_\infty, \quad a^\star \to a_0, \quad b^\star \to 0 \end{aligned} \tag{8}$$

In the above equation, subscript nf indicates the thermophysical characteristics of nanofluid, u, and v denote the velocity components along the $x-$ and $y-$ directions, respectively, $\nu(=\frac{\mu}{\rho})$ is the kinematic viscosity, μ is the dynamic viscosity, ρ is the density, k is the permeability of the porous medium, σ_e stands for the electrical conductivity, T indicate the temperature of nanofluid, C_p stands for the specific heat at constant pressure, κ is indicating the thermal conductivity, D_A, and D_B indicate diffusion coefficients, λ represent the latent heat of the nanofluid, c_s, and T_0 are the heat capacity of the solid surface and temperature, respectively, and a_0 is a positive constant.

Based on the theoretical model, physical properties of the $CNTs-$human blood nanofluid (represented in Table I) are mentioned by Khalid et al. (2018) as

$$\frac{\mu_{nf}}{\mu_{bf}} = \frac{1}{(1-\phi)^{5/2}} \tag{9}$$

$$\frac{\rho_{nf}}{\rho_{bf}} = 1-\phi+\frac{\rho_{CNT}}{\rho_{bf}}\phi \tag{10}$$

$$\frac{(\sigma_e)_{nf}}{(\sigma_e)_{bf}} = 1+\frac{3\left[\frac{(\sigma_e)_{CNT}}{(\sigma_e)_{bf}}-1\right]\phi}{2+\frac{(\sigma_e)_{CNT}}{(\sigma_e)_{bf}}-\left[\frac{(\sigma_e)_{CNT}}{(\sigma_e)_{bf}}-1\right]\phi} \tag{11}$$

$$\frac{(\rho C_p)_{nf}}{(\rho C_p)_{bf}} = 1-\phi+\frac{(\rho C_p)_{CNT}}{(\rho C_p)_{bf}}\phi \tag{12}$$

$$\frac{\kappa_{nf}}{\kappa_{bf}} = \frac{1-\phi+2\frac{\kappa_{CNT}}{\kappa_{CNT}-\kappa_{bf}}ln\frac{\kappa_{CNT}+\kappa_{bf}}{2\kappa_{bf}}\phi}{1-\phi+2\frac{\kappa_{bf}}{\kappa_{CNT}-\kappa_{bf}}ln\frac{\kappa_{CNT}+\kappa_{bf}}{2\kappa_{bf}}\phi} \tag{13}$$

where subscripts bf and CNT are used for base fluid human blood and carbon nanotubes, respectively, and ϕ indicates the volume fraction of $CNTs$.

3 Transformations

Utilizing the non-dimensional variables given by Hayat et al. (2016) are as follows.

$$\begin{aligned}&\psi = \left[\frac{2}{m+1}\nu_{bf}U_0(x+b)^{m+1}\right]^{\frac{1}{2}}F(\xi), \quad \xi = \left[\frac{m+1}{2}\frac{U_0(x+b)^{m-1}}{\nu_{bf}}\right]^{\frac{1}{2}}y,\\ &T = T_w+(T_\infty-T_w)\Theta(\xi), \quad a^\star = a_0\,\vartheta(\xi), \quad b^\star = a_0\,\Phi(\xi)\end{aligned} \tag{14}$$

here $\psi(x,y)$ denotes the stream function, which identically satisfies the mass conservation Eq. (3) along with $u=\frac{\partial\psi}{\partial y}$ and $v=-\frac{\partial\psi}{\partial x}$, $F(\xi)$ is the dimensionless stream function, ξ is the similarity variable, $\Theta(\xi)$ is the dimensionless temperature and, $\vartheta(\xi)$ and $\varphi(\xi)$ are the dimensionless concentrations. Because of the above similarity variables Eq. (14), the Eqs. (4) to (8) are reduced to

$$\begin{aligned}&\frac{1}{(1-\phi)^{5/2}}F'''+\left(1-\phi+\frac{\rho_{CNT}}{\rho_{bf}}\phi\right)\left(FF''-\frac{2m}{1+m}F'^2+\frac{2m}{1+m}A^2\right)\\ &\qquad-\frac{2k^\star}{1+m}\frac{1}{(1-\phi)^{5/2}}F'-\frac{(\sigma_e)_{nf}}{(\sigma_e)_{bf}}\frac{2}{1+m}Re_m\,(F'-A)=0\end{aligned} \tag{15}$$

$$\begin{aligned}&\frac{\kappa_{nf}}{\kappa_{bf}}\Theta''+Pr\left[1-\phi+\frac{(\rho C_p)_{CNT}}{(\rho C_p)_{bf}}\phi\right]F\Theta'+\frac{1}{(1-\phi)^{5/2}}BrF''^2\\ &\qquad+\frac{(\sigma_e)_{nf}}{(\sigma_e)_{bf}}\frac{2}{1+m}BrRe_m(F'-A)^2=0\end{aligned} \tag{16}$$

$$\frac{1}{Sc}\vartheta''+F\vartheta'-\frac{2K}{1+m}\Phi^2\vartheta=0 \tag{17}$$

$$\frac{\delta}{Sc}\Phi'' + F\Phi' + \frac{2K}{1+m}\vartheta\Phi^2 = 0 \tag{18}$$

with the transformed boundary conditions

$$\begin{aligned}
\alpha^\star = B\left(\frac{1+m}{2}\frac{U_0}{\nu_{bf}}\right)^{\frac{1}{2}}: \quad & F = \frac{1-m}{1+m}\alpha^\star, \quad F' = 1, \quad \Theta = 0, \\
& \frac{\kappa_{nf}}{\kappa_{bf}}M\Theta' + Pr\left(1-\phi+\frac{\rho_{CNT}}{\rho_{bf}}\phi\right)\left(F - \frac{1-m}{1+m}\alpha^\star\right) = 0, \\
& \vartheta' = \left(\frac{2}{1+m}\right)^{\frac{1}{2}} K_s\vartheta, \quad \Phi' = -\left(\frac{2}{1+m}\right)^{\frac{1}{2}}\frac{K_s}{\delta}\vartheta \\
\alpha^\star \to \infty: \quad & F' \to A, \quad \Theta \to 1, \quad \vartheta \to 1, \quad \Phi \to 0
\end{aligned} \tag{19}$$

In the above expressions, prime ($'$) represents the derivatives of functions with respect to ξ, $A\ (= \frac{U_\infty}{U_0})$ is the ratio parameter, $k^\star\ \left[= \frac{\nu_{bf}}{kU_0(x+b)^{m-1}}\right]$ is representing the permeability of the porous media, $Re_m\ \left[= \frac{(\sigma_e)_{bf}{B_0}^2(x+b)}{\rho_{bf}U_w}\right]$ is the magnetic parameter, $Pr\ \left[= \left(\frac{\nu\rho C_p}{\kappa}\right)_{bf}\right]$ is the Prandtl number, $Br\ (= PrEc)$ is the Brinkman number, $Ec\ \left[= \frac{U_w^2}{(C_p)_{bf}(T_\infty - T_w)}\right]$ stands for the Eckert number, $Sc\ \left(= \frac{\nu_{bf}}{D_A}\right)$ indicates the Schmidt number, $K\ \left[= \frac{k_1{a_0}^2(x+b)}{U_w}\right]$ is the homogeneous parameter, $\delta\ \left(= \frac{D_B}{D_A}\right)$ is the ratio of diffusion coefficients, $\alpha^\star\ (= \xi)$ is the wall thickness parameter, $M\ \left[= \frac{(C_p)_{bf}(T_\infty - T_w)}{[\lambda + c_s(T_w - T_0)]}\right]$ is the melting parameter, and $K_s\ \left\{= \frac{k_s}{D_A}\left[\frac{\nu_{bf}(x+b)}{U_w}\right]^{\frac{1}{2}}\right\}$ is the heterogeneous parameter. Additionally, in many applications, the diffusion coefficients D_A and D_B are equal, i.e., $\delta = 1$. Eqs. (17) and (18) are reduced to

$$\vartheta'' + Sc\,F\vartheta' - \frac{2}{1+m}K\,Sc\,\vartheta(1-\vartheta)^2 = 0 \tag{20}$$

with $\vartheta + \Phi = 1$

Applying $F(\xi) = f(\xi - \alpha^\star) = f(\eta), \quad \Theta(\xi) = \theta(\xi - \alpha^\star) = \theta(\eta)$
and $\Phi(\xi) = \varphi(\xi - \alpha^\star) = \varphi(\eta)$

Eqs. (15), (16) and (20) with boundary condition Eq. (19) give

$$\begin{aligned}
\frac{1}{(1-\phi)^{5/2}}f''' + \left(1-\phi+\frac{\rho_{CNT}}{\rho_{bf}}\phi\right)\left(ff'' - \frac{2m}{1+m}f'^2 + \frac{2m}{1+m}A^2\right) \\
- \frac{2k^\star}{1+m}\frac{1}{(1-\phi)^{5/2}}f' - \frac{(\sigma_e)_{nf}}{(\sigma_e)_{bf}}\frac{2}{1+m}Re_m\,(f'-A) = 0
\end{aligned} \tag{21}$$

$$\begin{aligned}
\frac{\kappa_{nf}}{\kappa_{bf}}\theta'' + Pr\left[1-\phi+\frac{(\rho C_p)_{CNT}}{(\rho C_p)_{bf}}\phi\right]f\theta' + \frac{1}{(1-\phi)^{5/2}}Brf''^2 \\
+ \frac{(\sigma_e)_{nf}}{(\sigma_e)_{bf}}\frac{2}{1+m}BrRe_m(f'-A)^2 = 0
\end{aligned} \tag{22}$$

$$\varphi'' + Sc\,f\varphi' - \frac{2}{1+m}K\,Sc\,\varphi(1-\varphi)^2 = 0 \tag{23}$$

along with the associated boundary conditions

$$\begin{aligned}
\eta = 0: \quad & f = \frac{1-m}{1+m}\alpha^{\star}, \quad f' = 1, \quad \theta = 0, \\
& \frac{\kappa_{nf}}{\kappa_{bf}} M\theta' + Pr\left(1 - \phi + \frac{\rho_{CNT}}{\rho_f}\phi\right)\left(f - \frac{1-m}{1+m}\alpha^{\star}\right) = 0, \\
& \varphi' = \left(\frac{2}{m+1}\right)^{1/2} K_s \varphi \\
\eta \to \infty: \quad & f' \to A \quad , \quad \theta \to 1 \quad , \quad \varphi \to 1
\end{aligned} \tag{24}$$

here, prime represents the differentiation with respect to η.

4 Physical Quantities

Here, we discuss the physical quantities such as the local skin friction coefficient (C_f) and local Nusselt number (Nu_x), which indicate the flow and heat transfer, respectively and symbolic as (mathematical notation)

$$C_f = \frac{2\mu_{nf}}{\rho_{bf}{U_w}^2}\left(\frac{\partial u}{\partial y}\right)_{y=B(x+b)^{(1-m)/2}}, \quad Nu_x = -\frac{\kappa_{nf}(x+b)}{\kappa_{bf}(T_\infty - T_w)}\left(\frac{\partial T}{\partial y}\right)_{y=B(x+b)^{(1-m)/2}} \tag{25}$$

By employing the similarity transformations Eq. (14), the Eq. (25) can be expressed as

$$\frac{C_f}{Re_x^{-1/2}} = \frac{2}{(1-\phi)^{5/2}}\left(\frac{1+m}{2}\right)^{1/2} f''(0), \quad \frac{Nu_x}{Re_x^{1/2}} = -\frac{\kappa_{nf}}{\kappa_{bf}}\left(\frac{1+m}{2}\right)^{1/2}\theta'(0) \tag{26}$$

where, $Re_x \left[= \frac{U_w(x+b)}{\nu_{bf}}\right]$ is the local Reynolds number.

5 Computational method and accuracy

Eqs. (21) to (23) with the boundary conditions Eq. (24) are handled numerically by employing the Galerkin finite element scheme as depicted by the flow diagram in Fig. 2, which is a well-known computational approach for handling differential equations. The basic idea behind this technique is that the whole domain is discretized into linear elements, and after that, equations are obtained for each element. Furthermore, element equations are assembled, and the equations have been reduced by applying boundary conditions. The remaining equations are handled by using the appropriate technique.

Assume

$$f' = p \tag{27}$$

then Eqs. (21) to (23) are reduced into the below form

$$\frac{1}{(1-\phi)^{5/2}}p'' + \left(1-\phi+\frac{\rho_{CNT}}{\rho_{bf}}\phi\right)\left(fp' - \frac{2m}{1+m}p^2 + \frac{2m}{1+m}A^2\right) - \frac{2k^\star}{1+m}\frac{1}{(1-\phi)^{5/2}}p - \frac{(\sigma_e)_{nf}}{(\sigma_e)_{bf}}\frac{2}{1+m}Re_m\,(p-A) = 0 \tag{28}$$

$$\frac{\kappa_{nf}}{\kappa_{bf}}\theta'' + Pr\left[1-\phi+\frac{(\rho C_p)_{CNT}}{(\rho C_p)_{bf}}\phi\right]f\theta' + \frac{1}{(1-\phi)^{5/2}}Br\,p'^2 + \frac{(\sigma_e)_{nf}}{(\sigma_e)_{bf}}\frac{2}{1+m}BrRe_m(p-A)^2 = 0 \tag{29}$$

$$\varphi'' + Sc\,f\varphi' - \frac{2K}{1+m}Sc\,\varphi(1-\varphi)^2 = 0 \tag{30}$$

and the changed boundary conditions are

$$\begin{aligned}\eta = 0: \quad & f = \left(\frac{1-m}{1+m}\right)\alpha^\star,\ p = 1,\ \theta = 0,\ \varphi' = \left(\frac{2}{1+m}\right)^{1/2}K_s\varphi,\\ & \frac{\kappa_{nf}}{\kappa_{bf}}M\theta' + \left(1-\phi+\frac{\rho_{CNT}}{\rho_{bf}}\phi\right)Pr\left[f - \frac{1-m}{1+m}\alpha^\star\right] = 0\\ \eta\to\infty: \quad & p\to A, \quad \theta\to 1, \quad \varphi\to 1\end{aligned} \tag{31}$$

If the values of η are taken larger than 6, then there are no further changes in the solutions of the system. Keeping this fact and limitations of computation, without loss of generality, $\eta\to\infty$ is taken numerically as $\eta_{max} = 6$. The flow domain is divided into 1,000 linear elements of equal sizes. A typical element (η_r, η_{r+1}) (say) is considered over this element, Eqs. (27) to (30) can be written in the variational form and are defined as follows

$$\int_{\eta_r}^{\eta_{r+1}} w_1(f'-p) = 0 \tag{32}$$

$$\int_{\eta_r}^{\eta_{r+1}} w_2\left[\frac{1}{(1-\phi)^{5/2}}p'' + \left(1-\phi+\frac{\rho_{CNT}}{\rho_{bf}}\phi\right)\left(fp' - \frac{2m}{1+m}p^2 + \frac{2m}{1+m}A^2\right) - \frac{2k^\star}{1+m}\frac{1}{(1-\phi)^{5/2}}p - \frac{(\sigma_e)_{nf}}{(\sigma_e)_{bf}}\frac{2}{1+m}Re_m\,(p-A)\right]d\eta = 0 \tag{33}$$

$$\int_{\eta_r}^{\eta_{r+1}} w_3\left\{\frac{\kappa_{nf}}{\kappa_{bf}}\theta'' + Pr\left[1-\phi+\frac{(\rho C_p)_{CNT}}{(\rho C_p)_{bf}}\phi\right]f\theta' + \frac{1}{(1-\phi)^{5/2}}Br\,p'^2 + \frac{(\sigma_e)_{nf}}{(\sigma_e)_{bf}}\frac{2}{1+m}BrRe_m(p-A)^2\right\}d\eta = 0 \tag{34}$$

$$\int_{\eta_r}^{\eta_{r+1}} w_4\left[\varphi'' + Sc\,f\varphi' - \frac{2K}{1+m}Sc\,\varphi(1-\varphi)^2\right]d\eta = 0 \tag{35}$$

here w_1, w_2, w_3, and w_4 are weight functions corresponding to the functions f, p, θ, and φ, respectively and these functions are given by:

$$\begin{aligned} f &= \sum_{t=1}^{2} f_t \psi_t, \qquad p = \sum_{t=1}^{2} p_t \psi_t, \qquad \theta = \sum_{t=1}^{2} \theta_t \psi_t, \\ \varphi &= \sum_{t=1}^{2} \varphi_t \psi_t \end{aligned} \tag{36}$$

While $w_1 = w_2 = w_3 = w_4 = \psi_s$, s = 1,2,3,4

The shape function ψ_s, for a typical element (η_r , η_{r+1}), is defined as:

$$\psi_1{}^{(r)} = \frac{\eta_{r+1} - \eta}{\eta_{r+1} - \eta_r}, \quad \psi_2{}^{(r)} = \frac{\eta - \eta_r}{\eta_{r+1} - \eta_r}, \quad \eta_r \le \eta \le \eta_{r+1} \tag{37}$$

In matrix form the system of Eqs. (32)-(35) are represented by

$$\begin{bmatrix} [A_{11}] & [A_{12}] & [A_{13}] & [A_{14}] \\ [A_{21}] & [A_{22}] & [A_{23}] & [A_{24}] \\ [A_{31}] & [A_{32}] & [A_{33}] & [A_{34}] \\ [A_{41}] & [A_{42}] & [A_{43}] & [A_{44}] \end{bmatrix} \begin{bmatrix} \{f\} \\ \{p\} \\ \{\theta\} \\ \{\varphi\} \end{bmatrix} = \begin{bmatrix} \{b^1\} \\ \{b^2\} \\ \{b^3\} \\ \{b^4\} \end{bmatrix} \tag{38}$$

where $[A^{ij}]$ and $\{b^i\}$, $i = 1, 2, 3, 4$, are as follows:

$$A_{st}^{11} = \int_{\eta_r}^{\eta_{r+1}} \psi_s \frac{d\psi_t}{d\eta} d\eta,$$

$$A_{st}^{12} = -\int_{\eta_r}^{\eta_{r+1}} \psi_s \psi_t d\eta,$$

$$A_{st}^{13} = A_{st}^{14} = A_{st}^{21} = 0,$$

$$\begin{aligned} A_{st}^{22} = \int_{\eta_r}^{\eta_{r+1}} \Bigg[& -\frac{1}{(1-\phi)^{5/2}} \frac{d\psi_s}{d\eta} \frac{d\psi_t}{d\eta} \\ & + \left(1 - \phi + \frac{\rho_{CNT}}{\rho_{bf}} \phi\right) \left(\bar{f} \psi_s \frac{d\psi_t}{d\eta} - \frac{2m}{1+m} \bar{p} \psi_s \psi_t\right) \\ & - \frac{2k^\star}{1+m} \frac{1}{(1-\phi)^{5/2}} \psi_s \psi_t - \frac{(\sigma_e)_{nf}}{(\sigma_e)_{bf}} \frac{2}{1+m} Re_m \psi_s \psi_t \Bigg] d\eta, \end{aligned}$$

$$A_{st}^{23} = A_{st}^{24} = A_{st}^{31} = 0,$$

$$\begin{aligned} A_{st}^{32} = \int_{\eta_r}^{\eta_{r+1}} \Bigg\{ & \frac{1}{(1-\phi)^{5/2}} Br\, \bar{p}'\, \psi_s \frac{d\psi_t}{d\eta} \\ & + \frac{(\sigma_e)_{nf}}{(\sigma_e)_{bf}} \frac{2}{1+m} Br Re_m \left(\bar{p} - 2A\right) \psi_s \psi_t \Bigg\} d\eta, \end{aligned}$$

$$A_{st}^{33} = \int_{\eta_r}^{\eta_{r+1}} \left\{ -\frac{\kappa_{nf}}{\kappa_{bf}} \frac{d\psi_s}{d\eta} \frac{d\psi_t}{d\eta} + Pr \left[1 - \phi + \frac{(\rho C_p)_{CNT}}{(\rho C_p)_{bf}} \phi \right] \bar{f} \psi_s \frac{d\psi_t}{d\eta} \right\} d\eta,$$

$$A_{st}^{34} = A_{st}^{41} = A_{st}^{42}, A_{st}^{43} = 0,$$

$$A_{st}^{44} = \int_{\eta_r}^{\eta_{r+1}} \left\{ -\frac{d\psi_s}{d\eta} \frac{d\psi_t}{d\eta} + Sc \bar{f} \psi_s \frac{d\psi_t}{d\eta} - \frac{2K}{1+m} Sc \left[(\bar{\varphi} - 2) \bar{\varphi} \psi_s \psi_t + \psi_s \psi_t \right] \right\} d\eta$$

and

$$b_s^1 = 0,$$

$$b_s^2 = -\frac{1}{(1-\phi)^{5/2}} \left(\psi_s \frac{dp}{d\eta} \right)_{\eta_r}^{\eta_{r+1}} - \frac{(\sigma_e)_{nf}}{(\sigma_e)_{bf}} \frac{2}{1+m} Re_m A \int_{\eta_r}^{\eta_{r+1}} \psi_s d\eta - \frac{2m}{1+m} A^2 \left(1 - \phi + \frac{\rho_{CNT}}{\rho_f} \phi \right) \int_{\eta_r}^{\eta_{r+1}} \psi_s d\eta,$$

$$b_s^3 = -\frac{\kappa_{nf}}{\kappa_{bf}} \left(\psi_s \frac{d\theta}{d\eta} \right)_{\eta_r}^{\eta_{r+1}} - \frac{(\sigma_e)_{nf}}{(\sigma_e)_{bf}} \frac{2}{1+m} Br Re_m A^2 \int_{\eta_r}^{\eta_{r+1}} \psi_s d\eta,$$

$$b_s^4 = -\left(\psi_s \frac{d\varphi}{d\eta} \right)_{\eta_r}^{\eta_{r+1}},$$

Where

$$\bar{f} = \sum_{s=1}^{s=2} \bar{f}_s \psi_s \quad , \quad \bar{p} = \sum_{s=1}^{s=2} \bar{p}_s \psi_s,$$

$$\bar{p'} = \sum_{s=1}^{s=2} \bar{p'_s} \psi_s \quad , \quad \bar{\varphi} = \sum_{s=1}^{s=2} \bar{\varphi}_s \psi_s$$

As mentioned, the whole domain is divided into 1,000 linear elements of equal sizes. There are 1001 nodes, and four functions are to be evaluated at each node. Hence, after assembling all the element equations, a matrix is obtained with the order of 4004×4004. After implementing boundary conditions, the system has 3,996 equations that are solved by the Gauss elimination technique while the accuracy of 10^{-7} is maintained.

To ensure precision, credibility, and consistency, we have compared our numerical outcomes with the reported data of Hayat et al. (2016) by imposing some conditions. The comparative results have been shown in Table II, and the accuracy of that validated our numerical computations.

6 Analysis of the Results

This part demonstrates the graphical rendition for viewing the effects of sundry parameters on the velocity, temperature, and concentration distributions of the SWCNT (single-wall carbon nanotube) and MWCNT (multi-wall carbon nanotube) suspended nanofluids by taking base fluid as blood. Also, the values of wall shear stress $f''(0)$, wall heat flux $\theta'(0)$

and concentration rate $\varphi'(0)$, corresponding to changes in physical parameters like power index parameter (m), wall thickness parameter $(\alpha^\star)$, ratio parameter (A), volume fraction parameter (ϕ), permeability parameter $(k^\star)$, magnetic parameter (Re_m), the Brinkman number (Br), the heterogeneous parameter (K_s), the Schmidt number (Sc), and the homogeneous parameter (K), keeping the Prandtl number $Pr(= 25)$ as constant are shown in Table III. Other parameters are taken as constant for unveiling the effect of specific parameters. It is noticed that for the considered profiles as the velocity, temperature, and concentration, MWCNT nanofluid is dominated when compared with SWCNT nanofluid.

Figs. 3−5 are sketched to see the behavior of flow velocity $f'(\eta)$, temperature $\theta(\eta)$, and concentration $\varphi(\eta)$ distributions for various values of power index parameter m, respectively. We notice that velocity $f'(\eta)$ decreases along with the increment in power index parameter m when $\eta < 1.5$ for both SWCNT and MWCNT, while the opposite behavior can be seen when $\eta \geq 1.5$. Increasing the power index parameter m reduces temperature distribution for SWCNT and MWCNT. The concentration profile is shown to have increments along with incremental changes in power index parameter m for both SWCNT and MWCNT. Physically, the enhancement in the power index parameter leads to an increase in the wall thickness parameter. Due to this, a reduction in the stretching of the surface occurs; hence the flow velocity $f'(\eta)$ decreases when $\eta < 1.5$, while if $\eta \geq 1.5$, there is an increment in the stretching of the surface, so the flow velocity $f'(\eta)$ increases. Furthermore, the reduction in the stretching surface leads to a reduction in the thermal boundary layer. Therefore the decrement happens in temperature. Similarly, the stretching of the surface is also a reason behind the increment in concentration profile.

The effect of wall thickness parameter $\alpha^\star$ on the velocity $f'(\eta)$, temperature $\theta(\eta)$, and concentration $\varphi(\eta)$ profiles are displayed in Figs. 6−8, respectively. The velocity of the fluid $f'(\eta)$ enlarges along with the rising values of the wall thickness parameter $\alpha^\star$, while a reduction in both temperature $\theta(\eta)$ and concentration $\varphi(\eta)$ is observed for both types of nanofluids. As the wall thickness parameter enhances, the dynamic viscosity increases and as a consequence, velocity $f'(\eta)$ grows significantly. In contrast, a reduction can be seen in temperature $\theta(\eta)$ and concentration $\varphi(\eta)$.

Figs. 9−11 portray the impact of ratio parameter A on the flow field $f'(\eta)$, temperature field $\theta(\eta)$, and concentration field $\varphi(\eta)$, respectively. It is noted that the flow field $f'(\eta)$, temperature field $\theta(\eta)$, and concentration field $\varphi(\eta)$ enhance along with the increasing values of ratio parameter A for both types of nanofluids. Due to the enlargement in the ratio parameter, the free stream velocity increases to the stretching velocity. Hence, the flow changed in inverted boundary layer fabrication, resulting in the rise in velocity profile $f'(\eta)$. At the same time, dynamic pressure increment leads to a fall off in the temperature profile $\theta(\eta)$.

The impacts of various values of volume fraction parameter ϕ on the dimensionless velocity $f'(\eta)$, temperature $\theta(\eta)$, and concentration $\varphi(\eta)$ are plotted in Figs. 12−14, respectively. These figures have shown that velocity $f'(\eta)$ and concentration $\varphi(\eta)$ have the behavior of acceleration with the enhancing values of volume fraction parameter ϕ. In contrast, the dimensionless temperature decelerates for SWCNT and MWCNT. The nanoparticle volume fraction is directly related to convective flow, so velocity increment happens. Due to the convection effect, the heat transfers from the hot fluid flow to a relatively colder surface. Hence a reduction can be seen in the temperature profile.

Figs. 15−17 exhibit the variation of the permeability parameter $k^\star$ on the velocity $f'(\eta)$, temperature $\theta(\eta)$, and concentration $\varphi(\eta)$ fields, respectively. As the permeability parameter $k^\star$ increases, the flow velocity $f'(\eta)$, temperature $\theta(\eta)$, and concentration $\varphi(\eta)$ decrease for SWCNT and MWCNT. Since the permeability is proportional to the fluid's dynamic viscosity, its booming values retards the motion of the fluid. While the permeability is reversely proportional to the pressure difference, so for the increasing values of $k^\star$, the pressure difference decreases, resulting in the reduction in the temperature profile.

The impact of magnetic parameter Re_m on the velocity, temperature, and concentration are demonstrated in Figs. 18−20, respectively. The rising values of magnetic parameter Re_m lead to a decrease in the velocity, temperature, and concentration profiles for SWCNT and MWCNT nanofluid. The fluid flow becomes more convective along with the escalating values of the magnetic parameter also it is generated by the Lorentz force. The Lorentz force and convective flow produce resistance for the fluidic flow which causes the de-escalation of fluid velocity, temperature, and concentration. Fig. 21 demonstrates the impact of Brinkman number Br on the temperature profile $\theta(\eta)$. The enlargement of Brinkman number Br leads to an increment in temperature $\theta(\eta)$. For both SWCNT and MWCNT, the increment in temperature has happened, so the thermal boundary layer also increases for both nanofluids. Physically, it occurs because the booming values of Brinkman number Br result in more heat generation by viscous dissipation and slower conduction of heat; subsequently, the temperature $\theta(\eta)$ increases significantly.

The impact of heterogeneous parameter K_s on the concentration profile $\varphi(\eta)$ is demonstrated in Fig. 22. It is monitored that the booming values of heterogeneous parameter K_s lead to a fall off in the concentration profile $\varphi(\eta)$ for both SWCNT and MWCNT nanofluids. Since the heterogeneous parameter K_s is reversely proportional to the mass diffusivity, the booming values of K_s cause the reduction in mass diffusivity. Consequently, the decay can be seen in the concentration profile $\varphi(\eta)$.

The variations of the concentration distribution $\varphi(\eta)$ for the distinct values of Schmidt number Sc are manifested in Fig. 23. The concentration profile $\varphi(\eta)$ grows along with the enlarging values of Schmidt number Sc for both nanofluids. It is to be noted that the Schmidt number Sc is the ratio of momentum diffusivity to mass diffusivity. Hence, the mass diffusivity decreases along with the increasing values of the Schmidt number Sc, and as a result, the concentration distribution $\varphi(\eta)$ reduces.

Fig. 24 depicts the impact of homogeneous parameter K on the concentration profile $\varphi(\eta)$. It is discovered that the rise of homogeneous parameter K results in a reduction in the concentration profile $\varphi(\eta)$ for both nanofluids. As homogeneous parameter K increases, the mass diffusion rate decays which in turn slows down the transportation of mass species which results in de-escalation of the mass distribution.

Table III has demonstrated the effects of various parameters like m, $\alpha^\star$, A, ϕ, $k^\star$, Re_m, Br, K_s, Sc, and K on the wall shear stress $f''(0)$, wall heat flux $\theta'(0)$, and the rate of concentration $\varphi'(0)$, with keeping $Pr = 25$ fixed. From Eq. (26), the skin friction coefficient and the local Nusselt number are proportional to the surface shear stress $f''(0)$ and the surface heat flux $\theta'(0)$, respectively. It is observed that the increment in parameters m, $k^\star$, and Re_m leads to a reduction in surface shear stress $f''(0)$ but reverse results are found if parameters $\alpha^\star$, A, and ϕ are taken into account. The heat transfer rate grows along with the booming values of A and Br, while the opposite phenomenon arises for parameters m,

$\alpha^\star$, ϕ, $k^\star$, and Re_m. Furthermore, the incremental changes in parameters A, ϕ, K_s, and Sc cause the enlargement in the rate of concentration $\varphi'(0)$. The reversal behavior is seen for parameters m, $\alpha^\star$, $k^\star$, Re_m, and K. The MWCNT-blood nanofluid has higher surface shear stress $f''(0)$, surface heat flux $\theta'(0)$, and rate of concentration $\varphi'(0)$ when compared with SWCNT-blood nanofluid.

7 Conclusions

In this work, the numerical examination of the influence of homogeneous-heterogeneous chemical reaction on the electro-hydrodynamic flow of nanofluid over a porous non-linear stretching sheet has been carried out. The effect of Joule heating and viscous dissipation on heat transfer has been considered. The Galerkin finite element scheme has been used to find the numerical solution. The main concluding remarks from this work are as follows.

1. The velocity, temperature, concentration, surface shear stress, surface heat flux, and rate of concentration profiles for MWCNT-blood nanofluid are higher than SWCNT-blood nanofluid for all controlling parameters.

2. The velocity reduces for enhancing values of the power index parameter when $\eta < 1.5$ for both types of nanofluids. However, the opposite phenomenon occurs when $\eta \geq 1.5$. The temperature, surface shear stress, surface heat flux, and rate of concentration decrease, while the concentration profile increases for both nanofluids.

3. There is a decrease in temperature, concentration, surface heat flux, and concentration rate as the wall thickness parameter is enhanced whereas the velocity and surface shear stress show opposite behavior for both nanofluids.

4. Velocity, temperature, concentration, surface shear stress, surface heat flux, and rate of concentration increase along with the increment in ratio parameter.

5. Velocity, concentration, surface shear stress, and rate of concentration are enhanced when the volume fraction parameter increases, but the temperature and surface heat flux decrease.

6. Enlargement in permeability parameter and magnetic parameter are results of reduction in the velocity, temperature, concentration, surface shear stress, surface heat flux, and rate of concentration profiles for SWCNT and MWCNT nanofluids.

7. The thermal boundary layer thickness and surface heat flux enhance along with the booming values of the Brinkman number.

8. Concentration profile declines while the concentration rate rises, corresponding to the rising values of the heterogeneous and homogeneous parameters whereas the opposite behavior can be seen for the Schimdt number.

Incorporating the Darcy-Forchheimer porous medium, inclined surface, adding hybrid nanofluids with different shapes, or calculating entropy generation could be the possible direction of future research.

Acknowledgements

Ajay Singh (09/964(0014)/2018-EMR-I) is grateful to CSIR, New Delhi, India, for financial favor in the form of Senior Research Fellowship.

References

[1] A. Mahdy, Unsteady mixed convection boundary layer flow and heat transfer of nanofluids due to stretching sheet, Nuclear Engineering and Design, 249, 248–255, (2012).

[2] A. Noghrehabadi, R. Pourrajab, M. Ghalambaz, Flow and heat transfer of nanofluids over stretching sheet taking into account partial slip and thermal convective boundary conditions, Heat and Mass Transfer, 49 (9), 1357–1366, (2013).

[3] Asma Khalid, Ilyas Khan, Arshad Khan, Sharidan Shafie, I. Tlili, Case study of MHD blood flow in a porous medium with CNTS and thermal analysis, Case Studies in Thermal Engineering, 12, 374–380, (2018).

[4] B. Jalilpour, S. Jafarmadar, D.D. Ganji, A.B. Shotorban, H. Taghavifar, Heat generation/absorption on MHD stagnation flow of nanofluid towards a porous stretching sheet with prescribed surface heat flux, Journal of Molecular Liquids, 195, 194–204 (2014).

[5] B. Mahanthesh, B.J. Gireesha, N.S. Shashikumar, S.A. Shehzad, Marangoni convective MHD flow of SWCNT and MWCNT nanoliquids due to a disk with solar radiation and irregular heat source, Physica E 94, 25–30, (2017).

[6] B.J. Gireesha, G.K. Ramesh, M.S. Abel, C.S. Bagewadi, Boundary layer flow and heat transfer of a dusty fluid flow over a stretching sheet with non-uniform heat source/sink, International Journal of Multiphase Flow, 37, 977–982, (2011).

[7] C. Bozkaya, M. Tezer-Sezgin, Fundamental solution for coupled magnetohydrodynamic flow equations, Journal of Computational and Applied Mathematics, 203, 125–144 (2007).

[8] D. Wen, Y. Ding, Effective thermal conductivity of aqueous suspensions of carbon nanotubes (Carbon Nanotube Nanofluids), Journal of Thermophysics and Heat Transfer, 18 (4), 481–485, (2004).

[9] K.L. Hsiao, Stagnation electrical MHD nanofluid mixed convection with slip boundary on a stretching sheet, Applied Thermal Engineering, 98, 850–861, (2016).

[10] L. Kumar, Finite element analysis of combined heat and mass transfer in hydromagnetic micropolar flow along a stretching sheet, Computational Materials Science, 46, 841–848, (2009).

[11] L. Wang, Q. Ni, M. Li, Q. Qian, The thermal effect on vibration and instability of carbon nanotubes conveying fluid, Physica E, 40, 3179–3182, (2008).

[12] L. Wang, Wave propagation of fluid-conveying single-walled carbon nanotubes via gradient elasticity theory, Computational Materials Science, 49, 761–766, (2010).

[13] L.J. Crane, Flow past a Stretching Plate, Journal of Applied Mathematics and Physics 21, 645–647, (1970).

[14] M. Ghalandari, E.M. Koohshahi, F. Mohamadian, S. Shamshirband, K.W. Chau, Numerical simulation of nanofluid flow inside a root canal, Engineering Applications of Computational Fluid Mechanics, 13 (1), 254–264, (2019).

[15] M. Sheikholeslami, D.D. Ganji, M.Y. Javed, R. Ellahi, Effect of thermal radiation on magnetohydrodynamics nanofluid flow and heat transfer by means of two phase model, Journal of Magnetism and Magnetic Materials, 374, 36–43, (2015).

[16] M. Turkyilmazoglu, Performance of direct absorption solar collector with nanofluid mixture, Energy Conversion and Management, 114, 1–10, (2016).

[17] M. Turkyilmazoglu, Thermal radiation effects on the time-dependent MHD permeable flow having variable viscosity, International Journal of Thermal Sciences, 50, 88–96, (2011).

[18] M. Whitby, N. Quirke, Fluid flow in carbon nanotubes and nanopipes, Nature Nanotechnology, 2 (2), 87–94, (2007).

[19] M.A. Ahmed, N.H. Shuaib, M.Z. Yusoff, A.H. Al-Falahi, Numerical investigations of flow and heat transfer enhancement in a corrugated channel using nanofluid, International Communications in Heat and Mass Transfer, 38, 1368–1375, (2011).

[20] M.M. Rashidi, M. Reza, S. Gupta, MHD stagnation point flow of micropolar nanofluid between parallel porous plates with uniform blowing, Powder Technology, 301, 876–885, (2016).

[21] M.M. Rashidi, N.V. Ganesh, A.K.A. Hakeem, B. Ganga, Buoyancy effect on MHD flow of nanofluid over a stretching sheet in the presence of thermal radiation, Journal of Molecular Liquids, 198, 234–238, (2014).

[22] N. Bachok, A. Ishak, I. Pop, Boundary-layer flow of nanofluids over a moving surface in a flowing fluid, International Journal of Thermal Sciences, 49, 1663–1668, (2010).

[23] N. Bachok, A. Ishak, I. Pop, Melting heat transfer in boundary layer stagnation-point flow towards a stretching/shrinking sheet, Physics Letters A, 374, 4075–4079, (2010).

[24] N.F.M. Noor, R.U. Haq, S. Nadeem, I. Hashim, Mixed convection stagnation flow of a micropolar nanofluid along a vertically stretching surface with slip effects, Meccanica, 50 (8), 2007–2022, (2015).

[25] P.A. Davidson, An introduction to Magnetohydrodynamics, Cambridge University Press (2001).

[26] R. Ellahi, The effects of MHD and temperature dependent viscosity on the flow of non-Newtonian nanofluid in a pipe: Analytical solutions, Applied Mathematical Modelling, 37, 1451–1467, (2013).

[27] R. Jain, R. Mehta, T. Mehta, J. Singh, D. Baleanu, MHD flow and heat and mass transport investigation over a decelerating disk with Ohmic heating and diffusive effect, Thermal Science, 27, 141–149, (2023).

[28] R. Kumar, J. Singh, R. Mehta, D. Kumar, D. Baleanu, Analysis of the impact of thermal radiation and velocity slip on the melting of magnetic hydrodynamic micropolar fluid-flow over an exponentially stretching sheet, Thermal Science, 27, 311–322, (2023).

[29] R. Mehta, R. Kumar, H. Rathore, J. Singh, Joule heating effect on radiating MHD mixed convection stagnation point flow along vertical stretching sheet embedded in a permeable medium and heat generation/absorption, Heat Transfer (Wiley), 51, 7369–7386, (2022).

[30] S. Chaudhary, Analysis of Cu water nanofluid flow with different particle shapes over an isothermal moving plate, Indian Journal of Chemical Technology, 29, 311–317, (2022).

[31] S. Chaudhary, K.K. Chouhan, Darcy-Forchheimer flow of Prandtl-Eyring nanofluid subjected to a Riga plate of varying thickness along with Brownian diffusion, thermophoresis and non-uniform heat source/sink effects, Numerical Heat Transfer, Part A: Applications, 84, 732–759, (2023).

[32] S. Chaudhary, KM Kanika, M.K. Choudhary, Newtonian heating and convective boundary condition on MHD stagnation point flow past a stretching sheet with viscous disipation and joule heating, Indian Journal of Pure and Applied Physics, 56, 931–940, (2018).

[33] S. Chaudhary, KM Kanika, Radiation heat transfer on SWCNT and MWCNT based magnetohydrodynamic nanofluid flow with Marangoni convection, Physica Scripta, 95 (2) (2019).

[34] S. Chaudhary, KM Kanika, Viscous dissipation and Joule heating in MHD Marangoni boundary layer flow and radiation heat transfer of Cu-water nanofluid along particle shapes over an exponential temperature, International Journal of Computer Mathematics, 97 (5), 943–958, (2020).

[35] S. Chaudhary, M.K. Choudhary, Partial slip and thermal radiation effects on hydromagnetic flow Over an exponentially stretching surface with suction or blowing, Thermal Science, 22 (2), 797–808, (2018).

[36] S. Jangid, R. Mehta, J. Singh, D. Baleanu, A.S. Alshomrani, Heat and mass transport of hydromagnetic williamson nanofluid passing through a permeable media across an extended sheet of varying thickness, Thermal Science, 27, 141-149, (2023).

[37] S. Lijima, Helical microtubules of graphitic carbon, Nature, 354, 56–58, (1991).

[38] S.-Q. Zhou, R. Ni, Measurement of the specific heat capacity of water-based Al_2O_3 nanofluid, Applied Physics Letters, 92 (9), 093123, (2008).

[39] S.A. Shehzad, T. Hayat, A. Alsaedi, Influence of convective heat and mass conditions in MHD flow of nanofluid, Bulletin of the Polish Academy of Sciences-Technical Sciences, 63, 465–474, (2015).

[40] S.U.S. Choi, J.A. Eastman, Enhancing thermal conductivity of fluids with nanoparticles, Publ. Fed 231ASME, 99–106, (1995).

[41] T. Hayat, Zakir Hussain, A. Alsaedi, S. Asghar, Carbon nanotubes effects in the stagnation point flow towards a nonlinear stretching sheet with variable thickness, Advanced Powder Technology, 27, 1677–1688, (2016).

[42] T.R. Mahapatra, A.S. Gupta, Heat transfer in stagnation-point flow towards a stretching sheet, Heat and mass transfer, 38, 517–521, (2002).

[43] W.A. Khan, Z.H. Khan, M. Rahi, Fluid flow and heat transfer of carbon nanotubes along a flat plate with Navier slip boundary, Applied Nanoscience, 4 (5), 633–641, (2013).

[44] Y. Ding, H. Alias, D. Wen, R.A. Williams, Heat transfer of aqueous suspensions of carbon nanotubes (CNT nanofluids), International Journal of Heat and Mass Transfer, 49, 240-250, (2006).

Table I: Thermophysical properties of used materials

Properties	Human Blood	SWCNT	MWCNT
$\rho(Kg/m^3)$	1053	2600	1600
$\sigma_e(S/m)$	0.8	$10^6 - 10^7$	1.9×10^{-4}
$C_p(J/KgK)$	3594	425	796
$\kappa(W/mK)$	0.492	6600	3000

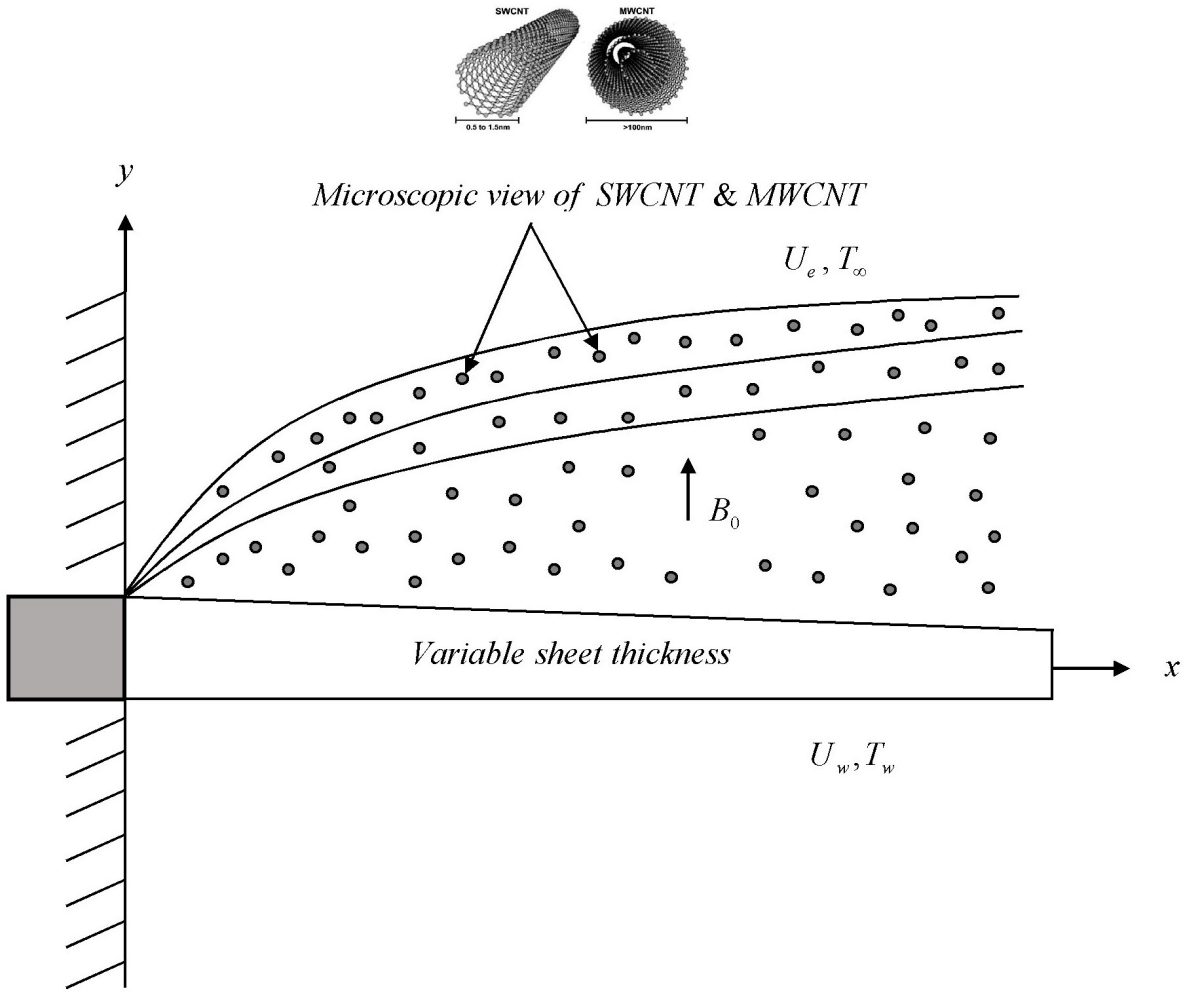

Figure 1: Sketch of the physical problem

Table II: Comparison of $-f''(0)$ with previously data when $m = 1$, $\alpha^\star =$ may have any value, $\phi = 0$, $Re_m = 0$

A	$k^\star$	Hayat et al. [2016]	Present results
0.1	0.0	0.969379	0.969436
0.2		0.918106	0.918113
0.5		0.667262	0.667264
0.0	0.5	1.2247	1.224776
	1.0	1.4142	1.414216
	1.5	1.5811	1.581139
	2.0	1.7320	1.732051
	5.0	2.4494	2.449490

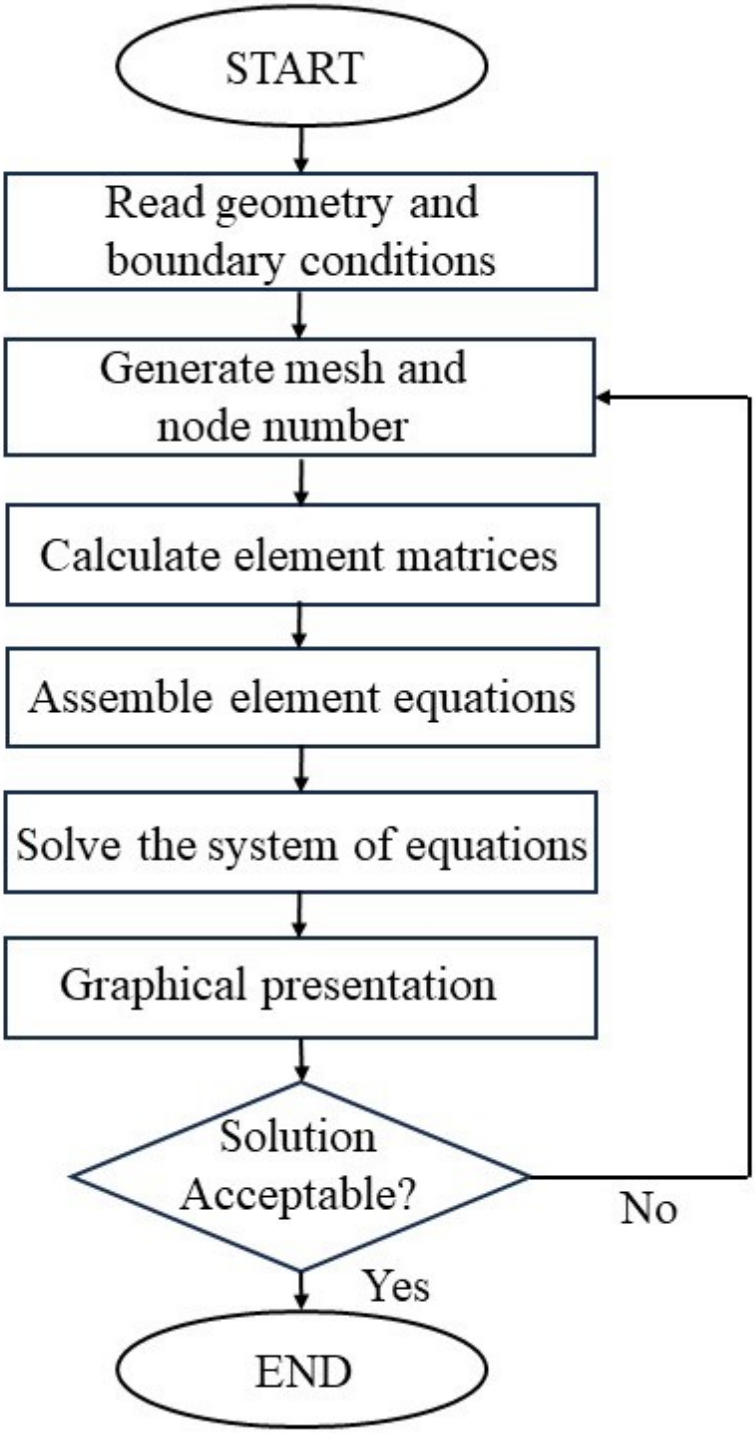

Figure 2: Flow chart of Galerkin finite element scheme

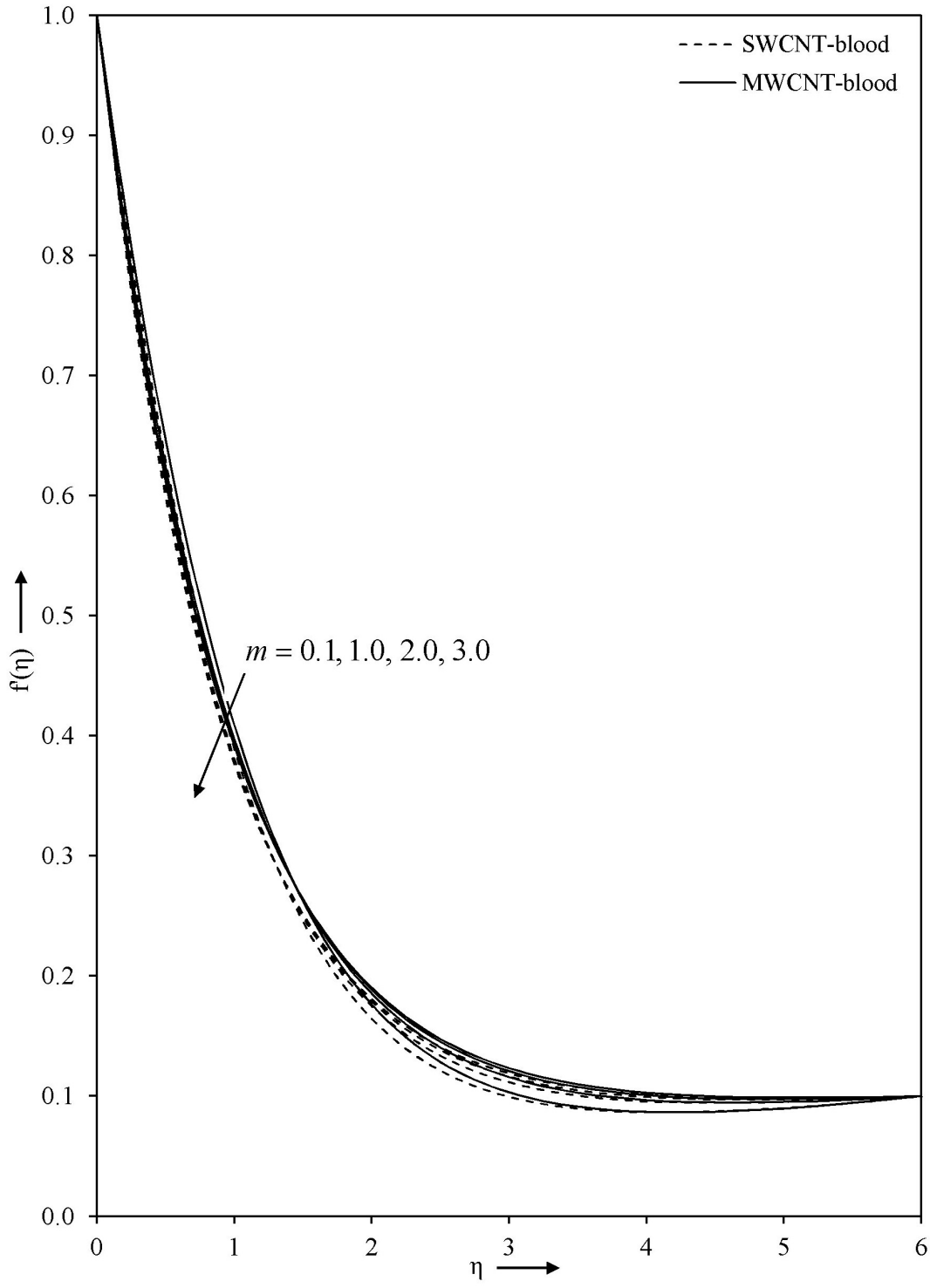

Figure 3: Impact of power index parameter m on velocity profile with $\alpha^\star = 0.1$, $A = 0.1$, $\phi = 0.1$, $k^\star = 0.1$ and $Re_m = 0.1$

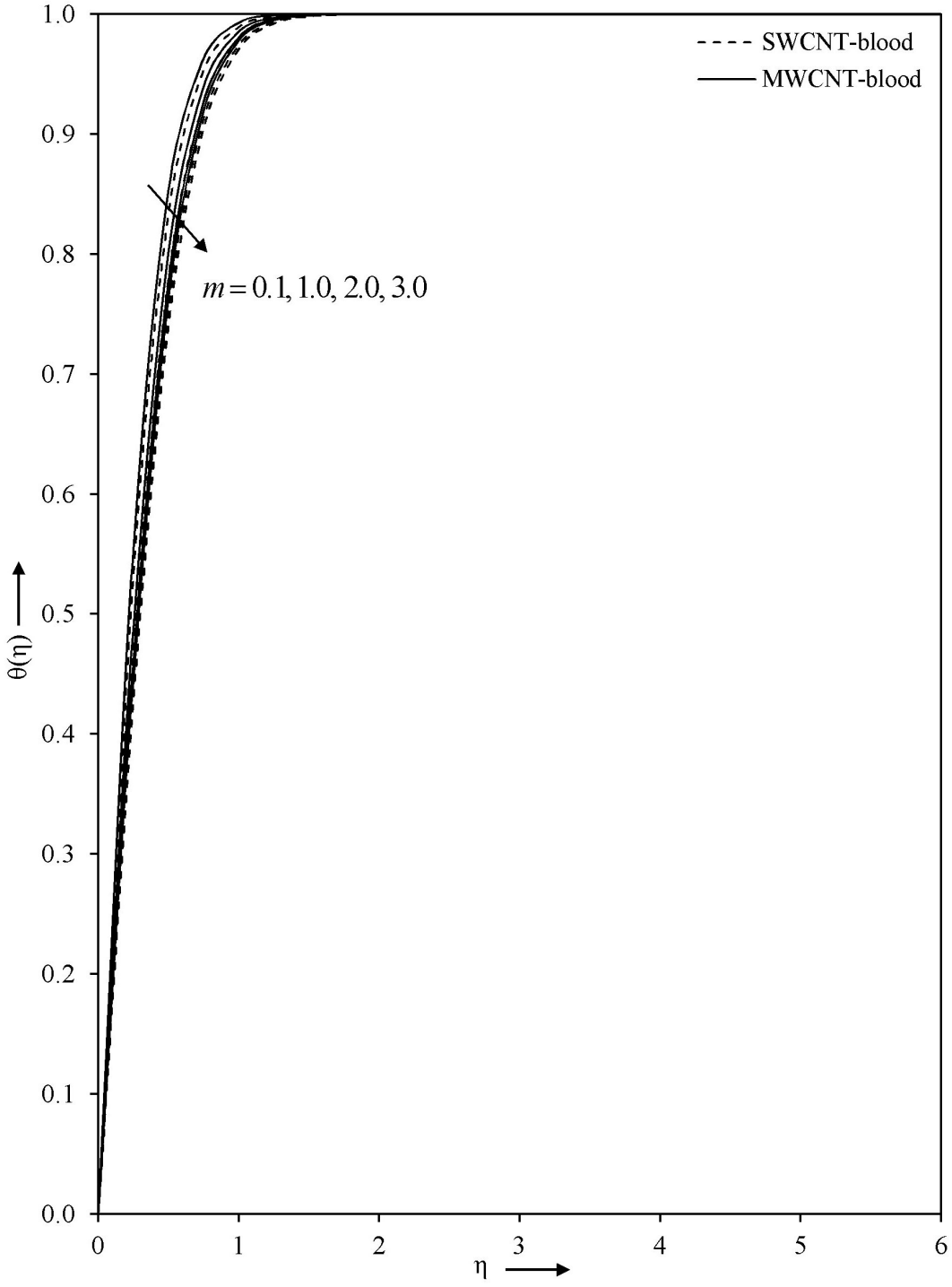

Figure 4: Impact of power index parameter m on temperature profile with $\alpha^{\star} = 0.1$, $A = 0.1$, $\phi = 0.1$, $k^{\star} = 0.1$, $Re_m = 0.1$, $Pr = 25$ and $Br = 0.1$

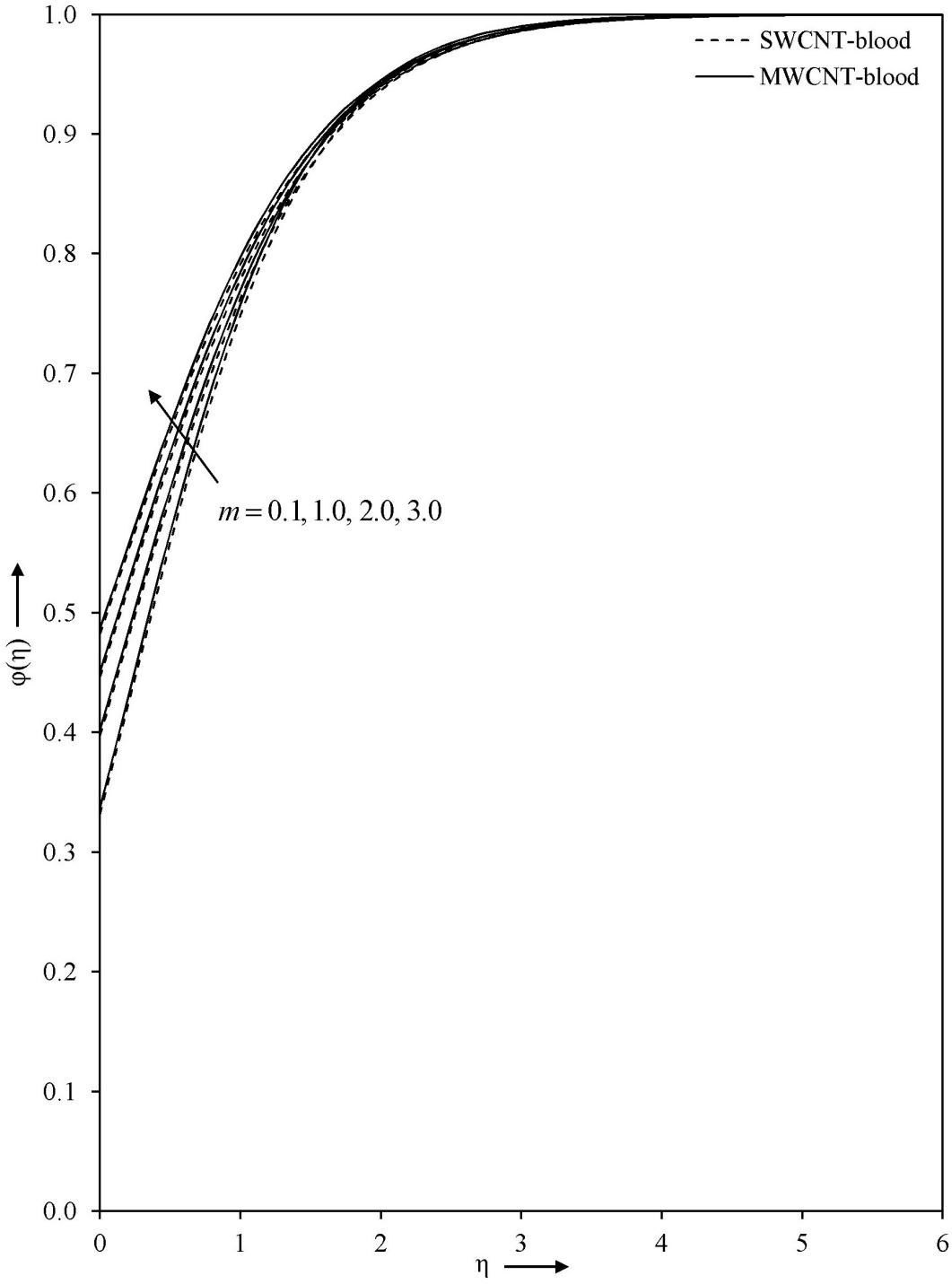

Figure 5: Impact of power index parameter m on concentration profile with $\alpha^{\star} = 0.1$, $A = 0.1$, $\phi = 0.1$, $k^{\star} = 0.1$, $Re_m = 0.1$, $K_s = 1.0$, $Sc = 1.5$ and $K = 0.5$

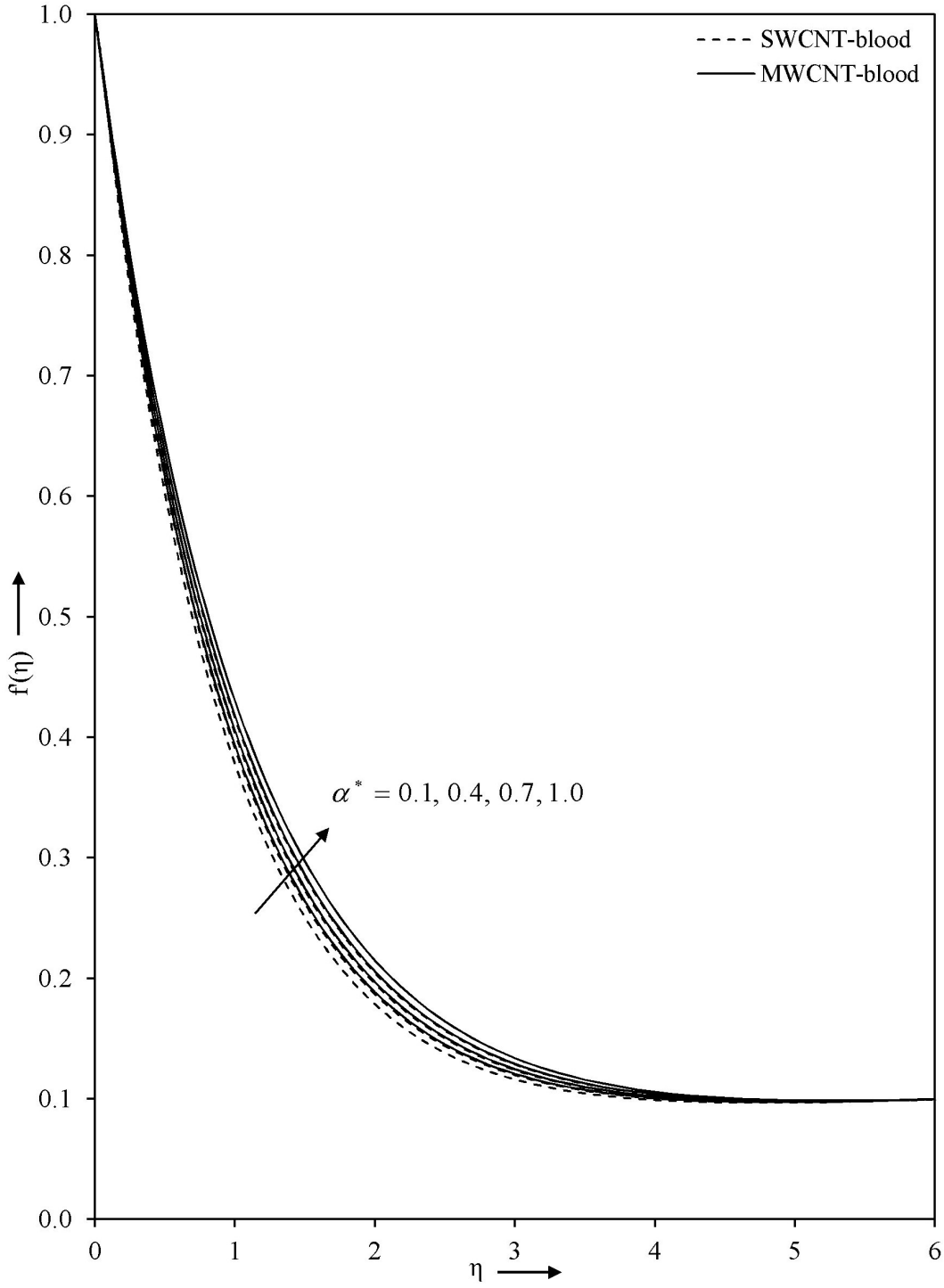

Figure 6: Impact of wall thickness parameter $\alpha^\star$ on velocity profile with $m = 2.0$, $A = 0.1$, $\phi = 0.1$, $k^\star = 0.1$ and $Re_m = 0.1$

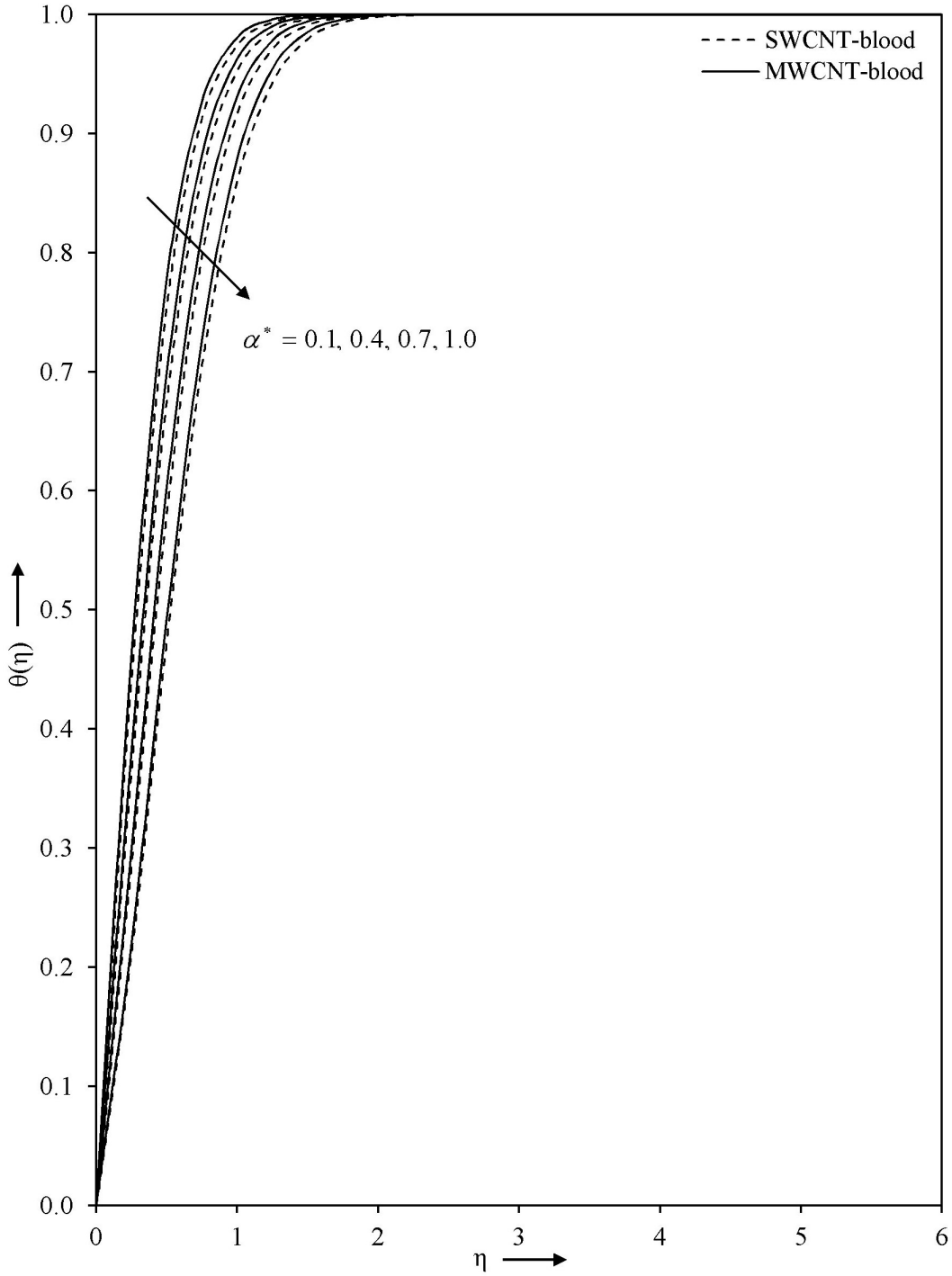

Figure 7: Impact of wall thickness parameter $\alpha^\star$ on temperature profile with $m = 2.0$, $A = 0.1$, $\phi = 0.1$, $k^\star = 0.1$, $Re_m = 0.1$, $Pr = 25$ and $Br = 0.1$

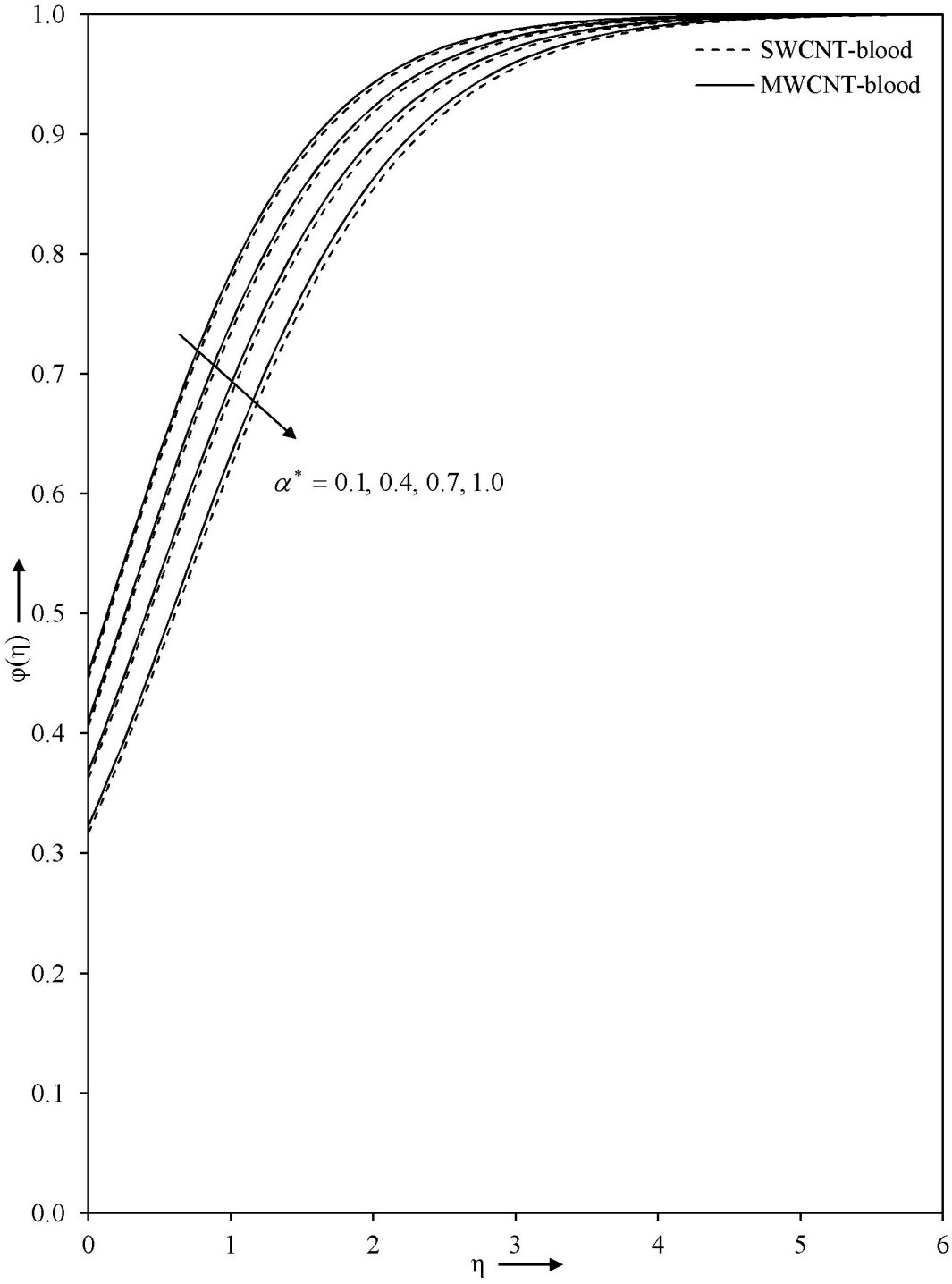

Figure 8: Impact of wall thickness parameter $\alpha^\star$ on concentration profile with $m = 2.0$, $A = 0.1$, $\phi = 0.1$, $k^\star = 0.1$, $Re_m = 0.1$, $K_s = 1.0$, $Sc = 1.5$ and $K = 0.5$

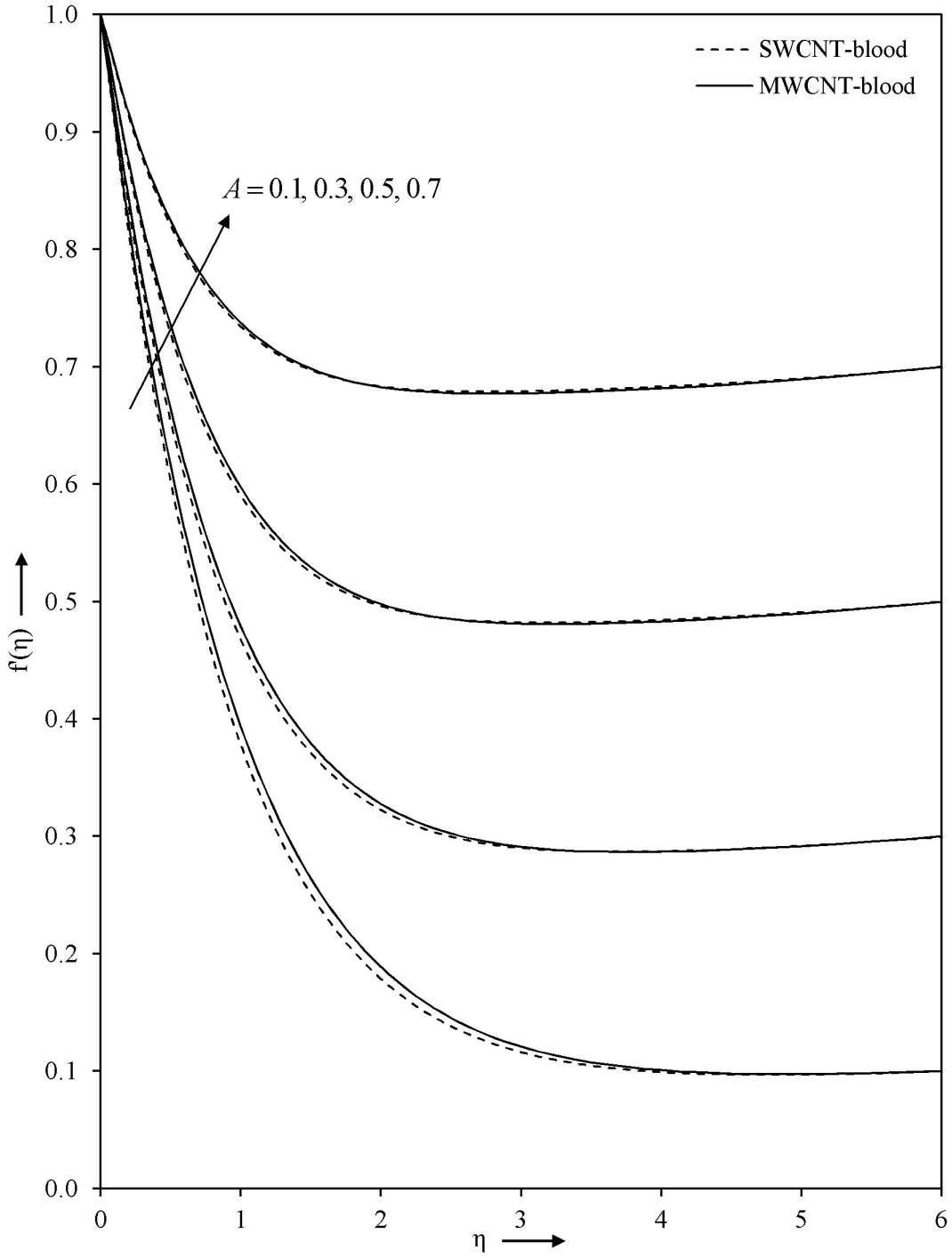

Figure 9: Impact of ratio parameter A on velocity profile with $m = 2.0$, $\alpha^{\star} = 0.1$, $\phi = 0.1$, $k^{\star} = 0.1$ and $Re_m = 0.1$

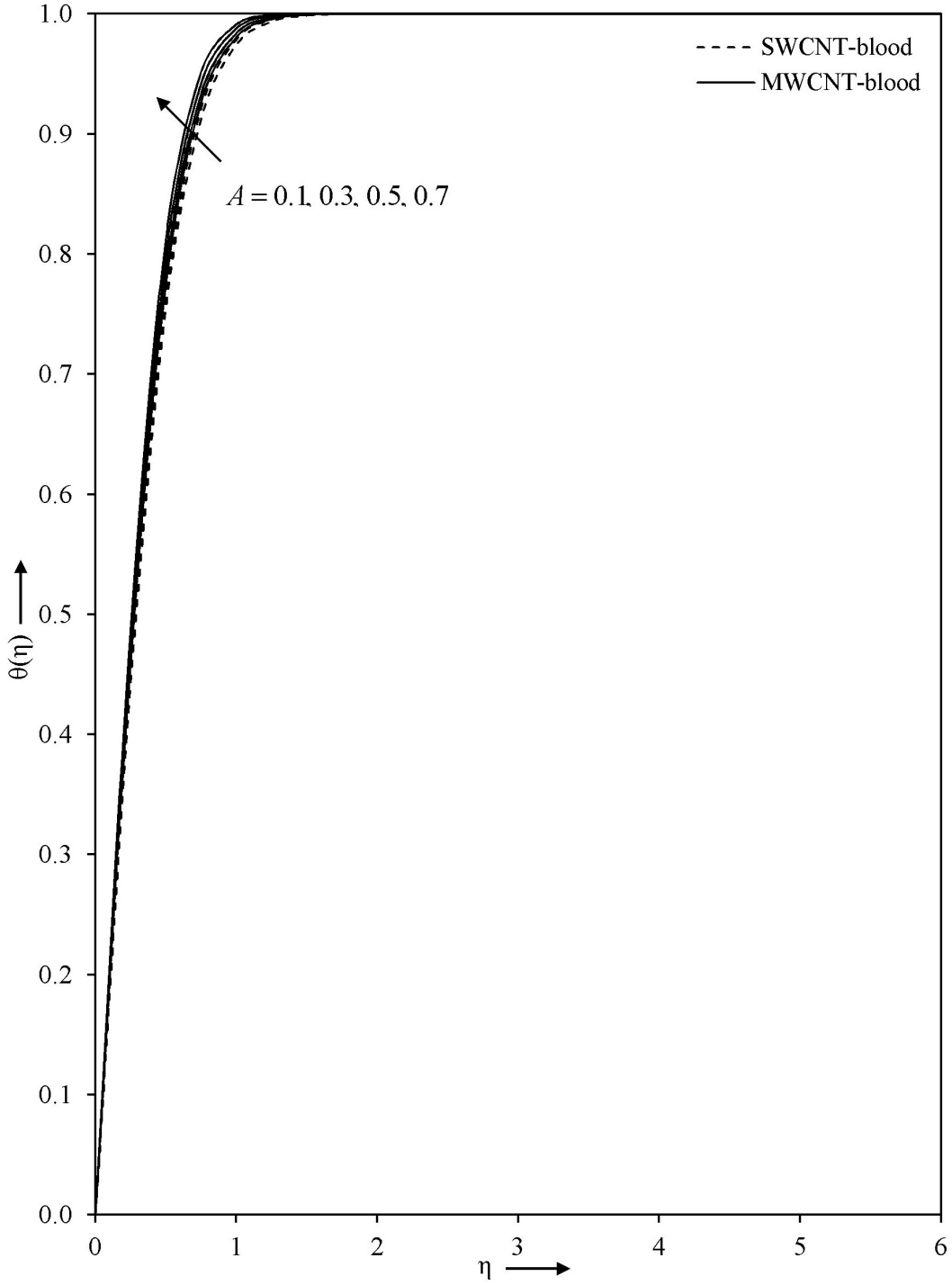

Figure 10: Impact of ratio parameter A on temperature profile with $m = 2.0$, $\alpha^{\star} = 0.1$, $\phi = 0.1$, $k^{\star} = 0.1$, $Re_m = 0.1$, $Pr = 25$ and $Br = 0.1$

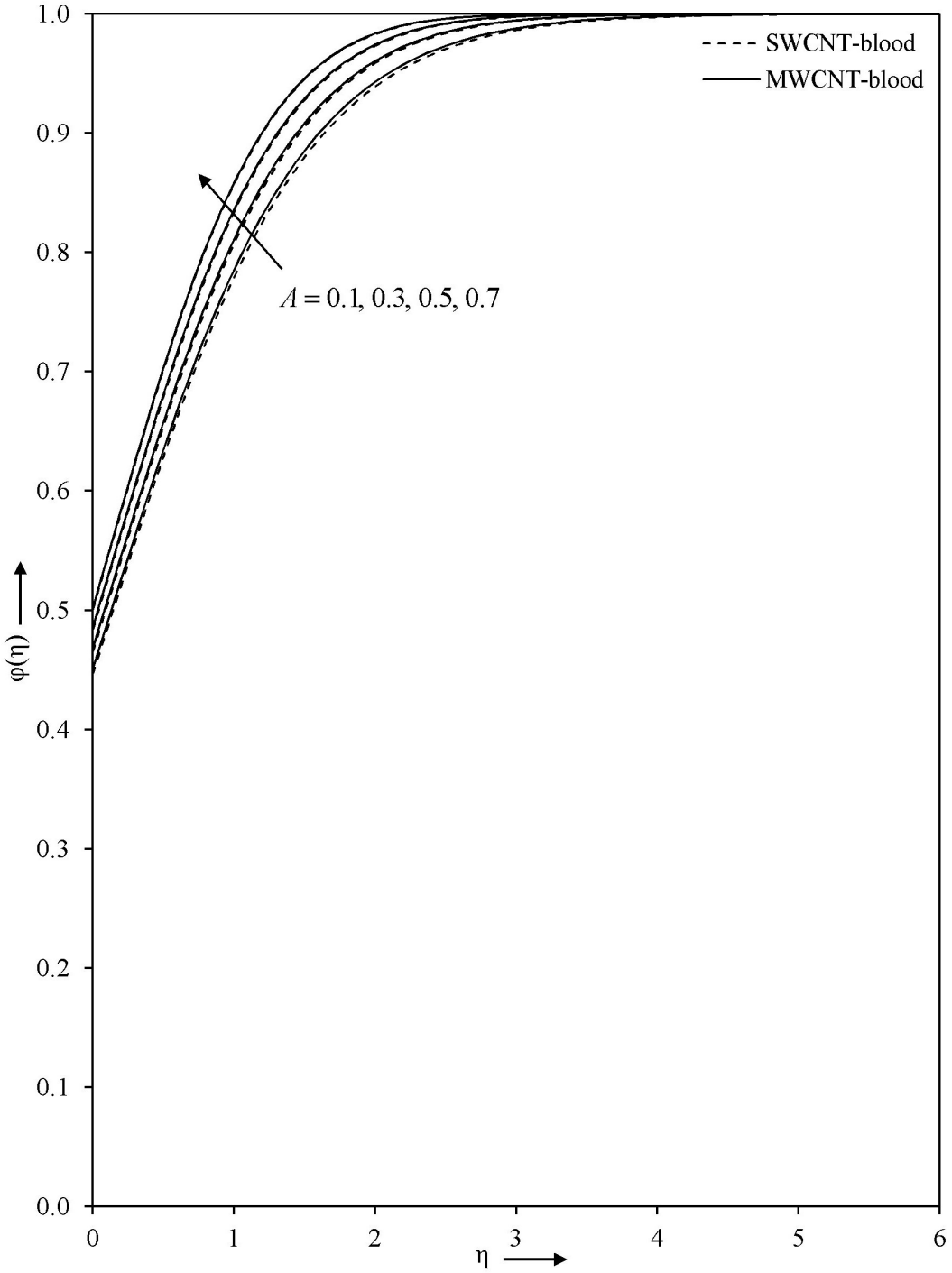

Figure 11: Impact of ratio parameter A on concentration profile with $m = 2.0$, $\alpha^{\star} = 0.1$, $\phi = 0.1$, $k^{\star} = 0.1$, $Re_m = 0.1$, $K_s = 1.0$, $Sc = 1.5$ and $K = 0.5$

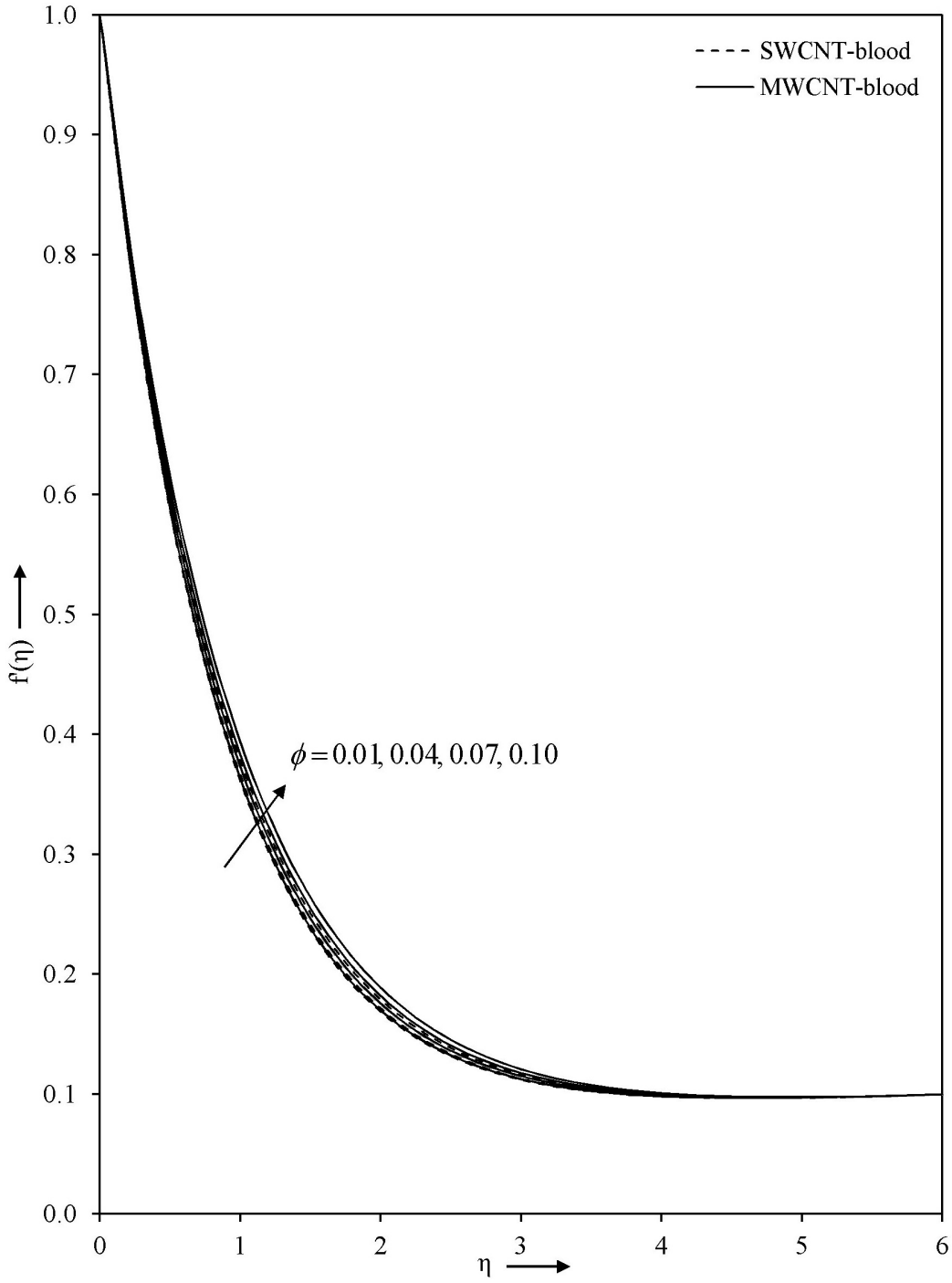

Figure 12: Impact of volume fraction parameter ϕ on velocity profile with $m = 2.0$, $\alpha^\star = 0.1$, $A = 0.1$, $k^\star = 0.1$ and $Re_m = 0.1$

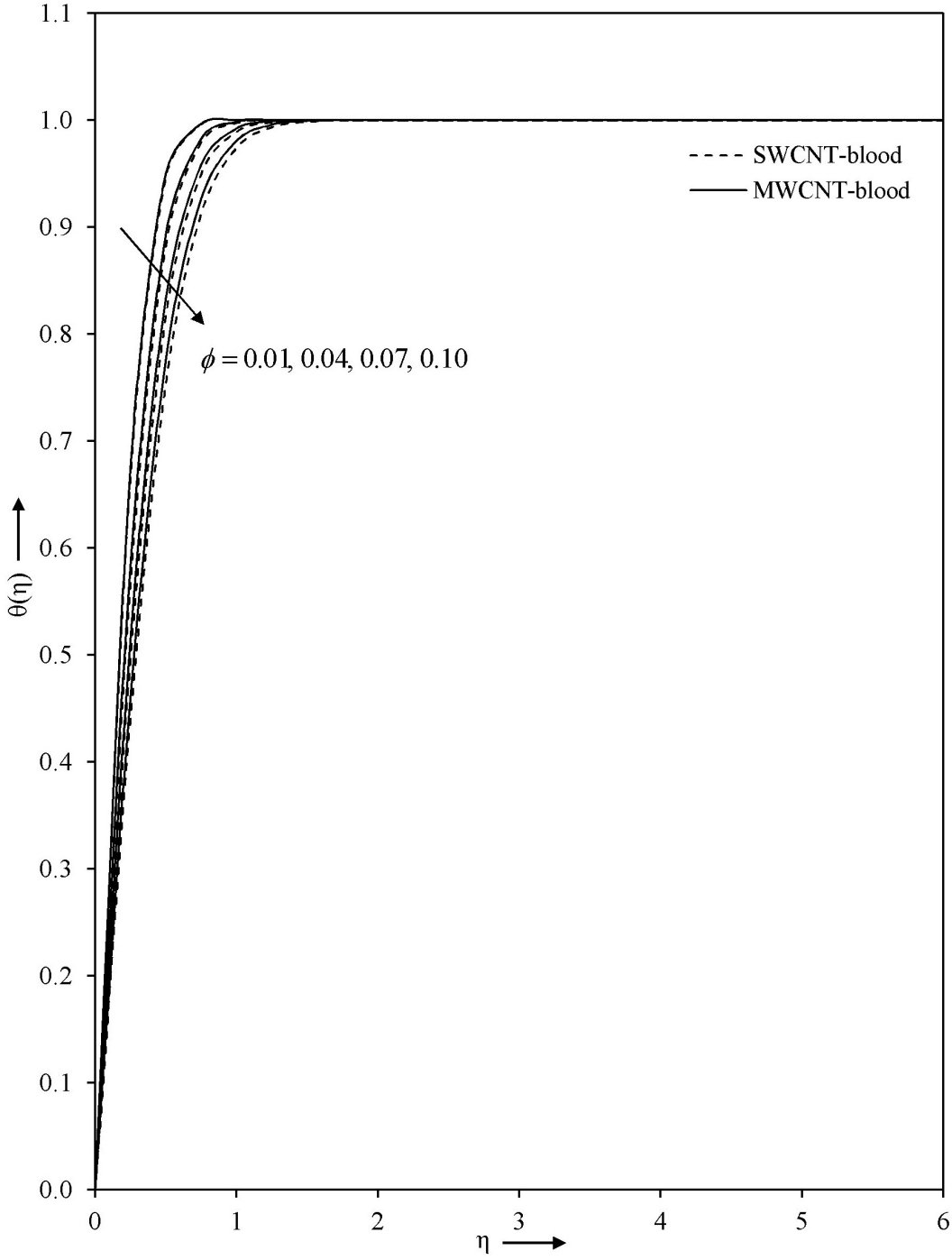

Figure 13: Impact of volume fraction parameter ϕ on temperature profile with $m = 2.0$, $\alpha^{\star} = 0.1$, $A = 0.1$, $k^{\star} = 0.1$, $Re_m = 0.1$, $Pr = 25$ and $Br = 0.1$

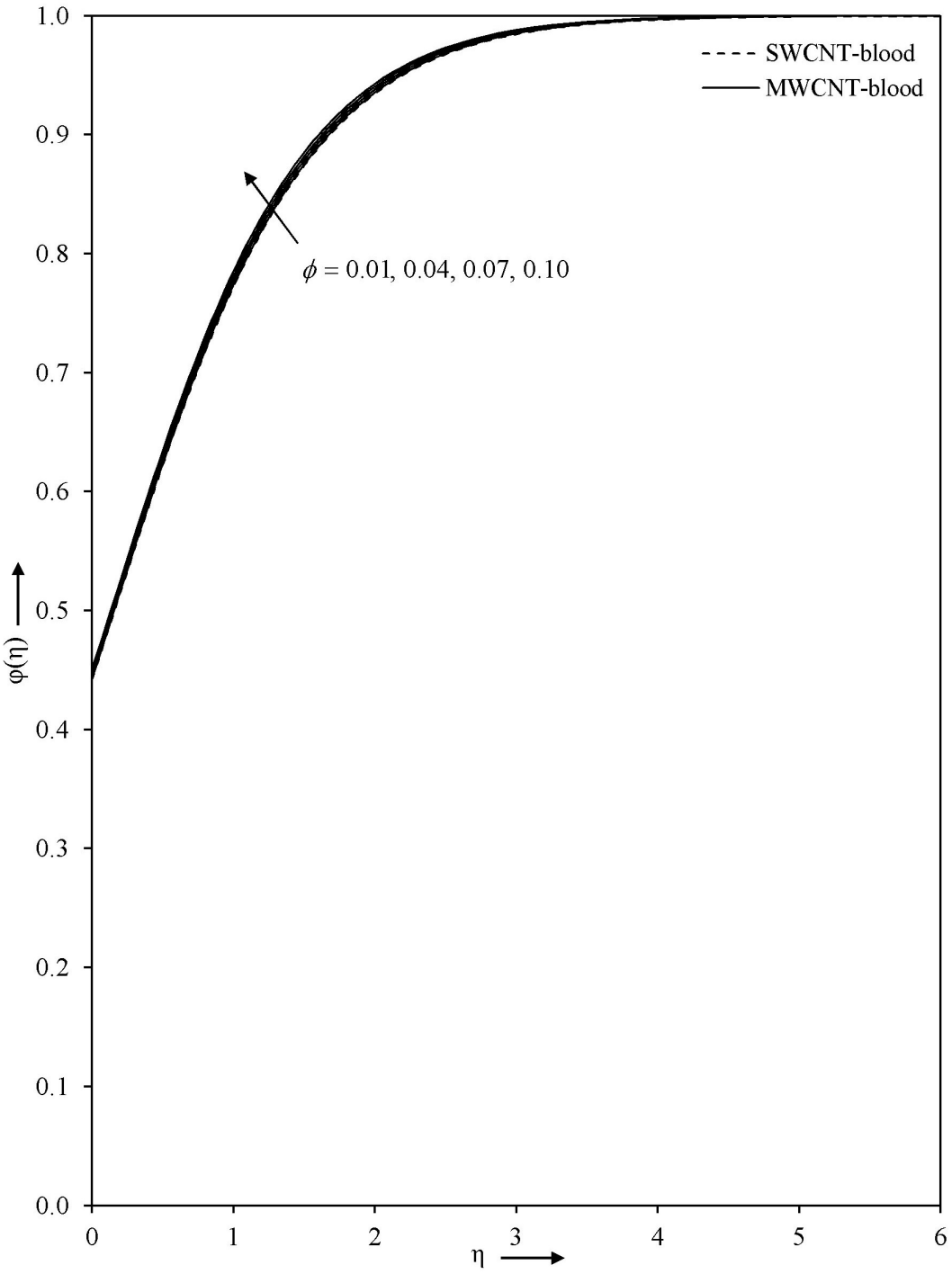

Figure 14: Impact of volume fraction parameter ϕ on concentration profile with $m = 2.0$, $\alpha^{\star} = 0.1$, $A = 0.1$, $k^{\star} = 0.1$, $Re_m = 0.1$, $K_s = 1.0$, $Sc = 1.5$ and $K = 0.5$

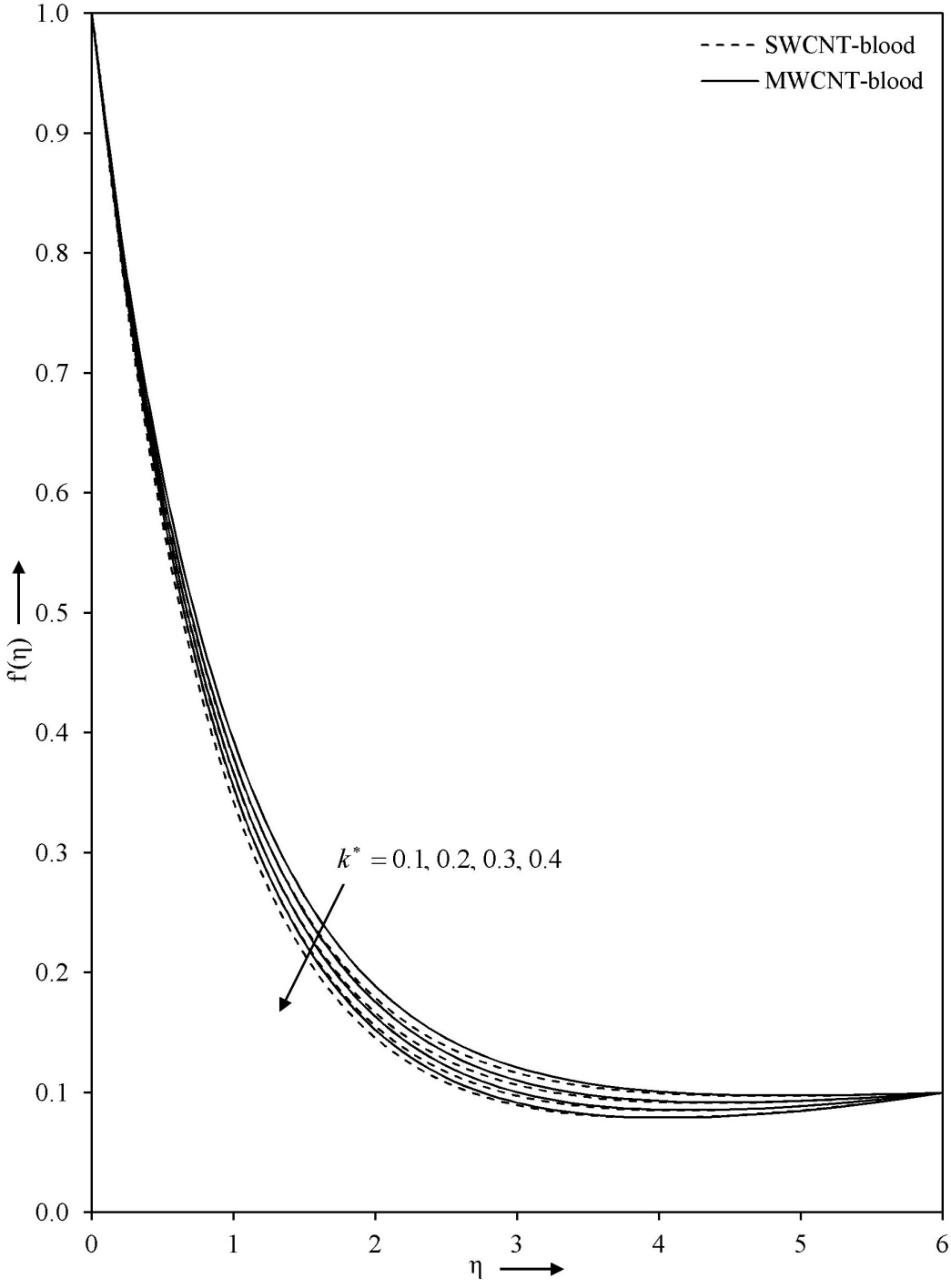

Figure 15: Impact of permeability parameter $k^\star$ on velocity profile with $m = 2.0$, $\alpha^\star = 0.1$, $A = 0.1$, $\phi = 0.1$ and $Re_m = 0.1$

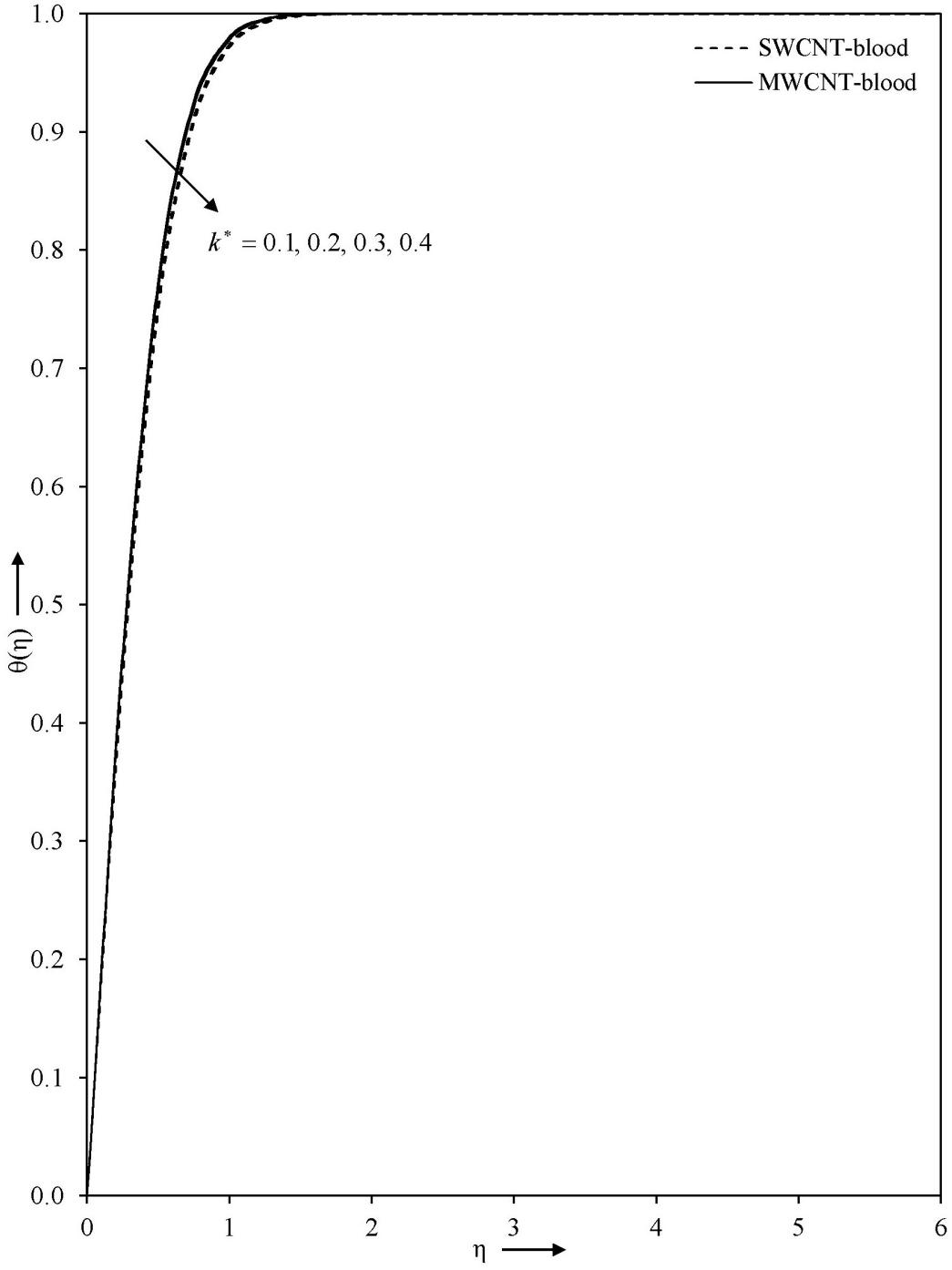

Figure 16: Impact of permeability parameter $k^\star$ on temperature profile with $m = 2.0$, $\alpha^\star = 0.1$, $A = 0.1$, $\phi = 0.1$, $Re_m = 0.1$, $Pr = 25$ and $Br = 0.1$

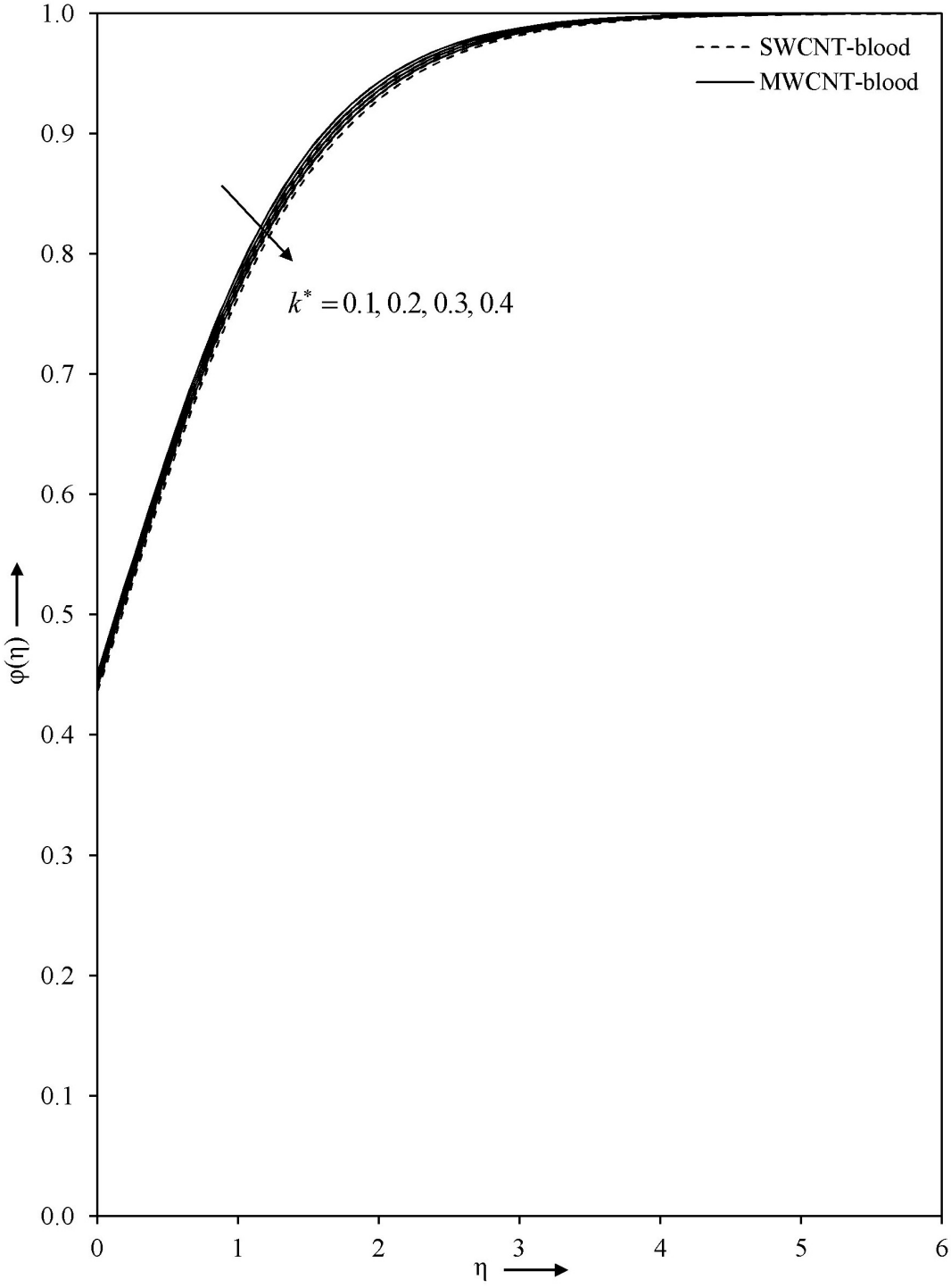

Figure 17: Impact of permeability parameter $k^\star$ on concentration profile with $m = 2.0$, $\alpha^\star = 0.1$, $A = 0.1$, $\phi = 0.1$, $Re_m = 0.1$, $K_s = 1.0$, $Sc = 1.5$ and $K = 0.5$

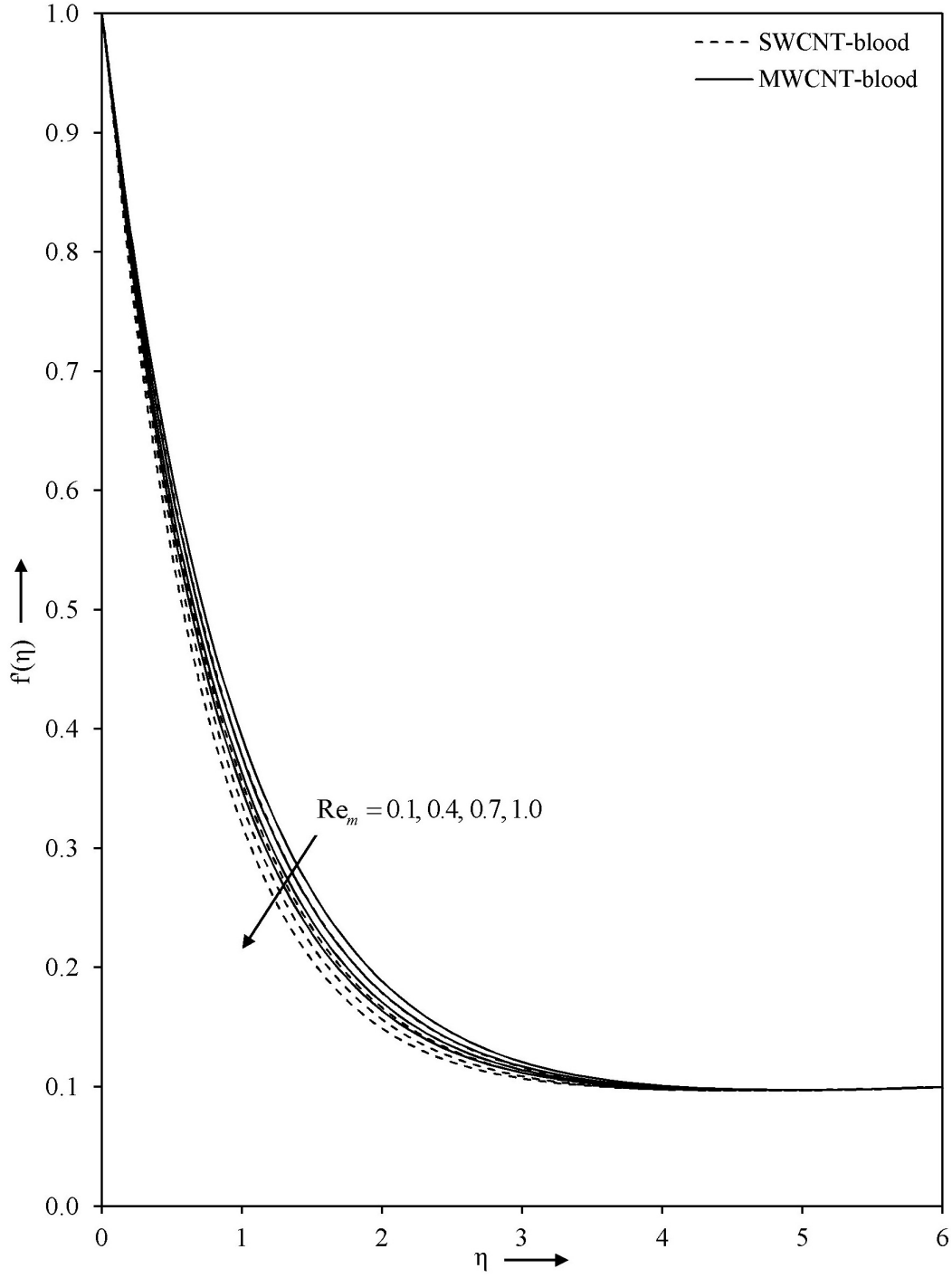

Figure 18: Impact of magnetic parameter Re_m on velocity profile with $m = 2.0$, $\alpha^\star = 0.1$, $A = 0.1$, $\phi = 0.1$ and $k^\star = 0.1$

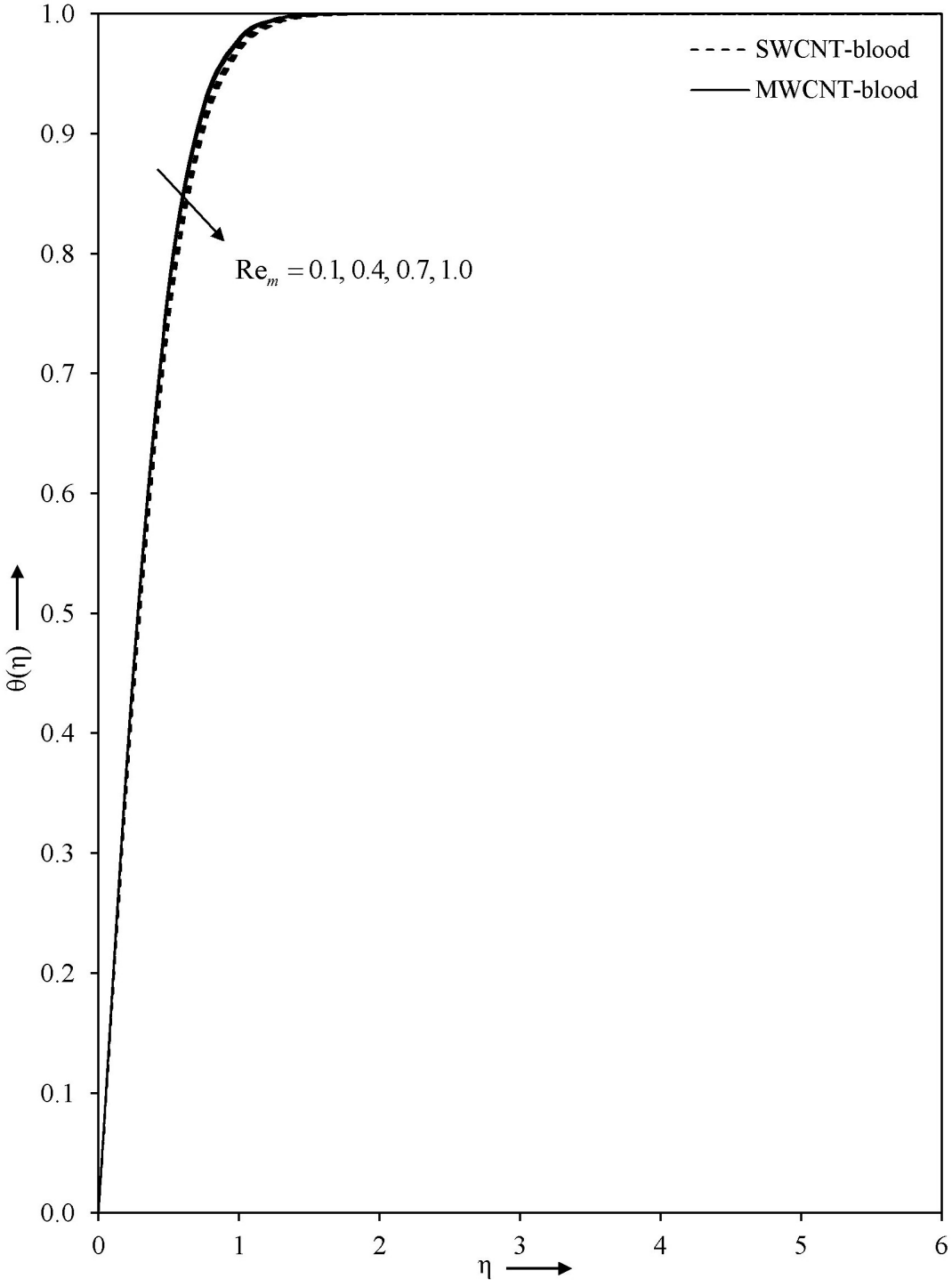

Figure 19: Impact of magnetic parameter Re_m on temperature profile with $m = 2.0$, $\alpha^\star = 0.1$, $A = 0.1$, $\phi = 0.1$, $k^\star = 0.1$, $Pr = 25$ and $Br = 0.1$

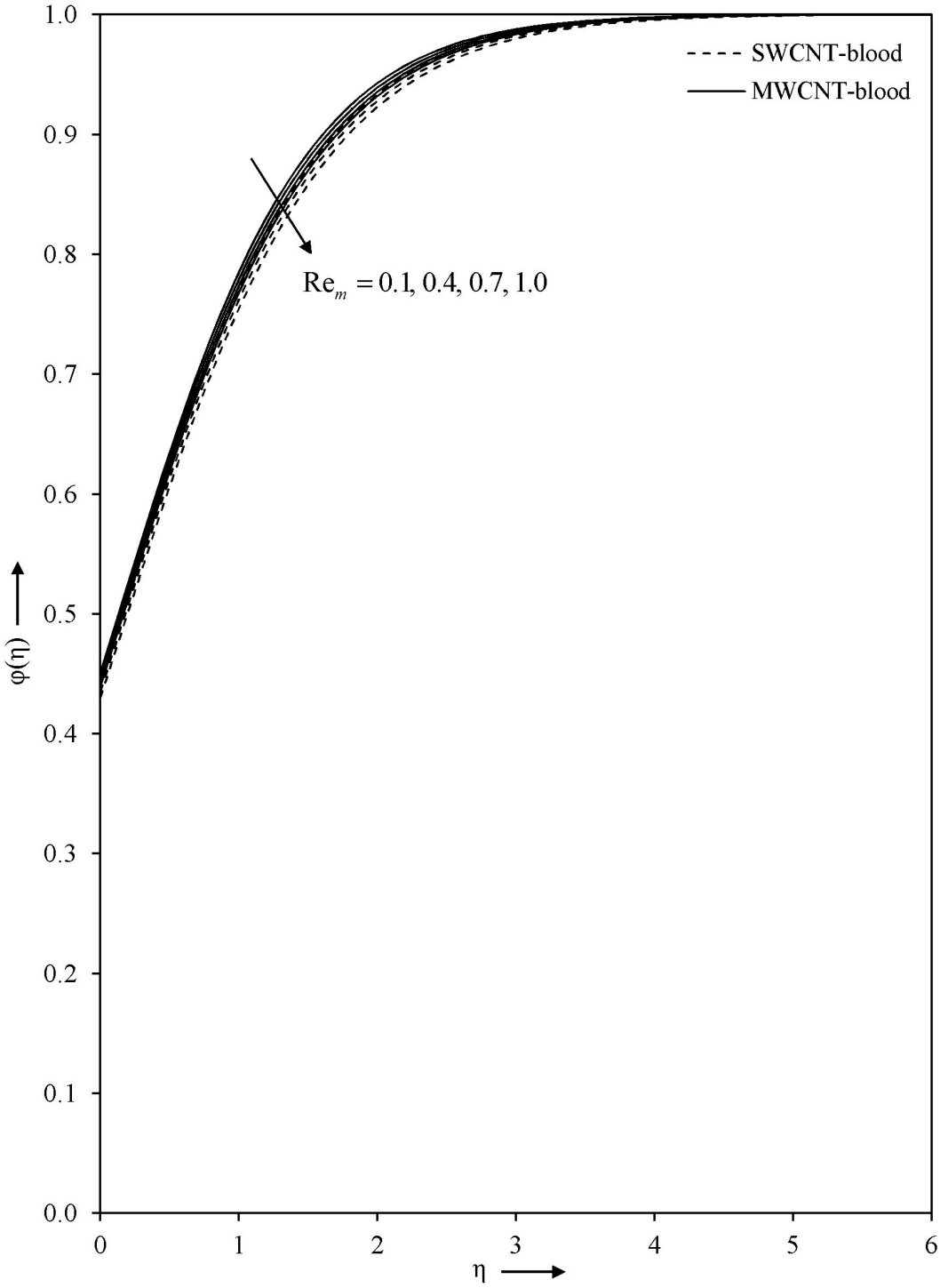

Figure 20: Impact of magnetic parameter Re_m on concentration profile with $m = 2.0$, $\alpha^\star = 0.1$, $A = 0.1$, $\phi = 0.1$, $k^\star = 0.1$, $K_s = 1.0$, $Sc = 1.5$ and $K = 0.5$

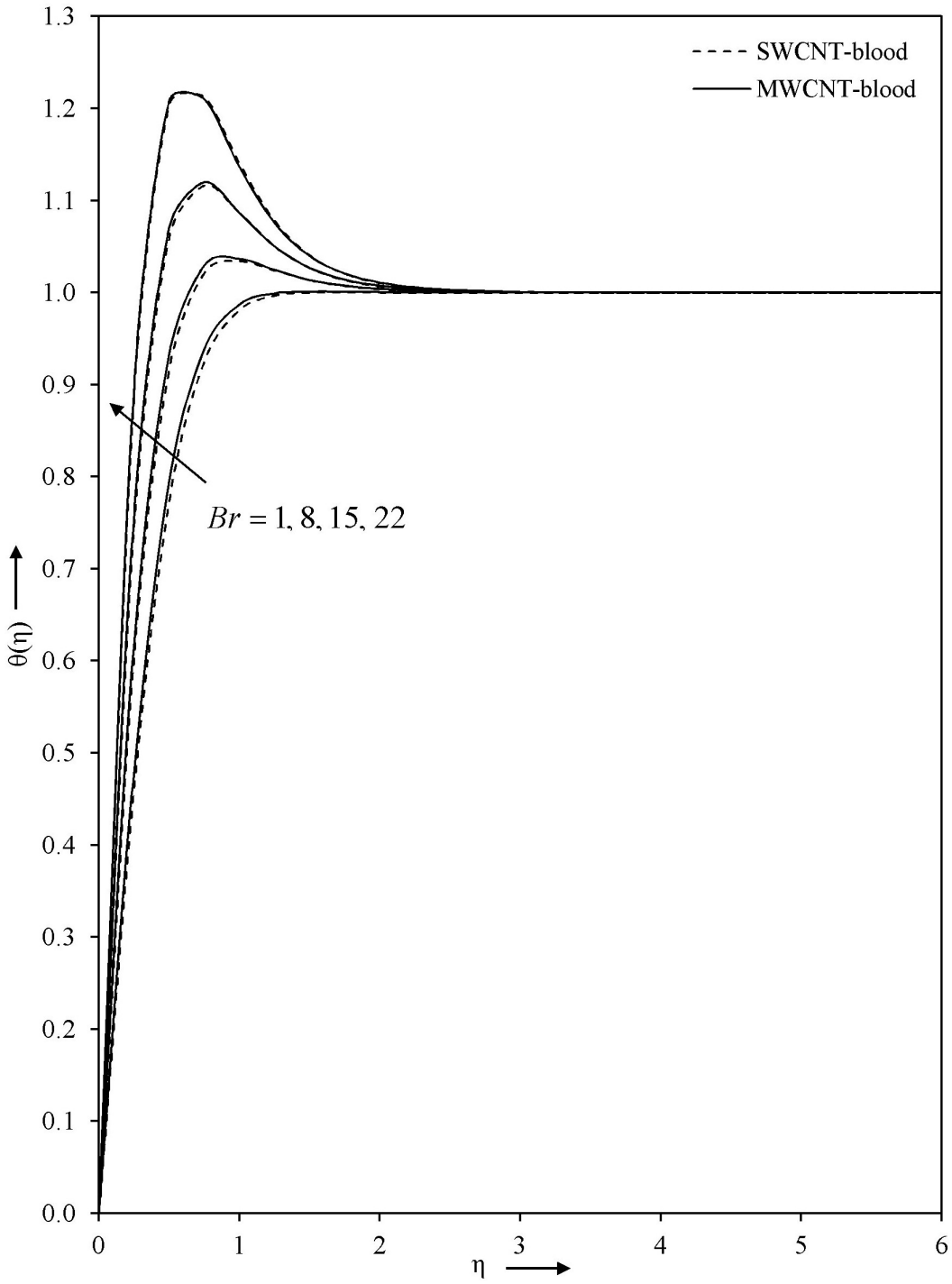

Figure 21: Impact of Brinkman number Br on temperature profile with $m = 2.0$, $\alpha^\star = 0.1$, $A = 0.1$, $\phi = 0.1$, $k^\star = 0.1$, $Re_m = 0.1$ and $Pr = 25$

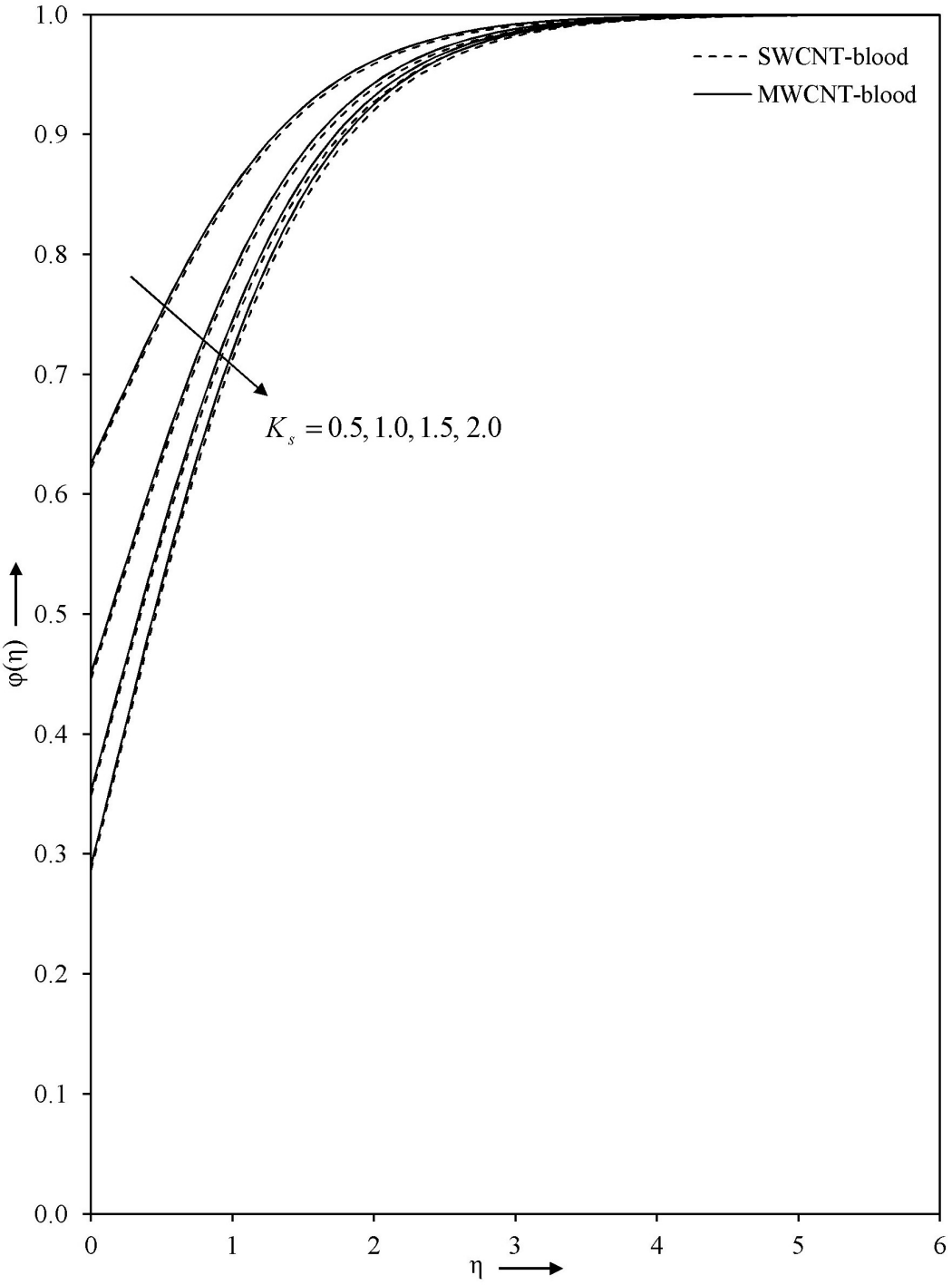

Figure 22: Impact of heterogeneous parameter K_s on concentration profile with $m = 2.0$, $\alpha^\star = 0.1$, $A = 0.1$, $\phi = 0.1$, $k^\star = 0.1$, $Re_m = 0.1$, $Sc = 1.5$ and $K = 0.5$

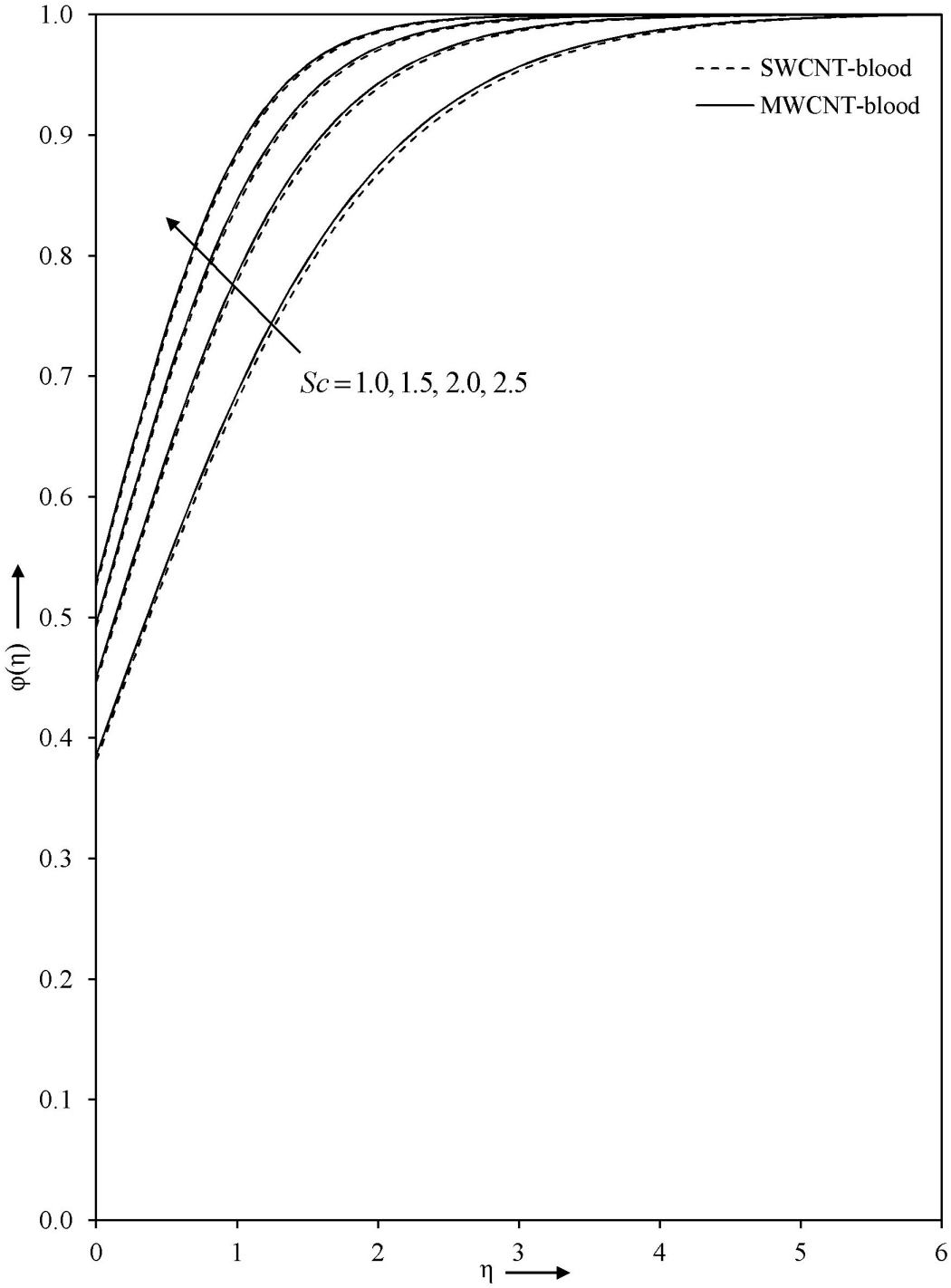

Figure 23: Impact of Schmidt number Sc on concentration profile with $m = 2.0$, $\alpha^{\star} = 0.1$, $A = 0.1$, $\phi = 0.1$, $k^{\star} = 0.1$, $Re_m = 0.1$, $K_s = 1.0$ and $K = 0.5$

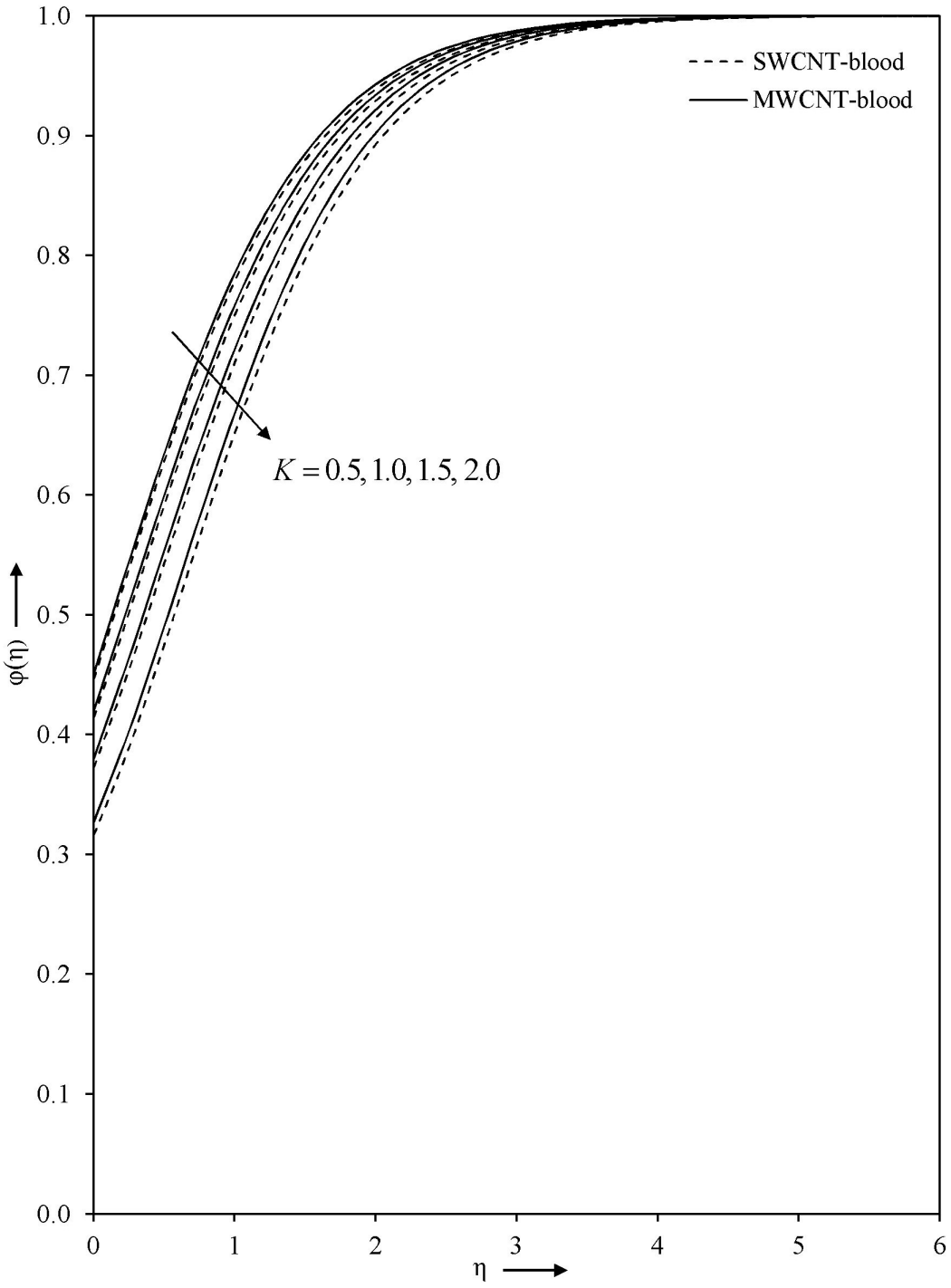

Figure 24: Impact of homogeneous parameter K on concentration profile with $m = 2.0$, $\alpha^{\star} = 0.1$, $A = 0.1$, $\phi = 0.1$, $k^{\star} = 0.1$, $Re_m = 0.1$, $K_s = 1.0$ and $Sc = 1.5$

Table III: Computed values of $f''(0)$, $\theta'(0)$ and $\varphi'(0)$ corresponding to various considered parameters for SWCNT−blood (SWCNT−b) and MWCNT−blood (MWCNT−b) with $Pr = 25$

m	$\alpha^\star$	A	ϕ	$k^\star$	Re_m	Br	K_s	Sc	K	$-f''(0)$		$\theta'(0)$		$\varphi'(0)$	
										SWCNT-b	MWCNT-b	SWCNT-b	MWCNT-b	SWCNT-b	MWCNT-b
0.1	0.1	0.1	0.10	0.1	0.1	0.1	1.0	1.5	0.5	0.885504	0.831434	2.4939	2.6089	0.44685	0.45354
1.0										1.007564	0.957639	2.0356	2.1204	0.39740	0.40156
2.0										1.053373	1.004705	1.8583	1.9318	0.36468	0.36780
3.0										1.075546	1.027434	1.7720	1.8400	0.34119	0.34375
2.0	0.4									1.014705	0.969169	1.3918	1.4357	0.33194	0.33556
	0.7									0.977555	0.934975	0.9902	1.0108	0.29657	0.30074
	1.0									0.941912	0.902115	0.6613	0.6658	0.25900	0.26372
	0.1	0.3								0.931354	0.890423	1.8888	1.9598	0.37987	0.38168
		0.5								0.742942	0.711969	1.9312	1.9997	0.39480	0.39580
		0.7								0.499347	0.480296	1.9810	2.0472	0.40845	0.40889
		0.1	0.01							1.108167	1.102490	3.0066	3.0276	0.36116	0.36152
			0.04							1.091644	1.070055	2.4754	2.5290	0.36220	0.36360
			0.07							1.073345	1.037454	2.1199	2.1870	0.36339	0.36569
			0.10	0.2						1.085488	1.038288	1.8515	1.9248	0.36200	0.36506
				0.3						1.116595	1.070738	1.8450	1.9180	0.35939	0.36237
				0.4						1.146767	1.102143	1.8386	1.9114	0.35680	0.35974
				0.1	0.4					1.128126	1.055586	1.8456	1.9232	0.35994	0.36457
					0.7					1.198385	1.104210	1.8336	1.9149	0.35550	0.36148
					1.0					1.264855	1.150847	1.8224	1.9070	0.35133	0.35853
					0.1	1.0				1.053373	1.004705	1.9820	2.0518	0.36468	0.36780
						8.0						2.9443	2.9850		
						15.0						3.9066	3.9183		
						22.0						4.8688	4.8515		
						0.1	0.5							0.25388	0.25532
							1.5							0.42743	0.43173
							2.0							0.46836	0.47350
							1.0	1.0						0.31166	0.31518
								2.0						0.40194	0.40468
								2.5						0.43004	0.43247
								1.5	1.0					0.33840	0.34258
									1.5					0.30425	0.31009
									2.0					0.25850	0.26700

An analysis of annular fin's thermal conductivity and heat production using the DTM-Pade approximation

Deepak Umarao Sarwe[1], Vishnu Sharma[2], Pradip Kumar Gaur*[2] and Stephan Antony Raj[3]

[1]Department of Mathematics, University of Mumbai, Maharastra, 40098, India

[2] Department of Mathematics, JECRC University, Jaipur, 303905, India

[3]Department of Mathematics, Rathinam Group of Institutions, Tamil nadu, 641107, India

[1] *deepaksarve@mathematica.mu.ac.in*

[2] *vishnu83.sharma@gmail.com*

*[2] *pradeep.gaur@jecrcu.edu.in*

[3] *stephanraj138@gmail.com*

Abstract

The DTM-Pade approximation is used in the current work to analyze the thermal behavior and thermal stresses of an annular fin while accounting for temperature-dependent thermal conductivity and internal heat generation. The energy problem is converted into a nonlinear ordinary differential equation (ODE) using non-dimensional parameters, and the DTM-Pade approximation is then utilized to provide an approximate analytical solution. The impacts of various settings on the temperature field are also graphically analyzed. It has been found that increasing the heat generation parameter causes the temperature distribution to improve. The growing thermo-geometric parameter values lead to an improvement in fin efficiency.

Keywords: Annular fin; DTM-Pade approximant method; Heat generation.

Nomenclature:

r_0	Outer radius	t	Thicknesses of the fin
Q	Actual heat transfer	$T_\star$	Temperature
h	Heat transfer coefficient	λ	Thermo-geometric parameter
α	Nondimensional heat generation	α	Heat generation parameter
κ_0	Thermal conductivity at ambient temperature	R	Dimensionless outer radius

θ	Dimensionless temperature	ν	Internal heat generation variation
q_0	Internal heat generation at ambient temperature	μ	Nondimensional heat generation variation
T_∞	Ambient temperature	k	Thermal conductivity of the fin
ζ	Dimensionless radius	T_b	Base temperature
$Q_{\max}$	Maximum possible heat transfer	r_i	Inner radius
η	Fin efficiency	κ	Thermal conductivity variation
σ_r, σ_ϕ	Radial and tangential stress	χ	Dimensionless coefficient of thermal expansion
$\alpha*$	linear coefficient of thermal expansion	ν	Poisson's ratio
$\varepsilon_r, \varepsilon_\phi$	Radial and tangential strain	$\bar{\sigma}_r, \bar{\sigma}_\phi$	Dimensionless radial and tangential stress
E	Young's modulus		

1 Introduction

Annular fins are typical heat transfer components that are employed in a variety of engineering applications to improve surface heat dissipation. The circular shape of these fins promotes effective heat transfer while using the least amount of material. In real-world situations, materials' thermal conductivities frequently change with temperature, and heat generation may take place within the fin structure for a variety of reasons. Optimizing the design and performance of annular fins with these complexities requires accurate analysis. Finned surfaces are widely used in electrical components, computer CPU heat sinks, heat exchangers, superheaters, electrical equipment, automobile radiators, compressor cylinders, and refrigeration because they can improve the convection heat transference between a solid surface and its surroundings. There are several ways to increase heat transfer, but one of the best is to mount a fin to the primary surface to offer more surface area. Numerous studies examine the behavior of thermal distribution through annular fins with standard profile shapes as triangular, rectangular, concave and hyperbolic, and convex parabolic fins. Recently, a number of researchers used numerical and analytical methods to examine the heat transfer properties of various fins. By taking into account the varied thermal conductivity, Darvishi et al. [1] investigated the thermal dispersion of an annular fin. Using a graphical illustration, Gaba et al. [2] addressed the heat transmission and effectiveness of annular fins with parabolic and exponential profiles. The differential evolution method was utilized by Ranjan et al. [3] to examine the radiative

phenomenon through an annular fin. By using the Durbin inverses Laplace transform approach, Bas and Keles [4] explained the thermal stress characteristics of one-dimensional annular extended surfaces. The property of temperature distribution across an annular fin was studied by Lee et al. in [5], and they also looked into the thermal stress of the fin. The heat distribution of a permeable fin submerged in a nanoliquid was examined by Sowmya et al. [6]. Baslem et al. [7] investigated the heat transfer of a straight porous fin positioned in a nanofluid while taking radiation and natural convection into account. The Homotopy Perturbation Method (HPM), Variational Iteration Method (VIM), Homotopy Analysis Method (HAM), and Adomian Decomposition Method (ADM) are some of the analytical techniques that can be used to address nonlinear differential problems. But the computations used in these methods are complicated. A technique that may effortlessly and without restrictions solve nonlinear terms is essential. This benefit is provided by the Differential Transformation Method (DTM), which may be used to expand a power series to find the analytical solution to differential equations that are both linear and nonlinear. By converting differential equations into algebraic equations, the numerical method known as DTM can solve differential equations. It offers an effective and precise approach to approximate the solutions of differential equations, particularly when closed-form solutions are not easily accessible. It is often used in conjunction with the Pade approximation. DTM with the Pade approximation can be used to get approximations of solutions for the temperature distribution T(r) in the context of the annular fin with temperature-dependent features. The Pade approximation is used to shorten the infinite series produced by DTM once the differential equation and boundary conditions are translated into algebraic equations. This approach expands the solution into Taylor's series form. DTM was initially used by Zhou [8] to examine an electrical circuit by solving both linear and nonlinear initial value issues. By taking varying thermal conductivity into account, Ghasemi et al. [9] were able to get at the analytical solution for the heat distribution through a fin using the DTM's attributes. In their study of the effects of radiation on a permeable extended surface (Moradi et al., [10], they used DTM to arrive at an analytical solution for the temperature field. Kundu and Lee [11] elaborated on heat transmission via an annular permeable extended surface, and DTM was used to solve the governing equation. For the temperature equation of the straight fin with varying thermal conductivity, Mosayebidorcheh et al. [12] used DTM. By using the DTM-Pade approximation, Christopher et al. [13] examined the hybrid nanoliquid stream across a cylindrical geometry. The creation of internal heat through a fin has been studied by several researchers. The significance of internal heat generation by an annular fin with temperature-dependent thermal conductivity was discussed by Ranjan and Mallick in [14]. The thermal behavior of a one-dimensional permeable rectangular fin with heat

generation was discussed by Hoseinzadeh et al. [15]. An analytical method was used by Ranjan et al. [16] to examine the thermal stresses and heat generation of an annular extended surface. By accounting for thermal conductivity, Kezzar et al. [17] investigated the features of heat generation over a longitudinal extended surface. Sowmya et al. [18] scrutinized the aspect of internal heat generation through a permeable fin immersed in a nanoliquid. The literature described above demonstrates that using the DTM-Pade approximant, no attempt has been made to examine the thermal distribution and thermal stresses of annular fins with internal heat generation and temperature-dependent thermal conductivity. A challenging issue in heat transfer and thermal engineering is analyzing the thermal behavior of an annular fin with temperature-dependent thermal conductivity and heat generation. Using a numerical method called the Differential Transformation Method (DTM) and Pade approximation, one can approximate the answers to such issues. Let's dissect the elements of this issue and talk about how DTM-Pade approximation might be used. Also, we refer [27–31] for more information. Therefore, the main goal of this inquiry is to use the DTM-Pade approximant, a sophisticated mathematical technique, to solve the annular fin's energy equation. Additionally, internal heat generation and thermal analysis of fins with temperature-dependent thermal conductivity are examined. The main advantage of this method is that it may be used directly on the issue without any linearization, perturbation, or discretization being necessary. Additionally, it offers more precise or exact solutions.

2 Formulation in mathematics

The following assumptions form the basis of the mathematical model:

1. This study takes into account an axisymmetric thin annular fin with uniform thickness, uniform inner and outer radii, and homogenous isotropic material, as shown in Figure 1.

2. The temperature of the surrounding liquid doesn't change while the heat is rejected.

3. At the tip of the fin, very little heat is lost.

4. Heat conduction only happens in the radial direction since there are no thermal gradients in the circumferential or axial orientations.

5. The base of the fin is maintained at a consistent temperature.

6. Convective heat transfer's coefficient is a fixed quantity.

7. By convection, the fin loses heat to its surroundings.

8. The fin functions in a steady condition.

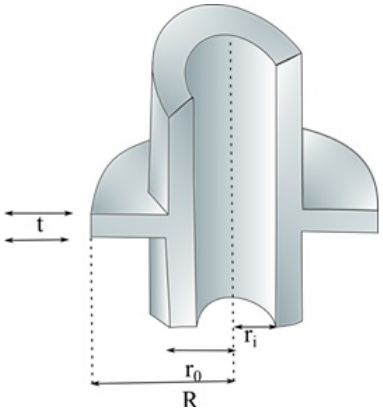

Figure 1: Schematic of an annular fin.

Under these assumptions, the energy equation derived from the law of conservation of energy for one-dimensional heat transfer is specified as [19]:

$$t\frac{d}{dr}\left[k(T_\star)r\frac{dT_\star}{dr}\right] - 2hr(T_\star - T_\infty) + q^*(T_\star)tr = 0 \tag{1}$$

The following values for the thermal conductivity and internal heat generation are assumed to change linearly with temperature:

$$\begin{aligned} k(T_\star) &= k_0\{1 + \kappa(T_\star - T_\infty)\}, \\ q^*(T_\star) &= q_0\{1 + \nu(T_\star - T_\infty)\}. \end{aligned} \tag{2}$$

Therefore, the following boundary conditions for the energy balance equation can be obtained by implementing zero conductive heat resistance at the fin wall.

$$\begin{aligned} r = r_i : T_\star = T_b, \\ r = r_0 : \tfrac{dT_\star}{dr} = 0. \end{aligned} \tag{3}$$

The following non-dimensional parameters are utilized.

$$\begin{aligned} &\theta = \frac{T_\star - T_\infty}{T_b - Ta},\ B_i = \frac{hr_i}{k_0},\ \beta = \kappa(T_b - T_\infty),\ \mu = \nu(T_b - T_\infty),\ \zeta = \frac{r - r_i}{r_i},\ R = \frac{r_0}{r_i}, \\ &\lambda^2 = \frac{2hr_i^2}{k_0 t},\ \alpha = \frac{q_0 r_i^2}{k_0(T_b - T_\infty)}. \end{aligned} \tag{4}$$

The governing equation (1) and boundary condition (3) are reduced into non-dimensional energy equation with the help of equation (2) and (4) and are given as:

$$\theta'' + \beta\theta\theta'' + \frac{\beta}{1+\zeta}\theta\theta' + \frac{1}{1+\zeta}\theta' + \beta(\theta')^2 - \lambda^2\theta + \alpha(1+\mu\theta) = 0, \tag{5}$$

$$\begin{aligned} \text{Here}, \zeta = 0 \quad &; \quad \theta = 1 \\ \text{and}, \zeta = R-1 \quad &; \quad \theta' = 0 \end{aligned} \tag{6}$$

3 Discussion on Differential Transformation Method (DTM)

The attributes of DTM were covered in this section. Using the Taylor's series expression, this method can be used to find solutions for a system of linear and nonlinear differential equations as well as adequate beginning and boundary conditions. Taylor's series has the following general form:

$$w(l) = \sum_{q=0}^{\infty} \frac{(l-l_0)^q}{q!} \left[\frac{d^q y(l)}{dx^q}\right]_{l=l_0} \tag{7}$$

The differential transformation $W(q)$ of a function $w(l)$ is expressed as follows:

$$W(q) = \frac{1}{q!}\left[\frac{d^q w(l)}{dx^q}\right]_{l=l_0} \tag{8}$$

In equation (7), $W(q)$ is the transformed function of the original function $w(l)$. Differential inverse transforms for $W(q)$ is defined as:

$$w(l) = \sum_{q=0}^{\infty} W(q)(l-l_0)^q \tag{9}$$

The fundamental properties of DTM are specified in Table. 2 (see Zhou [20], Hassan [21], Jawad and Hamody [22])

Table 2: Properties of DTM

Original function	**Transformed function**
$W(l) = g(l) \pm h(l)$	$W(q) = G(q) \pm H(q)$
$w(l) = \alpha g(l)$	$W(q) = CG(q)$, where C is the constant.

$W(l) = \frac{dh(l)}{dl}$	$W(q) = (q+1)H(q+1)$
$w(l) = \frac{d^n h(l)}{dl}$	$W(q) = (q+1)(q+1)\cdots(q+n)H(q+n)$
$w(l) = l^m$	$W(q) = \delta(q-m) = \left\{ \begin{array}{l} 1,\ q = m \\ 0,\ q \neq m \end{array} \right\}$
$w(l) = g(l)h(l)$	$W(q) = \sum_{r=0}^{q} G(r)H(q-r)$
$w(l) = f_1(l)f_2(l)\cdots$ $\cdots f_{s-1}(l)f_s(l)$	$W(q) = \sum_{q_{s-1}=0}^{q} \sum_{q_{s-2}=0}^{q_{s-1}=0} \cdots \sum_{q_2=0}^{q_3} \sum_{q_1=0}^{q_2} W_1(q_1)$ $W_2(q_2-q_1)\cdots W_{s-1}(q_{s-1}-q_{s-2})W_s(q-q_{s-1})$

4 Pade Approximant Method

The Pade approximant is a powerful approach that is frequently used in numerical analysis and scientific computing to approximate a polynomial function into rational functions of polynomials of a particular degree (see Boyd [23] and Rashidi et al. [24]). Compared to a straightforward polynomial fit, this method enables us to describe a given function with higher precision and adaptability. Assume that a power series represents the function $h(zeta)$. Using powers of a variable, in this case $zeta$, power series are a fundamental mathematics tool for expressing functions as an infinite sum of terms. When working with functions that may be roughly represented as a sum of polynomial terms, they are especially helpful.

$$h(\zeta) = \sum_{i=0}^{\infty} \gamma_i \zeta^i \tag{10}$$

Equation (4) is a vital initial step in any analysis using Pade approximants. The Pade approximant, a mathematical idea, is crucial to the discipline of numerical analysis. It is a rational fraction with a Maclaurin expansion that is intended to as closely match equation (3) as possible. In other words, Pade approximants use rational approximations, which are more computationally effective than attempting to directly compute or alter the actual equation, to provide an accurate representation of complicated functions.

$$\frac{\alpha_0 + \alpha_1\zeta + \alpha_2\zeta^2 + \cdots + \alpha_S\zeta^S}{\beta_0 + \beta_1\zeta + \beta_2\zeta^2 + \cdots + \beta_T\zeta^T} \tag{11}$$

It is believed that the numerator and denominator coefficients of equation (1) are of order $S+1$ and $T+1$, respectively. As a result, there is an independent T denominator, and independent $S+1$ numerator coefficients result in an overall $S+T+1$ unknown coefficient. This order suggests using the orders $1, \zeta, \zeta^2, \cdots, \zeta^{S+T}$ to usually fit the power series equation (3).

The representation of power series is given as:

$$\sum_{i=0}^{\infty}\gamma_i\zeta^i = \frac{\alpha_0+\alpha_1\zeta+\alpha_2\zeta^2+\cdots+\alpha_S\zeta^S}{\beta_0+\beta_1\zeta+\beta_2\zeta^2+\cdots+\beta_T\zeta^T}+o(\zeta^{S+T+1}) \quad (12)$$

$$(\beta_0+\beta_1\zeta+\beta_2\zeta^2+\cdots+\beta_S\zeta^T)(\gamma_0+\gamma_1\zeta+\gamma_2\zeta^2+\cdots) = \alpha_0+\alpha_1\zeta+\alpha_2\zeta^2+\cdots +\alpha_S\zeta^S+o(\zeta^{S+T+1}) \quad (13)$$

Comparing the coefficients of $\zeta^{S+1},\zeta^{S+2},\cdots,\zeta^{S+T}$

$$\begin{aligned}
\beta_T\gamma_{S-T+1}+\beta_{T-1}\gamma_{S-T+2}+\cdots+\beta_0\gamma_{S+1} &= 0,\\
\beta_T\gamma_{S-T+2}+\beta_{T-1}\gamma_{S-T+3}+\cdots+\beta_0\gamma_{S+2} &= 0,\\
&\cdots\cdots\\
&\cdots\cdots\\
&\cdots\cdots\\
\beta_T\gamma_T+\beta_{T-1}\gamma_{T+1}+\cdots+\beta_0\gamma_{S+T} &= 0,
\end{aligned} \quad (14)$$

To obtain the desired consistency in our mathematical framework, we define the parameter γ_i to be equal to zero. This choice plays a pivotal role in simplifying the system. When we set β_0 to be equal to 1, as stipulated in equation (5), this transforms the equation into a set of T linear equations. These linear equations represent the relationship between the various coefficients in our system, specifically, the T unknown denominator coefficients.

$$\begin{pmatrix}
\gamma_{S-T+1} & \gamma_{S-T+2} & \cdots & \gamma_{S+1}\\
\gamma_{S-T+2} & \gamma_{S-T+3} & \cdots & \gamma_{S+2}\\
\cdots & \cdots & \cdots & \cdots\\
\gamma_S & \gamma_{S+1} & \cdots & \gamma_{S+T}
\end{pmatrix}
\begin{pmatrix}
\beta_T\\ \beta_{T+1}\\ \cdots\\ \beta_S
\end{pmatrix}
=
\begin{pmatrix}
\gamma_{S+1}\\ \gamma_{S+2}\\ \cdots\\ \gamma_{S+T}
\end{pmatrix} \quad (15)$$

β_i is obtained from these equations. The numerator coefficients $\alpha_0,\alpha_1,\cdots,\alpha_S$ from equation (10) are found by equating the coefficients of $1,\zeta,\zeta^2,\cdots,\zeta^{S+T}$ such as,

$$\begin{aligned}
\alpha_0 &= \gamma_0, \\
\alpha_1 &= \gamma_1 + \beta_1\gamma_0, \\
\alpha_2 &= \gamma_2 + \beta_1\gamma_1 + \beta_2\gamma_0, \\
\cdots &\quad \cdots\cdots \\
\alpha_S &= \gamma_S + \sum_{i=1}^{min[S/T]} \beta_i\gamma_{S-i}.
\end{aligned} \tag{16}$$

The equations (15) and (16), also referred to as Pade equations, thereby yield the Pade numerator and denominator. These equations are crucial to numerical analysis, especially when it comes to approximating rational functions. They are effective tools for estimating complex functions using straightforward rational functions. In engineering and scientific computations, a particular kind of rational function approximation known as the $[S/T]$ Pade approximant is crucial. The trade-off between the degree of the numerator (S) and the degree of the denominator (T) is balanced in its development. A reference to another crucial equation that establishes the order of the Pade approximant is made in the phrase by the equation (10) . An approximation's accuracy and complexity are determined by its order. To ensure that the Pade approximant finds a compromise between accuracy and computational economy, the equation (10) offers a way for calculating its ideal order.

5 Applications of DTM-Pade method

The DTM-Pade method have several applications in a variety of scientific and technical fields. This potent mix of mathematical methods is essential for resolving difficult issues and simulating a wide range of phenomena. Applying DTM to the non-linear differential equation (2), we obtain the following expression

$$\begin{aligned}
(q+1)(q+2)\Theta[q+2] + \beta\sum_{r=0}^{q}\Theta[q-r](r+1)(r+2)\Theta[r+2] + \\
\beta\sum_{r+0}^{q}\sum_{m=0}^{r}\frac{1}{1+\delta[m-1]}\Theta[r-m](q-r+1)\Theta[q-r+1] + \\
\sum_{r=0}^{q}\frac{1}{1+\delta[m-1]}(q-r+1)\Theta[q-r+1] + \\
\beta\sum_{r=0}^{q}(q-r+1)\Theta[q-r+1](r+1)\Theta[r+1] - \lambda^2\Theta[k] + \alpha\delta[k] + \alpha\mu\Theta[k] = 0.
\end{aligned} \tag{17}$$

For the solution of difficult differential equations, the Differential Transformation Method (DTM) is applied to the boundary conditions of equations (6). With the aid of this groundbreaking mathematical method, we may better understand how the system behaves and create a precise expression that captures the complex interrelationships underlying the mathematical or physical events that are the subject of the inquiry. Applying DTM to the boundary conditions in equations (6) we obtain the following expression:

$$\Theta[0] = 1,\ \Theta[1] = a \tag{18}$$

Substituting $q = 0, 1, 2, \cdots$ so on and equation (18) in equation (17), we obtain the successive approximation as:

$$\Theta[2] = -\frac{1}{2}\frac{a^2\beta + \mu\alpha - \lambda^2 + a\beta + \alpha + a}{\beta + 1} \tag{19}$$

$$\Theta[3] = \frac{1}{12(\beta+1)^2}\begin{bmatrix} 6a^3\beta^2 + 4\mu\alpha a\beta - 4\lambda^2 a\beta + 6a^2\beta^2 - 2\mu\alpha a + 2\mu\alpha\beta \\ +6\alpha a\beta + 2\lambda^2 a - 2\lambda^2\beta + 6a^2\beta + a\beta^2 + 2\mu\alpha + 2\alpha\beta \\ -2\lambda^2 + 2a\beta + 2\alpha + a \end{bmatrix} \tag{20}$$

$$\Theta[4] = -\frac{1}{48(\beta+1)^3}\begin{bmatrix} 30a^4\beta^3 + 26\mu\alpha a^2\beta^2 - 26\lambda^2 a^2\beta^2 + 36a^3\beta^3 + 4\mu^2\alpha^2\beta \\ -8\mu\alpha\lambda^2\beta - 10\mu\alpha a^2 + 16\mu\alpha a\beta^2 + 36\alpha a^2\beta^2 + 4\lambda^4\beta \\ +10\lambda^2 a^2\beta - 16\lambda^2 a\beta^2 + 36a^3\beta^2 + 10a^2\beta^3 - 2\mu^2\alpha^2 \\ +10\mu\alpha^2\beta + 4\mu\alpha\lambda^2 + 12\mu\alpha a\beta - 10\alpha\lambda^2\beta + 20\alpha a\beta^2 - 2\lambda^2 \\ -12\lambda^2 a\beta + 20a^2\beta^2 + 3a\beta^3 - 2\mu\alpha^2 - 4\mu\alpha a + 6\alpha^2\beta \\ +2\alpha\lambda^2 + 20\alpha a\beta + 4\lambda^2 a + 10a^2\beta + 9a\beta^2 + 9a\beta + 3a \end{bmatrix} \tag{21}$$

and so on.

Where $\Theta[q]$ is the differential transform of $\theta(\zeta)$ and is the constant to be calculated by using boundary conditions.

Substituting the equations (18)-(21) in equation (9) comprising DTM, we obtain the

following equations:

$$\theta(\zeta) = 1 + a\zeta - \frac{1}{2}\frac{a^2\beta + \mu\alpha - \lambda_a^2\beta + \alpha + a}{\beta + 1}\zeta^2 + \frac{1}{12(\beta+1)^2}\begin{bmatrix} 6a^3\beta^2 + 4\mu\alpha a\beta - 4\lambda^2 a\beta \\ +6a^2\beta^2 - 2\mu\alpha a + 2\mu\alpha\beta \\ +6\alpha a\beta + 2\lambda^2 a - 2\lambda^2\beta \\ +6a^2\beta + a\beta^2 + a\beta^2 + 2\mu\alpha \\ +2\alpha\beta - 2\lambda + 2a\beta \\ +2\alpha + a \end{bmatrix}\zeta^3 - \frac{1}{48(\beta+1)^2}\begin{bmatrix} 30a^4\beta^3 + 26\mu\alpha a^2\beta^2 - 26\lambda^2 a^2\beta^2 + 36a^3\beta^3 + 4\mu^2\alpha^2\beta \\ -8\mu\alpha\lambda^2\beta - 10\mu\alpha a^2 + 16\mu\alpha a\beta^2 + 16\mu\alpha a\beta^2 + 36\alpha a^2\beta^2 \\ +4\lambda^4\beta + 10\lambda^2 a^2\beta - 16\lambda^2 a\beta^2 + 36a^3\beta^2 + 10a^2\beta^3 - 2\mu^2\alpha^2 \\ +10\mu\alpha^2\beta + 4\mu\alpha\lambda^2 + 12\mu\alpha a\beta - 10\alpha\lambda^2\beta + 20\alpha a\beta^2 - 2\lambda^4 \\ -12\lambda^2 a\beta + 20a^2\beta^2 + 3a\beta^3 - 2\mu\alpha^2 - 4\mu\alpha a + 6\alpha^2\beta + 2\alpha\lambda^2 \\ +20\alpha a\beta + 4\lambda^2 a + 10a^2\beta + 9a\beta^2 + 9a\beta + 3a \end{bmatrix}\zeta^4 + \cdots \tag{22}$$

To evaluate the value, we apply the Pade approximant to equation (22) along with boundary condition (6). We get the value of a and by substituting the constant value $a = -.9097156826,\ \alpha = 0.4,\ \mu = 0.4, \lambda = 1,\ \beta = 0.3$ in the equation (22) equation we get,

$$\theta(\zeta) = 1 - 0.9097256826\zeta + 0.5286012084\zeta^2 - 0.1192183969\zeta^3 + 0.05254461407\zeta^4 + \cdots$$

Table 3: Comparison of $\theta'(0)$ for the numerical method and DTM-Pade approximation

Parameters	**Numerical solution**	**DTM-Pade solution**
$\beta = 0.3$	-0.39096	-0.40052
$\alpha = 0.5$	-0.26968	-0.25435
$\mu = 0.8$	-0.26007	-0.26120
$\lambda = 1.5$	-1.13261	-1.12958

Table 4: Comparison of $\theta'(0)$ when $\mu = 0, \alpha = 0,\ \lambda = 1,\ \beta = 0.3$ for the numerical method and DTM-Pade approximation

Non dimensional radius ζ	**Arslanturk FDM [25]**	**Mallick et. al** HPM [26]	**Present DTM**
0	1.0	1.0	1.0
.1	.9477	.9455	.9489
.2	.9036	.9013	.9025
.3	.8668	.8659	.8608
.4	.8365	.8380	.8239

6 Fin Efficiency

The fin efficiency, a critical parameter for assessing a fin's thermal performance. Because it enables us to assess and improve the performance of heat exchangers, radiators, and other systems that depend on fins for heat transmission, the fin efficiency concept is useful in engineering and thermal design. Engineers can choose materials, fin geometry, and other design characteristics to increase heat transfer while minimizing energy use and material usage by having a thorough understanding of a fin's efficiency. In essence, it aids in the effective design of systems where heat absorption or dissipation is crucial for overall performance. Considerations for an annular fin's non-dimensional fin efficiency include its thickness, thermal conductivity, and outer and inner radii. We can use this equation to calculate the annular fin's efficiency at transferring heat from its base to the environment around it while taking into account its geometric and material characteristics. The non-dimensional form of fin efficiency is provided as follows for an annular fin:

$$\eta = \frac{Q}{Q_{max}} = \frac{4\pi h \int_{r_i}^{r_0} (T_\star - T_\infty) r dr}{2\pi h (r_0^2 - r_i^2)(T_b - T_\infty)} = \frac{2\int_0^{R-1} (1+\zeta)\theta d\zeta}{(R^2-1)} \tag{23}$$

7 Thermal stress formulation

A temperature gradient is applied to the annulus in the material under inquiry along its radial direction. The primary cause of stresses is an incompatible eigen-strain brought on by phase transformation, precipitation hardening, and temperature change brought on by the presence of a conduction-convection field. Furthermore, it is assumed that the only factor responsible for the evolution of the eigen-strain is the variation in temperature in the radial direction. Since the thickness of fin is significantly thinner than the radius of the fin, the difference in stress and displacement over the thickness is ignored. Additionally, due to the symmetric behavior of the issue, the radial and tangential stresses are independent of ϕ and cannot be influenced by it. As a result, the issue at hand is axisymmetrically

planar tension. The stress equilibrium equation in a cylindrical coordinate system derived from the classical theory of elasticity is as follows since the body force and inertia force are disregarded:

$$\frac{d\sigma_r}{dr} + \frac{\sigma_r - \sigma_\phi}{r} = 0 \tag{24}$$

Where σ_r and σ_ϕ are radial and tangential components of stress field.
The fin is subjected to thermal stresses, which causes the overall strain to evolve by two strains. While the second is a result of free thermal expansion, the first is caused by induced stresses. Using the traditional theory of elasticity, the stress-strain-temperature relationship is defined by the following expression:

$$\begin{aligned} \epsilon_r &= \frac{1}{E}[\sigma_r - v\sigma_\phi] + \alpha^* T_\star \\ \epsilon_\phi &= \frac{1}{E}[\sigma_\phi - v\sigma_r] + \alpha^* T_\star \end{aligned} \tag{25}$$

where ϵ_r and ϵ_ϕ represents the radial and tangential strain components, α^* is the coefficient of thermal expansion, v is the Poisson's ratio, and E is the modulus of elasticity of fin material. These parameters mentioned in the sentence play vital roles in characterizing the behavior of a material or a structural element.
Equation (25) can be written in the form

$$\begin{bmatrix} \sigma_r \\ \sigma_\phi \end{bmatrix} = \frac{E}{1-v^2} \begin{bmatrix} 1 & v \\ v & 1 \end{bmatrix} \begin{bmatrix} \epsilon_r \\ \epsilon_\phi \end{bmatrix} - \frac{E\alpha^* T_\star}{1-v} \begin{bmatrix} 1 \\ 1 \end{bmatrix} \tag{26}$$

Kinematics relations for the polar strain components, in a plane strain state, are

$$\epsilon_r = \frac{\partial u_r}{\partial r} \text{ and } \epsilon_\phi = \frac{u_r}{r} \tag{27}$$

Substituting Eqs. (27) and (26) into Eq. (24) and integrating twice, the following closed-form solution for the radial displacement is achieved as

$$u_r = \frac{(1+v)\alpha^*}{r} \int_a^r (T_\star - T_\infty)\eta d\eta + A_1 r + \frac{A_2}{r} \tag{28}$$

The traction-free boundary condition at outer and inner surfaces of the fin can be taken as

$$r = a, b : \sigma_r = 0 \tag{29}$$

Using Eqs. (28), (27), and (26), the constants of integration and can be appraised by applying the boundary conditions (Eq. 29)

$$A_1 = \frac{(1-v)a^*}{b^2-a^2}\int_a^b (T_\star - T_\infty)\eta d\eta + \alpha T_\infty \text{ and } A_2 = \frac{(1+v)a^* a^2}{b^2-a^2}\int_a^b (T_\star - T_\infty)\eta d\eta \quad (30)$$

Using the values of A_1 and A_2 from Eq. (30) in Eq. (28). We get,

$$\sigma_r = -\frac{\alpha^* E}{r^2}\int_a^r (T_\star - T_\infty)\eta d\eta + \frac{\alpha^* E}{b^2-a^2}\left(1-\frac{a^2}{r^2}\right)\int_a^b (T_\star - T_\infty)\eta d\eta \text{ and} \quad (31)$$

$$\sigma_\phi = 1\alpha^* E(T_\star - T_\infty)\int_a^r (T_\star - T_\infty)\eta d\eta + \frac{\alpha^* E}{b^2-a^2}\left(1+\frac{a^2}{r^2}\right)\int_a^b (T_\star - T_\infty)\eta d\eta. \quad (32)$$

Let us utilize the non-dimensional parameters:

$$\bar{\sigma}_r = \frac{\sigma_r}{E},\ \bar{\sigma}_\phi = \frac{\sigma_\phi}{E},\ \zeta_1 = \frac{r}{a},\ R = \frac{b}{a},\ \theta = \frac{T_\star - T_\infty}{T_b - T_\infty},\ \text{and } \chi = \alpha(T_b - T_\infty) \quad (33)$$

Using Eq. (33) in Eqs. (31) and (32) results as follows:

$$\begin{aligned}\bar{\sigma}_r &= -\frac{\alpha^*}{\zeta_1^2 a^2}(T_b - T_\infty)\int_1^{\zeta_1}\theta\cdot a\zeta_1\cdot a d\zeta_1 \\ &\quad + \frac{\alpha^*}{b^2-a^2}(T_b - T_\infty)\left(1-\frac{1}{\zeta_1^2}\right)\int_1^R \theta\cdot a\zeta_1\cdot a d\zeta_1 \quad (34)\\ \bar{\sigma}_\phi &= -\alpha^*(T_b - T_\infty) + \frac{\alpha^*}{\zeta_1^2 a^2}(T_b - T_\infty)\int_1^{\zeta_1}\theta\cdot a\zeta_1\cdot a d\zeta_1 + \\ &\quad \frac{\alpha^*}{b^2-a^2}(T_b - T_\infty)\left(1-\frac{1}{\zeta_1^2}\right)\int_1^R \theta\cdot a\zeta_1\cdot a d\zeta_1 \quad (35)\end{aligned}$$

Introduction of χ and R reduces Eqs. 34 and 35 to

$$\bar{\sigma}_r = \frac{\chi}{\zeta_1^2}\int_1^{\zeta_1}\theta\zeta_1 d\zeta_1 + \frac{\chi(\zeta_1^2-1)}{(R^2-1)\zeta_1^2}\int_1^R \theta\zeta_1 d\zeta_1 \quad (36)$$

$$\bar{\sigma}_\phi = -\chi\theta + \frac{\chi}{\zeta_1^2}\int_1^{\zeta_1}\theta\zeta_1 d\zeta_1 + \frac{\chi(\zeta_1^2+1)}{(R^2-1)\zeta_1^2}\int_1^R \theta\zeta_1 d\zeta_1 \quad (37)$$

The relation between ζ and ζ_1

$$\zeta = \zeta + 1 \quad (38)$$

Thus, the stress equations in terms of non-dimensional radius, ζ becomes

$$\bar{\sigma}_r = -\frac{\chi}{(\zeta+1)^2}\int_0^{\zeta}\theta(\zeta_+1)d\zeta + \frac{\chi(\zeta^2+2\zeta)}{(R^2-1)(\zeta+1)^2}\int_0^{R-1}\theta(\zeta+1)d\zeta \quad (39)$$

$$\bar{\sigma}_\phi = -\chi\theta + \frac{\chi}{(\zeta+1)^2}\int_0^{\zeta}\theta(\zeta_+1)d\zeta + \frac{\chi(\zeta^2+2\zeta+2)}{(R^2-1)(\zeta+1)^2}\int_0^{R-1}\theta(\zeta+1)d\zeta \quad (40)$$

8 Results and discussions

The impact of various non-dimensional parameters such as β, μ, α, and λ on dimensionless temperature field θ are elaborated graphically here. Additionally, the graphs are set up to talk about the effectiveness of an annular fin. Additionally, for the solutions found using both the DTM-Pade approximation method and the numerical method, graphs depicting variations in heat distribution are generated. The results of the numerical method will match the graphics produced by the DTM-Pade approximation method. The values of $\theta'(0)$ for various non-dimensional parameters are tabulated in Table 2 and the values obtained by DTM-Pade approximation method are closer to the values of numerical method. Table 3 epitomizes the numerical values of thermal field of an annular fin. The values obtained by DTM-Pade approximation method are tabulated and compared with existing work.

Figure 2 and Figure 3 show the effect of β on θ for both DTM-Pade approximation method and the numerical method. In Figure 2, the behavior of thermal distribution for different values of $\beta(= -0.4, -0.2, 0, 0.2, 0.4)$ is portrayed by plotting the graphs for both numerical and DTM-Pade approximation. From this figure, one can conclude that increase in the β value enhances the θ . The nature of θ for diverse values of $\beta(= 0.1, 0.2, 0.3, 0.4, 0.5)$ is explained via Figure 3 by using DTM-Pade approximation. It is found that θ upsurges for the rise in values. The variance in the thermal profile θ for various values of μ is exposed in Figure 4 and Figure 5. Figure 4 reveals the consequence of $\mu(= 0.3, 0.4, 0.5, 0.6)$ on θ for both numerical method and DTM-Pade approximation. This figure shows that as the μ values upsurges θ enhance rapidly. The aspect of θ for different values of $\mu(= 0.4, 0.5, 0.6, 0.7, 0.8)$ is explained via Figure 5 by using the DTM-Pade approximation. It indicates that increment of μ values improves the thermal distribution rate. Figure 6 and Figure 7 signify the influence of on temperature field θ by using both numerical and DTM-Pade approximation. The major impact of $\alpha(= 0.3, 0.4, 0.5, 0.6)$ on θ is elucidated in Figure 6. It denotes that, rise in the α values will enhance the temperature distribution. Furthermore, the impact of $\alpha(= 0.3, 0.4, 0.5, 0.6)$ on θ by implementing DTM-Pade approximation is shown in Figure 7. This figure reveals that, θ improves for enhanced α values.

The Three-dimensional (3D) and two-dimensional (2D) graphs are plotted (Figures 8 to Figure 15) for illustrating the variation of thermal profile for various increased values of non-dimensional parameters. Figure 8 and Figure 9 show the nature of θ for improved values of μ and β . These figures indicate that, θ enhances remarkably for enhanced values of μ and β. The major consequence of μ and α on θ is illustrated by utilizing 3D and 2D plots as shown in Figure 10 and Figure 11. These figures ensure that the improvement of μ and α values leads to the enhancement of θ . Figure 12 and Figure 13 demonstrate the behavior of μ for rising in α and values. These figures signify that, θ upsurges with the improvement of α and β values. The physical parameters influencing the efficiency of fin are discussed graphically as displayed in Figure 14 and Figure 15. The efficiency of fin is more for higher values of λ and β . Figures 16,17 and Figure 18,19 portray the aspects of thermal stresses caused due to heat transfer through the annular fin. Figure 16 and Figure 17 signifies the effect of non-dimensional parameters χ and β on radial stress distribution. Here, the radial stress magnitude upsurges with the decline of β. This happens due to the fact that, decrease in β values increases the thermal resistance. As a result, the fin material's local free expansion is hindered. Furthermore, the radial stress fields are unaffected by the heat generation factors α and
mu. Figures 10(a) and 10(b) show the impact of the non-dimensional parameters α and μ on the distribution of tangential stress. Tangential stress is significantly impacted by all non-dimensional parameters, including the heat generation parameters α and μ. For increased values of α and μ, the effect of heat generation on the tangential stresses remarkably increases.

9 Final remarks

In conclusion, it is a challenging task to analyze the thermal behavior of an annular fin with temperature-dependent thermal conductivity and heat generation. To achieve precise solutions, it is necessary to combine mathematical modeling, numerical techniques like DTM, and approximations like the Pade approximation. In many technical applications where effective heat transport and temperature control are critical, this analysis is crucial. The challenge of conducting a complex yet crucial thermal analysis of annular fins with temperature-dependent thermal conductivity and heat generation is one that engineers and designers must do. These fins can be optimized for better performance and efficiency with the use of accurate temperature distribution predictions within them. Engineers and scientists are able to effectively solve the governing equations and get insightful knowledge regarding the behavior of annular fins under real-world circumstances by using mathematical methods like the Differential Transformation Method (DTM) and Pade

approximation. Making informed judgments on the design and application of such heat transfer devices across a range of applications is made easier with the help of this analysis, which improves energy efficiency and system performance.

Utilizing the DTM-Pade approximant method, the current study investigates the heat transference analysis as well as the thermal stresses aspect of an annular fin with temperature-dependent thermal conductivity. Additionally, the current approach yields findings for the thermal field. According to the results of this study, the DTM-Pade approximant-based method offers fairly precise results and is easier to manage the nonlinear problem. From the current investigation, it is possible to draw the following conclusions:

- The thermal distribution is enhanced by the increasing values of β.
- The thermal distribution increases as μ values rise. Additionally, α is increased by the thermal distribution function.
- The effectiveness of the fin is increased by the rising values of non-dimensional parameters λ.
- The magnitude of the radial stress increases as β declines.
- For increased values of α and μ, the effect of heat generation on the tangential stresses remarkably increases.

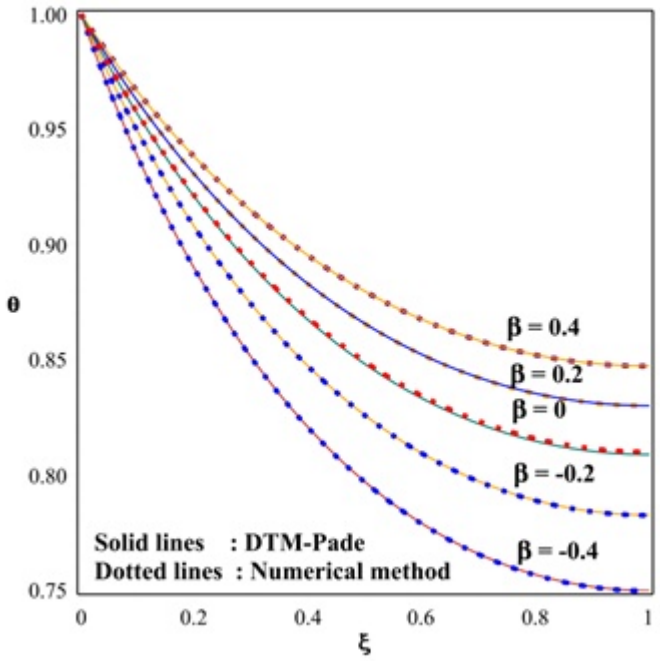

Figure 2: Influence of β on θ.

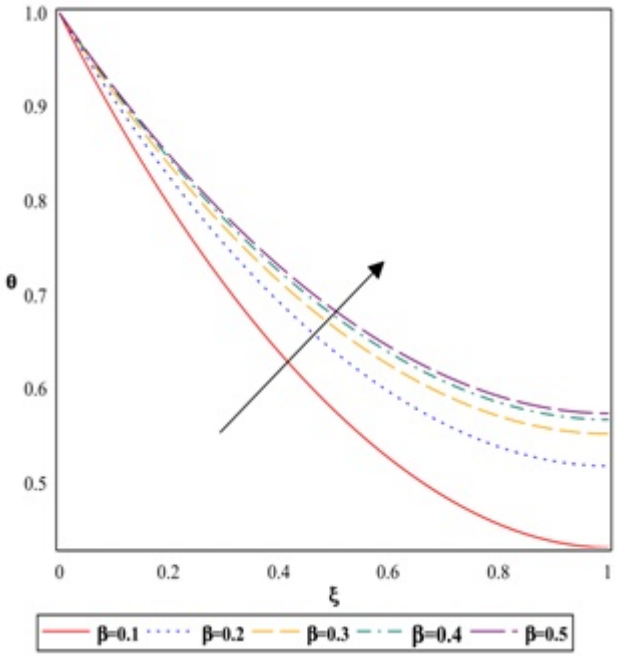

Figure 3: Influence of β on θ by using DTM-Pade Approximation.

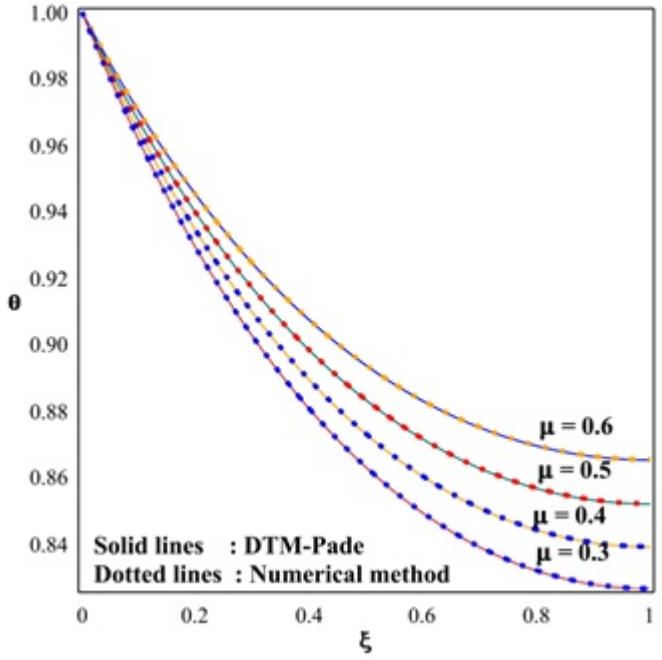

Figure 4: Influence of μ on θ.

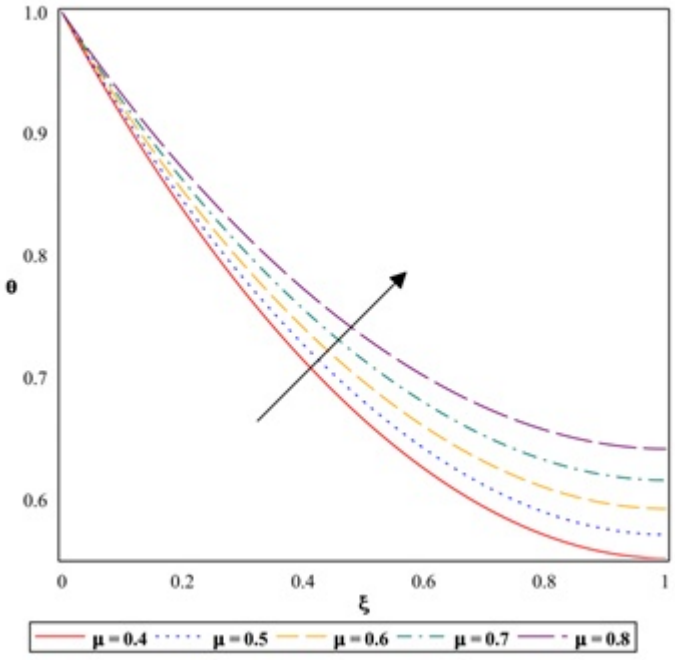

Figure 5: Influence of μ on θ by using DTM-Pade Approximation.

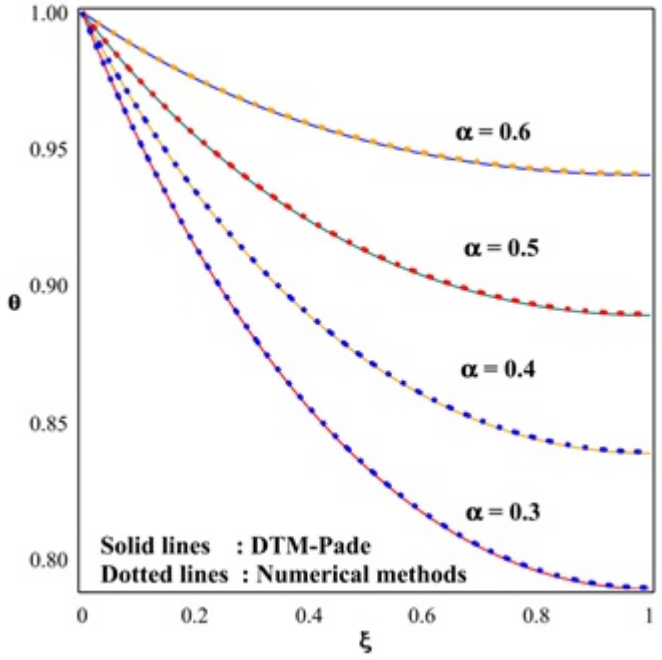

Figure 6: Influence of α on θ.

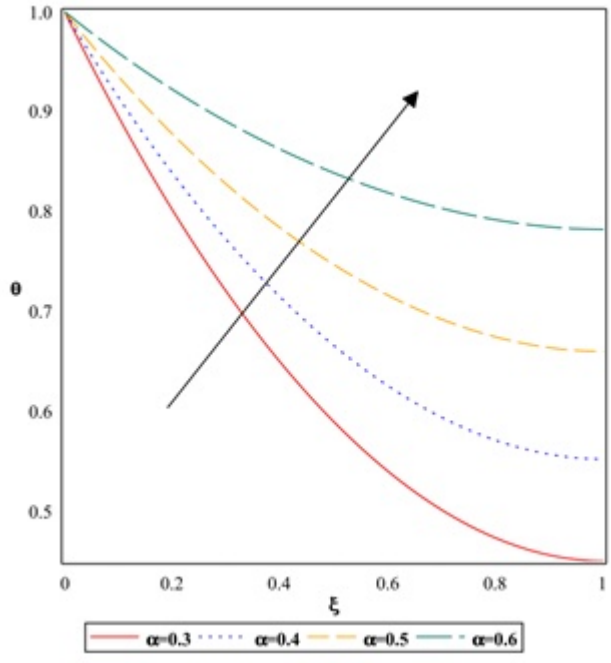

Figure 7: Influence of α on θ by using DTM-Pade Approximation.

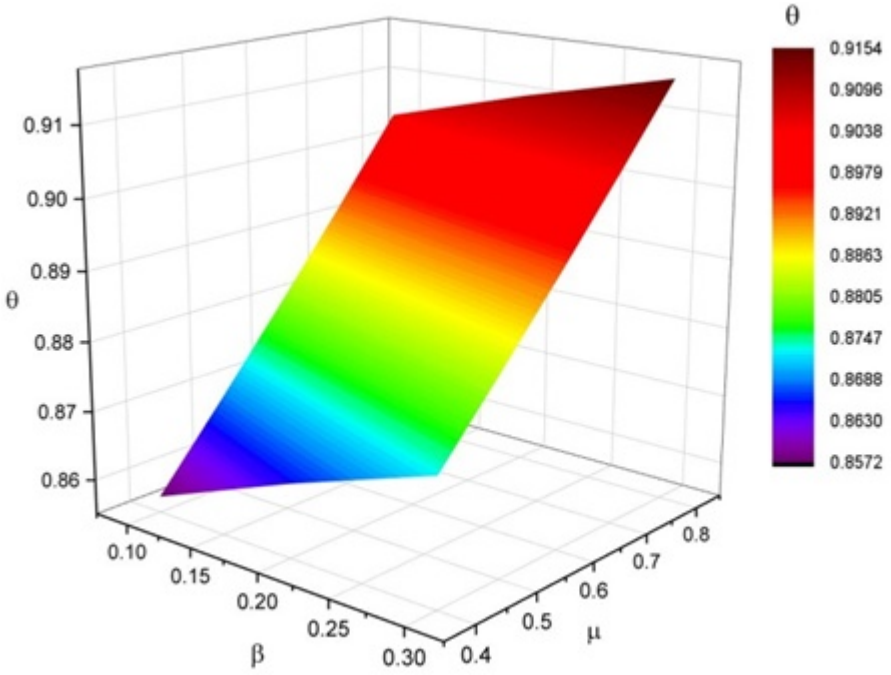

Figure 8: Deviance of θ for diverse values of μ against β.

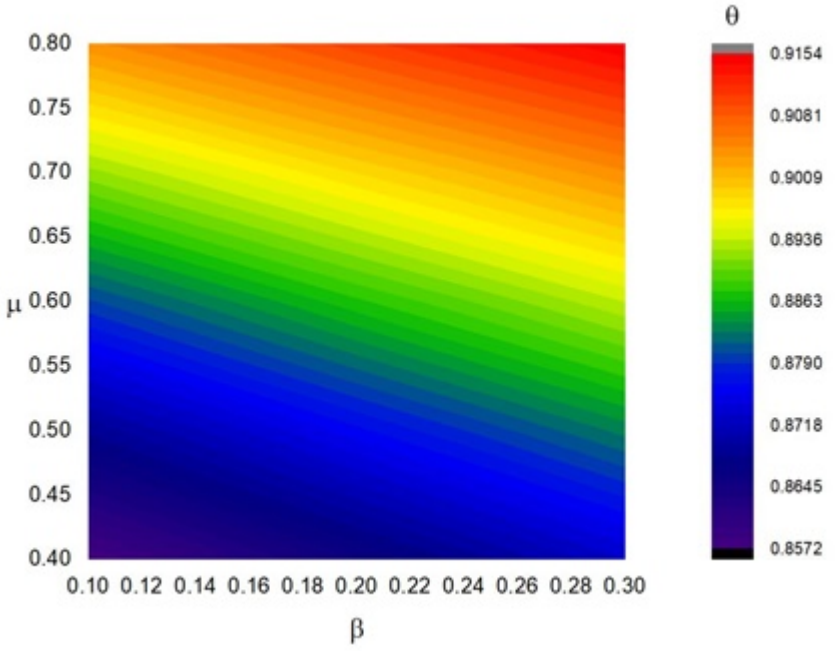

Figure 9: Deviance of θ for diverse values of μ against β.

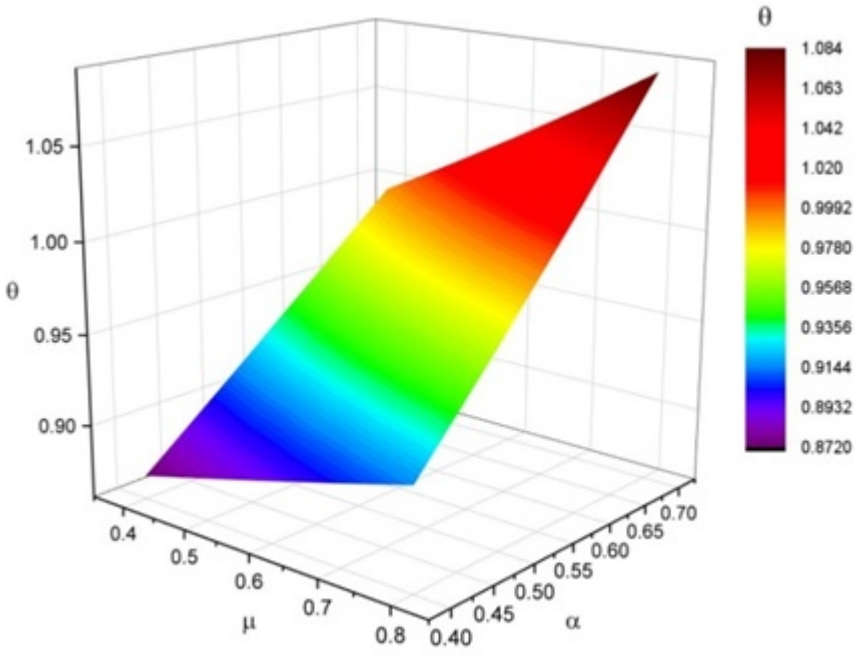

Figure 10: Deviance of θ for diverse values of μ against α.

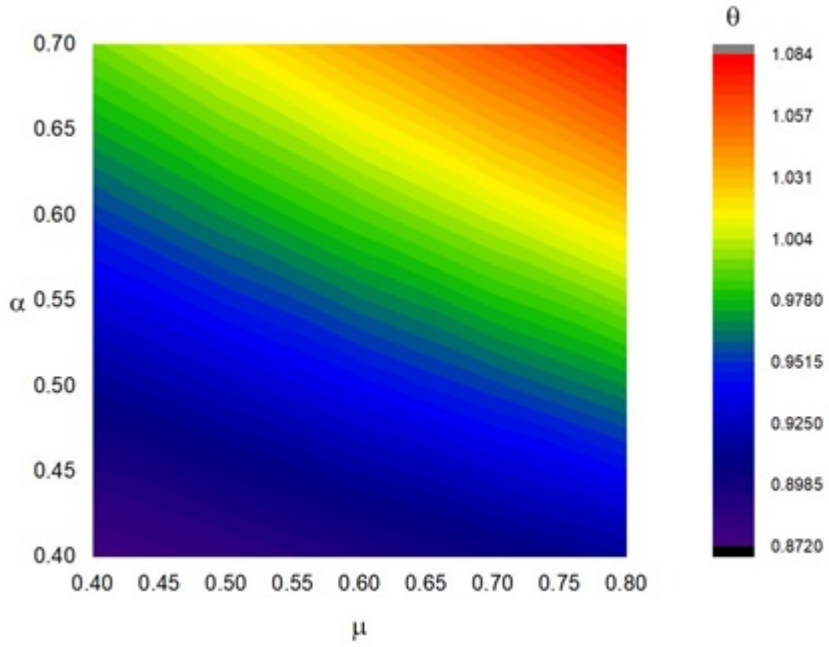

Figure 11: Deviance of θ for diverse values of μ against α.

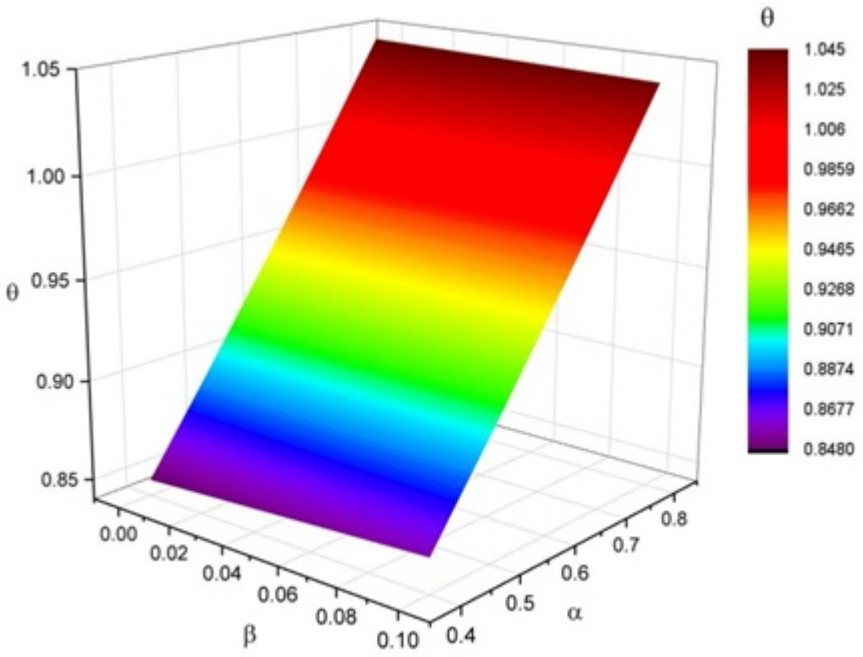

Figure 12: Deviance of θ for diverse values of α against β.

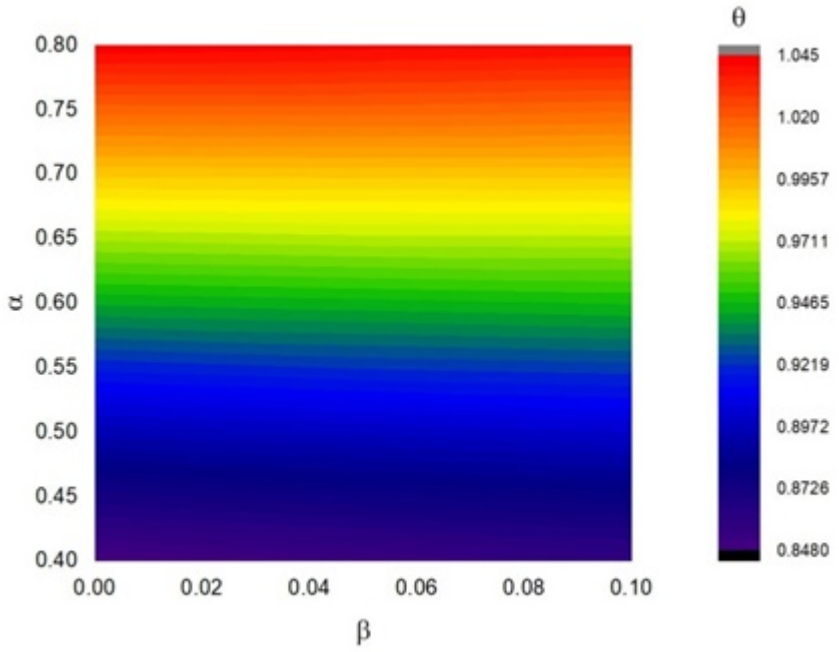

Figure 13: Deviance of θ for diverse values of α against β.

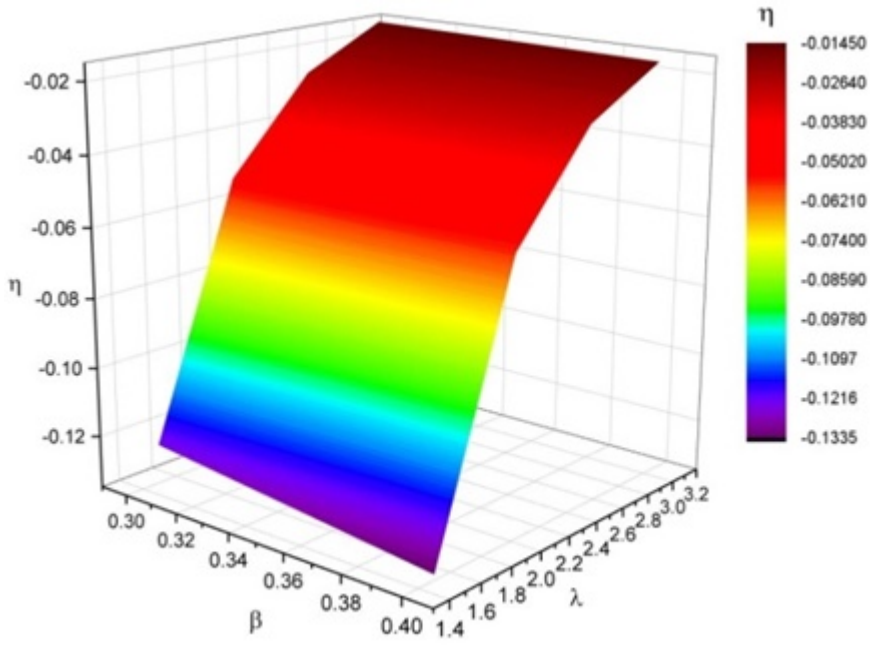

Figure 14: Efficiency of fin ν for diverse values of λ against β.

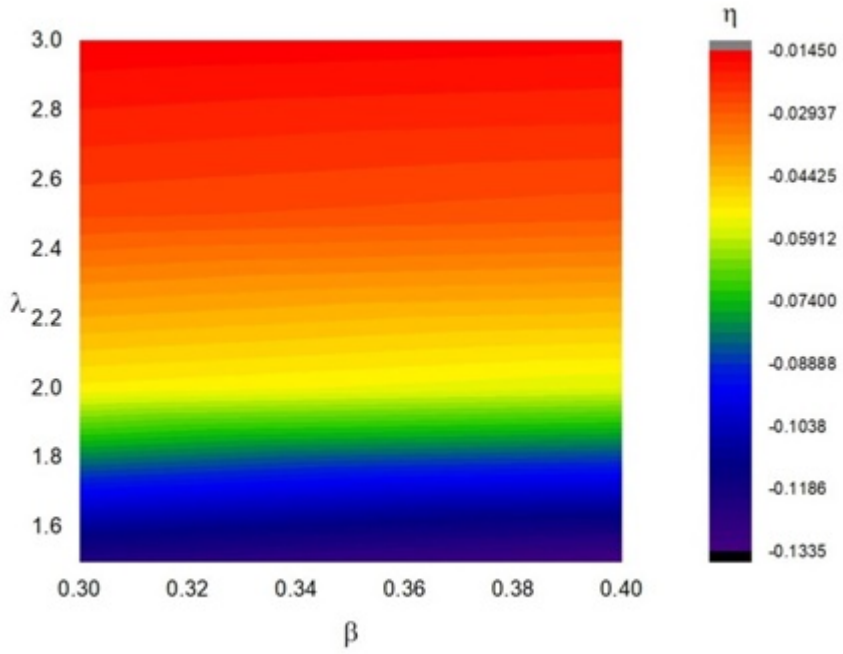

Figure 15: Efficiency of fin ν for diverse values of λ against β.

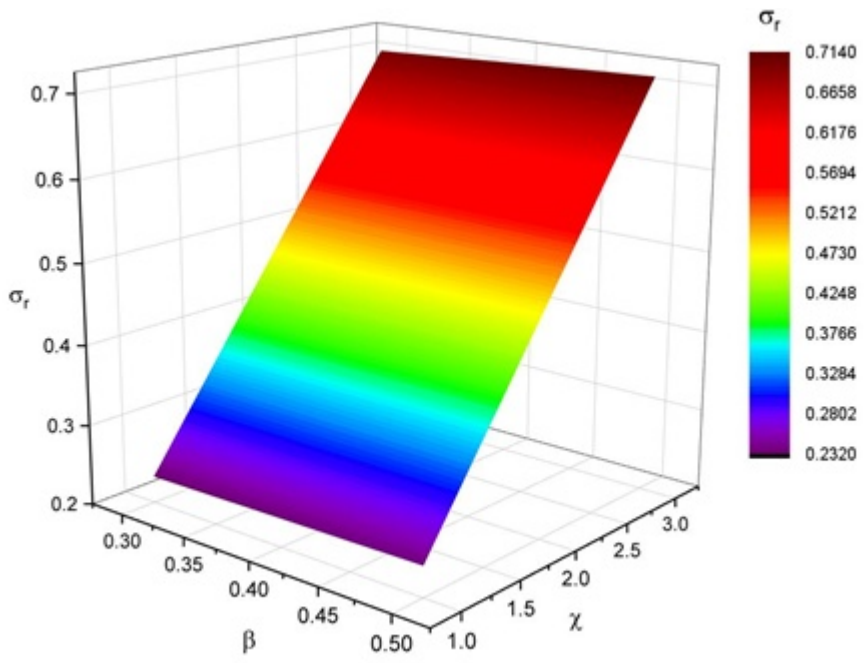

Figure 16: Impact of non-dimensional parameters χ and β on radial stress distribution.

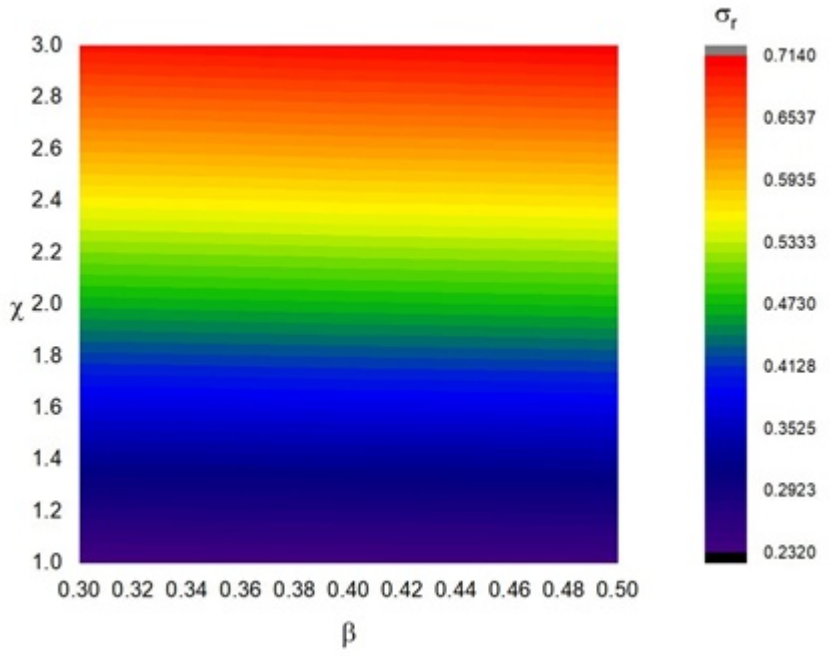

Figure 17: Impact of non-dimensional parameters χ and β on radial stress distribution.

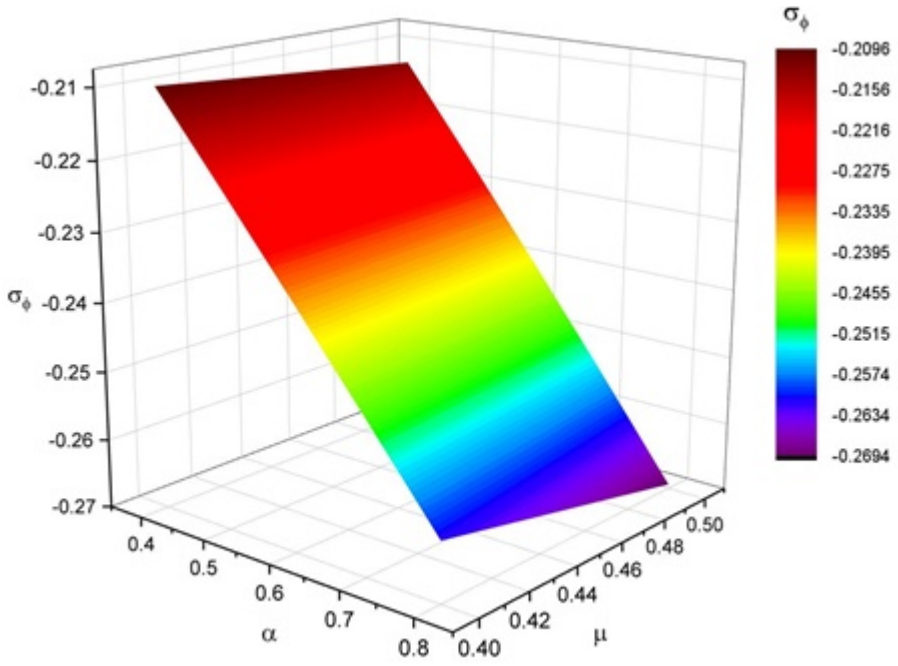

Figure 18: Impact of non-dimensional parameters α and μ on tangential stress distribution.

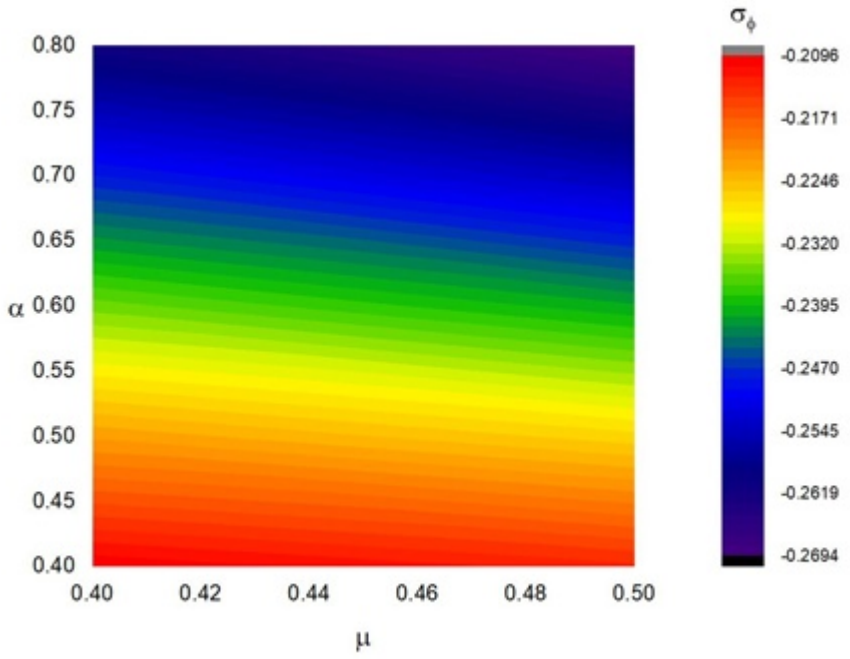

Figure 19: Impact of non-dimensional parameters α and μ on tangential stress distribution.

References

[1] M. T. Darvishi, F. Khani, and A. Aziz, "Numerical investigation for a hyperbolic annular fin with temperature-dependent thermal conductivity," Propuls. Power Res., vol. 5, no. 1, pp. 55–62, Mar. 2016, doi: 10.1016/j.jppr.2016.01.005.

[2] V. Gaba, A. Tiwari, and S. Bhowmick, "A report on performance of annular fins having varying thickness," J. Eng. Appl. Sci., vol. 11, pp. 5120–5125, Apr. 2016.

[3] R. Ranjan, A. Mallick, and D. K. Prasad, "Closed form solution for a conductive–convective–radiative annular fin with multiple nonlinearities and its inverse analysis," Heat Mass Transf., vol. 53, no. 3, pp. 1037–1049, Mar. 2017, doi: 10.1007/s00231-016-1872-8.

[4] H. Bas and İ. Keles, "Analysis of Transient Thermal Stresses in Annular Fin," presented at the The 2nd World Congress on Momentum, Heat and Mass Transfer, Apr. 2017, doi: 10.11159/ichtd17.103.

[5] S.-Y. Lee, L.-K. Chou, and C. K. Chen, "Nonlinear temperature and thermal stress analysis of annular fins with time dependent boundary condition," Eng. Comput., vol. 35, no. 3, pp. 1444–1459, Jan. 2018, doi: 10.1108/EC-07-2017-0289.

[6] G. Sowmya, B. J. Gireesha, B. C. Prasannakumara, "Scrutinization of different shaped nanoparticle of molybdenum disulfide suspended nanofluid flow over a radial porous fin," Int. J. Numer. Methods Heat Fluid Flow, vol. 30, no. 7, pp. 3685–3699, Jan. 2019, doi: 10.1108/HFF-08-2019-0622.

[7] A. Baslem, G. Sowmya, B. J. Gireesha, B. C. Prasannakumara, M. Rahimi-Gorji, and N. M. Hoang, "Analysis of thermal behavior of a porous fin fully wetted with nanofluids: convection and radiation," J. Mol. Liq., vol. 307, p. 112920, Jun. 2020, doi: 10.1016/j.molliq.2020.112920.

[8] J. K. Zhou, Differential transformation and its applications for electrical circuits. Huazhong University Press, Wuhan, China, 1986.

[9] S. E. Ghasemi, M. Hatami, and D. D. Ganji, "Thermal analysis of convective fin with temperature-dependent thermal conductivity and heat generation," Case Stud. Therm. Eng., vol. 4, pp. 1–8, Nov. 2014, doi: 10.1016/j.csite.2014.05.002.

[10] A. Moradi, T. Hayat, and A. Alsaedi, "Convection-radiation thermal analysis of triangular porous fins with temperature-dependent thermal conductivity by DTM," Energy Convers. Manag., vol. 77, pp. 70–77, Jan. 2014, doi: 10.1016/j.enconman.2013.09.016.

[11] B. Kundu and K.-S. Lee, "A proper analytical analysis of annular step porous fins for determining maximum heat transfer," Energy Convers. Manag., vol. 110, pp. 469–480, Feb. 2016, doi: 10.1016/j.enconman.2015.09.037.

[12] S. Mosayebidorcheh, M. Farzinpoor, and D. D. Ganji, "Transient thermal analysis of longitudinal fins with internal heat generation considering temperature-dependent properties and different fin profiles," Energy Convers. Manag., vol. 86, pp. 365–370, Oct. 2014, doi: 10.1016/j.enconman.2014.05.033.

[13] A. J. Christopher, N. Magesh, R. J. P. Gowda, R. N. Kumar, and R. S. V. Kumar, "Hybrid nanofluid flow over a stretched cylinder with the impact of homogeneous–heterogeneous reactions and Cattaneo–Christov heat flux: Series solution and numerical simulation," Heat Transf., vol. n/a, no. n/a, doi: https://doi.org/10.1002/htj.22052.

[14] R. Ranjan and A. Mallick, "An Efficient Unified Approach for Performance Analysis of Functionally Graded Annular Fin with Multiple Variable Parameters," Therm. Eng., vol. 65, no. 9, pp. 614–626, Sep. 2018, doi: 10.1134/S0040601518090082.

[15] S. Hoseinzadeh, A. Moafi, A. Shirkhani, and A. J. Chamkha, "Numerical Validation Heat Transfer of Rectangular Cross-Section Porous Fins," J. Thermophys. Heat Transf., vol. 33, no. 3, pp. 698–704, 2019, doi: 10.2514/1.T5583.

[16] R. Ranjan, A. Mallick, and P. Jana, "Thermoelastic study of a functionally graded annular fin with variable thermal parameters using semiexact solution," J. Therm. Stress., vol. 42, no. 10, pp. 1272–1297, Oct. 2019, doi: 10.1080/01495739.2019.1646617.

[17] M. Kezzar, I. Tabet, and M. R. Eid, "A new analytical solution of longitudinal fin with variable heat generation and thermal conductivity using DRA," Eur. Phys. J. Plus, vol. 135, no. 1, p. 120, Jan. 2020, doi: 10.1140/epjp/s13360-020-00206-0.

[18] G. Sowmya, B. J. Gireesha, S. Sindhu, and B. C. Prasannakumara, "Investigation of Ti6Al4V and AA7075 alloy embedded nanofluid flow over longitudinal porous fin in the presence of internal heat generation and convective condition," Commun. Theor. Phys., vol. 72, no. 2, p. 025004, Feb. 2020, doi: 10.1088/1572-9494/ab6904.

[19] A. Mallick, R. Ranjan, D. K. Prasad, and R. Das, "Inverse Prediction and Application of Homotopy Perturbation Method for Efficient Design of an Annular Fin with Variable Thermal Conductivity and Heat Generation," Math. Model. Anal., vol. 21, no. 5, Art. no. 5, Sep. 2016, doi: 10.3846/13926292.2016.1225606.

[20] J. K. Zhou, Differential transformation and its applications for electrical circuits. Huazhong University Press, Wuhan, China, 1986.

[21] I. H. Abdel-Halim Hassan, "Different applications for the differential transformation in the differential equations," Appl. Math. Comput., vol. 129, no. 2, pp. 183–201, Jul. 2002, doi: 10.1016/S0096-3003(01)00037-6.

[22] A. Jawad and A. Hamody, "Differential Transformation Method for Solving Nonlinear Heat Transfer Equations," Feb. 2013. doi: 10.13140/2.1.2858.4965.

[23] J. P. Boyd, "Padé approximant algorithm for solving nonlinear ordinary differential equation boundary value problems on an unbounded domain," Comput. Phys., vol. 11, no. 3, pp. 299–303, May 1997, doi: 10.1063/1.168606.

[24] M. M. Rashidi, N. Freidoonimehr, E. Momoniat, and B. Rostami, "Study of Nonlinear MHD Tribological Squeeze Film at Generalized Magnetic Reynolds Numbers Using DTM," PLOS ONE, vol. 10, no. 8, p. e0135004, Aug. 2015, doi: 10.1371/journal.pone.0135004

[25] C. Arslanturk, "Correlation equations for optimum design of annular fins with temperature dependent thermal conductivity," Heat Mass Transf., vol. 45, no. 4, pp. 519–525, Feb. 2009, doi: 10.1007/s00231-008-0446-9.

[26] A. Mallick, S. Ghosal, P. K. Sarkar, and R. Ranjan, "Homotopy Perturbation Method for Thermal Stresses in an Annular Fin with Variable Thermal Conductivity," J. Therm. Stress., vol. 38, no. 1, pp. 110–132, Jan. 2015, doi: 10.1080/01495739.2014.981120

[27] Jangid Sanju, Mehta Ruchika, Singh Jagdev, Baleanu Dumitru and Alshomrani Ali Saleh, "Heat and mass transport of hydromagnetic williamson nanofluid passing through a permeable media across an extended sheet of varying thickness", Thermal Science, vol. 27, pp. 129-140, 2023, doiserbia.nb.rs/Article.aspx?ID=0354-983623129J.

[28] Jain Ruchi, Mehta Ruchika, Mehta Tripti, Singh Jagdev and Baleanu Dumitru, "MHD flow and heat and mass transportinvestigation over a decelerating disk with ohmic heating and diffusive effect", Thermal Science, vol. 27 (1), pp. 141-149, 2023, doiserbia.nb.rs/Article.aspx?ID=0354-983623141J.

[29] Kumar Ravindra, Singh Jagdev, Mehta Ruchika, Kumar Devendra and Baleanu Dumitru, "Analysis of the impact of thermal radiation and velocity slip on the melting

of magnetic hydrodynamic micropolar fluid-flow over an exponentially stretching sheet", Thermal Science, vol. 27 (1), pp. 311-322, 2023, doi:10.2298/TSCI23S1311K.

[30] Ruchika Mehta, Ravindra Kumar, Himanshu Rathore and Jagdev Singh, "Joule heating effect on radiating MHD mixed convection stagnation point flow along vertical stretching sheet embedded in a permeable medium and heat generation/absorption", Heat Transfer (Wiley), vol. 51 (8), pp. 7369-7386, 2022, doi: 10.1002/htj.22648.

[31] Jagdev Singh, George A. Anastassiou, Dumitru Baleanu, Carlo Cattani, and Devendra Kumar, "Analysis of Soret and Dufour Effect on MHD Fluid Flow Over a Slanted Stretching Sheet with Chemical Reaction, Heat Source and Radiation", Advances in Mathematical Modelling, Applied Analysis and Computation. Lecture Notes in Networks and Systems, Springer, Singapore, vol. 415, Oct. 2022, doi.org/10.1007/978-981-19-0179-9.

Study of Heat Transfer in Porous Fin with Temperature Dependent Properties

Surjan Singh [1], Priti Sharma [2*], and Subrahamanyam Upadhaya [3]

[1] Department of Mathematics, Eternal Universty, Baru Sahib, Himachal Pradesh, India, Email:surjan.singhbhu@gmail.com

[2*] Corresponding Author: Department of Mathematics, Eternal University, Baru Sahib, Himachal Pradesh, India, Email:pritisharma251997@gmail.com

[3]Faculty of BS & H, INA, Ezhimal, India, Email:subabbu16@gmail.com

Abstract

In this paper, mathematical model of heat transfer in a porous fin with internal heat generation, and thermal conductivity is influenced by both spatial factors and temperature are examined. These two concepts are integrated into the model, which highlighting the originality of the current study. The equations and conditions that govern the system are expressed in a dimensionless manner. We examine three scenarios for thermal conductivity: constant, linear, and exponential dependence on temperature. We have utilized three different techniques to solve the problem, including the Legendre Wavelet Collocation, Finite Difference, and Least Square. Due to the nonlinearity of the presented problem, it is not possible to find an exact analytical solution. In this specific scenario, we calculate exact solution, which is then compared to these three methods and found to have a good agreement. The findings and error assessment are displayed in figures and tables. The Legendre wavelet collocation approach yields high accuracy. The novelty of the research is the implantation of space and temperature dependent thermal conductivity and solution of a complex nonlinear problem using a hybrid numerical technique, specifically the collocation method with Legendre Wavelet basis functions.

Keywords: Finite difference, Least square, Porous fin, Legendre Wavelet Collocation Method, Conductivity.

1. Introduction

Mechanical processes produce heat. The important question here is how is how to efficiently disperse this heat into the surrounding medium. In recent times, fins have gained popularity as efficient tools for dissipating heat into the surrounding environment due to their uncomplicated structure and ability to facilitate various forms of coupled heat transmission. Fins are appendages affixed to a primary item to augment the transfer of heat between the primary object and its environment. Firstly, Harper and Brown [1] presented mathematical analysis for extended surfaces. This surface was referred as a cooling fin, which later evolved into a fin. Further, Jakob [2] noted that the roots of the published mathematical analysis of fin can be traced back to early 1789. At that time, experiments were conducted to demonstrate the thermal conductivity of various metals. The fabrication of rods made from different metals

was coated with wax, and the resulting melting patterns were observed when the bases of the rods were heated. The mathematical analysis of temperature variations in rods was published by Fourier [3]. Fins are produced using metallic materials that possess a high level of thermal conductivity. Aluminum, copper, and stainless steel are the most often utilized materials. Kundu and Das [4] stated that maximizing the fin efficiency is largely dependent on its geometry. It is widely known that when the length of a fin rises, the heat transmission rate from the fin reduces, and the entire surface of the fin may not be used to its full potential. Because of this, designers are constantly working to discover the optimal fin that will either reduce the fin material's contribution to heat transfer or optimize the heat transmission rate over any specific fin region. An analysis of the fin shape and all of its dimensions can determine the amount of material required to make a fin as small as possible for the desired heat transfer. Alternatively, fin profile dimensions that fulfill the optimization conditions presented in reference [5]. Multiple fin forms are available for dissipating heat into the surroundings, such as rectangular, annular, elliptic, parabolic, and pin fins, etc. [6]. The applications of expanded surfaces are rising in various industries, including air conditioning, refrigeration, internal combustion engines, etc. [7]. Yunus [8] published a book that specifically examines heat transmission, providing a clear explanation of fundamental ideas. With the help of mathematical formulations, a novel fin design can be created, improving the overall quality of the fin, optimizing material costs, and maintaining fin efficiency.

Several researchers have conducted extensive research on various aspects of fins or heat exchangers. Bergman et al. [9] presented key concepts pertaining to the transfer of heat and mass, establishing a correlation between the principles of thermodynamics and heat transfer. Khatami and Rahbar [10] investigated the effectiveness of porous fins by integrating the concepts of the second law of thermodynamics into the governing differential equation. Hatami and colleagues [11] employed the differential transformation, the least square, and the moment techniques to analyze temperature variations in a porous fins with attributes that rely on temperature. Cuce and Cuce [12] utilized the homotopy perturbation method to evaluate the influence of heat transfer, efficiency, and efficacy on a porous fin. In addition, Venkitesh and Mallick [13] expanded the homotopy perturbation approach to analyze annular porous fins with two different geometries. Ma et al. [14] utilized the spectral element method to examine the heat transmission in rotating porous fins with various profiles. Kundu et al. [15] utilized the adomian decomposition approach to evaluate the performance and optimal design factors for porous fins. In a similar vein, Buonomo et al. [16] employed the adomian decomposition method to evaluate the influence of convection and radiation on a porous fin upon temperature. Although, Gireesha and Sowmya [17] utilized the differential transform approach to analyze the interaction between natural radiation and convection on an inclined extended porous fin. Hatami and Ganji [18] employed the RK4 method to investigate heat transfer and heat flux in circular convective and radiative porous fins. Ghasemi et al. [19]utilized the differential transformation method to investigate the heat transmission in solid and porous longitudinal fins, while considering the influence of temperature-dependent characteristics. Hatami and Ganji [20] utilized the RK4 technique and the Least Square method to analyze the variations in temperature and cooling effectiveness of totally wet porous fins. Bhanja et al. [21] utilized the adomian decomposition technique to examine the fluctuations in temperature, efficiency, and optimal design parameters for rotating porous fins. Hamdan and Al-Nimr [22] employed an implicit finite difference method to investigate forced convection between two parallel, isothermal plates with porous fins. Khani and Aziz [23] utilized Bessel function in study state for finding temperature variation and efficiency in longitudinal fin with space dependent thermal conductivity. Jangid et al. [24] applied RK4

to determine heat and mass transfer through fluid-flows extended sheets with variable thickness. Kumar et al. [25] examine the impact of thermal radiation and velocity slip on the melting of magnetic hydrodynamic micro-polar fluid flow over an exponentially stretching sheet fixed in a porous medium.

Recently, wavelet-weighted residual techniques have been successfully implemented to obtain solutions to the complicated problems. Singh et al. [26] employed the wavelet collocation technique to examine heat dissipation in a constantly rotating fin with properties that are temperature and wavelength dependent. Singh et al. [27] applied wavelet collocation and Galerkin techniques to examine heat transmission in a power-law-type fin. Oguntala et al. [28] examine the ideal layout, thermal efficiency, and stability of a rectangular fin via utilizing the haar wavelet collocation technique. Upadhyay et al. [29] employing the finite difference Legendre wavelet collocation technique along with the Galerkin approach to study heat and moisture transmission in the industrial drying of food goods. Recently, Kaur and Singh [30] utilized Legendre wavelet collocation and Least square techniques to study convective and radiative heat transfer in moving fin. The results findings concluded that Legendre wavelet collocation technique gives high accuracy in comparison to least square.

The objective of this study is to validate a mathematical model of heat transfer in a porous fin with internal heat generation, and thermal conductivity is influenced by both spatial factors and temperature. In order to achieve our research target, we utilize three separate methodologies: Legendre Wavelet Collocation, Finite Difference, and Least Square. In this specific scenario, we calculated a precise solution, compared it to the results of all these approaches, and saw a strong agreement. The findings and error assessment are displayed in figures and tables.

In existing studies, many numerical methods have been applied by researchers for finding temperature variation in porous or solid fins with temperature or space-dependent thermal conductivity, but this is the first time influences of thermal conductivity in both temperate and space are studied with the implementation of the Legendre wavelet collocation method. This creates interest for science or technology readers and can be applied in industries where thermal conductivity depends on both temperature and space. The novelty of the research is the implantation of space and temperature-dependent thermal conductivity and the solution of a complex nonlinear problem using a hybrid numerical technique, specifically the collocation method with Legendre wavelet basis functions. The present method has been successfully applied to linear and nonlinear problems.

2. Mathematical Formulation

Figure 1 depicts a graphical illustration of a rectangular porous fin. It has specific measurements, such as a length L, and a thickness t, is located in an environment, where heat is transferred through convection on both surfaces at a temperature T_∞. Oguntala and Abd-Alhameed [31] make the assumption that the porous media is uniform, isotropic, and completely surrounded by a single-phase fluid. The solid and fluid are assumed to have constant physical properties, with the exception of the liquid's fluctuating density, which may affect the buoyancy term. The fluid and porous media within the domain are in a state of thermodynamic equilibrium, whereas any surface radiative transfers and non-Darcian influences are deemed negligible. The temperature change within the fin is restricted to a one-dimensional distribution, meaning that it varies along its length while remaining constant over time. It is presumed that the tip of the fin maintains a constant temperature throughout.

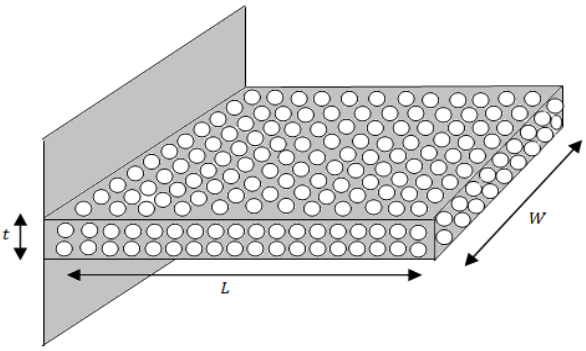

Figure 1: Rectangular porous fin geometry.

The mathematical model governing heat transmission in a one-dimensional fin is determined using Darcy's model and the assumption made before. This model is governed by [31], which is as follows:

$$\frac{d}{dx}[k_{eff}(T)\frac{dT}{dx}] - \frac{h(T-T_\infty)}{t} - \frac{\rho c_p g\beta' K(T-T_\infty)^2}{tv_f} + q_a(T) = 0, \tag{1}$$

and the specified boundary conditions (BC) are as follows:

$$x = L, \qquad T = T_b, \tag{2}$$

$$x = 0, \qquad \frac{dT}{dx} = 0, \tag{3}$$

here, our main emphasis is on the measurement of thermal conductivity and the internal heat generation. These factors are influenced by temperature and location-specific thermal conductivity [32], which can be described as:

$$k_{eff}(T) = k_a f\left(\frac{T-T_0}{T_b-T_\infty}\right), \tag{4}$$

$$q_a(T) = q_a[1+\psi(T-T_\infty)], \tag{5}$$

$$K_{eff}(T) = k_a(1+ax), \tag{6}$$

putting Eqs. (4-5) in Eq. (1), we get Eq. (7) and Eqs. (5-6) into Eq. (1), we get Eq. (8) as described below:

$$\frac{d}{dt}\left[f\left(\frac{T-T_0}{T_b-T_\infty}\right)\frac{dt}{dx}\right] - \frac{h(T-T_\infty)}{k_a t} - \frac{\rho c_p g\beta' K(T-T_\infty)^2}{k_a t v_f} + q_a[1+\psi(T-T_\infty)] = 0, \tag{7}$$

$$\frac{d}{dt}\left[f(x)\frac{dt}{dx}\right] - \frac{h(T-T_\infty)}{k_a t} - \frac{\rho c_p g\beta' K(T-T_\infty)^2}{k_a t v_f} + q_a[1+\psi(T-T_\infty)] = 0, \tag{8}$$

instigating dimensionless variables and parameters:

$$X = \frac{x}{L}, \quad \theta = \frac{T-T_\infty}{T_b-T_\infty}, \quad Ra = \left(\frac{\beta' g T_a t^3}{{v_f}^2}\right)\left(\frac{\rho c_p v_f}{k_{eff,a}}\right), \quad Q = \frac{q v_f t}{\rho c_p g\beta' K(T_b-T_\infty)^2},$$

$$M^2 = \frac{hL^2}{k_{eff,a}t} \quad Da = \frac{k}{t^2}, \quad S_h = \frac{RaDa\left(\frac{L}{t}\right)^2}{k_{eff,a}}, \quad \beta = \lambda(T_b-T_\infty), \quad \gamma = \psi(T_b-T_\infty), \tag{9}$$

the Eqs. (4), (5) and (6) can be converted into a dimensionless form as follows:

$$k_{eff}(\theta) = k_a f(\theta),$$
$$q_a(\theta) = q_a[1 + \gamma(\theta)],$$
$$K_{eff}(\theta) = k_a(1 + BX),$$

using Eq. (9), the dimensionless form of the model Eqs. (7) and (8) subjected to the boundary conditions Eqs. (2)-(3) come out to be:

$$f(\theta)\frac{d^2\theta}{dX^2} + f^{'}(\theta)\left(\frac{d\theta}{dX}\right)^2 - M^2\theta - S_h\theta^2 + S_hQ(1+\gamma\theta) = 0, \tag{10}$$

$$f(X)\frac{d^2\theta}{dX^2} + f^{'}(X)\left(\frac{d\theta}{dX}\right)^2 - M^2\theta - S_h\theta^2 + S_hQ(1+\gamma\theta) = 0, \tag{11}$$

the conditions at the boundaries are:

$$X = 1, \qquad \theta = 1, \tag{12}$$
$$X = 0, \qquad \frac{d\theta}{dX} = 0. \tag{13}$$

3. Solution of the problem

The concepts of matrix of integration, wavelet collocation method, Least Square method (LSM) and Finite Difference method (FDM) are given below:

3.1. Operational Matrix of integration

The matrix that represents the integration operational properties of the Legendre wavelet is given by:

$$\psi_{n,m} = \begin{cases} \sqrt{(m+1/2)}2^{k/2}P_m\left(2^kX - \hat{n}\right) & , \quad \frac{\hat{n}-1}{2^k} \le X \le \frac{\hat{n}+1}{2^k} \\ 0 & , \quad otherwise \end{cases}, \tag{14}$$

where $n = 1, 2, ..., 2^{k-1}, m = 0, 1, ..., S-1$ and k is the positive integer. Here, $P_m(X)$ signifies the Legendre polynomial of degree m, and $\psi(X)$, as defined in Eq. (14), is derived as follows:

$$\int_0^X \psi(t)dt = P\psi(X), \qquad \in [0, 1),$$

where P is the operational matrix of order $2^{k-1}M \times 2^{k-1}M$ and $k = 1$, which is investigated by Razzaghi and Yousefi [33].

3.2. Legendre Wavelet Collocation Method

Let

$$\theta^{''} = C^T \psi(X), \tag{15}$$

integrating Eq. (15) twice from 0 to X, and using BC, we obtain

$$\theta^{'}(X) = C^T P \psi(X), \tag{16}$$

and

$$\theta(X) = 1 - C^T P^2 \psi(1) + C^T P^2 \psi(X), \tag{17}$$

substituting Eqs. (15),(16) and (17) in Eqs. (10) and (11), we get

$$f(\theta)[C^T \psi X)] + f^{'}(\theta)[C^T P \psi(X)]^2 - M^2[1 - C^T P^2 \psi(1) + C^T P^2 \psi(X)] - S_h[1 - C^T P^2 \psi(1) + C^T P^2 \psi(X)]^2 + S_h Q[1 + \gamma(1 - C^T P^2 \psi(1) + C^T P^2 \psi(X))] = 0, \tag{18}$$

$$f(X)[C^T \psi X)] + f^{'}(X)[C^T P \psi(X)]^2 - M^2[1 - C^T P^2 \psi(1) + C^T P^2 \psi(X)] - S_h[1 - C^T P^2 \psi(1) + C^T P^2 \psi(X)]^2 + S_h Q[1 + \gamma(1 - C^T P^2 \psi(1) + C^T P^2 \psi(X))] = 0, \tag{19}$$

as $\theta(X)$ is an approximation of the results of the Eqs. (19). We choose n collocation points denoted as $(X_i, i = 1, 2, 3, ..., n)$, such that the residuals $R(X, c_1, c_2, ..., c_n)$ become zero. It is essential to note that the count of these collocation points and coefficients should be identical.

3.2.1. Temperature dependent thermal conductivity

For temperature dependent thermal conductivity we apply three cases in Eq. (18), we get

Case 1: Where thermal conductivity remains constant, the substitution of $f(\theta) = 1$ into Eq. (19) produces the following outcome:

$$[C^T \psi(X)] - M^2[1 - C^T P^2 \psi(1) + C^T P^2 \psi(X)] - S_h[1 - C^T P^2 \psi(1) + C^T P^2 \psi(X)]^2 + S_h Q[1 + \gamma(1 - C^T P^2 \psi(1) + C^T P^2 \psi(X))] = 0. \tag{20}$$

Case 2: Where thermal conductivity remains linear, the substitution of $f(\theta) = 1 + \beta\theta$ into Eq. (19), produces the following outcome:

$$[1 + \beta(1 - C^T P^2 \psi(1) + C^T P^2 \psi(X))][C^T \psi X)] + \beta[C^T P \psi(X)]^2 - M^2[1 - C^T P^2 \psi(1) + C^T P^2 \psi(X)] - S_h[1 - C^T P^2 \psi(1) + C^T P^2 \psi(X)]^2 + S_h Q[1 + \gamma(1 - C^T P^2 \psi(1) + C^T P^2 \psi(X))] = 0. \tag{21}$$

Case 3: Where thermal conductivity remains exponential, we put $f(\theta) = e^{\beta\theta}$ in Eq. (19), we get

$$e^{\beta\theta}[C^T\psi X)] + \beta e^{\beta\theta}[C^T P\psi(X)]^2 - M^2[1 - C^T P^2\psi(1) + C^T P^2\psi(X)] - S_h[1 - C^T P^2$$
$$\psi(1) + C^T P^2\psi(X)]^2 + S_h Q[1 + \gamma(1 - C^T P^2\psi(1) + C^T P^2\psi(X))] = 0. \tag{22}$$

3.2.2. Location dependent thermal conductivity

For location dependent thermal conductivity, we take $f(X) = 1 + BX$ as a linear function in Eq. (19), we get

$$(1 + BX)[C^T\psi(X)] + B[C^T P\psi(X)]^2 - M^2[1 - C^T P^2\psi(1) + C^T P^2\psi(X)] - S_h[1 - C^T P^2\psi(1) +$$
$$C^T P^2\psi(X)]^2 + S_h Q[1 + \gamma(1 - C^T P^2\psi(1) + C^T P^2\psi(X))] = 0. \tag{23}$$

This system consists of nine nonlinear algebraic equations, which are evaluated utilizing nine Legendre Wavelet basis functions and collocation points spanning the interval $(0, 1)$. Solving the resulting system of Eqs. (20), (21), (22) and (23) separately, by using Newton-Raphson Method. The system has nine nonlinear algebraic equations, which are computed using nine Legendre Wavelet basis functions and collocation points inside the interval $(0, 1)$. The values of the unknowns C_i were determined, and the dimensionless temperature was computed using the Eq. (17).

3.3. Least Square Method

The LSM, initially proposed by [34], is a weighted approach for minimizing the residuals of the test functions, which satisfies boundary conditions and is used to calculate the nonlinear differential equations. If all of the squared residuals are added up continuously [35], then

$$S = \int_X R(X)R(X)dX = \int_X R^2(X)dX, \tag{24}$$

in order to minimize this scalar function, all derivatives of S with respect to the unknown coefficients should be equated to zero, as stated in [35].

$$\frac{\delta S}{\delta c_i} = 2\int_X R(X)\frac{\delta R}{\delta c_i}dX = 0, \tag{25}$$

the weighted function is

$$W_i = 2\frac{\delta R}{\delta c_i}, \tag{26}$$

where, the equation's coefficient "2" will be eliminated. Then, Eq. (26) can be written as:

$$W_i = \frac{\delta R}{\delta c_i}, \tag{27}$$

to applying this method, we consider trial solution as follows

$$\theta(X) = 1 + c_1(1 - X^2) + c_2(1 - X^3) + c_3(1 - X^4) + c_4(1 - X^5) + c_5(1 - X^6), \tag{28}$$

which satisfies boundary conditions. Now putting the computed values of $\theta(X)$, $\theta'(X)$, and $\theta''(X)$ into Eqs. (10) and (11). We obtain residuals $R(X, c_1, c_2, ..., c_n)$ and evaluate the weighted function as described in Eq. (27). We substitute these residuals and weighted function $(W_i, i = 1, 2, ...n)$ in Eq. (25). Subsequently, we proceed to integrate Eq. (25) form 0 to 1, and we obtain a system of nonlinear equations in c_i. We employ the Newton-Raphson method to solve these systems of nonlinear equations and derive the values of ${c_i}'s$, which we subsequently substitute into the Eq. (28) in order to achieve the desired solution for the problem.

3.4. Finite Difference Method

Han *et al* [36] previously highlighted the use and validity of the finite element technique to examine the heat flow in fins for constant thermal properties. We used the central difference approximation to discretize X co-ordinate. Setting the central difference formulae as follows:

$$\begin{aligned}
&\theta(X) \approx \theta_i, \\
&\frac{d\theta}{dX} \approx \frac{\theta_{i+1} - \theta_{i-1}}{2h}, \\
&\frac{d^2\theta}{dX^2} \approx \frac{\theta_{i+1,j} - 2\theta_{i,j} + \theta_{i-1,j}}{h^2},
\end{aligned}$$

substituting above formulae in Eqs. (10) and (11) with BC Eqs. (12) and (13), we get eleven nonlinear algebraic equations. Solving this system of equations by well known method.

4. Results and Discussion

The present dimensionless model Eqs. (10)-(13) is a boundary value problem with a system of nonlinear differential equations. In order to find a resolution for this model, we utilized three separate methodologies: $LWCM$, LSM, and FDM. The approaches were employed to estimate the temperature distribution within a rectangular porous fin. The findings are displayed in figures 2-12 and tables 1-2.

4.1. Numerical validation of present method

A comparative analysis of the current approach with an exact results is required to validate the accuracy of the current methodology. In order to calculate the precise answer for a certain scenario, we substitute t $f(\theta) = f(X) = 1$ and $S_h = 0$ in Eqs. (10) and (11), we obtain

$$\frac{d^2\theta}{dX^2} - M^2\theta = 0, \tag{29}$$

and boundary conditions are provided in Eqs. (12) and (13).

The exact solution of Eq. (29) is:

$$\theta = \frac{coshMX}{coshM}. \tag{30}$$

Table 1 displays the comparison between the exact solution and the results obtained from the $LWCM$, LSM,

and FDM. the results produced by the $LWCM$, LSM, and FDM. In order to calculate the findings, we utilize the following reference values: $\gamma = 0.2, \beta = 0.0, Sh = 0.0, Q = 0.4$, and $M = 0.3$. From this table, it can be noticed that the findings obtained from these methods closely align with the exact results. In order to determine the highest level of accuracy among these methods, we do error analysis as presented in Table 2. An observation reveals that, the error in $LWCM$ is less as compared to LSM and FDM.This demonstrates the legitimacy of $LWCM$. So for further calculations, we employed the $LWCM$.

Table 1: A comparative analysis of Exact result with $LWCM, FDM$ and LSM in case 1.

X	Exact	LWCM	FDM	LSM
0.0	0.956627911900248	0.956627911900249	0.956628107692020	0.956627911900222
0.1	0.957058426747764	0.957058426747753	0.957058620610012	0.957058426749248
0.2	0.958350358782735	0.958350358782722	0.958350546851783	0.958350358783170
0.3	0.960504870831200	0.960504870831203	0.960505049233111	0.960504870828954
0.4	0.963523902099437	0.963523902099422	0.963524066941668	0.963523902096714
0.5	0.967410169919377	0.967410169919378	0.967410317284990	0.967410169919146
0.6	0.972167172194391	0.972167172194380	0.972167298133904	0.972167172196937
0.7	0.977799190547633	0.977799190547621	0.977799291072906	0.977799190550148
0.8	0.984311294175793	0.984311294175771	0.984311365252331	0.984311294175578
0.9	0.991709344411717	0.991709344411725	0.991709381990155	0.991709344410103
1.0	1.000000000000000	1.000000000000000	1.000000000000000	1.000000000000000

Table 2: Error analysis of Exact solution with LWCM, FDM and LSM for case 1.

X	Percentage Error		
	LWCM	FDM	LSM
0.0	1.0445×10^{-13}	$2.04669\ \times10^{-5}$	2.71571×10^{-12}
0.1	1.14844×10^{-12}	2.02561×10^{-5}	$1.55062\ \times10^{-10}$
0.2	1.35543×10^{-12}	1.96242×10^{-5}	$4.5389\ \times10^{-11}$
0.3	3.12086×10^{-13}	1.85738×10^{-5}	2.33833×10^{-10}
0.4	1.55554×10^{-12}	1.710×10^{-5}	2.82601×10^{-10}
0.5	1.03286×10^{-13}	1.5233×10^{-5}	$2.38821\ \times10^{-11}$
0.6	1.13058×10^{-12}	1.29545×10^{-5}	$2.61897\ \times10^{-10}$
0.7	1.22626×10^{-12}	1.02808×10^{-5}	$2.57209\ \times10^{-10}$
0.8	2.23328×10^{-12}	7.22094×10^{-6}	$2.18365\ \times10^{-11}$
0.9	8.06043×10^{-13}	3.78926×10^{-6}	$1.62742\ \times10^{-10}$
1.0	0	0	0

4.2. Effect of parameters

The preceding section (3) covered the development of a thermal conductivity model that takes into account the influence of location and temperature on a rectangular porous fin. We take thermal conductivity as temperature and location dependent to examine the temperature profile in porous fin. In this study, we consider one case for location-dependent thermal conductivity i.e., linear and three cases for temperature-dependent conductivity namely, constant, linear, and exponential function of temperature.

Figures 2-12 illustrate the impact of different parameters, such as thermal conductivity (β), thermo-geometric (M), porosity (S_h), heat transfer rate (Q), internal heat generation (γ), h value, and thermal conductivity gradient (B). The parameters are assigned reference values of $\beta = 0.5, S_h = 0.5, \gamma = 0.5, B = 0.5, M = 0.5$, and $Q = 0.5$.

4.2.1. Effects of parameters on temperature dependent porous fin

Figure 2 depicts the consequences of the thermal conductivity parameter (β) on the temperature profile in fin for case 1 and 2. From this figure, we deduced that the temperature in fin goes up with higher thermal conductivity values. Significantly, the temperature distribution for case 3 is higher than that of case 2. Consequently, in terms of

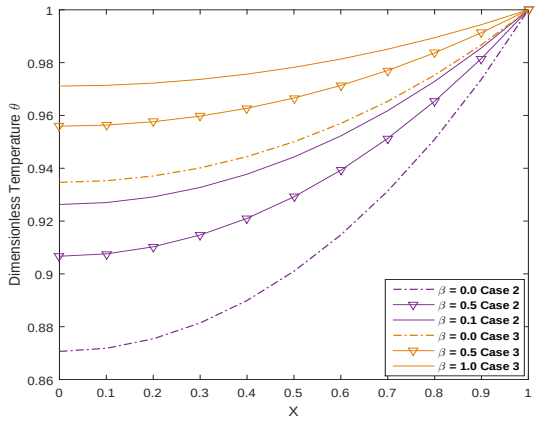

Figure 2: Effect of thermal conductivity parameter on temperature profile in fin for cases 2 and 3.

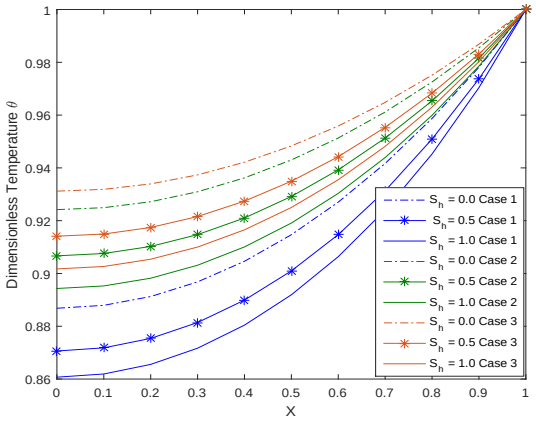

Figure 3: Impact of the porosity parameter on temperature profile in fin for cases 1, 2 and 3.

the cooling process, case 2 exhibits more efficiency compared to case 3. Figure 3 illustrates how the porosity parameter (S_h) affects the temperature profile in fin for cases 1, 2, and 3. We noticed that as the value of S_h rises, the temperature within the fin drops for cases 1, 2, and 3. This finding indicates that the fin's temperature tends to decrease with lower Darcy and Rayleigh numbers or higher effective thermal conductivity ratios. Figure 4 represented the impact of an internal heat generation parameter (γ) on the fin's temperature profile for cases 1, 2 and 3. Our observation revealed that the temperature within the fin goes up with higher values of γ for cases 1, 2,

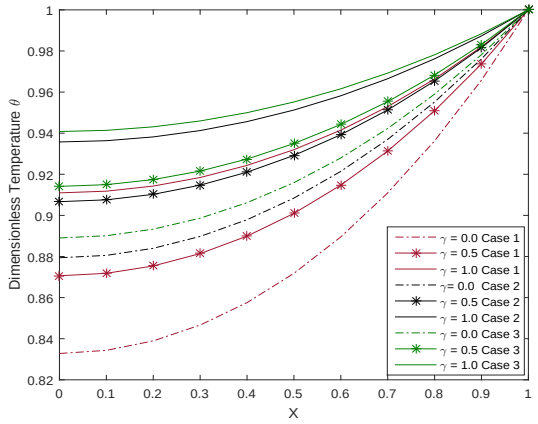

Figure 4: Consequences of internal heat generation parameter on temperature profile in fin for cases 1, 2 and 3.

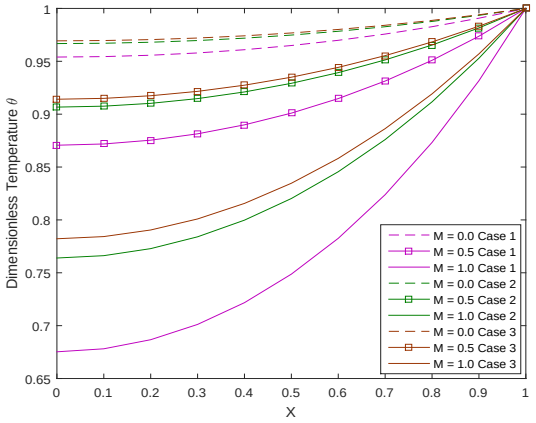

Figure 5: The impact of thermo-geometric parameter on temperature profile in the fin for cases 1, 2 and 3.

and 3. Figure 5 illustrated how thermo-geometric parameter M effect the fin temperature profile for case 1, 2 and 3. We concluded that as the value of M climbs for cases 1, 2, and 3, the temperature within the fin reduces. This suggests that, the fin's temperature goes down with higher effective thermal conductivity values or shorter fin lengths. Figure 6 displays the impact of heat transfer rate (Q) on the temperature profile within the fin for cases 1, 2, and 3. Our finding illustrates that as the value of Q grows, the temperature within the fin likewise rises for cases 1, 2, and 3. This shows that the fin's temperature goes up as both the kinematic viscosity and fin thickness grows, or as both the specific heat and coefficient of thermal expansion decrease. Figure 7 demonstrates the influence of varying h in FDM on temperature distribution in fin for case 1. We observed that, the accuracy of the results incre-

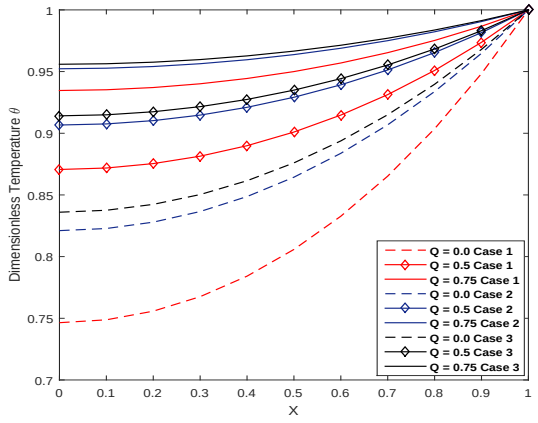

Figure 6: Effect of heat transfer rate on temperature profile in the fin for cases 1,2 and 3.

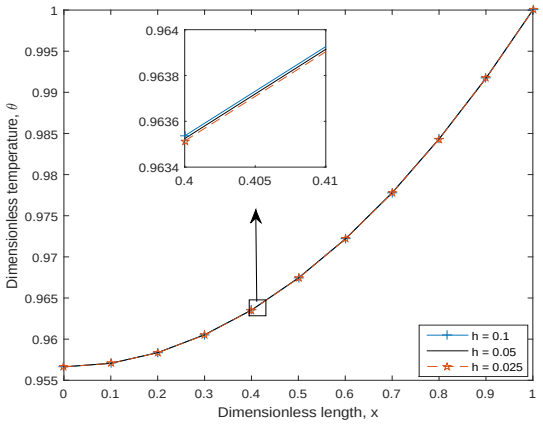

Figure 7: Impact of h on temperature distribution in fin for case 1.

-ased when the value of h decreased. Figures 3, 4, 5, 6, we noticed that, the temperature in porous fin for case 3 is greater as compared to case 2 and 1. It suggests that, case 1 is more efficient then other cases for cooling process.

4.2.2. Effects of parameters on location dependent porous fin

Figure 8 demonstrates the impact of thermal conductivity gradiant parameter (B) on the temperature profile in fin. We inferred that, the temperature within the fin rises with greater values of parameter B. Figure 9 exhibits the impact of the porosity parameter (S_h) on the temperature profile within the fin. Our observation indicates that as

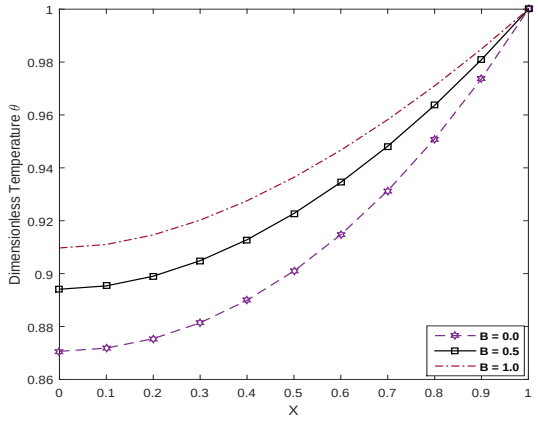

Figure 8: Effect of thermal conductivity gradiant B on temperature profile in fin.

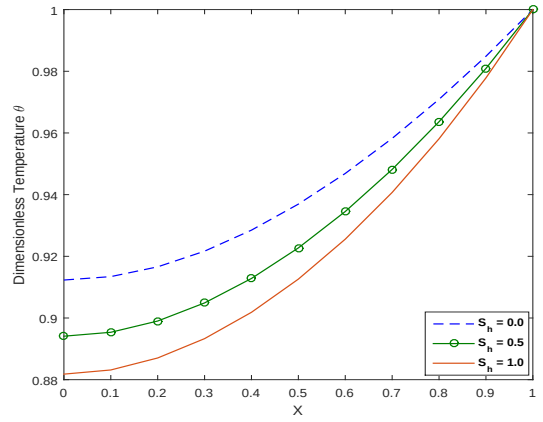

Figure 9: Effect of porosity parameter on temperature profile in fin.

the value of (S_h) rises, the temperature within the fin drops. This finding indicates that the fin's temperature tends to decrease with lower Darcy and Rayleigh numbers or higher effective thermal conductivity ratios. Figure 10 illustrates how internal heat generation parameter γ affects the temperature profile within the fin. It was noted that the temperature within the fin rises with higher values of γ. Figure 11 depicted the influence of heat transfer rate (Q) on the temperature profile within the fin. We deduced that, the temperature within the fin rises as the value of Q rises. This shows that the fin's temperature goes up as both the kinematic viscosity and fin thickness grows, or as both the specific heat and coefficient of thermal expansion decrease. Figure 12 illustrated the consequences of

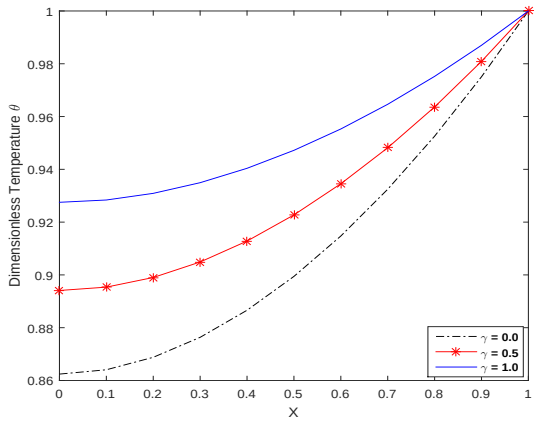

Figure 10: Effect of heat generation parameter on temperature profile in fin.

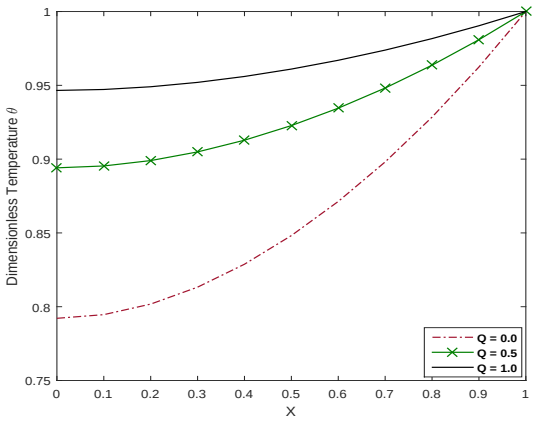

Figure 11: Effect of heat transfer rate on temperature profile in fin.

thermo-geometric parameter (M) on the temperature profile within the fin. We concluded that, the temperature within the fin goes down as the value of M rises. This suggests that, the fin's temperature goes down with higher effective thermal conductivity values or shorter fin lengths.

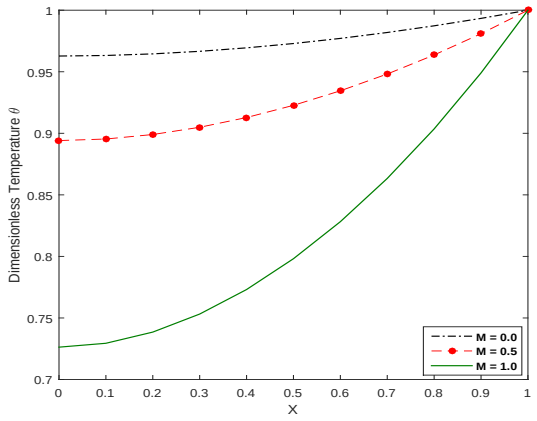

Figure 12: Impact of thermo-geometric parameter on temperature profile in fin.

5. Conclusions

In this paper, we consider a mathematical model and simulation technique for analyzing heat transfer in a porous fin, where the properties are influenced by temperature and location. The entire analysis has been done in dimensionless

form. To address our research objective, we employ three distinct methods: $LWCM, FDM$ and LSM. The main significant outcomes are summarized below:

- The results of $LWCM$ is correct up to twelve or thirteen decimal places with exact results as compared to FDM and LSM.
- The temperature in fin decreases when the values of S_h and M rises.
- The temperature in fin increases as the values of β, B, Q and γ increase.
- In case 1, the temperature is noticeably lower in comparison to cases 2 and 3. This observation implies that case 1 exhibits enhanced efficiency in the context of the cooling process within the fin.
- In the context of a linear case, it becomes evident that the temperature within a location-dependent porous fin is relatively lower than a temperature-dependent porous fin.

This research is novel for the incorporation of spatial and temperature-dependent thermal conductivity, as well as the solution of a complex nonlinear issue utilizing a hybrid numerical technique i.e., $LWCM$. As a result, the present method is applicable to highly nonlinear fin problems. It can be used in the engineering industry to improve the quality of fins. The future work can be extended for nanofluids with different shapes and size of the nano-particles.

NOMENCLATURE

P	Fin perimeter (m)
$\beta^{'}$	coefficient of thermal expansion (K^{-1})
K_{eff}	effective thermal conductivity ratio (W/mK)
T	local fin temperature (K)
T_b	fin base temperature (K)
T_∞	Sink temperature for convection (K)
t	thickness of the fin (mm)
h	heat transfer coefficient over the fin surface $(W(m^2K))$
L	length of the fin (m)
g	gravity constant (ms^2)
c_p	specific heat $(J(kg-K))$
K	permeability of the porous fin (m^2)
k_a	thermal conductivity at the base of the fin $(Wm^{-1}k^{-1})$
x	axial length measured from fin tip (m)
q	internal heat generation (W/in^3)
Da	Darcy number (m^2)
v	kinematic viscosity (m^2s)
a	constant, dimensions vary absorption coefficient (m^2)

Dimensionless parameter

β	thermal conductivity parameter
θ	temperature in fin
Ra	Rayleigh number
X	length of the fin
Q	heat transfer rate per unit area
γ	internal heat generation
S_h	porosity
M	thermo-geometric parameter
B	thermal conductivity gradiant parameter

Abbreviation

$LWCM$	Legendre Wavelet Collocation Method
FDM	Finite Difference Method
LSM	Least Square Method
BC	Boundary Conditions

References

[1] R. R. Harper and W. B. Brown, *Mathematical equations for heat conduction in the fins of air-cooled engines*, No. NACA-TR-158, 1923.

[2] M. Jakob, *Heat Transfer*, Wiley, New York, 1949.

[3] J. B. J. Fourier, *Analytical Theory of Heat*, Cambridge Uni. Press, London, 466, 1878.

[4] B. Kundu and P. K. Das, Performance analysis and optimization of straight taper fins with variable heat transfer coefficient, *Int. J. heat and mass trans.*, 45(24), 4739-4751 (2002).

[5] D. Q. Kern and A. D. Kraus, *Extended surface heat transfer*, McGraw Hill, New York, 1972.

[6] A. D. Kraus, A. Aziz, J. Welty and D. P. Sekulic, Extended surface heat transfer, *Appl. Mech. Rev.*, 54(5), B92-B92 (2001).

[7] H. G. Zhang, E. H. Wang and B. Y. Fan, Heat transfer analysis of a finned-tube evaporator for engine exhaust heat recovery, *Energy Conv. Manag.*, 65, 438-447 (2013).

[8] C. A. Yunus, *Heat transfer* (2nd ed.), McGraw-Hill, 2020.

[9] T. L. Bergman, F. P. Incropera, D. P. Dewitt and A. S. Lavine, *Fundamentals of heat and mass transfer*(7th ed.), John Wiley and Sons, 2011.

[10] S. Khatami and N. Rahbar, An analytical study of entropy generation in rectangular natural convective porous fins, *Therm. Sci. Eng. Prog.*, 11, 142-149 (2019).

[11] M. Hatami, A. Hasanpour and D. D. Ganji, Heat transfer study through porous fins (Si_3N_4 and AL) with temperature-dependent heat generation, *Energy Convers. Manag.*, 74, 9-16 (2013).

[12] E. Cuce, and P. M. Cuce, A successful application of homotopy perturbation method for efficiency and effectiveness assessment of longitudinal porous fins, *Energy Convers. Manag.*, 93, 92-99 (2015).

[13] V. Venkitesh and A. Mallick, Thermal analysis of a convectiveconductiveradiative annular porous fin with variable thermal parameters and internal heat generation, *J. Therm. Anal. Calorim.*, 1-15 (2020).

[14] J. Ma, Y. Sun and B. Li, Simulation of combined conductive, convective and radiative heat transfer in moving irregular porous fins by spectral element method, *Int. J. Therm. Sci.*, 118, 475-487 (2017).

[15] B. Kundu, D. Bhanja and K. S. Lee, A model on the basis of analytics for computing maximum heat transfer in porous fins, *Int. J. Heat Mass Transf.*, 55(25-26), 7611-7622 (2012).

[16] B. Buonomo, F. Cascetta, O. Manca and M. Sheremet, Heat transfer analysis of rectangular porous fins in local thermal non-equilibrium model, *Appl. Therm. Eng.*, 195, 117237 (2021).

[17] B. J. Gireesha and G. Sowmya, Heat transfer analysis of an inclined porous fin using Differential Transform Method, *Int. J. Ambient Energy*, 43(1), 3189-3195 (2022).

[18] M. Hatami and D. D. Ganji, Thermal performance of circular convectiveradiative porous fins with different section shapes and materials, *Energy Convers. Manag.*, 76, 185-193 (2013).

[19] S. E. Ghasemi, P. Valipour, M. Hatami and D. D. Ganji, Heat transfer study on solid and porous convective fins with temperature-dependent heat generation using efficient analytical method, *J. Cent. South Univ.*, 21(12), 4592-4598 (2014).

[20] M. Hatami and D. D. Ganji, Investigation of refrigeration efficiency for fully wet circular porous fins with variable sections by combined heat and mass transfer analysis, *Int. J. Refrig.*, 40, 140-151 (2014).

[21] D. Bhanja, B. Kundu and A. Aziz, Enhancement of heat transfer from a continuously moving porous fin exposed in convectiveradiative environment, *Energy Convers. Manag.*, 88, 842-853 (2014).

[22] M. Hamdan and M. D. A. Al-Nimr, The use of porous fins for heat transfer augmentation in parallel-plate channels, *Transp. Porous Media*, 84(2), 409-420 (2010).

[23] W. A. Khan and A. Aziz, Transient heat transfer in a functionally graded convecting longitudinal fin, *Heat Mass Transf.*, 48, 1745-1753 (2012).

[24] S. Jangid, R. Mehta, J. Singh, D. Baleanu and A. S. Alshomrani, Heat and mass transport of hydromagnetic Williamson nanofluid passing through a permeable media across an extended sheet of varying thickness, *Therm. Sci.*, 27, 129-140 (2023).

[25] R. Kumar, J. Singh, R. Mehta, D. Kumar and D. Baleanu, Analysis of the impact of thermal radiation and velocity slip on the melting of magnetic hydrodynamic micropolar fluid-flow over an exponentially stretching sheet, *Therm. Sci.*, 27, 311-322 (2023).

[26] S. Singh, D. Kumar and K. N. Rai, Convective-radiative fin with temperature dependent thermal conductivity, heat transfer coefficient and wavelength dependent surface emissivity, *Propuls. Power Res.*, 3(4), (2014).

[27] S. Singh, S. Upadhyay and K. N. Rai, comparative analysis of power-law type fin problem using wavelet collocation and Galerkin methods, *Int. J. Appl. Math.* 3(4), 534 (2014).

[28] G. Oguntala, R. Abd-Alhameed, G. Sobamowo and I. Danjuma, Performance, thermal stability and optimum design analyses of rectangular fin with temperature-dependent thermal properties and internal heat generation, *J. Appl. Comput. Mech.* 49(1), 37-43 (2018).

[29] S. Upadhyay, V. K. Singh and K. N. Rai, Finite difference Legendre wavelet collocation method applied to the study of heat mass transfer during food drying, *Heat Transf. Asian Res.* 48(7), 3079-3100 (2019).

[30] P. Kaur and S. Singh, Convective radiative moving fin with temperature-dependent thermal conductivity, *Pramana* 96(4), 216 (2022).

[31] G. A. Oguntala and R. A. Abd-Alhameed, Haar wavelet collocation method for thermal analysis of porous fin with temperature-dependent thermal conductivity and internal heat generation, *J. Appl. Comput. Mech.*, 3(3), 185-191 (2017).

[32] A. Bejan and A. D. Kraus, *Heat transfer handbook* (Vol. 1), John Wiley and Sons, 2003.

[33] M. Razzaghi and S. Yousefi, Legendre wavelets direct method for variational problems, *Math. Comput. Simul.* 53(3), 185-192 (2000).

[34] M. N. Azisik, M. N. Ozk and M. N. Ozsk, *Heat conduction*, John Wiley and Sons, 1993.

[35] M. Hatami and D. D. Ganji, Thermal and flow analysis of microchannel heat sink (MCHS) cooled by Cuwater nanofluid using porous media approach and least square method, *Energy Convers. Manag.*, 78, 347-358 (2014).

[36] Y. M. Han, J. S. Cho and H. S. Kang, Analysis of a one-dimensional fin using the analytic method and the finite difference method, *J. Korean Math. Soc.*, 9(1), 91-98 (2005).

Finite Sum Representation of Partial Derivatives of Multivariable Incomplete Aleph Functions

Rahul Sharma[1], Jagdev Singh[2,3,*], Devendra Kumar[4] and Yudhveer Singh[5]

January 8, 2024

[1]Department of Mathematics, University of Engineering and Management Jaipur-303807, Rajasthan, India
[2]Department of Mathematics, JECRC University, Jaipur-303905, Rajasthan, India
[3]Department of Computer Science and Mathematics, Lebanese American University, Beirut, Lebanon
[4]Department of Mathematics, University of Rajasthan, Jaipur-302004, Rajasthan, India
[5]Amity Institute of Information Technology, Amity University Rajasthan, Jaipur-303002, Rajasthan, India
*Corresponding author: jagdevsinghrathore@gmail.com

Abstract

Newly discovered, incomplete forms of special functions are increasing the interest of both pure and applied mathematicians. The main purpose of this work is to derive four theorems on partial derivatives with incomplete Aleph functions of two variables and generalize them up to r-variables. In addition to these theorems, we also established some novel formulae on the partial derivatives that play a key role in deriving the main results in terms of finite sum. Further, we generalize the result and obtain the finite sum for the incomplete Aleph functions with r-variables. Here, we also established some particular cases that are in most general character and including the results given earlier by Buschman and Deshpande and may prove significant in numerous interesting situations appearing in the literature on mathematical analysis, applied mathematics and mathematical physics.

Keywords: Partial Differentiation, Incomplete ℵ-functions, Mellin-Barnes Integral.
MSC2020: 26A24, 33B20, 33C60.

1 Introduction and Preliminaries

Recently, Tadesse et al. [7], Kumar et al. [5] and Oli et al. [3] have derived some results on partial derivatives and fractional order derivatives of multivariate Aleph function. Earlier to that, Buschman [11, 12] and Deshpande [18, 19] have generated some important results on partial derivatives of special functions of one variable, two variables and r-variables.
In the 18th century, some fundamental research was initiated in the field of special functions when Prym (1877) introduced incomplete gamma functions that were further studied by several authors. Sdland et al. [10] introduced and investigated the Aleph function in 1998. In 2020, the incomplete forms of the Aleph function were introduced by Bansal et al. [8].
The incomplete Aleph function with r-variables [6] defined using the Mellin Barnes type contour integral as given below:

$$
{}^{(\Gamma)}\aleph^{0,n:m_1,n_1,m_2,n_2;\ldots;m_r,n_r}_{p_i,q_i,\tau_i;R;p_{i^{(1)}},q_{i^{(1)}},\tau_{i^{(1)}};R_{(1)},\ldots,p_{i^{(r)}},q_{i^{(r)}},\tau_{i^{(r)}};R_{(r)}}
\left[\begin{array}{c|cc} z_1 & & \\ \vdots & W & W' \\ z_r & Z & Z' \end{array}\right]
$$

$$
= \frac{1}{(2\pi\omega)^r}\int_{L_1}\int_{L_2}\ldots\int_{L_r}\varphi\left(s_1,s_2,\ldots,s_r,y\right)\prod_{k=1}^{r}\left[\phi_k(s_k){z_k}^{s_k}\right]ds_1ds_2\ldots ds_r, \quad (1)
$$

where $\omega=\sqrt{-1}$,

$$
W=\left[a_1;\alpha_1^{(1)},\ldots,\alpha_1^{(r)},y\right],\left[a_j;\alpha_j^{(1)},\ldots,\alpha_j^{(r)}\right]_{2,n},\left[\tau_i\left(a_{ji};\alpha_{ji}^{(1)},\ldots,\alpha_{ji}^{(r)}\right)_{n+1,p_i}\right],
$$

$$
W'=\left[c_j^{(1)},\zeta_j^{(1)}\right]_{1,n_1},\left[\tau_{i^{(1)}}\left(c_{ji^{(1)}}^{(1)},\zeta_{ji^{(1)}}^{(1)}\right)_{n_1+1,p_i^{(1)}}\right],\ldots,\left[c_j^{(r)},\zeta_j^{(r)}\right]_{1,n_r},
$$

$$
\left[\tau_{i^{(r)}}\left(c_{ji^{(r)}}^{(r)},\zeta_{ji^{(r)}}^{(r)}\right)_{n_r+1,p_i^{(r)}}\right],
$$

$$
Z=\left[\ldots,\tau_i\left(b_{ji};\beta_{ji}^{(1)},\ldots,\beta_{ji}^{(r)}\right)_{m+1,q_i}\right],
$$

$$
Z'=\left[d_j^{(1)},\delta_j^{(1)}\right]_{1,m_1},\left[\tau_{i^{(1)}}\left(d_{ji^{(1)}}^{(1)},\delta_{ji^{(1)}}^{(1)}\right)_{m_1+1,q_i^{(1)}}\right],\ldots,\left[d_j^{(r)},\delta_j^{(r)}\right]_{1,m_r},
$$

$$
\left[\tau_{i^{(r)}}\left(d_{ji^{(r)}}^{(r)},\delta_{ji^{(r)}}^{(r)}\right)_{m_r+1,q_i^{(r)}}\right],
$$

$$
\varphi\left(s_1,s_2,\ldots,s_r,y\right)=\frac{\Gamma(1-a_1+\sum_{k=1}^{r}\alpha_1^{(k)}s_k,y)\prod_{j=2}^{n}\Gamma(1-a_j+\sum_{k=1}^{r}\alpha_j^{(k)}s_k)}{\sum_{i=1}^{R}\tau_i\left[\prod_{j=n+1}^{p_i}\Gamma\left(a_{ji}-\sum_{k=1}^{r}\alpha_{ji}^{(k)}s_k\right)\prod_{j=1}^{q_i}\Gamma\left(1-b_{ji}+\sum_{k=1}^{r}\beta_{ji}^{(k)}s_k\right)\right]},
$$

$$
\phi_k(s_k)=\frac{\prod_{j=1}^{m_k}\Gamma(d_j^{(k)}-\delta_j^{(k)}s_k)\prod_{j=1}^{n_k}\Gamma(1-c_j^{(k)}+\zeta_j^{(k)}s_k)}{\sum_{i^{(k)}=1}^{R^{(k)}}\tau_{i^{(k)}}\left[\prod_{j=m_k+1}^{q_{i^{(k)}}}\Gamma\left(1-d_{ji^{(k)}}^{(k)}+\delta_{ji^{(k)}}^{(k)}s_k\right)\prod_{j=n_k+1}^{p_{i^{(k)}}}\Gamma\left(c_{ji^{(k)}}^{(k)}-\zeta_{ji^{(k)}}^{(k)}s_k\right)\right]},
$$

$k=1,2,\ldots,r.$

Similarly, another form of incomplete Aleph function with r-variables is defined

by

$$ {}^{(\gamma)}\aleph^{0,n:m_1,n_1,m_2,n_2,\ldots,m_r,n_r}_{p_i,q_i,\tau_i;R;p_{i(1)},q_{i(1)},\tau_{i(1)};R_{(1)},\ldots,p_{i(r)},q_{i(r)},\tau_{i(r)};R_{(r)}} \left[\begin{array}{c|cc} z_1 & & \\ \vdots & W & W' \\ z_r & Z & Z' \end{array}\right] $$

$$ = \frac{1}{(2\pi\omega)^r}\int_{L_1}\int_{L_2}\ldots\int_{L_r}\varphi'(s_1,s_2,\ldots,s_r,y)\prod_{k=1}^{r}\left[\phi_k(s_k){z_k}^{s_k}\right]ds_1ds_2\ldots ds_r, \tag{2} $$

where

$$ \varphi'(s_1,s_2,\ldots,s_r,y) = \frac{\gamma(1-a_1+\sum_{k=1}^{r}\alpha_1^{(k)}s_k,y)\prod_{j=2}^{n}\Gamma(1-a_j+\sum_{k=1}^{r}\alpha_j^{(k)}s_k)}{\sum_{i=1}^{R}\tau_i\left[\prod_{j=n+1}^{p_i}\Gamma\left(a_{ji}-\sum_{k=1}^{r}\alpha_{ji}^{(k)}s_k\right)\prod_{j=1}^{q_i}\Gamma\left(1-b_{ji}+\sum_{k=1}^{r}\beta_{ji}^{(k)}s_k\right)\right]}. $$

Decomposition formula satisfying for incomplete Aleph functions with r-variables defined in (1) and (2) as ${}^{(\Gamma)}\aleph^{0,n:m_1,n_1,m_2,n_2,\ldots,m_r,n_r}_{p_i,q_i,\tau_i;R;p_{i(1)},q_{i(1)},\tau_{i(1)};R_{(1)},\ldots,p_{i(r)},q_{i(r)},\tau_{i(r)};R_{(r)}}[z_r] + {}^{(\gamma)}\aleph^{0,n:m_1,n_1,m_2,n_2,\ldots,m_r,n_r}_{p_i,q_i,\tau_i;R;p_{i(1)},q_{i(1)},\tau_{i(1)};R_{(1)},\ldots,p_{i(r)},q_{i(r)},\tau_{i(r)};R_{(r)}}[z_r]$
$= \aleph^{0,n:m_1,n_1,m_2,n_2,\ldots,m_r,n_r}_{p_i,q_i,\tau_i;R;p_{i(1)},q_{i(1)},\tau_{i(1)};R_{(1)},\ldots,p_{i(r)},q_{i(r)},\tau_{i(r)};R_{(r)}}[z_r]$.

Here, $a_j\ (j=1,\ldots,p)$; $b_j\ (j=1,\ldots,q)$; $c_j^{(k)}\ (j=1,\ldots,n_k)$; $c_{ji^{(k)}}^{(k)}\ (j=n_k+1,\ldots,p_{i^{(k)}})$; $d_j^{(k)}\ (j=1,\ldots,m_k)$; $d_{ji^{(k)}}^{(k)}\ (j=m_k+1,\ldots,q_{i^{(k)}})$; $k=1,\ldots,r$; $i=1,\ldots,R$ and $i^{(k)}=1,\ldots,R^{(k)}$ are complex numbers.

$$ \Omega_i^{(k)} = \sum_{j=1}^{n}\alpha_j^{(k)} + \tau_i\sum_{j=n+1}^{p_i}\alpha_{ji}^{(k)} + \sum_{j=1}^{n_k}\zeta_j^{(k)} + \tau_{i^{(k)}}\sum_{j=n_k+1}^{p_{i(k)}}\zeta_{ji^{(k)}}^{(k)} $$
$$ -\tau_i\sum_{j=1}^{q_i}\beta_{ji^{(k)}}^{(k)} - \sum_{j=1}^{m_k}\delta_j^{(k)} - \tau_{i^{(k)}}\sum_{j=m_k+1}^{q_{i(k)}}\delta_{ji^{(k)}}^{(k)} \le 0, $$

$\tau_i\ (i=1,\ldots,R)$, $\tau_{i^{(k)}}\ (i^{(k)}=1,\ldots,R^{(k)})$ are positive real numbers. The integral path $L_{il:\infty}$ is a contour starting from $l-i\infty$ to $l+i\infty$ and the poles of $\Gamma(d_j^{(k)}-\delta_j^{(k)}s_k)$, $j=1,\ldots,m_k$ are separated from those of $\Gamma(1-a_j+\sum_{k=1}^{r}\alpha_j^{(k)}s_k)$, $j=1,\ldots,n$ and $\Gamma(1-c_j^{(k)}+\zeta_j^{(k)}s_k)$, $j=1,\ldots,n_k$ to the left of the contour L_k. The existence conditions for multiple Mellin-Barnes contours (1) can be obtained with the bits of help of multivariable H-function as $|argz_k|<\frac{\pi}{2}\bar{\Omega}_i^{(k)}$, where

$$ \bar{\Omega}_i^{(k)} = \sum_{j=1}^{n}\alpha_j^{(k)} - \tau_i\sum_{j=n+1}^{p_i}\alpha_{ji}^{(k)} - \tau_i\sum_{j=1}^{q_i}\beta_{ji}^{(k)} + \sum_{j=1}^{n_k}\zeta_j^{(k)} - \tau_{i^{(k)}}\sum_{j=n_k+1}^{p_{i(k)}}\zeta_{ji^{(k)}}^{(k)} $$
$$ +\sum_{j=1}^{m_k}\delta_j^{(k)} - \tau_{i^{(k)}}\sum_{j=m_k+1}^{q_{i(k)}}\delta_{ji^{(k)}}^{(k)} > 0. $$

We can reduce incomplete Aleph functions with r-variables defined in (1) or (2) to the other well-known special functions by establishing values as given below:

(i) When we set $\tau_i = \tau_{i^{(k)}} = 1$ $(k = 1, \ldots, r)$, the multivariable incomplete Aleph functions reduce to the multivariable incomplete I-functions [16].
(ii) When we set $r = 1$, the incomplete Aleph functions with r-variables reduce to the incomplete Aleph-functions [8, 20, 17].
(iii) When we set $r = 1$ and $\tau_i = \tau_{i^{(k)}} = 1$ $(k = 1, \ldots, r)$, the multivariable incomplete Aleph functions reduce to the incomplete I-functions [9, 15].
(iv) By setting $y = 0$ and $\tau_i = \tau_{i^{(k)}} = 1$ $(k = 1, \ldots, r)$, the multivariable incomplete Aleph functions reduce to the multivariable I-function defined by Sharma et al. [4].
(v) By setting $y = 0$, $\tau_i = \tau_{i^{(k)}} = 1$ and $R = R^{(k)} = 1$ $(k = 1, \ldots, r)$, the multivariable incomplete Aleph-functions reduce to the multivariable H-function [14].
(vi) When we set $y = 0$ and $r = 1$, the multivariable incomplete Aleph functions reduce to the Aleph-function [10].

In the upcoming sections, we explore three formulas which serve as valuable tools for solving the theorems of sections 3 and 4. Within section 4, we generalized Theorem 1 and obtained the finite sum pertaining to the incomplete Aleph functions with r-variables. Additionally, some particular cases given by several authors are also discussed in section 5.

2 Formulas

In this particular section, we have developed three formulas that are intended to assist in resolving the theorems presented in sections 3 and 4.

The incomplete Aleph function can be expressed with two variables ${}^{(\Gamma)}\aleph_Q^P\left[\begin{array}{c} Z_1 \\ Z_2 \end{array}\right]$ as:

$$
\begin{aligned}
&{}^{(\Gamma)}\aleph_Q^P\left[\begin{array}{c|c} z_1 & X \\ z_2 & Y \end{array}\right] \\
&\qquad = \frac{1}{(2\pi\omega)^2}\int_{L_1}\int_{L_2}\varphi\left(s_1, s_2, y\right)\phi_1(s_1) z_1^{s_1}\phi_2(s_2) z_2^{s_2} ds_1 ds_2, \quad (3)
\end{aligned}
$$

where
$\omega = \sqrt{-1},\ P = 0, n : m_1, n_1, m_2, n_2,$
$Q = p_i, q_i, \tau_i; R; p_{i^{(1)}}, q_{i^{(1)}}, \tau_{i^{(1)}}; R_{(1)}; p_{i^{(2)}}, q_{i^{(2)}}, \tau_{i^{(2)}}; R_{(2)},$

$$
\varphi\left(s_1, s_2, y\right) = \frac{\Gamma(1-a_1+\sum_{k=1}^{2}\alpha_1^{(k)}s_k, y)\prod_{j=2}^{n}\Gamma(1-a_j+\sum_{k=1}^{2}\alpha_j^{(k)}s_k)}{\sum_{i=1}^{R}\tau_i\left[\prod_{j=n+1}^{p_i}\Gamma\left(a_{ji}-\sum_{k=1}^{2}\alpha_{ji}^{(k)}s_k\right)\prod_{j=1}^{q_i}\Gamma\left(1-b_{ji}+\sum_{k=1}^{2}\beta_{ji}^{(k)}s_k\right)\right]},
$$

$$
\phi_k(s_k) = \frac{\prod_{j=1}^{m_k}\Gamma(d_j^{(k)}-\delta_j^{(k)}s_k)\prod_{j=1}^{n_k}\Gamma(1-c_j^{(k)}+\zeta_j^{(k)}s_k)}{\sum_{i^{(k)}=1}^{R^{(k)}}\tau_{i^{(k)}}\left[\prod_{j=m_k+1}^{q_{i^{(k)}}}\Gamma\left(1-d_{ji^{(k)}}^{(k)}+\delta_{ji^{(k)}}^{(k)}s_k\right)\prod_{j=n_k+1}^{p_{i^{(k)}}}\Gamma\left(c_{ji^{(k)}}^{(k)}-\zeta_{ji^{(k)}}^{(k)}s_k\right)\right]},
$$

$k = 1, 2,$

$$
X = \left[a_1; \alpha_1^{(1)}, \alpha_1^{(2)}, y\right], \left[a_j; \alpha_j^{(1)}, \alpha_j^{(2)}\right]_{2,n}, \left[\tau_i\left(a_{ji}; \alpha_{ji}^{(1)}, \alpha_{ji}^{(2)}\right)_{n+1,p_i}\right],
$$

$\left[c_j^{(1)}, \zeta_j^{(1)}\right]_{1,n_1}, \left[\tau_{i^{(1)}}\left(c_{ji^{(1)}}^{(1)}, \zeta_{ji^{(1)}}^{(1)}\right)_{n_1+1,p_i^{(1)}}\right], \left[c_j^{(2)}, \zeta_j^{(2)}\right]_{1,n_2},$
$\left[\tau_{i^{(2)}}\left(c_{ji^{(2)}}^{(2)}, \zeta_{ji^{(2)}}^{(2)}\right)_{n_2+1,p_i^{(2)}}\right],$
$Y = \left[\ldots, \tau_i\left(b_{ji}; \beta_{ji}^{(1)}, \beta_{ji}^{(2)}\right)_{m+1,q_i}\right], \left[d_j^{(1)}, \delta_j^{(1)}\right]_{1,m_1},$
$\left[\tau_{i^{(1)}}\left(d_{ji^{(1)}}^{(1)}, \delta_{ji^{(1)}}^{(1)}\right)_{m_1+1,q_i^{(1)}}\right], \left[d_j^{(2)}, \delta_j^{(2)}\right]_{1,m_2}, \left[\tau_{i^{(2)}}\left(d_{ji^{(2)}}^{(2)}, \delta_{ji^{(2)}}^{(2)}\right)_{m_2+1,q_i^{(2)}}\right].$

Similarly, the lower form of the incomplete Aleph function of two variables ${}^{(\gamma)}\aleph_Q^P\left[\begin{array}{c} Z_1 \\ Z_2 \end{array}\right]$ as follows:

$$
\begin{aligned}
&{}^{(\gamma)}\aleph_Q^P\left[\begin{array}{c|c} z_1 & X \\ z_2 & Y \end{array}\right] \\
&\qquad = \frac{1}{(2\pi\omega)^2}\int_{L_1}\int_{L_2}\varphi'(s_1,s_2,y)\,\phi_1(s_1)z_1^{s_1}\phi_2(s_2)z_2^{s_2}ds_1ds_2, \quad (4)
\end{aligned}
$$

where
$\varphi'(s_1,s_2,y) = \frac{\gamma(1-a_1+\sum_{k=1}^{2}\alpha_1^{(k)}s_k,y)\prod_{j=2}^{n}\Gamma(1-a_j+\sum_{k=1}^{2}\alpha_j^{(k)}s_k)}{\sum_{i=1}^{R}\tau_i\left[\prod_{j=n+1}^{p_i}\Gamma\left(a_{ji}-\sum_{k=1}^{2}\alpha_{ji}^{(k)}s_k\right)\prod_{j=1}^{q_i}\Gamma\left(1-b_{ji}+\sum_{k=1}^{2}\beta_{ji}^{(k)}s_k\right)\right]}.$

Now, we derived the following formulas for the incomplete Aleph function with two variables that will be used for the proof of upcoming theorems.

Formula 1: We derive a formula for the incomplete Aleph function with two variables as follows:

$$
z_1^{\rho_1}z_2^{\rho_2}{}^{(\Gamma)}\aleph_Q^P\left[\begin{array}{c|c} z_1 & X \\ z_2 & Y \end{array}\right] = {}^{(\Gamma)}\aleph_Q^P\left[\begin{array}{c|c} z_1 & X_1 \\ z_2 & Y_1 \end{array}\right], \quad (5)
$$

where
$P = 0, n : m_1, n_1, m_2, n_2,$
$Q = p_i, q_i, \tau_i; R; p_{i^{(1)}}, q_{i^{(1)}}, \tau_{i^{(1)}}; R_{(1)}; p_{i^{(2)}}, q_{i^{(2)}}, \tau_{i^{(2)}}; R_{(2)},$
$X_1 = \left[a_1+\rho_1\alpha_1^{(1)}+\rho_2\alpha_1^{(2)}; \alpha_1^{(1)}, \alpha_1^{(2)}, y\right], \left[a_j+\rho_1\alpha_j^{(1)}+\rho_2\alpha_j^{(2)}; \alpha_j^{(1)}, \alpha_j^{(2)}\right]_{2,n},$
$\left[\tau_i\left(a_{ji}+\rho_1\alpha_{ji}^{(1)}+\rho_2\alpha_{ji}^{(2)}; \alpha_{ji}^{(1)}, \alpha_{ji}^{(2)}\right)_{n+1,p_i}\right], \left[c_j^{(1)}+\rho_1\zeta_j^{(1)}, \zeta_j^{(1)}\right]_{1,n_1},$
$\left[\tau_{i^{(1)}}\left(c_{ji^{(1)}}^{(1)}+\rho_1\zeta_{ji^{(1)}}^{(1)}, \zeta_{ji^{(1)}}^{(1)}\right)_{n_1+1,p_i^{(1)}}\right], \left[c_j^{(2)}+\rho_2\zeta_j^{(2)}, \zeta_j^{(2)}\right]_{1,n_2},$
$\left[\tau_{i^{(2)}}\left(c_{ji^{(2)}}^{(2)}+\rho_2\gamma_{ji^{(2)}}^{(2)}, \gamma_{ji^{(2)}}^{(2)}\right)_{n_2+1,p_i^{(2)}}\right],$
$Y_1 = \left[\ldots, \tau_i\left(b_{ji}+\rho_1\beta_{ji}^{(1)}+\rho_2\beta_{ji}^{(2)}; \beta_{ji}^{(1)}, \beta_{ji}^{(2)}\right)_{m+1,q_i}\right], \left[d_j^{(1)}+\rho_1\delta_j^{(1)}, \delta_j^{(1)}\right]_{1,m_1},$
$\left[\tau_{i^{(1)}}\left(d_{ji^{(1)}}^{(1)}+\rho_1\delta_{ji^{(1)}}^{(1)}, \delta_{ji^{(1)}}^{(1)}\right)_{m_1+1,q_i^{(1)}}\right], \left[d_j^{(2)}+\rho_2\delta_j^{(2)}, \delta_j^{(2)}\right]_{1,m_2},$
$\left[\tau_{i^{(2)}}\left(d_{ji^{(2)}}^{(2)}+\rho_2\delta_{ji^{(2)}}^{(2)}, \delta_{ji^{(2)}}^{(2)}\right)_{m_2+1,q_i^{(2)}}\right].$

To prove this formula, substitute $s_k + \rho_k = \mathfrak{s}_k$ ($\rho_k \in \mathbb{C}$) and use (3). After a small simplification, we get the desired result.

Formula 2: For $z_1 = \Lambda_1^{\gamma_1}$ and $z_2 = \Lambda_2^{\gamma_2}$, the partial derivatives of the incomplete Aleph function two variables with respect to Λ_1, Λ_2 defined as:

$$\Lambda_1^s \Lambda_2^t \frac{\partial^s}{\partial \Lambda_1^s} \frac{\partial^t}{\partial \Lambda_2^t} {}^{(\Gamma)}\aleph_Q^P \left[\begin{array}{c|c} z_1 & X \\ z_2 & Y \end{array} \right] = {}^{(\Gamma)}\aleph_{Q_2}^{P_2} \left[\begin{array}{c|c} z_1 & X_2 \\ z_2 & Y_2 \end{array} \right], \tag{6}$$

where

$P_2 = 0, n : m_1 + 1, n_1, m_2 + 1, n_2,$

$Q_2 = p_i, q_i, \tau_i; R; p_{i^{(1)}} + 1, q_{i^{(1)}} + 1, \tau_{i^{(1)}}; R_{(1)}; p_{i^{(2)}} + 1, q_{i^{(2)}} + 1, \tau_{i^{(2)}}; R_{(2)},$

$$X_2 = \left[a_1; \alpha_1^{(1)}, \alpha_1^{(2)}, y\right], \left[a_j; \alpha_j^{(1)}, \alpha_j^{(2)}\right]_{2,n}, \left[\tau_i \left(a_{ji}; \alpha_{ji}^{(1)}, \alpha_{ji}^{(2)}\right)_{n+1,p_i}\right],$$
$$\left[c_j^{(1)}, \zeta_j^{(1)}\right]_{1,n_1}, \left[\tau_{i^{(1)}} \left(c_{ji^{(1)}}^{(1)}, \zeta_{ji^{(1)}}^{(1)}\right)_{n_1+1,p_i^{(1)}}\right], [0, \gamma_1], \left[c_j^{(2)}, \zeta_j^{(2)}\right]_{1,n_2},$$
$$\left[\tau_{i^{(2)}} \left(c_{ji^{(2)}}^{(2)}, \zeta_{ji^{(2)}}^{(2)}\right)_{n_2+1,p_i^{(2)}}\right], [0, \gamma_2],$$
$$Y_2 = \left[\ldots, \tau_i \left(b_{ji}; \beta_{ji}^{(1)}, \beta_{ji}^{(2)}\right)_{m+1,q_i}\right], [s, \gamma_1], \left[d_j^{(1)}, \delta_j^{(1)}\right]_{1,m_1},$$
$$\left[\tau_{i^{(1)}} \left(d_{ji^{(1)}}^{(1)}, \delta_{ji^{(1)}}^{(1)}\right)_{m_1+1,q_i^{(1)}}\right], [t, \gamma_2], \left[d_j^{(2)}, \delta_j^{(2)}\right]_{1,m_2},$$
$$\left[\tau_{i^{(2)}} \left(d_{ji^{(2)}}^{(2)}, \delta_{ji^{(2)}}^{(2)}\right)_{m_2+1,q_i^{(2)}}\right].$$

Formula 3: For $z_1 = \Lambda_1^{-\gamma_1}$ and $z_2 = \Lambda_2^{-\gamma_2}$, the partial derivatives of the incomplete Aleph function two variables with respect to Λ_1, Λ_2 is as follows:

$$(-1)^{s+t} (\Lambda_1)^s (\Lambda_2)^t \frac{\partial^s}{\partial \Lambda_1^s} \frac{\partial^t}{\partial \Lambda_2^t} {}^{(\Gamma)}\aleph_Q^P \left[\begin{array}{c|c} z_1 & X \\ z_2 & Y \end{array} \right] = {}^{(\Gamma)}\aleph_{Q_3}^{P_3} \left[\begin{array}{c|c} z_1 & X_3 \\ z_2 & Y_3 \end{array} \right], \tag{7}$$

where

$P_3 = 0, n : m_1, n_1 + 1, m_2, n_2 + 1,$

$Q_3 = p_i, q_i, \tau_i; R; p_{i^{(1)}} + 1, q_{i^{(1)}} + 1, \tau_{i^{(1)}}; R_{(1)}; p_{i^{(2)}} + 1, q_{i^{(2)}} + 1, \tau_{i^{(2)}}; R_{(2)},$

$$X_3 = \left[a_1; \alpha_1^{(1)}, \alpha_1^{(2)}, y\right], \left[a_j; \alpha_j^{(1)}, \alpha_j^{(2)}\right]_{2,n}, \left[\tau_i \left(a_{ji}; \alpha_{ji}^{(1)}, \alpha_{ji}^{(2)}\right)_{n+1,p_i}\right],$$
$$[1 - s, \gamma_1], \left[c_j^{(1)}, \zeta_j^{(1)}\right]_{1,n_1}, \left[\tau_{i^{(1)}} \left(c_{ji^{(1)}}^{(1)}, \zeta_{ji^{(1)}}^{(1)}\right)_{n_1+1,p_i^{(1)}}\right], [1 - t, \gamma_2],$$
$$\left[c_j^{(2)}, \zeta_j^{(2)}\right]_{1,n_2}, \left[\tau_{i^{(2)}} \left(c_{ji^{(2)}}^{(2)}, \zeta_{ji^{(2)}}^{(2)}\right)_{n_2+1,p_i^{(2)}}\right],$$
$$Y_3 = \left[\ldots, \tau_i \left(b_{ji}; \beta_{ji}^{(1)}, \beta_{ji}^{(2)}\right)_{m+1,q_i}\right], \left[d_j^{(1)}, \delta_j^{(1)}\right]_{1,m_1},$$
$$\left[\tau_{i^{(1)}} \left(d_{ji^{(1)}}^{(1)}, \delta_{ji^{(1)}}^{(1)}\right)_{m_1+1,q_i^{(1)}}\right], [1, \gamma_1], \left[d_j^{(2)}, \delta_j^{(2)}\right]_{1,m_2},$$
$$\left[\tau_{i^{(2)}} \left(d_{ji^{(2)}}^{(2)}, \delta_{ji^{(2)}}^{(2)}\right)_{m_2+1,q_i^{(2)}}\right], [1, \gamma_2].$$

Similarly, we can derive all three formulas for the lower form of the incomplete Aleph function with two variables ${}^{(\gamma)}\aleph_{Q}^{P}\left[\begin{array}{c|c} z_1 & X \\ z_2 & Y \end{array}\right]$.

3 Main Results

In this section, we produce four theorems concerning the partial derivatives of incomplete Aleph functions with two variables, each having distinct parameters. Subsequently, we express these functions in terms of finite sums.

If we put $z = N \in Z^+$ in formula (30) of Erdelyi et al. ([1], P.19), we obtain the result as given:

$$\psi(e+N)-\psi(e)=\sum_{l=1}^{N}(-1)^{l-1}\frac{N!}{l(N-l)!}\frac{\Gamma(e)}{\Gamma(e+l)}, \tag{8}$$

where function $\psi(z)=\frac{d}{dz}log\left[\Gamma(z)\right]$.

Theorem 1: We derived the partial derivatives of the incomplete Aleph function with two variables in terms of finite sum for the given values of $\Lambda_1 = N_1,\ \Lambda_2 = N_2$ as:

$$\begin{aligned}&\frac{\partial}{\partial\Lambda_1}\frac{\partial}{\partial\Lambda_2}{}^{(\Gamma)}\aleph_{Q_4}^{P_4}\left[\begin{array}{c|c} z_1 & X_4 \\ z_2 & Y_4 \end{array}\right]_{\Lambda_1=N_1,\ \Lambda_2=N_2}\\ &\quad=\frac{N_1!N_2!}{4}\sum_{k_1=0}^{N_1-1}\sum_{k_2=0}^{N_2-1}\frac{1}{k_1!k_2!(N_1-k_1)(N_2-k_2)}{}^{(\Gamma)}\aleph_{Q_4}^{P_4}\left[\begin{array}{c|c} z_1 & X_5 \\ z_2 & Y_5 \end{array}\right],\end{aligned} \tag{9}$$

where
$P_4 = 0, n : m_1, n_1+2, m_2, n_2+2,$
$Q_4 = p_i, q_i, \tau_i; R; p_{i^{(1)}}+2, q_{i^{(1)}}, \tau_{i^{(1)}}; R_{(1)}; p_{i^{(2)}}+2, q_{i^{(2)}}, \tau_{i^{(2)}}; R_{(2)},$

$$X_4=\left[a_1;\alpha_1^{(1)},\alpha_1^{(2)},y\right],\left[a_j;\alpha_j^{(1)},\alpha_j^{(2)}\right]_{2,n},\left[\tau_i\left(a_{ji};\alpha_{ji}^{(1)},\alpha_{ji}^{(2)}\right)_{n+1,p_i}\right],$$
$$\left(1-\rho_1\pm\tfrac{\Lambda_1}{2},\gamma_1\right),\left[c_j^{(1)},\zeta_j^{(1)}\right]_{1,n_1},\left[\tau_{i^{(1)}},\left(c_{ji^{(1)}}^{(1)},\zeta_{ji^{(1)}}^{(1)}\right)_{n_1+1,p_i^{(1)}}\right],$$
$$\left(1-\rho_2\pm\tfrac{\Lambda_2}{2},\gamma_2\right),\left[c_j^{(2)},\zeta_j^{(2)}\right]_{1,n_2},\left[\tau_{i^{(2)}}\left(c_{ji^{(2)}}^{(2)},\zeta_{ji^{(2)}}^{(2)}\right)_{n_2+1,p_i^{(2)}}\right],$$
$$Y_4=\left[\ldots,\tau_i\left(b_{ji};\beta_{ji}^{(1)},\beta_{ji}^{(2)}\right)_{m+1,q_i}\right],\left[d_j^{(1)},\delta_j^{(1)}\right]_{1,m_1},$$
$$\left[\tau_{i^{(1)}}\left(d_{ji^{(1)}}^{(1)},\delta_{ji^{(1)}}^{(1)}\right)_{m_1+1,q_i^{(1)}}\right],\left[d_j^{(2)},\delta_j^{(2)}\right]_{1,m_2},\left[\tau_{i^{(2)}}\left(d_{ji^{(2)}}^{(2)},\delta_{ji^{(2)}}^{(2)}\right)_{m_2+1,q_i^{(2)}}\right],$$
$$X_5=\left[a_1;\alpha_1^{(1)},\alpha_1^{(2)},y\right],\left[a_j;\alpha_j^{(1)},\alpha_j^{(2)}\right]_{2,n},\left[\tau_i\left(a_{ji};\alpha_{ji}^{(1)},\alpha_{ji}^{(2)}\right)_{n+1,p_i}\right],$$

$\left[1-\rho_1+\frac{N_1}{2},\gamma_1\right],\left[1-\rho_1+\frac{N_1}{2}-k_1,\gamma_1\right],\left[c_j^{(1)},\zeta_j^{(1)}\right]_{1,n_1}$,
$\left[\tau_{i^{(1)}},\left(c_{ji^{(1)}}^{(1)},\zeta_{ji^{(1)}}^{(1)}\right)_{n_1+1,p_i^{(1)}}\right],\left[1-\rho_2+\frac{N_2}{2},\gamma_2\right],\left[1-\rho_2+\frac{N_2}{2}-k_2,\gamma_2\right]$,
$\left[c_j^{(2)},\zeta_j^{(2)}\right]_{1,n_2},\left[\tau_{i^{(2)}}\left(c_{ji^{(2)}}^{(2)},\zeta_{ji^{(2)}}^{(2)}\right)_{n_2+1,p_i^{(2)}}\right]$,
$Y_5=\left[\ldots,\tau_i\left(b_{ji};\beta_{ji}^{(1)},\beta_{ji}^{(2)}\right)_{m+1,q_i}\right],\left[d_j^{(1)},\delta_j^{(1)}\right]_{1,m_1}$,
$\left[\tau_{i^{(1)}}\left(d_{ji^{(1)}}^{(1)},\delta_{ji^{(1)}}^{(1)}\right)_{m_1+1,q_i^{(1)}}\right],\left[d_j^{(2)},\delta_j^{(2)}\right]_{1,m_2},\left[\tau_{i^{(2)}}\left(d_{ji^{(2)}}^{(2)},\delta_{ji^{(2)}}^{(2)}\right)_{m_2+1,q_i^{(2)}}\right]$.

Proof: In the first step, express the left-hand side of (9) in the form of the Mellin-Barnes integral as given in (3). Further, by using the chain rule of derivatives and result defined in (8), we have

$$\frac{\partial}{\partial\Lambda_1}\Gamma\left(\rho_1\pm\frac{\Lambda_1}{2}+\gamma_1 s_1\right)\Big|_{\Lambda_1=N_1}=\frac{1}{2}\Gamma\left(\rho_1\pm\frac{N_1}{2}+\gamma_1 s_1\right)\times$$
$$\left[\psi\left(\rho_1+\frac{N_1}{2}+\gamma_1 s_1\right)-\psi\left(\rho_1-\frac{N_1}{2}+\gamma_1 s_1\right)\right]=\frac{1}{2}\Gamma\left(\rho_1\pm\frac{N_1}{2}+\gamma_1 s_1\right)$$
$$\sum_{L_1=1}^{N_1}\frac{(-1)^{L_1-1}N_1!\Gamma\left(\rho_1-\frac{N_1}{2}+\gamma_1 s_1\right)}{L_1(N_1-L_1)!\Gamma\left(\rho_1-\frac{N_1}{2}+L_1+\gamma_1 s_1\right)}. \quad (10)$$

Similarly, we can write

$$\frac{\partial}{\partial\Lambda_2}\Gamma\left(\rho_2\pm\frac{\Lambda_2}{2}+\gamma_2 s_2\right)\Big|_{\Lambda_2=N_2}=\frac{1}{2}\Gamma\left(\rho_2\pm\frac{N_2}{2}+\gamma_2 s_2\right)\times$$
$$\left[\psi\left(\rho_2+\frac{N_2}{2}+\gamma_2 s_2\right)-\psi\left(\rho_2-\frac{N_2}{2}+\gamma_2 s_2\right)\right]=\frac{1}{2}\Gamma\left(\rho_2\pm\frac{N_2}{2}+\gamma_2 s_2\right)$$
$$\sum_{L_2=1}^{N_2}\frac{(-1)^{L_2-1}N_2!\Gamma\left(\rho_2-\frac{N_2}{2}+\gamma_2 s_2\right)}{L_2(N_2-L_2)!\Gamma\left(\rho_2-\frac{N_2}{2}+L_2+\gamma_2 s_2\right)}. \quad (11)$$

Now, we can write the left-hand side of (9) by using the above-given results in (10) and (11). We have

$$=\frac{N_1!N_2!}{4}\sum_{L_1=0}^{N_1}\sum_{L_2=0}^{N_2}\frac{(-1)^{L_1+L_2-2}}{L_1L_2(N_1-L_1)!(N_2-L_2)!}\times$$
$${}^{(\Gamma)}\aleph_{p_i,q_i,\tau_i;R;p_{i^{(1)}}+3,q_{i^{(1)}}+1,\tau_{i^{(1)}};R_{(1)};p_{i^{(2)}}+3,q_{i^{(2)}}+1,\tau_{i^{(2)}};R_{(2)}}^{0,n:m_1,n_1+3,m_2,n_2+3}\left[\begin{array}{c|c} z_1 & \left[a_1;\alpha_1^{(1)},\alpha_1^{(2)},y\right], \\ z_2 & \ldots, \end{array}\right.$$
$$\left[a_j;\alpha_j^{(1)},\alpha_j^{(2)}\right]_{2,n},\left[\tau_i\left(a_{ji};\alpha_{ji}^{(1)},\alpha_{ji}^{(2)}\right)_{n+1,p_i}\right],\left[1-\rho_1\pm\frac{N_1}{2},\gamma_1\right],$$
$$\left[\tau_i\left(b_{ji};\beta_{ji}^{(1)},\beta_{ji}^{(2)}\right)_{m+1,q_i}\right],\left[d_j^{(1)},\delta_j^{(1)}\right]_{1,m_1},\left[\tau_{i^{(1)}}\left(d_{ji^{(1)}}^{(1)},\delta_{ji^{(1)}}^{(1)}\right)_{m_1+1,q_i^{(1)}}\right],$$

$$\left[1-\rho_1+\tfrac{N_1}{2},\gamma_1\right],\left[c_j^{(1)},\zeta_j^{(1)}\right]_{1,n_1},\left[\tau_{i^{(1)}},\left(c_{ji^{(1)}}^{(1)},\zeta_{ji^{(1)}}^{(1)}\right)_{n_1+1,p_i^{(1)}}\right],$$
$$\left[1-\rho_1+\tfrac{N_1}{2}-L_1,\gamma_1\right],\left[d_j^{(2)},\delta_j^{(2)}\right]_{1,m_2},$$

$$\left[1-\rho_2\pm\tfrac{N_2}{2},\gamma_2\right],\left[1-\rho_2+\tfrac{N_2}{2},\gamma_2\right],\left[c_j^{(2)},\zeta_j^{(2)}\right]_{1,n_2},$$
$$\left[\tau_{i^{(2)}}\left(d_{ji^{(2)}}^{(2)},\delta_{ji^{(2)}}^{(2)}\right)_{m_2+1,q_i^{(2)}}\right],$$
$$\left[\begin{array}{c}\left[\tau_{i^{(2)}}\left(c_{ji^{(2)}}^{(2)},\zeta_{ji^{(2)}}^{(2)}\right)_{n_2+1,p_i^{(2)}}\right]\\ \left[1-\rho_2+\tfrac{N_2}{2}-L_2,\gamma_2\right]\end{array}\right]. \tag{12}$$

Now, consider the incomplete Aleph function with two variables portion of (12) and for the sake of convenience denote it by T. Thus we can write it as follows:

$$T={}^{(\Gamma)}\aleph^{0,n:m_1,n_1+3,m_2,n_2+3}_{p_i,q_i,\tau_i;R;p_{i^{(1)}}+3,q_{i^{(1)}}+1,\tau_{i^{(1)}};R_{(1)};p_{i^{(2)}}+3,q_{i^{(2)}}+1,\tau_{i^{(2)}};R_{(2)}}\left[\begin{array}{c|l}z_1 & \left[a_1;\alpha_1^{(1)},\right.\\ z_2 & \ldots,\end{array}\right.$$
$$\left.\alpha_1^{(2)},y\right],\left[a_j;\alpha_j^{(1)},\alpha_j^{(2)}\right]_{2,n},$$
$$\left[\ldots,\tau_i\left(b_{ji};\beta_{ji}^{(1)},\beta_{ji}^{(2)}\right)_{m+1,q_i}\right],$$
$$\left[\tau_i\left(a_{ji};\alpha_{ji}^{(1)},\alpha_{ji}^{(2)}\right)_{n+1,p_i}\right],\left[1-\rho_1\pm\tfrac{N_1}{2},\gamma_1\right],\left[1-\rho_1+\tfrac{N_1}{2},\gamma_1\right]$$
$$\left[d_j^{(1)},\delta_j^{(1)}\right]_{1,m_1},\left[\tau_{i^{(1)}}\left(d_{ji^{(1)}}^{(1)},\delta_{ji^{(1)}}^{(1)}\right)_{m_1+1,q_i^{(1)}}\right],$$

$$\left[c_j^{(1)},\zeta_j^{(1)}\right]_{1,n_1},\left[\tau_{i^{(1)}},\left(c_{ji^{(1)}}^{(1)},\zeta_{ji^{(1)}}^{(1)}\right)_{n_1+1,p_i^{(1)}}\right],\left[1-\rho_2\pm\tfrac{N_2}{2},\gamma_2\right],$$
$$\left[1-\rho_1+\tfrac{N_1}{2}-L_1,\gamma_1\right],\left[d_j^{(2)},\delta_j^{(2)}\right]_{1,m_2},\left[\tau_{i^{(2)}}\left(d_{ji^{(2)}}^{(2)},\delta_{ji^{(2)}}^{(2)}\right)_{m_2+1,q_i^{(2)}}\right],$$

$$\left[\begin{array}{l}\left[1-\rho_2+\tfrac{N_2}{2},\gamma_2\right],\left[c_j^{(2)},\zeta_j^{(2)}\right]_{1,n_2},\left[\tau_{i^{(2)}}\left(c_{ji^{(2)}}^{(2)},\zeta_{ji^{(2)}}^{(2)}\right)_{n_2+1,p_i^{(2)}}\right]\\ \left[1-\rho_2+\tfrac{N_2}{2}-L_2,\gamma_2\right]\end{array}\right]. \tag{13}$$

Now, evaluate the value of $Z_1^{-\frac{1}{\gamma_1}\left(\frac{N_1}{2}-\rho_1-L_1\right)}Z_2^{-\frac{1}{\gamma_2}\left(\frac{N_2}{2}-\rho_2-L_2\right)}\times T$, by using the formula 1 and formula 3, and after little simplification, we arrive at

$$(-1)^{N_1+N_2-L_1-L_2}(\Lambda_1)^{N_1/2+\rho_1}(\Lambda_2)^{N_2/2+\rho_2}\frac{\partial^{N_1-L_1}}{\partial\Lambda_1^{N_1-L_1}}\frac{\partial^{N_2-L_2}}{\partial\Lambda_2^{N_2-L_2}}\times\Lambda_1^{(N_1/2-\rho_1-L_1)}\times$$

$$\Lambda_2^{(N_2/2-\rho_2-L_2)(\Gamma)}\aleph^{0,n:m_1,n_1+2,m_2,n_2+2}_{p_i,q_i,\tau_i;R;p_{i(1)}+2,q_{i(1)},\tau_{i(1)};R_{(1)};p_{i(2)}+2,q_{i(2)},\tau_{i(2)};R_{(2)}}\left[\begin{array}{c|c} z_1 & [a_1; \\ z_2 & \ldots, \end{array}\right.$$

$$\left[\alpha_1^{(1)},\alpha_1^{(2)},y\right],\left[a_j;\alpha_j^{(1)},\alpha_j^{(2)}\right]_{2,n},\left[\tau_i\left(a_{ji};\alpha_{ji}^{(1)},\alpha_{ji}^{(2)}\right)_{n+1,p_i}\right],\left[1-\rho_1+\tfrac{N_1}{2},\gamma_1\right]^2,$$
$$\left[\tau_i\left(b_{ji};\beta_{ji}^{(1)},\beta_{ji}^{(2)}\right)_{m+1,q_i}\right],$$

$$\left[1-\rho_1+\tfrac{N_1}{2},\gamma_1\right]^2,\left[c_j^{(1)},\zeta_j^{(1)}\right]_{1,n_1},\left[\tau_{i^{(1)}},\left(c_{ji^{(1)}}^{(1)},\zeta_{ji^{(1)}}^{(1)}\right)_{n_1+1,p_i^{(1)}}\right],$$
$$\left[d_j^{(1)},\delta_j^{(1)}\right]_{1,m_1},\left[\tau_{i^{(1)}}\left(d_{ji^{(1)}}^{(1)},\delta_{ji^{(1)}}^{(1)}\right)_{m_1+1,q_i^{(1)}}\right],$$

$$\left.\begin{array}{l}\left[1-\rho_2+\tfrac{N_2}{2},\gamma_2\right]^2,\left[c_j^{(2)},\zeta_j^{(2)}\right]_{1,n_2},\left[\tau_{i^{(2)}}\left(c_{ji^{(2)}}^{(2)},\zeta_{ji^{(2)}}^{(2)}\right)_{n_2+1,p_i^{(2)}}\right] \\ \left[d_j^{(2)},\delta_j^{(2)}\right]_{1,m_2},\left[\tau_{i^{(2)}}\left(d_{ji^{(2)}}^{(2)},\delta_{ji^{(2)}}^{(2)}\right)_{m_2+1,q_i^{(2)}}\right]\end{array}\right], \quad (14)$$

where $z_1=\Lambda_1^{-\gamma_1}$ and $z_2=\Lambda_2^{-\gamma_2}$.
Now applying the Leibniz formula

$$\frac{\partial^{N-L}}{\partial\Lambda^{N-L}}\left(\Lambda^{-L}\Lambda^{N/2-\rho}\aleph\left[\begin{array}{c}\Lambda^{-\gamma}\\ z_2\end{array}\right]\right)$$
$$=\sum_{l=0}^{N-L}\binom{N-L}{l}\frac{\partial^{N-L-l}}{\partial\Lambda^{N-L-l}}(\Lambda^{-L})\frac{\partial^l}{\partial\Lambda^l}(\Lambda^{n/2-\rho})\aleph\left[\begin{array}{c}\Lambda^{-\gamma}\\ z_2\end{array}\right] \quad (15)$$

in (14) and after simplifying it, we have

$$=\sum_{l_1=0}^{N_1-L_1}\sum_{l_2=0}^{N_2-L_2}\frac{(N_1-L_1)!(N_2-L_2)!\Gamma(N_1-l_1)\Gamma(N_2-l_2)}{l_1!l_2!(N_1-L_1-l_1)!(N_2-L_2-l_2)!\Gamma(L_1)\Gamma(L_2)}\times$$

$$\aleph^{0,n:m_1,n_1+2,m_2,n_2+2}_{p_i,q_i,\tau_i;R;p_{i(1)}+2,q_{i(1)},\tau_{i(1)};R_{(1)};p_{i(2)}+2,q_{i(2)},\tau_{i(2)};R_{(2)}}\left[\begin{array}{c|c} z_1 & \left[a_1;\alpha_1^{(1)},\alpha_1^{(2)},y\right],[a_j; \\ z_2 & \ldots, \end{array}\right.$$

$$\alpha_j^{(1)},\alpha_j^{(2)}\Big]_{2,n},\left[\tau_i\left(a_{ji};\alpha_{ji}^{(1)},\alpha_{ji}^{(2)}\right)_{n+1,p_i}\right],\left[1-\rho_1+\tfrac{N_1}{2},\gamma_1\right],\left[1-\rho_1+\tfrac{N_1}{2}\right.$$
$$\left[\tau_i\left(b_{ji};\beta_{ji}^{(1)},\beta_{ji}^{(2)}\right)_{m+1,q_i}\right],\left[d_j^{(1)},\delta_j^{(1)}\right]_{1,m_1},$$

$$-k_1,\gamma_1],\left[c_j^{(1)},\zeta_j^{(1)}\right]_{1,n_1},\left[\tau_{i^{(1)}}\left(c_{ji^{(1)}}^{(1)},\zeta_{ji^{(1)}}^{(1)}\right)_{n_1+1,p_i^{(1)}}\right],\left[1-\rho_2+\tfrac{N_2}{2},\gamma_2\right],$$
$$\left[\tau_{i^{(1)}}\left(d_{ji^{(1)}}^{(1)},\delta_{ji^{(1)}}^{(1)}\right)_{m_1+1,q_i^{(1)}}\right],$$

$$\left.\begin{array}{l}\left[1-\rho_2+\frac{N_2}{2}-k_2,\gamma_2\right],\left[c_j^{(2)},\zeta_j^{(2)}\right]_{1,n_2},\left[\tau_{i^{(2)}}\left(c_{ji^{(2)}}^{(2)},\zeta_{ji^{(2)}}^{(2)}\right)_{n_2+1,p_i^{(2)}}\right]\\ \left[d_j^{(2)},\delta_j^{(2)}\right]_{1,m_2},\left[\tau_{i^{(2)}}\left(d_{ji^{(2)}}^{(2)},\delta_{ji^{(2)}}^{(2)}\right)_{m_2+1,q_i^{(2)}}\right]\end{array}\right]. \quad (16)$$

By using (13) and change the order of summations in $\sum_{L_1=1}^{N_1}\sum_{l_1=0}^{N_1-L_1}$ and $\sum_{L_2=1}^{N_2}\sum_{l_2=0}^{N_2-L_2}$ and inner sums then simplify to $L_1=L_2=1$. Consequently, we get the desired result.

Theorem 2: The incomplete Aleph function with two variables in terms of finite sum for the given values of $\Lambda_1=N_1,\ \Lambda_2=N_2$ as:

$$\frac{\partial}{\partial\Lambda_1}\frac{\partial}{\partial\Lambda_2}{}^{(\Gamma)}\aleph_{Q_5}^{P_5}\left[\begin{array}{c|c}z_1 & X_6\\ z_2 & Y_6\end{array}\right]_{\Lambda_1=N_1,\ \Lambda_2=N_2}$$
$$=\frac{N_1!N_2!}{4}\sum_{k_1=0}^{N_1-1}\sum_{k_2=0}^{N_2-1}\frac{1}{k_1!k_2!(N_1-k_1)(N_2-k_2)}{}^{(\Gamma)}\aleph_{Q_5}^{P_5}\left[\begin{array}{c|c}z_1 & X_7\\ z_2 & Y_7\end{array}\right], \quad (17)$$

where
$P_5=0,n:m_1+2,n_1,m_2+2,n_2,$
$Q_5=p_i,q_i,\tau_i;R;p_{i^{(1)}},q_{i^{(1)}}+2,\tau_{i^{(1)}};R_{(1)};p_{i^{(2)}},q_{i^{(2)}}+2,\tau_{i^{(2)}};R_{(2)},$

$X_6=\left[a_1;\alpha_1^{(1)},\alpha_1^{(2)},y\right],\left[a_j;\alpha_j^{(1)},\alpha_j^{(2)}\right]_{2,n},\left[\tau_i\left(a_{ji};\alpha_{ji}^{(1)},\alpha_{ji}^{(2)}\right)_{n+1,p_i}\right],$
$\left[c_j^{(1)},\zeta_j^{(1)}\right]_{1,n_1},\left[\tau_{i^{(1)}},\left(c_{ji^{(1)}}^{(1)},\zeta_{ji^{(1)}}^{(1)}\right)_{n_1+1,p_i^{(1)}}\right],\left[c_j^{(2)},\zeta_j^{(2)}\right]_{1,n_2},$
$\left[\tau_{i^{(2)}}\left(c_{ji^{(2)}}^{(2)},\zeta_{ji^{(2)}}^{(2)}\right)_{n_2+1,p_i^{(2)}}\right],$
$Y_6=\left[\ldots,\tau_i\left(b_{ji};\beta_{ji}^{(1)},\beta_{ji}^{(2)}\right)_{m+1,q_i}\right],\left[\rho_1\pm\frac{\Lambda_1}{2},\delta_1\right],\left[d_j^{(1)},\delta_j^{(1)}\right]_{1,m_1},$
$\left[\tau_{i^{(1)}}\left(d_{ji^{(1)}}^{(1)},\delta_{ji^{(1)}}^{(1)}\right)_{m_1+1,q_i^{(1)}}\right],\left[\rho_2\pm\frac{\Lambda_2}{2},\delta_2\right],\left[d_j^{(2)},\delta_j^{(2)}\right]_{1,m_2},$
$\left[\tau_{i^{(2)}}\left(d_{ji^{(2)}}^{(2)},\delta_{ji^{(2)}}^{(2)}\right)_{m_2+1,q_i^{(2)}}\right],$

$X_7=\left[a_1;\alpha_1^{(1)},\alpha_1^{(2)},y\right],\left[a_j;\alpha_j^{(1)},\alpha_j^{(2)}\right]_{2,n},\left[\tau_i\left(a_{ji};\alpha_{ji}^{(1)},\alpha_{ji}^{(2)}\right)_{n+1,p_i}\right],$
$\left[c_j^{(1)},\zeta_j^{(1)}\right]_{1,n_1},\left[\tau_{i^{(1)}},\left(c_{ji^{(1)}}^{(1)},\zeta_{ji^{(1)}}^{(1)}\right)_{n_1+1,p_i^{(1)}}\right],\left[c_j^{(2)},\zeta_j^{(2)}\right]_{1,n_2},$
$\left[\tau_{i^{(2)}}\left(c_{ji^{(2)}}^{(2)},\zeta_{ji^{(2)}}^{(2)}\right)_{n_2+1,p_i^{(2)}}\right],$
$Y_7=\left[\ldots,\tau_i\left(b_{ji};\beta_{ji}^{(1)},\beta_{ji}^{(2)}\right)_{m+1,q_i}\right],\left[\rho_1-\frac{N_1}{2},\delta_1\right],\left[\rho_1-\frac{N_1}{2}+k_1,\delta_1\right],$
$\left[d_j^{(1)},\delta_j^{(1)}\right]_{1,m_1},\left[\tau_{i^{(1)}}\left(d_{ji^{(1)}}^{(1)},\delta_{ji^{(1)}}^{(1)}\right)_{m_1+1,q_i^{(1)}}\right],\left[\rho_2-\frac{N_2}{2},\delta_2\right],\left[\rho_2-\frac{N_2}{2}+k_2,\delta_2\right],$

$$\left[d_j^{(2)},\delta_j^{(2)}\right]_{1,m_2},\left[\tau_{i^{(2)}}\left(d_{ji^{(2)}}^{(2)},\delta_{ji^{(2)}}^{(2)}\right)_{m_2+1,q_i^{(2)}}\right].$$

Proof: The proof for Theorem 2 follows a similar approach as that used for Theorem 1.

Theorem 3: A new variant of the partial derivatives of the incomplete Aleph function with two variables in terms of finite sum for the given values of $\Lambda_1 = N_1$ as:

$$\frac{\partial}{\partial\Lambda_1}{}^{(\Gamma)}\aleph_{Q_6}^{P_6}\left[\begin{array}{c|c} z_1 & X_8 \\ z_2 & Y_8 \end{array}\right]_{\Lambda_1=N_1} = \frac{N_1!}{2}\sum_{k_1=0}^{N_1-1}\frac{1}{k_1!(N_1-k_1)}{}^{(\Gamma)}\aleph_{Q_6}^{P_6}\left[\begin{array}{c|c} z_1 & X_9 \\ z_2 & Y_9 \end{array}\right], \quad (18)$$

where
$P_6 = 0, n : m_1, n_1 + 2, m_2, n_2,$
$Q_6 = p_i, q_i, \tau_i; R; p_{i^{(1)}} + 2, q_{i^{(1)}}, \tau_{i^{(1)}}; R_{(1)}; p_{i^{(2)}}, q_{i^{(2)}}, \tau_{i^{(2)}}; R_{(2)},$

$$X_8 = \left[a_1;\alpha_1^{(1)},\alpha_1^{(2)},y\right],\left[a_j;\alpha_j^{(1)},\alpha_j^{(2)}\right]_{2,n},\left[\tau_i\left(a_{ji};\alpha_{ji}^{(1)},\alpha_{ji}^{(2)}\right)_{n+1,p_i}\right],$$
$$\left[1-\rho_1\pm\tfrac{\Lambda_1}{2},\gamma_1\right],\left[c_j^{(1)},\zeta_j^{(1)}\right]_{1,n_1},\left[\tau_{i^{(1)}},\left(c_{ji^{(1)}}^{(1)},\zeta_{ji^{(1)}}^{(1)}\right)_{n_1+1,p_i^{(1)}}\right],\left[c_j^{(2)},\zeta_j^{(2)}\right]_{1,n_2},$$
$$\left[\tau_{i^{(2)}}\left(c_{ji^{(2)}}^{(2)},\zeta_{ji^{(2)}}^{(2)}\right)_{n_2+1,p_i^{(2)}}\right],$$
$$Y_8 = \left[\ldots,\tau_i\left(b_{ji};\beta_{ji}^{(1)},\beta_{ji}^{(2)}\right)_{m+1,q_i}\right],\left[d_j^{(1)},\delta_j^{(1)}\right]_{1,m_1},$$
$$\left[\tau_{i^{(1)}}\left(d_{ji^{(1)}}^{(1)},\delta_{ji^{(1)}}^{(1)}\right)_{m_1+1,q_i^{(1)}}\right],\left[d_j^{(2)},\delta_j^{(2)}\right]_{1,m_2},\left[\tau_{i^{(2)}}\left(d_{ji^{(2)}}^{(2)},\delta_{ji^{(2)}}^{(2)}\right)_{m_2+1,q_i^{(2)}}\right],$$
$$X_9 = \left[a_1;\alpha_1^{(1)},\alpha_1^{(2)},y\right],\left[a_j;\alpha_j^{(1)},\alpha_j^{(2)}\right]_{2,n},\left[\tau_i\left(a_{ji};\alpha_{ji}^{(1)},\alpha_{ji}^{(2)}\right)_{n+1,p_i}\right],$$
$$\left[1-\rho_1+\tfrac{N_1}{2},\gamma_1\right],\left[1-\rho_1+\tfrac{N_1}{2}-k_1,\gamma_1\right],\left[c_j^{(1)},\zeta_j^{(1)}\right]_{1,n_1},$$
$$\left[\tau_{i^{(1)}},\left(c_{ji^{(1)}}^{(1)},\zeta_{ji^{(1)}}^{(1)}\right)_{n_1+1,p_i^{(1)}}\right],\left[c_j^{(2)},\zeta_j^{(2)}\right]_{1,n_2},\left[\tau_{i^{(2)}}\left(c_{ji^{(2)}}^{(2)},\zeta_{ji^{(2)}}^{(2)}\right)_{n_2+1,p_i^{(2)}}\right],$$
$$Y_9 = \left[\ldots,\tau_i\left(b_{ji};\beta_{ji}^{(1)},\beta_{ji}^{(2)}\right)_{m+1,q_i}\right],\left[d_j^{(1)},\delta_j^{(1)}\right]_{1,m_1},$$
$$\left[\tau_{i^{(1)}}\left(d_{ji^{(1)}}^{(1)},\delta_{ji^{(1)}}^{(1)}\right)_{m_1+1,q_i^{(1)}}\right],\left[d_j^{(2)},\delta_j^{(2)}\right]_{1,m_2},\left[\tau_{i^{(2)}}\left(d_{ji^{(2)}}^{(2)},\delta_{ji^{(2)}}^{(2)}\right)_{m_2+1,q_i^{(2)}}\right].$$

Proof: The proof for Theorem 3 can be obtained using the same method employed in establishing Theorem 1.

Theorem 4: The partial derivatives of the incomplete Aleph function with

two variables in terms of finite sum for the given values of $\Lambda_1 = N_1$ as:

$$\frac{\partial}{\partial \Lambda_1}{}^{(\Gamma)}\aleph_{Q_7}^{P_7}\left[\begin{array}{c|c} z_1 & X_{10} \\ z_2 & Y_{10} \end{array}\right]_{\Lambda_1=N_1} = \frac{N_1!}{2}\sum_{k_1=0}^{N_1-1}\frac{1}{k_1!(N_1-k_1)}{}^{(\Gamma)}\aleph_{Q_7}^{P_7}\left[\begin{array}{c|c} z_1 & X_{11} \\ z_2 & Y_{11} \end{array}\right] \quad (19)$$

where
$P_7 = 0, n : m_1 + 2, n_1, m_2, n_2,$
$Q_7 = p_i, q_i, \tau_i; R; p_{i^{(1)}}, q_{i^{(1)}} + 2, \tau_{i^{(1)}}; R_{(1)}; p_{i^{(2)}}, q_{i^{(2)}}, \tau_{i^{(2)}}; R_{(2)},$

$$X_{10} = \left[a_1; \alpha_1^{(1)}, \alpha_1^{(2)}, y\right], \left[a_j; \alpha_j^{(1)}, \alpha_j^{(2)}\right]_{2,n}, \left[\tau_i\left(a_{ji}; \alpha_{ji}^{(1)}, \alpha_{ji}^{(2)}\right)_{n+1,p_i}\right],$$
$$\left[c_j^{(1)}, \zeta_j^{(1)}\right]_{1,n_1}, \left[\tau_{i^{(1)}}, \left(c_{ji^{(1)}}^{(1)}, \zeta_{ji^{(1)}}^{(1)}\right)_{n_1+1,p_i^{(1)}}\right], \left[c_j^{(2)}, \zeta_j^{(2)}\right]_{1,n_2},$$
$$\left[\tau_{i^{(2)}}\left(c_{ji^{(2)}}^{(2)}, \zeta_{ji^{(2)}}^{(2)}\right)_{n_2+1,p_i^{(2)}}\right],$$
$$Y_{10} = \left[\ldots, \tau_i\left(b_{ji}; \beta_{ji}^{(1)}, \beta_{ji}^{(2)}\right)_{m+1,q_i}\right], \left[\rho_1 \pm \tfrac{\Lambda_1}{2}, \delta_1\right], \left[d_j^{(1)}, \delta_j^{(1)}\right]_{1,m_1},$$
$$\left[\tau_{i^{(1)}}\left(d_{ji^{(1)}}^{(1)}, \delta_{ji^{(1)}}^{(1)}\right)_{m_1+1,q_i^{(1)}}\right], \left[d_j^{(2)}, \delta_j^{(2)}\right]_{1,m_2}, \left[\tau_{i^{(2)}}\left(d_{ji^{(2)}}^{(2)}, \delta_{ji^{(2)}}^{(2)}\right)_{m_2+1,q_i^{(2)}}\right],$$
$$X_{11} = \left[a_1; \alpha_1^{(1)}, \alpha_1^{(2)}, y\right], \left[a_j; \alpha_j^{(1)}, \alpha_j^{(2)}\right]_{2,n}, \left[\tau_i\left(a_{ji}; \alpha_{ji}^{(1)}, \alpha_{ji}^{(2)}\right)_{n+1,p_i}\right],$$
$$\left[c_j^{(1)}, \zeta_j^{(1)}\right]_{1,n_1}, \left[\tau_{i^{(1)}}, \left(c_{ji^{(1)}}^{(1)}, \zeta_{ji^{(1)}}^{(1)}\right)_{n_1+1,p_i^{(1)}}\right], \left[c_j^{(2)}, \zeta_j^{(2)}\right]_{1,n_2},$$
$$\left[\tau_{i^{(2)}}\left(c_{ji^{(2)}}^{(2)}, \zeta_{ji^{(2)}}^{(2)}\right)_{n_2+1,p_i^{(2)}}\right],$$
$$Y_{11} = \left[\ldots, \tau_i\left(b_{ji}; \beta_{ji}^{(1)}, \beta_{ji}^{(2)}\right)_{m+1,q_i}\right], \left[\rho_1 - \tfrac{N_1}{2}, \delta_1\right], \left[\rho_1 - \tfrac{N_1}{2} + k_1, \delta_1\right],$$
$$\left[d_j^{(1)}, \delta_j^{(1)}\right]_{1,m_1}, \left[\tau_{i^{(1)}}\left(d_{ji^{(1)}}^{(1)}, \delta_{ji^{(1)}}^{(1)}\right)_{m_1+1,q_i^{(1)}}\right], \left[d_j^{(2)}, \delta_j^{(2)}\right]_{1,m_2},$$
$$\left[\tau_{i^{(2)}}\left(d_{ji^{(2)}}^{(2)}, \delta_{ji^{(2)}}^{(2)}\right)_{m_2+1,q_i^{(2)}}\right].$$

Proof: The proof for Theorem 4 can be obtained using the same method employed in establishing Theorem 1.

4 Generalization of Main Result

In this section, we extend the primary outcome established in Theorem 1 to encompass the incomplete Aleph function considering r-variables ${}^{(\Gamma)}\aleph_Q^P[z_r]$ as

follows:

$$\prod_{k=1}^{r}\frac{\partial}{\partial\Lambda^{k}}{}^{(\Gamma)}\aleph^{0,n:m_1,n_1+2,m_2,n_2+2,\ldots,m_r,n_r+2}_{p_i,q_i,\tau_i;R:p_{i^{(1)}}+2,q_{i^{(1)}},\tau_{i^{(1)}};R_{(1)},\ldots,p_{i^{(r)}}+2,q_{i^{(r)}},\tau_{i^{(r)}};R_{(r)}}\left[\begin{array}{c|c} z_1 & [a_1; \\ \vdots & \ldots, \\ z_r & \end{array}\right.$$

$$\left.\alpha_1^{(1)},\ldots,\alpha_1^{(r)},y\right],\left[1-\rho_1\pm\tfrac{\Lambda_1}{2},\gamma_1\right],\left[a_j;\alpha_j^{(1)},\ldots,\alpha_j^{(r)}\right]_{2,n},$$
$$\left[\tau_i\left(b_{ji};\beta_{ji}^{(1)},\ldots\beta_{ji}^{(r)}\right)_{m+1,q_i}\right],\left[d_j^{(1)},\delta_j^{(1)}\right]_{1,m_1},\left[\tau_{i^{(1)}}\left(d_{ji^{(1)}}^{(1)},\delta_{ji^{(1)}}^{(1)}\right)_{m_1+1,q_i^{(1)}}\right],$$

$$\left[\tau_i\left(a_{ji};\alpha_{ji}^{(1)},\ldots,\alpha_{ji}^{(r)}\right)_{n+1,p_i}\right],\left[c_j^{(1)},\zeta_j^{(1)}\right]_{1,n_1},\left[\tau_{i^{(1)}},\left(c_{ji^{(1)}}^{(1)},\zeta_{ji^{(1)}}^{(1)}\right)_{n_1+1,p_i^{(1)}}\right],$$
$$\left[d_j^{(2)},\delta_j^{(2)}\right]_{1,m_2},\left[\tau_{i^{(2)}}\left(d_{ji^{(2)}}^{(2)},\delta_{ji^{(2)}}^{(2)}\right)_{m_2+1,q_i^{(2)}}\right],\ldots,$$

$$\ldots,\left[1-\rho_r\pm\tfrac{\Lambda_r}{2},\gamma_r\right],\left[c_j^{(r)},\zeta_j^{(r)}\right]_{1,n_r},\left[\tau_{i^{(r)}}\left(c_{ji^{(r)}}^{(r)},\zeta_{ji^{(r)}}^{(r)}\right)_{n_r+1,p_i^{(r)}}\right]$$
$$\left.\left[d_j^{(r)},\delta_j^{(r)}\right]_{1,m_r},\left[\tau_{i^{(r)}}\left(d_{ji^{(r)}}^{(r)},\delta_{ji^{(r)}}^{(r)}\right)_{m_r+1,q_i^{(r)}}\right]\right]_{\Lambda_k=N_k}$$

$$=\frac{\prod_{k=1}^{r}(N_k)!}{2^k}\sum_{k_1=0}^{N_1-1}\cdots\sum_{k_r=0}^{N_r-1}\frac{1}{\prod_{l=1}^{r}\left[k_l!(N_k-k_l)\right]}\times$$

$${}^{(\Gamma)}\aleph^{0,n:m_1,n_1+2,m_2,n_2+2,\ldots,m_r,n_r+2}_{p_i,q_i,\tau_i;R;p_{i^{(1)}}+2,q_{i^{(1)}},\tau_{i^{(1)}};R_{(1)},\ldots,p_{i^{(r)}}+2,q_{i^{(r)}},\tau_{i^{(r)}};R_{(r)}}\left[\begin{array}{c|c} z_1 & \left[a_1;\alpha_1^{(1)},\ldots,\alpha_1^{(r)},\right. \\ \vdots & \ldots, \\ z_r & \end{array}\right.$$

$$\left.y\right],\left[a_j;\alpha_j^{(1)},\ldots,\alpha_j^{(r)}\right]_{2,n},\left[\tau_i\left(a_{ji};\alpha_{ji}^{(1)},\ldots,\alpha_{ji}^{(r)}\right)_{n+1,p_i}\right],\left[1-\rho_1+\tfrac{N_1}{2},\gamma_1\right],$$
$$\left[\tau_i\left(b_{ji};\beta_{ji}^{(1)},\ldots\beta_{ji}^{(r)}\right)_{m+1,q_i}\right],$$

$$\left[1-\rho_1+\tfrac{N_1}{2}-k_1,\gamma_1\right],\left[c_j^{(1)},\zeta_j^{(1)}\right]_{1,n_1},\left[\tau_{i^{(1)}},\left(c_{ji^{(1)}}^{(1)},\zeta_{ji^{(1)}}^{(1)}\right)_{n_1+1,p_i^{(1)}}\right],\ldots,$$
$$\left[d_j^{(1)},\delta_j^{(1)}\right]_{1,m_1},\left[\tau_{i^{(1)}}\left(d_{ji^{(1)}}^{(1)},\delta_{ji^{(1)}}^{(1)}\right)_{m_1+1,q_i^{(1)}}\right],\ldots,$$

$$\left[1-\rho_r+\tfrac{N_r}{2},\gamma_r\right],\left[1-\rho_r+\tfrac{N_r}{2}-k_r,\gamma_r\right],\left[c_j^{(r)},\zeta_j^{(r)}\right]_{1,n_r},$$
$$\left[d_j^{(r)},\delta_j^{(r)}\right]_{1,m_r},$$

$$\left[\begin{matrix}\tau_{i^{(r)}}\left(c_{ji^{(r)}}^{(r)},\zeta_{ji^{(r)}}^{(r)}\right)_{n_r+1,p_i^{(r)}}\\ \tau_{i^{(r)}}\left(d_{ji^{(r)}}^{(r)},\delta_{ji^{(r)}}^{(r)}\right)_{m_r+1,q_i^{(r)}}\end{matrix}\right]\Bigg]. \tag{20}$$

Proof: Initially, we express the left-hand side of (20) in the form of the Mellin-Barnes integral as given in (1). Further, by applying the chain rule of derivatives and the result defined in (8), we get

$$\frac{\partial}{\partial\Lambda_1}\Gamma\left(\rho_1\pm\frac{\Lambda_1}{2}+\gamma_1 s_1\right)\Big|_{\Lambda_1=N_1}=\frac{1}{2}\Gamma\left(\rho_1\pm\frac{N_1}{2}+\gamma_1 s_1\right)\times$$
$$\left[\psi\left(\rho_1+\frac{N_1}{2}+\gamma_1 s_1\right)-\psi\left(\rho_1-\frac{N_1}{2}+\gamma_1 s_1\right)\right]=\frac{1}{2}\Gamma\left(\rho_1\pm\frac{N_1}{2}+\gamma_1 s_1\right)$$
$$\sum_{L_1=1}^{N_1}\frac{(-1)^{L_1-1}N_1!\Gamma\left(\rho_1-\frac{N_1}{2}+\gamma_1 s_1\right)}{L_1(N_1-L_1)!\Gamma\left(\rho_1-\frac{N_1}{2}+L_1+\gamma_1 s_1\right)}. \tag{21}$$

Similarly, we can generalize (21) for $\frac{\partial}{\partial\Lambda_k}\Gamma\left(\rho_k\pm\frac{\Lambda_k}{2}+\gamma_k s_k\right)\Big|_{\Lambda_k=N_k}$ $(k=1,\ldots,r-1)$. And the last term of the sequence is defined below by:

$$\frac{\partial}{\partial\Lambda_r}\Gamma\left(\rho_r\pm\frac{\Lambda_r}{2}+\gamma_r s_r\right)\Big|_{\Lambda_r=N_r}=\frac{1}{2}\Gamma\left(\rho_r\pm\frac{N_r}{2}+\gamma_r s_r\right)\times$$
$$\left[\psi\left(\rho_r+\frac{N_r}{2}+\gamma_r s_r\right)-\psi\left(\rho_r-\frac{N_r}{2}+\gamma_r s_r\right)\right]=\frac{1}{2}\Gamma\left(\rho_r\pm\frac{N_r}{2}+\gamma_r s_r\right)$$
$$\sum_{L_r=1}^{N_r}\frac{(-1)^{L_r-1}N_r!\Gamma\left(\rho_r-\frac{N_r}{2}+\gamma_r s_r\right)}{L_r(N_r-L_r)!\Gamma\left(\rho_r-\frac{N_r}{2}+L_r+\gamma_r s_r\right)}. \tag{22}$$

Now, we can write the left-hand side of (20) by using the above-given results in (21) and (22). After a bit of simplification, We have

$$=\frac{\prod_{k=1}^{r}(N_k)!}{2^k}\sum_{L_1=0}^{N_1}\cdots\sum_{L_r=0}^{N_r}\frac{(-1)^{L_1+L_2+\cdots+L_r-r}}{\prod_{k=1}^{r}L_k(N_k-L_k)!}\times$$

$${}^{(\Gamma)}\aleph_{p_i,q_i,\tau_i;R;p_{i^{(1)}}+3,q_{i^{(1)}}+1,\tau_{i^{(1)}};R_{(1)},\ldots,p_{i^{(r)}}+3,q_{i^{(r)}}+1,\tau_{i^{(r)}};R_{(r)}}^{0,n:m_1,n_1+3,\ldots,m_r,n_r+3}\left[\begin{matrix}z_1\\ \vdots\\ z_r\end{matrix}\;\middle|\;\begin{matrix}\left[a_1;\alpha_1^{(1)},\ldots,\right.\\ \ldots,\end{matrix}\right.$$

$$\left.\alpha_1^{(r)},y\right],\left[a_j;\alpha_j^{(1)},\ldots,\alpha_j^{(r)}\right]_{2,n},\left[\tau_i\left(a_{ji};\alpha_{ji}^{(1)},\ldots,\alpha_{ji}^{(r)}\right)_{n+1,p_i}\right],$$
$$\left[\tau_i\left(b_{ji};\beta_{ji}^{(1)},\ldots,\beta_{ji}^{(r)}\right)_{m+1,q_i}\right],\left[d_j^{(1)},\delta_j^{(1)}\right]_{1,m_1},\left[\tau_{i^{(1)}}\left(d_{ji^{(1)}}^{(1)},\delta_{ji^{(1)}}^{(1)}\right)_{m_1+1,q_i^{(1)}}\right],$$

$$\left[1-\rho_1 \pm \tfrac{N_1}{2}, \gamma_1\right], \left[1-\rho_1+\tfrac{N_1}{2}, \gamma_1\right], \left[c_j^{(1)}, \zeta_j^{(1)}\right]_{1,n_1},$$
$$\left[1-\rho_1+\tfrac{N_1}{2}-L_1, \gamma_1\right], \ldots, \left[d_j^{(r)}, \delta_j^{(r)}\right]_{1,m_r},$$

$$\left[\tau_{i^{(1)}}, \left(c_{ji^{(1)}}^{(1)}, \zeta_{ji^{(1)}}^{(1)}\right)_{n_1+1,p_i^{(1)}}\right], \ldots, \left[1-\rho_r \pm \tfrac{N_r}{2}, \gamma_r\right],$$
$$\left[\tau_{i^{(r)}} \left(d_{ji^{(r)}}^{(r)}, \delta_{ji^{(r)}}^{(r)}\right)_{m_r+1,q_i^{(r)}}\right],$$

$$\left[1-\rho_r+\tfrac{N_r}{2}, \gamma_r\right], \left[c_j^{(r)}, \zeta_j^{(r)}\right]_{1,n_r}, \left[\tau_{i^{(r)}} \left(c_{ji^{(r)}}^{(r)}, \zeta_{ji^{(r)}}^{(r)}\right)_{n_r+1,p_i^{(r)}}\right] \Bigg]. \quad (23)$$
$$\left[1-\rho_r+\tfrac{N_r}{2}-L_r, \gamma_r\right]$$

Now, consider the incomplete Aleph function with two variables portion of (23) and for the sake of convenience denote it by L. So, we can write it as follows:

$$L = {}^{(\Gamma)}\aleph_{p_i,q_i,\tau_i;R;p_{i^{(1)}}+3,q_{i^{(1)}}+1,\tau_{i^{(1)}};R_{(1)},\ldots,p_{i^{(r)}}+3,q_{i^{(r)}}+1,\tau_{i^{(r)}};R_{(r)}}^{0,n:m_1,n_1+3,m_2,n_2+3} \left[\begin{array}{c|c} z_1 & \left[a_1; \alpha_1^{(1)}, \right. \\ \vdots & \ldots, \\ z_r & \end{array}\right.$$

$$\left. \ldots, \alpha_1^{(r)}, y\right], \left[a_j; \alpha_j^{(1)}, \ldots, \alpha_j^{(r)}\right]_{2,n}, \left[\tau_i \left(a_{ji}; \alpha_{ji}^{(1)}, \ldots, \alpha_{ji}^{(r)}\right)_{n+1,p_i}\right],$$
$$\left[\tau_i \left(b_{ji}; \beta_{ji}^{(1)}, \ldots, \beta_{ji}^{(r)}\right)_{m+1,q_i}\right],$$

$$\left[1-\rho_1 \pm \tfrac{N_1}{2}, \gamma_1\right], \left[1-\rho_1+\tfrac{N_1}{2}, \gamma_1\right]$$
$$\left[d_j^{(1)}, \delta_j^{(1)}\right]_{1,m_1}, \left[\tau_{i^{(1)}} \left(d_{ji^{(1)}}^{(1)}, \delta_{ji^{(1)}}^{(1)}\right)_{m_1+1,q_i^{(1)}}\right],$$

$$\left[c_j^{(1)}, \zeta_j^{(1)}\right]_{1,n_1}, \left[\tau_{i^{(1)}}, \left(c_{ji^{(1)}}^{(1)}, \zeta_{ji^{(1)}}^{(1)}\right)_{n_1+1,p_i^{(1)}}\right], \ldots, \left[1-\rho_r \pm \tfrac{N_r}{2}, \gamma_r\right],$$
$$\left[1-\rho_1+\tfrac{N_1}{2}-L_1, \gamma_1\right], \ldots, \left[d_j^{(r)}, \delta_j^{(r)}\right]_{1,m_r}, \left[\tau_{i^{(r)}} \left(d_{ji^{(r)}}^{(r)}, \delta_{ji^{(r)}}^{(r)}\right)_{m_r+1,q_i^{(r)}}\right],$$

$$\left[1-\rho_r+\tfrac{N_r}{2}, \gamma_r\right], \left[c_j^{(r)}, \zeta_j^{(r)}\right]_{1,n_r}, \left[\tau_{i^{(r)}} \left(c_{ji^{(r)}}^{(r)}, \zeta_{ji^{(r)}}^{(r)}\right)_{n_r+1,p_i^{(r)}}\right] \Bigg]. \quad (24)$$
$$\left[1-\rho_r+\tfrac{N_r}{2}-L_r, \gamma_r\right]$$

Now, evaluate the value of $\prod_{k=1}^{r} Z_k^{-\frac{1}{\gamma_k}\left(\frac{N_k}{2}-\rho_k-L_k\right)} \times L$, by using the generalized form of formula 1 and 3, and after simplification. We obtain

$$(-1)^{\sum_{k=1}^{r}(N_k-L_k)}\prod_{k=1}^{r}\left[(\Lambda_k)^{N_k/2+\rho_k}\frac{\partial^{N_k-L_k}}{\partial\Lambda_k^{N_k-L_k}}\Lambda_1^{(N_k/2-\rho_k-L_k)}\right]\times$$

$${}^{(\Gamma)}\aleph^{0,n:m_1,n_1+2,\ldots,m_r,n_r+2}_{p_i,q_i,\tau_i;R;p_{i(1)}+2,q_{i(1)},\tau_{i(1)};R_{(1)},\ldots,p_{i(r)}+2,q_{i(r)},\tau_{i(r)};R_{(r)}}\left[\begin{array}{c|l} z_1 & \left[a_1;\alpha_1^{(1)},\ldots,\right. \\ z_2 & \ldots, \end{array}\right.$$

$$\left.\alpha_1^{(r)},y\right],\left[a_j;\alpha_j^{(1)},\ldots,\alpha_j^{(r)}\right]_{2,n},\left[\tau_i\left(a_{ji};\alpha_{ji}^{(1)},\ldots,\alpha_{ji}^{(r)}\right)_{n+1,p_i}\right],$$
$$\left[\tau_i\left(b_{ji};\beta_{ji}^{(1)},\ldots,\beta_{ji}^{(r)}\right)_{m+1,q_i}\right],$$

$$\left[1-\rho_1+\tfrac{N_1}{2},\gamma_1\right]^2,\left[c_j^{(1)},\zeta_j^{(1)}\right]_{1,n_1},\left[\tau_{i^{(1)}},\left(c_{ji^{(1)}}^{(1)},\zeta_{ji^{(1)}}^{(1)}\right)_{n_1+1,p_i^{(1)}}\right],\ldots,$$
$$\left[d_j^{(1)},\delta_j^{(1)}\right]_{1,m_1},\left[\tau_{i^{(1)}}\left(d_{ji^{(1)}}^{(1)},\delta_{ji^{(1)}}^{(1)}\right)_{m_1+1,q_i^{(1)}}\right],$$

$$\left[1-\rho_r+\tfrac{N_r}{2},\gamma_r\right]^2,\left[c_j^{(r)},\zeta_j^{(r)}\right]_{1,n_r},\left[\tau_{i^{(r)}}\left(c_{ji^{(r)}}^{(r)},\zeta_{ji^{(r)}}^{(r)}\right)_{n_r+1,p_i^{(r)}}\right]\Bigg],\qquad(25)$$
$$\left[d_j^{(r)},\delta_j^{(r)}\right]_{1,m_r},\left[\tau_{i^{(r)}}\left(d_{ji^{(r)}}^{(r)},\delta_{ji^{(r)}}^{(r)}\right)_{m_r+1,q_i^{(r)}}\right]$$

where $z_k=\Lambda_k^{-\gamma_k}$ $(k=1,\ldots,r)$.
Now applying the Leibniz formula (15) in (25) and simplify it, we have

$$=\sum_{l_1=0}^{N_1-L_1}\sum_{l_2=0}^{N_2-L_2}\cdots\sum_{l_r=0}^{N_r-L_r}\left[\prod_{k=1}^{r}\frac{(N_k-L_k)!\Gamma(N_k-l_k)}{l_k!(N_k-L_k-l_k)!\Gamma(L_k)}\right]\times$$

$$\aleph^{0,n:m_1,n_1+2,\ldots,m_r,n_r+2}_{p_i,q_i,\tau_i;R:p_{i(1)}+2,q_{i(1)},\tau_{i(1)};R_{(1)};\ldots,p_{i(r)}+2,q_{i(r)},\tau_{i(r)};R_{(r)}}\left[\begin{array}{c|l} z_1 & \left[a_1;\alpha_1^{(1)},\ldots,\alpha_1^{(r)},y\right], \\ z_2 & \ldots, \end{array}\right.$$

$$\left[a_j;\alpha_j^{(1)},\ldots,\alpha_j^{(r)}\right]_{2,n},\left[\tau_i\left(a_{ji};\alpha_{ji}^{(1)},\ldots,\alpha_{ji}^{(r)}\right)_{n+1,p_i}\right],\left[1-\rho_1+\tfrac{N_1}{2},\gamma_1\right],$$
$$\left[\tau_i\left(b_{ji};\beta_{ji}^{(1)},\ldots,\beta_{ji}^{(r)}\right)_{m+1,q_i}\right],\left[d_j^{(1)},\delta_j^{(1)}\right]_{1,m_1},$$

$$\left[1-\rho_1+\tfrac{N_1}{2}-k_1,\gamma_1\right]\left[c_j^{(1)},\zeta_j^{(1)}\right]_{1,n_1},$$
$$\left[d_j^{(1)},\delta_j^{(1)}\right]_{1,m_1},$$

$$\left[\tau_{i^{(1)}}\left(c_{ji^{(1)}}^{(1)},\zeta_{ji^{(1)}}^{(1)}\right)_{n_1+1,p_i^{(1)}}\right],\left[1-\rho_r+\tfrac{N_r}{2},\gamma_r\right],$$
$$\left[\tau_{i^{(1)}}\left(d_{ji^{(1)}}^{(1)},\delta_{ji^{(1)}}^{(1)}\right)_{m_1+1,q_i^{(1)}}\right],$$

$$\left.\begin{array}{l}\left[1-\rho_r+\frac{N_r}{2}-k_r,\gamma_r\right],\left[c_j^{(r)},\zeta_j^{(r)}\right]_{1,n_r},\left[\tau_{i^{(r)}}\left(c_{ji^{(r)}}^{(r)},\zeta_{ji^{(r)}}^{(r)}\right)_{n_r+1,p_i^{(r)}}\right]\\ \left[d_j^{(r)},\delta_j^{(r)}\right]_{1,m_r},\left[\tau_{i^{(r)}}\left(d_{ji^{(r)}}^{(r)},\delta_{ji^{(r)}}^{(r)}\right)_{m_r+1,q_i^{(r)}}\right]\end{array}\right]. \quad (26)$$

By using (24) and change the order of summations in $\sum_{L_k=1}^{N_k}\sum_{l_k=0}^{N_k-L_k}$ $(k=1,\ldots,r)$ and inner sums then simplify to $L_k=1$ $(k=1,\ldots,r)$. Finally, we obtain the desired result.
Similarly, We can derive all the theorems for the incomplete Aleph function with r-variables ${}^{(\gamma)}\aleph_Q^P[z_r]$ as we derived for ${}^{(\Gamma)}\aleph_Q^P[z_r]$ and generalized it also as given in section 4.

5 Particular Cases

In this part, we discuss some important cases of Theorem 1 which can also comfortably obtain the results identically to Theorem 2, 3 and 4. Further, if we assign specific values to the parameters in the incomplete Aleph functions of two variables then we have the following cases.

5.1 In terms of H-function with two variables

By setting $y=0,\tau_i=\tau_{i^{(1)}}=\tau_{i^{(2)}}=1$ and $R=R^{(1)}=R^{(2)}=1$ in Theorem 1, we get a known result derived by Deshpande [19] as follows:

$$\frac{\partial}{\partial\Lambda_1}\frac{\partial}{\partial\Lambda_2}H_{Q^*}^{P^*}\left[\begin{array}{c|c}z_1 & X^*\\ z_2 & Y^*\end{array}\right]_{\Lambda_1=N_1,\,\Lambda_2=N_2}$$
$$=\frac{N_1!N_2!}{4}\sum_{k_1=0}^{N_1-1}\sum_{k_2=0}^{N_2-1}\frac{1}{k_1!k_2!(N_1-k_1)(N_2-k_2)}H_{Q^*}^{P^*}\left[\begin{array}{c|c}z_1 & X^{**}\\ z_2 & Y^{**}\end{array}\right], \quad (27)$$

where
$P^*=0,n:m_1,n_1+2,m_2,n_2+2,$
$Q^*=p,q:p_{(1)}+2,q_{(1)},p_{(2)}+2,q_{(2)},$

$X^*=\left[a_j;\alpha_j^{(1)},\alpha_j^{(2)}\right]_{1,n},\left[1-\rho_1\pm\frac{\Lambda_1}{2},\gamma_1\right],\left[c_j^{(1)},\zeta_j^{(1)}\right]_{1,n_1},\left[1-\rho_2\pm\frac{\Lambda_2}{2},\gamma_2\right],$
$\left[c_j^{(2)},\zeta_j^{(2)}\right]_{1,n_2},$

$$Y^{*}=\left[b_{ji};\beta_{ji}^{(1)},\beta_{ji}^{(2)}\right]_{m+1,q_i},\left[d_j^{(1)},\delta_j^{(1)}\right]_{1,m_1},\left[d_j^{(2)},\delta_j^{(2)}\right]_{1,m_2},$$
$$X^{**}=\left[a_j;\alpha_j^{(1)},\alpha_j^{(2)}\right]_{1,n},\left[1-\rho_1+\tfrac{N_1}{2},\gamma_1\right),\left(1-\rho_1+\tfrac{N_1}{2}-k_1,\gamma_1\right],$$
$$\left[c_j^{(1)},\zeta_j^{(1)}\right]_{1,n_1},\left[1-\rho_2+\tfrac{N_2}{2},\gamma_2\right],\left[1-\rho_2+\tfrac{N_2}{2}-k_2,\gamma_2\right],\left[c_j^{(2)},\zeta_j^{(2)}\right]_{1,n_2},$$
$$Y^{**}=\left[b_{ji};\beta_{ji}^{(1)},\beta_{ji}^{(2)}\right]_{m+1,q_i},\left[d_j^{(1)},\delta_j^{(1)}\right]_{1,m_1},\left[d_j^{(2)},\delta_j^{(2)}\right]_{1,m_2}.$$

Similarly, we get more results by setting $y=0,\tau_i=\tau_{i^{(1)}}=\tau_{i^{(2)}}=1$ and $R=R^{(1)}=R^{(2)}=1$, thus convert Multivariable incomplete Aleph function to Multivariable H-function in all theorems of section 3.

5.2 In terms of G-function with two variables

By substituting $\alpha_j^{(1)}=\alpha_j^{(2)}=\zeta_j^{(1)}=\zeta_j^{(2)}=\beta_{ji}^{(1)}=\beta_{ji}^{(2)}=\delta_j^{(1)}=\delta_j^{(2)}=1$ in the result 5.1, we can transform that result in G-function [13, 2, 14] as follows:

$$\frac{\partial}{\partial\Lambda_1}\frac{\partial}{\partial\Lambda_2}G_{p,q:p_{(1)}+2,q_{(1)},p_{(2)}+2,q_{(2)}}^{0,n:m_1,n_1+2,m_2,n_2+2}\left[\begin{array}{c|l} z_1 & (a_j)_{1,n},\left(1-\rho_1\pm\frac{\Lambda_1}{2},\gamma_1\right),\left(c_j^{(1)}\right), \\ z_2 & (b_{ji})_{m+1,q_i},\left(d_j^{(1)}\right)_{1,m_1}, \end{array}\right.$$

$$\left.\begin{array}{l} \left(1-\rho_2\pm\frac{\Lambda_2}{2},\gamma_2\right),\left(c_j^{(2)}\right) \\ \left(d_j^{(2)}\right)_{1,m_2} \end{array}\right]_{\Lambda_1=N_1,\,\Lambda_2=N_2}$$
$$=\frac{N_1!N_2!}{4}\sum_{k_1=0}^{N_1-1}\sum_{k_2=0}^{N_2-1}\frac{1}{k_1!k_2!(N_1-k_1)(N_2-k_2)}\times$$

$$G_{p,q:p_{(1)}+2,q_{(1)},p_{(2)}+2,q_{(2)}}^{0,n:m_1,n_1+2,m_2,n_2+2}\left[\begin{array}{c|l} z_1 & (a_j)_{1,n},\left[1-\rho_1+\frac{N_1}{2},\gamma_1\right],\left[1-\rho_1+\frac{N_1}{2}-k_1,\right. \\ z_2 & \left.(b_{ji})_{m+1,q_i},\left(d_j^{(1)}\right)_{1,m_1},\right. \end{array}\right.,$$

$$\left.\begin{array}{l} \gamma_1\right],\left(c_j^{(1)}\right)_{1,n_1},\left[1-\rho_2+\frac{N_2}{2},\gamma_2\right],\left[1-\rho_2+\frac{N_2}{2}-k_2,\gamma_2\right],\left(c_j^{(2)}\right)_{1,n_2} \\ \left(d_j^{(2)}\right)_{1,m_2} \end{array}\right]. \quad (28)$$

By putting suitable values to the parameters, we arrived at the known results given by Buschman and Despande [11, 12, 18].

6 Conclusions

We summed up this analysis by considering the utility and prospective applications of the newly derived special functions. Several known and novel outcomes

involving special functions follow as specific cases of our main findings due to the most fundamental character of the functions involved in the present work. The significance of our results lies in many fold generality. Because of the generality of the incomplete Aleph functions with r-variables, on suitable specializing the various parameters and variables in these functions from our results, we can establish extensive varieties of useful results, which are expressible in terms of families of the incomplete H-functions, incomplete generalized hypergeometric functions, incomplete I-functions, I-function, Aleph function and many more. This work will remove the constraints of special functions and these results may be used to solve a variety of problems in mathematical analysis.

References

[1] A. Erdelyi, W. Magnus, F. Oberhettinger, F. G. Tricomi, *Higher Transcendental Functions Vol. 1*, McGraw-Hill Book Co., Inc., New York, 1953.

[2] A. Verma, A note on expansions involving Meijers G-functions, *Mathematics of Computation*, 21(97), 107-112, (1967).

[3] A. Oli, K. Tilahun, G. V. Reddy, The Multivariable Aleph-function involving the Generalized Mellin-Barnes Contour Integrals, *Cubo (Temuco)*, 22(3), 351-359, (2020).

[4] C. K. Sharma, S. S. Ahmad, On the multivariable I-function, *Acta ciencia Indica Math.*, 20(2), 113116, (1994).

[5] D. Kumar, F. Y. Ayant, S. D. Purohit, F. Ucar, On Partial Derivatives of the I-function of r-variables, *Azerbaijan Journal of Mathematics*, 10, 49-61, (2020).

[6] F. Ayant, P. Kumar, Incomplete Multivariable Aleph-function and Integral of Three Parameters Calculus, *The Mathematics Education*, 55. 12-27, (2021).

[7] H. Tadesse, D. L. Suthar, M. Ayalew, Finite Integral Formulas Involving Multivariable Aleph-Functions, *Journal of Applied Mathematics*, Article ID: 6821797, (2019).

[8] M. K. Bansal, D. Kumar, K. S. Nisar, J. Singh, Certain fractional calculus and integral transform results of incomplete Aleph-functions with applications, *Mathematical Methods in the Applied Sciences*, 43(8), 5602-5614, (2020).

[9] M. K. Bansal, D. Kumar, On the integral operators pertaining to a family of incomplete I-functions, *AIMS-Math.*, (2), 1247-1259, (2020).

[10] N. Sdland, B. Baumann, T. F. Nannenmacher, Open problem: who knows about the aleph-function?, *Appl Anal*, 1, 401402, (1998).

[11] R. G. Buschman, Finite sum representations for partial derivatives of special functions with respect to parameters, *Mathematics of Computation*, 28(127), 817-824, (1974).

[12] R. G. Buschman, Partial derivatives of the H-function with respect to parameters expressed as finite sum and integrals, *Univ. Nac. Tucuman, Rev. Ser. A*, 24, 149-155, (1974).

[13] R. P. Agarwal, An extention of Meijer's G-function, *Proc. Nat. Inst. Sei. India. Sect. A*, 32, (1965).

[14] R. Panda, H. M. Srivastava, Some bilateral generating functions for a class of generalized hypergeometric polynomials, *J. Reine Angew. Math.*, 283/284, 265-274, (1976).

[15] R. Sharma, J. Singh, D. Kumar, Y. Singh, Certain Unified Integrals Associated with Product of the General Class of Polynomials and Incomplete I-Functions, *Int. J. Appl. Comput. Math.*, 8(7), (2021).

[16] R. Sharma, J. Singh, D. Kumar, Y. Singh, An Application of Incomplete I-Functions with Two Variables to Solve the Nonlinear Differential Equations Using S-Function, *J. Computational Analysis And Applications*, 31(1), 80-95, (2023).

[17] S. Momani, R. Sharma, J. Singh, Y. Singh, S. Hadid, Fractional Order Mathematical Modelling for Studying the Impact on the Emergence of Pollution and Biodiversity Pertaining to Incomplete Aleph Functions, *Progress in Fractional Differentiation and Applications*, 10(1), 15-22, (2024)

[18] V. L. Deshpande, Partial derivatives of hypergeometric functions of two variables with respect to parameters,*To appear in the J. Indian Acad. Math., Indore*, (1978).

[19] V. L. Deshpande, Finite sum representations of the H-function of two and more variables with respect to parameters,*Indian J. pure appl. Math*, 10, 1514-1524, (1979).

[20] Y. Singh, R. Sharma, R. Maanju, Beer-Lamberts law as an application of incomplete Aleph (ℵ) functions, *AIP Conf. Proc*, 2768 (1): 020038, (2023).

A Study on Fractional SIR Epidemic Model with Vital Dynamics and Variable Population Size using the Residual Power Series Method

Rakesh Kumar Meena[1], Sushil Kumar[2]
Department of Mathematics,
S. V. National Institute of Technology, Surat-395007 (Gujarat), India.
[1]rakeshkumarmeena318@gmail.com, [2]sushilk@amhd.svnit.ac.in

December 31, 2023

Abstract

In this paper, we develop an integer and fractional-order susceptible, infectious, and recovery (SIR) epidemic model based on vital dynamics, i.e., birth, death, immigration, and variable population size, including infection and recovery rates. We investigate the stability analysis for the fractional SIR model on the disease-free and endemic equilibrium points. The existence and uniqueness conditions of solutions for a stable model are also discussed. The residual power series (RPS) approach is used to get the semi-analytical solutions of the proposed model in the form of convergent fractional power series. The convergence analysis of the RPS method is also discussed. Numerical results demonstrate the effect of distinct fractional orders $\alpha \in (0, 1]$ on the population density. The obtained results are exciting and may be beneficial for medical experts to control the epidemic disease.
Keywords: SIR model, Caputo derivative, Fractional power series, and Residual power series.

1 Introduction

Fractional calculus is a powerful tool for the mathematical modelling of physical problems [1, 2, 3]. It has been applied in many research areas, such as science, economics, engineering, etc. Additionally, fractional differential equations in nonlinear dynamics have been studied by many researchers [4, 5, 6, 7]. In classical integer-order epidemic models, the disease spreads between compartments of the model with an equal chance. The rates of contact and illness transmission should be constant. A fractional derivative could replace a classical derivative to learn more about the dynamics of the model [8, 9, 10].

There is no long-lasting protection against several infectious illnesses. Some infections recover, and some people become susceptible after an infection. The SIR model studies this kind of illness. The schematic of the susceptible, infectious, and recovery (SIR) model is shown in Fig. 1. Here, $S(t)$, $I(t)$, and $R(t)$ represent the number of susceptible individuals, the number of infectious individuals, and the number of recovery individuals, respectively, at time t. λ is the number of births per unit time. μ_1, μ_2, and μ_3 are the numbers of immigration and deaths per unit of time for S, I, and R, respectively. r_1 and r_2 are the numbers of infectious people per infected person per unit of time and the number of recovered people per unit of time, respectively. The considered population size at time t is $N(t) = S(t) + I(t) + R(t)$.

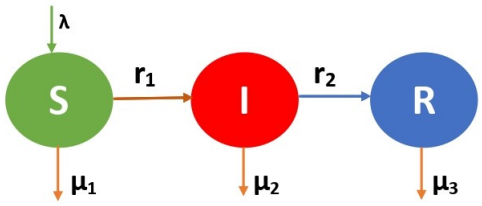

Figure 1: SIR Epidemic Model.

Researchers have successfully investigated several generalized variations of the classical and fractional-order epidemic models. Hethcote and Driessche [11] studied an susceptible-infectious-susceptible (SIS) epidemic model with variable population size. Ackleh and Allen [12] and Zaman et al. [13] discussed the SIR epidemic model with varying population sizes. El-Saka [14] addressed fractional epidemic models like SIR and susceptible-infectious-recovery-susceptible with varying population sizes. The SIR model with varying population sizes and continuous recruitment was examined by Bakare et al. [15]. Hassouna et al. [16] studied a fractional SIS epidemic model with varying population sizes. Fractional-order SIR epidemiological models were examined by Tafhvaei et al. [17]. Koziol et al. [18] discussed the influence of fractional order values on the dynamic properties of the SIR model. The SIR, susceptible-exposive-infectious-recovery, and susceptible-exposive-infective-asymptomatic-recovery models with fractional orders were reviewed by Chen et al. [19]. Balzotti et al. [20] studied the fractional SIS epidemic model with varying population sizes. Meena and Kumar [21, 22] discussed the fractional SIR and SIS epidemic models with constant population size. Sidi Ammi et al. [23] studied the diffusive SIR epidemic model described by reaction-diffusion equations involving a fractional derivative. A fractional SIR epidemic model with treatment cure rate was discussed by Sadki et al. [24].

The above-cited articles considered SIR models with constant population sizes. To the best of the author's knowledge, the study of the integer and

fractional order SIR models, considering the model's vital dynamics and variable population size, is lacking in the literature. So, in this paper, we develop integer and fractional order SIR epidemic models consisting of susceptible, infectious, and recovery groups with birth, immigration, death, infection, and recovery rates for variable population sizes. Moreover, parameters (i.e., λ, μ_1, μ_2, and μ_3) are added to discuss more insight into the model's dynamics. These parameters are directly associated with particular groups and also affect the population sizes during the disease.

In the present study, we deal with the aforementioned integer and fractional-order SIR epidemic models. The linearization procedure is used to discuss the stability analysis of the fractional model with disease-free and endemic equilibrium points. The existence and uniqueness of the solutions for the stable model are also examined. Semi-analytical solutions of the proposed model are obtained in the form of a fast-convergent series with the help of the RPS method. The absolute errors between the semi-analytical and numerical solutions using the Runge-Kutta (RK) method for $\alpha = 1$ are obtained to show the RPS method's effectiveness. The effect of the fractional order (α) on population densities is also discussed. The numerical and graphical results show that this study can benefit researchers, policy-makers, and medical experts understand the dynamics of epidemic models.

The structure of the paper is as follows: After the introduction in Section 1, some basic definitions of fractional calculus are listed in Section 2. A mathematical model is formulated in Section 3. The stability and existence of a uniformly stable solution for the proposed model are discussed in Section 4 and Section 5, respectively. Section 6 discusses the procedures of the RPS Method and the solution of the model. Numerical results and graphs are discussed in Section 7, and the outcomes of the study are concluded in Section 8.

2 Preliminaries

This section discusses the definitions and properties of fractional calculus. The fractional derivative has a variety of fascinating definitions. Yet, given their advantage over issues with an initial value, we use the well-known Caputo derivatives in the present study.

Definition 2.1 *[25] The Caputo fractional derivative of order α of function $r(y)$ is defined as:*

$$ {}_0^C D_y^\alpha r(y) = \begin{cases} \dfrac{1}{\Gamma(q-\alpha)} \displaystyle\int_0^y \frac{r^{(q)}(v)}{(y-v)^{\alpha+1-q}} dv, & \text{if } (q-1) < \alpha < q,\ q \in \mathbb{N}, \\ \dfrac{d^q}{dy^q} r(y), & \text{if } \alpha = q,\ q \in \mathbb{N}. \end{cases} $$

Definition 2.2 *[26, 27] The fractional power series (FPS) about $y = y_0$ can be*

defined as

$$\sum_{j=0}^{\infty} l_j (y-y_0)^{j\alpha} = l_0 + l_1(y-y_0)^{\alpha} + l_2(y-y_0)^{2\alpha} + \ldots;$$

$(q-1) < \alpha \leq q,\ q \in N,\ y \geq y_0$. *Where* $l_j,\ j = 0, 1, 2, \ldots$ *are the coefficients of the FPS.*

Theorem 2.1 *[26, 27] A FPS of the function* $r(y)$ *about* $y = y_0$ *can be defined as*

$$r(y) = \sum_{j=0}^{\infty} l_j (y-y_0)^{j\alpha},\ y_0 \leq y < (y_0 + \rho).$$

It was found that if ${}_0^C D_{y_0}^{j\alpha} r(y),\ \forall j = 0, 1, 2, \ldots$ *are continuous on* $(y_0, y_0 + \rho)$, *then* $l_j = \dfrac{D_{y_0}^j r(y_0)}{\Gamma(1+j\alpha)}$. *Where* ρ *is the radius of convergence and* ${}_0^C D_{y_0}^{j\alpha} = {}_0^C D_{y_0}^{\alpha}\, {}_0^C D_{y_0}^{\alpha} \ldots {}_0^C D_{y_0}^{\alpha}$ *(j-times).*

Property 2.1 *[25] Let* $r(y) = y^q$, $q \geq 0$,

$${}_0^C D_y^{\alpha} y^q = \begin{cases} \dfrac{\Gamma(q+1)}{\Gamma(q+1-\alpha)} y^{q-\alpha}, & \text{if } q \geq \lceil \alpha \rceil, \\ 0, & \text{if } q < \lceil \alpha \rceil. \end{cases}$$

3 Mathematical Model

A mathematical model is vital in analyzing the physical, chemical, linguistic, etc., systems. The SIR model is general and can be used for the mathematical study of any disease like influenza, measles, chicken pox, mumps, etc. The assumption of a fractional-order SIR model in the epidemic has essential implications for the time domain. The fractional order model gives a better way to understand the physical behavior of the SIR epidemic model than the integer order model. Following are the assumptions to construct the SIR epidemic model at time t.

3.1 Assumptions

1. The disease spreads in a particular region with a variable population size $N(t)$, i.e., $S(t) + I(t) + R(t) = N(t)$.
2. $r_1 S(t) I(t)$ is total newly infected people from susceptible at time t.
3. $r_2 I(t)$ is the number of recovered infected persons at time t. The recovered person has ongoing immunity.
4. The number of births per unit of time t in the susceptible compartment is $\lambda N(t)$ at the rate λ.

5. The number of deaths and immigration in susceptible, infectious, and recovered compartments is $\mu_1 S(t)$, $\mu_2 I(t)$, and $\mu_3 R(t)$, respectively, with rates of μ_1, μ_2, and μ_3.

For integer order, the SIR model with vital dynamics can be formulated as

$$\left.\begin{aligned} \frac{dS(t)}{dt} &= \lambda N(t) - r_1 S(t) I(t) - \mu_1 S(t), \\ \frac{dI(t)}{dt} &= r_1 S(t) I(t) - r_2 I(t) - \mu_2 I(t), \\ \frac{dR(t)}{dt} &= r_2 I(t) - \mu_3 R(t), \\ \frac{dS(t)}{dt} &+ \frac{dI(t)}{dt} + \frac{dR(t)}{dt} = \frac{dN(t)}{dt}. \end{aligned}\right\} \tag{1}$$

At $t = 0$, the initial conditions of the model (Eq. (1)) are given as

$$S(0) = S_0,\ I(0) = I_0,\ R(0) = R_0,\ \text{and } N(0) = N_0. \tag{2}$$

By replacing the integer order derivative with the Caputo derivatives of order $\alpha \in (0, 1]$ in model (Eq. (1)), we have the following model

$$\left.\begin{aligned} {}_0^C D_t^\alpha S(t) &= \lambda N(t) - r_1 S(t) I(t) - \mu_1 S(t), \\ {}_0^C D_t^\alpha I(t) &= r_1 S(t) I(t) - r_2 I(t) - \mu_2 I(t), \\ {}_0^C D_t^\alpha R(t) &= r_2 I(t) - \mu_3 R(t), \\ {}_0^C D_t^\alpha S(t) &+ {}_0^C D_t^\alpha I(t) + {}_0^C D_t^\alpha R(t) = {}_0^C D_t^\alpha N(t). \end{aligned}\right\} \tag{3}$$

At $t = 0$, the initial conditions of the model (Eq. (3)) are

$$S(0) = S_0,\ I(0) = I_0,\ R(0) = R_0,\ \text{and } N(0) = N_0. \tag{4}$$

Where parameters r_1, r_2, λ, μ_1, μ_2, and μ_3 are the positive constants.

4 Stability Analysis of the Fractional SIR Epidemic Model

In this section, we discuss disease-free and endemic equilibrium points of the model (Eq. (3)) as

$${}_0^C D_t^\alpha S(t) = 0,\ {}_0^C D_t^\alpha I(t) = 0,\ {}_0^C D_t^\alpha R(t) = 0.$$

4.1 Disease-free Equilibrium Point

The disease-free equilibrium point (i.e., $I = 0$) is $(S_{Eq}, I_{Eq}, R_{Eq}) = (0, 0, 0)$. We find matrix

$$A = \begin{bmatrix} \lambda - \mu_1 & \lambda & \lambda \\ 0 & -(r_2 + \mu_2) & 0 \\ 0 & r_2 & -\mu_3 \end{bmatrix}$$

and its eigenvalues are

$$\lambda_1 = \lambda - \mu_1,$$
$$\lambda_2 = -r_2 - \mu_2,$$
$$\lambda_3 = -\mu_3.$$

Hence, (S_{Eq}, I_{Eq}, R_{Eq}) is local asymptotically stable if $(\lambda - \mu_1) < 0$.

4.2 Endemic Equilibrium Point

The endemic equilibrium point $(S_{Eq}, I_{Eq}, R_{Eq}) = (S_\star, I_\star, R_\star)$, which is characterized by the existence of infected nodes, i.e., $I \neq 0$ is given as

$$S_\star = \frac{r_2 + \mu_2}{r_1}, I_\star = \frac{\mu_3(\mu_1 - \lambda)(r_2 + \mu_2)}{r_1\left[(\lambda - r_2 - \mu_2) * \mu_3 - \lambda r_2\right]}, R_\star = \frac{r_2(\mu_1 - \lambda)(r_2 + \mu_2)}{r_1\left[(\lambda - r_2 - \mu_2) * \mu_3 - \lambda r_2\right]}.$$

We find matrix

$$A = \begin{bmatrix} \lambda - \mu_1 - \dfrac{\mu_3(r_2 + \mu_2)(\lambda - \mu_1)}{r_2 + \mu_3(r_2 + \mu_1 - \lambda)} & \lambda - r_2 - \mu_2 & \lambda \\ \dfrac{\mu_3(r_2 + \mu_2)(\lambda - \mu_1)}{r_2 + \mu_3(r_2 + \mu_1 - \lambda)} & 0 & 0 \\ 0 & r_2 & -\mu_3 \end{bmatrix}$$

and if real parts of its all eigenvalues of matrix A are negative, then (S_{Eq}, I_{Eq}, R_{Eq}) is local asymptotically stable.

5 Existence and Uniqueness of Stable Solution

Let $y_1(t) = S(t)$, $y_2(t) = I(t)$, and $y_3(t) = R(t)$, then

$$f_1(y_1(t), y_2(t), y_3(t)) = (\lambda - \mu_1)y_1(t) - (\lambda + r_1 y_1(t))y_2(t) - \lambda y_3(t),$$
$$f_2(y_1(t), y_2(t), y_3(t)) = r_1 y_1(t)y_2(t) - (r_2 + \mu_2)y_2(t),$$
$$f_3(y_1(t), y_2(t), y_3(t)) = r_2 y_2(t) - \mu_3 y_3(t).$$

Let $D = \{y_1, y_2, y_3 \in R : |y_i(t)| \leq a, t \in [0, \rho]\}$ and $|f_i(y_1(t), y_2(t), y_3(t))| \leq M_i$, $i = 1, 2, 3$. Each function f_1, f_2, and f_3 is continuous with respect to the three parameters y_1, y_2, and y_3. Then on D we have

$$\left|\frac{\partial}{\partial y_1} f_1(y_1, y_2, y_3)\right| \leq k_1, \quad \left|\frac{\partial}{\partial y_2} f_1(y_1, y_2, y_3)\right| \leq k_2, \quad \left|\frac{\partial}{\partial y_3} f_1(y_1, y_2, y_3)\right| \leq k_3,$$
$$\left|\frac{\partial}{\partial y_1} f_2(y_1, y_2, y_3)\right| \leq l_1, \quad \left|\frac{\partial}{\partial y_2} f_2(y_1, y_2, y_3)\right| \leq l_2, \quad \left|\frac{\partial}{\partial y_3} f_2(y_1, y_2, y_3)\right| \leq l_3,$$
$$\left|\frac{\partial}{\partial y_1} f_3(y_1, y_2, y_3)\right| \leq m_1, \quad \left|\frac{\partial}{\partial y_2} f_3(y_1, y_2, y_3)\right| \leq m_2, \quad \left|\frac{\partial}{\partial y_3} f_3(y_1, y_2, y_3)\right| \leq m_3,$$

where k_i, l_i, and m_i, $i = 1, 2, 3$ are positive constants.
Consider the following initial value problem which represents the proposed model (Eq. (3))

$$\begin{aligned} {}_0^C D_t^\alpha y_1(t) &= f_1(y_1(t), y_2(t), y_3(t)),\ t > 0,\ \text{and } y_1(0) = y_{10}, \\ {}_0^C D_t^\alpha y_2(t) &= f_2(y_1(t), y_2(t), y_3(t)),\ t > 0,\ \text{and } y_2(0) = y_{20}, \\ {}_0^C D_t^\alpha y_3(t) &= f_3(y_1(t), y_2(t), y_3(t)),\ t > 0,\ \text{and } y_3(0) = y_{30}. \end{aligned} \tag{5}$$

Definition 5.1 *By a solution of the system (Eq. (5)), we mean a column vector* $(y_1(t), y_2(t), y_3(t))^\tau$, y_1, y_2, *and* $y_3 \in C[0, T]$, $T < \infty$ *where* $C[0, T]$ *is the class of continuous functions defined on the interval* $[0, T]$ *and* τ *denote the transpose of the matrix, and*

$$F(Y(t)) = (f_1(y_1(t), y_2(t), y_3(t)), f_2(y_1(t), y_2(t), y_3(t)), f_3(y_1(t), y_2(t), y_3(t)))^\tau.$$

Now, applying Theorem 2.1 [28], we deduce that the considered system has a unique solution. Also, this solution is uniformly Lyapunov stable by Theorem 3.2 [28].

6 Solution using RPS Method

6.1 RPS Methodology

In this section, we apply the RPS method [21, 29, 30, 31, 32, 33] to solve the proposed model (Eq. (3)) using following steps

Step 1: The FPS for $S(t)$, $I(t)$, $R(t)$, and $N(t)$ about $t = 0$ can be written as

$$\left.\begin{aligned} S(t) &= \sum_{j=0}^{\infty} \frac{a_j t^{j\alpha}}{\Gamma(j\alpha + 1)}, \quad I(t) = \sum_{j=0}^{\infty} \frac{b_j t^{j\alpha}}{\Gamma(j\alpha + 1)}, \\ R(t) &= \sum_{j=0}^{\infty} \frac{c_j t^{j\alpha}}{\Gamma(j\alpha + 1)}, \quad N(t) = \sum_{j=0}^{\infty} \frac{d_j t^{j\alpha}}{\Gamma(j\alpha + 1)}, \end{aligned}\right\} 0 \le t < \rho. \tag{6}$$

The n^{th}-truncated series of $S(t)$, $I(t)$, $R(t)$, and $N(t)$ denoted by $S_n(t)$, $I_n(t)$, $R_n(t)$, and $N_n(t)$, respectively, are defined as

$$\left.\begin{aligned} S_n(t) &= \sum_{j=0}^{n} \frac{a_j t^{j\alpha}}{\Gamma(j\alpha + 1)}, \quad I_n(t) = \sum_{j=0}^{n} \frac{b_j t^{j\alpha}}{\Gamma(j\alpha + 1)}, \\ R_n(t) &= \sum_{j=0}^{n} \frac{c_j t^{j\alpha}}{\Gamma(j\alpha + 1)}, \quad N_n(t) = \sum_{j=0}^{n} \frac{d_j t^{j\alpha}}{\Gamma(j\alpha + 1)}, \end{aligned}\right\} 0 \le t < \rho. \tag{7}$$

For $n = 0$, from Eqs. (4) and (7), we obtain

$$\begin{aligned} S_0(t) &= a_0 = S_0(0) = S_0, \quad I_0(t) = b_0 = I_0(0) = I_0, \\ R_0(t) &= c_0 = R_0(0) = R_0, \quad N_0(t) = d_0 = N_0(0) = N_0. \end{aligned} \tag{8}$$

Now, from Eqs. (7) and (8) the n^{th}-truncated series of Eq. (7) can be defined as

$$\begin{aligned} S_n(t) &= a_0 + \sum_{j=1}^{n} \frac{a_j t^{j\alpha}}{\Gamma(j\alpha+1)}, \quad I_n(t) = b_0 + \sum_{j=1}^{n} \frac{b_j t^{j\alpha}}{\Gamma(j\alpha+1)}, \\ R_n(t) &= c_0 + \sum_{j=1}^{n} \frac{c_j t^{j\alpha}}{\Gamma(j\alpha+1)}, \quad N_n(t) = d_0 + \sum_{j=1}^{n} \frac{d_j t^{j\alpha}}{\Gamma(j\alpha+1)}. \end{aligned} \tag{9}$$

Step 2: Define the residual functions for model (Eq. (3)) as

$$\left.\begin{aligned} Res_S(t) &= {}_0^{\mathbf{C}}D_t^{\alpha} S(t) - \lambda N(t) + r_1 S(t) I(t) + \mu_1 S(t), \\ Res_I(t) &= {}_0^{\mathbf{C}}D_t^{\alpha} I(t) - r_1 S(t) I(t) + (r_2 + \mu_2) I(t), \\ Res_R(t) &= {}_0^{\mathbf{C}}D_t^{\alpha} R(t) - r_2 I(t) + \mu_3 R(t), \\ Res_N(t) &= {}_0^{\mathbf{C}}D_t^{\alpha} N(t) - \lambda N(t) + \mu_1 S(t) + \mu_2 I(t) + \mu_3 R(t). \end{aligned}\right\} \tag{10}$$

Hence, the n^{th}-residual functions of $S(t)$, $I(t)$, $R(t)$, and $N(t)$, respectively, are

$$\left.\begin{aligned} Res_{S_n}(t) &= {}_0^{\mathbf{C}}D_t^{\alpha} S_n(t) - \lambda N_n(t) + r_1 S_n(t) I_n(t) + \mu_1 S_n(t), \\ Res_{I_n}(t) &= {}_0^{\mathbf{C}}D_t^{\alpha} I_n(t) - r_1 S_n(t) I_n(t) + (r_2 + \mu_2) I_n(t), \\ Res_{R_n}(t) &= {}_0^{\mathbf{C}}D_t^{\alpha} R_n(t) - r_2 I_n(t) + \mu_3 R_n(t), \\ Res_{N_n}(t) &= {}_0^{\mathbf{C}}D_t^{\alpha} N_n(t) - \lambda N_n(t) + \mu_1 S_n(t) + \mu_2 I_n(t) + \mu_3 R_n(t). \end{aligned}\right\} \tag{11}$$

The residual function satisfies the properties, $Res_S(t) = Res_I(t) = Res_R(t) = Res_N(t) = 0,\ \forall t \geq 0$. Also,

$$\begin{aligned} \lim_{n\to\infty} Res_{S_n}(t) &= Res_S(t), \quad \lim_{n\to\infty} Res_{I_n}(t) = Res_I(t), \\ \lim_{n\to\infty} Res_{R_n}(t) &= Res_R(t), \quad \lim_{n\to\infty} Res_{N_n}(t) = Res_N(t). \end{aligned}$$

From [29], we have

$$\left.\begin{aligned} {}_0^{\mathbf{C}}D_t^{(j-1)\alpha} Res_S(0) &= {}_0^{\mathbf{C}}D_t^{(j-1)\alpha} Res_{S_i}(0), \\ {}_0^{\mathbf{C}}D_t^{(j-1)\alpha} Res_I(0) &= {}_0^{\mathbf{C}}D_t^{(j-1)\alpha} Res_{I_i}(0), \\ {}_0^{\mathbf{C}}D_t^{(j-1)\alpha} Res_R(0) &= {}_0^{\mathbf{C}}D_t^{(j-1)\alpha} Res_{R_i}(0), \\ {}_0^{\mathbf{C}}D_t^{(j-1)\alpha} Res_N(0) &= {}_0^{\mathbf{C}}D_t^{(j-1)\alpha} Res_{N_i}(0), \end{aligned}\right\} \ \forall j = 1, \ldots, n.$$

Step 3: To determine the coefficients a_j, b_j, c_j, and d_j for $j = 1, 2, 3, \ldots, n$, we substitute the n^{th}-truncated series of $S(t)$, $I(t)$, $R(t)$, and $N(t)$ in Eq. (11), and then use the Caputo fractional derivative operator $D_0^{(n-1)\alpha}$

on $Res_S(t)$, $Res_I(t)$, $Res_R(t)$, and $Res_N(t)$. It gives the equations

$$\left.\begin{array}{l} {}_0^{\mathbf{C}}D_t^{(n-1)\alpha} Res_S(0) = {}_0^{\mathbf{C}}D_t^{(n-1)\alpha} Res_{S_n}(0) = 0, \\ {}_0^{\mathbf{C}}D_t^{(n-1)\alpha} Res_I(0) = {}_0^{\mathbf{C}}D_t^{(n-1)\alpha} Res_{I_n}(0) = 0, \\ {}_0^{\mathbf{C}}D_t^{(n-1)\alpha} Res_R(0) = {}_0^{\mathbf{C}}D_t^{(n-1)\alpha} Res_{R_n}(0) = 0, \\ {}_0^{\mathbf{C}}D_t^{(n-1)\alpha} Res_N(0) = {}_0^{\mathbf{C}}D_t^{(n-1)\alpha} Res_{N_n}(0) = 0, \end{array}\right\} \forall n = 1, 2, 3, \ldots, . \quad (12)$$

Step 4: Now, the values of a_j, b_j, c_j, and d_j for $j = 1, 2, 3, \ldots, n$ are obtained using Eq. (12).

Step 5: The higher accuracy can be obtained by evaluating more coefficients in Eq. (9).

6.2 Convergence Analysis

This section discusses the convergence analysis of semi-analytical solutions obtained using the RPS method. Let us consider two FPS about $z = z_0$

$$r(z) = \sum_{j=0}^{\infty} l_i (z - z_0)^{j\alpha}, \; r_n(z) = \sum_{j=0}^{n} l_j (z - z_0)^{j\alpha}, \; z_0 \le z < (z_0 + \rho). \quad (13)$$

Theorem 6.1 *[27] If for $0 < P < 1$, $|r_{n+1}(z)| \le P|r_n(z)|$, $\forall n \in \mathbb{N}$ and $0 < z < \rho < 1$, then the solution of an FPS converges to an exact solution.*
Proof: *We have*

$$\begin{aligned} |r(z) - r_n(z)| &= \left| \sum_{j=n+1}^{\infty} r_j(z) \right| \\ &\le \sum_{j=n+1}^{\infty} |r_j(z)|, \quad \forall \; 0 < z < \rho < 1. \\ &\le |j_0| \left| \sum_{j=n+1}^{\infty} P^j \right| \\ &= \frac{P^{n+1}}{(1-P)} |j_0| \to 0 \; \text{as} \; n \to \infty. \end{aligned}$$

Theorem 6.2 *[27] The FPS $\sum_{j=0}^{\infty} l_j z^{j\alpha}$, $z \ge 0$ has a radius of convergence $\rho^{\frac{1}{\alpha}}$, if the classical power series expansion $\sum_{j=0}^{\infty} l_j z^i$, $-\infty < z < \infty$ has a radius of convergence ρ.*

6.3 Solution

The parameters and initial conditions of the model (Eq. (3)) are taken as $r_1 = 0.002$, $r_2 = 0.02$, $\lambda = 0.007$, $\mu_1 = 0.009$, $\mu_2 = 0.001$, $\mu_3 = 0.003$, $N_0 = 100$, $S_0 = 75$, $I_0 = 10$, and $R_0 = 15$.

For $n = 1$, from Eq. (7), we get

$$S_1(t) = a_0 + \frac{a_1 t^\alpha}{\Gamma(\alpha+1)}, \quad I_1(t) = b_0 + \frac{b_1 t^\alpha}{\Gamma(\alpha+1)},$$
$$R_1(t) = c_0 + \frac{c_1 t^\alpha}{\Gamma(\alpha+1)}, \quad N_1(t) = d_0 + \frac{d_1 t^\alpha}{\Gamma(\alpha+1)}.$$

Using Step (3), 1^{st}-residual functions of $S(t)$, $I(t)$, $R(t)$, and $N(t)$ are obtained as

$$Res_{S_1}(t) = {}_0^{\mathbf{C}}D_t^\alpha S_1(t) - 0.007N_1(t) + 0.002S_1(t)I_1(t) + 0.009S_1(t),$$
$$Res_{I_1}(t) = {}_0^{\mathbf{C}}D_t^\alpha I_1(t) - 0.002S_1(t)I_1(t) + 0.021I_1(t),$$
$$Res_{R_1}(t) = {}_0^{\mathbf{C}}D_t^\alpha R_1(t) - 0.02I_1(t) + 0.003R_1(t),$$
$$Res_{N_1}(t) = {}_0^{\mathbf{C}}D_t^\alpha N_1(t) - 0.007N_1(t) + 0.009S_1(t) + 0.001I_1(t) + 0.003R_1(t).$$

On substituting $S_1(t)$, $I_1(t)$, $R_1(t)$ and $N_1(t)$ into the previous expression and equating $Res_{S_1}(0)$, $Res_{I_1}(0)$, $Res_{R_1}(0)$, and $Res_{N_1}(0)$ to zero, the values of a_1, b_1, c_1, and d_1 are obtained as

$$a_1 = -0.1250,\ b_1 = -0.0600,\ c_1 = 0.1948,\ \text{and}\ d_1 = 0.0098.$$

Hence, $S_1(t)$, $I_1(t)$, $R_1(t)$, and $N_1(t)$ can be written as

$$S_1(t) = 75 - \frac{0.1250t^\alpha}{\Gamma(\alpha+1)},\ I_1(t) = 10 - \frac{0.0600t^\alpha}{\Gamma(\alpha+1)},$$
$$R_1(t) = 15 + \frac{0.1948t^\alpha}{\Gamma(\alpha+1)},\ N_1(t) = 100 + \frac{0.0098t^\alpha}{\Gamma(\alpha+1)}.$$

For $n = 2$, from Eq. (7), we get

$$S_2(t) = 75 - \frac{0.1250t^\alpha}{\Gamma(\alpha+1)} + \frac{a_2 t^{2\alpha}}{\Gamma(2\alpha+1)}, \quad I_2(t) = 10 - \frac{0.0600t^\alpha}{\Gamma(\alpha+1)} + \frac{b_2 t^{2\alpha}}{\Gamma(2\alpha+1)},$$
$$R_2(t) = 15 + \frac{0.1948t^\alpha}{\Gamma(\alpha+1)} + \frac{c_2 t^{2\alpha}}{\Gamma(2\alpha+1)}, \quad N_2(t) = 100 + \frac{0.0098t^\alpha}{\Gamma(\alpha+1)} + \frac{d_2 t^{2\alpha}}{\Gamma(2\alpha+1)}.$$

Now, from Eqs. (11) and (12), we obtain

$$a_2 = 0.0023,\ b_2 = 0.0001,\ c_2 = -0.0013,\ \text{and}\ d_2 = 0.0012.$$

Thus, $S_2(t)$, $I_2(t)$, $R_2(t)$, and $N_2(t)$ can be written as

$$S_2(t) = 75 - \frac{0.1250t^\alpha}{\Gamma(\alpha+1)} + \frac{0.0023t^{2\alpha}}{\Gamma(2\alpha+1)}, \quad I_2(t) = 10 - \frac{0.0600t^\alpha}{\Gamma(\alpha+1)} + \frac{0.0001t^{2\alpha}}{\Gamma(2\alpha+1)},$$
$$R_2(t) = 15 + \frac{0.1948t^\alpha}{\Gamma(\alpha+1)} - \frac{0.0013t^{2\alpha}}{\Gamma(2\alpha+1)}, \quad N_2(t) = 100 + \frac{0.0098t^\alpha}{\Gamma(\alpha+1)} + \frac{0.0012t^{2\alpha}}{\Gamma(2\alpha+1)}.$$

The rest coefficients of Eq. (9) can be obtained using the following recurrence relations

$$\left.\begin{aligned} a_{j+1} &= \lambda d_j - r_1 \sum_{r=0}^{j} \frac{a_r b_{j-r} \Gamma(j\alpha+1)}{\Gamma(r\alpha+1)\Gamma((j-r)\alpha+1)} - \mu_1 a_j, \\ b_{j+1} &= r_1 \sum_{r=0}^{j} \frac{a_r b_{j-r} \Gamma(j\alpha+1)}{\Gamma(r\alpha+1)\Gamma((j-r)\alpha+1)} - (r_2+\mu_2) b_j, \\ c_{j+1} &= r_2 b_j - \mu_3 c_j,\ d_{j+1} = \lambda d_j - \mu_1 a_j - \mu_2 b_j - \mu_3 c_j, \end{aligned}\right\} \forall j = 1, 2 \ldots, n. \quad (14)$$

7 Results and Discussion

To show the convergence of the method (From Eqs. (6), (7) and (13)), values of $|S(t) - S_n(t)|$, $|I(t) - I_n(t)|$, $|R(t) - R_n(t)|$, and $|N(t) - N_n(t)|$ at $t = 0.99$ with respect to n are plotted in Figs. 2a to 2d for different values of $\alpha = 1.0, 0.99, 0.95, 0.9$, and 0.85. It is observed that maximum absolute error $\mathcal{O}(10^{-45})$ is obtained for $n = 20$. For $n = 10$, the maximum absolute errors is $\mathcal{O}(10^{-20})$. In subsequent calculations, we use $n = 10$, as it gives sufficient accuracy.

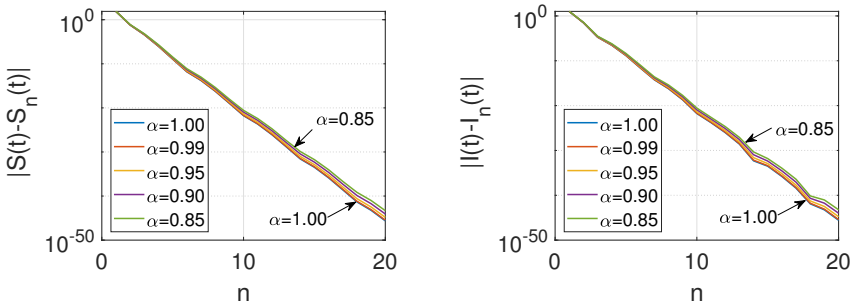

(a) $|S(t) - S_{n(t)}|$ vs n (b) $|I(t) - I_{n(t)}|$ vs n

(c) $|R(t) - R_{n(t)}|$ vs n (d) $|N(t) - N_{n(t)}|$ vs n

Figure 2: Convergence analysis of the RPS approach at $t = 0.99$ for distinct fractional orders $\alpha \in (0, 1]$.

For $\alpha = 1$ and $n = 10$, the absolute errors between RK and RPS methods in $S(t)$, $I(t)$, $R(t)$, and $N(t)$ are denoted by $Abs_S(t)$, $Abs_I(t)$, $Abs_R(t)$, and $Abs_N(t)$, respectively, which are defined as

$$\left.\begin{array}{ll} Abs_S(t) = |S(t)_{RK} - S(t)_{RPS}|, & Abs_I(t) = |I(t)_{RK} - I(t)_{RPS}|, \\ Abs_R(t) = |R(t)_{RK} - R(t)_{RPS}|, & Abs_N(t) = |N(t)_{RK} - N(t)_{RPS}|, \end{array}\right\} t \geq 0. \tag{15}$$

For fractional order $\alpha = 1$ and $n = 10$, comparison between the RK and RPS solutions in $S(t)$, $I(t)$, $R(t)$, and $N(t)$ are shown in Table I. Further, the absolute errors in $S(t)$, $I(t)$, $R(t)$, and $N(t)$ using the RPS and RK methods for $\alpha = 1$ are depicted in Figs. 3a to 3d. Here, maximum absolute errors in $S(t)$, $I(t)$, $R(t)$, and $N(t)$ are $\mathcal{O}(10^{-13})$ for $t \in (0, 1]$.

Table I and Figs. 3a to 3d show that the RPS method gives accurate and reliable results for a minimal computational coefficients.

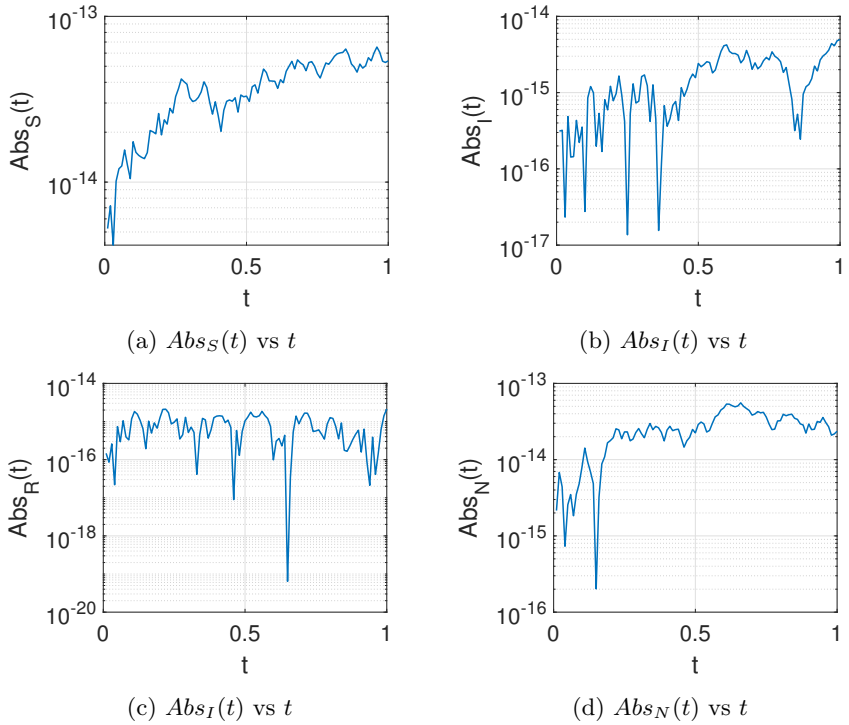

(a) $Abs_S(t)$ vs t

(b) $Abs_I(t)$ vs t

(c) $Abs_I(t)$ vs t

(d) $Abs_N(t)$ vs t

Figure 3: Absolute error of $S(t)$, $I(t)$, $R(t)$, and $N(t)$ using RK and RPS methods, respectively, for $\alpha = 1$ and $n = 10$.

Table I: The values of $S(t)$, $I(t)$, $R(t)$, and $N(t)$ using RK and RPS methods for $\alpha = 1$ (upto 3 decimal places).

	RK method				RPS method			
t	$S(t)$	$I(t)$	$R(t)$	$N(t)$	$S(t)$	$I(t)$	$R(t)$	$N(t)$
0	75.0	10.0	15.0	100.0	75.0	10.0	15.0	100.0
0.1	74.988	9.994	15.019	100.001	74.988	9.994	15.019	100.001
0.2	74.975	9.988	15.039	100.002	74.975	9.988	15.039	100.002
0.3	74.963	9.982	15.058	100.003	74.963	9.982	15.058	100.003
0.4	74.950	9.976	15.078	100.004	74.950	9.976	15.078	100.004
0.5	74.938	9.970	15.097	100.005	74.938	9.970	15.097	100.005
0.6	74.925	9.964	15.117	100.006	74.925	9.964	15.117	100.006
0.7	74.913	9.958	15.136	100.007	74.913	9.958	15.136	100.007
0.8	74.901	9.952	15.155	100.008	74.901	9.952	15.155	100.008
0.9	74.888	9.946	15.175	100.009	74.888	9.946	15.175	100.009
1.0	74.876	9.940	15.194	100.010	74.876	9.940	15.194	100.010

Table II: The values of $S(t)$, $I(t)$, $R(t)$, and $N(t)$ via RPS method (upto 3 decimal places).

	RPS ($\alpha = 0.80$)				RPS ($\alpha = 0.70$)			
t	$S(t)$	$I(t)$	$R(t)$	$N(t)$	$S(t)$	$I(t)$	$R(t)$	$N(t)$
0	75.0	10.0	15.0	100.0	75.0	10.0	15.0	100.0
0.1	74.979	9.990	15.033	100.001	74.973	9.987	15.043	100.002
0.2	74.963	9.982	15.058	100.003	74.956	9.979	15.069	100.004
0.3	74.949	9.975	15.080	100.004	74.941	9.972	15.092	100.005
0.4	74.936	9.969	15.100	100.005	74.928	9.965	15.112	100.006
0.5	74.923	9.963	15.120	100.006	74.916	9.959	15.132	100.007
0.6	74.912	9.957	15.138	100.007	74.905	9.954	15.149	100.008
0.7	74.900	9.952	15.157	100.008	74.894	9.949	15.166	100.009
0.8	74.889	9.946	15.174	100.009	74.884	9.944	15.182	100.010
0.9	74.878	9.941	15.191	100.010	74.874	9.939	15.198	100.011
1.0	74.867	9.936	15.208	100.011	74.864	9.934	15.213	100.012

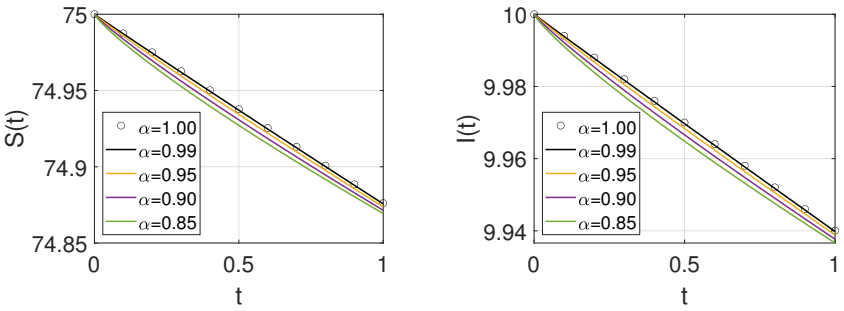

(a) $S(t)$ vs t (b) $I(t)$ vs t

(c) $R(t)$ vs t (d) $N(t)$ vs t

Figure 4: The semi-analytical solutions of $S(t)$, $I(t)$, $R(t)$, $N(t)$ for distinct fractional orders $\alpha \in (0, 1]$ and $n = 10$.

The RPS solution of $S(t)$, $I(t)$, $R(t)$, and $N(t)$ for $\alpha = 0.80$ and 0.70 are

listed in Table II. The behavior of $S(t)$, $I(t)$, $R(t)$, and $N(t)$ for distinct fractional order $\alpha \in (0, 1]$ is depicted in Figs. 4a to 4d, respectively. These figures show that the number of susceptible and infected individuals decreases with a decrease in α. At the same time, an increase in the recovered and total population is observed with a decrease in α.

8 Conclusion

In this paper, we have developed the SIR model (Eq. (3)) with vital dynamics and variable population sizes for integer and fractional orders. Further, we have discussed the existence and uniqueness of the solutions for the stable model. After that, the semi-analytical solutions for the proposed model are obtained by the RPS approach. For $\alpha = 1$, we have compared the results obtained by RPS and the RK methods. The convergence analysis of the RPS technique is also discussed. It is also observed that with the decline in fractional order (α), the numbers of susceptible and infected decrease, while the numbers of recovered personnel and the total population increase. Numerical simulation and graphs show that the fractional SIR epidemic model with vital dynamics and variable population size gives a better understanding and produces outstanding results than an integer SIR epidemic model without vital dynamics and varying population size. The results indicate that the RPS technique can be used as an alternative method for solving linear and nonlinear differential equations of any arbitrary order. This study may be helpful for medical experts in controlling the infection during the disease.

Acknowledgements

The Junior Research Fellowship (JRF) provided by the Council of Scientific & Industrial Research (CSIR), New Delhi, India, via file no: $09/1007(0011)/2021-EMR-I$ during the study of present work is acknowledged by the first author.

References

[1] S. Dubey, V. P. Dubey, J. Singh, A. M. Alshehri, D. Kumar, Computational study of a local fractional Tricomi equation occurring in fractal transonic flow, *J. Comput. Nonlinear Dyn.* 17 (8) (2022) 081006.

[2] V. P. Dubey, D. Kumar, H. M. Alshehri, J. Singh, D. Baleanu, Generalized invexity and duality in multiobjective variational problems involving nonsingular fractional derivative, *Open Phys.* 20 (1) (2022) 939–962.

[3] Akshey, T. R. Singh, A robust iterative approach for space-time fractional multidimensional telegraph equation, *Int. J. Appl. Comput.* 9 (5) (2023) 84.

[4] I. Podlubny, A. Chechkin, T. Skovranek, Y. Chen, B. M. V. Jara, Matrix approach to discrete fractional calculus II: partial fractional differential equations, *J. Comput. Phys.* 228 (8) (2009) 3137–3153.

[5] V. P. Dubey, J. Singh, S. Dubey, D. Kumar, Some integral transform results for Hilfer–Prabhakar fractional derivative and analysis of free-electron laser equation, *Iranian J. Sci.* 47 (4) (2023) 1333–1342.

[6] V. P. Dubey, J. Singh, S. Dubey, D. Kumar, Analysis of cauchy problems and diffusion equations associated with the Hilfer–Prabhakar fractional derivative via Kharrat–Toma transform, *Fractal fract.* 7 (5) (2023) 413.

[7] D. Kumar, V. P. Dubey, S. Dubey, J. Singh, A. M. Alshehri, Computational analysis of local fractional partial differential equations in realm of fractal calculus, *Chaos Solit. Fractals* 167 (2023) 113009.

[8] V. P. Dubey, D. Kumar, S. Dubey, A modified computational scheme and convergence analysis for fractional order hepatitis E virus model, in: *Advanced Numerical Methods for Differential Equations*, CRC Press, 2021, pp. 279–312.

[9] V. P. Dubey, J. Singh, A. M. Alshehri, S. Dubey, D. Kumar, Forecasting the behavior of fractional order Bloch equations appearing in NMR flow via a hybrid computational technique, *Chaos Solit. Fractals* 164 (2022) 112691.

[10] V. P. Dubey, J. Singh, A. M. Alshehri, S. Dubey, D. Kumar, Numerical investigation of fractional model of phytoplankton–toxic phytoplankton–zooplankton system with convergence analysis, *Int. J. Biomath.* 15 (04) (2022) 2250006.

[11] H. W. Hethcote, P. van den Driessche, An SIS epidemic model with variable population size and a delay, *J. Math. Biol.* 34 (1995) 177–194.

[12] A. S. Ackleh, L. J. Allen, Competitive exclusion and coexistence for pathogens in an epidemic model with variable population size, *J. Math. Biol.* 47 (2003) 153–168.

[13] G. Zaman, Y. H. Kang, I. H. Jung, Stability analysis and optimal vaccination of an SIR epidemic model, *BioSystems* 93 (3) (2008) 240–249.

[14] H. El-Saka, The fractional-order SIR and SIRS epidemic models with variable population size, *Math. Sci. Lett.* 2 (3) (2013) 195.

[15] E. A. Bakare, A. Nwagwo, E. Danso-Addo, Optimal control analysis of an SIR epidemic model with constant recruitment, *Int. J. Appl. Math. Research* 3 (3) (2014) 273.

[16] M. Hassouna, A. Ouhadan, E. El Kinani, On the solution of fractional order SIS epidemic model, *Chaos Solit. Fractals* 117 (2018) 168–174.

[17] A. Taghvaei, T. T. Georgiou, L. Norton, A. Tannenbaum, Fractional SIR epidemiological models, *Sci. Reports* 10 (1) (2020) 20882.

[18] K. Kozioł, R. Stanisławski, G. Bialic, Fractional-order SIR epidemic model for transmission prediction of covid-19 disease, *Appl. Sci.* 10 (23) (2020) 8316.

[19] Y. Chen, F. Liu, Q. Yu, T. Li, Review of fractional epidemic models, *Appl. Math. Model.* 97 (2021) 281–307.

[20] C. Balzotti, M. D'Ovidio, A. C. Lai, P. Loreti, Effects of fractional derivatives with different orders in SIS epidemic models, *Computation* 9 (8) (2021) 89.

[21] R. K. Meena, S. Kumar, Solution of fractional order SIR epidemic model using residual power series method, *Palest. J. Math.* 11 (2022).

[22] R. K. Meena, S. Kumar, A study on fractional SIS epidemic model using RPS method, in: *International Conference on Mathematics and Computing*, Springer, 2023, pp. 293–309.

[23] M. R. Sidi Ammi, M. Tahiri, M. Tilioua, A. Zeb, I. Khan, M. Andualem, Global analysis of a time fractional order spatio-temporal SIR model, *Sci. Rep.* 12 (1) (2022) 5751.

[24] M. Sadki, S. Harroudi, K. Allali, Fractional-order SIR epidemic model with treatment cure rate, *Partial Differ. Equ. Appl. Math.* 8 (2023) 100593.

[25] I. Podlubny, Fractional differential equations: an introduction to fractional derivatives, fractional differential equations, to methods of their solution and some of their applications, Elsevier, (1998).

[26] A. A. Kilbas, H. M. Srivastava, J. J. Trujillo, Theory and applications of fractional differential equations, Vol. 204, Elsevier, 2006.

[27] A. El-Ajou, O. A. Arqub, Z. A. Zhour, S. Momani, New results on fractional power series: theories and applications, *Entropy* 15 (12) (2013) 5305–5323.

[28] A. M. El-Sayed, On the existence and stability of positive solution for a nonlinear fractional-order differential equation and some applications, *Alex. J. Math.* 1 (1) (2010) 1–10.

[29] A. El-Ajou, O. A. Arqub, M. Al-Smadi, A general form of the generalized Taylor's formula with some applications, *Appl. Math. Comput.* 256 (2015) 851–859.

[30] K. Moaddy, M. Al-Smadi, I. Hashim, A novel representation of the exact solution for differential algebraic equations system using residual power-series method, *Discrete Dyn. Nat. Soc.* 2015 (2015).

[31] L. Wang, X. Chen, Approximate analytical solutions of time fractional Whitham–Broer–Kaup equations by a residual power series method, *Entropy* 17 (9) (2015) 6519–6533.

[32] R. Abu-Gdairi, M. Al-Smadi, G. Gumah, An expansion iterative technique for handling fractional differential equations using fractional power series scheme, *J. Math. Stat.* 11 (2) (2015) 29.

[33] I. Komashynska, M. Al-Smadi, A. Al-Habahbeh, A. Ateiwi, Analytical approximate solutions of systems of multi-pantograph delay differential equations using residual power-series method, arXiv preprint arXiv:1611.05485 (2016).

A novel computational analysis of diabetes model with Caputo-Katugampola memory

Jagdev Singh[1,2,*] and Rashmi Agrawal[1]

[1]Department of Mathematics, JECRC University, Jaipur 303905, Rajasthan, India, Email: jagdevsinghrathore@gmail.com
[2]Department of Computer Science and Mathematics, Lebanese American University, Beirut, Lebanon

Abstract

In this study, we have investigated a diabetes model and its complication using the Katugampola fractional derivative in Caputo sense. We studied a deterministic mathematical model that uses non integer derivatives to precisely depict the dynamics of diabetes mellitus. We have employed q-homotopy analysis generalized transform method (q-HAGTM) to find analytical approximate solution for presented model. Furthermore, the fixed-point theorem is employed to present the existence as well as uniqueness analysis of obtained solution for the discussed model. The obtained results are further complemented by conducting numerical simulations, providing graphical demonstrations that support and illustrate the findings. This approach enables us to understand and develop efficient ways to cure these diseases.

Keywords: Diabetes model; Caputo-Katugampola fractional derivative; Generalized Laplace transform

1 Introduction

Diabetes is a rapidly growing global concern, with its occurrence and prevalence on the rise worldwide. This chronic condition imposes a substantial burden not only on individuals but also on society as a whole due to the numerous complications associated with the disease. It is a chronic metabolic disorder characterized by high levels of glucose in the blood. It occurs when the body either does not produce enough insulin or cannot effectively use the insulin it produces. There are mainly 2 types of diabetes, Type 1 diabetes, often referred to as insulin-dependent diabetes mellitus (IDDM), typically manifests in individuals below the age of 40, although it can occur at any age. It accounts for approximately 10 to 15 percent of the diabetic population. Type 1 diabetes is characterized by an autoimmune response in which the body's immune system

mistakenly attacks and destroys the insulin-producing cells in the pancreas. As a result, people with Type 1 diabetes require lifelong insulin treatment to regulate their blood sugar levels. Type 2 diabetes, previously known as non-insulin-dependent diabetes mellitus (NIDDM), is the most common form of diabetes, accounting for approximately 85 to 90 percent of all cases. In this the body either does not produce enough insulin or becomes resistant to its effects, leading to elevated blood sugar levels. Prolonged hyperglycemia (having blood glucose concentration higher than 70-180 mg/dl), can result in long-term complications, such as neuropathy, retinopathy, and cardiovascular and heart diseases and pose significant risks to individuals and impact their quality of life and overall health [30, 24, 1]. In 2003, around 194 million people had diabetes, making up over 3% (5.1% for ages 20 to 79) of the global population. The prevalence of diabetes is on the rise, and it is projected to reach approximately 333 million people (6.3%) by 2025 [5]. Researchers have produced a multitude of studies aimed at developing mathematical models for predicting the proliferation of diabetes and issues coherent with it, such as Pandit et al. [20], Makroglou et al. [17], Patil et al. [21] and others. Numerous scientists and mathematicians have empirically validated the usefulness of fractional extensions of integer-order mathematical models in systematically representing natural phenomena, exemplified by methodologies such as the Caputo approach, which adeptly captures and represents the inherent characteristics of real-world processes [28, 10]. Singh et al. [26] presented analysis of fractional diabetes model with exponential law using Caputo–Fabrizio fractional derivative. Miller and Ross [18], Podlubny [22] authored their work namely "An introduction to the fractional calculus and fractional differential equations" and "fractional differential equation" respectively in which they focused on derivatives and integrals of fractional order and highlighted the evolution of fractional calculus and its application in modelling physical problems. In this paper we have used Katugampola fractional derivative in Caputo sense to formulate fractional diabetes model including its inherent complication factors such as its occurrence, spreading, healing and natural mortality rate. The Caputo derivative [6] and the Riemann-Liouville derivative [9] are two often used fractional derivatives. A novel fractional order derivative, introduced by Katugampola [14, 13], provides a generalized fractional derivative encompassing both the Riemann-Liouville and Hadamard fractional integrals and derivatives. Lately, Katugampola fractional derivative in Caputo sense has been used due to its ability to capture both local differentiation and integration properties and provides framework for handling systems with fractional exponents, which makes it well-suited for modeling and analyzing systems with fractional dynamics. Almeida et al. in [4] introduced a fractional operator of new kind, namely Katugampola derivative in Caputo type with special cases being the Caputo and the Caputo–Hadamard fractional derivatives. In this article, the diabetes model is developed with the main goal of examining the diabetes model using a novel non integer order derivative and to studying the specifications regarding the existence and uniqueness of the diabetes model's solution. In this work, we study the fractional diabetes model by applying the q-HAGTM. The q-HAGTM [25], which is related to fractional order diabetes modeling is used to find approximate analytical solution. The generalized Laplace transform (GLT) [12] and the q-homotopy analysis method (q-HAM) [7, 8] are combined in the utilized methodology to produce an effective result. An advancement of HAM is called q-HAM, which is a more gener-

alized approach than HAM [15, 16], has been established the search for more elegant methods to enlarge the convergence region. The q-homotopy analysis method has been exploited by the authors and used to interpret non-linear arbitrary PDEs [3, 2, 23]. By Singh et al [27], the q-HATM methodology was presented. In this, unlike prior approaches no discretization, linearization, or perturbation is required. The q-HAGTM employs two convergence parameters denoted as n and $\hbar$ which allows greater flexibility in modifying and regulating the convergence rate and region of convergence for the series solutions. The studied method is novel in sense that it yields a simple optimal solution, a significant region of convergence, and a non-local effect in the attained solution. Hence, In presented work we have utilized the novel Katumgampola based fractional derivative model to simulate spread of diabetes in human populus while also presenting the effect of external factors on it's occurrence, spreading, healing and natural mortality rate. This article is presented in following order- we introduce the definitions of Caputo derivative, Caputo-Katugampola fractional derivative, generalized Laplace transform,Katugampola integral opreator in Section 2. In Section 3, fundamental procedure of the implemented analytical technique that is q-HAGTM is given. Description of discussed model is presented in mathematical form in Section 4. In Section-5, we have obtained analytical solution to fractional order diabetes model and its complication by using q-HAGTM. In Section 6, the fixed-point theory is used to investigate the existence and uniqueness of the system's solutions. Numerical simulation with graphical representation is shown in Section 7. Finally, the conclusion of this research article is presented in Section 8.

2 Mathematical preliminaries

Definition 1: The fractional order (ρ) Caputo derivative [6] is described as follows,

$$ {}_{a}^{C}D_{\tau}^{\rho}\xi(\tau) = \frac{1}{\Gamma(l-\rho)}\int_{a}^{\tau}\frac{\xi^{(l)}(v)\,dv}{(\tau-v)^{\rho+1-l}}, \quad (l-1<\rho\leq l),\ l\in\mathbb{N}. \tag{1} $$

Definition 2: The Katugampola fractional derivative (KFD) [14, 13] in Caputo kind of order $0<\rho\leq 1$ of the function $\xi(\tau)$ can be given as

$$ {}_{a}^{kc}D_{\tau}^{\rho,\eta}\xi(\tau) = \frac{1}{\Gamma(1-\rho)}\int_{a}^{\tau}\left(\frac{\tau^{\eta}-v^{\eta}}{\eta}\right)^{-\rho}\zeta\frac{\xi(v)}{v^{1-\eta}}dv, \tag{2} $$

where the differential operator ζ is defined by $\zeta = \tau^{1-\eta}\frac{d}{d\tau}$. If we consider $\eta = 1$, the fractional derivative (FD) in Eq. (2) becomes the Caputo fractional derivative with order ρ . If η approaches 0, then the FD of Eq. (2) results into Caputo-Hadamard FD of order ρ.

Definition 3: Let $\xi, m : [a,\infty) \to R$ be real valued function s.t. $m(\tau)$ is continuous and $m'(\tau) > 0$ on $[a,\infty)$. Now, if the GLT [12] of $\xi(\tau)$ exists, then

$$ L_m\{\xi(\tau)\}(s) = \int_{a}^{\infty} e^{-s(m(\tau)-m(a))}\xi(\tau)\,m'(\tau)\,d\tau, \tag{3} $$

$'s'$ being the GLT parameter.

Note that if we set $a = 0$ and $m(\tau)=\tau$ in Eq. (3), then GLT transforms into the classical Laplace transform (LT) but if we set $m(\tau) = \frac{\tau^\eta}{\eta}$ and $a = 0$, then GLT reduces to η−LT [11]. This inclusive study is represented as the GLT with $m(\tau) = \frac{\tau^\eta}{\eta}$ with $a = 0$ by $\frac{\tau^\eta}{\eta}$−LT. Henceforth, the $\frac{\tau^\eta}{\eta}$- LT is described as

$$L_{\frac{\tau^\eta}{\eta}}\{\xi(\tau)\}(s) = \int_a^\infty e^{-s\frac{\tau^\eta}{\eta}}\xi(\tau)\frac{d\tau}{\tau^{1-\eta}}. \tag{4}$$

The $\frac{\tau^\eta}{\eta}$−LT of the KFD in Caputo kind [11, 29] can be stated as follows

$$L_{\frac{\tau^\eta}{\eta}}\left\{\left(\frac{\tau^\eta}{\eta}\right)^\rho\right\}(s) = \frac{\Gamma(1+\rho)}{s^{1+\rho}},$$

$$L_{\frac{\tau^\eta}{\eta}}\left\{\left(kc D_\tau^{\rho,\eta}\xi(\tau)\right)\right\}(s) = s^\rho L_{\frac{\tau^\eta}{\eta}}\xi(\tau)(s) - s^{\rho-1}\xi(0). \tag{5}$$

Definition 4: The Katugampola integral operator [14] of fractional order ρ is defined as

$$({}_a+I^{\rho,\eta}\xi)(\tau) = \frac{\eta^{1-\rho}}{\Gamma(\rho)}\int_a^\tau \frac{v^{\eta-1}}{(\tau^\eta - v^\eta)^{1-\rho}}\xi(v)dv. \tag{6}$$

3 Fundamental plan of *q*-homotopy analysis generalized transform method (*q*-HAGTM)

Principal scheme of proposed method is discussed by studying a nonlinear differential equation associated to the Katugampola derivative. It can be stated as follows

$$kc D_\tau^{\rho,\eta}\xi(\tau) + M\xi(\tau) + Q\xi(\tau) = f(\tau), \qquad l-1 < \rho \le l, \tag{7}$$

here $\xi(\tau)$ is a function in time τ and $kc D_\tau^{\rho,\eta}$ represents the Caputo-Katugamopla derivative of order ρ, R denotes the linear bounded operator, Q denotes common nonlinear differential operator,which is Lipschitz continuous and $f(\tau)$ stands for source term. Apply GLT operator on Eq. (7), we have

$$L_{\frac{\tau^\eta}{\eta}}\left[kc D_\tau^{\rho,\eta}\xi(t)\right] + L_{\frac{\tau^\eta}{\eta}}\left[M\xi(\tau) + Q\xi(\tau)\right] = L_{\frac{\tau^\eta}{\eta}}[f(\tau)]. \tag{8}$$

On using the GLT of Caputo-Katugampola fractional derivative, we have

$$s^\rho L_{\frac{\tau^\eta}{\eta}}\left[\xi(\tau)\right](s) - s^{\rho-1}\xi(0) + L_{\frac{\tau^\eta}{\eta}}\left[M\xi(\tau) + Q\xi(\tau)\right] - L_{\frac{\tau^\eta}{\eta}}[f(\tau)] = 0. \tag{9}$$

On refining the Eq. (9), we get

$$L_{\frac{\tau^\eta}{\eta}}\left[\xi(\tau)\right](s) - \frac{1}{s}\xi(0) + \frac{1}{s^\rho}\left[L_{\frac{\tau^\eta}{\eta}}\left[M\xi(\tau) + Q\xi(\tau)\right] - L_{\frac{\tau^\eta}{\eta}}[f(\tau)\right] = 0. \tag{10}$$

Now, we present a nonlinear operator which is given as follows

$$\begin{aligned} Q[\phi(\tau;q)] = L_{\frac{\tau^\eta}{\eta}}[\phi(\tau;q)] - \frac{1}{s}\phi(0;q)(0^+) \\ + \frac{1}{s^\rho}\left[L_{\frac{\tau^\eta}{\eta}}\left[M\phi(\tau;q) + Q\phi(\tau;q)\right] - L_{\frac{\tau^\eta}{\eta}}[f(\tau,q)\right]. \end{aligned} \tag{11}$$

Here $q \in \left[0, \frac{1}{n}\right]$ and $\phi(\tau; q)$ denotes a real valued function. Further, in subsequent approach, we set a homotopy

$$(1 - nq) L_{\frac{\tau^\eta}{\eta}} \left[\phi(\tau; q) - \xi_0(\tau)\right] = \hbar q Q[\phi(\tau; q)], \tag{12}$$

where $L_{\frac{\tau^\eta}{\eta}}$ indicates that the GLT operator, the auxiliary parameter $\hbar \neq 0$ and $\phi(\tau; q)$ is an unknown function, $\xi_0(\tau)$ is an initial approximation of $\xi(\tau)$. Furthermore, by substituting the embedding parameter values of $q = 0$ and $q = 1/n$, it gives

$$\phi(\tau; 0) = \xi_0(\tau) \qquad \phi\left(\tau; \frac{1}{n}\right) = \xi(\tau). \tag{13}$$

Therefore, when q progresses from 0 to $\frac{1}{n}$, $\phi(\tau; q)$ transforms from $\xi_0(\tau)$ to the solution $\xi(\tau)$. Expanding $\phi(\tau; q)$ into a series form by employing Taylor's theorem about parameter q, we get

$$\phi(\tau; q) = \xi_0(\tau) + \sum_{k=1}^{\infty} \xi_k(\tau) q^k, \tag{14}$$

where,

$$\xi_k(\tau) = \frac{1}{k!} \frac{\partial^k}{\partial q^k} \{\phi(\tau; q)\}\Big|_{q=0}. \tag{15}$$

If the initial condition $\xi_0(\tau)$, asymptotic parameter n and convergence control parameter $\hbar$ are expressed appropriately, then Eq. (15) converges at $q = \frac{1}{n}$, then, we obtain the subsequent equation

$$\xi(\tau) = \xi_0(\tau) + \sum_{k=1}^{\infty} n^{-k} \xi_k(\tau). \tag{16}$$

The solution given by Eq. (16) is a solution of discussed Eq. (7). Using Eq. (16) and Eq. (12). Solution of governing equation can be attained as

$$\xi_k(\tau) = \{\xi_0(\tau), \xi_1(\tau), \ldots \xi_k(\tau)\}. \tag{17}$$

On differentiating Eq. (12) k-times w.r.t q and then multiplying by $1/k!$ and substituting $q = 0$, we get

$$L_{\frac{\tau^\eta}{\eta}} \left[\xi_k(\tau) - \alpha_k \xi_{k-1}(\tau)\right] = \hbar[\Re_k(\xi_{k-1})]. \tag{18}$$

Employing the inverse GLT operator on Eq. (18), we attain the subsequent result

$$\xi_k(\tau) = \alpha_k \xi_{k-1}(\tau) + \hbar L^{-1}_{\frac{\tau^\eta}{\eta}}[\Re_k(\xi_{k-1})]. \tag{19}$$

Where α_k is defined as

$$\alpha_k = \begin{cases} 0, & \text{if } k \leq 1 \\ n, & k > 1 \end{cases} \tag{20}$$

and we represent the value of $\Re_k(\xi_{k-1})$ as follows

$$\Re_k(\xi_{k-1}) = L_{\frac{\tau^\eta}{\eta}} \left[\xi_{k-1}(\tau)\right] - \left(1 - \frac{\alpha_k}{n}\right)\left[s^{-1}\xi(0) + s^{-\rho} L_{\frac{\tau^\eta}{\eta}} f(\tau)\right] + s^{-\rho} L_{\frac{\tau^\eta}{\eta}} \left[R\xi_{k-1} + A_{k-1}\right]. \tag{21}$$

In Eq. (21) A_k exhibit the homotopy polynomial [19] and given as

$$A_k = \frac{1}{\Gamma k}\left[\frac{\partial^k}{\partial q^k} Q\phi(\tau;q)\right]_{q=0}, \tag{22}$$

and

$$\phi(\tau;q) = \phi_0 + q\phi_1 + q^2\phi_2 + \ldots. \tag{23}$$

On utilizing Eq. (21) in Eq. (19), we attain the subsequent equation

$$\xi_k(\tau) = (\alpha_k + \hbar)\,\xi_{k-1}(\tau) - \hbar\left(1 - \frac{\alpha_k}{n}\right) L^{-1}_{\frac{\tau^\eta}{\eta}}\left[s^{-1}\xi(0) + s^{-\rho} L_{\frac{\tau^\eta}{\eta}} f(\tau)\right] + \hbar L^{-1}_{\frac{\tau^\eta}{\eta}}\left[s^{-\rho} L_{\frac{\tau^\eta}{\eta}}\left[R\xi_{k-1} + A_{k-1}\right]\right]. \tag{24}$$

Hence, by utilizing Eq. (24), we can determine various components of $\xi_k(\tau)$ for $n \geq 1$ and q-HAGTM solution can be given by the following equation

$$\xi(\tau) = \sum_{k=0}^{\infty}\left(\frac{1}{n}\right)^k \xi_k(\tau). \tag{25}$$

4 Fractional diabetes mathematical model

The diabetes model in classical form, along with its complications [5] can be given as

$$\begin{aligned}\frac{dD}{d\tau} &= P - (\gamma + \varpi) D + C,\\ \frac{dC}{d\tau} &= P + \gamma D - (\eta + \varpi + \alpha + \beta) C.\end{aligned} \tag{26}$$

Here C indicates number of diabetics with complications. D denotes number of diabetics without complications at time τ. $N = N(\tau) = C(\tau) + D(\tau)$ represents size of population having diabetes at the time τ. The occurrence of diabetic mellitus is denoted by P. γ indicates probability of developing a complication. α shows rate at which patients with complications become severely disabled. β denotes the mortality rate due to complications. ϖ indicates the rate of natural mortality. η shows rate at which complications are cured.

$$\begin{aligned}\frac{dC}{d\tau} &= -(\gamma + \sigma) C + \gamma N,\\ \frac{dN}{d\tau} &= P - (\alpha + \beta) C - \varpi N.\end{aligned} \tag{27}$$

Where $\sigma = \eta + \varpi + \alpha + \beta$, with the initial condition

$$C(0) = C_0, N(0) = N_0. \tag{28}$$

As the classical order derivative does not attribute memory to the system, hence, in order to contain the whole memory of the system, we change the model (27) from integer order derivative to the Katugampola fractional derivative in the Caputo sense.

$$\begin{aligned}{}_{k}c D_\tau^{\rho,\eta} C(\tau) &= -(\gamma + \sigma) C + \gamma N,\\ {}_{k}c D_\tau^{\rho,\eta} N(\tau) &= P - (\alpha + \beta) C - \varpi N.\end{aligned} \tag{29}$$

5 q-HAGTM algorithm for fractional diabetes model and its complication

In this section, we solve the fractional order diabetes model and its complication Eq. (29) subjecting to the initial condition Eq. (28) by q-HAGTM, we get

$$L_{\frac{\tau^\eta}{\eta}}\left[{}_{kc}D_\tau^{\rho,\eta}C(\tau)\right](s) = L_{\frac{\tau^\eta}{\eta}}\left[-(\gamma+\sigma)C+\gamma N\right],$$

$$L_{\frac{\tau^\eta}{\eta}}\left[{}_{kc}D_\tau^{\rho,\eta}N(\tau)\right](s) = L_{\frac{\tau^\eta}{\eta}}\left[P-(\alpha+\beta)C-\varpi N\right]. \tag{30}$$

After employing the GLT formula for the Katugampola fractional derivative and further simplification, we get

$$s^\rho L_{\frac{\tau^\eta}{\eta}}\{C(\tau)\}(s) - s^{\rho-1}C(0) = L_{\frac{\tau^\eta}{\eta}}\left[-(\gamma+\sigma)C+\gamma N\right],$$

$$s^\rho L_{\frac{\tau^\eta}{\eta}}\{N(\tau)\}(s) - s^{\rho-1}N(0) = L_{\frac{\tau^\eta}{\eta}}\left[P-(\alpha+\beta)C-\varpi N\right]. \tag{31}$$

On simplification Eq. (31), we have

$$L_{\frac{\tau^\eta}{\eta}}\{C(\tau)\}(s) - \frac{C_0}{s} - \frac{1}{s^\rho}\left\{L_{\frac{\tau^\eta}{\eta}}\left[-(\gamma+\sigma)C+\gamma N\right]\right\},$$

$$L_{\frac{\tau^\eta}{\eta}}\{N(\tau)\}(s) - \frac{N_0}{s} - \frac{1}{s^\rho}\left\{L_{\frac{\tau^\eta}{\eta}}\left[P-(\alpha+\beta)C-\varpi N\right]\right\} = 0. \tag{32}$$

We present the non-linear operator given as follows

$$Q_1\{C,\tau;q\} = L_{\frac{\tau^\eta}{\eta}}\{C,\tau;q\}(s) - \frac{C_0}{s} - \frac{1}{s^\rho}\left\{L_{\frac{\tau^\eta}{\eta}}\left[-(\gamma+\sigma)\{C,\tau;q\}+\gamma\{N,\tau;q\}\right]\right\},$$

$$Q_2\{N,\tau;q\} = L_{\frac{\tau^\eta}{\eta}}\{N,\tau;q\}(s) - \frac{N_0}{s} - \frac{1}{s^\rho}\left\{L_{\frac{\tau^\eta}{\eta}}\left[P-(\alpha+\beta)\{C,\tau;q\}-\varpi\{N,\tau;q\}\right]\right\}. \tag{33}$$

The term of the k^{th} order deformation equation are as follows

$$L_{\frac{\tau^\eta}{\eta}}\{C_k(\tau)-\alpha_k C_{k-1}(\tau)\} = \hbar\Re_{1,k}(C_{k-1}(\tau)),$$

$$L_{\frac{\tau^\eta}{\eta}}\{N_k(\tau)-\alpha_k N_{k-1}(\tau)\} = \hbar\Re_{2,k}(N_{k-1}(\tau)). \tag{34}$$

Where

$$\Re_{1,k}(C_{k-1}) = L_{\frac{\tau^\eta}{\eta}}\{C_{k-1}\} - \left(1-\frac{\alpha_k}{n}\right)\left(\frac{C_0}{s}\right) - \frac{1}{s^\rho}\left\{L_{\frac{\tau^\eta}{\eta}}\left[-(\gamma+\sigma)C_{k-1}+\gamma N_{k-1}\right]\right\},$$

$$\Re_{2,k}(N_{k-1}) = L_{\frac{\tau^\eta}{\eta}}\{N_{k-1}\} - \left(1-\frac{\alpha_k}{n}\right)\left(\frac{N_0}{s}\right) - \frac{1}{s^\rho}\left\{L_{\frac{\tau^\eta}{\eta}}\left[P-(\alpha+\beta)C_{k-1}-\varpi N_{k-1}\right]\right\}. \tag{35}$$

By using the inverse GLT on Eq. (34), we get

$$C_k(\tau) = \alpha_k C_{k-1}(\tau) + \hbar L^{-1}_{\frac{\tau^\eta}{\eta}}\Re_{1,k}(C_{k-1}(\tau)),$$

$$N_k(\tau) = \alpha_k N_{k-1}(\tau) + \hbar L^{-1}_{\frac{\tau^\eta}{\eta}} \Re_{2,k}(N_{k-1}(\tau)). \tag{36}$$

Solution to the k^{th} order deformation equation is expressed by

$$C_k(\tau) = \alpha_k C_{k-1}(\tau) + \hbar L^{-1}_{\frac{\tau^\eta}{\eta}} \left\{ L_{\frac{\tau^\eta}{\eta}} \{C_{k-1}\} - \left(1 - \frac{\alpha_k}{n}\right)\left(\frac{C_0}{s}\right) - \frac{1}{s^\rho} \left\{ L_{\frac{\tau^\eta}{\eta}} \left[-(\gamma+\sigma) C_{k-1} + \gamma N_{k-1} \right] \right\} \right\},$$

$$N_k(\tau) = \alpha_k N_{k-1}(\tau) + \hbar L^{-1}_{\frac{\tau^\eta}{\eta}} \left\{ L_{\frac{\tau^\eta}{\eta}} \{N_{k-1}\} - \left(1 - \frac{\alpha_k}{n}\right)\left(\frac{N_0}{s}\right) - \frac{1}{s^\rho} \left\{ L_{\frac{\tau^\eta}{\eta}} \left[P - (\alpha+\beta) C_{k-1} - \varpi N_{k-1} \right] \right\} \right\}. \tag{37}$$

Putting $k = 1, 2\ldots$ in Eq. (37), we obtain

$$C_1(\tau) = \hbar \left[(\gamma+\sigma) C_0 - \gamma N_0 \right] \frac{1}{\Gamma(1+\rho)} \left(\frac{\tau^\eta}{\eta}\right)^\rho,$$

$$N_1(\tau) = \hbar \left[-P + (\alpha+\beta) C_0 + \varpi N_0 \right] \frac{1}{\Gamma(1+\rho)} \left(\frac{\tau^\eta}{\eta}\right)^\rho. \tag{38}$$

Similarly

$$C_2(\tau) = (n+\hbar) \{ \hbar (\gamma+\sigma) C_0 - \gamma N_0 \} \frac{1}{\Gamma(1+\rho)} \left(\frac{\tau^\eta}{\eta}\right)^\rho + \hbar^2 \left\{ \left[(\gamma+\sigma)^2 C_0 - \gamma(\gamma+\sigma) N_0 \right] - \gamma \left[-P + (\alpha+\beta) C_0 + \varpi N_0 \right] \right\} \frac{1}{\Gamma(1+2\rho)} \left(\frac{\tau^\eta}{\eta}\right)^{2\rho},$$

$$N_2(\tau) = (n+\hbar) \{ \hbar \left[-P + (\alpha+\beta) C_0 + \varpi N_0 \right] \} \frac{1}{\Gamma(1+\rho)} \left(\frac{\tau^\eta}{\eta}\right)^\rho - \hbar \{P\} \frac{1}{\Gamma(1+\rho)} \left(\frac{\tau^\eta}{\eta}\right)^\rho + \hbar^2 \{ (\alpha+\beta) \left[(\gamma+\sigma) C_0 - \gamma N_0 \right] + \mu \left[-P + (\alpha+\beta) C_0 + \varpi N_0 \right] \} \frac{1}{\Gamma(1+2\rho)} \left(\frac{\tau^\eta}{\eta}\right)^{2\rho}. \tag{39}$$

By following the same procedure remaining terms for $k \geq 2$ find the series solution of model. So, the solution of fractional order diabetes and its complication model Eq. (29) is given by

$$C_k(\tau) = C_0(\tau) + \frac{1}{n} C_1(\tau) + \left(\frac{1}{n}\right)^2 C_2(\tau) + \ldots,$$

$$N_k(\tau) = N_0(\tau) + \frac{1}{n} N_1(\tau) + \left(\frac{1}{n}\right)^2 N_2(\tau) + \ldots. \tag{40}$$

6 Analysis of existence and uniqueness of the obtained solution

Here, we investigate the existence of a solution for the fractional diabetic model through the fixed point assumption.

Now, using the Katugamola integral oprator given by Eq. (4) to the system (29), we obtain the subsequent integral equations

$$C(\tau) - C(0) = \frac{\eta^{1-\rho}}{\Gamma\rho} \int_0^\tau [-(\gamma+\sigma) C + \gamma N] \cdot v^{\eta-1}(\tau^\eta - v^\eta)^{\rho-1} dv,$$

$$N(\tau) - N(0) = \frac{\eta^{1-\rho}}{\Gamma\rho} \int_0^\tau [P - (\alpha+\beta) C - \varpi N] \cdot v^{\eta-1}(\tau^\eta - v^\eta)^{\rho-1} dv. \tag{41}$$

For ingenuity, we find out

$$K_1(\tau, C) = [-(\gamma+\sigma) C + \gamma N],$$

$$K_2(\tau, N) = [P - (\alpha+\beta) C - \varpi N]. \tag{42}$$

Theorem 1: The kernels K_i, $i = 1, 2$ satisfy the Lipschitz condition, when $0 \leq \Psi_1 < 1$, $i = 1, 2$.

Proof. Suppose $K_1(\tau, C) = [-(\gamma+\sigma) C + \gamma N]$, is the kernel and $C(\tau)$ and $C_1(\tau)$ be two functions, consequently we obtain the following

$$\|K_1(\tau, C) - K_1(\tau, C_1)\| = \left\|[-(\gamma+\sigma) C + \gamma N] - [-(\gamma+\sigma) C_1 + \gamma N]\right\|,$$

$$= \|-(\gamma+\sigma) \cdot (C(\tau) - C_1(\tau))\|$$

$$\leq -(\gamma+\sigma) \cdot \|(C(\tau) - C_1(\tau))\|$$

$$\leq \Psi_1 \|(C(\tau) - C_1(\tau))\|. \tag{43}$$

Now consider $\Psi_1 = -(\gamma+\sigma) < 1$, let $P_1 = max_{t\in R}\|C(\tau)\|$ and $P_2 = max_{t\in R}|N(\tau)\|$ are bounded function then, we find

$$\|K_1(\tau, C) - K_1(\tau, C_1)\| \leq \Psi_1 \|(C(\tau) - C_1(\tau))\|. \tag{44}$$

Obviously, which is Lipschitz condition for K_1. In addition if $0 \leq \Psi_1 < 1$. Then $C(\tau)$ has an upper bound.

In the same way, we can show that

$$\|K_2(\tau, N) - K_2(\tau, N_1)\| \leq \Psi_2 \|(N(\tau) - N_1(\tau))\|. \tag{45}$$

From Eq. (42) K_1 and K_2 are the kernels. Then the associate integrals are found

$$C(\tau) = C(0) + \frac{\eta^{1-\rho}}{\Gamma\rho} \int_0^\tau K_1(v, C) \cdot v^{\eta-1}(\tau^\eta - v^\eta)^{\rho-1} dv,$$

$$N(\tau) = N(0) + \frac{\eta^{1-\rho}}{\Gamma\rho} \int_0^\tau K_2(v, N) \cdot v^{\eta-1}(\tau^\eta - v^\eta)^{\rho-1} dv. \tag{46}$$

Further, we get

$$C_n(\tau) = C(0) + \frac{\eta^{1-\rho}}{\Gamma\rho} \int_0^\tau K_1(v, C_{n-1}) \cdot v^{\eta-1}(\tau^\eta - v^\eta)^{\rho-1} dv,$$

$$N_n(\tau) = N(0) + \frac{\eta^{1-\rho}}{\Gamma\rho}\int_0^\tau K_2(v, N_{n-1})\cdot v^{\eta-1}(\tau^\eta - v^\eta)^{\rho-1}dv. \tag{47}$$

Where the initial conditions are

$$C(0) = C_0 \quad and\ N(0) = N_0. \tag{48}$$

After subtracting consecutive terms, we have

$$\Xi_n = C_n(\tau) - C_{n-1}(\tau) = \frac{\eta^{1-\rho}}{\Gamma\rho}\int_0^\tau (K_1(v, C_{n-1}) - K_1(v, C_{n-2}))\times v^{\eta-1}(\tau^\eta - v^\eta)^{\rho-1}\,dv,$$

$$\Delta_n = N_n(\tau) - N_{n-1}(\tau) = \frac{\eta^{1-\rho}}{\Gamma\rho}\int_0^\tau (K_2(v, N_{n-1}) - K_2(v, N_{n-2}))\times v^{\eta-1}(\tau^\eta - v^\eta)^{\rho-1}\,dv. \tag{49}$$

Taking the below

$$C_n(\tau) = \sum_{j=1}^{n}\Xi_j(\tau),$$

$$N_n(\tau) = \sum_{j=1}^{n}\Delta_j(\tau). \tag{50}$$

Hence forth by applying the tri-angular and norm properties on equation of (49), we arrive at the following equation

$$\|\Xi_n\| = \|\,C_n(\tau) - C_{n-1}(\tau)\| \le \frac{\eta^{1-\rho}}{\Gamma\rho}\left\|\int_0^\tau (K_1(v, C_{n-1}) - K_1(v, C_{n-2}))\times v^{\eta-1}(\tau^\eta - v^\eta)^{\rho-1}\,dv\right\|,$$

$$\|\Delta_n\| = \|\,N_n(\tau) - N_{n-1}(\tau)\| \le \frac{\eta^{1-\rho}}{\Gamma\rho}\left\|\int_0^\tau (K_2(v, N_{n-1}) - K_2(v, N_{n-2}))\times v^{\eta-1}(\tau^\eta - v^\eta)^{\rho-1}\,dv\right\|. \tag{51}$$

While satisfying the Lipschitz conditions the kernels yield the following outcomes

$$\begin{aligned}\|\,C_n(\tau) - C_{n-1}(\tau)\| &\le \frac{\eta^{1-\rho}}{\Gamma\rho}\int_0^\tau \|(K_1(v, C_{n-1}) - K_1(v, C_{n-2}))\|\times v^{\eta-1}(\tau^\eta - v^\eta)^{\rho-1}\,dv\\ &\le \Psi_1\frac{\eta^{1-\rho}}{\Gamma\rho}\int_0^\tau \|C_{n-1} - C_{n-2}\|\times v^{\eta-1}(\tau^\eta - v^\eta)^{\rho-1}\,dv,\\ \|\,N_n(\tau) - N_{n-1}(\tau)\| &\le \frac{\eta^{1-\rho}}{\Gamma\rho}\int_0^\tau \|(K_2(v, N_{n-1}) - K_2(v, N_{n-2}))\|\times v^{\eta-1}(\tau^\eta - v^\eta)^{\rho-1}\,dv\\ &\le \Psi_2\frac{\eta^{1-\rho}}{\Gamma\rho}\int_0^\tau \|N_{n-1} - N_{n-2}\|\times v^{\eta-1}(\tau^\eta - v^\eta)^{\rho-1}\,dv.\end{aligned} \tag{52}$$

Therefore, we obtain the following

$$\|\Xi_n\| \le \Psi_1\frac{\eta^{1-\rho}}{\Gamma\rho}\int_0^\tau \|\Xi_{n-1}(\tau)\|\times v^{\eta-1}(\tau^\eta - v^\eta)^{\rho-1}\,dv,$$

$$\|\Delta_n\| \leq \Psi_2 \frac{\eta^{1-\rho}}{\Gamma\rho} \int_0^\tau \|\Delta_{n-1}(\tau)\| \times v^{\eta-1} (\tau^\eta - v^\eta)^{\rho-1} \, dv. \tag{53}$$

Theorem 2. The Katugampola fractional derivative non-integer order fractional diabetic model has unique solution provided that the following conditions are satisfied for τ_{max}.

$$\frac{\Psi_i}{\Gamma\rho + 1} \left(\frac{\tau^\eta{}_{max}}{\eta} \right)^\rho < 1, i = 1, 2. \tag{54}$$

Proof. Here, we assume that $C(\tau)$ and $N(\tau)$ are bounded functions and fulfills the Lipschitz condition, then using Eq. (53), and using recursive techniques, we have

$$\|\Xi_n\| \leq \|C_0\| \left[\frac{\Psi_1}{\Gamma\rho + 1} \left(\frac{\tau^\eta{}_{max}}{\eta} \right)^\rho \right]^n,$$

$$\|\Delta_n\| \leq \|N_0\| \left[\frac{\Psi_2}{\Gamma\rho + 1} \left(\frac{\tau^\eta{}_{max}}{\eta} \right)^\rho \right]^n. \tag{55}$$

All above functions exist and result in Eq. (55), therefore, we will show that these functions are the solutions to the diabetic model. Then, we have

$$C(\tau) - C(0) = C_n(\tau) - A_n(\tau),$$

$$N(\tau) - N(0) = N_n(\tau) - B_n(\tau). \tag{56}$$

Further, we calculate the following norms of $A_n(\tau)$

$$\begin{aligned} \|A_n(\tau)\| &\leq \frac{\eta^{1-\rho}}{\Gamma\rho} \left\| \int_0^\tau (K_1(v, C) - K_1(v, C_{n-1})) \times v^{\eta-1} (\tau^\eta - v^\eta)^{\rho-1} \, dv \right\| \\ &\leq \frac{\eta^{1-\rho}}{\Gamma\rho} \int_0^\tau \|(K_1(v, C) - K_1(v, C_{n-1}))\| \times v^{\eta-1} (\tau^\eta - v^\eta)^{\rho-1} \, dv \\ &\leq \Psi_1 \frac{\eta^{1-\rho}}{\Gamma\rho} \int_0^\tau \|C - C_{n-1}\| \times v^{\eta-1} (\tau^\eta - v^\eta)^{\rho-1} \, dv \\ &\leq \frac{\Psi_1}{\Gamma\rho + 1} \left(\frac{\tau^\eta}{\eta} \right)^\rho \|C - C_{n-1}\|. \end{aligned} \tag{57}$$

The following equation follows a recursive process

$$\|A_n(\tau)\| \leq \|C_0\| \left[\frac{1}{\Gamma\rho + 1} \left(\frac{\tau^\eta}{\eta} \right)^\rho \right]^{n+1} {\Psi_1}^n F.$$

At τ_{max} we obtain

$$\|A_n(\tau)\| \leq \|C_0\| \left[\frac{1}{\Gamma\rho + 1} \left(\frac{\tau^\eta_{max}}{\eta} \right)^\rho \right]^{n+1} {\Psi_1}^n F. \tag{58}$$

On the above equation, when we take the limits of both sides, we get $\|A_n(\tau)\| \to 0$ at $n \to \infty$. It is possible to attain $\|B_n(\tau)\| \to 0$. Hence, the proof is concluded.

Uniqueness of Solution: The uniqueness of solutions that is attained in this segment of the diabetic mathematical model is considered. We assume $C_1(\tau)$ and $N_1(\tau)$ are the other solutions of the proposed system, then we have

$$C(\tau) - C_1(\tau) = \frac{\eta^{1-\rho}}{\Gamma\rho} \int_0^\tau (K_1(v, C) - K_1(v, C_1)) \times v^{\eta-1} (\tau^\eta - v^\eta)^{\rho-1} \, dv. \tag{59}$$

The following result is obtained by applying the norm to each side of Eq. (59)

$$\|C(\tau) - C_1(\tau)\| \leq \frac{\eta^{1-\rho}}{\Gamma\rho} \int_0^\tau \|(K_1(v, C) - K_1(v, C_1))\| \times v^{\eta-1} (\tau^\eta - v^\eta)^{\rho-1} \, dv. \tag{60}$$

Lipschitz condition applied to the kernel gives us

$$\|C(\tau) - C_1(\tau)\| \leq \Psi_1 \frac{\eta^{1-\rho}}{\Gamma\rho} \int_0^\tau \|C - C_1\| \times v^{\eta-1} (\tau^\eta - v^\eta)^{\rho-1} \, dv, \tag{61}$$

$$\leq \frac{\Psi_1}{\Gamma\rho + 1} \left(\frac{\tau^\eta}{\eta}\right)^\rho \|C - C_1\|. \tag{62}$$

The following result are obtained

$$\|C(\tau) - C_1(\tau)\| \cdot \left[1 - \frac{\Psi_1}{\Gamma\rho + 1} \left(\frac{\tau^\eta}{\eta}\right)^\rho\right] \leq 0,$$

$$\|C(\tau) - C_1(\tau)\| = 0,$$

$$\implies C(\tau) = C_1(\tau) \tag{63}$$

Considering the above, we can conclude that the first differential equation of the diabetic model has a unique solution. Similarly, we also prove that $N(\tau)$ have unique solutions.

7 Numerical simulations

In this section, we have examined the results of numerical simulations for fractional order diabetes model by using effective and powerful method q-HAGTM. Numerical values have been computed for $C(\tau)$ and $N(\tau)$ at $\rho = 0.85, 0.90$ and 1. Fig.1 explains the nature of trend followed by diabetic population inhibiting complications C corresponding to time τ for discrete values of fractional derivative order ρ. It shows that with increase in time, diabetic population having complications increases. Fig. 2 indicates that the size of diabetic N at time τ also shows incremental behavior with w.r.t time for distinct values of ρ.

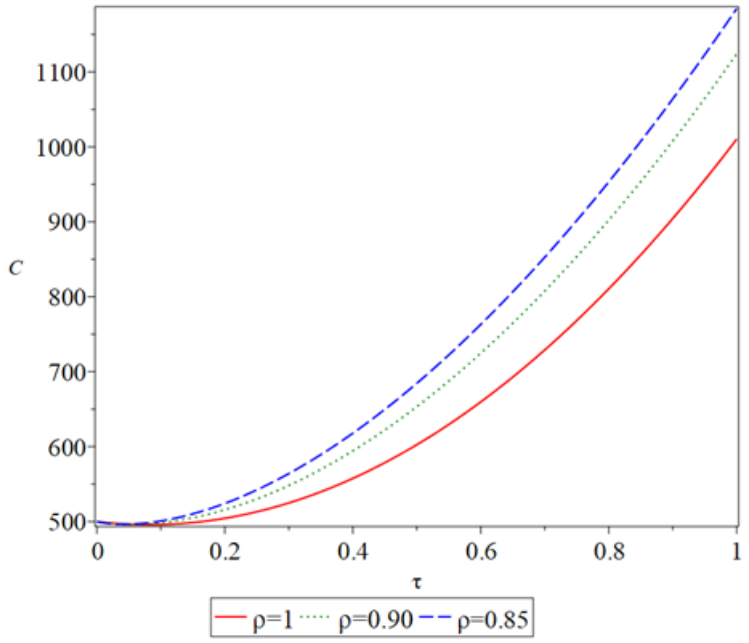

Figure 1: Nature of $C(\tau)$ w.r.t to time τ for distinct values of ρ

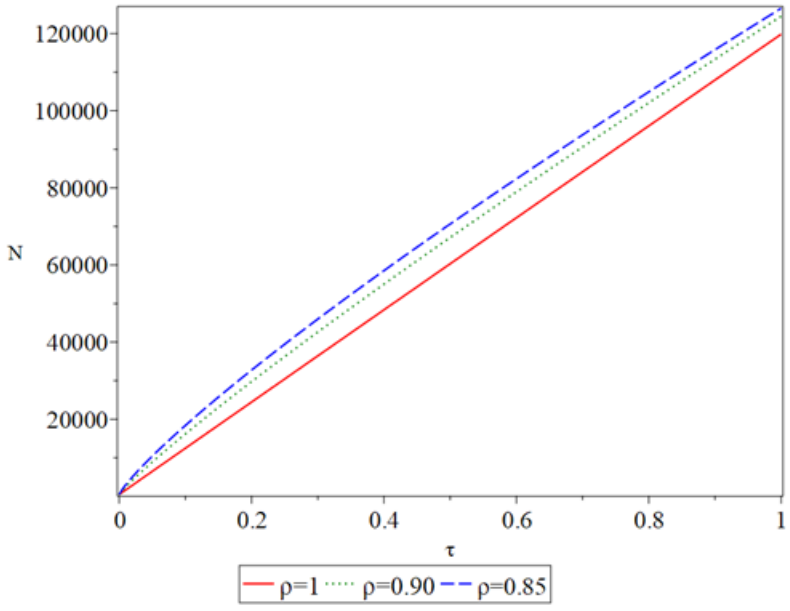

Figure 2: Responses of $N(\tau)$ w.r.t to time τ for distinct values of ρ

8 Conclusions

In this study, the nonlinear fractional diabetic model is investigated with the help of q-HAGTM. The existence and uniqueness of the obtained results are presented using fixed point theory and the Katugampola fractional integral operator. Some numerical results are analyzed to describe the effect of the arbitrary order. The effect of various parameters on the number of diabetic patients with complications and the size of diabetic patients over time is shown graphically. The results of this study are very helpful for medical practitioners dealing with diabetes and related problems. Thus, we have concluded that the implemented technique is efficient for analyzing the behavior of these types of problems arising in various fields.

References

[1] E. Ackerman, L. Gatewood, J. Rosevear, and G. Molnar. Blood glucose regulation and diabetes. *Concepts and Models of Biomathematics*, pages 131–156, 1969.

[2] L. Akinyemi and O. S. Iyiola. A reliable technique to study nonlinear time-fractional coupled korteweg–de vries equations. *Advances in Difference equations*, 2020(1):1–27, 2020.

[3] L. Akinyemi, O. S. Iyiola, and U. Akpan. Iterative methods for solving fourth- and sixth-order time-fractional cahn-hillard equation. *Mathematical Methods in the Applied Sciences*, 43(7):4050–4074, 2020.

[4] R. Almeida, A. B. Malinowska, and T. Odzijewicz. Fractional differential equations with dependence on the caputo–katugampola derivative. *Journal of Computational and Nonlinear Dynamics*, 11(6):061017, 2016.

[5] A. Boutayeb, E. Twizell, K. Achouayb, and A. Chetouani. A mathematical model for the burden of diabetes and its complications. *Biomedical engineering online*, 3:1–8, 2004.

[6] M. Caputo. Elasticità e dissipazione, zanichelli, bologna, 1969.

[7] M. A. El-Tawil and S. N. Huseen. The q-homotopy analysis method (q-ham). *International Journal of Applied Mathematics and Mechanics*, 8(15):51–75, 2012.

[8] M. A. El-Tawil and S. N. Huseen. On convergence of the q-homotopy analysis method. *International Journal of Contemporary Mathematical Sciences*, 8(10):481–497, 2013.

[9] N. Heymans and I. Podlubny. Physical interpretation of initial conditions for fractional differential equations with riemann-liouville fractional derivatives. *Rheologica Acta*, 45:765–771, 2006.

[10] Ö. İlhan and G. Şahin. A numerical approach for an epidemic sir model via morgan-voyce series. *International Journal of Mathematics and Computer in Engineering*, 2024.

[11] F. Jarad and T. Abdeljawad. A modified laplace transform for certain generalized fractional operators. *Results in Nonlinear Analysis*, 1(2):88–98, 2018.

[12] F. Jarad and T. Abdeljawad. Generalized fractional derivatives and laplace transform. 2020.

[13] U. Katugampola. A new approach to generalized fractional derivatives. 6:1–15, 2014.

[14] U. N. Katugampola. New approach to a generalized fractional integral. *Applied mathematics and computation*, 218(3):860–865, 2011.

[15] S. Liao. *Beyond perturbation: introduction to the homotopy analysis method*. CRC press, 2003.

[16] S. Liao. On the homotopy analysis method for nonlinear problems. *Applied mathematics and computation*, 147(2):499–513, 2004.

[17] A. Makroglou, J. Li, and Y. Kuang. Mathematical models and software tools for the glucose-insulin regulatory system and diabetes: an overview. *Applied numerical mathematics*, 56(3-4):559–573, 2006.

[18] K. S. Miller and B. Ross. An introduction to the fractional calculus and fractional differential equations. *Wiley, New York*, 1993.

[19] Z. Odibat and A. Sami Bataineh. An adaptation of homotopy analysis method for reliable treatment of strongly nonlinear problems: construction of homotopy polynomials. *Mathematical methods in the Applied Sciences*, 38(5):991–1000, 2015.

[20] S. V. Pandit, W. R. Giles, and S. S. Demir. A mathematical model of the electrophysiological alterations in rat ventricular myocytes in type-i diabetes. *Biophysical journal*, 84(2):832–841, 2003.

[21] B. M. Patil, R. C. Joshi, and D. Toshniwal. Hybrid prediction model for type-2 diabetic patients. *Expert systems with applications*, 37(12):8102–8108, 2010.

[22] I. Podlubny. Fractional differential equations, mathematics in science and engineering. *Academic press New York*, 1999.

[23] M. Şenol, O. S. Iyiola, H. Daei Kasmaei, and L. Akinyemi. Efficient analytical techniques for solving time-fractional nonlinear coupled jaulent–miodek system with energy-dependent schrödinger potential. *Advances in Difference Equations*, 2019(1):1–21, 2019.

[24] A. A. Sharief and A. Sheta. Developing a mathematical model to detect diabetes using multigene genetic programming. *International Journal of Advanced Research in Artificial Intelligence*, 3(10), 2014.

[25] J. Singh and A. Gupta. Computational analysis of fractional modified degasperis-procesi equation with caputo-katugampola derivative. *AIMS Mathematics*, 8(1):194–212, 2022.

[26] J. Singh, D. Kumar, and D. Baleanu. On the analysis of fractional diabetes model with exponential law. *Advances in Difference Equations*, 2018(1):1–15, 2018.

[27] J. Singh, D. Kumar, and R. Swroop. Numerical solution of time-and space-fractional coupled burgers' equations via homotopy algorithm. *Alexandria Engineering Journal*, 55(2):1753–1763, 2016.

[28] R. Singh, J. Mishra, and V. K. Gupta. The dynamical analysis of a tumor growth model under the effect of fractal fractional caputo-fabrizio derivative. *International Journal of Mathematics and Computer in Engineering*, 2023.

[29] S. Thanompolkrang, W. Sawangtong, and P. Sawangtong. Application of the generalized laplace homotopy perturbation method to the time-fractional black–scholes equations based on the katugampola fractional derivative in caputo type. *Computation*, 9(3):33, 2021.

[30] C. Zecchin, A. Facchinetti, G. Sparacino, G. De Nicolao, and C. Cobelli. A new neural network approach for short-term glucose prediction using continuous glucose monitoring time-series and meal information. In *2011 Annual International Conference of the IEEE Engineering in Medicine and Biology Society*, pages 5653–5656. IEEE, 2011.

Heat and Mass transfer on 3D Radiative MHD Casson Fluid Flow over a Stretching Permeable Sheet with Chemical Reaction and Heat Source/Sink

*R*avindra Kumar[1], *Sarook Khan*[1], *Deepak Kumar*[1] *and Sushila*[2*]
[1]*Department of Mathematics, Vivekananda Global University*,
Jaipur-303012, India
Email: rkmath1982@gmail.com, khansarook@gmail.com,deepak120786@gmail.com
[2]*Department of Physics, Vivekananda Global University*,
Jaipur-303012, India
Email: sushila.jag@gmail.com

Abstract

The objective of this research is to ascertain how 3D MHD heat transfer Casson fluid flow over a linearly porous stretched surface is affected by chemical reaction, radiation, and heat source/sink. The Roseland approximation is used to account for the radiation impact in the energy equation when examining the impacts of thermal radiation. Recently, there has been interest in heat transmission past a stretched sheet because of its numerous commercial applications and substantial impact on a variety of industrial processes. These consist of metal spinning, plastic sheet extrusion, condensation, heat exchangers, MHD generators, and power plants. The governing equations and related boundary conditions are reduced to a dimensionless form using similarity variables, and the Runge-Kutta-Fehlberg method is then used to solve the problem. An increase in the Casson fluid parameter, magnetic field parameter and Permeability parameter causes the velocity field to decrease in x and y directions and improve the temperature and concentration dispersion. Sherwood number and Skin friction coefficient over x and y direction are increasing function of Casson fluid parameter and Nusselt number is decreasing function while the reverse effect is seen in streatching sheet parameter. Nusselt number is increasing function of chemical reaction parameter, Schmidt number, Radiation parameter and heat heat source/sink parameters while the reverse effect is seen in Sherwood number.

Keywords: Chemical reaction, MHD Casson fluid , Stretching surface, Permeability, Heat Source/Sink.

1 Introduction:

The scientific literature has recently shown a great deal of interest in the vast array of biological uses for non-Newtonian fluids, including muds, low-shear rate blood, emulsions, apple sauce, sugar solutions, and shampoos. Fluids that do not flow in a Newtonian manner are referred to as non-Newtonian fluids. The International Atomic Energy Agency classifies them as actual non-Newtonian fluids that occur in nature. Numerous mathematical models have been proposed and examined in the

academic community, and many more are being developed. For instance, a greater variety of industrial applications employ Casson fluids. This model works well for researching the mechanics of yield-stress liquids with pseudo-plastic properties.[18] Thermal radiation, slip velocity, and MHD effects at the stagnation point flow across the stretched surface were examined. [15] the investigation of MHD in three dimensions of Casson fluid flow through a porous sheet that is linearly stretched is done. [9] focused on the impact of double dispersion, non-uniform heat source/sink, higher-order chemical processes, and MHD Casson fluid flow over a vertical cone and flat plate saturated with porous material on unstable, free convective flow. [21] A Casson fluid flow with magnetic nanoparticles incorporated is analyzed. It is believed that the flow is across a paraboloid of revolutions top surface. Nonlinear thermal radiation and viscous dissipation effects are taken into account. [29] examined the three-dimensional Newtonian and non-Newtonian MHD fluid flow. The investigation focuses on mass and heat transmission over a stretched surface when thermophoresis and Brownian motion are present. [6] Numerous biological activities, including the distribution of food, endoscopic procedures, the pumping of blood from the heart to different areas of the body, and the regulation of heat transport phenomena, depend heavily on multiple slips. [17] examined how heat, mass transport, and thermal radiation affected the three-dimensional Casson nanofluid's unstable MHD flow. Partial slip and convective circumstances might affect the flow. [22] examined the three-dimensional MHD Casson fluid flow across a stretched sheet using a non-Darcy porous material and a heat source/sink. [30] An unstable Casson fluid with mixed convection flow with slip and convective boundary conditions approaches a nonlinearly stretched sheet. Additionally examined are the impacts of Soret Dufour, viscous dissipation, and heat source/sink. [27] The effects of warm diffusion, chemical response, and heat radiation on the hydromagnetic pulsating flow of Casson fluid in a porous medium are investigated. [28] Investigations are conducted into the effects of heat radiation, chemical reactions, and thermal diffusion on the hydromagnetic pulsing flow of Casson fluid in a porous medium. [7] Discover the two-dimensional MHD movement of the Casson fluid and the dual solutions of heat transfer over the extension sheet. [14] aimed at describing the characteristics of melting heat transfer on Casson fluid flow in MHD flow in a porous medium under thermal radiation effect. [20] analyzed the impact of nonlinear thermal radiation with an non-uniform heat source and sink in the context of homogeneous-heterogeneous interactions on the three-dimensional Carreau and Casson fluid flow across a stretched surface in an unstable manner. [24] The study examines the consistent movement of a hybrid that is incompressible Casson nanofluid on an exponential stretching sheet that is permeable vertically.[8] The topic discussed is the unstable free convection slip flow of a second-grade fluid across an infinitely heated inclined plate. Additionally eligible are the impacts of mass diffusions in the flow. The constitutive equations for mass transport and heat employ the Caputo-Fabrizio fractional derivative, respectively.[26] examined the thin-film flow down an inclined plane of a third-grade fluid. The homotopy perturbation Elzaki transform technique is an efficient and well-organized computational methodology that is used to determine the solution of a nonlinear boundary value problem (BVP).[4] Single-walled carbon nanotubes are solid, microscopic materials found in nature that have good thermal conductivity and are valuable in many biological applications, particularly in the creation of biological nanofluid are examined.[12] investigated the features of heat transmission of a stationary 2D MHD Casson shear thickening liquid through a perpendicularly extended glass placed in a Variable heat sink/source combined with a permeable medium. [19] examined a rotating system's natural convection MHD Casson fluid flow via an oscillating vertical plate. Using a ramping wall temperature, the properties of thermal radiation, heat production, Hall current, and chemical reactions are examined. [23] examined how magneto-Casson nanofluid

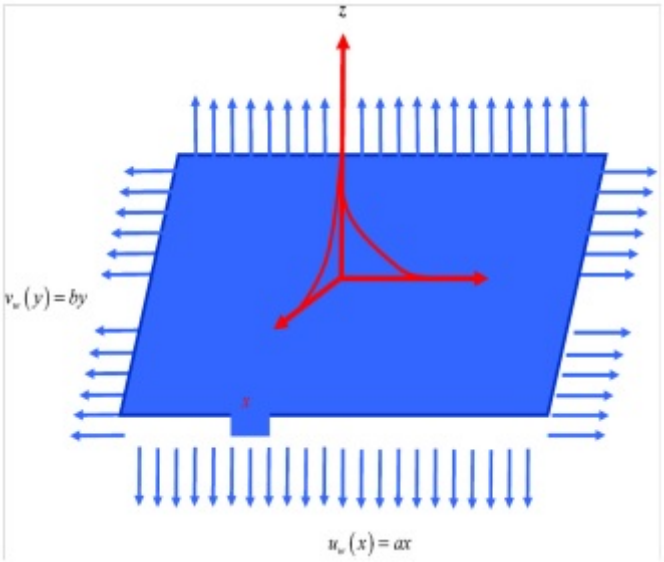

Figure 1: Schematic diagram of the Problem

phenomena, which result in thermal radiation passing through a porous inclined stretched sheet, are affected by chemical reactions and Joule heating. [25] Research was conducted under the stagnation zone to examine the heat and mass transfer of a hybrid nanomaterial Casson fluid with time-dependent flow across a vertical Riga sheet. With this formulation, Lorentz forces were introduced into the system when the Riga sheet was included in fluid flow models. [1] The investigation concentrated on the flow over a vertical stretching sheet near the stagnation point of a compressible, unstable Casson hybrid nanofluid flow. [5] achieved to uncover the novelty of a stretchable sheet with convective boundary conditions driving an incompressible MHD Casson liquid flow. [11] conducted a numerical investigation of the heat transfer of an electrically directed fluid across a radially extending sheet fixed in a permeable medium, as well as the axisymmetric mixed convection boundary layer flow. [16] examined the use of a vertically extended sheet embedded in a permeable material to explore MHDs varying convective stagnation point stream. [31] Measured the impact of radiation, Prandtl number, and chemical reaction on the Casson fluid flow during 3-D MHD heat transfer over a stretched surface with linear porosity. [2] The discussion focuses on Sutterby nanofluid flow at a nonlinear stretching cylinder with an induced magnetic field. Discussion is held on the impacts of viscous dissipation, Darcy resistance, and changing thermal conductivity. [3] Uncompressible We study Sutterby fluid flows across a cylinder that is stretched. When thermal slip, Darcy resistance, and sponginess are present, the impact of varying thermal conductivity is taken into account. [10] examined the effects of heat Source/Sink, joule heating, and thermal radiation on the two-dimensional nanofluid stagnation point flow above a stretched sheet anchored in a spongy medium. [13] Accessible properties include the transfer of melting heat through an exponentially stretched sheet placed in a porous material with a heat source and sink, as well as radiation and velocity slip on an MHD stream.

2 Construction of the Problem:

Consider the incompressible, electrically conducting steady 3D viscous Casson fluid movement on a surface that is extending. It is considered that the sheet is enlarged along xy-plane and stretched with velocities $U_w = ax$,$V_w = by$ in x- and y -directions (where a, b, are stretching constants), while the fluid is place along z-axis. let (u,v,w) denotes the components of velocity along the (x,y,z) paths correspondingly. The physical coordinate system and geometry of this model are exposed in Fig. 1. The Hall current and the Joule dissipation are not taken into consideration and both the consequences of chemical response and the effects of radiation are taken into account.The rheological equation of a Casson fluid can be articulated as

$$\begin{aligned} \tau_{ij} &= 2\left(\mu_B + \frac{p_z}{\sqrt{2\pi}}\right) e_{ij}, \pi > \pi_c \\ &= 2\left(\mu_B + \frac{p_z}{\sqrt{2\pi_c}}\right) e_{ij}, \pi < \pi_c \end{aligned} \tag{1}$$

where $\pi = e_{ij}e_{ji}$, e_{ij} is the (i,j)ˆth component of the deformation rate with itself, π_c is the decisive value of this product based on the shear thickening model, μ_B is the plastic dynamic viscosity of Casson fluid, and p_y is the yield stress of the fluid Equation of Continuity

$$\frac{\partial u}{\partial x} + \frac{\partial v}{\partial y} + \frac{\partial w}{\partial z} = 0, \tag{2}$$

Equation of Momentum

$$u\frac{\partial u}{\partial x} + v\frac{\partial u}{\partial y} + w\frac{\partial u}{\partial z} = \nu\left(1 + \frac{1}{\beta}\right)\frac{\partial^2 u}{\partial z^2} - \frac{\sigma {B_0}^2 u}{\rho} - \frac{\nu}{k}u, \tag{3}$$

$$u\frac{\partial v}{\partial x} + v\frac{\partial v}{\partial y} + w\frac{\partial v}{\partial z} = \nu\left(1 + \frac{1}{\beta}\right)\frac{\partial^2 v}{\partial z^2} - \frac{\sigma {B_0}^2 v}{\rho} - \frac{\nu}{k}v, \tag{4}$$

Equation of Energy

$$\begin{aligned} u\frac{\partial T}{\partial x} + v\frac{\partial T}{\partial y} + w\frac{\partial T}{\partial z} &= \frac{k}{\rho C_p}\frac{\partial^2 T}{\partial z^2} - \frac{1}{\rho c_p}\frac{\partial q_r}{\partial z} \\ +\tau\left(D_b\frac{\partial T}{\partial y}\frac{\partial C}{\partial y} + \frac{D_T}{T_\infty}\left(\frac{\partial T}{\partial y}\right)^2\right) &+ \frac{Q^*(T - T_\infty)}{\rho c_p} \end{aligned} \tag{5}$$

Equation of Species Diffusion

$$u\frac{\partial C}{\partial x} + v\frac{\partial C}{\partial y} + w\frac{\partial C}{\partial z} = D_b\frac{\partial^2 C}{\partial z^2} + \frac{D_T}{T_\infty}\frac{\partial^2 T}{\partial z^2} - {C_r}^*\left(C - C_\infty\right) \tag{6}$$

The boundary conditions for this flow are

$$\begin{gathered} u = u_w(x) = ax, v = V_w(x) = by, C = C_w, T = T_w, at\ z = 0, and \\ u \to 0, v \to 0,\ \ T \to T_\infty, C \to C_\infty, as\ z \to \infty \end{gathered} \tag{7}$$

The radiative heat flux, according to the Rosseland's estimate, is

$$q_r = -\frac{4}{3}\frac{\sigma^*}{k^*}\frac{\partial T^4}{\partial z} \tag{8}$$

Where the Stefan-Boltzmann constant σ^* and the mean absorption coefficient k^*, respectively, are the values. The growth of T^4 near T_∞ in the Tailor series is

$$T^4 = 4TT_\infty{}^3 - 3T_\infty{}^4 \tag{9}$$

Now let us utilize the ensuing similarity conversions
The velocity components can be defined as follows in terms of the stream function ψ as

$$\begin{gathered}\eta = \sqrt{\frac{a}{\nu}}y\ , u = axf'(\eta),\ v = byg'(\eta),\ ,\ w = -\sqrt{a\nu}(f(\eta)+cg(\eta)) \\ \theta(\eta) = \frac{(T-T_\infty)}{(T_w-T_\infty)}, \phi(\eta) = \frac{(C-C_\infty)}{(C_w-C_\infty)}\end{gathered} \tag{10}$$

Here $c = \frac{b}{a}$, is the velocity ratio among the x and y axes, and ($\hat{}$) denotes diff. w. r. to η
By use of Eq. (8), (9), and (10), Eqs. (3), (4), (5), and (6) take the below form

$$\left(1+\frac{1}{\beta}\right)f''' + (f+cg)f'' - f'^2 - (M+K)f' = 0, \tag{11}$$

$$\left(1+\frac{1}{\beta}\right)g''' + (f+cg)g'' - cg'^2 - (M+K)g' = 0, \tag{12}$$

$$(1+Ra)\theta'' + Pr[Nb\theta'\phi' + Nt\theta'^2 + (f+cg)\theta' + \delta\theta] = 0 \tag{13}$$

$$\phi'' + \frac{Nt}{Nb}\theta'' + Sc\left[(f+cg)\phi' - Cr\phi\right] = 0, \tag{14}$$

the corresponding boundary conditions (7) become

$$\begin{gathered}f(0)=0, g(0)=0, f'(0)=1, g'(0)=c, \theta(0)=1, \phi(0)=1, \\ f'(\infty)\to 0, g'(\infty)\to 0, \theta(\infty)\to 0, \phi(\infty)\to 0,\end{gathered} \tag{15}$$

with respect to the relevant physical characteristics
where $M = \frac{\sigma {B_0}^2}{\rho a}$, hint to the magnetic restriction, $K = \frac{\nu}{ka}$ is the permeability parameter, $Pr = \frac{\nu}{\alpha}$ is Prandtl number, $Ra = \frac{16\sigma^* {T_\infty}^3}{3kk^*}$ is radiation parameter, $Nb = \frac{\tau D_b(C_w-C_\infty)}{\nu}$ shows the Brownian motion parameter, $Nt = \frac{\tau D_T(T_w-T_\infty)}{\nu T_\infty}$ is thermophoresis parameter, $\delta = \frac{Q^*}{\rho C_p U_w}$ heat source/sink, parameter, $Sc = \frac{\nu}{D_b}$ Schmidt number, and $Cr = \frac{{C_r}^*}{a}$ is the chemical reaction.
Quantities of physical interest, the physical parameters of the friction factor over x, y paths, and the Nusselt number and Sherwood numbers are shown.

$$C_{f_x} = \frac{\tau_{wx}}{\rho {U_w}^2} \Rightarrow C_{f_x}{Re_x}^{\frac{1}{2}} = \left(1+\frac{1}{\beta}\right)f''(0) \tag{16}$$

$$C_{f_y} = \frac{\tau_{wy}}{\rho {V_w}^2} \Rightarrow C_{f_y}{Re_y}^{\frac{1}{2}} = \left(1+\frac{1}{\beta}\right)\frac{1}{c}g''(0) \tag{17}$$

$$Nu_x = \frac{xq_w}{k(T_w-T_\infty)} \Rightarrow Nu_x{Re_x}^{\frac{-1}{2}} = -\theta'(0) \tag{18}$$

$$Sh_x = \frac{xq_m}{D_b(C_w-C_\infty)} \Rightarrow Sh_x{Re_x}^{\frac{-1}{2}} = -\phi'(0) \tag{19}$$

where

$$q_w = -k\left(\frac{\partial T}{\partial z}\right)_{z=0}, q_m = -\left(D_b\frac{\partial C}{\partial z}\right)_{z=0} \tag{20}$$

$Re_x = \frac{xU_w}{\nu}$ and $Re_y = \frac{yV_w}{\nu}$ are the local Reynolds numbers.

Mathematical process for result:
The result of equations. (11), (12), (13), and (14) jointly through borderline circumstances (15) is determined through a systematic numerical method be aware shooting technique. We translate the nonlinear equivalences into first-order regular differential equivalences by labeling the variable quantity i.e.
$f = f_1, f^{'} = f_2, f^{''} = f_3, g = f_4, g^{'} = f_5, g^{''} = f_6, \theta = f_7, \theta^{'} = f_8, \phi = f_9, \phi^{'} = f_10,$
Hence, the system of equations becomes

$$f_1^{'} = f_2, \tag{22}$$

$$f_2^{'} = f_3, \tag{23}$$

$$f_3^{'} = \left(1+\frac{1}{\beta}\right)^{-1}[f_2^2 - (f_1+cf_4)f_3 + (M+K)f_2] \tag{24}$$

$$f_4^{'} = f_5, \tag{25}$$

$$f_5^{'} = f_6, \tag{26}$$

$$f_6^{'} = \left(1+\frac{1}{\beta}\right)^{-1}[cf_5^2 - (f_1+cf_4)f_6 + (M+K)f_5] \tag{27}$$

$$f_7^{'} = f_8, \tag{28}$$

$$f_8^{'} = (1+Ra)^{-1}[Nbf_8f_{10} + Nt{f_8}^2 + (f_1+cf_4)f_8 + \delta f_7] \tag{29}$$

$$f_9^{'} = f_{10}, \tag{30}$$

$${f_{10}}^{'} = Sc[Crf_9 - (f_1+cf_4)f_{10}] - \frac{Nt}{Nb}f_8^{'}, \tag{31}$$

Subject to the following conditions

$$f_1(0)=0, f_2(0)=1, f_3(0)=S_1, f_4(0)=0, f_5(0)=c, f_6(0)=S_2, f_7(0)=1, \\ f_8(0)=S_3, f_9(0)=0, f_{10}(0)=S_4, \tag{32}$$

$$f_2(\infty)=0, f_4(\infty)=0, f_6(\infty)=0, f_8(\infty)=0,\ as\ \eta\to\infty \tag{33}$$

Now Runge Kutta Fehlberg (RKF45) for stepwise integration, a numerical technique with shooting method is used, and MATLAB software is used for the computations.

3 Results and discussion

Figs. 2, 3, 4, and 5 show how the magnetic parameter affects velocity along the x- and y-directions, temperature, and concentration. Here, we observed that the temperature and concentration increased as they increased, but the velocity profile decreased. It has been observed that a stronger magnetic field makes flow more difficult. The momentum boundary layer thickness decreased as a result of the change in velocity profile, as illustrated in Figs. 2 and 3.

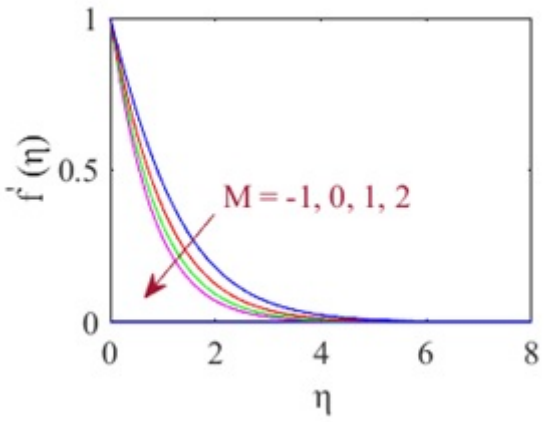

Figure 2: Behaviour of the magnetic parameter M on velocity along the x direction.

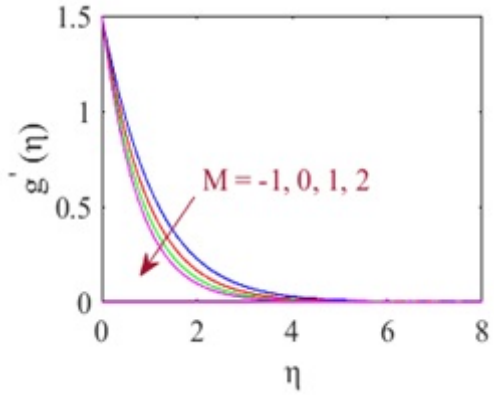

Figure 3: Behaviour of the magnetic parameter M on velocity along the y direction.

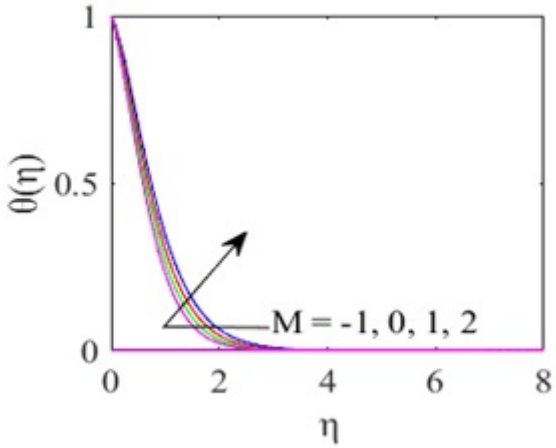

Figure 4: Behaviour of the magnetic parameter M on temperature.

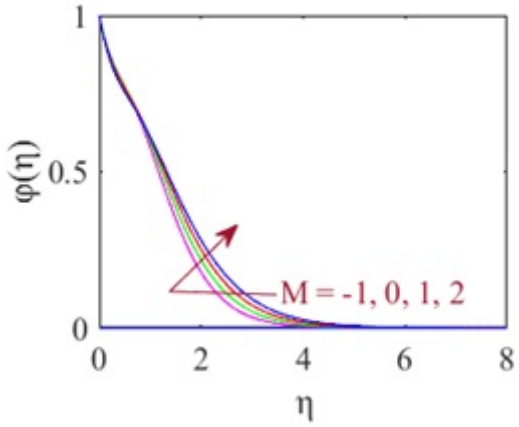

Figure 5: Behaviour of the magnetic parameter M on concenteration.

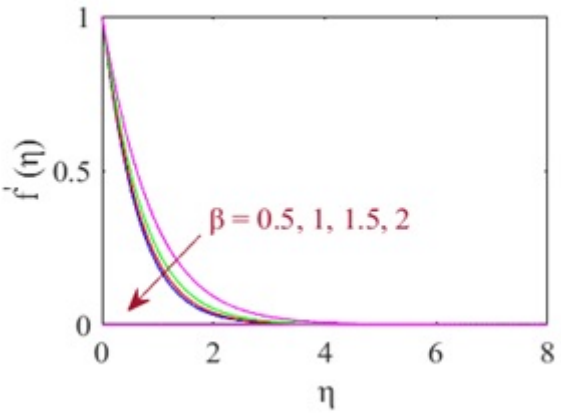

Figure 6: Behaviour of the Casson fluid parameter β on velocity along the x direction.

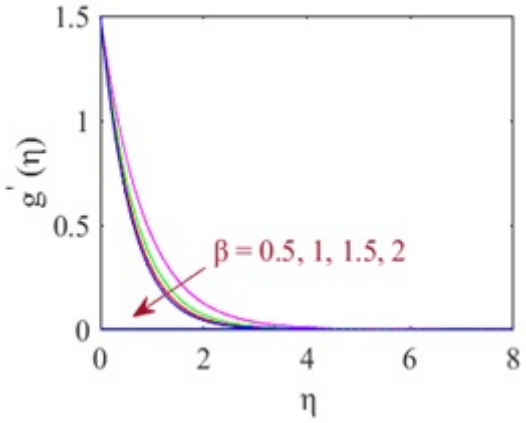

Figure 7: Behaviour of the Casson fluid parameter β on velocity along the y direction.

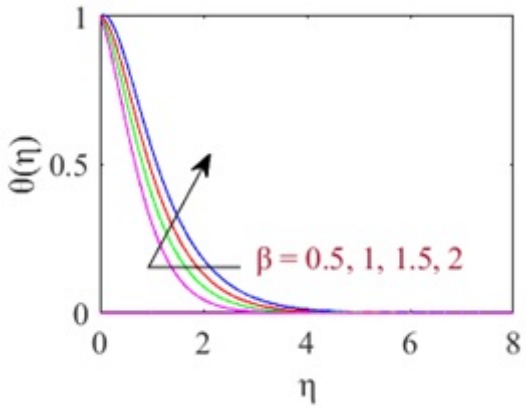

Figure 8: Behaviour of the Casson fluid parameter β on temperature.

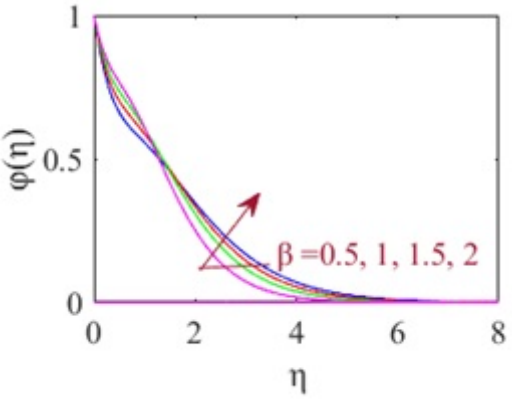

Figure 9: Behaviour of the Casson fluid parameter β on concenteration.

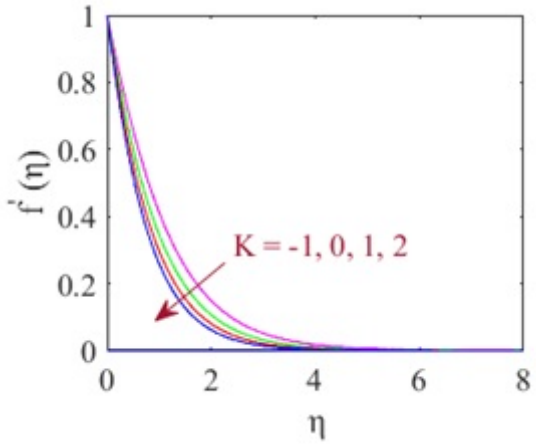

Figure 10: Behaviour of the permeability parameter K velocity along the x direction.

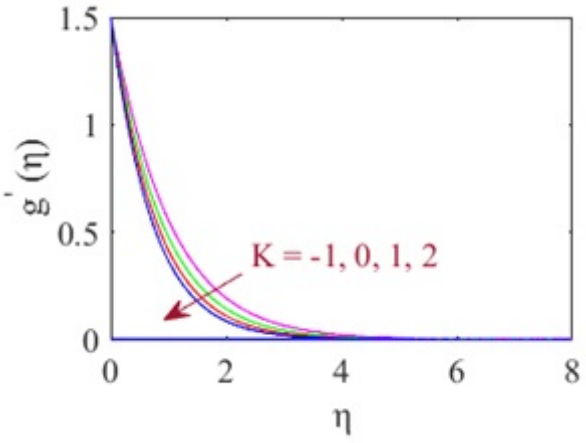

Figure 11: Behaviour of the permeability parameter K velocity along the y direction.

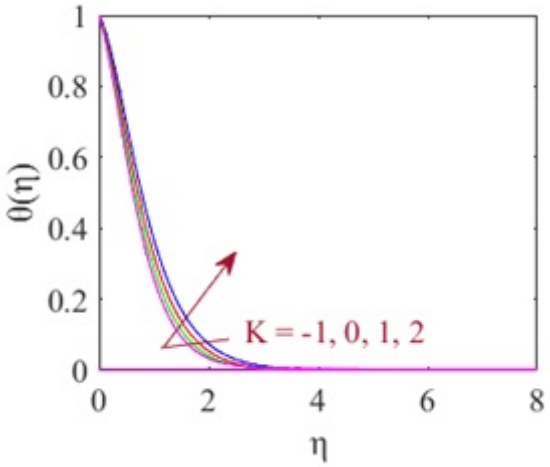

Figure 12: Behaviour of the permeability parameter K on temperature.

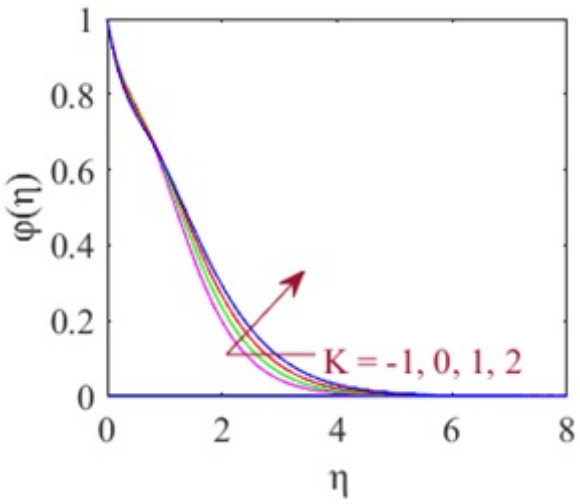

Figure 13: Behaviour of the permeability parameter K on concentration.

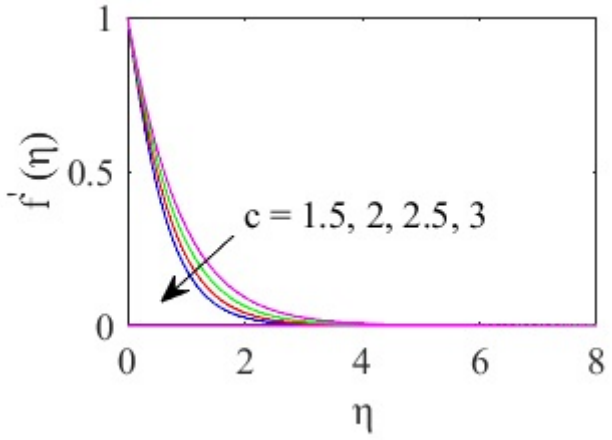

Figure 14: Behaviour of the Stretching sheet parameter c on velocity along the x direction.

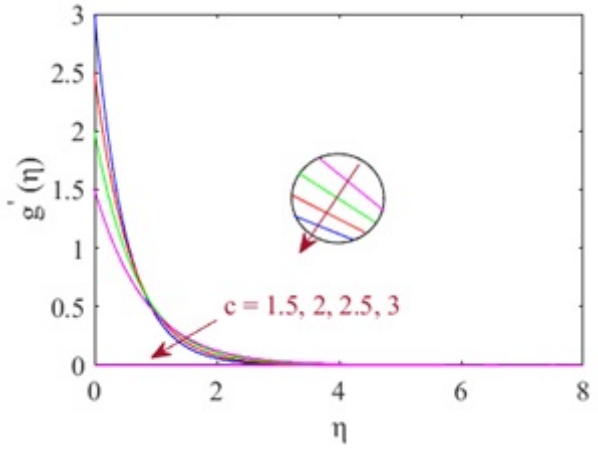

Figure 15: Behaviour of the Stretching sheet parameter c on velocity along the y direction.

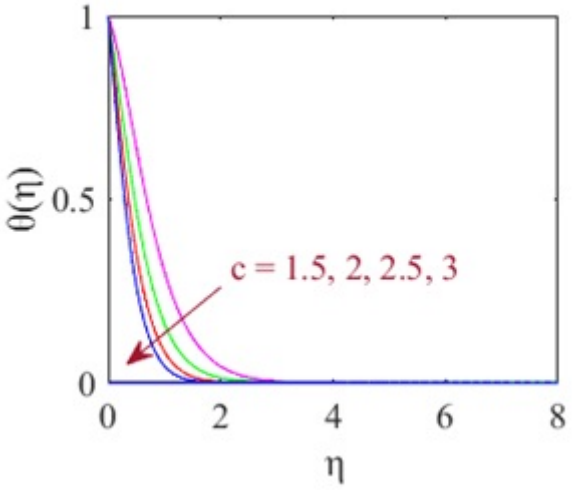

Figure 16: Behaviour of the Stretching sheet parameter c on temperature.

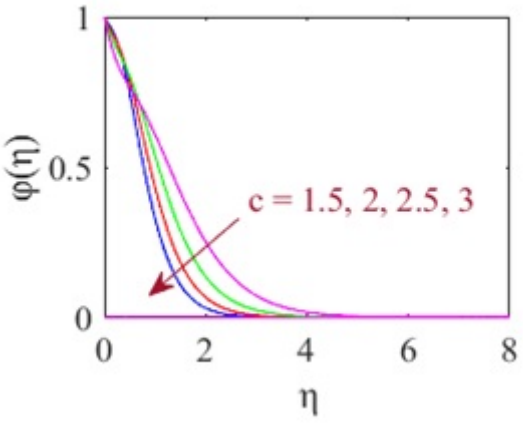

Figure 17: Behaviour of the Stretching sheet parameter c on on concenteration.

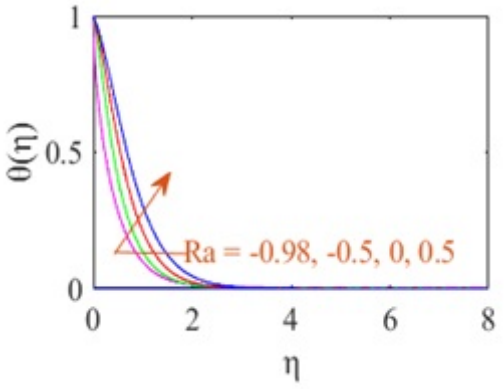

Figure 18: Behaviour of the radiation parameter Ra on temperature.

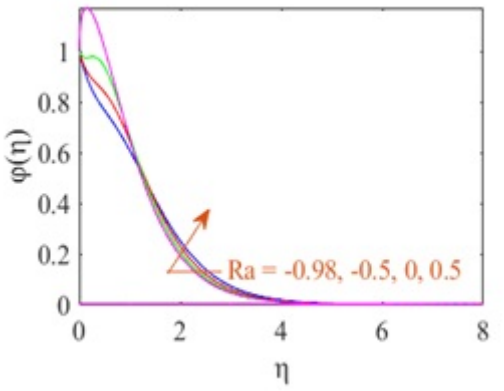

Figure 19: Behaviour of the radiation parameter Ra on concenteration.

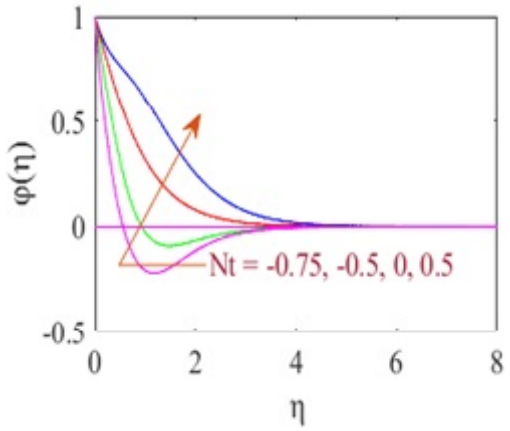

Figure 20: Thermoplastics parameter Nt behavior with respect to temperature.

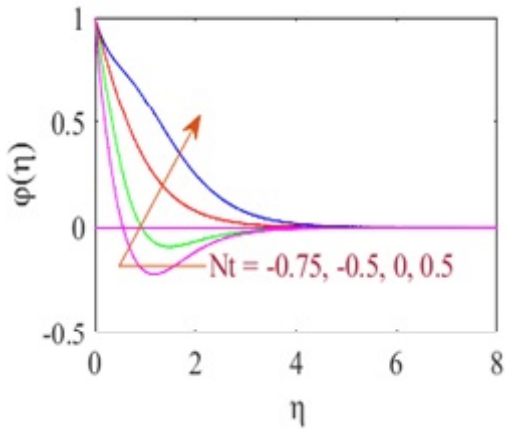

Figure 21: Behaviour of the thermophoresis parameter Nt on concentration.

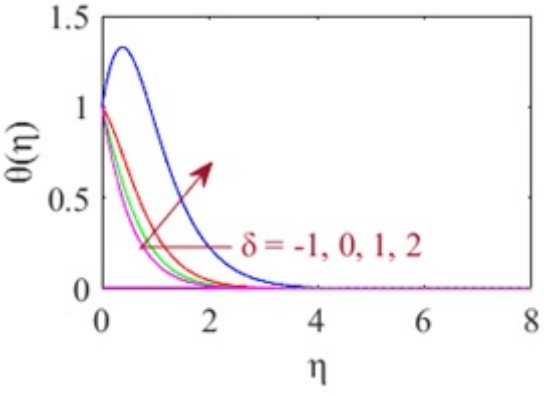

Figure 22: Behaviour of the heat source/sink parameter δ on temperature.

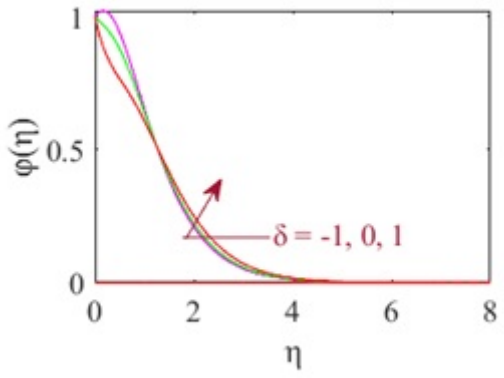

Figure 23: Behaviour of the heat source/sink parameter δ on concentration.

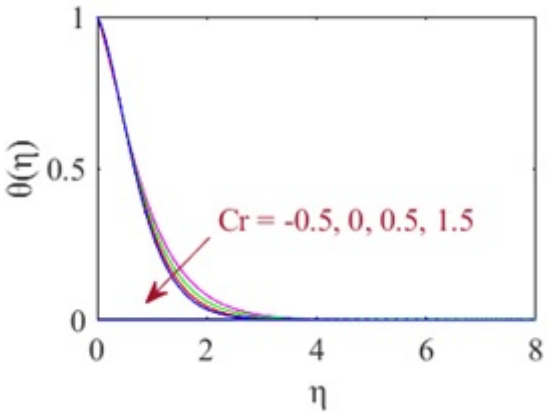

Figure 24: Behaviour of the chemical reaction Cr on temperature.

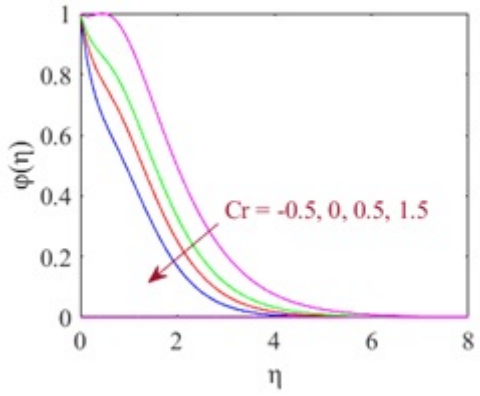

Figure 25: Behaviour of the chemical reaction Cr on concentration.

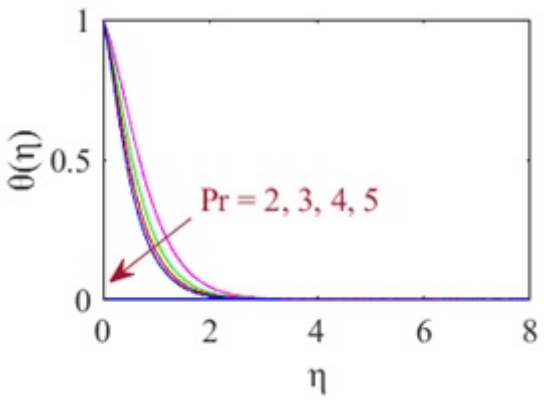

Figure 26: Behaviour of the Prandtl number Pr on temperature.

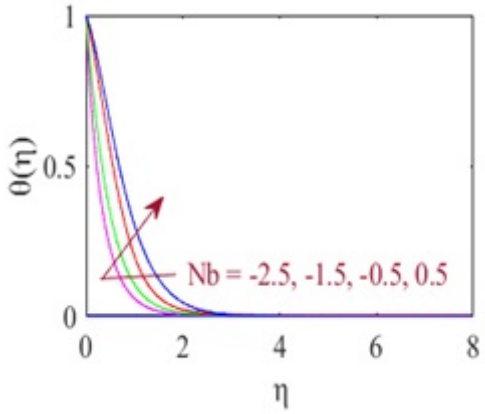

Figure 27: Behaviour of the Brownian motion restriction Nb on concentration.

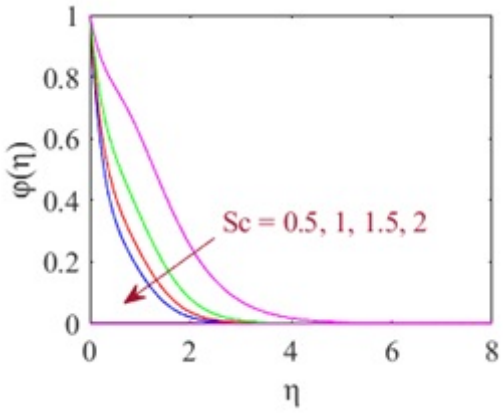

Figure 28: . Behaviour of the Schmidt number Sc on on concentration.

Table 1: Impact of different non-dimensional controlling factors on friction factors C_{f_x}, C_{f_y}, Nusselt number N_{u_x} and Sherwood number S_{u_x}.

Parameter	C_{f_x}	C_{f_y}	N_{u_x}	S_{u_x}
$M = -1$	-2.005746	-2.544402	0.580582	0.801173
$M = 0$	-2.629326	-3.064782	0.500582	0.818533
$M = 1$	-3.140856	-3.51485	0.417652	0.848203
$M = 2$	-3.583068	-3.915582	0.326602	0.891835
$K = -1$	-2.334816	-2.815062	0.521082	0.823045
$K = 0$	-2.895696	-3.297062	0.451682	0.838045
$K = 1$	-3.368973	-3.720438	0.372052	0.869313
$K = 2$	-3.785391	-4.101684	0.275052	0.920523
$\beta = 0.5$	-3.140856	-3.51485	0.417652	0.848203
$\beta = 1$	-2.564498	-2.8698667	0.208992	0.958713
$\beta = 1.5$	-2.341055	-2.6198178	0.044302	1.066831
$\beta = 2$	-2.2209195	-2.485376	-0.1243	1.189151
$c = 1.5$	-3.140856	-3.51485	0.417652	0.848203
$c = 2$	-3.416166	-4.199868	0.931302	0.608003
$c = 2.5$	-3.738744	-4.9411452	1.375402	0.448203
$c = 3$	-4.097244	-5.717001	1.775402	0.338553

Table 2: Impact of different non-dimensional controlling factors on Nusselt number N_{u_x} and Sherwood number S_{u_x}.

Parameter	N_{u_x}	S_{u_x}
$Pr = 2$	0.417652	0.848203
$Pr = 3$	0.573052	0.740903
$Pr = 4$	0.703052	0.641503
$Pr = 5$	0.830052	0.537983
$Cr = -0.5$	0.510152	0.121503
$Cr = 0$	0.457652	0.556253
$Cr = 0.5$	0.417652	0.848203
$Cr = 1$	0.307652	1.307885
$Sc = 0.5$	0.417652	0.848203
$Sc = 1$	0.155712	1.617803
$Sc = 1.5$	-0.05071	2.188503
$Sc = 2$	-0.18071	2.632103
$Ra = -0.98$	9.510052	-8.020473
$Ra = -0.5$	0.915052	0.466403
$Ra = 0$	0.580052	0.735203
$Ra = 0.5$	0.417652	0.848203
$\delta = -1$	1.658502	-0.259983
$\delta = 0$	1.152222	0.197903
$\delta = 1$	0.417652	0.848203
$\delta = 2$	-1.75765	2.671003
$Nb = -2.5$	3.325092	1.469253
$Nb = -1.5$	1.957652	1.404003
$Nb = -0.5$	0.657652	1.183203
$Nb = 0.5$	0.417652	0.848203
$Nt = -0.75$	1.940152	3.092603
$Nt = -0.5$	1.007152	1.500203
$Nt = 0$	0.512552	0.920423
$Nt = 0.5$	0.417652	0.848203

Higher values result in a larger Lorentz force in the magnetic field, which increases the thickness of the thermal boundary layer. Evidently, the Lorentz force is generated by a magnetic field with antagonistic/resistive strength. That causes the fluid velocity to decrease and causes the flow boundary layer to narrow. Figs. 6, 10, 7, 11, 8, 9, and 12, 13 show how Casson fluid parameter and permeability parameter affect velocity along the x- and y-directions, temperature, and concentration. Here, we observed that in figures 8, 9, and 12, 13, the temperature and concentration increased as they increased, but in figures 6, 10, and 7, 11 the velocity profile decreased because the yield stress of the fluid is represented by the Casson fluid parameter. The lowest tension that a fluid has to have in order to flow is known as yield stress. With an increase in the Casson fluid parameter, the fluid yield stress decreases and its viscosity increases. The velocity decreases more gradually as a result. Figs. 14, 15, 16, and 17 show how the stretching sheet parameter affects velocity along the x- and y-directions, temperature, and concentration. Here, we observed that the velocity along the x- and y-directions, temperature, and concentration increased as they increased. Figs. 18, 19, 20, 21, 22, and 23 shows how the radiation parameter, thermophoresis parameter, and heat source/sink parameter affect temperature and concentration. Here, we observed that the temperature and concentration increased as increased, and a reverse effect is seen in Figs. 24 and 25 for chemical reactions. Fig. 26 shows how the Prandtl number affects temperature. Here, we observed that the temperature decreased as it increased.When heat is transferred in relation to momentum, a higher Prandtl number denotes slower heat transfer, and a lower Prandtl number implies faster heat transfer. A fluid with a high Prandtl number often has a relatively short temperature gradient and a smooth, well-mixed temperature profile. Figs. 27 and 28 show how the Brownian motion parameter and Schmidt number affect concentration. Here, we observed that concentration increased as the Brownian motion parameter increased, and a reverse effect is seen in the Schmidt number.

4 Conclusions

This study investigated the effects of radiation and the Prandtl number on the three-dimensional Casson fluid flow across a stretched surface when a magnetic field is present with chemical reaction, and heat source/sink. Prior to being numerically solved, this model is transformed and compressed into a dimensionless form. The numerical data has been used to create graphs and tables that show the flow characteristics.
The principal conclusions drawn from this study are:

- An increase in the magnetic field parameter, Casson fluid parameter, and permeability parameter leads to a decrease in the velocity field in the x and y directions and enhances the distribution of temperature and concentration.
- Increase in Stretching the sheet parameter increases the temperature, concentration, and velocity field in the x and y directions.
- An increase in the radiation parameter, heat source/sink parameter, and thermophoresis parameter increases temperature and concentration, and a reverse effect is seen in the chemical reaction parameter.
- Increase in stretching sheet parameter decrease in temperature, concentration, and velocity field in x and y directions.
- An increase in Prandtl number decreases the temperature.
- An increase in the Schmidt number decreases the concentration.

- The Nusselt number and skin friction coefficient over x and y directions are decreasing functions, while the Sherwood number is an increasing function of the magnetic field parameter and radiation parameter.
- Sherwood number and skin friction coefficient over x and y directions are increasing functions of the Casson fluid parameter, and Nusselt number is a decreasing function, while the reverse effect is seen in the stretching sheet parameter.
- The Nusselt number is an increasing function of the chemical reaction parameter, Schmidt number, radiation parameter, and heat source/sink parameters, while the reverse effect is seen in the Sherwood number.
- The Nusselt number and the Sherwood number are both decreasing functions of the Brownian motion parameter and the thermophoresis parameter.

[1] [2] [3] [5] [6] [7] [9] [12] [11] [13] [10] [14] [15] [16] [17] [18] [19] [20] [21] [22] [23] [24] [25] [27] [28] [29] [30] [31] [4] [26] [8]

References

[1] Abbas, N., Shatanawi, W., and Abodayeh, K. Computational analysis of mhd nonlinear radiation casson hybrid nanofluid flow at vertical stretching sheet. *Symmetry 14*, 7 (2022), 1494.

[2] Abbas, N., Shatanawi, W., Hasan, F., and Shatnawi, T. A. Numerical analysis of darcy resistant sutterby nanofluid flow with effect of radiation and chemical reaction over stretching cylinder: induced magnetic field. *AIMS Math 8* (2023), 11202–11220.

[3] Abbas, N., Shatanawi, W., Shatnawi, T. A., and Hasan, F. Theoretical analysis of induced mhd sutterby fluid flow with variable thermal conductivity and thermal slip over a stretching cylinder. *AIMS Mathematics 8*, 5 (2023), 10146–10159.

[4] Ahmad, M., Asjad, M. I., and Singh, J. Application of novel fractional derivative to heat and mass transfer analysis for the slippage flow of viscous fluid with single-wall carbon nanotube subject to newtonian heating. *Mathematical Methods in the Applied Sciences* (2021).

[5] Anantha Kumar, K., Venkata Ramudu, A., Sugunamma, V., and Sandeep, N. Effect of non-linear thermal radiation on mhd casson fluid flow past a stretching surface with chemical reaction. *International Journal of Ambient Energy 43*, 1 (2022), 8400–8407.

[6] Gopal, D., Kishan, N., and Raju, C. Viscous and joule's dissipation on casson fluid over a chemically reacting stretching sheet with inclined magnetic field and multiple slips. *Informatics in medicine Unlocked 9* (2017), 154–160.

[7] Hamid, M., Usman, M., Khan, Z., Ahmad, R., and Wang, W. Dual solutions and stability analysis of flow and heat transfer of casson fluid over a stretching sheet. *Physics Letters A 383*, 20 (2019), 2400–2408.

[8] Haq, S. U., Jan, S. U., Shah, S. I. A., Khan, I., and Singh, J. Heat and mass transfer of fractional second grade fluid with slippage and ramped wall temperature using caputo-fabrizio fractional derivative approach. *AIMS Mathematics 5*, 4 (2020), 3056–3088.

[9] Jasmine Benazir, A., Sivaraj, R., and Makinde, O. D. Unsteady magnetohydrodynamic casson fluid flow over a vertical cone and flat plate with non-uniform heat source/sink. *International Journal of Engineering Research in Africa 21* (2016), 69–83.

[10] Kumar, R., Mehta, R., Mehta, T., et al. Mhd stagnation point flow and heat transfer of a nanofluid over a stretching sheet fixed in porous medium with effect of thermal radiation, joule heating and heat source/sink. *Journal of Computational Analysis & Applications 31*, 1 (2023).

[11] Kumar, R., Mehta, R., Rathore, H., and Kumar, M. Effect of axisymmetric mixed convection boundary layer flow and heat transmission over exponentially stretching sheet fixed in porous medium with heat source/sink and radiation effect. *International Journal of Energy for a Clean Environment 23*, 7 (2022).

[12] Kumar, R., Mehta, R., Sharma, K., and Kumar, D. Effect of suction/injection on the stream of a magnetohydrodynamic casson fluid over a vertical stretching surface installed in a porous medium with a variable heat sink/source. *Science & Technology Asia* (2021), 13–26.

[13] Kumar, R., Singh, J., Mehta, R., Kumar, D., and Baleanu, D. Analysis of the impact of thermal radiation and velocity slip on the melting of magnetic hydrodynamic micropolar fluid-flow over an exponentially stretching sheet. *Thermal Science 27*, Spec. issue 1 (2023), 311–322.

[14] Mabood, F., and Das, K. Outlining the impact of melting on mhd casson fluid flow past a stretching sheet in a porous medium with radiation. *Heliyon 5*, 2 (2019).

[15] Mahanta, G., and Shaw, S. 3d casson fluid flow past a porous linearly stretching sheet with convective boundary condition. *Alexandria Engineering Journal 54*, 3 (2015), 653–659.

[16] Mehta, R., Kumar, R., Rathore, H., and Singh, J. Joule heating effect on radiating mhd mixed convection stagnation point flow along vertical stretching sheet embedded in a permeable medium and heat generation/absorption. *Heat Transfer 51*, 8 (2022), 7369–7386.

[17] Mondal, S., Oyelakin, I., and Sibanda, P. Unsteady mhd three-dimensional casson nanofluid flow over a porous linear stretching sheet with slip condition. *Frontiers in heat and mass transfer (FHMT) 8* (2017).

[18] Nadeem, S., Haq, R. U., Akbar, N. S., and Khan, Z. H. Mhd three-dimensional casson fluid flow past a porous linearly stretching sheet. *Alexandria Engineering Journal 52*, 4 (2013), 577–582.

[19] Nayak, M., Mahanta, G., Karmakar, K., Mohanty, P., and Shaw, S. Effects of thermal radiation and stability analysis on mhd stagnation casson fluid flow over the stretching surface with slip velocity. In *AIP Conference Proceedings* (2022), vol. 2435, AIP Publishing.

[20] Patel, H. R. Effects of heat generation, thermal radiation, and hall current on mhd casson fluid flow past an oscillating plate in porous medium. *Multiphase Science and Technology 31*, 1 (2019).

[21] Raju, C., and Sandeep, N. Unsteady three-dimensional flow of casson–carreau fluids past a stretching surface. *Alexandria Engineering Journal 55*, 2 (2016), 1115–1126.

[22] Reddy, J. R., Sugunamma, V., and Sandeep, N. Enhanced heat transfer in the flow of dissipative non-newtonian casson fluid flow over a convectively heated upper surface of a paraboloid of revolution. *Journal of Molecular liquids 229* (2017), 380–388.

[23] Reddy, Y. D., Goud, B. S., Chamkha, A. J., and Kumar, M. A. Influence of radiation and viscous dissipation on mhd heat transfer casson nanofluid flow along a nonlinear stretching surface with chemical reaction. *Heat Transfer 51*, 4 (2022), 3495–3511.

[24] Shankar, D. G., Raju, C., Kumar, M. J., and Makinde, O. D. Cattaneo-christov heat flux on an mhd 3d free convection casson fluid flow over a stretching sheet. *Engineering Transactions 68*, 3 (2020), 223–238.

[25] Shatnawi, T. A., Abbas, N., and Shatanawi, W. Comparative study of casson hybrid nanofluid models with induced magnetic radiative flow over a vertical permeable exponentially stretching sheet. *AIMS Math 7*, 12 (2022), 20545–20564.

[26] Singh, J., Kumar, D., Baleanu, D., et al. A hybrid analytical algorithm for thin film flow problem occurring in non-newtonian fluid mechanics. *Ain Shams Engineering Journal 12*, 2 (2021), 2297–2302.

[27] Sobamowo, M., et al. Combined effects of thermal radiation and nanoparticles on free convection flow and heat transfer of casson fluid over a vertical plate. *International Journal of Chemical Engineering 2018* (2018).

[28] Srinivas, S., Kumar, C. K., and Reddy, A. S. Pulsating flow of casson fluid in a porous channel with thermal radiation, chemical reaction and applied magnetic field. *Nonlinear Analysis: Modelling and Control 23*, 2 (2018), 213–233.

[29] Sulochana, C., Ashwinkumar, G., and Sandeep, N. Similarity solution of 3d casson nanofluid flow over a stretching sheet with convective boundary conditions. *Journal of the Nigerian Mathematical Society 35*, 1 (2016), 128–141.

[30] Ullah, I., Khan, I., and Shafie, S. Soret and dufour effects on unsteady mixed convection slip flow of casson fluid over a nonlinearly stretching sheet with convective boundary condition. *Scientific Reports 7*, 1 (2017), 1113.

[31] Yanala, D. R., Kumar, M. A., Bejawada, S. G., Nisar, K. S., Raju, R. S., and Rao, V. S. Exploration of heat and mass transfer on 3-d radiative mhd casson fluid flow over a stretching permeable sheet with chemical reaction. *Case Studies in Thermal Engineering 51* (2023), 103527.

Study and mathematical analysis of the novel fractional bone mineralization model

Ritu Agarwal[1*], Chhaya Midha[2]

[1,2]Department of Mathematics, Malaviya National Institute of Technology, Jaipur-302017, INDIA

E-mail: [1]*ragarwal.maths@mnit.ac.in,* [2]*midhachhaya@gmail.com*

Abstract

Different biological models can be evaluated using mathematical models in both qualitative and quantitative ways. A fractional bone mineralization model involving Caputo's fractional derivative is presented in this work. The fractional mathematical model is beneficial because of its memory carrying property. An appropriate fractional order of the derivative can be chosen that is more closely related to experimental or actual data. The dynamical system of equations for the process of bone mineralization is examined qualitatively and quantitatively in this article. A numerical simulation has been performed for the model. The model's parameters have undergone sensitivity analysis and their effects on the model variables have been explored. By studying the mineralization patterns in bone, different diseases can be cured, and it can also be examined how the deviations from healthy mineral distributions lead to specific bone diseases.

Keywords Bone mineralization, mineralization dynamics, Caputo fractional derivative, critical points

2020 Mathematics subject classification:92-10, 34A34

1 Introduction

In the last decades fractional calculus had a remarkable journey in the field of science, mathematics, and physics. Numerous fractional calculus applications include biophysics, polymer material research, heat transmission in biological systems, random walk problems, and chaotic systems description. (see, e.g [7, 8, 13, 21]). Dynamics of some other models have also been studied like the Ebola virus model [15], malaria transmission model [20], and tumour growth model[9, 19]. Some other biological models and their mathematical analysis can be found in [16, 17, 18].

*Corresponding Author

The Riemann-Liouville fractional integral of order ϱ, $0 < \varrho \leq 1$ of the function $f \in \mathrm{L}_1[\mathrm{a}, \mathrm{b}]$ is defined as

$$I_x^{\varrho}\mathfrak{f}(x) = \frac{1}{\Gamma(\varrho)} \int_0^x (x-t)^{\varrho-1}\mathfrak{f}(t)dt. \tag{1}$$

Caputo fractional derivative, named after Michele Caputo, was first mentioned in his research article [5] in 1967.

Definition 1.1 (Caputo Fractional Derivative)**.** *Suppose that $\varrho > 0$, $a < x < b$, $x \in \mathbb{R}$ and $f(x) \in AC^n[a, b]$, the fractional operator*

$${}_a^C D_x^{\varrho}\mathfrak{f}(x) = \frac{1}{\Gamma(n-\varrho)} \int_a^x (x-t)^{n-\varrho-1}\mathfrak{f}^{(n)}(t)dt, \quad n = [Re(\varrho)] + 1, \tag{2}$$

is called the Caputo fractional derivative of order ϱ.

Equivalently, in the convolution form

$${}_a^C D_x^{\varrho}\mathfrak{f}(x) = \frac{1}{\Gamma(n-\varrho)}\mathfrak{f}^{(n)}(x) * (x^{n-\varrho-1}), \;\; n = [Re(\varrho)] + 1, \; x \in (a, b). \tag{3}$$

The Caputo derivative of the power function x^n is given by

$${}_0^C D_x^{\varrho}(x^n) = \frac{\Gamma(1+n)}{\Gamma(n+1-\varrho)} x^{n-\varrho}. \tag{4}$$

The composition of the Caputo fractional derivative and Riemann-Liouville fractional integral gives the following results:

$$\left({}_0^C D_x^{\varrho} \; I_x^{\varrho}\mathfrak{f}\right)(x) = \mathfrak{f}(x), \tag{5}$$

$$\left(I_x^{\varrho} \; {}_0^C D_x^{\varrho}\mathfrak{f}\right)(x) = \mathfrak{f}(x) - \textstyle\sum_{k=0}^{n-1} \mathfrak{f}^k(0^+)\frac{(x-\varrho)^k}{k!}. \tag{6}$$

We aim to study the dynamics of bone mineralization by fractionalising it in the Caputo sense, followed by finding its solution and graphical analysis.

2 Bone mineralization

Bone is a multidimensional system that functions as a mechanical shield to provide support and security. The involvement of bone in haemostasis (cessation of bleeding from a blood vessel) is also crucial. The process of developing inorganic precipitation over an organic foundation is known as bone mineralization. Basically, it is a process of deposition of minerals on the bone matrix for the growth and development of the bone [6]. Disease that can cause disorders of bone mineralization in children includes rickets, renal disease, and tumour-induced osteomalacia. The core idea of studying the mathematical model for bone mineralization is to know more about how to solve this numerically in order to forecast the reaction of the system, which could result in major clinical signs like bone abnormalities and fractures. In this article, we have studied the mathematical model of the

bone mineralization process, which is described in detail by Komarova [11] and the references cited therein.
Attempts have been made to do quantitative formulation in terms of mathematical laws that relate the mineralization process with predefined parameters. Furthermore, it is explained how this mineralization is measured together with the mathematical formulation of the model and how this can be influenced by several impacts. This helps us to deal with bone diseases and drug therapies. For a fruitful interplay between theory and simulation, considerable efforts have been made to make both outputs comparable. We validate the accuracy of model predictions using bone diseases associated with dramatic changes in mineralization dynamics due to key parameters.

2.1 Mathematical Model

An important and effective way to understand the biological problems is by establishing the mathematical models and analyzing their dynamical behaviors. Various types of mathematical models of biological processes were discussed previously by many authors (see, e.g. [4, 9, 10, 14]). In the present framework, we consider the model for bone mineralization that was given by Komarova [11]. The following system of equations describes the dynamics of bone mineralization:

$$\frac{d\mathfrak{x}_1}{dt} = -k_1\mathfrak{x}_1, \tag{7}$$

$$\frac{d\mathfrak{x}_2}{dt} = k_1\mathfrak{x}_1, \tag{8}$$

$$\frac{d\mathfrak{I}}{dt} = v_1\mathfrak{x}_1 - r_1\mathfrak{x}_2\mathfrak{I}, \tag{9}$$

$$\frac{d\mathfrak{N}}{dt} = k_2\frac{d\mathfrak{x}_2}{dt} - r_2\frac{d\mathfrak{y}}{dt}\mathfrak{N}, \tag{10}$$

$$\frac{d\mathfrak{y}}{dt} = k_3\left(\frac{\rho}{\rho + \mathfrak{I}^\sigma}\right)\mathfrak{N}. \tag{11}$$

The notations and various terms of the equations used in the model are as follows:
$\mathfrak{x}_1$: Concentration of naive collagen.
$\mathfrak{x}_2$: Concentration of mature collagen.
$\mathfrak{I}$: Inhibitor of mineralization.
$\mathfrak{N}$: Number of the nucleators that help in the process of mineralization and act on mature collagen.
$\mathfrak{y}$: Mineral
k_1: It is the rate at which collagen cross-linking takes place and is inversely related to time lag.
The relationships are defined by the equations (7) and (8), and the collagen matrix is created from raw osteoblasts (bone-forming cells) that develop into fully constructed collagen matrix ($\mathfrak{x}_2$).
v_1: It refers to the rate at which inhibitors permeate through immature collagen and into the extracellular compartment close to the cells. It has an inverse relationship with time and directly influences the maximum value of $\mathfrak{I}$. As a result,

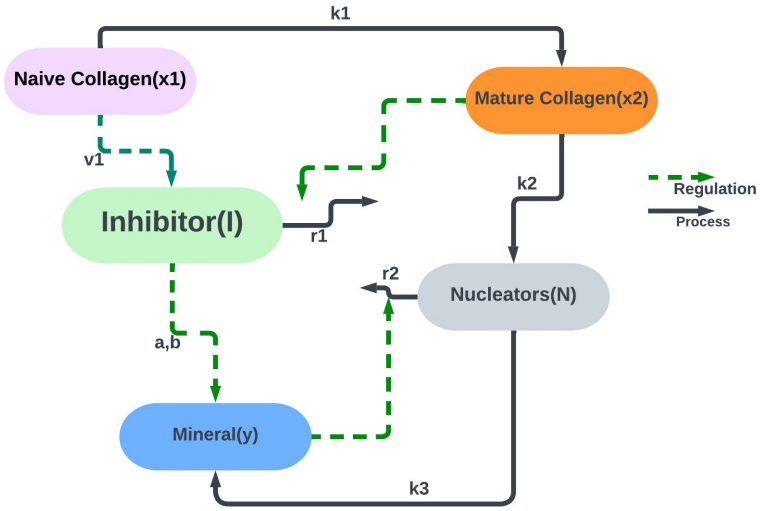

Figure 1: Schematic representation of the model dynamics for bone mineralization.

the amount of inhibitor is proportional to the availability of naive or raw collagen, as indicated by the term $v_1\mathfrak{x}_1$.
The idea is to stimulate the mature collagen because naive collagen can not be mineralized. Inhibitor prevent the conversion of the naive collagen into mature collagen.
r_1: It is the rate by which the inhibitor removal or reduction takes place.
In equation (9), $r_1\mathfrak{x}_2\mathfrak{I}$ represents reduction of inhibitors with rate constant r_1 and is induced by the involvement of mature collagen $\mathfrak{x}_2$.
k_2: The number of nucleators present in each mature collagen molecule.
Each collagen molecule has only one intrafibrillar nucleator when $k_2 = 1$, although interfibrillar nucleators behave similarly.
There is a mixture of intrafibrillar and interfibrillar nucleators when $k_2 \geq 1$. As a result, the rate of nucleator appearance, which is proportional to matrix maturation, is represented by $k_2\dfrac{d\mathfrak{x}_2}{dt}$.
r_2: It is the rate by which mineral mask the nucleator. The number of nucleators diminishes as the mineral covers them up when a certain nucleator starts the mineralization. The rate of decrease of nucleators in equation (10), is thought to be proportional to both the concentration of nucleators present and the rate at which mineralized crystals emerge i.e. $\dfrac{d\mathfrak{y}}{dt}$.
k_3: The rate at which mineralization takes place.
From a physiological perspective, the process of forming bone tissues starts when osteoblasts secrete an organic bone matrix made up of collagen. This raw collagen matrix must be treated to accommodate mineralization once it is deposited into the extracellular compartment; this process is known as matrix maturation.
This model and its simulations have been done by considering the following assumptions:

1. Nucleators generated during collagen maturation are eliminated from the

system in proportion to the rate of mineralization.

2. The model does not define the elaborate process of matrix maturation.
3. Different types of inhibitors are utilized, but they are treated as a single entity.
4. Similarly, interfibrillar and intrafibrillar nucleators are not properly distinguished.

The analysis and observations of the model may help us to find the cure for numerous bone-related diseases like Osteogenesis imperfecta (OI), which is usually caused due to increased bone mineralization resulting in high bone fragility, low bone mass, and brittleness of bones. Mathematically, it can be interpreted as increase in mineralization degree and a decrease in mineralization lag time which has been explained in later sections of this paper through graphical representation. Osteomalacia and Osteoporosis are disease that are caused by to decrease in the degree of bone mineralization and low mineral content respectively.

3 Fractional bone mineralization model

Recently, in the chapter [1], the authors have studied the qualitative analysis and numerical simulation of the integer order model defined by (7)– (11).

Since the recent research involving the fractional-order derivatives has produced superior results in simulating real-world occurrences, we investigate the process of bone mineralization using the Caputo fractional-order derivative. The fractional-order derivative is the generalization of the integer-order derivative and is capable of carrying the memory of the system. It is also helpful in the detection of any lag in the process. Motivated by the work in the field of fractional modeling, we moderate this dynamical system by substituting the time derivative with the Caputo-fractional time derivative.

On fractionalizing the model (7)- (11) using the Caputo fractional derivative of order $0 < \alpha \leq 1$, we get

$$ {}_0^C D_t^\alpha \ \mathfrak{x}_1 = -k_1^\alpha \ \mathfrak{x}_1, \tag{12} $$

$$ {}_0^C D_t^\alpha \ \mathfrak{x}_2 = k_1^\alpha \ \mathfrak{x}_1, \tag{13} $$

$$ {}_0^C D_t^\alpha \ \mathfrak{I} = v_1^\alpha \ \mathfrak{x}_1 - {r_1}^\alpha \ \mathfrak{x}_2 \mathfrak{I}, \tag{14} $$

$$ {}_0^C D_t^\alpha \ \mathfrak{N} = k_2 \ ({}_0^C D_t^\alpha \ \ \mathfrak{x}_2) - r_2 \ ({}_0^C D_t^\alpha \ \mathfrak{y}) \ \mathfrak{N}, \tag{15} $$

$$ {}_0^C D_t^\alpha \ \mathfrak{y} = k_3^\alpha \left(\frac{\rho}{\rho + \mathfrak{I}^\sigma} \right) \mathfrak{N}. \tag{16} $$

The ordinary derivative has an inverse second dimension s^{-1} and the fractional derivative has a dimension of $s^{-\alpha}$. For the non-dimensionlization, making the substitutions

$X_1 = \frac{\mathfrak{x}_1}{\hat{\mathfrak{x}_1}}$, $X_2 = \frac{\mathfrak{x}_2}{\hat{\mathfrak{x}_2}}$, $Y = \frac{\mathfrak{y}}{\hat{\mathfrak{y}}}$, $\tilde{I} = \frac{\mathfrak{I}}{\hat{\mathfrak{x}_1}}$, $\tilde{N} = \frac{\mathfrak{N}}{\hat{\mathfrak{x}_1}}$, $r_1^\alpha \hat{\mathfrak{x}_1} = \hat{r_1}$, $r_2 \hat{\mathfrak{y}} = \hat{r_2}$, $\hat{b} = \frac{b}{\hat{\mathfrak{x}_1}^a}$, $\frac{k_3^\alpha \ \hat{\mathfrak{x}_1}}{\hat{\mathfrak{y}}} =$

$\hat{k_3}$, $k_1^\alpha = \hat{k_1}$, $v_1^\alpha = \hat{v_1}$, $\hat{\mathfrak{x}_1} = \hat{\mathfrak{x}_2} = 10^6 molecules/\mu m^3$, $\hat{\mathfrak{y}_1} = 10^9 molecules/\mu m^3$ in the system (12)-(16), it gets transformed into:

$$ {}_0^C D_t^\alpha \ X_1 = -\hat{k_1} X_1, \tag{17} $$

$$ {}_0^C D_t^\alpha \ X_2 = \hat{k_1} X_1, \tag{18} $$

$$ {}_0^C D_t^\alpha \ \tilde{I} = \hat{v_1} X_1 - \hat{r_1} X_2 \tilde{I}, \tag{19} $$

$$ {}_0^C D_t^\alpha \ \tilde{N} = k_2 \ ({}_0^C D_t^\alpha \ X_2) - \hat{r_2} \ ({}_0^C D_t^\alpha \ Y)\tilde{N}, \tag{20} $$

$$ {}_0^C D_t^\alpha \ Y = \hat{k_3} \left(\frac{\tilde{\rho}}{\tilde{\rho} + \tilde{I^\sigma}} \right) \tilde{N}. \tag{21} $$

For this fractional model, we perform the qualitative analysis i.e. the existence and uniqueness of the solution of the defined coupled system is proved. The model is simulated for observing the behavior of the variable under the impact of fractional order derivative. A comparison with integer order derivative helps in understanding the phenomenon in a better way. The sensitivity analysis for the fractional model is done with respect to the parameters of the model.

4 Qualitative analysis of the model

In this section, the qualitative analysis of the model has been done. We shall first prove the existence and uniqueness of the solution of the system (17)-(21). The existence and uniqueness of the solution are the key ideas in the field of differential equations as they ensure that a solution to the fractional order model exists and can be found by one or the other method. It also guarantees that if the solution exists, it is unique.

4.1 Existence and Uniqueness of Solution

If $C(J)$ is the collection of continuous real-valued functions defined on the interval $J \subset R$. Then $V = C(J) * C(J) * C(J) * C(J) * C(J)$ is the Banach space with the norm for $(X_1, X_2, \tilde{I}, \tilde{N}, Y) \in V$ defined as $\|(X_1, X_2, \tilde{I}, \tilde{N}, Y)\| = \|X_1\| + \|X_2\| + \|\tilde{I}\| + \|\tilde{N}\| + \|Y\|$, where $X_1, X_2, \tilde{I}, \tilde{N}, Y \in C(J)$ and $\| \cdot \| = \sup_{t \in J} \ | \cdot |$. With the application of the fixed point theorem, we shall prove that the solution of the system of differential equations (17)-(21) exists.
Applying the integral operator (5) upon the equation (17),

$$ I_t^\alpha \ {}_0^C D_t^\alpha \ X_1 = I_t^\alpha (-\hat{k_1} X_1), \tag{22} $$

we obtain

$$ X_1(t) - X_1(0) = \frac{1}{\Gamma(\alpha)} \int_0^t (t-\tau)^{\alpha-1} (-\hat{k_1} X_1(\tau)) d\tau. \tag{23} $$

Similarly,

$$ X_2(t) - X_2(0) = \frac{1}{\Gamma(\alpha)} \int_0^t (t-\tau)^{\alpha-1} (\hat{k_1} X_1(\tau)) d\tau, \tag{24} $$

$$\tilde{I}(t) - \tilde{I}(0) = \frac{1}{\Gamma(\alpha)} \int_0^t (t-\tau)^{\alpha-1} (\hat{v_1} X_1 - \hat{r_1} X_2 \tilde{I}) d\tau, \tag{25}$$

$$\tilde{N}(t) - \tilde{N}(0) = \frac{1}{\Gamma(\alpha)} \int_0^t (t-\tau)^{\alpha-1} (k_2 \hat{k_1} X_1 - \hat{r_2} \ ({}_0^C D_t^\alpha \ Y) \ \tilde{N}) d\tau, \tag{26}$$

$$Y(t) - Y(0) = \frac{1}{\Gamma(\alpha)} \int_0^t (t-\tau)^{\alpha-1} \left(\hat{k_3} \left(\frac{\tilde{\rho}}{\tilde{\rho} + \tilde{I^\sigma}} \right) \tilde{N} \right) d\tau. \tag{27}$$

Denote,

$$\begin{aligned} \mathcal{K}_1 &= -\hat{k_1} X_1, \\ \mathcal{K}_2 &= \hat{k_1} X_1, \\ \mathcal{K}_3 &= \hat{v_1} X_1 - \hat{r_1} X_2 \tilde{I}, \\ \mathcal{K}_4 &= k_2 \ ({}_0^C D_t^\alpha \ X_2) - \hat{r_2} \ ({}_0^C D_t^\alpha \ Y) \tilde{N}, \\ \mathcal{K}_5 &= \hat{k_3} \left(\frac{\tilde{\rho}}{\tilde{\rho} + \tilde{I^\sigma}} \right) \tilde{N}. \end{aligned} \tag{28}$$

The kernels $\mathcal{K}_i$, $i = 1, 2, 3, 4, 5$ satisfy certain requirements, as stated in the following theorem [2].

Theorem 4.1. *The Lipschitz condition and contraction would be satisfied by $\mathcal{K}_1$, $\mathcal{K}_2$, $\mathcal{K}_3$, $\mathcal{K}_4$, $\mathcal{K}_5$, for the Lipschitz constants $0 \leq \hat{k_1} < 1$, $0 \leq \hat{r_1} c_1 < 1$, $0 \leq 2\hat{r_2} k_2 \hat{k_3} c_1 < 1$.*

Proof. Let us start with $\mathcal{K}_1$. Let X_1 and $X_1^{(1)}$ are two functions, then

$$\begin{aligned} \|\mathcal{K}_1(t, X_1) - \mathcal{K}_1(t, X_1^{(1)})\| &= \| - \hat{k_1} X_1 + \hat{k_1} X_1^{(1)} \| \\ &= \hat{k_1} \ \| X_1 - X_1^{(1)} \|. \end{aligned} \tag{29}$$

Clearly, $\hat{k_1}$ is a fixed parameter and $\|X_1\|$ is a bounded function.
Hence the Lipschitz condition is satisfied for $\mathcal{K}_1$, and it is contraction mapping. Similarly, the other four kernels also satisfy the Lipschitz condition, i.e.,

$$\begin{aligned} \|\mathcal{K}_2(t, X_2) - \mathcal{K}_2(t, X_2^{(1)})\| &= \hat{k_1} \|X_2 - X_2^{(1)}\|, \\ \|\mathcal{K}_3(t, \tilde{I}) - \mathcal{K}_3(t, \tilde{I}^{(1)})\| &= \hat{r_1} c_1 \|\tilde{I} - \tilde{I}^{(1)}\|, \\ \|\mathcal{K}_4(t, \tilde{N}) - \mathcal{K}_4(t, \tilde{N}^{(1)})\| &= 2\hat{r_2} k_2 \hat{k_3} c_1 \|\tilde{N} - \tilde{N}^{(1)}\|, \\ \|\mathcal{K}_5(t, Y) - \mathcal{K}_5(t, Y^{(1)})\| &= 0, \end{aligned} \tag{30}$$

On using the above kernels from (28) in the equations (23) - (27), we get

$$\begin{aligned} X_1(t) &= X_1(0) + \int_0^t \mathcal{K}_1(\tau, X_1(\tau)) d\tau, \\ X_2(t) &= X_2(0) + \int_0^t \mathcal{K}_2(\tau, X_2(\tau)) d\tau, \\ \tilde{I}(t) &= \tilde{I}(0) + \int_0^t \mathcal{K}_3(\tau, \tilde{I}(\tau)) d\tau, \\ \tilde{N}(t) &= \tilde{N}(0) + \int_0^t \mathcal{K}_4(\tau, \tilde{N}(\tau)) d\tau, \\ Y(t) &= Y(0) + \int_0^t \mathcal{K}_5(\tau, Y(\tau)) d\tau. \end{aligned} \tag{31}$$

Corresponding recursive formulas are given by

$$\begin{aligned} X_1^{(n)}(t) &= \int_0^t \mathcal{K}_1(\tau, X_1^{(n-1)}(\tau))d\tau, \\ X_2^{(n)}(t) &= \int_0^t \mathcal{K}_2(\tau, X_2^{(n-1)}(\tau))d\tau, \\ \tilde{I}^{(n)}(t) &= \int_0^t \mathcal{K}_3(\tau, \tilde{I}^{(n-1)}(\tau))d\tau, \\ \tilde{N}^{(n)}(t) &= \int_0^t \mathcal{K}_4(\tau, \tilde{N}^{(n-1)}(\tau))d\tau, \\ Y^{(n)}(t) &= \int_0^t \mathcal{K}_5(\tau, Y^{(n-1)}(\tau))d\tau. \end{aligned} \tag{32}$$

The initial conditions are $X_1^{(0)} = X_1(0), X_2^{(0)} = X_2(0), \tilde{I}^{(0)} = \tilde{I}(0), \tilde{N}^{(0)} = \tilde{N}(0), Y^{(0)} = Y(0)$.

The following expressions represent respectively the difference of the terms in (32) with their succeeding terms,

$$\begin{aligned} \psi_{1n}(t) &= X_1^{(n)}(t) - X_1^{(n-1)}(t) \\ &= \frac{1}{\Gamma(\alpha)} \int_0^t \big(\mathcal{K}_1(\tau, X_1^{(n-1)}(\tau)) - \mathcal{K}_1(\tau, X_1^{(n-2)}(\tau))\big)(x-\tau)^{\alpha-1}d\tau, \end{aligned} \tag{33}$$

$$\begin{aligned} \psi_{2n}(t) &= X_2^{(n)}(t) - X_2^{(n-1)}(t) \\ &= \frac{1}{\Gamma(\alpha)} \int_0^t \big(\mathcal{K}_2(\tau, X_2^{(n-1)}(\tau)) - \mathcal{K}_2(\tau, X_2^{(n-2)}(\tau))\big)(x-\tau)^{\alpha-1}d\tau, \end{aligned} \tag{34}$$

$$\begin{aligned} \psi_{3n}(t) &= \tilde{I}^{(n)}(t) - \tilde{I}^{(n-1)}(t) \\ &= \frac{1}{\Gamma(\alpha)} \int_0^t \big(\mathcal{K}_3(\tau, \tilde{I}^{(n-1)}(\tau)) - \mathcal{K}_3(\tau, \tilde{I}^{(n-2)}(\tau))\big)(x-\tau)^{\alpha-1}d\tau, \end{aligned} \tag{35}$$

$$\begin{aligned} \psi_{4n}(t) &= \tilde{N}^{(n)}(t) - \tilde{N}^{(n-1)}(t) \\ &= \frac{1}{\Gamma(\alpha)} \int_0^t \big(\mathcal{K}_4(\tau, \tilde{N}^{(n-1)}(\tau)) - \mathcal{K}_4(\tau, \tilde{N}^{(n-2)}(\tau))\big)(x-\tau)^{\alpha-1}d\tau, \end{aligned} \tag{36}$$

$$\begin{aligned} \psi_{5n}(t) &= Y^{(n)}(t) - Y^{(n-1)}(t) \\ &= \frac{1}{\Gamma(\alpha)} \int_0^t \big(\mathcal{K}_5(\tau, Y^{(n-1)}(\tau)) - \mathcal{K}_5(\tau, Y^{(n-2)}(\tau))\big)(x-\tau)^{\alpha-1}d\tau. \end{aligned} \tag{37}$$

Now, on taking norm of (33),

$$\begin{aligned} |\psi_{1n}(t)| &= \Big\| X_1^{(n)}(t) - X_1^{(n-1)}(t) \Big\| \\ &= \| \frac{1}{\Gamma(\alpha)} \int_0^t \big(\mathcal{K}_1(\tau, X_1^{(n-1)}(\tau)) - \mathcal{K}_1(\tau, X_1^{(n-2)}(\tau))\big)d\tau \| \\ &\leq \int_0^t \| \big(\mathcal{K}_1(\tau, X_1^{(n-1)}(\tau)) - \mathcal{K}_1(\tau, X_1^{(n-2)}(\tau))\big) \| d\tau. \end{aligned} \tag{38}$$

As the kernel $\mathcal{K}_1$ fulfill the Lipschitz condition, we have

$$\|X_1^{(n)}(t) - X_1^{(n-1)}(t)\| \leq \hat{k_1} \int_0^t \|X_1^{(n-1)}(t) - X_1^{(n-2)}(t)\| d\tau, \tag{39}$$

and hence,

$$\|\psi_{1n}(t)\| \leq \gamma_1 \int_0^t \|\psi_{1(n-1)}(t)(\tau)\| d\tau. \tag{40}$$

Similarly,

$$\|\psi_{2n}(t)\| \leq \gamma_2 \int_0^t \|\psi_{2(n-1)}(\tau)\| d\tau, \tag{41}$$

$$\|\psi_{3n}(t)\| \leq \gamma_3 \int_0^t \|\psi_{3(n-1)}(\tau)\| d\tau, \tag{42}$$

$$\|\psi_{4n}(t)\| \leq \gamma_4 \int_0^t \|\psi_{4(n-1)}(\tau)\| d\tau, \tag{43}$$

$$\|\psi_{5n}(t)\| \leq \gamma_5 \int_0^t \|\psi_{5(n-1)}(\tau)\| d\tau, \tag{44}$$

where, $\gamma_1 = \gamma_2 = \hat{k_1}$, $\gamma_3 = \hat{r_1} c_1$, $\gamma_4 = 2\hat{r_2} k_2 \hat{k_3} c_1$, $\gamma_5 = 0$.
Hence,

$$X_1^{(n)}(t) = \sum_{i=0}^{n} \psi_{1n}(t), \tag{45}$$

$$X_2^{(n)}(t) = \sum_{i=0}^{n} \psi_{2n}(t), \tag{46}$$

$$\tilde{I}^{(n)}(t) = \sum_{i=0}^{n} \psi_{3n}(t), \tag{47}$$

$$\tilde{N}^{(n)}(t) = \sum_{i=0}^{n} \psi_{4n}(t), \tag{48}$$

$$Y^{(n)}(t) = \sum_{i=0}^{n} \psi_{5n}(t). \tag{49}$$

□

In the following theorem we prove the existence and uniqueness of the solution [12].

Theorem 4.2. *The system of fractional bone mineralization model has an exact coupled solution under the condition that we can find* t_1 *such that* $\frac{\hat{k_1} t_1}{\Gamma(\alpha)} \leq 1$, $\frac{\hat{r_1} c_1 t_1}{\Gamma(\alpha)} \leq 1$, $\frac{\hat{r_2} \hat{k_3} t}{\Gamma(\alpha)} \leq 1$ *and also the solution is unique.*

Proof. The functions $X_1(t)$, $X_2(t)$, $\tilde{I}(t)$, $\tilde{N}(t)$, and $Y(t)$ are bounded and the Lipschitz condition is satisfied by the kernels $\mathcal{K}_i$, $i = 1, 2, 3, 4, 5$,

$$\begin{aligned} X_1(t) - X_1(0) &= X_1^{(n)}(t) - \mathcal{H}_1^{(n)}(t), \\ X_2(t) - X_2(0) &= X_2^{(n)}(t) - \mathcal{H}_2^{(n)}(t), \\ \tilde{I}(t) - \tilde{I}(0) &= \tilde{I}^{(n)}(t) - \mathcal{H}_3^{(n)}(t), \\ \tilde{N}(t) - \tilde{N}(0) &= \tilde{N}^{(n)}(t) - \mathcal{H}_4^{(n)}(t), \\ Y(t) - Y(0) &= Y^{(n)}(t) - \mathcal{H}_5^{(n)}(t). \end{aligned} \tag{50}$$

Now,

$$\begin{aligned} \mathcal{H}_1^{(n)}(t) &= X_1^{(n)}(t) - X_1(t) + X_1(0) \\ \implies \|\mathcal{H}_1^{(n)}(t)\| &= \left\| \frac{1}{\Gamma(\alpha)} \int_0^t \mathcal{K}_1(\tau, X_1^{(n-1)}(\tau)) d\tau - X_1(t) + X_1(0) \right\| \\ &= \frac{1}{\Gamma(\alpha)} \left\| \int_0^t \mathcal{K}_1(\tau, X_1^{(n-1)}(\tau)) d\tau + X_1(0) - X_1(0) - \int_0^t \mathcal{K}_1(\tau, X_1(\tau)) d\tau \right\| \\ &= \frac{1}{\Gamma(\alpha)} \int_0^t \|(\mathcal{K}_1(\tau, X_1^{(n-1)}(\tau)) - \mathcal{K}_1(\tau, X_1(\tau)))\| d\tau \\ &\leq \frac{\hat{k_1}}{\Gamma(\alpha)} \|(X_1^{(n-1)} - X_1)\| \int_0^t d\tau \\ &\leq \frac{\hat{k_1}}{\Gamma(\alpha)} \|X_1^{(n-1)} - X_1\| t. \end{aligned} \tag{51}$$

On repeated use of above process, we get

$$\|\mathcal{H}_1^{(n)}(t)\| \leq (\hat{k_1})^{n+1} \left(\frac{t}{\Gamma(\alpha)} \right)^{n+1} \lambda. \tag{52}$$

Thus, $\exists\ t_1$ such that

$$\|\mathcal{H}_1^{(n)}(t)\| \leq (\hat{k_1})^{n+1} \left(\frac{t_1}{\Gamma(\alpha)} \right)^{n+1} \lambda. \tag{53}$$

Taking the limit $n \to \infty$, since, $0 \leq \hat{k_1} t < 1$,

$$\|\mathcal{H}_1^{(n)}(t)\| \to 0. \quad \implies X_1(t) - X_1(0) = \lim_{n \to \infty} X_1^{(n)}(t) \tag{54}$$

Similarly,

$$\begin{aligned} \|\mathcal{H}_2^{(n)}(t)\| &\leq \frac{\hat{k_1} t}{\Gamma(\alpha)} \|X_2^{(n-1)} - X_2\| \\ \|\mathcal{H}_3^{(n)}(t)\| &\leq \frac{\hat{r_1} c_1 t}{\Gamma(\alpha)} \|\tilde{I}^{(n-1)} - \tilde{I}\| \\ \|\mathcal{H}_4^{(n)}(t)\| &\leq \frac{\hat{r_2} \hat{k_3} t}{\Gamma(\alpha)} \|\tilde{N}^{(n-1)} - \tilde{N}\| \\ \|\mathcal{H}_5^{(n)}(t)\| &= 0, \end{aligned} \tag{55}$$

and hence, we have

$$\begin{aligned}
\|\mathcal{H}_2^{(n)}(t)\| \to 0. \quad &\implies X_2(t) - X_2(0) = \lim_{n\to\infty} X_2^{(n)}(t), \\
\|\mathcal{H}_3^{(n)}(t)\| \to 0. \quad &\implies \tilde{I}(t) - \tilde{I}(0) = \lim_{n\to\infty} \tilde{I}^{(n)}(t), \\
\|\mathcal{H}_4^{(n)}(t)\| \to 0. \quad &\implies \tilde{N}(t) - \tilde{N}(0) = \lim_{n\to\infty} \tilde{N}^{(n)}(t), \\
\|\mathcal{H}_5^{(n)}(t)\| \to 0. \quad &\implies Y(t) - Y(0) = \lim_{n\to\infty} Y^{(n)}(t).
\end{aligned} \tag{56}$$

This proves that the solution to the given system exists.

To prove that the solution is unique, let us assume that X_1', X_2', $\tilde{I}'$, $\tilde{N}'$, Y' be another set of solutions of the system (7)-(11). Then from (32)

$$\begin{aligned}
& X_1(t) - X_1'(t) = \int_0^t (\mathcal{K}_1(\tau, X_1) - \mathcal{K}_1(\tau, X_1'))d\tau \\
\implies & \|X_1(t) - X_1'(t)\| \leq \hat{k_1} t \|X_1(t) - X_1'(t)\| \\
\implies & \|X_1(t) - X_1'(t)\| = 0 \quad \text{since } \hat{k_1} t < 1 \\
\implies & X_1(t) = X_1'(t).
\end{aligned} \tag{57}$$

Uniqueness can be proved for the other variables $X_2, \tilde{I}, \tilde{N}, Y$ in the similar way. □

4.2 Stability Analysis

Since the system of equations is a model of the physical behavior of the simulation's objects, the stability of the system of differential equations is defined as the physical stability of the system. In the model $(17) - (21)$, defining the functions as follows

$$\mathfrak{f}_1 = -\hat{k_1} X_1, \tag{58}$$

$$\mathfrak{f}_2 = \hat{k_1} X_1, \tag{59}$$

$$\mathfrak{f}_3 = \hat{v_1} X_1 - \hat{r_1} X_2 \tilde{I}, \tag{60}$$

$$\mathfrak{f}_4 = k_2 \left({}_0^C D_t^\alpha\right) X_2 - \hat{r_2} \left({}_0^C D_t^\alpha\right) Y\tilde{N}, \tag{61}$$

$$\mathfrak{f}_5 = \hat{k_3} \left(\frac{\tilde{\rho}}{\tilde{\rho} + \tilde{I}^\sigma}\right) \tilde{N}. \tag{62}$$

The critical points will be obtained for $\mathfrak{f}_i$=0, $i = 1, 2, 3, 4, 5$.

$$\mathfrak{f}_1 = -\hat{k_1} X_1 = 0 \implies X_1 = 0$$

Since, $X_1 + X_2 = K$, we have $X_2 = K$. Now,

$$\mathfrak{f}_3 = \hat{v_1} X_1 - \hat{r_1} X_2 \tilde{I} = 0 \quad \implies \hat{v_1} X_1 - \hat{r_1} K \tilde{I} = 0 \quad \implies \tilde{I} = 0.$$

Also,

$$\mathfrak{f}_5 = \hat{k_3} \left(\frac{\tilde{\rho}}{\tilde{\rho} + \tilde{I}^\sigma}\right) \tilde{N} = 0 \quad \implies \tilde{N} = 0.$$

$$\mathfrak{f}_4 = k_2\hat{k_1}X_1 - \hat{r_2}\ ({}_0^C D_t^\alpha\ Y)\tilde{N} = 0 \quad \implies \hat{r_2}\ ({}_0^C D_t^\alpha\ Y)\tilde{N} = 0.$$

${}_0^C D_t^\alpha\ Y$ may or may not be zero. Hence, the system has infinitely many critical points $(X_1, X_2, \tilde{I}, \tilde{N}, Y) = (0, K, 0, 0, Y)$.
Now, we will check whether the given system is stable or unstable at the critical points. So, for this, we will find the Jacobian matrix.
The general form of the Jacobian matrix for the given system of bone mineralization will be:

$$J = \frac{\partial(\mathfrak{f}_1, \mathfrak{f}_2, \mathfrak{f}_3, \mathfrak{f}_4, \mathfrak{f}_5)}{\partial(X_1, X_2, \tilde{I}, \tilde{N}, Y)} = \begin{bmatrix} \frac{\partial \mathfrak{f}_1}{\partial X_1} & \frac{\partial \mathfrak{f}_1}{\partial X_2} & \frac{\partial \mathfrak{f}_1}{\partial \tilde{I}} & \frac{\partial \mathfrak{f}_1}{\partial \tilde{N}} & \frac{\partial \mathfrak{f}_1}{\partial Y} \\ \frac{\partial \mathfrak{f}_2}{\partial X_1} & \frac{\partial \mathfrak{f}_2}{\partial X_2} & \frac{\partial \mathfrak{f}_2}{\partial \tilde{I}} & \frac{\partial \mathfrak{f}_2}{\partial \tilde{N}} & \frac{\partial \mathfrak{f}_2}{\partial Y} \\ \frac{\partial \mathfrak{f}_3}{\partial X_1} & \frac{\partial \mathfrak{f}_3}{\partial X_2} & \frac{\partial \mathfrak{f}_3}{\partial \tilde{I}} & \frac{\partial \mathfrak{f}_3}{\partial \tilde{N}} & \frac{\partial \mathfrak{f}_3}{\partial Y} \\ \frac{\partial \mathfrak{f}_4}{\partial X_1} & \frac{\partial \mathfrak{f}_4}{\partial X_2} & \frac{\partial \mathfrak{f}_4}{\partial \tilde{I}} & \frac{\partial \mathfrak{f}_4}{\partial \tilde{N}} & \frac{\partial \mathfrak{f}_4}{\partial Y} \\ \frac{\partial \mathfrak{f}_5}{\partial X_1} & \frac{\partial \mathfrak{f}_5}{\partial X_2} & \frac{\partial \mathfrak{f}_5}{\partial \tilde{I}} & \frac{\partial \mathfrak{f}_5}{\partial \tilde{N}} & \frac{\partial \mathfrak{f}_5}{\partial Y} \end{bmatrix}. \tag{63}$$

Substituting for $\mathfrak{f}_i,\ i = 1, 2, 3, 4, 5$ in the matrix, we get the following Jacobian Matrix:

$$\begin{bmatrix} -\hat{k_1} & 0 & 0 & 0 & 0 \\ \hat{k_1} & 0 & 0 & 0 & 0 \\ \hat{v_1} & -\hat{r_1}\tilde{I} & 0 & 0 & 0 \\ \hat{k_1}k_2 & 0 & 0 & 0 & 0 \\ 0 & 0 & 0 & \frac{\hat{k_3}\tilde{\rho}}{\tilde{\rho} + \tilde{I}^\sigma} & 0 \end{bmatrix}. \tag{64}$$

The eigen values corresponding to above matrix are $0, 0, 0, -\hat{k_1}, -\hat{k_1}\hat{r_1}$. Observing the eigenvalues, we can conclude that the system is *marginally stable* at the critical points $(0, K, 0, 0, Y)$, which occur after a short span of time period just after the start of the mineralization process. Thus, the mineralization will not suddenly explode and the system will always have bounded solution but no steady state output.

5 Simulation and discussion

The numerical simulation has been done using the Lagrange's two-step method . Applying Lagrange's two-step method for the Caputo fractional derivative [3, Eq.

2.89], we get the following numerical scheme for (23).

$$X_1(n+1) = X_1(1) + \frac{h^\alpha}{\Gamma(\alpha+2)} \times \left(\sum_{k=2}^{n} \left[(n-k+1)^\alpha (n-k+2+\alpha) - (n-k)^\alpha (n-k+2+2\alpha) \right] f\left(t(k), X_1(k)\right) - \sum_{k=2}^{n} \left[(n-k+1)^{\alpha+1} - (n-k)^\alpha (n-k+1+\alpha) \right] f(t(k-1), X_1(k-1)) \right) \tag{65}$$

Similarly, expression for other variables $X_2, \tilde{I}, \tilde{N}, Y$ can be obtained.
The values of the parameters are mentioned in Table 1 as provided in [11] and are used for the purpose of simulation. These values are relevant to the mineralization process in human bone and also agree with the theoretical analysis of human disorders of bone mineralization.

Table 1: Model parameters

Parameter	Description	Value
k_1	Collagen cross-linking rate	0.1/ day
k_2	Nucleator count per collagen molecule	1
k_3	rate of mineral formation of mineral	1000/day
r_1	rate of inhibitors degradation	2×10^{-7}/day
v_1	rate of production of inhibitors by osteoblasts	0.1 per day
r_2	nucleators covered by mineral	1.7×10^{-8}/mol
σ	Hill coefficient	10
ρ	Hill function parameter	10^{57}

The plots are created for different values of the order α of the Caputo fractional operator. In Figure 2, it is observed that raw collagen, which initially constituted 100 percent of the total collagen in the system, decreases with the passage of time as it gets converted into mature collagen. The figure explores the temporal change of concentration of raw collagen for different values of α and shows a similar pattern with integer order suggesting that the fractional order model is well-posed, effective, and precise.

Figure 3 explores the temporal change of mature collagen for different values of α. which leads to $70-80$ percent conversion in 20 days and complete maturation in $45-60$ days. Figure 4 depicts the impact of inhibitors for different values of α. Inhibitors were initially present in raw collagen frameworks for 10 days before being rapidly destroyed with the development of mature collagen.
Figure 5 depicts the impact of nucleators for different values of α with respect to time. As the process gets started and paces up nucleator distribution into the system is sluggish. Figure 6 depicts the impact of mineralization for different values of α and graph also shows the lag time which is required for mineralization which is approximately 10 days and mineralization then gradually increases with

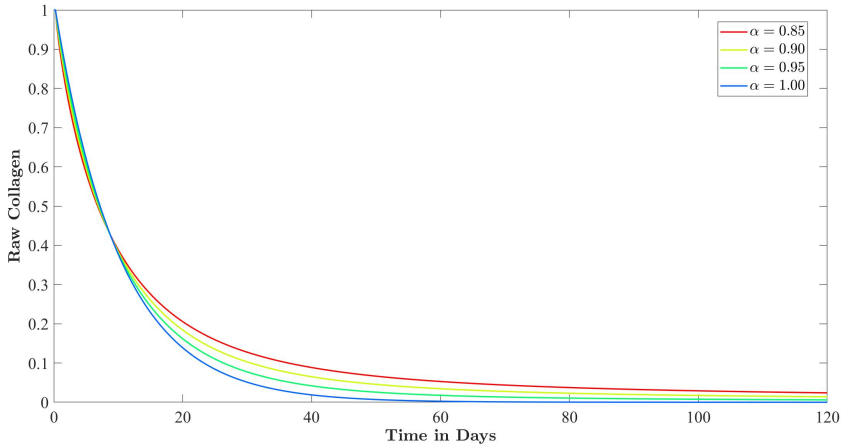

Figure 2: Variation in raw collagen with time for different value of $\alpha = 0.85, 0.90, 0.95, 1$.

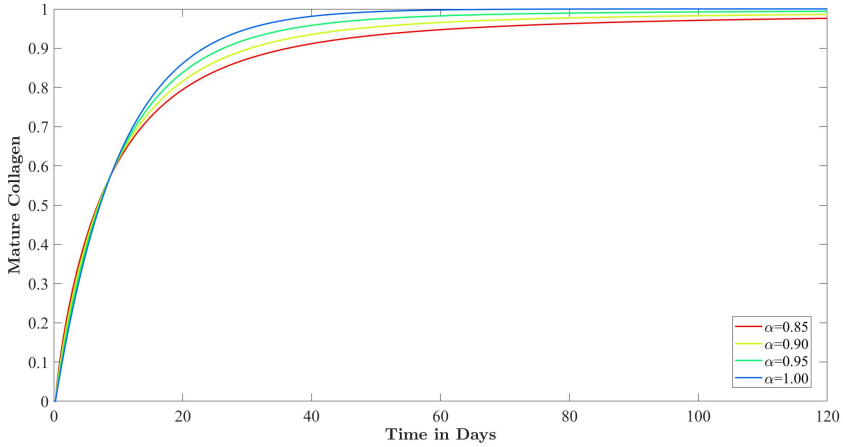

Figure 3: Variation in mature collagen with time for different values of $\alpha = 0.85, 0.90, 0.95, 1$.

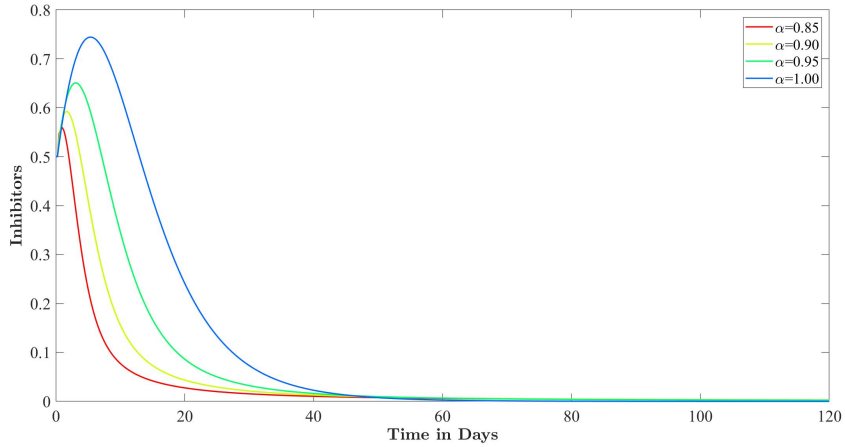

Figure 4: Variation in inhibitors with time for different value of $\alpha = 0.85, 0.90, 0.95, 1$.

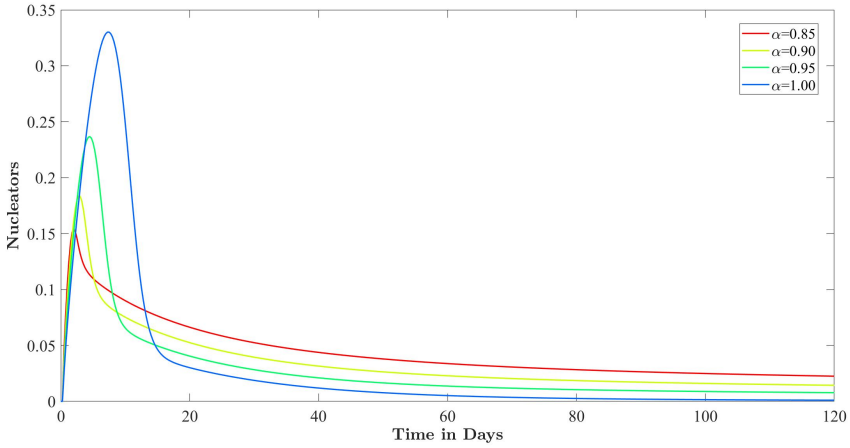

Figure 5: Variation in the nucleator quantity with time for different value of $\alpha = 0.85, 0.90, 0.95, 1$.

time. The normalized mineralization degree of 1 is attained in 100 days after the deposition of raw collagen takes place.

The graphs plotted provide the variation in the values of the variable when the values of α are changed. The value of the order α of fractional derivative can be chosen to fit the experimental data, if available.

Mineralization lag time is the amount of time required to start the mineralization process. In a healthy human bone, it takes approximately 10 days. After the lag was completed mineralization began quickly, followed by a steady decline in mineral formation whereas, the mineralization degree is the greatest amount of mineralization that may occur. The normalized mineralization degree of 1 (i.e., full mineralization) was obtained 100 days after the deposition of raw collagen. It is further observed from Figure 6 that, the fractional model can help in detecting any anomaly in mineralization at an early stage compared to the integer order model.

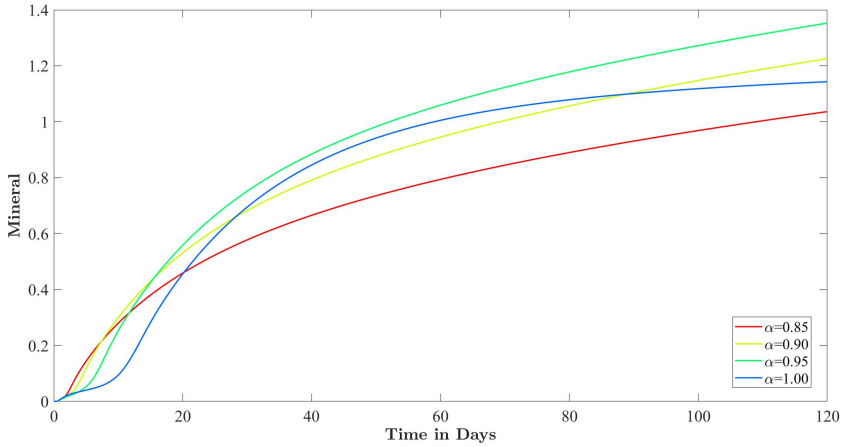

Figure 6: Variation in the quantity of the mineral with time for different value of $\alpha = 0.85, 0.90, 0.95, 1$.

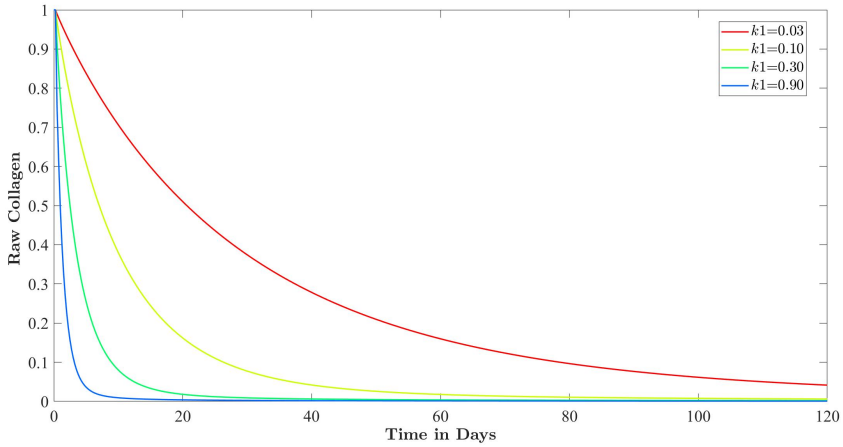

Figure 7: Impact of parameter k_1(collagen cross-linking rate) on raw collagen for fractional order $\alpha = 0.95$.

5.1 Sensitivity Analysis

Parameters play a vital role in the dynamics of any system. Here, the impact of the various parameters k_1, k_2, v_1, r_1, r_2 has been studied on the model variables.

In figure 7, sensitivity with respect to parameter k_1 has been explored which concludes that as the rate k_1 increases (i.e. collagen cross-linking rate) raw collagen takes less number of days to transform into mature collagen. Here, precisely the effect is observed by increasing the rate to threefold.
Figure 8 provides a visual representation of how the parameter k_1 impacts the dynamic of mature collagen. So, we find that for different values of k_1 mature collagen reach equilibrium at a different level, and in general the number of mature collagen increases with time, and at a certain time, it reaches equilibrium, With the increase in the value of k_1, the rate of formation of mature collagen increases. Figure 9 explores the impact of parameter v_1 on inhibitors. It highlights that as

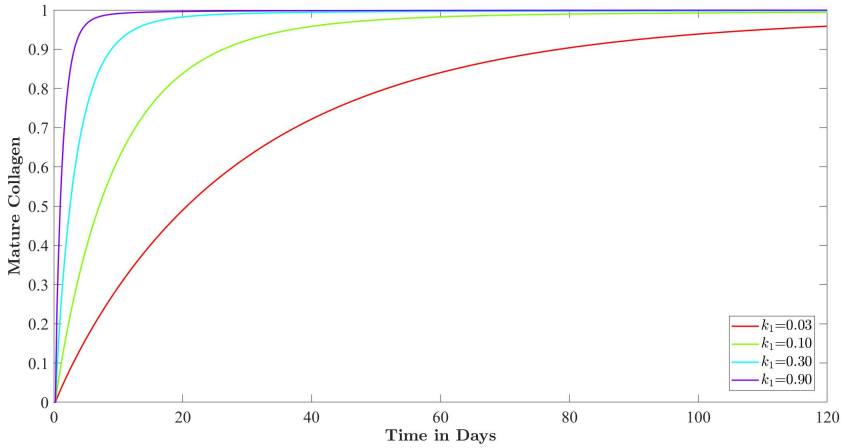

Figure 8: Impact of parameter k_1 (collagen cross-linking rate) on mature collagen for fractional order $\alpha = 0.95$.

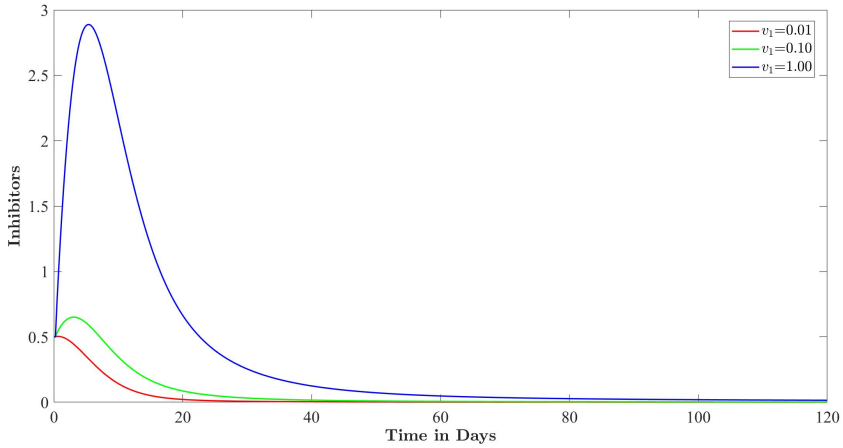

Figure 9: Impact of parameter v_1(rate at which inhibitors diffuse) on inhibitor for fractional order $\alpha = 0.95$.

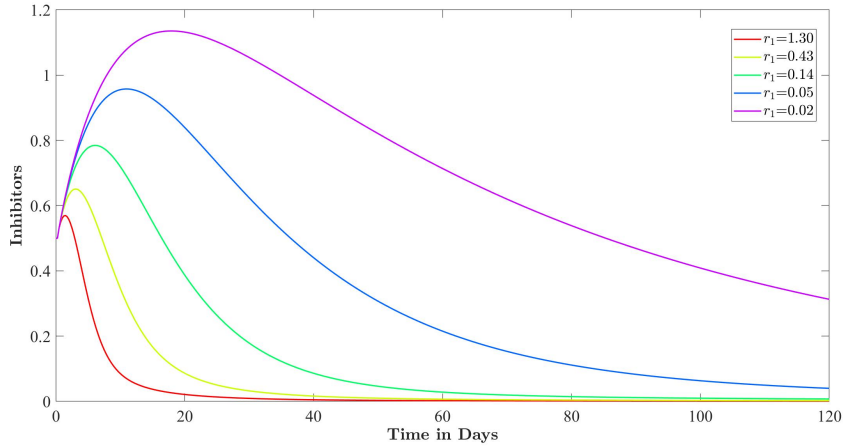

Figure 10: Impact of parameter r_1(rate of inhibitor removal) on inhibitor for fractional order $\alpha = 0.95$.

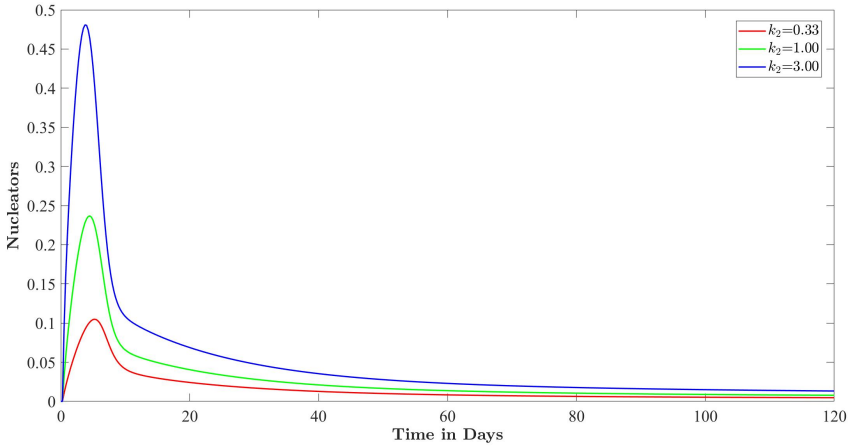

Figure 11: Impact of parameter k_2 on nucleators for fractional order $\alpha = 0.95$.

the parameter v_1 rises, more inhibitors will begin to diffuse into raw collagen. It is observable that there is a direct relationship between v_1 and inhibitor supply. There is a drastic increase in the concentration of active inhibitors for $v_1 = 1.0$.
Figure 10 explores the impact of parameter r_1 on inhibitors. It depicts that the inhibitor's concentration drops as the parameter r_1 increases because r_1 is the rate of removal of inhibitors and hence deterioration takes place largely.
Figure 11 explores the impact of parameter k_2 on nucleators. The nucleation process accelerates as the number of nucleators per mature collagen increases.
Figure 12 explores the impact of parameter r_2 on the nucleators. The number of nucleators grows as r_2 increases. As we increase the rate of r_2 three times we observe that the number of nucleators begins to diminish as they are masked by minerals.
Figure 13 explores the impact of parameter k_3 on mineralization. Mineralization is strongly linked to the parameter k_3; as the rate k_3 rises, so does mineralization. Changes in k_3 had a predictable effect on the pace of mineral production, but they also had a dramatic and proportionate effect on the degree of mineralization. A

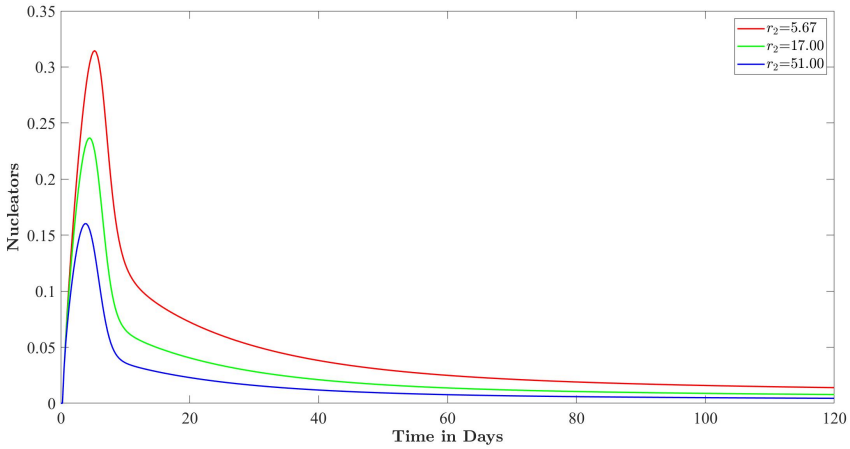

Figure 12: Impact of parameter r_2 on nucleators for fractional order $\alpha = 0.95$.

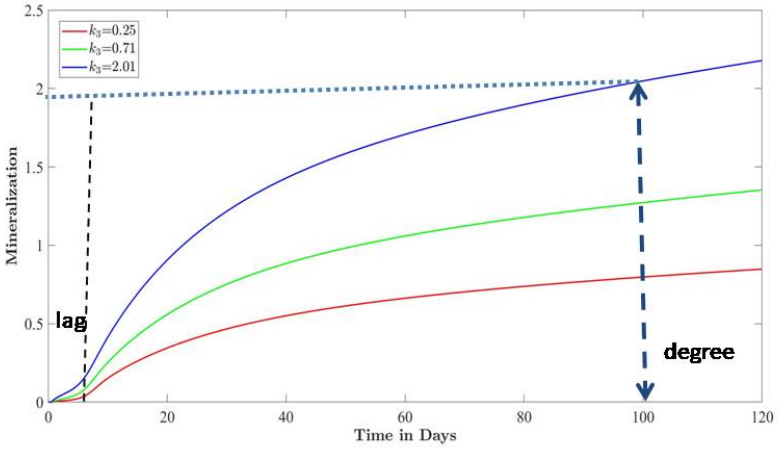

Figure 13: Impact of parameter k_3 on mineralization for fractional order $\alpha = 0.95$.

threefold drop in the rate of mineral formation k_3 resulted in a threefold decrease in mineralization degree.
The impact of all the parameters have been tested with raw collagen, mature collagen, inhibitors, nucleators, and mineralization but it is found that k_1 is the key parameter for raw and mature collagen whereas v_1 and r_1 are the key parameter for inhibitors k_2 and r_2 for nucleators and k_3 for mineralization respectively. Thus, it can be winded up with a graphical representation in the context of these parameters only. The CPU time taken for the computation in the code varies depending on the specific hardware and processing capabilities of the machine running the MATLAB code. The computation for the solution of this dynamical system took 1.9034 seconds of CPU time.

6 Conclusion

In this work, bone mineralization is studied with mathematical and numerical tools by considering bone at the micrometer level and thus provides vital support for the interpretation of experimental results. Furthermore, fixed point theory has been used to demonstrate the existence of a unique solution to the model. Also, the efficiency of the proposed scheme is drowned in terms of numerical simulations which are shown in graphs and it is clear that the proposed method is very accurate. Sensitivity analysis shows how the stiffness of bone depends on the inhibitor, nucleator, or raw or mature collagen and also to what extent bone does not get deformed under load. The use of fractional calculus helps in the early detection of any unusual patterns in the mineralization process. We can use this model to investigate more bone-related diseases by considering more assumptions. The obtained results will be useful for orthopedists to have a rough guess of the days needed for the mineralization of bone. Also, this model can be helpful for studying bone mineralization in other species too. A further important application is the study of how pharmaceutical therapies interfere with bone mineralization. The model can be modified to investigate the mineralization of additional calcified tissues, including the enamel, cementum, and dentin of teeth, etc.

Acknowledgement

The authors express their gratitude to the anonymous reviewers for their insightful recommendations aimed at raising the article's quality.

References

[1] Agarwal, R., Airan, P., and Midha, C. (2023). Mathematical analysis of the dynamics of bone mineralization. In Singh, H., editor, *Mathematical Methods in Medical and Biological Sciences*. Elsevier, In press.

[2] Agarwal, R., Purohit, S. D., and Kritika (2019). A mathematical fractional model with nonsingular kernel for thrombin receptor activation in calcium signalling. *Mathematical Methods in the Applied Sciences*, 42(18):7160–7171.

[3] Atangana, A. and İğret Araz, S. (2021). 2 - two-steps lagrange polynomial interpolation: numerical scheme. In Atangana, A. and İğret Araz, S., editors, *New Numerical Scheme with Newton Polynomial*, pages 11–112. Academic Press.

[4] Bozkurt, F., Yousef, A., Baleanu, D., and Alzabut, J. (2020). A mathematical model of the evolution and spread of pathogenic coronaviruses from natural host to human host. *Chaos, Solitons & Fractals*, 138:109931.

[5] Caputo, M. (1967). Linear models of dissipation whose Q is almost frequency independent—II. *Geophysical Journal International*, 13(5):529–539.

[6] Dey, P. (2020). Bone mineralisation. In Churchill, D. G., Sikirić, M. D., Čolović, B., and Milhofer, H. F., editors, *Contemporary Topics about Phosphorus in Biology and Materials*, chapter 3. IntechOpen, Rijeka.

[7] Diethelm, K. and Ford, N. J. (2002). Analysis of fractional differential equations. *Journal of Mathematical Analysis and Applications*, 265(2):229–248.

[8] Feng, Y.-Y., Yang, X.-J., and Liu, J.-G. (2020). On overall behavior of Maxwell mechanical model by the combined Caputo fractional derivative. *Chinese Journal of Physics*, 66:269–276.

[9] Friedman, A. (2007). Mathematical analysis and challenges arising from models of tumor growth. *Mathematical Models and Methods in Applied Sciences*, 17:1751–1772.

[10] Grodins, F. S., Buell, J., and Bart, A. J. (1967). Mathematical analysis and digital simulation of the respiratory control system. *Journal of Applied Physiology*, 22(2):260–276.

[11] Komarova, S. V., Safranek, L., Gopalakrishnan, J., Ou, M.-j. Y., McKee, M. D., Murshed, M., Rauch, F., and Zuhr, E. (2015). Mathematical model for bone mineralization. *Frontiers in cell and developmental biology*, 3:51.

[12] Kritika, Agarwal, R., and Purohit, S. D. (2021). A fractional model to study the diffusion of cytosolic calcium. In *Congress on Intelligent Systems: Proceedings of CIS 2020, Volume 2*, pages 585–597. Springer.

[13] Sene, N. (2022). Analytical solutions of a class of fluids models with the Caputo fractional derivative. *Fractal and Fractional*, 6(1):35.

[14] Shaikh, A. S., Shaikh, I. N., and Nisar, K. S. (2020). A mathematical model of COVID-19 using fractional derivative: outbreak in India with dynamics of transmission and control. *Advances in Difference Equations*, 2020(1):373.

[15] Singh, H. (2020). Analysis for fractional dynamics of Ebola virus model. *Chaos, Solitons & Fractals*, 138:109992.

[16] Singh, H. and Dutta, H. (2023). *Computational Methods for Biological Models*, volume 1109. Springer Nature.

[17] Singh, J., Gupta, A. D., and Baleanu, D. (2023a). Fractional dynamics and analysis of coupled Schrödinger-kdv equation with Caputo-Katugampola type memory. *Journal of Computational and Nonlinear Dynamics*, 18(9):091001.

[18] Singh, J., Gupta, A. D., and Kumar, D. (2023b). Computational analysis of the fractional Riccati differential equation with Prabhakar-type memory. *Mathematics*, 11(3):644.

[19] Singh, R., Mishra, J., and Gupta, V. K. (2023c). The dynamical analysis of a tumor growth model under the effect of fractal fractional Caputo-Fabrizio derivative. *International Journal of Mathematics and Computer in Engineering*, 1(1):115–126.

[20] ul Rehman, A., Singh, R., and Singh, J. (2022). Mathematical analysis of multi-compartmental malaria transmission model with reinfection. *Chaos, Solitons & Fractals*, 163:112527.

[21] Veeresha, P., Prakasha, D., and Baskonus, H. M. (2019). New numerical surfaces to the mathematical model of cancer chemotherapy effect in Caputo fractional derivatives. *Chaos: An Interdisciplinary Journal of Nonlinear Science*, 29(1):013119.

NUMERICAL STUDY OF TRIPLE DIFFUSIVE MHD RADIATIVE CASSON FLUID FLOW OVER A VERTICAL WALL WITH CHEMICAL REACTION & HEAT SOURCE/SINK IMPACTS

Atiya Ali[1] , Ruchika Mehta[1*], Renu Sharma[2] and Sushila[3]
[1,1*] Department of Mathematics and Statistics,
Manipal University Jaipur,
Jaipur-303007, Rajasthan, India
[2]Department of Physics, JECRC University,
Jaipur-303905, Rajasthan, India
[3]Department of Physics, Vivekananda Global University,
Jaipur-303012, Rajasthan,India
[1*]ruchika.mehta1981@gmail.com

Abstract

The present study focuses on the MHD Radiative Casson fluid flow with the effect of triple diffusivity over a vertical porous wall along with convective boundary conditions. The governing equations for detecting the nature of the fluid under the influence of solutal diffusivity and thermal conductivity in triple diffusive boundary layer flow are derived. Non-linear partial differential equations are reduced to ordinary differential equations via similarity transformation. The BVP4C method in MATLAB software is then used to solve them. The outcomes of several physical dimensionless parameters like permeability, convective parameter, buoyancy ratio parameter, Casson parameter and chemical reaction parameter with source/sink impacts established by graphics. Also, the impression of the local skin friction coefficient, Nusselt number, and local Sherwood number are presented through the tables.
Key words: MHD; Vertical wall; Casson fluid; Mixed Convection; Buoyancy; Triple diffusive; Brownian motion.

Table 1: Symbols List:

B_0	Magnetic induction	π	deformation rate Multiple factors
Sc_1	Schmidt parameter for concentration profile 1	π_c	Critical value of πfounded on non-Newtonian model
Sc_2	Schmidt parameter for concentration profile 2	e_{ij}	$(i,j)^{th}$ deformation rate factor
C_n	Concentration profile n,(n=1,2)	Nr	Radiation parameter
$C_{n\infty}$	Ambient concentration n,(n=1,2) as y tends to infinity	Ec	Eckert number
C_{nw}	reference concentration profile n,(n=1,2)	M	Magnetic field parameter
C_p	Specific heat capacity	Pr	Prandtl number
D_{B1}	Brownian diffusion coefficient for concentration profile 1	Re_x	Local Reynolds number
D_{B2}	Brownian diffusion coefficient for concentration profile 2	G_T	local temperature Grashof number
D_m	Mass diffusivity	G_{C1}	local Grashof number for concentration profile 1
K	parameter of Porous media	G_{C2}	local Grashof number for concentration profile 2
k	the porous medium Permeability	R_0	Chemical reaction coefficient
Sh_{x1}	Local Sherwood number for concentration profile 1	R_1	Chemical reaction parameter for concentration profile 1
Sh_{x2}	Local Sherwood number for concentration profile 2	R_2	Chemical reaction parameter for concentration profile 2
n	viscosity factor (Constant)	T	Temperature of the nanofluid within the boundary layer
Q_0	The heat Source/sink coefficient(dimensional)	T_W	Reference temperature
q	Radiative heat flux	T_∞	Ambient fluid Temperature
N_1	The Buoyancy force parameter for concentration profile 2	T_f	constant fluid temperature
N_2	The Buoyancy force parameter for concentration profile 2	Nu_x	Local Nusselt number
C_{fx}	The Skin friction coefficient	h_f	variable heat transfer

	Greek Symbols
θ	Dimensionless temperature
ϕ_n	Dimensionless concentration(n-1,2)
ν	viscosity Kinematic coefficient
α	Thermal Diffusivity
β	parameter of Casson Fluid
σ	The electrical conductivity
λ	The heat source/sink parameter
λ_1	Mixed convection parameter
η	Similarity variable
τ	Heat capacity ratio
τ_w	wall shear stress of the fluid
μ_B	Non-Newtonian plastic dynamic viscosity

u, v	components of Velocity along x- and y- directions, respectively
u_w	Reference velocity
$x.y$	Cartesian coordinates along and normal to the plate, respectively
Subscripts	
w	Surface conditions
∞	Conditions far away from the surfaces
Superscripts	
$'$	Differentiation with respect to η

1 Introduction

The non-Newtonian fluid is an essential part of our daily lives and is utilized in various applications. These fluids are used as drag-reducing agents, in printing technology, and as damping and braking devices. They are also used in personal protective equipment and food products. These versatile fluids have many uses and are an essential part of modern technology. In the Engineering sector, Industries and the Research area use different applications for studying mass and heat transfer known in various theoretical and practical aspects. Triple diffusive magnetohydrodynamic (MHD) fluid flow involves the study of fluid motion that includes three distinct types of diffusion processes: thermal diffusion, mass diffusion, and magnetic diffusion. This type of flow is encountered in various physical systems and finds applications in astrophysics, geophysics, and engineering. In the case of the study of anomalies in fatty acid, uses of convection of triple diffusive observed in the modelling of medical airing tools, triglycerides and surrounding several components such as saturated fat (high-density lipoproteins, low-density-Cholesterol lipoproteins), which hold different diffusivities. Many industries, technical applications and different sectors depend on MHD fluxes and MHD generators. Devi, & Devi, (2) conducted a numerical parametric study to compare the heat transfer characteristics of nano-fluid and hybrid nano-fluid. Through these observations, they found that the rate of heat transfer of hybrid nano-fluid (Cu–Al2O3/water) is higher than that of nano-fluid (Cu/water) when a magnetic field is present. Gireesha, B.J. et al. (4) studied heat and mass transfer in a three-dimensional, double-diffusive, hydromagnetic boundary layer flow of an electrically conducted Casson nano-fluid over a stretched surface. The researchers conducted this study to take into account a variety of factors to define convective boundaries, including unsynchronized thermal radiation, electromagnetic fields, buoyancy forces, thermophoresis, and Brownian motion. Hayat, T. et al. (7) explained the study of the effects of Soret and Dufour on the magnetohydrodynamic three-dimensional 3D flow of second-grade fluid in the existence of heat radiation and effects from Soret and Dufour. The second-grade fluid is taken to be electrically conductive by means of a uniform magnetic field. Isa, et al.(9) illustrated how the exponentially permeable fabric affects the Mixed convection magnetohydrodynamic (MHD) boundary layer flow for Casson fluid. Jena, S. et al.(13) noticed the MHD viscoelastic fluid flow subject to variable magnetic field implanted in a porous medium in the existence of chemical reaction and heat source or sink with soret and Dofour effect over a porous vertical stretching sheet. Patil, et al.(25) investigated numerically on steady boundary layer flow with triple diffusive and mixed convection past a vertical plate moving corresponding to the free stream in the upward direction. Patil, et al.(25) considered solutal components like sodium chloride and sucrose which are added to the flow stream from below with various concentration levels and investigated the thermal and species concentration fields. Raghunatha, et al.(27) investigated the weakly non-linear constancy of the convection of triple diffusive in a Maxwell fluid-saturated porous layer and found that depending on the alternative of the physical parameters the bifurcating

oscillatory solution is either supercritical or subcritical. In terms of time and area-averaged Nusselt numbers Heat and mass transfers are predictable. Manjappa, et al. (21) examined the impact of non-linear triple diffusive thermal radiation on the convective boundary layer flow of Casson nano-fluid along a flat plate. The free convection of triple diffusive in triangular, square and trapezoidal permeable chambers under an effect of interior volumetric heat production was examined by Khan, et al.(14). Here the chambers with the peak surface and pedestal surfaces are supposed to be adiabatic and impenetrable. Khan, et al.(15) analyzed the entropy for triple diffusive flow and due to various effects, they found that as compared to opposing flows the assisting flows entropy generation rates are higher. Simultaneously, these entropy generation rates are reduced with some other effect. Lund, et al.(19) examined numerically a study of magnetohydrodynamic (MHD) micro polar fluid flow in the presence of joule heating effect and viscous dissipation effects on a shrinking surface. Nawaz, and Awais, (23) discussed double diffusion of nanoparticles and solute presuming using adapting finite element method for the numerical effects of diffusion thermo and thermal diffusion. Rao, et al.(29) analyzed Dufour and thermophoresis effects in magnetohydrodynamic (MHD) three-dimensional fluid motion of Newtonian and non-Newtonian and calculated the mass & heat transfer above a stretching surface with Brownian motion. Umavathi, et al.(34) explored that when heat is exchanged from the external fluid with the plates, the flow does not depend on time on triple diffusive convection in a vertical channel. Farooq, et al.(3) experimented with the essential quantities modified in the streamwise direction in the Darcy-Forchheimer-Brinkman framework. Therefore, in non-Darcy porous media, the Casson nano-fluid steady flow over a flat plate is installed and developed non-similar boundary layer model for forced convection. Parvin, et al.(24) studied the numerical solutions of magnetohydrodynamics (MHD) casson fluid flow which considers the temperature and concentration gradients. Calculated the effects of nondimensional parameters on velocity, temperature and concentration profile via graph. Ramesh, K. et al.(28) discussed the essential flows of a Casson fluid in flat parallel plates and considered three primary situations such as the plate walls progressing in contradictory directions, the growth of inferior plate in the flow direction and others in a rigid location, the growth of the plates in the flow direction respectively. It was quite interesting to study the behaviour of the fluid in these different scenarios. Shaheen, N. et al.(31) analyzed electrically conducting two-dimensional radiative casson nanofluid flow through a deformable cylinder fixed in a porous medium with the impact of unpredictable characteristics compound with chemical reaction and Arrhenius activation energy. Shankar, S. et al.(32) studied the Casson fluid numerically with MHD through a vertical permeable wall with impacts of triple diffusive on a viscous flow with mixed convection. The fluids nature is examined by the triple diffusive boundary layer stream under the pressure of solutal diffusivity and thermal conductivity. Abbas, N. et al.(1) analyzed unsteady compressible Casson hybrid nanofluid flow over an erect stretching sheet with a stagnation point. Also studied the nonlinear radiation impact in this manner. Gnanaprasanna, K. and Singh, A. K.(5) explained that nanofluid with more shear thinning effects and rheological properties with variable viscosity on a vertical plate using the Prandtl number numerically. Hameed, N. et al.(6) examined the two-dimensional flow of Casson hybrid nanofluid flow on a non-linear extending surface using absorption and heat generation, Magnetic field and viscous dissipation. Irfan, and Khan,(8) examined the two-dimensional magnetohydrodynamic (MHD) casson fluid flow with shear thickening properties for a vertical stretching sheet in the presence of variable heat source and heat transfer characteristics. This paper also considers the velocity slip conditions and the effect of thermal radiation. Jain et al.(10) studied MHD laminar flow with heat, mass, magnetic flux, buoyancy ratio, thermal conduction, radiation, and convective boundary conditions for an electromagnetic fluid. Khashi'ie,

et al.(16) examined how viscous dissipation and MHD affect the transfer of heat radiative of fluid flow of Reiner-Philippoff across a nonlinearly contracting sheet. Lanjwani, et al.(18) studied the two-dimensional steady boundary layer flow, heat transfer, and mass transfer properties of micropolar nanofluids over surfaces that are exponentially expanding and contracting. Mehta et al.(22) studied the magnetohydrodynamics of a convective stagnation point flow with a vertical sheet embedded in a permeable medium. The effects of heat generation/absorption, radiation, and viscous dissipation were all taken into account. Prasad, et al.(26) illustrated the flow of nano-convective magnetohydrodynamic radiation over a cone. Xia, et al. (35) examined the flow of a micropolar hybrid nano-fluid in a 3D nonlinear mixed convective boundary layer under multiple slip conditions and microorganism presence across the thin surface.Jain et al.(11) conducted a study on the spinning fluid flow that occurs when a disk revolves with an inverse linear angular velocity in a magnetic unsteady Brownian motion of viscous nanofluids. Jangid et al.(12) modelled heat and mass transfer in fluid sheets of varying thickness, and stagnant sheets considering heat source/sink, permeability, magnetic fields, radiation, Joule heating, buoyancy force and chemical reactions.The belongings of radiation and velocity slip on MHD stream and melting warmth transmission of a micropolar liquid over an exponentially stretched sheet which is fixed in a porous medium with heat source/sink are accessibled by Kumar et al.(17) Makkar, et al. (20) experimented in the presence of convective conditions and gyrotactic microorganisms with MHD Casson fluid flow and calculated the influence of different fundamental fluid parameters. Reddy, et al. (32) analyzed the MHD casson nanofluid on variable radiative flow with a joule heating effect on a stretching sheet. Sneha, et al.(33) explained two-dimensional MHD incompressible flow which does not depend on time and in this term also calculated the heat transfer of the flow. In the fluid, nanoparticles were added to improve thermal efficiency and also applied a strong transverse magnetic field. As per the authors' conclusion and some research on triple diffusive Casson fluid flow with MHD and convective boundary conditions. Here the motive of this research is to find out the triple diffusive Casson fluid flow with MHD in the existence of radiation and chemical reaction parameters. These studies can also help in developing more accurate and predictive models for various scientific and engineering applications, contributing to advancements in multiple fields. This study helps to find Triple MHD Casson fluid flow with Radiation, source/sink parameter and chemical reaction impacts over a vertical wall with convective boundary conditions. It helps to develop new technologies and experiments. It also has further applications in the fields of security, medicine, engineering, bioscience and industrialized methods such as the refining of waste from plastic, the oil recovery process, polymer extrusion and transpiration cooling process and many more.

2 Problem Structure:

In a two-dimensional MHD Casson mixed convective fluid flow with radiation and joule heating effect, considered temperature T_∞ and free stream velocity U_∞ which is constant over a static porous plane surface. To solve the geometry problem, take the x-axis upwards along with the vertical plate, and the y-axis taken perpendicular to it. Also, consider the velocity components u and v to determine the solution to this problem accurately. [Figure1].
In the solution of two distinguished elements S_n (n=1,2) with concentration, C_n (n=1,2) is assumed. A constant fluid temperature T_f is maintained by the left side of the plate which gives a variable heat transfer h_f. Here ($T_f > T_\infty$) shows the supplementary flow corresponds to the shield being heated by the liquid, and ($T_f < T_\infty$) shows the opposing flow corresponds to the shield being cooled by the fluid.

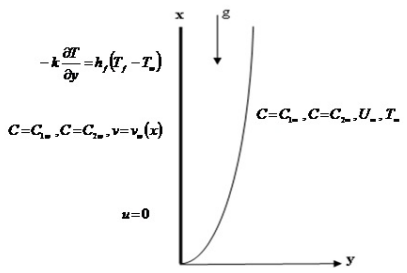

Figure 1: Physical Diagram

The buoyancy approximation is factored in and integrated with the flow region. On the surface, a moving magnetic field $B_0(x)$ is forced. The imposed magnetic field can't be compared to the induced one due to the low magnetic Reynolds number. Above all preliminaries, The fundamental governing PDE's equations are:

$$\frac{\partial u}{\partial x}+\frac{\partial v}{\partial y}=0 \tag{1}$$

$$\begin{aligned} u\frac{\partial u}{\partial x}+v\frac{\partial v}{\partial y} =&\nu(1+\frac{1}{\beta})\frac{\partial^2 u}{\partial y^2}-\frac{\sigma B^2(x)u}{\rho}+g_0[\beta_T(T-T_\infty) \\ &+\beta_{C1}(C_1-C_{1\infty})+\beta_{C1}(C_2-C_{2\infty})] \end{aligned} \tag{2}$$

$$u\frac{\partial T}{\partial x}+v\frac{\partial T}{\partial y}=\alpha\frac{\partial^2 T}{\partial y^2}+\frac{Q_0}{\rho c_p}(T-T_\infty)-\frac{1}{\rho c_p}\frac{\partial q_r}{\partial y} \tag{3}$$

$$u\frac{\partial C_1}{\partial x}+v\frac{\partial C}{\partial y}=D_{B1}\frac{\partial^2 C}{\partial y^2}-R_1(C_1-C_{1\infty}) \tag{4}$$

$$u\frac{\partial C_1}{\partial x}+v\frac{\partial C}{\partial y}=D_{B2}\frac{\partial^2 C}{\partial y^2}-R_2(C_2-C_{2\infty}) \tag{5}$$

The suitable Boundary conditions are:

$$\begin{cases} u=0, v=V_w(x), C_1=C_{1w}, C_2=C_{2w}, -K\frac{\partial T}{\partial y}=h_f(T_f-T_w) & \text{at} \quad y=0 \\ u\to U_\infty, v\to 0, T\to T_\infty, C_1\to C_{1\infty}, C_2\to C_{2\infty} & \text{at} \quad y\to\infty \end{cases} \tag{6}$$

Where, $V_w(x)<0$ and $V_w(x)>0$ represent suction and injection, respectively.

$$\tau_{ij}=\begin{cases} 2(\mu_B+\frac{\tau_y}{\sqrt{2\pi}})e_{ij} & \text{if} \quad \pi>\pi_c \\ 2(\mu_B+\frac{\tau_y}{\sqrt{2\pi}})e_{ij} & \text{if} \quad \pi<\pi_c \end{cases} \tag{7}$$

where τ_{ij} is known as share stress and the yield stress of non-Newtonian fluid is represented by τ_y $\pi=e_{ij}e_{ij}$

Using transformation Similarity in classify to express PDE's(1)-(6) in linear form

$$\begin{cases} u = U_\infty f'(\eta), v = -\frac{1}{2}\sqrt{\frac{U_\infty}{x}}\nu(f(\eta) - \eta f'(\eta)), \eta = y\sqrt{\frac{U_\infty}{(\nu x)}}, \\ \psi = \sqrt{(U_\infty \nu x)} f(\eta), \theta(\eta) = \frac{T - T_\infty}{T_f - T_\infty}, \phi_{1(\eta)} = \frac{C_1 - C_{1\infty}}{C_{1w} - C_{2\infty}}, \phi_{2(\eta)} = \frac{C_2 - C_{2\infty}}{C_{2w} - C_{2\infty}} \end{cases} \tag{8}$$

Where ψ is the stream function and u and v are the velocity components. Reducing the equations (1)-(6) in the form of non-dimensional with the help of equation (8)

$$(1 + \frac{1}{\beta})f''' + \frac{1}{2}ff'' - M^2 f' + \lambda\theta + N_1\phi_1 + N_2\phi_2 = 0 \tag{9}$$

$$(1 + \frac{Nr}{Pr})\theta'' + (\frac{Pr}{2})f\theta' + \lambda_1\theta = 0 \tag{10}$$

$$\phi_1{}'' + \tfrac{1}{2}Sc_1 f\phi_1{}' - R_1 Sc_1\phi_1 = 0 \tag{11}$$

$$\phi_2{}'' + \tfrac{1}{2}Sc_2 f\phi_2{}' - R_2 Sc_2\phi_2 = 0 \tag{12}$$

The boundary conditions are :

$$\begin{cases} f(\eta) = f_w, f'(\eta) = 0, \theta'(\eta) = -a[1 - \theta(\eta)], \phi_1(\eta) = 1, \phi_2(\eta) = 1; & \text{at} \quad \eta = 0 \\ f'(\eta) = 1, \theta(\eta) = 0, \phi_1(\eta) = 0, \phi_2(\eta) = 0; & \text{at} \quad \eta \to \infty \end{cases} \tag{13}$$

where η_∞ is the edge of the boundary layer;

Local Concentration Grashof number$(G_{C1}) = g_0\beta_{C1}(C_1 - C_{1\infty})x^3/\nu^2$
Local Concentration Grashof number$(G_{C2}) = g_0\beta_{C2}(C_2 - C_{2\infty})x^3/\nu^2$
Local Temperature Grashof number$(G_T) = g_0\beta_T(T_f - T_w)x^3/\nu^2$
Prandtl number$(Pr) = \frac{\nu}{\alpha}$
Buoyancy force parameter$(N_1) = \frac{D_{C1}}{{Re_X}^2}$
Buoyancy force parameter$(N_2) = \frac{D_{C2}}{{Re_X}^2}$
Schmidt number$(Sc_1) = \frac{\nu}{D_{B1}}$
Schmidt number$(Sc_2) = \frac{\nu}{D_{B2}}$
Mixed convection Parameter$(\lambda_1) = \frac{G_T}{{Re_X}^2}$
Magnetic parameter$(M) = B_0\sqrt{\frac{\sigma}{\rho U_\infty}}$

When $\lambda_1 > 0$ then the Mixed convection parameter corresponds to assisting flow and when $\lambda_1 < 0$ then it is opposing flow.The coefficient of Skin friction (C_{fx}), the Nusselt number(Nu_x), and the Sherwood numbers (Sh_{x1}),(Sh_{x2}), are defined as,

$$C_{fx} = 2{Re_x}^{-\frac{1}{2}}f''(0), \quad {Re_x}^{-\frac{1}{2}}Nu_x = \theta'(0),$$
$$Sh_{x1} = -{Re_x}^{-\frac{1}{2}}\phi_1{}'(0)), \quad Sh_{x2} = -{Re_x}^{-\frac{1}{2}}\phi_2{}'(0)), \tag{14}$$

3 Results and Discussion:

In this segment, results are calculated with the help of the above equation (9)-(12) and are solved with equation (9) using the BVP4C technique and the outcome are

discussed through graphs. This study numerically calculated the velocity f', temperature θ, concentrations ϕ_1&ϕ_2, skin friction as well as heat transfer for different non-dimensional parameters which are demonstrated in figs (2-18). For the verification of this study, current results are compared to the previous study shown in Table **??** with the Ref. papers (18), (27). The effect of Convective parameter(a) on the profile of velocity. From Fig. 2, It is noticed that if the value of the Convective parameter(a) increased, then the velocity profiles also increased. Also from the boundary condition it is perceived that if 'a' is raised to infinity then the outcomes of surface temperature get a higher value as well. In the profile of velocity, Temperature and concentrations if the suction injection effect is applied, then according to the suction ($f_w > 0$) the fluid is being removed from the flow, which creates a local pressure region in the flow field. elsewhere, in the injection ($f_w < 0$) fluid is added to the flow or the extra fluid is counted. Come to Fig.3 which states the temperature profile, it is easy to understand that when the amount of the fluid is less then the temperature mid between the particle of fluid flow is higher or it is stated that in the impact of suction ($f_w > 0$) creates a lower pressure region in the flow, which can lead to a decrease in temperature due to the decrease in overall energy content of the fluid. This is a result of the reduced enthalpy associated with the lower pressure. The temperature profile near the injection ($f_w < 0$) point can be influenced by the temperature of the injected fluid. If the injected fluid is warmer, it can lead to an increase in temperature in the vicinity of the injection point. The presence of heat sources and sinks can significantly influence fluid flow patterns and temperature distributions within a system. From Fig. 4 and 5, in the presence of the heat source/ sink parameter (λ), the velocity and temperature profile increases when the value of the heat source/sink parameter increases due to variation of thermal energies in the fluid flow. [h]

Table 2: Relative study of Heat Transfer rate at the sheet for numerous ranges of a When f_w= M= $\lambda = 0$ and $Pr = 10$ between Shankar S., et al[27] and the current work.

$constant$	$Ref.(18)$	$Ref.(27)$	$PresentWork$
a	$(-\theta')(0))$	$(-\theta')(0))$	$(-\theta')(0))$
0.8	0.381191	0.381201	0.381186
1	0.421344	0.421252	0.421338
5	0.635583	0.635601	0.635571
10	0.678721	0.678711	0.678707
20	0.702563	0.702601	0.702549

The mixed Convection Parameter (λ_1), inside the Boundary layer wall, increases the velocity as the buoyancy force is added ($\lambda_1 > 0$), the concentration profile decreases when the value of the mixed convection parameter increases which is presented in Fig.6 and Fig.7. The impact of the Magnetic field parameter (M) for the velocity profile is shown in Fig.8 which states that the velocity decreases as the magnetic field is increased. Lorentz force increases as increases the magnetic field, resulting in the resistance increasing as well and due to this the velocity decreases inside the boundary layer. Temperature profile and Concentration profile presented in Fig.9, 10 and 11 give the impact of the Magnetic field (M). The temperature and concentration profiles are observed in the existence of a Magnetic field (M), as the Magnetic field increases in the fluid flow the temperature is increased. The concentration profile also behaves the same as temperature with the magnetic field. Both the Temperature and Concentration profile are increased as increases with the Magnetic field (M). Fig.12 displayed the graph between the temperature profile and Radiation parameter, stating that with the effect of radiation in fluid flow, the

Table 3: Properties of Thermo physical of NaCl and Sucrose at $25°C$ from Shankar S., et al[27].

Components	*Morality*	*Weights%*	$\nu(\times 10^{-}6)$	$D_s(\times 10^{-}6)$	*Sc*	ΔC	*Nc*
	0.01	0.0584	1.003	1.545	649.19	0.0108	-2.48
Nacl	0.05	0.2922	1.007	1.502	670.43	0.03	-6.86
	0.1	0.05844	1.011	1.483	681.72	0.05	-11.43
	0.5	2.922	1.031	1.472	700.4	0.48	-91.51
	1.0	5.844	1.058	1.484	712.93	0.5	-114.3
	0.01	0.342	1.014	0.521	1946.25	0.0108	-1.36
Sucrose	0.05	1.7115	1.043	0.468	2226.4	0.03	-3.77
	0.1	3.423	1.08	0.451	2597.4	0.05	-6.28
	0.5	17.115	1.610	0.442	3635.95	0.4	-50.3
	1.0	34.23	3.535	0.466	7585.83	0.5	-62.87

Table 4: : The rate of coefficient of skin friction, coefficient of transfer of mass, and coefficient of transfer of heat for assorted non-dimensional parameters:

a	f_w	λ	λ_1	N_1	N_2	Nr	β	Pr	M	R_1	R_2	Sc_1	Sc_2	$f"(0)$	$-\theta'(0)$	$-\phi_1{}'(0)$	$-\phi_2{}'(0)$
1														0.941407	0.326776	0.42599	0.456568
2	0.1	0.1	1	1	1.5	0.1	0.5	2	1	0.1	0.1	2.5	3	0.968986	0.393397	0.432001	0.393395
3														0.98079	0.42336	0.434546	0.466287
	-0.2													1.03431	0.256811	0.225586	0.225586
1	-0.1	0.1	1	1	1.5	0.1	0.5	2	1	0.1	0.1	2.5	3	1.0036	0.277131	0.294636	0.294636
	0.1													0.941407	0.326776	0.42599	0.456568
	0.2													0.910529	0.35146	0.500845	0.54919
		0.2												0.955528	0.28894	0.4299	0.460984
1	0.1	0.3	1	1	1.5	0.1	0.5	2	1	0.1	0.1	2.5	3	0.880178	0.37584	0.581348	0.6492
		0.5												1.02367	0.111128	0.448566	0.481968
			2											1.07854	0.336191	0.454996	0.489426
1	0.1	0.1	3	1	1.5	0.1	0.5	2	1	0.1	0.1	2.5	3	1.20887	0.344437	0.480658	0.518284
			4											1.3335	0.351762	0.50368	0.544025
				2										1.4568	0.340277	0.467695	0.503785
1	0.1	0.1	1	2.5	1.5	0.1	0.5	2	1	0.1	0.1	2.5	3	1.24404	0.346181	0.486147	0.52452
				3										1.34026	0.351635	0.50332	0.543742
					2									1.04101	0.33333	0.446169	0.47952
1	0.1	0.1	1	1	2.5	0.1	0.5	2	1	0.1	0.1	2.5	3	1.13785	0.339313	0.46471	0.500502
					3									1.23229	0.344812	0.481884	0.519855
						0.5								0.939397	0.332216	0.425434	0.455939
1	0.1	0.1	1	1	1.5	2.5	0.5	2	1	0.1	0.1	2.5	3	0.934938	0.344333	0.4242	0.454545
						7								0.932304	0.351524	0.423472	0.453721
							1							1.18766	0.337913	0.460554	0.496715
1	0.1	0.1	1	1	1.5	0.1	1.5	2	1	0.1	0.1	2.5	3	1.32315	0.343131	0.476998	0.515822
							2							1.40955	0.346187	0.486713	0.527118
								5						0.890574	0.438856	0.410308	0.438856
1	0.1	0.1	1	1	1.5	0.1	0.5	7	1	0.1	0.1	2.5	3	0.874273	0.487666	0.405927	0.433851
								10						0.858763	0.537411	0.402169	0.429533
									2					0.686251	0.283281	0.293155	0.304612
1	0.1	0.1	1	1	1.5	0.1	0.5	2	2.5	0.1	0.1	2.5	3	0.598314	0.238594	0.238594	0.26554
									3					0.529289	0.182999	0.1943327	0.251155
										0.1				0.965534	0.329515	0.193649	0.466009
1	0.1	0.1	1	1	1.5	0.1	0.5	2	1	0.2	0.1	2.5	3	0.999693	0.333354	0.108434	0.479209
										0.3				0.941407	0.326776	0.42599	0.456568
											0			0.913539	0.323714	0..41661	0.665877
1	0.1	0.1	1	1	1.5	0.1	0.5	2	1	0.1	0.1	2.5	3	0.941407	0.326776	0.42599	0.456568
											0.2			0.978782	0.330841	0.438473	0.199103
												3		0.933673	0.335694	0.452877	0.452877
1	0.1	0.1	1	1	1.5	0.1	0.5	2	1	0.1	0.1	5	3	0.910704	0.322609	0.442281	0.457293
												7		0.895246	0.320677	0.435594	0.62798
													4	0.922117	0.324165	0.417999	0.503224
1	0.1	0.1	1	1	1.5	0.1	0.5	2	1	0.1	0.1	2.5	5	0.906819	0.322148	0.411826	0.545151
													6	0.894242	0.320534	0.406893	0.583771

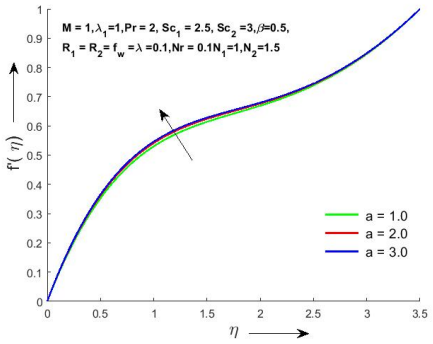

Figure 2: Change in $f'(\eta)$ with assorted values of a(Convective parameter)

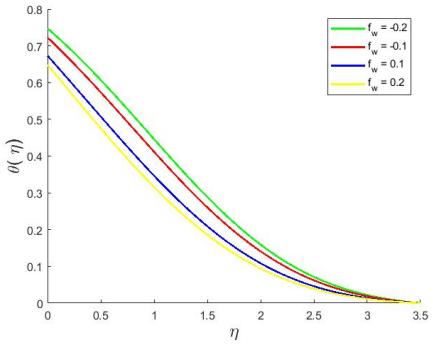

Figure 3: Change in $\theta(\eta)$ with various values of f_w(Injection/Suction Parameter)

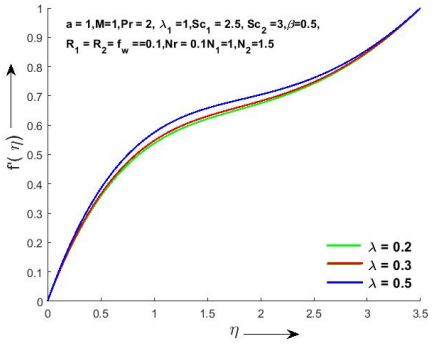

Figure 4: Change in $f'(\eta)$ with assorted values of λ(Heat Source/sink Parameter)

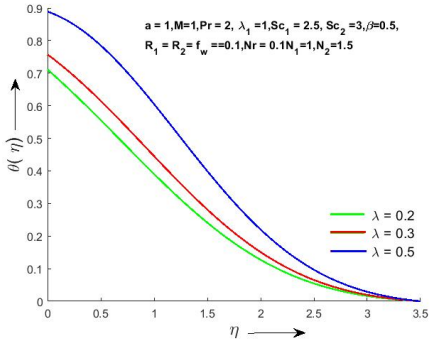

Figure 5: Change in $\theta(\eta)$ with various values of λ(Heat Source/sink Parameter)

temperature decreases. It is noticed that chemical reaction parameters R_1 and R_2 affect the density of fluid flow, which in turn can impact buoyancy forces, pressure gradients, and fluid flow velocity. These changes are particularly relevant in combustion processes, where chemical reactions can release energy and result in changes in temperature, density, and velocity. In Fig.13 to 16 observed that the velocity and concentration profiles increase as R_1 and R_2 increase. Concentration profile ϕ_1 has been taken for R_1, while concentration profile ϕ_2 has been taken for R_2. Based on the earlier study, a higher Schmidt number impacts diffusion and leads to thicker concentration boundary layers, slower mass transport, and potentially different mixing characteristics. Looking at the data presented in Fig.17 and Fig.18, it appears that there are various values of the Schmidt numbers Sc_1 and Sc_1 that impact velocity profiles. Specifically, if the Schmidt number increases, all profiles of velocities decrease.

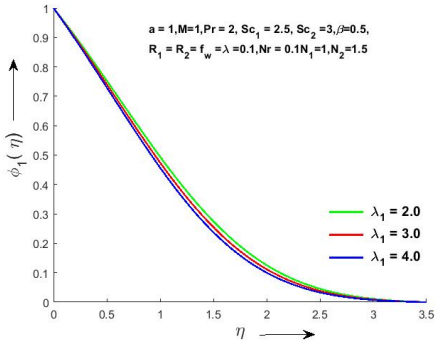

Figure 6: Change in $\phi_1(\eta)$ with assorted values of λ_1(Convection Parameter)

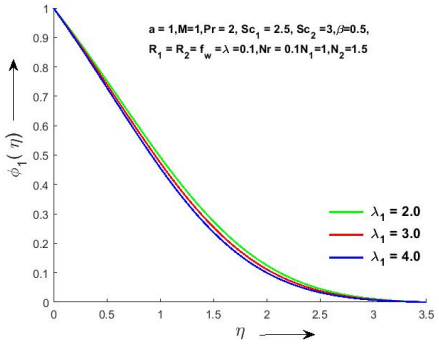

Figure 7: Change in $\phi_1(\eta)$ with assorted values of λ_1(Convection Parameter)

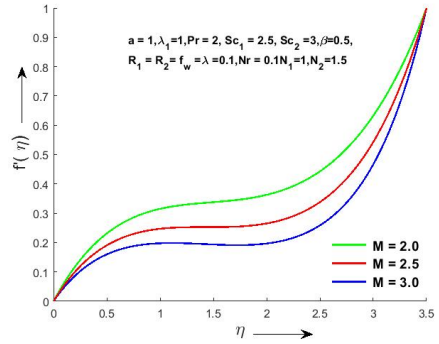

Figure 8: Change in $f'(\eta)$ with assorted values of M(Magnetic Field)

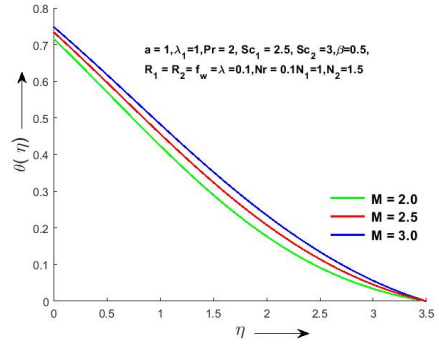

Figure 9: Change in $\theta(\eta)$ with assorted values of M(Magnetic Field)

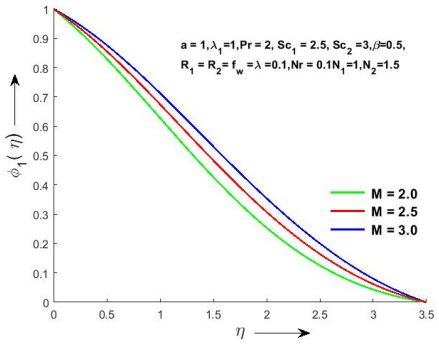

Figure 10: Change in $\phi_1(\eta)$ with assorted values of M(Magnetic Field)

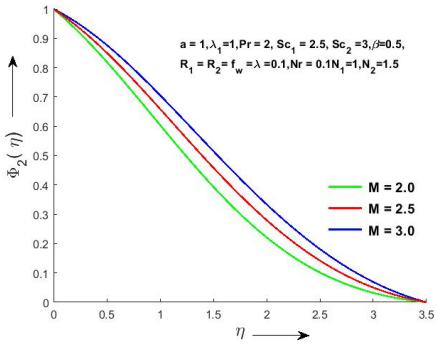

Figure 11: Change in $\phi_2(\eta)$ with assorted values of M(Magnetic Field)

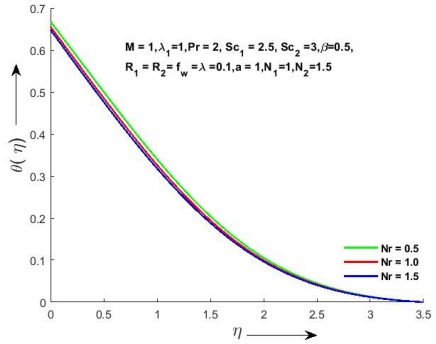

Figure 12: Change in $\theta(\eta)$ with assorted values of Nr(Radiation Parameter)

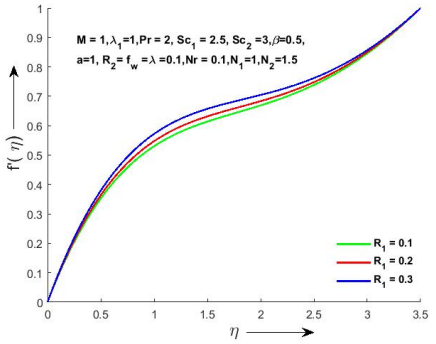

Figure 13: Change in $f'(\eta)$ with assorted values of R_1(Parameter of Chemical Reaction)

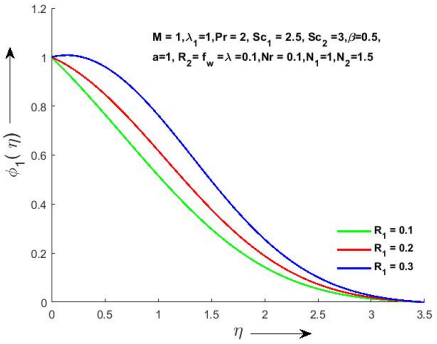

Figure 14: Change in $\phi_1(\eta)$ with assorted values of R_1(Parameter of Chemical Reaction)

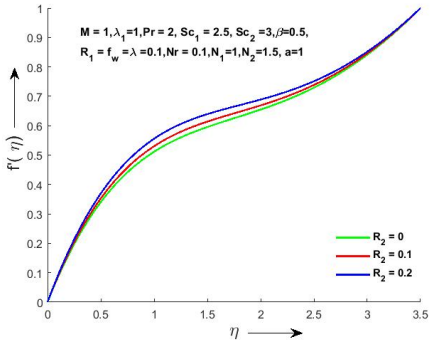

Figure 15: Change in $f'(\eta)$ with assorted values of R_2(Parameter of Chemical Reaction)

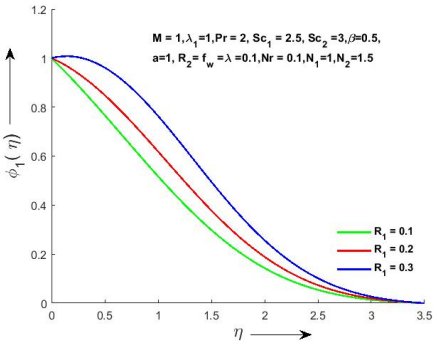

Figure 16: Change in $\phi_1(\eta)$ with assorted values of R_1(Parameter of Chemical Reaction)

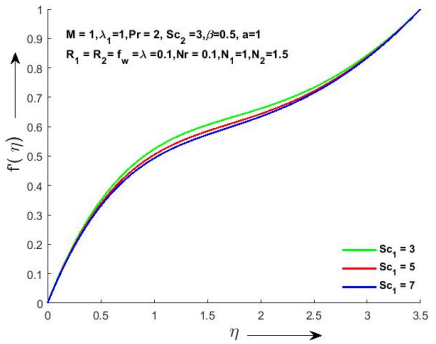

Figure 17: Change in $f'(\eta)$ with assorted values of Sc_1(Schmidt number)

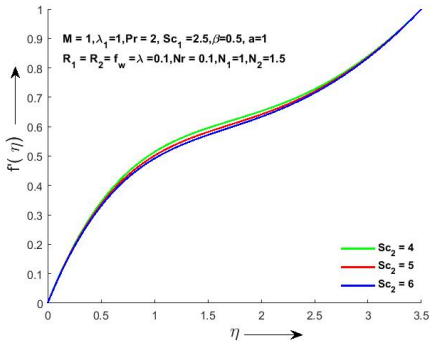

Figure 18: Change in $f'(\eta)$ with assorted values of Sc_2(Schmidt number)

4 Conclusion:

Triple diffusive MHD fluid flow with radiation can lead to valuable insights that can improve technology, resource utilization and our understanding of complex physical phenomena.This numerical study shows that a Casson fluid flows with triple MHD, in the existence of radiation, Chemical reaction and Heat source or sink. The presence of all parameters gets results numerically and graphically, and these are the subsequent results:

- The sucrose concentration boundary layer is thinner than NaCl. Due to the smaller size of NACl ions, the diffusion of NACl particles in the liquid is deeper than that of sucrose.
- The Temperature Profile goes down when Suction/Injection Parameter(f_w) upsurges.
- Boundary layer thickness is upsurged in both velocity and temperature profiles when heat source/sink parameter(λ) enlarges due to variation of thermal energies in the fluid flow,
- When we applied the Magnetic parameter (M), it enhanced the temperature profile and concentration profile but decreased the velocity by raising the value of M.
- The fluid temperature decays when the Radiation parameter (Nr) enlarges.
- The chemical reaction parameters R_1 andR_2 significantly affect the density of fluid flow, the velocity and concentration boost with rising R_1 and R_2.
- The velocity profile increases by the convection parameter 'a' increased.
- In the future, we will extend this flow model to convective heating scenarios including a variety of geometries such as Riga plates, cylindrical sheets, etc.

References

[1] Abbas, N., Shatanawi, W.,& Abodayeh, K. (2022). Computational analysis of MHD nonlinear radiation casson hybrid nanofluid flow at vertical stretching sheet. Symmetry, 14(7), 1494.

[2] Devi, S. S. U., & Devi, S. A. (2016). Numerical investigation of three-dimensional hybrid Cu–Al2O3/water nanofluid flow over a stretching sheet with effecting Lorentz force subject to Newtonian heating. Canadian Journal of Physics, 94(5), 490-496.

[3] Farooq, U., Hussain, M., Ijaz, M. A., Khan, W. A., & Farooq, F. B. (2021). Impact of non-similar modeling on Darcy-Forchheimer-Brinkman model for forced convection of Casson nano-fluid in non-Darcy porous media. International Communications in Heat and Mass Transfer, 125, 105312.

[4] Gireesha, B. J., Archana, M., Prasannakumara, B. C., Gorla, R. R., & Makinde, O. D. (2017). MHD three dimensional double diffusive flow of Casson nanofluid with buoyancy forces and nonlinear thermal radiation over a stretching surface. International Journal of Numerical Methods for Heat & Fluid Flow, 27(12), 2858-2878.

[5] Gnanaprasanna, K., & Singh, A. K. (2022). A numerical approach of forced convection of Casson nanofluid flow over a vertical plate with varying viscosity and thermal conductivity. Heat Transfer, 51(7), 6782-6800.

[6] Hameed, N., Noeiaghdam, S., Khan, W., Pimpunchat, B., Fernandez-Gamiz, U., Khan, M. S., & Rehman, A. (2022). Analytical analysis of the magnetic field, heat generation and absorption, viscous dissipation on couple stress casson hybrid nanofluid over a nonlinear stretching surface. Results in Engineering, 16, 100601.

[7] Hayat, T., Ullah, I., Muhammad, T., & Alsaedi, A. (2017). Radiative three-dimensional flow with Soret and Dufour effects. International Journal of Mechanical Sciences, 133, 829-837.

[8] Irfan, H. M., Khan, A. (2022). Numerical Investigation of Suction/Injuction on Triple Diffusive MHD Casson Fluid Flow over a Vertical Stretching Surface. International Journal of Advancements in Mathematics, 2(2), 105-122.

[9] Isa, S. S. P. M., Arifin, N. M., Nazar, R., Bachok, N., Ali, F. M., & Pop, I. (2017). MHD mixed convection boundary layer flow of a Casson fluid bounded by permeable shrinking sheet with exponential variation. Scientia Iranica, 24(2), 637-647.

[10] Jain, R., Mehta, R., Rathore, H., Singh, J. (2022). Analysis of Soret and Dufour Effect on MHD Fluid Flow Over a Slanted Stretching Sheet with Chemical Reaction, Heat Source and Radiation. In Advances in Mathematical Modelling, Applied Analysis and Computation: Proceedings of ICMMAAC 2021 (pp. 571-597). Singapore: Springer Nature Singapore.

[11] Jain, R., Mehta, R., Mehta, T., Singh, J., Baleanu, D. (2023). MHD flow and heat and mass transport investigation over a decelerating disk with ohmic heating and diffusive effect. Thermal Science, 27(Spec. issue 1), 141-149.

[12] Jangid, S., Mehta, R., Singh, J., Baleanu, D., Alshomrani, A. S. (2023). Heat and mass transport of hydromagnetic Williamson nanofluid passing through a permeable media across an extended sheet of varying thickness. Thermal Science, 27(Spec. issue 1), 129-140.

[13] Jena, S., Dash, G. C., & Mishra, S. R. (2018). Chemical reaction effect on MHD viscoelastic fluid flow over a vertical stretching sheet with heat source/sink. Ain Shams Engineering Journal, 9(4), 1205-1213.

[14] Khan, Z.H.; Khan, W.A.; Sheremet, M.A.(2020). Enhancement of heat and mass transfer rates through various porous cavities for triple convective-diffusive free convection. Energy, 201, https://doi.org/10.1016/j.energy.2020.117702.

[15] Khan, Z.H.; Khan, W.A.; Tang, J.; Sheremet, M.A. (2020). Entropy generation analysis of triple diffusive flow past a horizontal plate in porous medium. Chemical Engineering Science,228,https://doi.org/10.1016/j.ces.2020.115980.

[16] Khashi'ie, N. S., Waini, I., Kasim, A. R. M., Zainal, N. A., Ishak, A., & Pop, I. (2022). Magnetohydrodynamic and viscous dissipation effects on radiative heat transfer of non-Newtonian fluid flow past a nonlinearly shrinking sheet: Reiner–Philippoff model. Alexandria Engineering Journal, 61(10), 7605-7617.

[17] Kumar, R., Singh, J., Mehta, R., Kumar, D.,& Baleanu, D. (2023). Analysis of the impact of thermal radiation and velocity slip on the melting of magnetic hydrodynamic micropolar fluid-flow over an exponentially stretching sheet. Thermal Science, 27(Spec. issue 1), 311-322.

[18] Lanjwani, H. B., Chandio, M. S., Anwar, M. I., Al-Johani, A. S., Khan, I., & Alam, M. (2022). Triple Solutions with Stability Analysis of MHD Mixed Convection Flow of Micropolar Nanofluid with Radiation Effect. Journal of Nanomaterials, 2022.

[19] Lund, L. A., Omar, Z., Khan, I., Raza, J., Sherif, E. S. M., & Seikh, A. H. (2020). Magnetohydrodynamic (MHD) flow of micropolar fluid with effects of viscous dissipation and joule heating over an exponential shrinking sheet: triple solutions and stability analysis. Symmetry, 12(1), 142.

[20] Makkar, V., Poply, V., & Sharma, N. (2023). Three-dimensional magnetohydrodynamic non-Newtonian bioconvective nanofluid flow influenced by gyrotactic microorganisms over stretching sheet. Heat Transfer,vol 52,issue1 pg.548-562.

[21] Manjappa, A.; Jayanna, G.B.; Chandrappa, P.B. (2019). Triple diffusive flow of Casson nanofluid with buoyancy forces and non-linear thermal radiation over a horizontal plate. Archives of Thermodynamics, 40, 49-69,https://doi.org/10.24425/ather.2019.12828.

[22] Mehta, R., Kumar, R., Rathore, H., Singh, J. (2022). Joule heating effect on radiating MHD mixed convection stagnation point flow along vertical stretching sheet embedded in a permeable medium and heat generation/absorption. Heat Transfer, 51(8), 7369-7386.

[23] Nawaz, M.; Awais, M. (2020). Triple diffusion of species in fluid regime using tangent hyperbolic rheology. Journal of Thermal Analysis and Calorimetry, https://doi.org/10.1007/s10973-020-10026-0.

[24] Parvin, S., Balakrishnan, N., & Isa, S. S. P. M. (2021). MHD Casson fluid flow under the temperature and concentration gradients. Magnetohydrodynamics (0024-998X), 57(3).

[25] Patil, P.M.; Roy, M.; Roy, S.; Momoniat, E. (2018). Triple diffusive mixed convection along a vertically moving surface. International Journal of Heat and Mass Transfer, 117, 287-295, https://doi.org/10.1016/j.ijheatmasstransfer.2017.09.106.

[26] Prasad, J. R., Rao, I. V., Balamurugan, K. S., & Dharmaiah, G. (2022). Radiative Magnetohydrodynamic Flow Over a Vertical Cone Filled With Convective Nanofluid. Communications in Mathematics and Applications, 13(2), 449.

[27] Raghunatha, K.R.; Shivakumara, I.S.; Shankar, B.M. (2018). Weakly nonlinear stability analysis of triple diffusive convection in a Maxwell fluid saturated porous layer. Applied Mathematics and Mechanics, 39, 153-168, https://doi.org/10.1007/s10483-018-2298-6.

[28] Ramesh, K., Riaz, A., & Dar, Z. A. (2021). Simultaneous effects of MHD and Joule heating on the fundamental flows of a Casson liquid with slip boundaries. Propulsion and Power Research, 10(2), 118-129.

[29] Rao, P. S., Prakash, O., Mishra, S. R., & Sharma, R. P. (2020). Similarity solution of three-dimensional MHD radiative Casson nanofluid motion over a stretching surface with chemical and diffusion-thermo effects. Heat Transfer, 49(4), 1842-1862.

[30] Reddy, B. N., & Maddileti, P. (2023). Casson nanofluid and joule parameter effects on variable radiative flow of MHD stretching sheet. Partial Differential Equations in Applied Mathematics, 100487.

[31] Shaheen, N., Alshehri, H. M., Ramzan, M., Shah, Z., & Kumam, P. (2021). Soret and Dufour effects on a Casson nanofluid flow past a deformable cylinder with variable characteristics and Arrhenius activation energy. Scientific Reports, 11(1), 19282.

[32] Shankar, S., Ramakrishna, S. R., Gullapalli, N., & Samuel, N. (2021). Triple diffusive MHD Casson fluid flow over a vertical wall with convective boundary conditions. Biointerface Res Appl Chem, 11, 13765-13778.

[33] Sneha, K. N., Bognar, G., Mahabaleshwar, U. S., Singh, D. K., & Singh, O. P. (2023). Magnetohydrodynamics Effect of Marangoni Nano Boundary Layer Flow And Heat Transfer With CNT And Radiation. Journal of Magnetism and Magnetic Materials, 170721.

[34] Umavathi, J.C.; Ali, H.M.; Patil, S.L. (2020). Triple diffusive mixed convection flow in a duct using convective boundary conditions. Mathematical Methods in the Applied Sciences, 43, 9223-9244, https://doi.org/10.1002/mma.6617.

[35] Xia, W. F., Ahmad, S., Khan, M. N., Ahmad, H., Rehman, A., Baili, J., & Gia, T. N. (2022). Heat and mass transfer analysis of nonlinear mixed convective hybrid nanofluid flow with multiple slip boundary conditions. Case Studies in Thermal Engineering, 32, 101893.

FRACTIONAL CALCULUS OPERATORS OF THE GENERALIZED HURWITZ-LERCH ZETA FUNCTION

SHILPA KUMAWAT[‡] AND HEMLATA SAXENA[§]

ABSTRACT. In this paper, our aim is to establish certain generalized Marichev-Saigo-Maeda fractional integral and derivative formulas involving generalized p–extended Hurwitz-Lerch zeta function by using the Hadamard product (or the convolution) of two analytic functions. We then obtain their composition formulas by using fractional integral and derivative formulas and certain Integral transforms associated with Beta, Laplace and Whittaker transforms involving generalized p–extended Hurwitz-Lerch Zeta function.

1. INTRODUCTION

Fractional calculus is the field of mathematical analysis which deals with the investigation and applications of integrals and derivatives of arbitrary order. The study of fractional integrals and fractional derivatives has a long history, and they have many real-world applications due to their properties of interpolation between operators of integer order and its applications in various fields of science and engineering, such as fluid flow, rheology, diffusive transport akin to diffusion, electrical networks, and probability. This field has covered classical fractional operators such as Riemann-Liouville, Weyl, Caputo, Grnwald-Letnikov, etc. Also, especially in the last two decades, many new operators have appeared, often defined using integrals with special functions in the kernel, such as Atangana-Baleanu, Prabhakar, Marichev-Saigo-Maeda, and tempered, as well as their extended or multivariable forms. These have been intensively studied because they can also be useful in modelling and analysing real-world processes because of their different properties and behaviours, which are comparable to those of the classical operators[8, 22, 23, 24]. Special functions, such as the Hurwitz-Lerch Zeta function, Mittag-Leffler functions, hypergeometric functions, Foxs H-functions, Wright functions, Bessel and hyper-Bessel functions, etc., also have some more classical and fundamental connections with fractional calculus [13]. Some of them, such as the Mittag-Leffler function and its generalisations, appear naturally as solutions of fractional differential equations or fractional difference equations. Furthermore, many interesting relationships between different special functions may be discovered using the operators of fractional calculus. Because of their significance and potential for applications, fractional calculus operators (such as the Riemann-Liouville, Weyl, Liouville-Caputo, and other operators of

2010 *Mathematics Subject Classification.* Primary 26A33, 33B15; Secondary 33C05, 33C99, 44A20.

Key words and phrases. Hurwitz-Lerch Zeta Function; p–extended Hurwitz-Lerch Zeta Function; Fractional Calculus operators.

fractional integrationandfractional derivative) have undergone extensive development and study (for more information, seein [12], [18] and [26]).

We begin by recalling a general pair of fractional integral operators known as Marichev-Saigo-Maeda that have the third-order Appell'stwo-variable hypergeometric function $F_3(.)$ as their kernel (see for more information, [15, 20, 21]), which is defined by:

Definition 1. *Let $\varpi_1, \varpi_1', \nu_1, \nu_1', \xi \in \mathrm{C}$ and $x > 0$, then for $\Re(\xi) > 0$,*

$$\left(I_{0,x}^{\varpi_1,\varpi_1',\nu_1,\nu_1',\xi} f\right)(x) = \frac{x^{-\varpi_1}}{\Gamma(\xi)} \int_0^x (x-t)^{\xi-1}\, t^{-\varpi_1'} \times F_3\left(\varpi_1, \varpi_1', \nu_1, \nu_1'; \xi; 1-\frac{t}{x}, 1-\frac{x}{t}\right) f(t)\, \mathrm{d}t. \tag{1.1}$$

and

$$\left(I_{x,\infty}^{\varpi_1,\varpi_1',\nu_1,\nu_1',\xi} f\right)(x) = \frac{x^{-\varpi_1'}}{\Gamma(\xi)} \int_x^\infty (t-x)^{\xi-1}\, t^{-\varpi_1} \times F_3\left(\varpi_1, \varpi_1', \nu_1, \nu_1'; \xi; 1-\frac{x}{t}, 1-\frac{t}{x}\right) f(t)\, \mathrm{d}t. \tag{1.2}$$

Here, the Appell's hypergeometric function of two variables, [25], is denoted by $F_3(.)$.

Definition 2. *Let $\varpi_1, \varpi_1', \nu_1, \nu_1', \xi \in \mathrm{C}$ and $x > 0$, then for $\Re(\xi) > 0$,*

$$\begin{aligned}\left(D_{0,x}^{\varpi_1,\varpi_1',\nu_1,\nu_1',\xi} f\right)(x) &= \left(I_{0+}^{-\varpi_1',-\varpi_1,-\nu_1',-\nu_1,-\xi} f\right)(x) \\ &= \left(\frac{d}{dx}\right)^n \left(I_{0+}^{-\varpi_1',-\varpi_1,-\nu_1'+n,-\nu_1,-\xi+n} f\right)(x) \quad (n = [\Re(\xi)] + 1) \\ &= \frac{1}{\Gamma(n-\xi)} \left(\frac{d}{dx}\right)^n x^{\varpi_1'} \int_0^x (x-t)^{n-\xi-1}\, t^{\sigma} \\ &\qquad \times F_3\left(-\varpi_1', -\varpi_1, n-\nu_1', -\nu_1; n-\xi; 1-\frac{t}{x}, 1-\frac{x}{t}\right) f(t)\, \mathrm{d}t. \end{aligned} \tag{1.3}$$

and

$$\begin{aligned}\left(D_{x,\infty}^{\varpi_1,\varpi_1',\nu_1,\nu_1',\xi} f\right)(x) &= \left(I_{-}^{-\varpi_1',-\varpi_1,-\nu_1',-\nu_1,-\xi} f\right)(x) \\ &= \left(-\frac{d}{dx}\right)^n \left(I_{-}^{-\varpi_1',-\varpi_1,-\nu_1',-\nu_1'+n,-\xi+n} f\right)(x) \quad (n = [\Re(\xi)] + 1) \\ &= \frac{1}{\Gamma(n-\xi)} \left(-\frac{d}{dx}\right)^n x^{\varpi_1'} \int_x^\infty (t-x)^{n-\xi-1}\, t^{\sigma'} \\ &\qquad \times F_3\left(-\varpi_1', -\varpi_1, \nu_1', n-\nu_1; n-\xi; 1-\frac{x}{t}, 1-\frac{t}{x}\right) f(t)\, \mathrm{d}t. \end{aligned} \tag{1.4}$$

These operators include Riemann-Liouville, Erdélyi-Kober, and Saigo hypergeometric fractional calculus operators as special examples for various parameter choices (see for more information, [12], [18] and [26]). Early on, the p–extended Bessel function, p–modified Bessel function, p–extended Sturve function,and p–extended Mathieu series were used by a number of authors to create some intriguing generalized fractional formulas, (see, for details, [5, 10]).

The more generalized form of Hurwitz-Lerch zeta function has been considered very recently by Luo *et al.* [17] in the following form

$$\Phi_{\lambda,\vartheta;\nu}^{(\theta,\theta')}(z,s,a;p) := \sum_{n=0}^{\infty} \frac{(\lambda)_n}{n!} \frac{B^{(\theta,\theta')}(\vartheta+n,\, \nu-\vartheta\,;\, p)}{B(\vartheta,\, \nu-\vartheta)} \frac{z^n}{(n+a)^s} \tag{1.5}$$

$$\big(\Re(\theta)>0, \Re(\theta')>0, \Re(p)\geq 0;\ p, \lambda, \vartheta, s\in\mathbb{C};\, \nu,\, a\in\mathbb{C}\setminus\mathbb{Z}_0^-; |z|<1\big).$$

where $\mathrm{B}^{(\theta,\theta')}(x,y;p)$ denotes the generalized Beta function, that is introduced by Chaudhry *et al.* [2]

$$\mathrm{B}^{(\theta,\theta')}(x,y;p) = \mathrm{B}_p^{(\theta,\theta')}(x,y) = \int_0^1 t^{x-1}(1-t)^{y-1}\, {}_1F_1(\theta;\theta';-\frac{p}{t})\mathrm{d}t\,, \tag{1.6}$$

when $\min\{\Re(\theta)>0, \Re(\theta')>0, \Re(x), \Re(y)\}>0; \Re(p)\geq 0$. They also introduced p-extended of hypergeometric function as [3]:

$$F_p^{(\theta,\theta')}(a,b;c;z) = \sum_{n\geq 0} (a)_n \frac{\mathrm{B}^{(\theta,\theta')}(b+n,\, c-b\,;\, p)}{\mathrm{B}(b,\, c-b)} \frac{z^n}{n!} \qquad p\geqq 0; |z|<1;\, \Re(c)>\Re(b)>0\,, \tag{1.7}$$

Additionally provided in [4]are related properties, multiple integral representations, differentiation formulæ, Mellin transforms, recurrence relations, and summations.

The definition of the Hadamard product (or convolution) of two analytical functions, such as in[5], is necessary for the present study. If the R_f and R_g be the radii of convergence of the two power series

$$f(z) := \sum_{n=0}^{\infty} a_n z^n \ (|z|<R_f) \ \text{ and } \ g(z) := \sum_{n=0}^{\infty} b_n z^n \ (|z|<R_g),$$

respectively. Then the Hadamard product is the new emerged series defined by

$$(f\ *\ g)(z) := \sum_{n=0}^{\infty} a_n\, b_n z^n = (g\ *\ f)(z) \ (|z|<R) \tag{1.8}$$

where

$$R = \lim_{n\to\infty}\left|\frac{a_n\, b_n}{a_{n+1}\, b_{n+1}}\right| = \left(\lim_{n\to\infty}\left|\frac{a_n}{a_{n+1}}\right|\right).\left(\lim_{n\to\infty}\left|\frac{b_n}{b_{n+1}}\right|\right) = R_f\,.R_g,$$

so that, in general, we have $R\geqq R_f\cdot R_g$.

In the following study, we seek to broaden the compositions of the generalized fractional integral and differential operators (1.1), (1.2), (1.3) and (1.4) for the p–extended Hurwitz-Lerch zeta function (1.5) by using the Hadamard product (1.8) in terms of p–extended Hurwitz-Lerch zeta function and Wright hypergeometric function.

2. Fractional formulas of the p–extended Hurwitz-Lerch zeta function

The Wright hypergeometric function ${}_r\Psi_s(z)$ ($r,\, s\in\mathbb{N}_0$) having numerator and denominator parameters r and s, respectively, defined for $\zeta_1,\ldots,\,\zeta_r\in\mathbb{C}$ and $\kappa_1,\ldots,\,\kappa_s\in\mathbb{C}\setminus\mathbb{Z}_0^-$ by (see, for example, [11, 14, 18, 25]):

$${}_r\Psi_s\left[\begin{array}{l}(\zeta_1,A_1),\cdots,(\zeta_r,A_r);\\ (\kappa_1,B_1),\cdots,(\kappa_s,B_s);\end{array}\ z\right] = \sum_{n=0}^{\infty} \frac{\Gamma(\zeta_1+A_1n)\cdots\Gamma(\zeta_r+A_rn)}{\Gamma(\kappa_1+B_1n)\cdots\Gamma(\kappa_s+B_sn)}\ \frac{z^n}{n!} \tag{2.1}$$

$$\left(A_j \in \mathbb{R}^+ \ (j=1,\ldots,r);\ B_j \in \mathbb{R}^+ \ (j=1,\ldots,s);\ 1+\sum_{j=1}^{s} B_j - \sum_{j=1}^{r} A_j \geqq 0\right),$$

with

$$|z| < \nabla := \left(\prod_{j=1}^{r} A_j^{-A_j}\right) \cdot \left(\prod_{j=1}^{s} B_j^{B_j}\right).$$

Also, if we take $A_j = B_k = 1$ $(j = 1,\ldots,r; \quad k = 1,\ldots,s)$ in (2.1), reduces to the generalized hypergeometric function ${}_rF_s$ $(r,\ s \in \mathbb{N}_0)$ (see, *e.g.*, [25]):

$${}_rF_s\left[\begin{array}{c} \zeta_1,\ldots,\zeta_r; \\ \kappa_1,\ldots,\kappa_s; \end{array} z\right] = \frac{\Gamma(\kappa_1)\cdots\Gamma(\kappa_s)}{\Gamma(\zeta_1)\cdots\Gamma(\zeta_r)}\ {}_r\Psi_s\left[\begin{array}{c} (\zeta_1,1),\cdots,(\zeta_r,1); \\ (\kappa_1,1),\cdots,(\kappa_s,1); \end{array} z\right]. \tag{2.2}$$

In the context of our investigation, the image formulas or power functions below, referencing [1],are significant.

Lemma 1. *Let $\varpi_1, \varpi_1', \nu_1, \nu_1', \xi, \varrho \in \mathrm{C}$ and $x > 0$. The relation that follows is then:*

(a) *If $\Re(\xi) > 0$ and $\Re(\varrho) > \max\{0, \Re(\varpi_1 + \varpi_1' + \nu_1 - \xi), \Re(\varpi_1' - \nu_1')\}$, then*

$$\left(I_{0,x}^{\varpi_1,\varpi_1',\nu_1,\nu_1',\xi} t^{\varrho-1}\right)(x) = \frac{\Gamma(\varrho)\Gamma(\varrho+\xi-\varpi_1-\varpi_1'-\nu_1)\Gamma(\varrho+\nu_1'-\varpi_1')}{\Gamma(\varrho+\nu_1')\Gamma(\varrho+\xi-\varpi_1-\varpi_1')\Gamma(\varrho+\xi-\varpi_1'-\nu_1)} x^{\varrho+\xi-\varpi_1-\varpi_1'-1} \tag{2.3}$$

(b) *If $\Re(\xi) > 0$ and $\Re(\varrho) < 1 + \min\{\Re(-\nu_1), \Re(\varpi_1 + \varpi_1' - \xi), \Re(\varpi_1 + \nu_1' - \xi)\}$, then*

$$\left(I_{x,\infty}^{\varpi_1,\varpi_1',\nu_1,\nu_1',\xi} t^{\varrho-1}\right)(x) = \frac{\Gamma(1-\varrho-\nu_1)\Gamma(1-\varrho-\xi+\varpi_1+\varpi_1')\Gamma(1-\varrho-\xi+\varpi_1+\nu_1')}{\Gamma(1-\varrho)\Gamma(1-\varrho-\xi+\varpi_1+\varpi_1'+\nu_1')\Gamma(1-\varrho+\varpi_1-\nu_1)} x^{\varrho+\xi-\varpi_1-\varpi_1'-1}. \tag{2.4}$$

Lemma 2. *Let $\varpi_1, \varpi_1', \nu_1, \nu_1', \xi, \varrho \in \mathrm{C}$ and $x > 0$. The relation that follows is then:*

(a) *If $\Re(\xi) > 0$ and $\Re(\varrho) > \max\{0, \Re(\xi - \varpi_1 - \varpi_1' + \nu_1'), \Re(\nu_1 - \varpi_1)\}$, then*

$$\left(D_{0,x}^{\varpi_1,\varpi_1',\nu_1,\nu_1',\xi} t^{\varrho-1}\right)(x) = \frac{\Gamma(\varrho)\Gamma(\varrho-\xi+\varpi_1+\varpi_1'+\nu_1')\Gamma(\varrho-\nu_1+\varpi_1)}{\Gamma(\varrho-\nu_1)\Gamma(\varrho-\xi+\varpi_1+\varpi_1')\Gamma(\varrho-\xi+\varpi_1+\nu_1')} x^{\varrho-\xi+\varpi_1+\varpi_1'-1} \tag{2.5}$$

(b) *If $\Re(\xi) > 0$ and $\Re(\varrho) < 1 + \min\{\Re(\nu_1'), \Re(\xi - \varpi_1 - \varpi_1'), \Re(\xi - \varpi_1' - \nu_1)\}$, then*

$$\left(D_{x,\infty}^{\varpi_1,\varpi_1',\nu_1,\nu_1',\xi} t^{\varrho-1}\right)(x) = \frac{\Gamma(1-\varrho-\nu_1')\Gamma(1-\varrho+\xi-\varpi_1-\varpi_1')\Gamma(1-\varrho+\xi-\varpi_1'-\nu_1)}{\Gamma(1-\varrho)\Gamma(1-\varrho+\xi-\varpi_1-\varpi_1'-\nu)\Gamma(1-\varrho-\varpi_1'-\nu_1')} x^{\varrho-\xi+\varpi_1+\varpi_1'-1}. \tag{2.6}$$

We begin the key outcomes exposition with showing the composition formulae for generalized fractional operators (1.1), (1.2), (1.3) and (1.4) involving the p–extended Hurwitz-Lerch zeta function by making use of the Hadamard product (1.8) in terms of p–extended Hurwitz-Lerch zeta function (1.5) and Fox-Wright function (2.1).

Theorem 1. *Let $\varpi_1, \varpi_1', \nu_1, \nu_1', \xi, \varrho, p, \lambda, \vartheta, s \in \mathbb{C}$ with $\gamma \in \mathbb{R}^+$ and $\nu,\ a \in \mathbb{C}\backslash\mathbb{Z}_0^-$ such that $\Re(\xi) > 0$ and $\Re(\varrho) > \max\{0, \Re(\varpi_1 + \varpi_1' + \nu_1 - \xi), \Re(\varpi_1' - \nu_1')\}$ with $|t| < 1$. Then for $\Re(p) \geq 0$, the fractional integration formula shown below is valid:*

$$\left(I_{0,x}^{\varpi_1,\varpi_1',\nu_1,\nu_1',\xi}\left\{t^{\varrho-1}\ \Phi_{\lambda,\vartheta;\nu}^{(\theta,\theta')}(t^\gamma, s, a; p)\right\}\right)(x)$$

$$= x^{\varrho+\xi-\varpi_1-\varpi_1'-1}\,\Phi_{\lambda,\vartheta;\nu}^{(\theta,\theta')}(x^\gamma,s,a;p)$$
$$* \ {}_4\Psi_3\left[\begin{array}{c}(1,1),(\varrho,\gamma),(\varrho+\xi-\varpi_1-\varpi_1'-\nu_1,\gamma),(\varrho+\nu_1'-\varpi_1',\gamma);\\(\varrho+\nu_1',\gamma),(\varrho+\xi-\varpi_1-\varpi_1',\gamma),(\varrho+\xi-\varpi_1'-\nu_1,\gamma);\end{array}\ x^\gamma\right].$$

Proof. Using the relation (2.3) and the definitions (1.5) and (1.1),we can shift the order of integration. Thus, we obtain for $x>0$

$$\left(I_{0,x}^{\varpi_1,\varpi_1',\nu_1,\nu_1',\xi}\left\{t^{\varrho-1}\,\Phi_{\lambda,\vartheta;\nu}^{(\theta,\theta')}(t^\gamma,s,a;p)\right\}\right)(x)$$
$$=\sum_{k=0}^{\infty}\frac{(\lambda)_k\,\mathrm{B}^{(\theta,\theta')}(\vartheta+k,\,\nu-\vartheta\,;\,p)}{(k+a)^s\,\mathrm{B}(\vartheta,\,\nu-\vartheta)\,k!}\ \left(I_{0,x}^{\varpi_1,\varpi_1',\nu_1,\nu_1',\xi}\{t^{\varrho+\gamma k-1}\}\right)(x)$$
$$= x^{\varrho+\xi-\varpi_1-\varpi_1'-1}\sum_{k=0}^{\infty}\frac{(\lambda)_k\ \mathrm{B}(\vartheta+k,\,\nu-\vartheta\,;\,p)}{(k+a)^s\,\mathrm{B}(\vartheta,\,\nu-\vartheta)\,k!}$$
$$\times\frac{\Gamma(\varrho+\gamma k)\Gamma(\varrho+\xi-\varpi_1-\varpi_1'-\nu_1+\gamma k)\Gamma(\varrho+\nu_1'-\varpi_1'+\gamma k)}{\Gamma(\varrho+\nu_1'+\gamma k)\Gamma(\varrho+\xi-\varpi_1-\varpi_1'+\gamma k)\Gamma(\varrho+\xi-\varpi_1'-\nu_1+\gamma k)}x^{\gamma k}. \quad (2.7)$$

Subsequently,the necessary formula is obtained by utilizing the Hadamard product (1.8)in (2.7), which, in light of (1.5) and (2.1). □

Theorem 2. *Let $\varpi_1,\varpi_1',\nu_1,\nu_1',\xi,\varrho,p,\lambda,\vartheta,s\in\mathbb{C}$ with $\gamma\in\mathbb{R}^+$ and $\nu,\ a\in\mathbb{C}\backslash\mathbb{Z}_0^-$ such that $\Re(\xi)>0$ and $\Re(\varrho)<1+\min\{\Re(-\nu_1),\Re(\varpi_1+\varpi_1'-\xi),\Re(\varpi_1+\nu_1'-\xi)\}$ with $|1/t|<1$. Then for $\Re(p)\geq 0$, the fractional integration formula shown below is valid:*

$$\left(I_{x,\infty}^{\varpi_1,\varpi_1',\nu_1,\nu_1',\xi}\left\{t^{\varrho-1}\,\Phi_{\lambda,\vartheta;\nu}^{(\theta,\theta')}\left(\frac{1}{t^\gamma},s,a;p\right)\right\}\right)(x)$$
$$= x^{\varrho+\xi-\varpi_1-\varpi_1'-1}\,\Phi_{\lambda,\vartheta;\nu}^{(\theta,\theta')}\left(\frac{1}{x^\gamma},s,a;p\right)$$
$$* \ {}_4\Psi_3\left[\begin{array}{c}(1,1),(1-\varrho-\nu_1,\gamma),(1-\varrho-\xi+\varpi_1+\varpi_1',\gamma),(1-\varrho-\xi+\varpi_1+\nu_1',\gamma);\\(1-\varrho,\gamma),(1-\varrho-\xi+\varpi_1+\varpi_1'+\nu_1',\gamma),(1-\varrho+\varpi_1-\nu_1,\gamma);\end{array}\ \frac{1}{x^\gamma}\right].$$

Theorem 3. *Let $\varpi_1,\varpi_1',\nu_1,\nu_1',\xi,\varrho,p,\lambda,\vartheta,s\in\mathbb{C}$ with $\gamma\in\mathbb{R}^+$ and $\nu,\ a\in\mathbb{C}\backslash\mathbb{Z}_0^-$ such that $\Re(\xi)>0$ and $\Re(\varrho)>\max\{0,\Re(\xi-\varpi_1-\varpi_1'-\nu_1'),\Re(\nu_1-\varpi_1)\}$ with $|t|<1$. Then for $\Re(p)\geq 0$, the fractional integration formula shown below is valid:*

$$\left(D_{0,x}^{\varpi_1,\varpi_1',\nu_1,\nu_1',\xi}\left\{t^{\varrho-1}\,\Phi_{\lambda,\vartheta;\nu}^{(\theta,\theta')}(t^\gamma,s,a;p)\right\}\right)(x)$$
$$= x^{\varrho-\xi+\varpi_1+\varpi_1'-1}\,\Phi_{\lambda,\vartheta;\nu}^{(\theta,\theta')}(x^\gamma,s,a;p)$$
$$* \ {}_4\Psi_3\left[\begin{array}{c}(1,1),(\varrho,\gamma),(\varrho-\xi+\varpi_1+\varpi_1'+\nu_1',\gamma),(\varrho-\nu_1+\varpi_1,\gamma);\\(\varrho-\nu_1,\gamma),(\varrho-\xi+\varpi_1+\varpi_1',\gamma),(\varrho-\xi+\varpi_1+\nu_1',\gamma);\end{array}\ x^\gamma\right].$$

Proof. Using the relation (2.5), and the definitions (1.5), (1.3), we can shift the order of integration. Thus, we obtain for $x>0$

$$\left(D_{0,x}^{\varpi_1,\varpi_1',\nu_1,\nu_1',\xi}\left\{t^{\varrho-1}\,\Phi_{\lambda,\vartheta;\nu}^{(\theta,\theta')}(x^\gamma,s,a;p)\right\}\right)(x)$$

$$= \sum_{k=0}^{\infty} \frac{(\lambda)_k \, \mathrm{B}^{(\theta,\theta')}(\vartheta+k,\, \nu-\vartheta\,;\, p)}{(k+a)^s \, \mathrm{B}(\vartheta,\, \nu-\vartheta)\, k!} \left(D_{0,x}^{\varpi_1,\varpi_1',\nu_1,\nu_1',\xi} \{ t^{\varrho+\gamma k-1} \} \right)(x)$$

$$= x^{\varrho-\xi+\varpi_1+\varpi_1'-1} \sum_{k=0}^{\infty} \frac{(\lambda)_k \, \mathrm{B}(\vartheta+k,\, \nu-\vartheta\,;\, p)}{(k+a)^s \, \mathrm{B}(\vartheta,\, \nu-\vartheta)\, k!}$$

$$\times \frac{\Gamma(\varrho+\gamma k)\Gamma(\varrho-\xi+\varpi_1+\varpi_1'+\nu_1'+\gamma k)\Gamma(\varrho-\nu_1+\varpi_1+\gamma k)}{\Gamma(\varrho-\nu_1+\gamma k)\Gamma(\varrho-\xi+\varpi_1+\varpi_1'+\gamma k)\Gamma(\varrho-\xi+\varpi_1+\nu_1'+\gamma k)} x^{\gamma k}. \quad (2.8)$$

Subsequently,the necessary formula (1.3) is obtained by utilizing the Hadamard product (1.8) in (2.8), which in light of (1.5) and (2.1). □

Theorem 4. *Let* $\varpi_1, \varpi_1', \nu_1, \nu_1', \xi, \varrho, p, \lambda, \vartheta, s \in \mathbb{C}$ *with* $\gamma \in \mathbb{R}^+$ *and* $\nu,\, a \in \mathbb{C}\backslash\mathbb{Z}_0^-$ *such that* $Re(\xi) > 0$ *and* $Re(\varrho) < 1+\min\{Re(\nu_1'), Re(\xi-\varpi_1-\varpi_1', Re(\xi-\varpi_1'-\nu_1)\}$ *with* $|1/t| < 1$. *Then for* $\Re(p) \geq 0$, *the fractional integration formula shown below is valid:*

$$\left(D_{x,\infty}^{\varpi_1,\varpi_1',\nu_1,\nu_1',\xi} \left\{ t^{\varrho-1} \, \Phi_{\lambda,\vartheta;\nu}^{(\theta,\theta')} \left(\frac{1}{t^\gamma}, s, a; p \right) \right\} \right)(x)$$

$$= x^{\varrho-\xi+\varpi_1+\varpi_1'-1} \, \Phi_{\lambda,\vartheta;\nu}^{(\theta,\theta')} \left(\frac{1}{x^\gamma}, s, a; p \right)$$

$$* \; {}_4\Psi_3 \left[\begin{matrix} (1,1), (1-\varrho-\nu_1', \gamma), (1-\varrho+\xi-\varpi_1-\varpi_1', \gamma), (1-\varrho+\xi-\varpi_1'-\nu_1, \gamma); \\ (1-\varrho, \gamma), (1-\varrho+\xi-\varpi_1-\varpi_1'-\nu_1, \gamma), (1-\varrho-\varpi_1'-\nu_1', \gamma); \end{matrix} \frac{1}{x^\gamma} \right].$$

3. Certain integral transforms

With the aid of the findings from the previous section, we will give severalextremely intriguing theorems relating to the Beta, Laplace, and Whitaker transformations in this section. First, we would like to define these transformations for this.

Definition 3. *As is customary, the Euler-Beta transform* [19]*of the function* $f(z)$ *is set forth by*

$$\mathcal{B}\{f(z); a, b\} = \int_0^1 z^{a-1}(1-z)^{b-1} f(z)\, dz. \quad (3.1)$$

Definition 4. *As is customary, the Laplace transform (see,* e.g., [19]*) of the function* $f(z)$ *is set forth by*

$$L\{f(z); t\} = \int_0^\infty e^{-tz} f(z)\, dz. \quad (Re(t) > 0) \quad (3.2)$$

The following integral involving Whittaker function (see Mathai *et al.* [14, p. 79]):

$$\int_0^\infty t^{\rho-1} e^{-\frac{1}{2}at} \, W_{\kappa,\nu}(at)\, dt = a^{-\rho} \frac{\Gamma(\frac{1}{2} \pm \nu + \rho)}{\Gamma(1-\kappa+\rho)} \quad (Re(a) > 0,\; Re(\rho \pm \nu) > -\frac{1}{2}), \quad (3.3)$$

is significant to the subject at hand, where $W_{\kappa,\nu}$ is the Whittaker function [16, p. 334].

In this portion, the following captivating results in the form of theorems shall be demonstrated. These findings are put forward here without further justification because they follow directly from the definitions (3.1), (3.2), (3.3)and Theorems 1 to 4.

Theorem 5. *Let $\varpi_1, \varpi_1', \nu_1, \nu_1', \xi, \varrho, p, \lambda, \vartheta, s \in \mathbb{C}$ with $\gamma \in \mathbb{R}^+$ and ν, $a \in \mathbb{C}\backslash\mathbb{Z}_0^-$ such that $Re(\xi) > 0$ and $Re(\varrho) > \max\{0, Re(\varpi_1 + \varpi_1' + \nu_1 - \xi), Re(\varpi_1' - \nu_1')\}$ with $|t| < 1$. Then for $\Re(p) \geq 0$, the Beta-transform formula shown below is valid:*

$$B\left\{\left(I_{0,x}^{\varpi_1,\varpi_1',\nu_1,\nu_1',\xi}\left\{t^{\varrho-1}\,\Phi_{\lambda,\vartheta;\nu}^{(\theta,\theta')}((tz)^\gamma, s, a; p)\right\}\right)(x) : l, m\right\}$$
$$= x^{\varrho+\xi-\varpi_1-\varpi_1'-1}\,\Gamma(m)\,\Phi_{\lambda,\vartheta;\nu}^{(\theta,\theta')}(x^\gamma, s, a; p)$$
$$* \ {}_5\Psi_4\left[\begin{matrix}(1,1),(l,\gamma),(\varrho,\gamma),(\varrho+\xi-\varpi_1-\varpi_1'-\nu_1,\gamma),(\varrho+\nu_1'-\varpi_1',\gamma);\\(l+m,\gamma),(\varrho+\nu_1',\gamma),(\varrho+\xi-\varpi_1-\varpi_1',\gamma),(\varrho+\xi-\varpi_1'-\nu_1+\gamma,\gamma);\end{matrix}\ x^\gamma\right].$$

Theorem 6. *Let $\varpi_1, \varpi_1', \nu_1, \nu_1', \xi, \varrho, p, \lambda, \vartheta, s \in \mathbb{C}$ with $\gamma \in \mathbb{R}^+$ and ν, $a \in \mathbb{C}\setminus\mathbb{Z}_0^-$ such that $Re(\xi) > 0$ and $Re(\varrho) < 1 + \min\{Re(-\nu_1), Re(\varpi_1 + \varpi_1' - \xi), Re(\varpi_1 + \nu_1' - \xi)\}$ with $|1/t| < 1$. Then for $\Re(p) \geq 0$, the Beta-transform formula shown below is valid:*

$$B\left\{\left(I_{x,\infty}^{\varpi_1,\varpi_1',\nu_1,\nu_1',\xi}\left\{t^{\varrho-1}\,\Phi_{\lambda,\vartheta;\nu}^{(\theta,\theta')}\left(\left(\frac{z}{t}\right)^\gamma, s, a; p\right)\right\}\right)(x) : l, m\right\}$$
$$= x^{\varrho+\xi-\varpi_1-\varpi_1'-1}\,\Gamma(m)\,\Phi_{\lambda,\vartheta;\nu}^{(\theta,\theta')}\left(\frac{1}{x^\gamma}, s, a; p\right)$$
$$* \ {}_5\Psi_4\left[\begin{matrix}(1,1),(l,\gamma),(1-\varrho-\nu_1,\gamma),\\(l+m,\gamma),(1-\varrho,\gamma),\\(1-\varrho-\xi+\varpi_1+\varpi_1',\gamma),(1-\varrho-\xi+\varpi_1+\nu_1',\gamma);\\(1-\varrho-\xi+\varpi_1+\varpi_1'+\nu_1',\gamma),(1-\varrho+\varpi_1-\nu_1,\gamma);\end{matrix}\ \frac{1}{x^\gamma}\right].$$

Theorem 7. *Let $\varpi_1, \varpi_1', \nu_1, \nu_1', \xi, \varrho, p, \lambda, \vartheta, s \in \mathbb{C}$ with $\gamma \in \mathbb{R}^+$ and ν, $a \in \mathbb{C}\backslash\mathbb{Z}_0^-$ such that $Re(\xi) > 0$ and $Re(\varrho) > \max\{0, Re(\xi - \varpi_1 - \varpi_1' - \nu_1'), Re(\nu_1 - \varpi_1)\}$ with $|t| < 1$. Then for $\Re(p) \geq 0$, the Beta-transform formula shown below is valid:*

$$B\left\{\left(D_{0,x}^{\varpi_1,\varpi_1',\nu_1,\nu_1',\xi}\left\{t^{\varrho-1}\,\Phi_{\lambda,\vartheta;\nu}^{(\theta,\theta')}((tz)^\gamma), s, a; p\right\}\right)(x) : l, m\right\}$$
$$= x^{\varrho-\xi+\varpi_1+\varpi_1'-1}\,\Gamma(m)\,\Phi_{\lambda,\vartheta;\nu}^{(\theta,\theta')}(x^\gamma, s, a; p)$$
$$* \ {}_5\Psi_4\left[\begin{matrix}(1,1),(l,\gamma),(\varrho,\gamma),(\varrho-\xi+\varpi_1+\varpi_1'+\nu_1',\gamma),(\varrho-\nu_1+\varpi_1,\gamma);\\(l+m,\gamma),(\varrho-\nu_1,\gamma),(\varrho-\xi+\varpi_1+\varpi_1',\gamma),(\varrho-\xi+\varpi_1+\nu_1'+\gamma,\gamma);\end{matrix}\ x^\gamma\right].$$

Theorem 8. *Let $\varpi_1, \varpi_1', \nu_1, \nu_1', \xi, \varrho, p, \lambda, \vartheta, s \in \mathbb{C}$ with $\gamma \in \mathbb{R}^+$ and ν, $a \in \mathbb{C}\backslash\mathbb{Z}_0^-$ such that $Re(\xi) > 0$ and $Re(\varrho) < 1 + \min\{Re(\nu_1'), Re(\xi - \varpi_1 - \varpi_1', Re(\xi - \varpi_1' - \nu_1)\}$ with $|1/t| < 1$. Then for $\Re(p) \geq 0$, the Beta-transform formula shown below is valid:*

$$B\left\{\left(D_{x,\infty}^{\varpi_1,\varpi_1',\nu_1,\nu_1',\xi}\left\{t^{\varrho-1}\,\Phi_{\lambda,\vartheta;\nu}^{(\theta,\theta')}\left(\left(\frac{z}{t}\right)^\gamma, s, a; p\right)\right\}\right)(x) : l, m\right\}$$
$$= x^{\varrho-\xi+\varpi_1+\varpi_1'-1}\,\Gamma(m)\,\Phi_{\lambda,\vartheta;\nu}^{(\theta,\theta')}\left(\frac{1}{x^\gamma}, s, a; p\right)$$
$$* \ {}_5\Psi_4\left[\begin{matrix}(1,1),(l,\gamma),(1-\varrho-\nu_1',\gamma),\\(1-\varrho,\gamma),(1-\varrho+\xi-\varpi_1-\varpi_1'-\nu_1,\gamma),\end{matrix}\right.$$

$$(1-\varrho+\xi-\varpi_1-\varpi_1',\gamma),(1-\varrho+\xi-\varpi_1'-\nu_1,\gamma);\ \frac{1}{x^\gamma}\Big].$$
$$(l+m,\gamma),(1-\varrho-\varpi_1'-\nu_1',\gamma);$$

Theorem 9. *Let $\varpi_1,\varpi_1',\nu_1,\nu_1',\xi,\varrho,p,\lambda,\vartheta,s\in\mathbb{C}$ with $\gamma\in\mathbb{R}^+$ and $\nu,a\in\mathbb{C}\backslash\mathbb{Z}_0^-$ such that $Re(\xi)>0$ and $Re(\varrho)>\max\{0,Re(\varpi_1+\varpi_1'+\nu_1-\xi),Re(\varpi_1'-\nu_1')\}$ with $|t|<1$. Then for $\Re(p)\geq 0$, the Laplace-transform formula shown below is valid:*

$$L\left\{z^{l-1}\left(I_{0,x}^{\varpi_1,\varpi_1',\nu_1,\nu_1',\xi}\left\{t^{\varrho-1}\,\Phi_{\lambda,\vartheta;\nu}^{(\theta,\theta')}((tz)^\gamma),s,a;p\right\}\right)(x)\right\}$$
$$=\frac{x^{\varrho+\xi-\varpi_1-\varpi_1'-1}}{s^l}\,\Phi_{\lambda,\vartheta;\nu}^{(\theta,\theta')}\left(\left(\frac{x}{s}\right)^\gamma,s,a;p\right)$$
$$*\ {}_5\Psi_3\left[\begin{matrix}(1,1),(l,\gamma),(\varrho,\gamma),(\varrho+\xi-\varpi_1-\varpi_1'-\nu_1,\gamma),(\varrho+\nu_1'-\varpi_1',\gamma);\\(\varrho+\nu_1',\gamma),(\varrho+\xi-\varpi_1-\varpi_1',\gamma),(\varrho+\xi-\varpi_1'-\nu_1,\gamma);\end{matrix}\ \left(\frac{x}{s}\right)^\gamma\right].$$

Theorem 10. *Let $\varpi_1,\varpi_1',\nu_1,\nu_1',\xi,\varrho,p,\lambda,\vartheta,s\in\mathbb{C}$ with $\gamma\in\mathbb{R}^+$ and $\nu,a\in\mathbb{C}\setminus\mathbb{Z}_0^-$ such that $Re(\xi)>0$ and $Re(\varrho)<1+\min\{Re(-\nu_1),Re(\varpi_1+\varpi_1'-\xi),Re(\varpi_1+\nu_1'-\xi)\}$ with $|1/t|<1$. Then for $\Re(p)\geq 0$, the Laplace-transform formula shown below is valid:*

$$L\left\{z^{l-1}\left(I_{x,\infty}^{\varpi_1,\varpi_1',\nu_1,\nu_1',\xi}\left\{t^{\varrho-1}\,\Phi_{\lambda,\vartheta;\nu}^{(\theta,\theta')}\left(\left(\frac{z}{t}\right)^\gamma,s,a;p\right)\right\}\right)(x)\right\}$$
$$=\frac{x^{\varrho+\xi-\varpi_1-\varpi_1'-1}}{s^l}\,\Phi_{\lambda,\vartheta;\nu}^{(\theta,\theta')}\left(\left(\frac{1}{xs}\right)^\gamma,s,a;p\right)$$
$$*\ {}_5\Psi_3\Big[\begin{matrix}(1,1),(l,\gamma),(1-\varrho-\nu_1,\gamma),(1-\varrho-\xi+\varpi_1+\varpi_1',\gamma),\\(1-\varrho,\gamma),(1-\varrho-\xi+\varpi_1+\varpi_1'+\nu_1',\gamma),\end{matrix}$$
$$\begin{matrix}(1-\varrho-\xi+\varpi_1+\nu_1',\gamma);\\(1-\varrho+\varpi_1-\nu_1,\gamma);\end{matrix}\ \left(\frac{1}{xs}\right)^\gamma\Big].$$

Theorem 11. *Let $\varpi_1,\varpi_1',\nu_1,\nu_1',\xi,\varrho,p,\lambda,\vartheta,s\in\mathbb{C}$ with $\gamma\in\mathbb{R}^+$ and $\nu,a\in\mathbb{C}\setminus\mathbb{Z}_0^-$ such that $Re(\xi)>0$ and $Re(\varrho)>\max\{0,Re(\xi-\varpi_1-\varpi_1'-\nu_1'),Re(\nu_1-\varpi_1)\}$ with $|t|<1$. Then for $\Re(p)\geq 0$, the Laplace-transform formula shown below is valid:*

$$L\left\{z^{l-1}\left(D_{0,x}^{\varpi_1,\varpi_1',\nu_1,\nu_1',\xi}\left\{t^{\varrho-1}\,\Phi_{\lambda,\vartheta;\nu}^{(\theta,\theta')}((tz)^\gamma,s,a;p)\right\}\right)(x):\right\}$$
$$=\frac{x^{\varrho-\xi+\varpi_1+\varpi_1'-1}}{s^l}\,\Phi_{\lambda,\vartheta;\nu}^{(\theta,\theta')}\left(\left(\frac{x}{s}\right)^\gamma,s,a;p\right)$$
$$*\ {}_5\Psi_3\left[\begin{matrix}(1,1),(l,\gamma),(\varrho,\gamma),(\varrho-\xi+\varpi_1+\varpi_1'+\nu_1',\gamma),(\varrho-\nu_1+\varpi_1,\gamma);\\(\varrho-\nu_1,\gamma),(\varrho-\xi+\varpi_1+\varpi_1',\gamma),(\varrho-\xi+\varpi_1+\nu_1',\gamma);\end{matrix}\ \left(\frac{x}{s}\right)^\gamma\right].$$

Theorem 12. *Let $\varpi_1,\varpi_1',\nu_1,\nu_1',\xi,\varrho,p,\lambda,\vartheta,s\in\mathbb{C}$ with $\gamma\in\mathbb{R}^+$ and $\nu,a\in\mathbb{C}\setminus\mathbb{Z}_0^-$ such that $Re(\xi)>0$ and $Re(\varrho)<1+\min\{Re(\nu_1'),Re(\xi-\varpi_1-\varpi_1',Re(\xi-\varpi_1'-\nu_1)\}$ with $|1/t|<1$. Then for $\Re(p)\geq 0$, the Laplace-transform formula shown below is valid:*

$$L\left\{z^{l-1}\left(D_{x,\infty}^{\varpi_1,\varpi_1',\nu_1,\nu_1',\xi}\left\{t^{\varrho-1}\,\Phi_{\lambda,\vartheta;\nu}^{(\theta,\theta')}\left(\left(\frac{z}{t}\right)^\gamma,s,a;p\right)\right\}\right)(x)\right\}$$
$$=\frac{x^{\varrho-\xi+\varpi_1+\varpi_1'-1}}{s^l}\,\Phi_{\lambda,\vartheta;\nu}^{(\theta,\theta')}\left(\left(\frac{1}{xs}\right)^\gamma,s,a;p\right)$$

$$* \ {}_5\Psi_3\Big[\begin{matrix} (1,1),(l,\gamma),(1-\varrho-\nu_1',\gamma), \\ (1-\varrho,\gamma),(1-\varrho+\xi-\varpi_1-\varpi_1'-\nu_1,\gamma), \\ (1-\varrho+\xi-\varpi_1-\varpi_1',\gamma),(1-\varrho+\xi-\varpi_1'-\nu_1,\gamma); \\ (1-\varrho-\varpi_1'-\nu_1',\gamma); \end{matrix} \Big(\frac{1}{xs}\Big)^{\gamma}\Big].$$

Theorem 13. *Let* $\varpi_1,\varpi_1',\nu_1,\nu_1',\xi,\varrho,p,\lambda,\vartheta,s \in \mathbb{C}$ *with* $\gamma \in \mathbb{R}^+$ *and* $\nu, a \in \mathbb{C}\setminus\mathbb{Z}_0^-$ *such that* $Re(\xi) > 0$ *and* $Re(\varrho) > \max\{0, Re(\varpi_1+\varpi_1'+\nu_1-\xi), Re(\varpi_1'-\nu_1')\}$ *with* $|t|<1$ *. Then for* $\Re(p)\geq 0$*, the Laplace-transform formula shown below is valid:*

$$\int_0^{\infty} z^{l-1}e^{-\frac{1}{2}\delta z}\, W_{\tau,\varsigma}(\delta z)\left\{\left(I_{0,x}^{\varpi_1,\varpi_1',\nu_1,\nu_1',\xi}\left\{t^{\varrho-1}\,\Phi_{\lambda,\vartheta;\nu}^{(\theta,\theta')}((wtz)^{\gamma}),s,a;p\right\}\right)(x)\right\}\mathrm{d}z$$
$$= \frac{x^{\varrho+\xi-\varpi_1-\varpi_1'-1}}{\delta^l}\,\Phi_{\lambda,\vartheta;\nu}^{(\theta,\theta')}\left(\Big(\frac{wx}{\delta}\Big)^{\gamma},s,a;p\right)$$
$$* \ {}_6\Psi_4\Big[\begin{matrix} (1,1),(\frac{1}{2}+\zeta+l,\gamma),(\frac{1}{2}-\zeta+l,\gamma), \\ (\frac{1}{2}-\tau+l,\gamma),(\varrho+\nu_1',\gamma), \\ (\varrho,\gamma),(\varrho+\xi-\varpi_1-\varpi_1'-\nu_1,\gamma),(\varrho+\nu_1'-\varpi_1',\gamma); \\ (\varrho+\xi-\varpi_1-\varpi_1',\gamma),(\varrho+\xi-\varpi_1'-\nu_1,\gamma); \end{matrix} \Big(\frac{wx}{\delta}\Big)^{\gamma}\Big].$$

Theorem 14. *Let* $\varpi_1,\varpi_1',\nu_1,\nu_1',\xi,\varrho,p,\lambda,\vartheta,s \in \mathbb{C}$ *with* $\gamma \in \mathbb{R}^+$ *and* $\nu, a \in \mathbb{C}\setminus\mathbb{Z}_0^-$ *such that* $Re(\xi) > 0$ *and* $Re(\varrho) < 1+\min\{Re(-\nu_1), Re(\varpi_1+\varpi_1'-\xi), Re(\varpi_1+\nu_1'-\xi)\}$ *with* $|1/t|<1$*. Then for* $\Re(p)\geq 0$*, the integral formula shown below is valid:*

$$\int_0^{\infty} z^{l-1}e^{-\frac{1}{2}\delta z}\, W_{\tau,\varsigma}(\delta z)\left\{\left(I_{x,\infty}^{\varpi_1,\varpi_1',\nu_1,\nu_1',\xi}\left\{t^{\varrho-1}\,\Phi_{\lambda,\vartheta;\nu}^{(\theta,\theta')}\left(\Big(\frac{wz}{t}\Big)^{\gamma},s,a;p\right)\right\}\right)(x)\right\}\mathrm{d}z$$
$$= \frac{x^{\varrho+\xi-\varpi_1-\varpi_1'-1}}{\delta^l}\,\Phi_{\lambda,\vartheta;\nu}^{(\theta,\theta')}\left(\Big(\frac{w}{x\delta}\Big)^{\gamma},s,a;p\right)$$
$$* \ {}_6\Psi_4\Big[\begin{matrix} (1,1),(\frac{1}{2}+\zeta+l,\gamma),(\frac{1}{2}-\zeta+l,\gamma),(1-\varrho-\nu_1,\gamma), \\ (\frac{1}{2}-\tau+l,\gamma),(1-\varrho,\gamma), \\ (1-\varrho-\xi+\varpi_1+\varpi_1',\gamma),(1-\varrho-\xi+\varpi_1+\nu_1',\gamma); \\ (1-\varrho-\xi+\varpi_1+\varpi_1'+\nu_1',\gamma),(1-\varrho+\varpi_1-\nu_1,\gamma); \end{matrix} \Big(\frac{w}{x\delta}\Big)^{\gamma}\Big].$$

Theorem 15. *Let* $\varpi_1,\varpi_1',\nu_1,\nu_1',\xi,\varrho,p,\lambda,\vartheta,s\in\mathbb{C}$ *with* $\gamma\in\mathbb{R}^+$ *and* $\nu, a\in\mathbb{C}\setminus\mathbb{Z}_0^-$ *such that* $Re(\xi)>0$ *and* $Re(\varrho)>\max\{0, Re(\xi-\varpi_1-\varpi_1'-\nu_1'), Re(\nu_1-\varpi_1)\}$ *with* $|t|<1$*. Then for* $\Re(p)\geq 0$*, the integral formula shown below is valid:*

$$\int_0^{\infty} z^{l-1}e^{-\frac{1}{2}\delta z}\, W_{\tau,\varsigma}(\delta z)\left\{\left(D_{0,x}^{\varpi_1,\varpi_1',\nu_1,\nu_1',\xi}\left\{t^{\varrho-1}\,\Phi_{\lambda,\vartheta;\nu}^{(\theta,\theta')}((wtz)^{\gamma}),s,a;p\right\}\right)(x)\right\}$$
$$= \frac{x^{\varrho-\xi+\varpi_1+\varpi_1'-1}}{\delta^l}\,\Phi_{\lambda,\vartheta;\nu}^{(\theta,\theta')}(\Big(\frac{wx}{\delta}\Big)^{\gamma},s,a;p)$$
$$* \ {}_6\Psi_4\Big[\begin{matrix} (1,1),(\frac{1}{2}+\zeta+l,\gamma),(\frac{1}{2}-\zeta+l,\gamma) \\ (\frac{1}{2}-\tau+l,\gamma),(\varrho-\nu_1,\gamma), \\ (\varrho+\gamma,\gamma),(\varrho-\xi+\varpi_1+\varpi_1'+\nu_1',\gamma),(\varrho-\nu_1+\varpi_1,\gamma); \\ (\varrho-\xi+\varpi_1+\varpi_1',\gamma),(\varrho-\xi+\varpi_1+\nu_1',\gamma) \end{matrix} \Big(\frac{wx}{\delta}\Big)^{\gamma}\Big].$$

Theorem 16. *Let* $\varpi_1, \varpi_1', \nu_1, \nu_1', \xi, \varrho, p, \lambda, \vartheta, s \in \mathbb{C}$ *with* $\gamma \in \mathbb{R}^+$ *and* $\nu, a \in \mathbb{C} \setminus \mathbb{Z}_0^-$ *such that* $Re(\xi) > 0$ *and* $Re(\varrho) < 1 + \min\{Re(\nu_1'), Re(\xi - \varpi_1 - \varpi_1', Re(\xi - \varpi_1' - \nu_1)\}$ *with* $|1/t| < 1$. *Then for* $\Re(p) \geq 0$, *the integral formula shown below is valid:*

$$\int_0^\infty z^{l-1} e^{-\frac{1}{2}\delta z}\, W_{\tau,\varsigma}(\delta z) \left\{ \left(D_{x,\infty}^{\varpi_1,\varpi_1',\nu_1,\nu_1',\xi} \left\{ t^{\varrho-1}\, \Phi_{\lambda,\vartheta;\nu}^{(\theta,\theta')} \left(\left(\frac{wz}{t} \right)^\gamma, s, a; p \right) \right\} \right)(x) \right\}$$

$$= \frac{x^{\varrho-\xi+\varpi_1+\varpi_1'-1}}{\delta^l}\, \Phi_{\lambda,\vartheta;\nu}^{(\theta,\theta')} \left(\left(\frac{w}{x\delta} \right)^\gamma, s, a; p \right)$$

$$* \; {}_6\Psi_4 \Big[\begin{matrix} (1,1), (\frac{1}{2}+\zeta+l, \gamma), (\frac{1}{2}-\zeta+l, \gamma), (1-\varrho-\nu_1', \gamma), \\ (\frac{1}{2}-\tau+l, \gamma), (1-\varrho, \gamma), \end{matrix}$$

$$\begin{matrix} (1-\varrho+\xi-\varpi_1-\varpi_1', \gamma), (1-\varrho+\xi-\varpi_1'-\nu_1, \gamma)p; \\ (1-\varrho+\xi-\varpi_1-\varpi_1'-\nu_1, \gamma), (1-\varrho-\varpi_1'-\nu_1', \gamma); \end{matrix} \left(\frac{w}{x\delta} \right)^\gamma \Big].$$

4. Concluding Remarks and Observations

In the current study, we have found the composition formulas for the generalized Marichev-Saigo-Maeda fractional integrals and differential operators (1.1), (1.2), (1.3) and (1.4) involving the p–extended Hurwitz-Lerch zeta function $\Phi_{\lambda,\vartheta;\nu}^{(\theta,\theta')}(z, s, a; p)$ in terms of the Hadamard product (1.8) of the p–extended Hurwitz-Lerch zeta function $\Phi_{\lambda,\vartheta;\nu}^{(\theta,\theta')}(z, s, a; p)(z, s, a)$ and the Fox–Wright function ${}_r\Psi_s(z)$ employing the Hadamard product (or convolution) of two analytic functions. Additionally, we have derived some image formulas in connection with integral transformations such asthe Euler-Beta, Laplace, and Whittaker transforms. Then, as special cases, we can construct as corollaries the specific image formulas for the Erdélyi-Kober(E-K), Riemann-Liouville(R-L), and Saigo's fractional integral and differential operators. We have left this as an exercise for the readers. The results obtained in this paper are assumed to be have applications in various field of Physical and Engineering Sciences. Another application in real world problems can be developed in recents papers[22, 23]

References

[1] R. P. Agarwal, A. Kılıçman, R. K. Parmar and A. K. Rathie, Certain generalized fractional calculus formulas and integral transforms involving (p, q)–Mathieu-type series, *Adv. Differ. Equ.* **221**, (2019), 1–11 , https://doi.org/10.1186/s13662-019-2142-0.

[2] M.A. Chaudhry, A. Qadir, M. Rafique and S.M. Zubair, Extension of Euler's Beta function, *J. Comput. Appl. Math.* **78** (1997), 19–32.

[3] M.A. Chaudhry, A. Qadir, H.M. Srivastava and R.B. Paris, Extended hypergeometric and confluent hypergeometric functions, *Appl. Math. Comput.* **159** (2004), 589–602.

[4] J. Choi, A.K. Rathie, R.K. Parmar, *Extension of extended beta, hypergeometric and confluent hypergeometric functions*. Honam Math. J. **36(2)** (2014), 339–367.

[5] J. Choi and Rakesh K. Parmar, Fractional Integration And Differentiation of the (p, q)–extended Bessel function, *Bulletin of the Korean Mathematical Society*, **55**(2) (2018), 599–610. https://doi.org/10.4134/BKMS.b170193

[6] J. Choi and Rakesh K. Parmar, Fractional calculus of the (p, q)–extended Struve function, *Far East Journal of Mathematical Sciences*, **103**(2) (2018), 541–559. http://dx.doi.org/10.17654/MS103020541

[7] J. Choi, R.K. Parmar and T.K. Pogány, Mathieu-type series built by (p, q)–extended Gaussian hypergeometric function, *Bull. Korean Math. Soc.* **54**(3) (2017), 789–797. https://doi.org/10.4134/BKMS.b160313

[8] D. Kumar, V. P. Dubey, S. Dubey, J. Singh, A. M. Alshehri eComputational analysis of local fractional partial differential equations in realm of fractal calculus, *Chaos, Solitons & Fractals*, **167**, **2023**, 113009, https://doi.org/10.1016/j.chaos.2022.113009

[9] M.J. Luo, R.K. Parmar and R.K. Raina, On extended HurwitzLerch zeta function, *J. Math. Anal. Appl.* **448** (2017), 12811–1304.

[10] D. Jankov Maširević, Rakesh K. Parmar and T. K. Pogány, (p, q)–extended Bessel and modified Bessel functions of the first kind,*Results in Mathematics*, **72)** (2017), 617–632. https://doi.org/10.1007/s00025-016-0649-1

[11] A. A. Kilbas, H. M. Srivastava, and J.J. Trujillo, *Theory and Applications of Fractional Differential Equations*, North-Holland Mathematical Studies, Vol. **204**, Elsevier (North-Holland) Science Publishers, Amsterdam, London and New York, 2006.

[12] V. Kiryakova, *Generalized Fractional Calculus and Applications*, Pitman Research Notes in Mathematics Series, 301, Longman Scientific and Technical, Harlow; copublished in the United States with John Wiley and Sons, Inc., New York (1994).

[13] A Guide to Special Functions in Fractional Calculus, *Mathematics*, **9(1)**,(**2021),106; https://doi.org/10.3390/math9010106**

[14] A. M. Mathai, R. K. Saxena and H. J. Haubold, *The H-Functions: Theory and Applications*, Springer, New York, 201

[15] O. I. Marichev, "Volterra Equation of Mellin Convolution Type with a Horn Function in the Kernel," Izv. AN BSSR Ser. Fiz.-Mat. Nauk. 1, 128–129 (1974) [in Russian].

[16] F.W.J. Olver, D.W. Lozier, R.F. Boisvert and C.W. Clark (eds.), *NIST Handbook of Mathematical Functions*, Cambridge University Press, Cambridge, 2010.

[17] Parmar, R.K.; Choi, J.; Purohit, S.D. Further generalization of the extended Hurwitz-Lerch Zeta functions. *Bol. Soc. Paran. Mat.* 2019, *37*, 177–190.

[18] S. G. Samko, A. A. Kilbas, and O. I. Marichev, *Fractional Integrals and Derivatives*: *Theory and Applications*, Translated from the Russian: *Integrals and Derivatives of Fractional Order and Some of Their Applications* ("Nauka i Tekhnika", Minsk, 1987); Gordon and Breach Science Publishers: Reading, UK, 1993.

[19] I. N. Sneddon, *The use of the Integral Transforms*, Tata McGraw-Hill, New Delhi, 1979.

[20] M. Saigo, "On Generalized Fractional Calculus Operators," in *Recent Advances in Applied Mathematics*, Proceedings of the International Workshop held at Kuwait University (Kuwait; May 4–7, 1996), Kuwait University, Department of Mathematics and Computer Science, Kuwait, 441–450 (1996).

[21] M. Saigo and N. Maeda, "More Generalization of Fractional Calculus," in *Transform Methods and Special Functions*, Proceedings of the Second International Workshop Dedicated to the 100th Anniversary of the Birth of Nikola Obreschkoff (Varna; August 23–30, 1996) (P. Rusev, I. Dimovski and V. Kiryakova, Editors) (Bulgarian Academy of Sciences, Institute of Mathematics and Informatics, Sofia, 1998) pp. 386–400.

[22] J. Singh, A. Gupta, D. Kumar, Computational Analysis of the Fractional Riccati Differential Equation with Prabhakar-type Memory, *Mathematics* 2023, *11(3)* :644, https://doi.org/10.3390/math11030644

[23] J. Singh, A. Gupta, D. Baleanu, Fractional Dynamics and Analysis of Coupled Schrödinger-KdV Equation With Caputo-Katugampola Type Memory, *J. Comput. Nonlinear Dynam.*, 2023, 18(9): 091001, https://doi.org/10.1115/1.4062391

[24] J. Singh, A. M. Alshehri, Sushila, D. Kumar, Computational Analysis of Fractional Liénard's Equation With Exponential Memory, *J. Comput. Nonlinear Dynam.*, 2023, 18(4): 041004, https://doi.org/10.1115/1.4056858

[25] H.M. Srivastava and P.W. Karlsson, *Multiple Gaussian Hypergeometric Series*, Halsted Press, (Ellis Horwood Limited, Chichester), John Wiley and Sons, New York, Chichester, Brisbane and Toronto, 1985.

[26] H. M. Srivastava and R. K. Saxena, Operators of fractional integration and their applications, *Applied Mathematics and Computation*, 118, (2001), 1–52.

‡ Department of Mathematics, Career Point University, Kota-325003, Rajasthan, India
E-mail address: shilpaprajapat786@gmail.com

§ Department of Mathematics, Career Point University, Kota-325003, Rajasthan, India
E-mail address: saxenadrhemlata@gmail.com

A Novel Family of Distribution with Application in Engineering Problems: A Simulation Study

Kanak Modi[1] and Yudhveer Singh*[2]

[1] *Amity School of Applied Sciences, Amity University Rajasthan, Jaipur-303002, India.*
Email: mangalkanak@gmail.com
*[2] *Amity Institute of information Technology, Amity University Rajasthan, Jaipur-303002, India.*
Email: yudhvir.chahal@gmail.com

Abstract

We establish a novel family of Kumaraswamy-X probability distributions in the present investigation. We discussed the Kumaraswamy-Exponential univariate probability distribution. The new distribution with three parameters possesses density function with unimodal and reverse J-shape and hazard rate function of bathtub shaped. We study various statistical properties for it and derive the expressions for its density function, distribution function, survival and hazard rate function, Probability weighted Moments, lth moment, moment generating function, quantile function and Shannon entropy. For the derived distribution order statistics is also discussed. The parameters are estimated using the maximum likelihood estimation approach, and the performance of the estimators was evaluated using a Monte Carlo simulation. Through extensive Monte Carlo simulations and comparative analyses, we assess the performance of the Kumaraswamy-X distribution against other common probability distributions used in engineering contexts. When we apply it to real datasets, it offers a more suitable fit than other existing distributions. We explore the characteristics and potential applications of the Kumaraswamy-X distribution in the context of engineering problems through a comprehensive simulation-based investigation.

Keywords: T-X family of distributions, Probability weighted Moments, Shannon entropy, Order Statistics, Monte Carlo simulation, Maximum likelihood estimation.
AMS 2000 Subject Code: 62F10, 62F03.

1 Introduction

In probability distribution theory, the selection of a specific probability distribution for modeling real-world phenomena depends on the flexibility of the distribution. It is practice to apply probability distributions that better match the set of data that is available, instead of transforming the current data collected. Because of this, there have been numerous recent attempts to guarantee that the classical probability distributions are updated and developed, since this could boost their adaptability and improve their ability to predict real-world data sets. The Kumaraswamy-X probability distribution, an extension of the well-known Kumaraswamy distribution, has application in modeling a wide range of lifetime problems. This study explores the characteristics and potential applications of the Kumaraswamy-X distribution in the context of engineering problems through a comprehensive simulation-based investigation.

The concept of creating customised distributions is still a hot topic in the literature today. Several approaches could be used to extend an existing standard distribution. For instance, generalization, which entails leveraging the widely available generalized family of distributions, can boost a distribution's adaptability. To generalize the distribution an additional shape parameter(s) may be added to the family of distributions. These extra shape parameter(s) are responsible for altering the tail weight of the resulting compound distribution and introducing skewness. The extension of classical distributions is a long-standing practice and an important issue in statistics, just like many other real-world issues.

The distributions could be used in different domains, like engineering, economics, industrial and physical fields, among a great number of others. To increase the flexibility of traditional distributions, statisticians developed methods for creating new probability distribution families. In many relevant fields, these improvements give practitioners more flexible model options for results that fit them better and are ultimately more accurate. For instance, some of the well-known families are the beta-G family (B-G) by Eugene et al. [8], Kumaraswamy-G family (Kw-G) by Cordeiro and de Castro [6], McDonald-G family (Mc-G) by Alexander et al. [2], T-X family introduced by Alzaatreh et al. [4], gamma-X family by Alzaatreh et al. [3], Exponentiated T-X family by Alzaghal et al. [5], Logistic-X family by Tahir et al. [15], new Weibull-X family by Ahmad et al. [1] and some new member of T-X family by Jamal and Nasir [10] among others. A new family of Distribution with application on two real datasets on survival problem by Modi et al. [12]. Power Exponentiated Family of Distributions proposed by Modi [11]. In this article, we have proposed a new lifetime family of distributions which can be used to fit data in different fields. The paper is organized as follows. In **Section 2**, we define T-X family of distributions. Kumaraswamy distribution and Exponential distribution in **Section 3** and **Section 4** respectively. In **Section 5**, we provide the probability density function (pdf) and the cumulative distribution function (cdf) of the Kumaraswamy-Exponential distribution. In **Section 6**, we examine the survival function and hazard rate function for the new distribution. Formulas

for moments, moment generating function and probability weighted moments of the Kumaraswamy-Exponential distribution (KED) are given in **Section 7**, **Section 8** & **Section 9** respectively. Mean, median and mode are discussed in **Section 10** and quantile function in **Section 11**. The Simulation study and Shannon entropy in **Section 12** & **Section 13** respectively. The distribution of the order statistics for the new distribution are discussed in **Section 14**. In **Section 15**, we estimate its parameters using the method of maximum likelihood estimation. In **Section 16**, we show the application of Kumaraswamy-Exponential distribution on two real datasets and compare it with some well known distributions. We need the following Lemmas to complete the derivations:

Lemma 1.1. *From Gradshteyn and Ryzhik [9], Equation (1.110), Page 25. If q is a positive real non integer and $|z| \leq 1$, then by binomial series expansion we have:*

$$(1-z)^{\Upsilon-1} = \sum_{p=0}^{\infty} (-1)^p \binom{\Upsilon-1}{p} z^p.$$

Lemma 1.2. *From Prudnikov et al. [14], Equation (18), Page 241, the integral expression is defined as follows:*

$$\int z^{\zeta} \ln z \, dz = z^{\zeta+1} \left[\frac{\ln z}{\zeta+1} - \frac{1}{(\zeta+1)^2} \right].$$

Lemma 1.3. *From Gradshteyn and Ryzhik [9], Equation (3.383.1), Page 347. For $Re\Omega > 0$, $Re\varsigma > 0$*

$$\int_0^{\kappa} x^{\Omega-1} (\kappa - x)^{\varsigma-1} e^{\beta x} \, dx = B(\varsigma, \Omega) \, \kappa^{\varsigma+\Omega-1} {}_1F_1(\Omega; \varsigma+\Omega; \beta\kappa).$$

Lemma 1.4. *From Gradshteyn and Ryzhik [9], Equation (2.729.1), Page 239, the integral expression is defined as follows:*

$$\int x^{\xi} \ln(a+bx) \, dx = \frac{1}{\xi+1} \left[x^{\xi+1} - \frac{(-a)^{\xi+1}}{b^{\xi+1}} \right] \ln(a+bx) + \frac{1}{\xi+1} \sum_{k=1}^{\xi+1} \frac{(-1)^k \, x^{\xi-k+2} a^{k-1}}{(\xi-k+2) \, b^{k-1}}.$$

2 T-X family of distributions

The cumulative distribution function (cdf) of the T-X family introduced by Alzaatreh et al. [4], is given by $U\{W(Q(x))\}$. Let T be a continuous random

variable (r.v.) with pdf u(t) defined on [0, 1], can be defined as:

$$G_X(x) = \int_0^{W(Q_X(x))} u(t)\,dt,$$

where Q is the cdf of X, U(t) is the cdf of a r.v. T and W is a non-decreasing function having the support of U as its range defined on [0, 1]. Thus, we have:

$$G_X(x) = U\left[-\log\left(1 - Q_X(x)\right)\right] \qquad x > 0, \tag{2.1}$$

$$g_X(x) = \frac{q_X(x)}{(1 - Q_X(x))} u\left[-\log\left(1 - Q_X(x)\right)\right]. \tag{2.2}$$

Thus substituting the different cdf Q(x)and pdf q(x), we can obtain a number of distributions.

3 Kumaraswamy distribution

A continuous random variable X is said to have Kumaraswamy distribution, if its pdf $f_X(x)$ and cdf $F_X(x)$ are, respectively, given by:

$$f(x) = \kappa b x^{\kappa-1}\left(1 - x^{\kappa}\right)^{b-1}, \qquad 0 \le x \le 1, b > 0, \kappa > 0 \tag{3.1}$$

and

$$F(x) = 1 - \left(1 - x^{\kappa}\right)^{b}. \tag{3.2}$$

4 Exponential distribution

A continuous random variable X is said to have Exponential distribution, if its pdf $f_X(x)$ and cdf $F_X(x)$ are, respectively, given by:

$$f(x) = \eta e^{-\eta x}, \quad x \ge 0,\ \eta > 0, \tag{4.1}$$

and

$$F(x) = 1 - e^{-\eta x}. \tag{4.2}$$

5 Kumaraswamy - Exponential distribution

Using Kumaraswamy distribution in T-X family, we obtain the Kumaraswamy-X family of distributions:

$$G_X(x) = 1 - \left[1 - \left(-\log\left(1 - Q\left(x\right)\right)\right)^{\kappa}\right]^{b}.$$

Using cdf given in equation (4.2), we obtain cdf of Kumaraswamy - Exponential distribution as:

$$G_X(x) = 1 - \left[1 - (\eta x)^{\kappa}\right]^{b}. \tag{5.1}$$

Using Kumaraswamy distribution in T-X family density given in equation (2.2), we obtain the pdf of Kumaraswamy-X family of distributions:

$$g_X(x) = \frac{q(x)}{1-Q(x)} \kappa b \left(-\log\left(1-Q(x)\right)\right)^{\kappa-1} \left[1-\left(-\log\left(1-Q(x)\right)\right)^{\kappa}\right]^{b-1}.$$

Using pdf in equation (4.1) and cdf in equation (4.2), we obtain pdf of Kumaraswamy - Exponential distribution

$$g_X(x) = \eta^{\kappa} \kappa b x^{\kappa-1} \left[1-(\eta x)^{\kappa}\right]^{b-1}, \tag{5.2}$$

Using Lemma 1, in the above expression then we have

$$g_X(x) = \eta^{\kappa} \kappa b x^{\kappa-1} \sum_{v=0}^{\infty} (-1)^v \binom{b-1}{v} (\eta x)^{v\kappa} \quad x>0, b>0, \eta>0, \kappa>0. \tag{5.3}$$

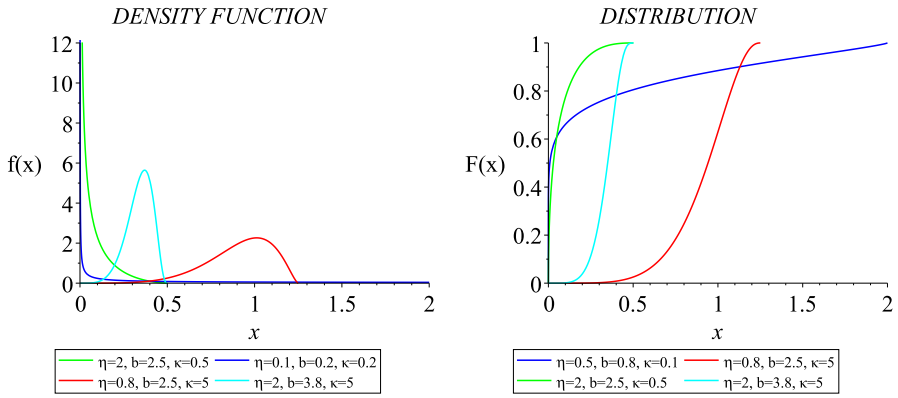

Figure 1: Density function (Left) and distribution function (Right) graphs of Kumaraswamy - Exponential distribution for different values of its parameters η, b, κ.

6 Hazard Rate Function and Survival Function

To study the life phenomena we can use hazard rate function as an important characteristic. Using the pdf defined in equation (5.2), we define h(x) as:

$$h(x) = \frac{\eta^{\kappa} \kappa b x^{\kappa-1}}{1-(\eta x)^{\kappa}}, \tag{6.1}$$

also, its survival function obtained as:

$$S(x) = \left[1-(\eta x)^{\kappa}\right]^{b}. \tag{6.2}$$

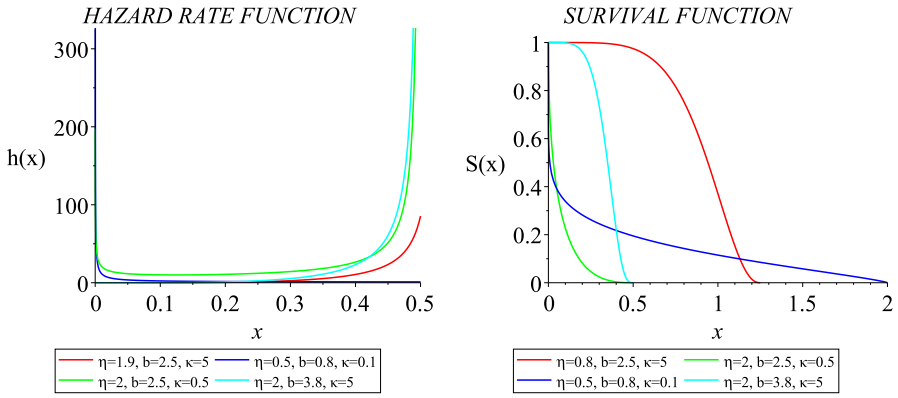

Figure 2: Hazard rate function (Left) and survival function (Right) graphs of Kumaraswamy - Exponential distribution for different values of its parameters η, b, κ.

7 Moments

The l^{th} moment of a random variable X with pdf defined in equation (5.2), can be calculated as:

$$\mu_l^{'} = E(x^l) = \eta^{\kappa}\kappa b \int_0^1 x^{l+\kappa-1} \sum_{v=0}^{\infty} (-1)^v \binom{b-1}{v} (\eta x)^{v\kappa}\, dx,$$

$$= \kappa b \sum_{v=0}^{\infty} (-1)^v \binom{b-1}{v} \eta^{v\kappa+\kappa} \int_0^1 x^{l+v\kappa+\kappa-1} dx.$$

On integration, we obtain

$$\mu_l^{'} = \kappa b \sum_{v=0}^{\infty} (-1)^v \binom{b-1}{v} \eta^{v\kappa+\kappa} \frac{1}{l+v\kappa+\kappa}. \tag{7.1}$$

8 Moment Generating Function

The mgf for the pdf defined in equation (5.2), is given by:

$$M_X(t) = E(e^{tx}) = \int_0^\infty e^{tx} f(x)dx$$

$$= \eta^\kappa \kappa b \int_0^1 e^{tx}.x^{\kappa-1} \sum_{v=0}^\infty (-1)^v \binom{b-1}{v} (\eta x)^{v\kappa} dx$$

$$= \kappa b \sum_{v=0}^\infty (-1)^v \binom{b-1}{v} \eta^{v\kappa+\kappa} \int_0^1 e^{tx} x^{v\kappa+\kappa-1} dx$$

Using Lemma 3, in the above expression then we have

$$E\left(e^{tx}\right) = \kappa b \sum_{v=0}^\infty (-1)^v \binom{b-1}{v} \times$$
$$\eta^{v\kappa+\kappa} B(1, \kappa+v\kappa) (1)^{\kappa+v\kappa} .{}_1F_1(\kappa+v\kappa; 1+\kappa+v\kappa; t.1)$$

$$E\left(e^{tx}\right) = \kappa b \sum_{v=0}^\infty (-1)^v \binom{b-1}{v} \frac{\eta^{v\kappa+\kappa}}{(\kappa+v\kappa)} .{}_1F_1(\kappa+v\kappa; 1+\kappa+v\kappa; t) \quad (8.1)$$

9 Probability Weighted Moments

For the pdf of the proposed distribution, corresponding p^{th} probability weighted moment is given by:

$$\rho = E\left(x^p (G(x))^\phi\right) = \int_0^1 x^p (G(x))^\phi .g(x) dx,$$

$$= \kappa b \eta^\kappa \int_0^1 x^{p+\kappa-1} \left(1 - [1-(\eta x)^\kappa]^b\right)^\phi . [1-(\eta x)^\kappa]^{b-1} dx,$$

using Lemma 1, in the above expression then we have

$$= \eta^\kappa \kappa b \sum_{t=0}^\infty (-1)^t \binom{\phi}{t} \int_0^1 x^{p+\kappa-1} [1-(\eta x)^\kappa]^{bt+b-1} dx,$$

again we apply Lemma 1, then we obtained

$$= \kappa b \sum_{t=0}^\infty \sum_{u=0}^\infty (-1)^{t+u} \binom{\phi}{t} \binom{bt+b-1}{u} \eta^{\kappa+\kappa u} \int_0^1 x^{p+\kappa+\kappa u-1} dx.$$

$$\rho = \kappa b \sum_{t=0}^{\infty} \sum_{u=0}^{\infty} (-1)^{t+u} \left(\begin{array}{c} \phi \\ t \end{array} \right) \left(\begin{array}{c} bt+b-1 \\ u \end{array} \right) \frac{\eta^{\kappa+\kappa u}}{p+\kappa+\kappa u}. \tag{9.1}$$

10 Mean, Median and Mode

The mean of a probability distribution is defined as:

$$E(x) = \int_0^{\infty} x.g\,(x)\,dx$$

$$E\,(x) = \kappa b \sum_{d=0}^{\infty} (-1)^d \left(\begin{array}{c} b-1 \\ d \end{array} \right) \eta^{d\kappa+\kappa} \frac{1}{1+d\kappa+\kappa}. \tag{10.1}$$

The median of the proposed distribution is given by

$$G_X(M) = \frac{1}{2} \text{ and } M = \frac{1}{\eta}\left[1 - \{0.5\}^{1/b}\right]^{1/\kappa}. \tag{10.2}$$

The mode of the proposed distribution given in equation (5.2), can be obtained as

$$g_X(x) = \eta^{\kappa}\kappa b x^{\kappa-1}\left[1-(\eta x)^{\kappa}\right]^{b-1}$$

$$g'(x) = g\,(x)\,.\left[\frac{\kappa-1}{x} - \frac{\eta^{\kappa}\kappa x^{\kappa-1}\,(b-1)}{1-(\eta x)^{\kappa}}\right] \tag{10.3}$$

Thus $g(x)$ has mode at $x = \frac{1}{\eta}\left[\frac{\kappa-1}{b\kappa-1}\right]^{1/\kappa}$ with $g(0) = 0$, $g(\infty) = \infty$. Clearly $g'(x) > 0$, $\forall b, \kappa, \eta$ this shows that $g(x)$ is a growing function of x.

11 Quantile Function

Using equation (5.1) the quantile function of proposed distribution is given by:

$$Q\,(x) = \frac{1}{\eta}\left[1 - \{1-U\}^{1/b}\right]^{1/\kappa}. \tag{11.1}$$

where for interval [0,1], U follows the Uniform distribution.

12 Simulation Study

To judge the MLEs estimators performance for a finite sample of size n, here we carry out a Monte Carlo simulation analysis. To explore the average biases (ABs), root mean square errors (RMSEs), mean square errors (MSEs) and maximum likelihood estimates (MLEs), a simulation study based on the Kumaraswamy - Exponential distribution is conducted for the distribution parameters η, b and κ. Multiple simulations with different sample sizes and parameter

settings were used to conduct the simulation experiment. We use the quantile function to produce random samples for the KED. The simulation study was performed for sample sizes $n = 50, 100, ..., 1500$ each repeated 1500 times, for the following parameter values $\eta = 2.2,\ b = 3.9,\ \kappa = 4.8$.
The MLEs of the KE model are calculated using the optim ( ) R-function with method = "SANN ". For every set of simulated data, say, (estimates) for $i = 1,\ 2,\ \ldots, 1500$, the AB, MSE, and RMSE of the parameters were computed for $\eta = 2.2,\ b = 3.9,\ \kappa = 4.8$. For different sample sizes, the AB, MLE and RMSE of the parameters, $\eta,\ b$ and κ are shown. These results lead us to the conclusion that the MLEs are best to estimate the model parameters, with more stability and closer to the genuine values. Table 1 and Fig. 3 demonstrate that the RMSE, AB, and MSE drop as sample size grows as would be predicted. The MLEs of the model's parameters are also quite near to their actual values. Thus even small samples can be fitted with derived distribution with better precision.

Table 1: Results obtained for Monte Carlo simulation of MLE, AB and RMSE for the KE Distribution.

Para.	n	MLE	AB	RMSE
η	50	0.7829606	-1.4170393	1.518000
	100	0.8087420	-1.3912579	1.555102
	300	1.0488439	-1.1511561	1.544286
	600	1.5011235	-0.6988764	1.269147
	900	1.8463882	-0.3536118	0.973826
	1200	2.0019255	-0.1980744	0.792184
	1500	2.1223060	-0.0776939	0.615142
b	50	1.009512	-2.8904885	3.968965
	100	3.642784	-0.2572159	5.646243
	300	5.213961	1.3139606	5.896080
	600	5.129874	1.2298743	4.692855
	900	4.670879	0.7708793	3.495491
	1200	4.528949	0.6289491	2.829144
	1500	4.269290	0.3692901	2.041111
κ	50	13.287630	8.48763013	10.84302
	100	11.627627	6.82762727	9.0838924
	300	7.172703	2.37270337	3.9406621
	600	5.465790	0.66579011	2.0529831
	900	4.919511	0.11951053	1.2649680
	1200	4.738959	-0.06104107	0.9195160
	1500	4.633040	-0.16696001	0.7118000

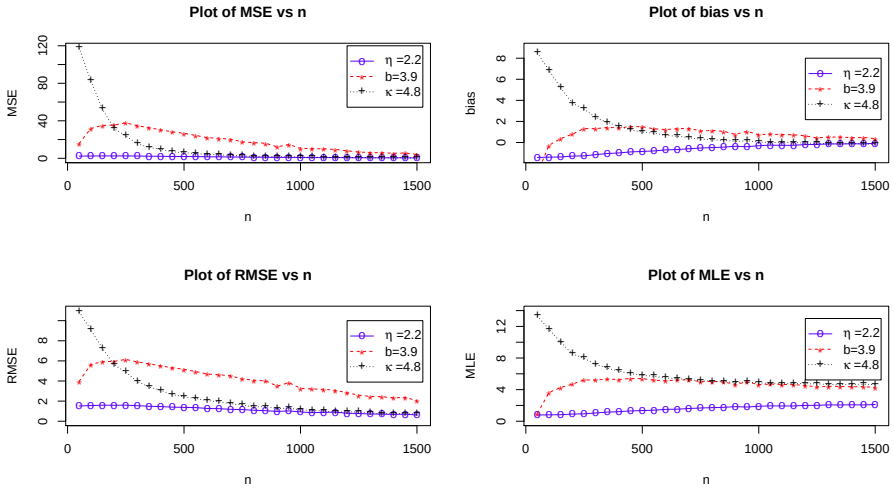

Figure 3: Plots for MLE, bias, MSE, and RMSE for Kumaraswamy - Exponential distribution for parameter values $\eta = 2.2, b = 3.9, \kappa = 4.8$.

13 Shannon Entropy

The entropy of a random variable is a measure of deviation of the uncertainty. The Shannon entropy defined as:

$$E\left[-\ln g_X(x)\right] = -\int_0^\infty \ln g_X(x).g_X(x)dx$$

Using pdf defined in equation (5.2), we get

$$\begin{aligned} E\left[-\ln g_X(x)\right] = & \\ & -\eta^\kappa \kappa b \int_0^1 \ln\left[\eta^\kappa \kappa b x^{\kappa-1}\left[1-(\eta x)^\kappa\right]^{b-1}\right] x^{\kappa-1}\left[1-(\eta x)^\kappa\right]^{b-1} dx \\ & = -\eta^\kappa \kappa b \ln\left(\eta^\kappa \kappa b\right) \int_0^1 x^{\kappa-1}\left[1-(\eta x)^\kappa\right]^{b-1} dx - \eta^\kappa \kappa b\left(\kappa-1\right) \times \\ & \int_0^1 \ln\left(x\right).x^{\kappa-1}\left[1-(\eta x)^\kappa\right]^{b-1} dx - \eta^\kappa \kappa b\left(b-1\right) \times \\ & \int_0^1 \ln\left(1-(\eta x)^\kappa\right).x^{\kappa-1}\left[1-(\eta x)^\kappa\right]^{b-1} dx \end{aligned}$$

$$= I_1 + I_2 + I_3. \tag{13.1}$$

where,

$$I_1 = -\eta^{\kappa}\kappa b \ln\left(\eta^{\kappa}\kappa b\right) \int_0^1 x^{\kappa-1}\left[1-(\eta x)^{\kappa}\right]^{b-1} dx,$$

$$= -\kappa b \ln\left(\eta^{\kappa}\kappa b\right) \sum_{i=0}^{\infty} (-1)^i \begin{pmatrix} b-1 \\ i \end{pmatrix} \eta^{\kappa+i\kappa} \int_0^1 x^{\kappa+i\kappa-1} dx$$

$$I_1 = -\kappa b \ln\left(\eta^{\kappa}\kappa b\right) \sum_{i=0}^{\infty} (-1)^i \begin{pmatrix} b-1 \\ i \end{pmatrix} \frac{\eta^{\kappa+i\kappa}}{\kappa+i\kappa}.$$

$$I_2 = -\eta^{\kappa}\kappa b\left(\kappa-1\right) \int_0^1 \ln\left(x\right).x^{\kappa-1}\left[1-(\eta x)^{\kappa}\right]^{b-1} dx,$$

putting $1-(\eta x)^{\kappa} = t \Rightarrow -\kappa\eta^{\kappa}x^{\kappa-1}dx = dt$ and $x = \frac{1}{\eta}\left(1-t\right)^{1/\kappa}$, we get

$$I_2 = -\eta^{\kappa}\kappa b\left(\kappa-1\right) \int_{1-\eta^{\kappa}}^1 \ln\left(\frac{(1-t)^{1/\kappa}}{\eta}\right) t^{b-1}\frac{dt}{\eta^{\kappa}\kappa},$$

$$= -b\left(\kappa-1\right) \int_{1-\eta^{\kappa}}^1 \left[\ln\left(\frac{1}{\eta}\right) + \frac{1}{\kappa}\ln\left(1-t\right)\right] t^{b-1}dt,$$

$$= -b\left(\kappa-1\right)\ln\left(\frac{1}{\eta}\right) \int_{1-\eta^{\kappa}}^1 t^{b-1}dt - b\frac{(\kappa-1)}{\kappa} \int_{1-\eta^{\kappa}}^1 \ln\left(1-t\right).t^{b-1}dt,$$

by using Lemma 4, we found that

$$I_2 = -\left(\kappa-1\right)\ln\left(\frac{1}{\eta}\right)\left[1-\left(1-\eta^{\kappa}\right)^b\right] - b\frac{(\kappa-1)}{\kappa b} \left[\left(t^b-1\right)\ln\left(1-t\right) - \sum_{g=1}^{b}\frac{t^{b-g+1}}{(b-g+1)}\right]_{1-\eta^{\kappa}}^1 \tag{13.2}$$

$$= -\left(\kappa-1\right)\ln\left(\frac{1}{\eta}\right)\left[1-\left(1-\eta^{\kappa}\right)^b\right] - \frac{(\kappa-1)}{\kappa} \left[-\sum_{g=1}^{b}\frac{1}{(b-g+1)} - \left(\left(1-\eta^{\kappa}\right)^b-1\right)\ln\left(\eta^{\kappa}\right) + \sum_{g=1}^{b}\frac{\left(1-\eta^{\kappa}\right)^{b-g+1}}{(b-g+1)}\right].$$

$$I_3 = -\eta^{\kappa}\kappa b\,(b-1)\int_0^1 \ln\left(1-(\eta x)^{\kappa}\right).x^{\kappa-1}\left[1-(\eta x)^{\kappa}\right]^{b-1}dx,$$

putting $1-(\eta x)^{\kappa} = t \Rightarrow -\kappa\eta^{\kappa}x^{\kappa-1}dx = dt$ and $x = \frac{1}{\eta}(1-t)^{1/\kappa}$, we get

$$I_3 = -b\,(b-1)\int_{1-\eta^{\kappa}}^1 \ln(t).t^{b-1}dt,$$

by using Lemma 2, we found that

$$I_3 = -(b-1)\left[t^b\ln(t) - \frac{t^b}{b}\right]_{1-\eta^{\kappa}}^1$$
$$= (b-1)\left[\frac{1}{b} + (1-\eta^{\kappa})^b\ln(1-\eta^{\kappa}) - \frac{(1-\eta^{\kappa})^b}{b}\right].$$

putting values of I_1, I_2 and I_3 in equation (13.1) we can obtain required result.

14 Order statistics

In this section, we develop the distribution of the q^{th} order statistic of the Kumaraswamy-Exponential distribution (KED). Let $X_{(1:n)} \leq \ldots \leq X_{(r:n)} \leq \ldots \leq X_{(n:n)}$ represents the ordered sample of n random variables for KED. The distribution of the q^{th} order statistics $X_{q:p}, q = 1, 2, \ldots, p$ can be defined as:

$$g_{q:p}(x) = C_{q:p}\left[G(x;\eta,b,\kappa)\right]^{q-1} g(x;\eta,b,\kappa)\left[1-G(x;\eta,b,\kappa)\right]^{p-q} \quad x>0 \quad (14.1)$$

where $G(.)$ and $g(.)$ are given by equation (5.1) and equation (5.2) respectively, thus

$$C_{q:p}(x) = \frac{p!}{(q)!\,(p-q)!}.$$

Thus, Using binomial expansion given in Lemma 1, we get

$$g_{q:p}(x) = C_{q:p}\sum_{k=0}^{\infty}(-1)^k\binom{p-q}{k}\left[G(x;\eta,b,\kappa)\right]^{q+k-1} g(x;\eta,b,\kappa),$$

$$g_{q:p}(x) = C_{q:p}\sum_{k=0}^{\infty}(-1)^k\binom{p-q}{k}\left[1-\left[1-(\eta x)^{\kappa}\right]^b\right]^{q+k-1}\times$$
$$\eta^{\kappa}\kappa b x^{\kappa-1}\left[1-(\eta x)^{\kappa}\right]^{b-1},$$

now using Lemma 1, we obtained

$$g_{q:p}(x) = C_{q:p} \sum_{k=0}^{\infty} \sum_{u=0}^{\infty} (-1)^{k+u} \left(\begin{array}{c} p-q \\ k \end{array} \right) \left(\begin{array}{c} q+k-1 \\ u \end{array} \right) \times \eta^{\kappa} \kappa b x^{\kappa-1} \left[1-(\eta x)^{\kappa}\right]^{b+bu-1}. \quad (14.2)$$

It's s^{th} moment can be calculated as:

$$E(x^s) = C_{q:p} \sum_{w=0}^{\infty} \sum_{u=0}^{\infty} (-1)^{w+u} \left(\begin{array}{c} p-q \\ w \end{array} \right) \left(\begin{array}{c} q+w-1 \\ u \end{array} \right) \times \eta^{\kappa} \kappa b. \int_0^1 x^{\kappa+s-1} \left[1-(\eta x)^{\kappa}\right]^{b+bu-1} dx,$$

Again applying Lemma 1, we have

$$E(x^s) = C_{q:p} \sum_{w=0}^{\infty} \sum_{u=0}^{\infty} \sum_{r=0}^{\infty} (-1)^{w+u+r} \left(\begin{array}{c} p-q \\ w \end{array} \right) \left(\begin{array}{c} q+w-1 \\ u \end{array} \right) \times \left(\begin{array}{c} b+bu-1 \\ r \end{array} \right) \eta^{\kappa+\kappa r} \kappa b. \int_0^1 x^{\kappa+\kappa r+s-1} dx,$$

$$= C_{q:p} \sum_{w=0}^{\infty} \sum_{u=0}^{\infty} \sum_{r=0}^{\infty} (-1)^{w+u+r} \left(\begin{array}{c} p-q \\ w \end{array} \right) \left(\begin{array}{c} q+w-1 \\ u \end{array} \right) \times \left(\begin{array}{c} b+bu-1 \\ r \end{array} \right) \frac{\eta^{\kappa+\kappa r} \kappa b}{\kappa+\kappa r+s} \quad (14.3)$$

15 Maximum Likelihood Estimators

Let X is a random variable having the pdf of Kumaraswamy-Exponential distribution defined as:

$$g_X(x) = \eta^{\kappa} \kappa b x^{\kappa-1} \left[1-(\eta x)^{\kappa}\right]^{b-1}.$$

Then its log-likelihood function can be written as:

$$L(x;\eta,b,\kappa) = n \ln \kappa + n\kappa \ln \eta + n \ln b + (\kappa-1) \sum_{i=1}^{n} \ln (x_i) + (b-1) \sum_{i=1}^{n} \ln \left(1-(\eta x_i)^{\kappa}\right). \quad (15.1)$$

Thus the non-linear normal equations are given as follows:

$$\frac{\partial L(x;\eta,b,\kappa)}{\partial \eta} = \frac{n\kappa}{\eta} - (b-1)\sum_{i=1}^{n} \frac{\kappa \eta^{\kappa-1} x_i^{\kappa}}{(1-(\eta x_i)^{\kappa})}. \tag{15.2}$$

$$\frac{\partial L(x;\eta,b,\kappa)}{\partial \kappa} = n\ln\eta + \frac{n}{\kappa} + \sum_{i=1}^{n} \ln(x_i) - (b-1)\sum_{i=1}^{n} \frac{\eta^{\kappa} x_i^{\kappa} \ln(\eta x_i)}{(1-(\eta x_i)^{\kappa})}. \tag{15.3}$$

$$\frac{\partial L(x;\eta,b,\kappa)}{\partial b} = \frac{n}{b} + \sum_{i=1}^{n} \ln(1-(\eta x_i)^{\kappa}). \tag{15.4}$$

To find the estimate of the unknown parameters by using the maximum likelihood method equate the equation (15.2) - equation (15.4) to zero and we can obtain solution.

16 Application To Real Life Data

Now we apply the proposed Kumaraswamy-Exponential distribution on two engineering data sets. We compare its flexibility with some pre-defined distributions. To analyse the present study, we obtain the results using R software. Following distributions are considered for discussion:
Exponentiated Exponential Distribution

$$f(j) = r\varpi\left(1-e^{-\varpi.j}\right)^{r-1}.e^{-\varpi.j}$$

Exponentiated Weibull distribution

$$f(w) = a\beta\sigma^{\beta}w^{\beta-1}.\exp\left(-(\sigma w)^{\beta}\right)\left(1-\exp\left(-(\sigma w)^{\beta}\right)\right)^{a-1}$$

Beta distribution

$$f(x) = \frac{\Gamma(\alpha+b)}{\Gamma(\alpha).\Gamma(b)}x^{\alpha-1}(1-x)^{b-1}$$

Burr-XII exponential distribution

$$f(l) = cp\varpi.\left(e^{\varpi l}-1\right)^{c-1}e^{\varpi l}\left(1+\left(e^{\varpi l}-1\right)^{c}\right)^{-p-1}$$

Gompertz distribution

$$f(x) = \lambda\exp\left[\alpha x - \frac{\lambda}{\alpha}(e^{\alpha x}-1)\right]$$

At $\alpha = 1\%$ LOS assume the hypothesis as,
H_0: The data fit the Kumaraswamy Exponential distribution
H_1: The data do not fit the Kumaraswamy Exponential distribution

Table 2: Table containing estimates and AIC values.

Distributions	Estimates	p-value	D	LL	AIC
Kumaraswamy exponential distribution	$\eta = 0.583923$ $b = 54.427161$ $\kappa = 1.596120$	0.1178	0.26605	-26.13379	58.26758
Beta distribution	$\alpha = 3.11202$ $b = 21.81905$	0.1521	0.25378	-27.8813	59.7626
Exponentiated Weibull distribution	$a = 9.388397$ $\beta = 0.975218$ $\sigma = 24.898336$	0.5196	0.18229	-32.83807	71.67614
Exponentiated exponential distribution	$\alpha = 13.82227$ $\theta = 27.75196$	0.6835	0.16024	-3297643	69.95286
Burr-XII exponential distribution	$c = 12.2957340$ $p = 0.1133163$ $\tau = 9.6519132$	0.924	0.12272	-37.99018	81.98036

Data Set1: The data from Murthy et al. [13] representing of the breakdown time of 20 mechanical parts. The records are:
0.085, 0.114, 0.068, 0.085, 0.086, 0.089, 0.098, 0.098, 0.114, 0.121, 0.115, 0.125, 0.131, 0.081, 0.149, 0.076, 0.160, 0.084, 0.485, 0.067.

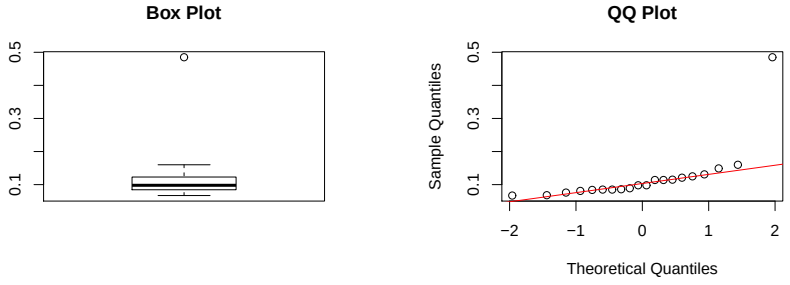

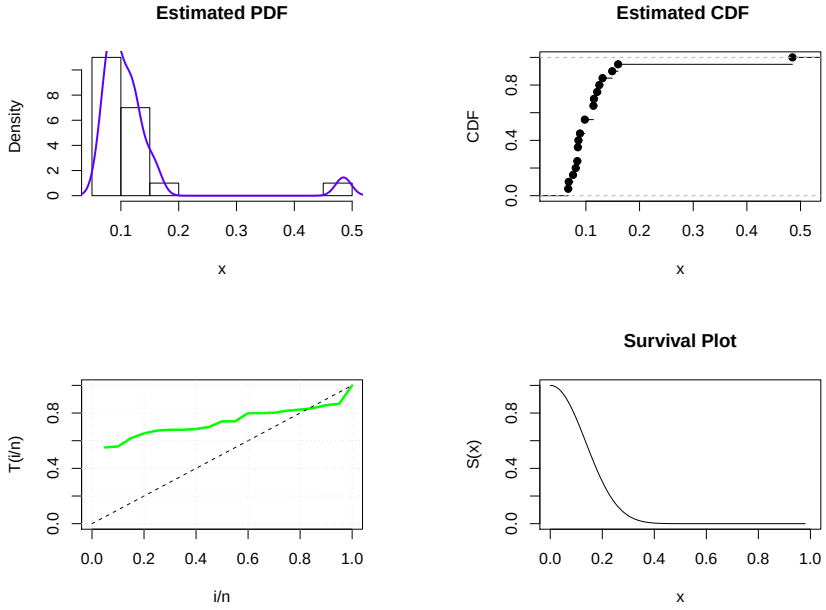

Figure 4: Plots of fitted Kumaraswamy Exponential distribution for breakdown time data.

Plots of fitted KE distribution for breakdown time data are displayed in Figure 4. Box plot revels that data is positively skewed. The TTT plot in Figure 4 for data 1 has concave than convex shape which suggests that hazard shape is upside-down bathtub (unimodal). The empirical visualization suggests that the KE distribution provides an improved fit for the breakdown time data.

Data Set2: This data set referred from Dasgupta [7] for the 50 observations with opening of 12 mm and sheet thickness of 3.15 mm by the drilling machine. The records are:
0.32, 0.04, 0.02, 0.24, 0.08, 0.22, 0.12, 0.14, 0.08, 0.22, 0.12, 0.08, 0.26, 0.24, 0.04, 0.14, 0.08, 0.32, 0.28, 0.14, 0.24, 0.26, 0.24, 0.22, 0.12, 0.18, 0.16, 0.06, 0.24, 0.14, 0.26, 0.16, 0.14, 0.16, 0.24, 0.16, 0.32, 0.18, 0.16, 0.12, 0.06, 0.02, 0.18, 0.22, 0.16, 0.06, 0.04, 0.14, 0.18, 0.16.

From Table 2 and Table 3, the Kumaraswamy-Exponential distribution has the AIC with lowest value and greater log-likelihood value for three parameter distribution, thus providing better fit than the Burr-XII exponential distribution, Exponentiated exponential distribution, Beta distribution, Exponentiated Weibull distribution and Gompertz distribution. So, since $p - value > \alpha$, we suppose that data follows the Kumaraswamy-Exponential distribution and can-

Table 3: Table containing estimates and AIC values.

Distributions	Estimates	p-value	D	LL	AIC
Kumaraswamy exponential distribution	$\eta = 1.011943$ $b = 33.421670$ $\kappa = 2.099506$	0.613	0.10726	-56.06933	118.13866
Burr-XII exponential distribution	$c = 1.991607$ $p = 17.947926$ $\tau = 1.161502$	0.5666	0.1112	-56.12203	118.24406
Gompertz distribution	$\lambda = 1.590379$ $\alpha = 10.274716$	0.6522	0.10397	-57.07532	118.15064
Exponentiated Weibull distribution	$a = 0.2970342$ $\beta = 4.9819583$ $\sigma = 3.8439353$	0.7083	0.09924	-57.53448	121.06896

not reject the null hypothesis.

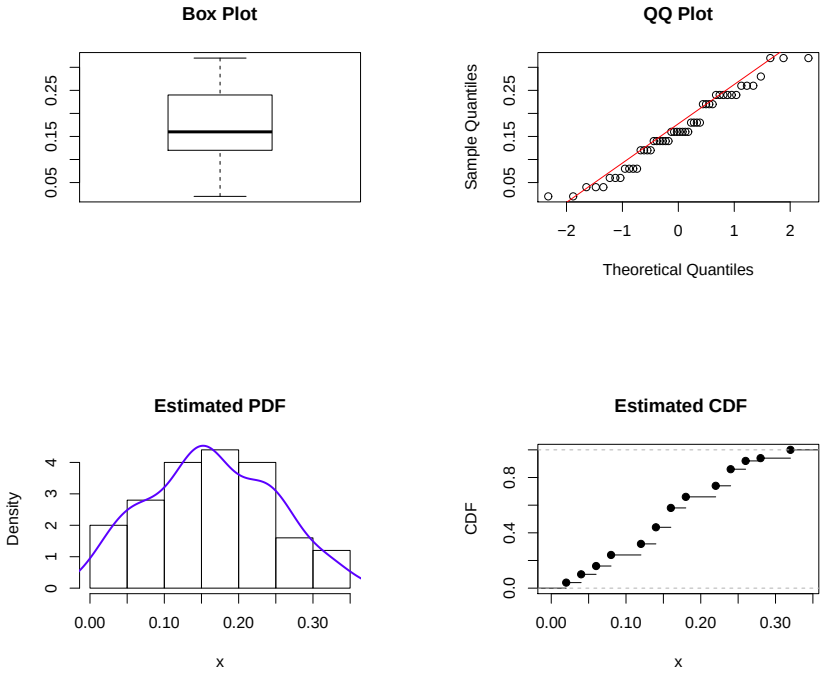

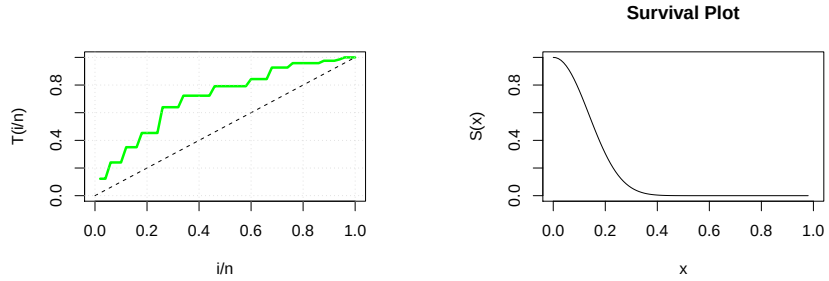

Figure 5: Plots of fitted Kumaraswamy Exponential distribution for drilling machine data.

Plots of fitted KE distribution for drilling machine data are displayed in Fig. 5. Box plot revels that data is normal. The TTT plot in Fig. 5 for data 2 has a concave shape which suggests hrf is increasing. The empirical visualization suggests that the KE distribution provides an improved fit for the drilling machine data.

Conclusion

In this manuscript, we establish a new family of Kumaraswamy-X probability distributions. Particularly, we developed the Kumaraswamy exponential distribution's cdf and pdf expressions. We have studied characteristic properties for the proposed distribution. From density graph, we conclude the proposed distribution has reverse-J shape or unimodal. The graphs for survival and hazard rate function for new distribution are also given. Further the mean, median and mode are discussed. The formulae for the l^{th} moment, probability weighted moments and moment generating function are also derived. We derived the Shannon entropy formula and the distribution of its q^{th} order statistics for proposed distribution. The MLE technique is used to estimate its parameters. We measure the accuracy of the estimators for a finite sample of size n using a Monte Carlo simulation analysis. The distribution is applied on two real datasets and its efficiency measured with some existing distributions. It is clearly visible from findings that the Kumaraswamy Exponential distribution exhibits a better fit for the considered data sets. This study contributes to the expanding body of knowledge on the Kumaraswamy-X probability distribution by offering insights into its theoretical foundations and practical applications in engineering problems. The simulation-based evaluation highlights its potential to enhance the accuracy and reliability of probabilistic modelling in various engineering disciplines, promoting its adoption as a valuable tool in engineering research and practice.
Furthermore, the simulation study has demonstrated that the Kumaraswamy-X distribution can provide a suitable alternative to other well-established distri-

butions, offering a fresh perspective and potentially improving the accuracy of predictive models. Its robust performance in various scenarios, as evidenced by our study, suggests that it should be considered an essential and important tool for the scientist and engineers.
Our future work will also focus on the determination of Bayesian estimators of the proposed distribution. One aspect that will also be the focus of our attention will be the determination of the performance of estimators using various estimation methods.

References

[1] Z.Ahmad, M. Elgarhy, & G.G.Hamedani, A new Weibull-X family of distributions: properties, characterizations and applications, *J Stat Distrib Appl.* , 5(1), 1-18(2018).

[2] C. Alexander, G.M.Cordeiro, E.M. Ortega, & J.M. Sarabia, Generalized beta-generated distributions, *Comput. Stat. Data Anal.* ,56(6), 1880-1897(2012).

[3] A. Alzaatreh, F. Famoye, & C. Lee, The gamma-normal distribution: properties and applications, *Comput. Stat. Data Anal.* , 69, 67-80(2014).

[4] A. Alzaatreh, F. Famoye, & C. Lee, A new method for generating families of continuous distributions, *Metron*, 71, 6379(2013).

[5] A. Alzaatreh, F. Famoye, & C. Lee, Exponentiated TX family of distributions with some applications, *Int.J.Stat. Probab.*, 2(3), 31-49(2013).

[6] G.M.Cordeiro, M. de Castro, A new family of generalized distributions, *J Stat Comput Simul.* , 81(7), 883-898(2011).

[7] R. Dasgupta, On the distribution of Burr with applications, *Sankhya*, 73, 1-19(2011).

[8] N.Eugene, C. Lee, and F. Famoye, Beta-normal distribution and its applications, *Commun. Stat. Theory Methods*,31, 497-512(2002).

[9] Gradshteyn, I. S. and Ryzhik, I. M. *Table of integrals, series and products,* 7th edition. Academic Press,2007.

[10] F.Jamal and M. Nasir, Some new members of the T-X family of distributions, *Proc. 17th International Conference on Statistical Sciences Lahore, Pakistan*,January 21-23, 33, 113-120(2019).

[11] K. Modi, Power Exponentiated Family of Distributions with Application on Two Real-Life Datasets, *Thai Stat.*,19(3), 536-546(2021).

[12] K.Modi, D. Kumar, & Y. Singh, A new family of Distribution with application on two real datasets on survival problem, *Sci & Technology Asia*,25(1), 1-10(2020).

[13] D.N.P. Murthy, M. Xie, & R. Jiang, Weibull models. *Wiley series in probability and statistics: John Wiley and Sons*,2004.

[14] A.P.Prudnikov, Y.A. Brychkov, & O.I. Marichev, Integrals and Series. *New York: Gordon and Breach Science Publishers*, vol.1,1986.

[15] M.H. Tahir, G.M. Cordeiro, A.Y. Alzaatreh, M. Mansoor, & M. Zubair, The Logistic-X family of distributions and its applications, *Commun. Stat. Theory Methods*,45(24), 7326-7349(2016).

The Mohand Transform Approach to Fractional Integro-Differential Equations

Tharmalingam Gunasekar*, †; Prabakaran Raghavendran ‡

December 28, 2023

This research investigates specific classes of fractional integro-differential equations using a straightforward fractional calculus technique. The employed methodology yields a variety of compelling outcomes, including a generalized version of the well-established classical Frobenius method. The approach presented in this study primarily relies on fundamental theorems concerning the specific solutions of fractional integro-differential equations, utilizing the Mohand transform and binomial series extension coefficients. Additionally, advanced techniques for solving fractional integro-differential equations effectively are showcased.

Keywords: Riemann-Liouville (RL) fractional integrals; fractional-order differential equation; gamma function; Mittag-Leffler function; Wright function; Mohand transform of the fractional derivative

2010 Subject Classification: 26A33; 31A10; 33C10; 34A05; 35K37.

1 Introduction

Fractional calculus, an exploration of non-integer order integrals and derivatives, has garnered significant attention in mathematics owing to its diverse applications in scientific and engineering domains [4]. Its profound impact arises from robust mathematical foundations and practical implementations. More and more people are interested in making transforms that can solve fractional integro-differential equations. These transforms are often linked to basic ideas like the gamma function, beta function, error function, Mittag-Leffler function, and Mellin-Ross function [8].

*Department of Mathematics, Vel Tech Rangarajan Dr. Sagunthala R&D Institute of Science and Technology, Chennai, Email: tguna84@gmail.com

†School of Artificial Intelligence & Data Science, Indian Institute of Technology (IIT), Jodhpur, Rajasthan, India.

‡Department of Mathematics, Vel Tech Rangarajan Dr. Sagunthala R&D Institute of Science and Technology, Chennai, Email: rockypraba55@gmail.com

Integral transformations stand as fundamental mathematical tools crucial in addressing various differential equations, including partial differential equations, partial integro-differential equations, delay differential equations, and models describing population dynamics. Out of these, the Mohand transform, which comes from the classical Fourier integral, stands out as a simple and mathematically sound way to solve ordinary differential equations in the time domain. Alongside the Mohand transform, the Fourier, Laplace, Aboodh, and Elzaki transforms [2, 5, 6, 7] constitute the principal mathematical arsenal for solving differential equations. Notably, the Mohand transform shares a close relationship with the Laplace transform.

In recent research, Dubey et al. [12, 13, 14, 15, 16] have extensively explored various aspects of fractional calculus, employing computational techniques to forecast behavior, analyze integral transforms, investigate generalized invexity and duality in optimization problems, and delve into fractal dynamics within the physical sciences. Alongside these contributions, Singh, Purohit, and Kumar [17] compiled a comprehensive book discussing advanced numerical methods for differential equations, while Kumar et al. [18] conducted a computational analysis using fractal calculus to study local fractional partial differential equations.

The Mohand transform [1], like other integral transformations, exhibits certain limitations in its applicability. Its effectiveness often hinges on specific conditions and assumptions, potentially restricting its scope when solving differential equations. Some things about the Mohand approach are the same as the Laplace transform, but it might be hard to get closed-form solutions, especially when there are complicated boundary conditions or nonlinear equations. Recognizing and addressing these limitations is crucial when evaluating its usefulness in solving fractional integro-differential equations.

Aruldoss and Anusuya Devi expanded the use of binomial series extension coefficients and the Aboodh transform of fractional derivatives in 2020 to find exact solutions for fractional differential equations that are not homogeneous [3]. Moreover, Sumudu-based algorithms for differential equations have been extensively explored [9, 10].

We use the Mohand transform of fractional derivatives and binomial series extension coefficients in our research to come up with new ways to solve a number of fractional integro-differential equations. Furthermore, we elucidate properties relevant to our focal investigation.

2 Preliminaries

In this section, we are listing some preliminaries that are useful throughout the paper.

1. For the function $f(t)$, the RL fractional integral [3] of order $\varpi > 0$ is defined as,

$$I^{\varpi}{}_{t} f\left(t\right) = \frac{1}{\Gamma(\varpi)} \int_{a}^{t} \left(t-\zeta\right)^{\varpi-1} \, f\left(\zeta\right) d\zeta.$$

2. Caputo fractional derivative [2] of the function $f(t)$ is defined by

$$D^{\varpi}{}_{t}f\left(t\right)=\begin{cases} f^{m}\left(t\right) & ;\quad if\ \varpi=m\in\mathbb{N}, \\ \frac{1}{\Gamma(m-\varpi)}\int_{0}^{\zeta}\frac{f^{m}(t)}{(t-x)^{\varpi-m+1}}dt & ;if\ m-1<\varpi<m, \end{cases}$$

where the Euler gamma function $\Gamma(\cdot)$ is defined by

$$\Gamma\left(\phi\right)=\int_{0}^{\infty}t^{\phi-1}e^{-t}\ dt \qquad (\mathbb{R}>0)\,.$$

3. The Mohand transform [1] of a function $f(t)$, $t\in(0,\infty)$ is defined by

$$M\left[f\left(t\right)\right]\left(s\right)=F\left(s\right)=s^{2}\int_{0}^{\infty}e^{-st}\ f\left(t\right)\ dt(\mathrm{s}\in\mathbb{C}).$$

4. The Mittag-Leffler function [11] is defined by

$$E_{\gamma,\delta}\left(\phi\right)=\sum_{\wp=0}^{\infty}\frac{\phi^{\wp}}{\Gamma\left(\gamma\wp+\delta\right)} \qquad (\gamma,\delta,\phi\in\mathbb{C},\ \mathbb{R}(\gamma)>0).$$

5. The Simplest wright function [11] is defined by

$$\rho\left(\omega,\phi;\varphi\right)=\sum_{\wp=0}^{\infty}\frac{1}{\Gamma(\omega\wp+\phi)}.\frac{\varphi^{\wp}}{\wp!} \qquad (\varphi.\phi,\omega\in\mathbb{C}\ )\,.$$

6. The general Wright function [11] ${}_{i}\lambda_{j}\left(\varphi\right)$ is classified as $\varphi\in\mathbb{C}$, $\nu_{1p},\nu_{2p}\in\mathbb{C}$, and real $\omega_{p},\phi_{q}\in\mathbb{R}$ $(p=1,\ldots,\ i,\ q=1,\ldots,\ j)$ by the series

$${}_{i}\lambda_{j}\left(\nu\right)=\ {}_{i}\lambda_{j}\left(\begin{array}{c}(\nu_{1p},\omega_{p})_{1,i}\\(\nu_{2q},\phi_{q})_{1,j}\end{array}\ \middle|\ \varphi\right)=\sum_{r=0}^{\infty}\frac{\prod_{p=1}^{i}\Gamma(\nu_{1p}+\omega_{p}r)}{\prod_{q=1}^{j}\Gamma(\nu_{2q}+\phi_{q}r)}.\frac{\varphi^{r}}{r!}.$$

7. The convolution integral of Mohand transform is

$$M\left[\left(f*g\right)\left(t\right)\right]=\frac{1}{s^{2}}M[f\left(t\right)]M[g\left(t\right)].$$

8. The inverse Mohand transform is defined by

$$M^{-1}\Big[\frac{\Gamma(n+1)}{s^{n-1}}\Big]=t^{n}.$$

9. The derivatives of the Mohand transform are

$$M[f^{'}(t)]=sF(s)-s^{2}f(0),$$

$$M[f^{''}(t)]=s^{2}F(s)-s^{3}f(0)-s^{2}f^{'}(0).$$

Remark 2.1

$$M\left[D^{\varpi}f\left(t\right)\right]\left(s\right)=s^{2}\int_{0}^{\infty}e^{-st}\ \left[D^{\varpi}\ f\left(t\right)\right]dt$$

$$
\begin{aligned}
&= s^2 \int_0^\infty e^{-st} \frac{1}{\Gamma(n-\varpi)} \int_0^t \frac{f^{(n)}(\zeta)}{(t-\zeta)^{\varpi-n+1}} \, d\zeta \, dt \\
&= \frac{s^2}{\Gamma(n-\varpi)} \int_0^\infty \int_\zeta^\infty e^{-st} \frac{f^{(n)}(\zeta)}{(t-\zeta)^{\varpi-n+1}} \, dt \, d\zeta \\
&= \frac{s^2}{\Gamma(n-\varpi)} \int_0^\infty f^{(n)}(\zeta) \int_0^\infty e^{-s(u+t)} \, u^{n-\varpi-1} \, du \, d\zeta \\
&= \frac{s^2}{\Gamma(n-\varpi)} \int_0^\infty e^{-s\zeta} f^{(n)}(\zeta) \int_0^\infty e^{-su} \, u^{n-\varpi-1} \, du \, d\zeta \\
&= \frac{s^2}{\Gamma(n-\varpi)} \int_0^\infty e^{-s\zeta} f^{(n)}(\zeta) \frac{\Gamma(\mathrm{n}-\varpi)}{s^{n-\varpi}} d\zeta \\
&= s^{\varpi-n+2} \int_0^\infty e^{-s\zeta} \, f^{(n)}(\zeta) \, d\zeta = s^{\varpi-n+2} \, M\left[f^{(n)}(\zeta)\right](s) \\
&= s^{\varpi-n+2}.s^n \left[F(s) - \left(sf(0) + f'(0) + \cdots + s^{2-n} f^{(n-1)}(0)\right)\right] \\
&= s^{\varpi+2} \left[F(s) - sf(0) - f'(0) - \cdots - s^{2-n} f^{(n-1)}(0)\right] \\
&= s^{\varpi+2} \left[M[f(t)] - \sum_{\mathfrak{K}=0}^{n} s^{1-\mathfrak{K}} f^{(\mathfrak{K}-1)}(0)\right].
\end{aligned}
$$

Note: To change the order of integration in the preceding derivative we use Fubini's theorem.

3 Solutions of fractional integro-differential equations

We can strongly suspect thus far in this section that $y(t)$ is enough to ensure that the Mohand transform $M[y(t)]$ proceeds for some value of the parameter s.

Theorem 3.1 Let $1 < \varpi < 2$ and a and $b \in \mathbb{R}$. Then the fractional integro-differential equation

$$
y''(t) + a \, y^{\varpi}(t) + by(t) = \int_0^s \frac{g(t)}{(s-t)^{\varrho}} \, dt \quad ; \quad 0 < \varrho < 1 \tag{1}
$$

With $y(0) = \aleph_0$ and $y'(0) = \aleph_1$ its proposal is provided by

$$
\begin{aligned}
y(t) = \; & \aleph_0 \sum_{\mathfrak{K}=0}^{\infty} \frac{(-b)^{\mathfrak{K}} \, t^{2\mathfrak{K}}}{\mathfrak{K}!} \sum_{\wp=0}^{\infty} \frac{\Gamma(\mathfrak{K}+\wp+1) \, \left(-at^{(2-\varpi)}\right)^{\wp}}{\Gamma[(2-\varpi)\wp + 2\mathfrak{K}+1] \; \wp!} \\
& + \aleph_1 \sum_{\mathfrak{K}=0}^{\infty} \frac{(-b)^{\mathfrak{K}} \, t^{2\mathfrak{K}+1}}{\mathfrak{K}!} \sum_{\wp=0}^{\infty} \frac{\Gamma(\mathfrak{K}+\wp+1) \, \left(-at^{(2-\varpi)}\right)^{\wp}}{\Gamma[(2-\varpi)\wp + 2\mathfrak{K}+2] \; \wp!}
\end{aligned}
$$

$$+\ a\aleph_0 \sum_{\mathfrak{K}=0}^{\infty} \frac{(-b)^{\mathfrak{K}}\ t^{2\mathfrak{K}-\varpi+2}}{\mathfrak{K}!} \sum_{r=0}^{\infty} \frac{\Gamma(\mathfrak{K}+\wp+1)\ \left(-at^{(2-\varpi)}\right)^{\wp}}{\Gamma[(2-\varpi)\wp+2\mathfrak{K}-\varpi+3]\ \wp!}$$

$$+\ a\aleph_1 \sum_{\mathfrak{K}=0}^{\infty} \frac{(-b)^{\mathfrak{K}}\ t^{2\mathfrak{K}-\varpi+3}}{\mathfrak{K}!} \sum_{\wp=0}^{\infty} \frac{\Gamma(\mathfrak{K}+\wp+1)\ \left(-at^{(2-\varpi)}\right)^{\wp}}{\Gamma[(2-\varpi)\wp+2\mathfrak{K}-\varpi+4]\ \wp!}$$

$$+\frac{\sin\varrho\pi}{\pi}\frac{d}{ds}\int_0^s (s-t)^{\varrho-1} f(t)\,dt \sum_{\mathfrak{K}=0}^{\infty} \frac{(-b)^{\mathfrak{K}}\ t^{2\mathfrak{K}+1}}{\mathfrak{K}!} \sum_{\wp=0}^{\infty} \frac{\Gamma(\mathfrak{K}+\wp+1)\ \left(-at^{(2-\varpi)}\right)^{\wp}}{\Gamma[(2-\varpi)\wp+2\mathfrak{K}+2]\ \wp!}\ . \tag{2}$$

Proof:
Utilizing the Mohand transform in (1) and taking into consideration, we have

$$s^2F(s)-s^3f(0)-s^2f'(0)+a\left[s^{\varpi}F(s)-s^{\varpi+1}f(0)-s^{\varpi}f'(0)\right]+bF(s)=M[f(t)]$$

where $f(t)=\int_0^s \frac{g(t)}{(s-t)^{\varrho}}\ dt$,

$$s^2M[y(t)]-s^3y(0)-s^2y'(0)+as^{\varpi}M[y(t)]-as^{\varpi+1}y(0)-as^{\varpi}y'(0)+b\,M[y(t)]=M[f(t)]$$

$$\left(s^2+as^{\varpi}+b\right)\ M[y(t)]=s^3\aleph_0+s^2\aleph_1+as^{\varpi+1}\aleph_0+as^{\varpi}\aleph_1+M[f(t)]$$

$$M[y(t)]=\frac{s^3\aleph_0+s^2\aleph_1+as^{\varpi+1}\aleph_0+as^{\varpi}\aleph_1+M[f(t)]}{(s^2+as^{\varpi}+b)}. \tag{3}$$

Since

$$\begin{aligned}
\frac{1}{(s^2+as^{\varpi}+b)} &= \frac{s^{-\varpi}}{s^{2-\varpi}+a+bs^{-\varpi}} \\
&= \frac{s^{-\varpi}}{(s^{2-\varpi}+a)\left(1+\frac{bs^{-\varpi}}{s^{2-\varpi}+a}\right)} \\
&= \frac{s^{-\varpi}}{s^{2-\varpi}+a}\sum_{\mathfrak{K}=0}^{\infty}\left(\frac{-bs^{-\varpi}}{s^{2-\varpi}+a}\right)^{\mathfrak{K}} \\
&= \sum_{\mathfrak{K}=0}^{\infty}\frac{(-b)^k s^{-\varpi\mathfrak{K}-\varpi}}{(s^{2-\varpi}+a)^{\mathfrak{K}+1}} \\
&= \sum_{\mathfrak{K}=0}^{\infty}\frac{(-b)^{\mathfrak{K}}s^{-2\mathfrak{K}-2}}{\left(1+a\ s^{\varpi-2}\right)^{\mathfrak{K}+1}} \\
&= \sum_{\mathfrak{K}=0}^{\infty}(-b)^{\mathfrak{K}}s^{-2\mathfrak{K}-2}\sum_{\wp=0}^{\infty}\left(-as^{\varpi-2}\right)^{\wp}\begin{pmatrix}\mathfrak{K}+\wp\\ \wp\end{pmatrix} \\
&= \sum_{\mathfrak{K}=0}^{\infty}(-b)^{\mathfrak{K}}\sum_{\wp=0}^{\infty}\begin{pmatrix}\mathfrak{K}+\wp\\ \wp\end{pmatrix}(-a)^{\wp}\ s^{(\varpi-2)\wp-2\mathfrak{K}-2}
\end{aligned} \tag{4}$$

and

$$M\left[f\left(t\right)\right]=M\left[\int_{0}^{s}\frac{g\left(t\right)}{\left(s-t\right)^{\varrho}}\,dt\right].$$

This is Convolution integral,

$$F\left(P\right)=\frac{1}{s^{2}}\;K\left(P\right)\;G(P)$$

Where $K(P)$ is the Mohand transform of $K(s)=s^{-\varrho}$

$$M\left[K\left(s\right)\right]=s^{-\varrho}$$

$$K\left(P\right)=\frac{\Gamma(-\varrho+1)}{s^{-\varrho-1}}=s^{\varrho+1}\;\Gamma\left(-\varrho+1\right)$$

$$G\left(P\right)=\frac{p^{2}F(P)}{p^{\varrho+1}\;\Gamma(1-\varrho)}$$

$$G\left(P\right)=\frac{p^{1-\varrho}F\left(P\right)}{\Gamma\left(1-\varrho\right)}$$

$$G\left(P\right)=\frac{\sin\pi\;\varrho}{\pi}p\;.\;p^{-\varrho}\Gamma\left(\varrho\right)F(P)$$

$$G\left(P\right)=\frac{\sin\pi\;\varrho}{\pi}p\;.M\left[\int_{0}^{s}\left(s-t\right)^{\varrho}\;f'(t)\;dt\right]\tag{5}$$

Substituting the above two equations (4) and (5) in (3), we get

$$\begin{aligned}M[y\left(t\right)]=\;&\aleph_{0}\sum_{\mathfrak{K}=0}^{\infty}\left(-b\right)^{\mathfrak{K}}\sum_{\wp=0}^{\infty}\left(\begin{array}{c}\mathfrak{K}+\wp\\ \wp\end{array}\right)\;\left(-a\right)^{\wp}\;s^{(\varpi-2)\wp-2\mathfrak{K}-1}\\&+\aleph_{1}\sum_{\mathfrak{K}=0}^{\infty}\left(-b\right)^{\mathfrak{K}}\sum_{\wp=0}^{\infty}\left(\begin{array}{c}\mathfrak{K}+\wp\\ \wp\end{array}\right)\;\left(-a\right)^{\wp}\;s^{(\varpi-2)\wp-2\mathfrak{K}-2}\\&+a\aleph_{0}\sum_{\mathfrak{K}=0}^{\infty}\left(-b\right)^{\mathfrak{K}}\sum_{\wp=0}^{\infty}\left(\begin{array}{c}\mathfrak{K}+\wp\\ \wp\end{array}\right)\;\left(-a\right)^{\wp}\;s^{(\varpi-2)\wp-2\mathfrak{K}+\varpi-3}\\&+a\aleph_{1}\sum_{\mathfrak{K}=0}^{\infty}\left(-b\right)^{\mathfrak{K}}\sum_{\wp=0}^{\infty}\left(\begin{array}{c}\mathfrak{K}+\wp\\ \wp\end{array}\right)\;\left(-a\right)^{\wp}\;s^{(\varpi-2)\wp-2\mathfrak{K}+\varpi-4}\\+\frac{\sin\pi\;\varrho}{\pi}p\;.M&\left[\int_{0}^{s}\frac{g\left(t\right)}{\left(s-t\right)^{\varrho}}\;dt\right]\sum_{\mathfrak{K}=0}^{\infty}\left(-b\right)^{\mathfrak{K}}\sum_{\wp=0}^{\infty}\left(\begin{array}{c}\mathfrak{K}+\wp\\ \wp\end{array}\right)\;\left(-a\right)^{\wp}\;s^{(\varpi-2)\wp-2\mathfrak{K}-2}\;.\end{aligned}$$

(6)

Thus, providing inverse Mohand transform on both sides in equation (6), we get

$$y\left(t\right)=\;\aleph_{0}\sum_{\mathfrak{K}=0}^{\infty}\frac{\left(-b\right)^{\mathfrak{K}}\;t^{2\mathfrak{K}}}{\mathfrak{K}!}\sum_{\wp=0}^{\infty}\frac{\Gamma\left(\mathfrak{K}+\wp+1\right)\;\left(-at^{(2-\varpi)}\right)^{\wp}}{\Gamma\left[\left(2-\varpi\right)\wp+2\mathfrak{K}+1\right]\;\wp!}$$

$$+\aleph_1\sum_{\mathfrak{K}=0}^{\infty}\frac{(-b)^{\mathfrak{K}}\ t^{2\mathfrak{K}+1}}{\mathfrak{K}!}\sum_{\wp=0}^{\infty}\frac{\Gamma\left(\mathfrak{K}+\wp+1\right)\ \left(-at^{(2-\varpi)}\right)^{\wp}}{\Gamma\left[\left(2-\varpi\right)\wp+2\mathfrak{K}+2\right]\ \wp!}$$

$$+\ a\aleph_0\sum_{\mathfrak{K}=0}^{\infty}\frac{(-b)^{\mathfrak{K}}\ t^{2\mathfrak{K}-\varpi+2}}{\mathfrak{K}!}\sum_{\wp=0}^{\infty}\frac{\Gamma\left(\mathfrak{K}+\wp+1\right)\ \left(-at^{(2-\varpi)}\right)^{\wp}}{\Gamma\left[\left(2-\varpi\right)\wp+2\mathfrak{K}-\varpi+3\right]\ \wp!}$$

$$+\ a\aleph_1\sum_{\mathfrak{K}=0}^{\infty}\frac{(-b)^{\mathfrak{K}}\ t^{2\mathfrak{K}-\varpi+3}}{\mathfrak{K}!}\sum_{\wp=0}^{\infty}\frac{\Gamma\left(\mathfrak{K}+\wp+1\right)\ \left(-at^{(2-\varpi)}\right)^{\wp}}{\Gamma\left[\left(2-\varpi\right)\wp+2\mathfrak{K}-\varpi+4\right]\ \wp!}$$

$$+\frac{\sin\varrho\pi}{\pi}\frac{d}{ds}\int_0^s(s-t)^{\varrho-1}f\left(t\right)dt\sum_{\mathfrak{K}=0}^{\infty}\frac{(-b)^{\mathfrak{K}}\ t^{2\mathfrak{K}+1}}{\mathfrak{K}!}\sum_{\wp=0}^{\infty}\frac{\Gamma\left(\mathfrak{K}+\wp+1\right)\ \left(-at^{(2-\varpi)}\right)^{\wp}}{\Gamma\left[\left(2-\varpi\right)\wp+2\mathfrak{K}+2\right]\ \wp!}\ .$$

Example 3.1 The fractional integro-differential equation is

$$y^{''}\left(t\right)+\sqrt{6}\ y^{\left(\frac{3}{2}\right)}\left(t\right)+11y\left(t\right)=\int_0^s\frac{g\left(t\right)}{\left(s-t\right)^{\left(\frac{1}{2}\right)}}\ dt$$

With $y\left(0\right)=1$ and $y'\left(0\right)=1$ its proposal is provided by

$$y\left(t\right)=\ \sum_{\mathfrak{K}=0}^{\infty}\frac{(-11)^{\mathfrak{K}}\ t^{2\mathfrak{K}}}{\mathfrak{K}!}\sum_{\wp=0}^{\infty}\frac{\Gamma\left(\mathfrak{K}+\wp+1\right)\ \left(-\sqrt{6}\ t^{\left(\frac{1}{2}\right)}\right)^{\wp}}{\Gamma\left[\left(\frac{1}{2}\right)\wp+2\mathfrak{K}+1\right]\ \wp!}$$

$$+\sum_{\mathfrak{K}=0}^{\infty}\frac{(-11)^{\mathfrak{K}}\ t^{2\mathfrak{K}+1}}{\mathfrak{K}!}\sum_{\wp=0}^{\infty}\frac{\Gamma\left(\mathfrak{K}+\wp+1\right)\ \left(-\sqrt{6}t^{\left(\frac{1}{2}\right)}\right)^{\wp}}{\Gamma\left[\left(\frac{1}{2}\right)\wp+2\mathfrak{K}+2\right]\ \wp!}$$

$$+\ \sqrt{6}\sum_{\mathfrak{K}=0}^{\infty}\frac{(-11)^{\mathfrak{K}}\ t^{2\mathfrak{K}+\frac{1}{2}}}{\mathfrak{K}!}\sum_{\wp=0}^{\infty}\frac{\Gamma\left(\mathfrak{K}+\wp+1\right)\ \left(-\sqrt{6}t^{\left(\frac{1}{2}\right)}\right)^{\wp}}{\Gamma\left[\left(\frac{1}{2}\right)\wp+2\mathfrak{K}+\frac{3}{2}\right]\ \wp!}$$

$$+\ \sqrt{6}\sum_{\mathfrak{K}=0}^{\infty}\frac{(-11)^{\mathfrak{K}}\ t^{2\mathfrak{K}+\frac{3}{2}}}{\mathfrak{K}!}\sum_{\wp=0}^{\infty}\frac{\Gamma\left(\mathfrak{K}+\wp+1\right)\ \left(-\sqrt{6}t^{\left(\frac{1}{2}\right)}\right)^{\wp}}{\Gamma\left[\left(\frac{1}{2}\right)\wp+2\mathfrak{K}+\frac{5}{2}\right]\ \wp!}$$

$$+\frac{1}{\pi}\frac{d}{ds}\int_0^s(s-t)^{-\frac{1}{2}}f\left(t\right)dt\sum_{\mathfrak{K}=0}^{\infty}\frac{(-11)^{\mathfrak{K}}\ t^{2\mathfrak{K}+1}}{\mathfrak{K}!}\sum_{\wp=0}^{\infty}\frac{\Gamma\left(\mathfrak{K}+\wp+1\right)\ \left(-at^{\left(\frac{1}{2}\right)}\right)^{\wp}}{\Gamma\left[\left(\frac{1}{2}\right)\wp+2\mathfrak{K}+2\right]\ \wp!}\ ,$$

Figure 1 illustrates the solution behavior of the fractional integro-differential equation of example 1 at various values of ϖ.

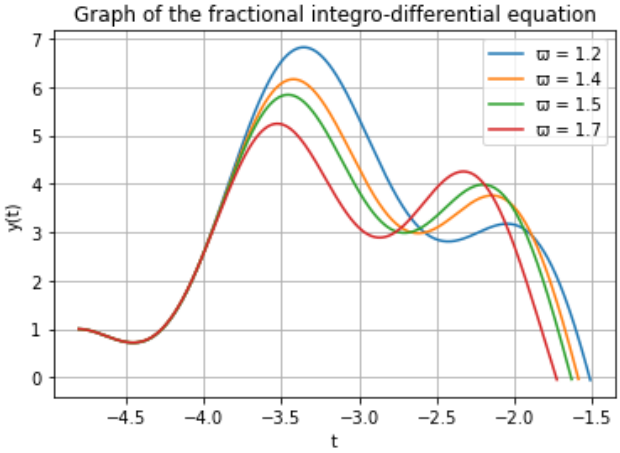

Figure 1: The solution behavior of Example 1.

Theorem 3.2 Let $1 < \varpi < 2$ and a and $b \in \mathbb{R}$. Then the fractional integro-differential equation is

$$y^{\varpi}(t) + a\, y'(t) + by(t) = \int_0^s \frac{g(t)}{(s-t)^{\varrho}}\, dt \quad ; \quad 0 < \varrho < 1 \tag{7}$$

with $y(0) = \aleph_0$ and $y'(0) = \aleph_1$ its proposal is provided by

$$\begin{aligned} y(t) = {} & \aleph_0 \sum_{\mathfrak{K}=0}^{\infty} \frac{(-b)^{\mathfrak{K}}}{\mathfrak{K}!} \sum_{\wp=0}^{\infty} \frac{\Gamma(\mathfrak{K}+\wp+1)\ (-a)^{\wp} t^{(\varpi-1)\wp+\varpi\mathfrak{K}}}{\Gamma[(\varpi-1)\wp+\varpi\mathfrak{K}+1]\ \wp!} \\ & + \aleph_1 \sum_{\mathfrak{K}=0}^{\infty} \frac{(-b)^{\mathfrak{K}}}{\mathfrak{K}!} \sum_{\wp=0}^{\infty} \frac{\Gamma(\mathfrak{K}+\wp+1)\ (-a)^{\wp} t^{(\varpi-1)\wp+\varpi\mathfrak{K}+1}}{\Gamma[(\varpi-1)\wp+\varpi\mathfrak{K}+2]\ \wp!} \\ & + a\aleph_0 \sum_{\mathfrak{K}=0}^{\infty} \frac{(-b)^{\mathfrak{K}}}{\mathfrak{K}!} \sum_{\wp=0}^{\infty} \frac{\Gamma(\mathfrak{K}+\wp+1)\ (-a)^{\wp} t^{(\varpi-1)\wp+\varpi\mathfrak{K}+\varpi-1}}{\Gamma[(\varpi-1)\wp+\varpi\mathfrak{K}+\varpi]\ \wp!} \\ & + \frac{\sin\varrho\pi}{\pi} \frac{d}{ds} \int_0^s (s-t)^{\varrho-1} f(t)\, dt \sum_{\mathfrak{K}=0}^{\infty} \frac{(-b)^{\mathfrak{K}}}{\mathfrak{K}!} \sum_{\wp=0}^{\infty} \frac{\Gamma(\mathfrak{K}+\wp+1)\ (-a)^{\wp} t^{(\varpi-1)\wp+\varpi\mathfrak{K}+\varpi-1}}{\Gamma[(\varpi-1)\wp+\varpi\mathfrak{K}+\varpi]\ \wp!}. \end{aligned} \tag{8}$$

Proof: Utilizing the Mohand transform in (7) and taking into consideration, we have

$$s^{\varpi} F(s) - s^{\varpi+1} f(0) - s^{\varpi} f'(0) + a\left[s\, F(s) - s^2 f(0)\right] + b\, F(s) = M[f(t)]$$

where $f(t) = \int_0^s \frac{g(t)}{(s-t)^{\varrho}}\, dt$,

$$s^{\varpi} M[y(t)] - s^{\varpi+1} y(0) - s^{\varpi} y'(0) + a\, s\, M[y(t)] - as^2 y(0) + b\, M[y(t)] = M[f(t)]$$

$$s^{\varpi}M\left[y\left(t\right)\right]-s^{\varpi+1}\aleph_0-s^{\varpi}\aleph_1+a\ s\ M\left[y\left(t\right)\right]-as^2\aleph_0+b\ M\left[y\left(t\right)\right]=M\left[f\left(t\right)\right]$$

$$M\left[y\left(t\right)\right]=\frac{s^{\varpi+1}\aleph_0+s^{\varpi}\aleph_1+as^2\aleph_0+M\left[f\left(t\right)\right]}{\left(s^{\varpi}+a\ s+b\right)}. \tag{9}$$

Since

$$\begin{aligned}\frac{1}{\left(s^{\varpi}+a\ s+b\right)}&=\frac{s^{-1}}{s^{\varpi-1}+a+bs^{-1}}\\&=\frac{s^{-1}}{\left(s^{\varpi-1}+a\right)\left(1+\frac{b\ s^{-1}}{s^{\varpi-1}+a}\right)}\\&=\frac{s^{-1}}{s^{\varpi-1}+a}\sum_{\mathfrak{K}=0}^{\infty}\left(\frac{-bs^{-1}}{s^{\varpi-1}+a}\right)^{\mathfrak{K}}\\&=\sum_{\mathfrak{K}=0}^{\infty}\frac{(-b)^{\mathfrak{K}}s^{-\mathfrak{K}-1}}{\left(s^{\varpi-1}+a\right)^{\mathfrak{K}+1}}\\&=\sum_{\mathfrak{K}=0}^{\infty}\frac{(-b)^{\mathfrak{K}}s^{-\varpi\mathfrak{K}-\varpi}}{\left(1+a\ s^{1-\varpi}\right)^{\mathfrak{K}+1}}\\&=\sum_{\mathfrak{K}=0}^{\infty}(-b)^{\mathfrak{K}}s^{-\varpi\mathfrak{K}-\varpi}\sum_{\wp=0}^{\infty}\left(-as^{1-\varpi}\right)^{\wp}\left(\begin{array}{c}\mathfrak{K}+\wp\\ \wp\end{array}\right)\\&=\sum_{\mathfrak{K}=0}^{\infty}(-b)^{\mathfrak{K}}\sum_{\wp=0}^{\infty}\left(\begin{array}{c}\mathfrak{K}+\wp\\ \wp\end{array}\right)\ (-a)^{\wp}\ s^{(1-\varpi)\wp-\varpi\mathfrak{K}-\varpi}\end{aligned} \tag{10}$$

and we know that,

$$M\left[f\left(t\right)\right]=M\left[\int_0^s\frac{g\left(t\right)}{\left(s-t\right)^{\varrho}}\ dt\right].$$

This gives that,

$$G\left(P\right)=\frac{\sin\pi\ \varrho}{\pi}p\ .M\left[\int_0^s\left(s-t\right)^{\varrho}\ f'(t)\ dt\right]. \tag{11}$$

Substituting the above two equations (10) and (11) in (9), we get

$$\begin{aligned}y\left(t\right)=\ &\aleph_0\sum_{\mathfrak{K}=0}^{\infty}\frac{(-b)^{\mathfrak{K}}}{\mathfrak{K}!}\sum_{\wp=0}^{\infty}\frac{\Gamma\left(\mathfrak{K}+\wp+1\right)\ (-a)^{\wp}t^{(\varpi-1)\wp+\varpi\mathfrak{K}}}{\Gamma\left[\left(\varpi-1\right)\wp+\varpi\mathfrak{K}+1\right]\ \wp!}\\&+\aleph_1\sum_{\mathfrak{K}=0}^{\infty}\frac{(-b)^{\mathfrak{K}}}{\mathfrak{K}!}\sum_{\wp=0}^{\infty}\frac{\Gamma\left(\mathfrak{K}+\wp+1\right)\ (-a)^{\wp}t^{(\varpi-1)\wp+\varpi\mathfrak{K}+1}}{\Gamma\left[\left(\varpi-1\right)\wp+\varpi\mathfrak{K}+2\right]\ \wp!}\\&+a\aleph_0\sum_{\mathfrak{K}=0}^{\infty}\frac{(-b)^{\mathfrak{K}}}{\mathfrak{K}!}\sum_{\wp=0}^{\infty}\frac{\Gamma\left(\mathfrak{K}+\wp+1\right)\ (-a)^{\wp}t^{(\varpi-1)\wp+\varpi\mathfrak{K}+\varpi-1}}{\Gamma\left[\left(\varpi-1\right)\wp+\varpi\mathfrak{K}+\varpi\right]\ \wp!}\end{aligned}$$

$$+\frac{\sin\varrho\pi}{\pi}\frac{d}{ds}\int_0^s (s-t)^{\varrho-1} f(t)\,dt \sum_{\mathfrak{K}=0}^{\infty}\frac{(-b)^{\mathfrak{K}}}{\mathfrak{K}!}\sum_{\wp=0}^{\infty}\frac{\Gamma(\mathfrak{K}+\wp+1)\ (-a)^{\wp}t^{(\varpi-1)\wp+\varpi\mathfrak{K}+\varpi-1}}{\Gamma[(\varpi-1)\wp+\varpi\mathfrak{K}+\varpi]\ \wp!}.$$

The Wright function can express this solution as

$$\begin{aligned} y(t) = {} & \aleph_0\sum_{\mathfrak{K}=0}^{\infty}\frac{(-b)^{\mathfrak{K}}\ t^{\varpi\mathfrak{K}}}{\mathfrak{K}!}1\lambda 1\left(\begin{array}{c}(\mathfrak{K}+1,\ 1\\ (\varpi\mathfrak{K}+1,\ \varpi-1)\end{array}\Big|-a\ t^{\varpi-1}\right)\\ & +\aleph_1\sum_{\mathfrak{K}=0}^{\infty}\frac{(-b)^{\mathfrak{K}}t^{\varpi\mathfrak{K}+1}}{\mathfrak{K}!}1\lambda 1\left(\begin{array}{c}(\mathfrak{K}+1,\ 1\\ (\varpi\mathfrak{K}+2,\ \varpi-1)\end{array}\Big|-a\ t^{\varpi-1}\right)\\ & +a\aleph_0\sum_{\mathfrak{K}=0}^{\infty}\frac{(-b)^{\mathfrak{K}}t^{\varpi\mathfrak{K}+\varpi-1}}{\mathfrak{K}!}1\lambda 1\left(\begin{array}{c}(\mathfrak{K}+1,\ 1\\ (\varpi\mathfrak{K}+\varpi,\ \varpi-1)\end{array}\Big|-a\ t^{\varpi-1}\right)\\ & +\frac{\sin\varrho\pi}{\pi}\frac{d}{ds}\int_0^s (s-t)^{\varrho-1} f(t)\,dt\sum_{\mathfrak{K}=0}^{\infty}\frac{(-b)^{\mathfrak{K}}t^{\varpi\mathfrak{K}+\varpi-1}}{\mathfrak{K}!}\ 1\lambda 1\left(\begin{array}{c}(\mathfrak{K}+1,\ 1\\ (\varpi\mathfrak{K}+\varpi,\ \varpi-1)\end{array}\Big|-a\ t^{\varpi-1}\right). \end{aligned} \tag{12}$$

Example 3.2 The fractional integro-differential equation is

$$y^{\frac{3}{2}}(t)-4y'(t)-5\ y(t)=\int_0^s\frac{g(t)}{(s-t)^{\frac{1}{2}}}\ dt$$

with $y(0)=1$ and $y'(0)=1$ its proposal is provided by

$$\begin{aligned} y(t) = {} & \sum_{\mathfrak{K}=0}^{\infty}\frac{(5)^{\mathfrak{K}}}{\mathfrak{K}!}\sum_{\wp=0}^{\infty}\frac{\Gamma(\mathfrak{K}+\wp+1)\ (4)^{\wp}t^{(\varpi-1)\wp+\varpi\mathfrak{K}}}{\Gamma\left[\left(\frac{1}{2}\right)\wp+\frac{3}{2}\mathfrak{K}+1\right]\ \wp!}\\ & +\sum_{\mathfrak{K}=0}^{\infty}\frac{(5)^{\mathfrak{K}}}{\mathfrak{K}!}\sum_{\wp=0}^{\infty}\frac{\Gamma(\mathfrak{K}+\wp+1)\ (4)^{\wp}t^{\left(\frac{1}{2}\right)\wp+\frac{3}{2}\mathfrak{K}+1}}{\Gamma\left[\left(\frac{1}{2}\right)\wp+\frac{3}{2}\mathfrak{K}+2\right]\ \wp!}\\ & -4\sum_{\mathfrak{K}=0}^{\infty}\frac{(5)^{\mathfrak{K}}}{\mathfrak{K}!}\sum_{\wp=0}^{\infty}\frac{\Gamma(\mathfrak{K}+\wp+1)\ (4)^{\wp}t^{\left(\frac{1}{2}\right)\wp+\frac{3}{2}\mathfrak{K}+\frac{1}{2}}}{\Gamma\left[\left(\frac{1}{2}\right)\wp+\frac{3}{2}\mathfrak{K}+\frac{3}{2}\right]\ \wp!}\\ & +\frac{1}{\pi}\frac{d}{ds}\int_0^s (s-t)^{-\frac{1}{2}} f(t)\,dt\sum_{\mathfrak{K}=0}^{\infty}\frac{(5)^{\mathfrak{K}}}{\mathfrak{K}!}\sum_{\wp=0}^{\infty}\frac{\Gamma(\mathfrak{K}+\wp+1)\ (4)^{\wp}t^{\left(\frac{1}{2}\right)\wp+\frac{3}{2}\mathfrak{K}+\frac{1}{2}}}{\Gamma\left[\left(\frac{1}{2}\right)\wp+\frac{3}{2}\mathfrak{K}+\frac{3}{2}\right]\ \wp!} \end{aligned}$$

Figure 2 illustrates the solution behavior of the fractional integro-differential equation of example 1 at various values of ϖ.

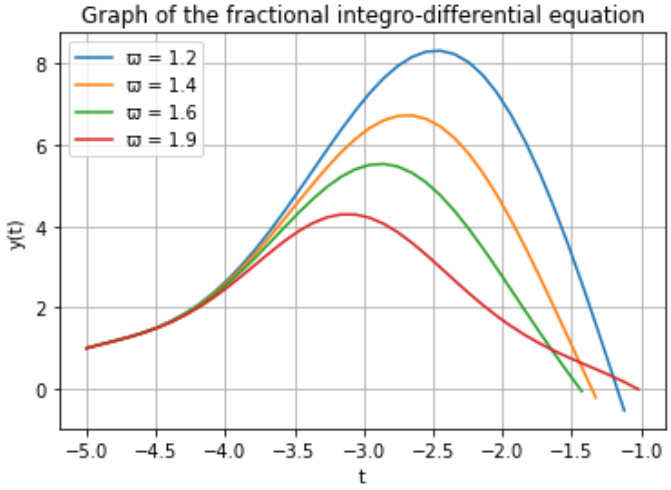

Figure 2: The solution behavior of Example 2.

Proposition 3.1 Let $1 < \varpi, \varrho < 2$ and $b \in \mathbb{R}$. Then the fractional integro-differential equation is

$$y^{\varpi}(t) - by(t) = \int_0^s \frac{g(t)}{(s-t)^{\varrho}}\, dt \quad ; \quad 0 < \varrho < 1 \tag{13}$$

With $y(0) = \aleph_0$ its proposal is provided by

$$y(t) = \aleph_0 \sum_{\Re=0}^{\infty} b^{\Re} \frac{t^{\varpi\Re}}{\Gamma(\varpi\Re+1)} + \frac{\sin\varrho\pi}{\pi} \frac{d}{ds} \int_0^s (s-t)^{\varrho-1} f(t)\, dt \sum_{\Re=0}^{\infty} \frac{(-b)^{\Re} t^{\varpi+\varpi\Re-1}}{\Gamma(\varpi+\varpi\Re)}$$

$$= \aleph_0 E_{\alpha}(bt^{\varpi}) + \frac{\sin\varrho\pi}{\pi} \frac{d}{ds} \int_0^s (s-t)^{\varrho-1} f(t)\, dt\, t^{\varpi-1} E_{\varpi,\varpi}(bt^{\varpi}). \tag{14}$$

Proof: The proof of this proposition as like as previous theorem.

Remark 3.1 Accordingly, $a = 0$ in (7), then the derivative is

$$y^{\varpi}(t) + by(t) = \int_0^s \frac{g(t)}{(s-t)^{\varrho}}\, dt \quad ; \; 1 < \varpi \leq 2, \; 0 < \varrho < 1 \tag{15}$$

With $y(0) = \aleph_0$ and $y'(0) = \aleph_1$ its proposal is provided by

$$y(t) = \aleph_0 E_{\varpi,1}(-bt^{\varpi}) + \aleph_1 E_{\varpi,2}(-bt^{\varpi}) + \frac{\sin\varrho\pi}{\pi} \frac{d}{ds} \int_0^s (s-t)^{\varrho-1} f(t)\, dt\, t^{\varpi-1} E_{\varpi,\varpi}(-bt^{\varpi}). \tag{16}$$

Proposition 3.2 A nearly simple harmonic vibration integro-differential equation

$$y^{\varpi}(t) + z^2 y(t) = \int_0^s \frac{g(t)}{(s-t)^{\varrho}}\, dt \quad ; \; 1 < \varpi \leq 2, \; 0 < \varrho < 1 \tag{17}$$

With $y(0) = \aleph_0$ and $y'(0) = \aleph_1$ its proposal is provided by

$$y(t) = \aleph_0 E_{\varpi,1}\left(-z^2 t^{\varpi}\right) + \aleph_1 E_{\varpi,2}\left(-z^2 t^{\varpi}\right) + \frac{\sin\varrho\pi}{\pi}\frac{d}{ds}\int_0^s (s-t)^{\varrho-1} f(t)\, dt\, t^{\varpi-1} E_{\varpi,\varpi}\left(-z^2 t^{\varpi}\right).$$

Proof: The above proof is accomplished by implanting $b = z^2$ in equation (16).

4 Conclusion

The utilization of the Mohand transform to solve fractional integro-differential equations stands as a pivotal focus of this article. Exploring the intricate relationship between the Mohand transform and the Laplace transform has yielded invaluable insights, enriching our comprehension of these integral transformations. This study uses a unique method that combines the Mohand transform with binomial series extension coefficients to come up with a new way to solve fractional integro-differential equations. Beyond its mere application, this research delves into elucidating various properties and providing illustrative examples, substantiating the efficacy and adaptability of the proposed methodology. Looking ahead, future research endeavors aim to refine the Mohand transform's applicability by addressing its limitations in specific scenarios. Also, looking into how it can be used in different scientific fields and combining different types of methods are both good ways to improve how differential equations are solved. In conclusion, this study not only introduces a novel approach but also sets the stage for broader investigations, seeking to expand the practical utility and deepen the understanding of the Mohand transform in diverse mathematical problem-solving domains.

References

[1] M. M. Abdelrahim, The New Integral Transform Mohand Transform, *Adv Theoret Appl Mathe*, 12, 2, 113-120 (2017).

[2] K. S. Aboodh, The New Integral transform Aboodh transform, *Global Journal of Pure and Applied Mathematics*, 9, 1, 35 - 43 (2013).

[3] R. Aruldoss, and R. Anusuya Devi, Aboodh Transform for Solving Fractional Differential Equations, *Global Journal of Pure and Applied Mathematics*, 16, 2, 145-153 (2020).

[4] M. Caputo, Elasticity dissipazione (Elasticity and anelastic dissipation), *Zanichelli, Bologna,* 4, 98(1969).

[5] A.E. Elsayed Mohamed, Elzaki transformation for Linear Fractional Differential Equations, *Journal of Computational and Theoretical Nanoscience*, 12, 2303 - 2315 (2015).

[6] A. Kashuri, A. Fundo, R. Liko, New Integral transform for solving some fractional differential equations, *International Journal of Pure and Applied Mathematics*, 103, 4, 675-682, (2015).

[7] S. Lin, C. Lu, Laplace transform for solving some families of fractional differential equations and its applications, *Advances in Difference Equations*, 1-9 (2013).

[8] I. Podlubny, Fractional Differential Equation, *Academic Press, San Diego*, (1999).

[9] F. S. Silva, D. M. Moreira, and M. A. Moret, Conformable Laplace transform of fractional differential equations, *Axioms*, 7, 3, 55 (2018).

[10] J. A. Zhang, Sumudu based algorithm for solving differential equations, *Computer Science Journal of Moldova*, 15, 3, 45-53 (2007).

[11] P. Raghavendran, T. Gunasekar, H. Balasundaram, S. S. Santra, D. Majumder, and D. Baleanu, Solving fractional integro-differential equations by Aboodh transform. *J. Math. Computer Sci*, 229-240, 32 (2023).

[12] V.P. Dubey, J. Singh, A.M. Alshehri, S. Dubey, and D. Kumar, Forecasting the behavior of fractional order Bloch equations appearing in NMR flow via a hybrid computational technique. *Chaos, Solitons & Fractals*, 164, 112691, (2022).

[13] V.P. Dubey, J. Singh, A.M. Alshehri, S. Dubey, and D. Kumar, Some integral transform results for Hilfer–Prabhakar fractional derivative and analysis of free-electron laser equation. *Iranian Journal of Science*, 1333-1342, 47, 4 (2023).

[14] V.P. Dubey, J. Singh, A.M. Alshehri, S. Dubey, and D. Kumar, Analysis of Cauchy Problems and Diffusion Equations Associated with the Hilfer–Prabhakar Fractional Derivative via Kharrat–Toma Transform. *Fractal and Fractional*, 413, 7, 5 (2023).

[15] V.P. Dubey, D. Kumar, A.M. Alshehri, J. Singh, and D. Baleanu, Generalized invexity and duality in multiobjective variational problems involving non-singular fractional derivative. *Open Physics*, 939-962, 20, 1 (2022).

[16] V.P. Dubey, J. Singh, A.M. Alshehri, S. Dubey, and D. Kumar, Analysis and Fractal Dynamics of Local Fractional Partial Differential Equations Occurring in Physical Sciences. *Journal of Computational and Nonlinear Dynamics*, 031001, 18, 3 (2023).

[17] H. Singh, J. Singh, S. D. Purohit, & D. Kumar, (Eds.). Advanced Numerical Methods for Differential Equations: Applications in Science and Engineering (1st ed.), (2021) CRC Press. https://doi.org/10.1201/9781003097938.

[18] D. Kumar, V.P. Dubey, S. Dubey, J. Singh, and A.M. Alshehri, Computational analysis of local fractional partial differential equations in realm of fractal calculus. *Chaos, Solitons & Fractals*, 113009, 167 (2023).

Solving multi-choice solid stochastic multi objective transportation problem with supply, demand and conveyance capacity involving Newton divided difference interpolations

Vishwas Deep Joshi[1], Medha Sharma[1] and
Jagdev Singh[1,2,*]

[1] Department of Mathematics, JECRC University Jaipur, Rajasthan, INDIA

[2]Department of Computer Science and Mathematics,

Lebanese American University, Beirut, Lebanon

Email: vdjoshi.or@gmail.com, medhasharma1997@gmail.com,

jagdevsinghrathor@gmail.com

*Corresponding author

January 7, 2024

Abstract

The main concern is the uncertainty in the real-world solid transportation problem. This study examines a supply, demand, and conveyance capacity-based multi-choice solid stochastic multi-objective transportation problem (MCSS-MOTP). Due to uncertainty, the concrete objective function coefficients of the proposed model are of multivariate type. Furthermore, the parameters of the constraints are treated as independent multivariate random variables with normal distribution. First, a Newton divided difference method-based interpolation polynomial is described that extends an interpolation polynomial using practical properties at non-negative integer nodes to deal with any multiple-choice parameter. Second, the probabilistic constraints are converted into precise ones utilizing a stochastic programming approach. In the end, ranking procedure was used to compare the existing approach with the old models. The proposed model's applicability was confirmed using a numerical example.

Keywords- Solid transportation problem; Newton divided difference; Stochastic programming; multi-choice random parameter; Ranking of solutions

1 Introduction

The first and most significant use of the linear programming problem is in transportation [20]. It has numerous applications in inventory control, supply management, logistics systems, and production planning, among others. By taking into account the standard transportation problem's parameters are cost, supply, and demand. However, given the level of market competition today, it's possible that the criteria aren't presented precisely. The price of the product may change occasionally or it may depend on how the product is made. Additionally, because information on the shipping goods is unavailable, supply and demand may be ambiguous in nature. For these reasons and to deal with ambiguous information, Zadeh[16]developed the idea of ambiguity.

In numerous fields including Economics, Psychology, Philosophy, Mathematics, and Statistics, decision-making is crucial. The necessity of transportation as a component of distribution networks must be acknowledged. The main objective of the transportation problem (TP) is to reduce the price of transferring goods between consumers and producers so that manufacturers may more easily satisfy consumers' demands. The TP's parameters are price, supply, and demand. We may transfer goods from sources to destinations using different modes of transportation even though there are many modes of transportation accessible for shipments of commodities in a transportation system if we want to save money or meet deadlines. The fundamental TP was first expressed by Hitchcock [13] and later, according to the literature, it was widely discussed by many authors.

When there are random parameters involved in an optimization problem, stochastic programming (SP) techniques are applied. This indicates that some of the parameters in the model coefficients have known probability distributions that indicate they are known with uncertainty. Typically, SP arises frequently in a wide range of real-world management science, engineering, and technology challenges that contain some stochastic factors, i.e., uncertain input data, and models built on unreliable information. Because of the rapid advancement of computers and contemporary optimization techniques over the past five decades, there have been an increasing number of stochastic optimization applications to various challenging real-world decision-making situations. SP models have been effectively used to a number of applications, including supply chain management, environmental planning, telecommunications, transportation, and planning for energy and financial resources.

A mathematical method called stochastic programming is used to resolve optimization problem with uncertainty. Stochastic programming considers the randomness or variability of these values as opposed to conventional optimization techniques, which assume deterministic values for variables. By taking into account a variety of potential outcomes and the corresponding probabilities, it enables decision-makers to make educated decisions. For instance, stochastic

programming in finance can be used to choose the best investment portfolio by taking into account various market conditions and their probabilities. It can be used in supply chain management to optimize inventory levels by taking uncertain demand and supply disruptions into account. A potent tool for making decisions in complicated and uncertain contexts is stochastic programming.

The solid transportation problem (STP), also known as three-dimensional TP or three-dimensional TP, is a developed version of the well-known TP that was first modelled by Schell [11]and developed by Haley [15]. The objective of STP is to transport homogeneous goods from their origin to their final destination using different modes of transportation to minimize the total cost of transportation. A three-dimensional TP's parameters include the product's availability at source points, the product's needs at destination points, and the carrying capacity of different modes of transportation (such as trucks, cargo planes, goods trains, ships, etc.) used to move the product from sources to destinations. Due to the inclusion of multiple variables, such as equipment failure and labor concerns for manufacturing, market mode, road condition, and weather conditions for transportation, the problem's parameters are not deterministic in real life. Random variables are occasionally used to describe these uncertainties, particularly stochastic ones. When formulating a real-world STP, we must take into account the optimization of a number of goals, including minimizing transportation time, minimizing loss during transit, and minimizing transportation cost. This knowledge prompts us to take into account a stochastic multi-objective STP. The STP is a significant study area from both a theoretical and a practical standpoint. In this field of study, numerous researchers have made substantial contributions. Supply, demand, transportation capacity, direct costs, and fixed charges are all unknown variables in the fixed charge STP that Zhang et al.[9] discussed.

An urgent situation in the transportation sector that needs immediate attention and a solution is referred to as a "solid transportation problem." When there is a lack of dependable and effective transportation infrastructure, it can cause delays, traffic, or poor connectivity. For instance, if a city's public transportation infrastructure is out of date and unable to handle the rising demand, the city may have a serious transportation issue. As a result, travellers may experience crowded buses, protracted waits, and frustration. To ensure a smooth and efficient movement of people and commodities, solving solid transportation issues needs thoughtful planning, investment in infrastructure development, and competent management.

The majority of real-world, practical decision-making issues are modelled using multiple choices. The use of multi-choice optimization techniques has grown in importance in a variety of fields, including technology, business, transportation, and military applications. The price indices the objective function's C_{ijk} might stand in for the price of moving a unit of production from source i to destination j by conveyance k . Due to rising fuel prices and other important

factors, let us present a multiple-choice version of the cost coefficient of the objective function for the transportation problem. Supply and demand parameters should also be multi-choice in order to account for market price fluctuations for all items. Multiple choice programming, which Healy [25] initially invented, is a method for solving linear programming problems with zero-one variables.

Mathematicians and computer scientists utilize Newton's divided difference interpolation as a numerical technique to approximate a function from a collection of data points. Its foundation is the idea of divided differences, which entails figuring out the variations between related data points. This method enables the construction of a polynomial function that traverses each of the provided data points. Newton's Divided Difference a multi-choice fractional stochastic transport problem can be solved using interpolation by transforming it into a deterministic model [14]. A method for solving MCFS-MOTPs by interpolating multi-choice parameters, transforming probabilistic constraints, linearizing the problem, and solving using fuzzy goal programming and ϵ-constraint method [4]. A method for solving MOSSTP under uncertainty by formulating it as a chance-constrained programming problem and using global criterion method and fuzzy goal programming approach to find good solutions in a reasonable amount of time [17]. A new approach for analysing STP by combining multi-choice programming and stochastic programming, and using a transformation technique to find an optimal solution [18]. A weighted goal programming approach for multi-objective transportation problems that can obtain compromise solutions according to the decision-maker's priorities [2]. A weighted goal programming approach for multi-objective transportation problems that finds compromise solutions according to the decision-maker's priorities, illustrated with a numerical example [21]. A method for solving multi-choice stochastic transportation problems by using Lagrange's interpolating polynomial to select an appropriate choice and transforming stochastic supply constraints into deterministic constraints [24].

A new transformation technique for solving multi-choice stochastic transportation problems with exponential distribution by introducing binary variables for each aspiration level of each cost coefficient, transforming probabilistic constraints into deterministic constraints, and formulating a non-linear deterministic model [8]. A method for solving multi-choice transportation problems by using Lagrange's interpolating polynomial and chance technique to select an appropriate choice and formulate a non-linear mathematical model [7, 23]. A mathematical model for a transportation problem with nonlinear cost and multi-choice demand is proposed by developing a general transformation technique and formulating a multi-objective decision making model [19]. A solution procedure for multi-choice stochastic transportation problem with extreme value distribution by transforming probabilistic constraints into deterministic constraints, handling multi-choice type cost coefficients using binary variables [6].

Table 1: Comparison of the approach to the present models

Reference	S	D	C	MO	MC	Methodology
Joshi[21]	✓	✓		✓		**GP using WS**
Agrawal[14]	✓	✓			✓	**NDD**
Das[17]	✓	✓	✓	✓		**WD**
Roy[18]	✓	✓			✓	**CD**
Sayed[4]	✓	✓		✓	✓	**NDD**
Roy[22]	✓	✓			✓	**WD**
Proposed Approach	✓	✓	✓	✓	✓	**NDD**

S*= Supply, **D*= Demand**,**C*= Conveyance**,
MO*=Multi-Objective, **MC*= Multi-Choice**,
GP*= Goal programming,**WS*= Weighted Sum**,**WD*= Weibull Distribution**,**CD*= Cauchy' Distribution**,**NDD*= Newton's divided difference**,

A solution procedure for multi-objective stochastic unbalanced transportation problem by changing the problem into deterministic scenario using fuzzy theory [5]. A solution procedure for multi-choice stochastic transportation problem with Weibull distribution by transforming probabilistic constraints into deterministic [10]. A solution procedure for multi-objective capacitated transportation problem with uncertain input information by transforming the uncertain information into deterministic form and solving the resultant MOCTP for the compromise solution [25]. A method for solving linear programming problems with multi-choice parameters by interpolating technique [1]. A multi-choice stochastic transportation problem with extreme value distribution is solved by transforming probabilistic constraints into deterministic constraints [6]. A two-phase solution procedure for multi-objective capacitated transportation problem with uncertain input information is proposed [3]. A solution methodology for multi-choice stochastic transportation problem with Weibull distribution and multi-choice cost coefficients is proposed [22].

The paper is organized as follows. Section 1 presents a review of the relevant literature and introduction. Basic definitions that are related to this article presents in section 2. This paper's notation is covered in section 3. Section 4 presents the exhaustive problem statement. Section 5 illustrates the process for solving the given problem. Section 6 proposes a new solution method for the problem. Section 7 evaluates the performance of the proposed solution method on a set of numerical examples. Section 8 discusses the theoretical and practical implications of the proposed method. Section 9 concludes the paper and suggests directions for future research.

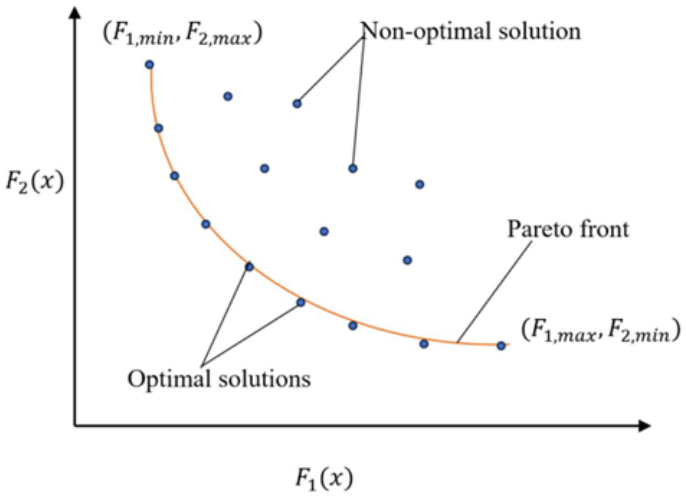

Figure 1: Pareto optimal solution

2 Basic definitions

2.1 Feasible solution:

A feasible solution to an optimization problem is a set of values for the decision variables that satisfies all of the constraints of the problem.

2.2 Pareto optimal solution:

A set of "non-inferior" solutions in the objective space that specify a limit beyond which none of the objectives can be improved without compromising at least one of the other objectives is known as a pareto optimum solution.

2.3 Compromise solution:

A compromise solution is a balanced outcome that takes into account multiple conflicting factors or goals. It involves finding a middle ground that satisfies different objectives without fully favouring one over the others. It's like reaching a fair agreement that considers everyone's preferences. Decision-makers prioritize the compromise option over all other solutions when taking into account all the criteria in the multi-objective.

2.4 Ideal solution:

When a problem involves minimization, the ideal solution is one in which each objective function achieves its optimal minimum.

2.5 Anti-ideal solution:

When a problem involves minimization, the anti-ideal solution is one in which each objective function achieves its maximum value.

3 Notations

- R**:** number of objective functions
- m**:** number of supply sources
- n**:** number of demand destinations
- l**:** number of conveyances
- x_{ijk}**:** amount of shipment from i^{th} supply source to j^{th} demand destination using k^{th} transportation mode
- Z_r**:** r^{th} objective functions
- c_{ijk}^r**:** unit cost in the r^{th} objective function
- a_i**:** amount of supply at the i^{th} supply source
- b_j**:** amount of demand at the j^{th}demand destination
- e_k**:** amount of conveyance capacity of the k^{th} transportation mode
- ϕ**:** the cumulative distribution functions
- θ_i**:** probability for a_i
- δ_j**:** probability forb_j
- σ_k**:** probability for e_k
- g_{θ_i}**:** the value of standard normal variable for a_i
- g_{δ_j}**:** the value of standard normal variable for b_j
- g_{σ_k}**:** the value of standard normal variable for e_k
- $E(F_{a_i}(w_{a_i}))$**:** the mean of supply of interpolating polynomial $F_{a_i}(w_{a_i})$
- $E(F_{b_j}(w_{b_j}))$**:** the mean of demand of interpolating polynomial $F_{b_j}(w_{b_j})$
- $E(F_{e_k}(w_{e_k}))$**:** the mean of conveyance of interpolating polynomial $F_{e_k}(w_{e_k})$
- $V(F_{a_i}(w_{a_i}))$**:** the variance of supply of interpolating polynomial $F_{a_i}(w_{a_i})$
- $V(F_{b_j}(w_{b_j}))$**:** the variance of demand of interpolating polynomial $F_{b_j}(w_{b_j})$
- $V(F_{e_k}(w_{e_k}))$**:** the variance of conveyance of interpolating polynomial $F_{e_k}(w_{e_k})$

4 Problem Statement:

A transportation company must convey its products from numerous production facilities to numerous retail locations. There are m production houses, n retail stores, and l vehicles, assuming that a homogeneous product is conveyed from the i^{th} production house to the j^{th} retail store by the k^{th} vehicle. Let x_{ijk} serve as a representation of the product's unit quantity. The parameters for supplies, demand, and conveyance capacity are thought of as multi-choice random parameters since the values of the parameters are not always set due to the environment's uncertainty and variety of possibilities. As a result, the defined problem's constraints are probabilistic with regard to their degree of want. The mathematical formulation of the aforementioned problem is as follows because the objective function is in linear form and the transportation cost is considered to be of the multi-choice variety:

$$Min\ Z_r = \sum_{i=1}^{m}\sum_{j=1}^{n}\sum_{k=1}^{l}(c_{ijk}^1, c_{ijk}^2, \ldots, c_{ijk}^R)x_{ijk}, \tag{1}$$

Subject to:

$$P\{\sum_{j=1}^{n}\sum_{k=1}^{l} x_{ijk} \leq (a_i^1, a_i^2, \ldots, a_i^u)\} \geq 1-\theta_i, \qquad i = 1, 2, \ldots, m \tag{2}$$

$$P\{\sum_{i=1}^{m}\sum_{k=1}^{l} x_{ijk} \geq (b_j^1, b_j^2, \ldots, b_j^v)\} \geq 1-\delta_j, \qquad j = 1, 2, \ldots, n \tag{3}$$

$$P\{\sum_{i=1}^{m}\sum_{j=1}^{n} x_{ijk} \leq (e_k^1, e_k^2, \ldots, e_k^q)\} \geq 1-\sigma_k, \qquad k = 1, 2, \ldots, l \tag{4}$$

$$x_{ijk} \geq 0, \forall\ i, j\ and\ k \tag{5}$$

Where the multi-choice random parameters for the total availability a_i at the i^{th} manufacturing house, regarded as an independent random variable, are $(a_i^1, a_i^2, \ldots, a_i^u)$.The multi-choice random parameters $(b_j^1, b_j^2, \ldots, b_j^v)$ for the overall quantity b_j of the product at the j^{th} retail outlets are regarded as independent random variables. The multi-choice random parameters for the total capacity e_k of the conveyance at the k^{th} vehicle, which is regarded as an independent random variable, are $(e_k^1, e_k^2, \ldots, e_k^q)$. The probability of meeting the constraints is represented by the values θ_i, δ_j and σ_k.

5 Solutions Methodology

5.1 Newton's divided difference interpolating polynomial for multi-choice parameters

The Newton's divided Difference Interpolation numerical approximation technique is used to convert the multi-choice parameter into the best option. Introduce an integer variable so that the interpolating polynomial can be defined for each option of a multi-choice parameter. The integer variables $w^t_{c_{ijk}}, (t = 0, 1, \ldots, s-1)$ are used since there are s possible cost options in the problem above.

For each alternative, the integer variables $w^p_{a_i}(p = 0, 1, \ldots, u-1)$, $w^h_{b_j}(h = 0, 1, \ldots, v-1)$ and $w^g_{e_k}(g = 0, 1, \ldots, q-1)$ are introduced since supplies, demands, and conveyance capacity are multi-choice random parameters. Each multi-choice parameter has a different divided difference that is determined based on the alternatives. Using Table 2, which lists various divided difference orders, Newton's divided difference (NDD) interpolation polynomial is created for the cost parameter in equation (6).

Table 2: Divided difference (DD)

$w^t_{c_{ij1}}$	$F_{c_{ijk}}(w^t_{c_{ijk}}$	**First DD**	**Second DD**	**Third DD**
0	c^1_{ijk}	$f[w^0_{c_{ijk}}, w^1_{c_{ijk}}]$		
1	c^2_{ijk}	$f[w^1_{c_{ijk}}, w^2_{c_{ijk}}]$	$f[w^0_{c_{ijk}}, w^1_{c_{ijk}}, w^1_{c_{ijk}}]$	$f[w^0_{c_{ijk}}, w^1_{c_{ijk}}, w^2_{c_{ijk}}, w^3_{c_{ijk}}]$
2	c^3_{ijk}	$f[w^2_{c_{ijk}}, w^3_{c_{ijk}}]$	$f[w^1_{c_{ijk}}, w^2_{c_{ijk}}, w^3_{c_{ijk}}]$	
3	c^4_{ijk}			

$$F_{c_{ijk}}(w_{c_{ijk}}) = f[w^0_{c_{ijk}}] + (w_{c_{ijk}} - w^0_{c_{ijk}}) f[w^0_{c_{ijk}}, w^1_{c_{ijk}}] + (w_{c_{ijk}} - w^0_{c_{ijk}})(w_{c_{ijk}} - w^1_{c_{ijk}}) f[w^0_{c_{ijk}}, w^1_{c_{ijk}}, w^2_{c_{ijk}}] + (w_{c_{ijk}} - w^0_{c_{ijk}})(w_{c_{ijk}} - w^1_{c_{ijk}}), \ldots, (w_{c_{ijk}} - w^{s-1}_{c_{ijk}}) f[w^0_{c_{ijk}}, w^1_{c_{ijk}}, \ldots, w^{s-1}_{c_{ijk}}] \quad (6)$$

$$F_{c_{ijk}} = c^1_{ijk} + (w_{c_{ijk}} - w^0_{c_{ijk}})(c^2_{ijk} - c^1_{ijk}) + (w_{c_{ijk}} - w^0_{c_{ijk}})(w_{c_{ijk}} - w^1_{c_{ijk}}) (\frac{c^3_{ijk} - 2c^2_{ijk} + c^1_{ijk}}{(w^2_{c_{ijk}} - w^0_{c_{ijk}})} + \cdots + \sum_{t=1}^{s} \frac{c^t_{ijk}}{\substack{s-1 \\ t \neq p+1, p=0}} (w^{t-1}_{c_{ijk}} - w^p_{c_{ijk}}) \quad (7)$$

Similarly, by replacing the multiple choice parameters in the program with its interpolated polynomials for supply, demand, and transportation capacity,

represented by $F_{a_i}(w_{a_i}), F_{b_j}(w_{b_j})$ and $F_{e_k}(w_{e_k})$ Respectively, the mathematical model can be formulated as follows.

$$Min\ Z_r = \sum_{i=1}^{m}\sum_{j=1}^{n}\sum_{k=1}^{l} F_{ijk}(w_{ijk})x_{ijk}, \tag{8}$$

Subject to:

$$P\{\sum_{j=1}^{n}\sum_{k=1}^{l} x_{ijk} \leq F_{a_i}(w_{a_i})\} \geq 1-\theta_i, \qquad i=1,2,\ldots,m \tag{9}$$

$$P\{\sum_{i=1}^{m}\sum_{k=1}^{l} x_{ijk} \geq F_{b_j}(w_{b_j})\} \geq 1-\delta_j, \qquad j=1,2,\ldots,n \tag{10}$$

$$P\{\sum_{i=1}^{m}\sum_{j=1}^{n} x_{ijk} \leq F_{e_k}(w_{e_k})\} \geq 1-\sigma_k, \qquad k=1,2,\ldots,l \tag{11}$$

$$x_{ijk} \geq 0, \forall\ i,j\ and\ k \tag{12}$$

5.2 The transformation of probabilistic constraints

The multi-choice parameters were transformed into their interpolating polynomials so that the resulting probabilistic constraints would be transformed into their deterministic form. To transform its deterministic restrictions into probabilistic ones, we consider the supply's constraints.

Consider the constraint (9) for every, $i=1,2,\ldots,m$

$$P\{\sum_{j=1}^{n}\sum_{k=1}^{l} x_{ijk} \leq F_{a_i}(w_{a_i})\} \geq 1-\theta_i$$

or

$$1-P\{\sum_{j=1}^{n}\sum_{k=1}^{l} x_{ijk} \leq F_{a_i}(w_{a_i})\} \geq 1-\theta_i$$

Applying Chance constrained technique, this implies

$$P\{\frac{F_{a_i}(w_{a_i})-E(F_{a_i}(w_{a_i}))}{\sqrt{V(F_{a_i}(w_{a_i}))}} \leq \frac{\sum_{j=1}^{n}\sum_{k=1}^{l} x_{ijk}-E(F_{a_i}(w_{a_i}))}{\sqrt{V(F_{a_i}(w_{a_i}))}}\} \leq \theta_i$$

$$P\{\xi_{a_i} \leq \frac{\sum_{j=1}^{n}\sum_{k=1}^{l} x_{ijk}-E(F_{a_i}(w_{a_i}))}{\sqrt{V(F_{a_i}(w_{a_i}))}}\} \leq \theta_i$$

$$\phi\{\frac{\sum_{j=1}^{n}\sum_{k=1}^{l} x_{ijk}-E(F_{a_i}(w_{a_i}))}{\sqrt{V(F_{a_i}(w_{a_i}))}}\} \leq \phi(-g_{\theta_i})$$

$$\{\frac{\sum_{j=1}^{n}\sum_{k=1}^{l} x_{ijk} - E(F_{a_i}(w_{a_i}))}{\sqrt{V(F_{a_i}(w_{a_i}))}}\} \leq -g_{\theta_i}$$

$$\sum_{j=1}^{n}\sum_{k=1}^{l} x_{ijk} \leq E(F_{a_i}(w_{a_i})) - g_{\theta_i}\sqrt{V(F_{a_i}(w_{a_i}))} \tag{13}$$

The mean and variance of the interpolating polynomial $F_{a_i}(w_{a_i})$ are, respectively, denoted by $E(F_{a_i})(w_{a_i})$ and $V(F_{a_i})(w_{a_i})$ accordingly. Additionally, let ϕ be the standard normal distribution's cumulative distribution function and g_{θ_i} stand for the standard normal variable's value. Equation (13) thus expresses the deterministic constraint of the probabilistic constraint (9).

The analogous deterministic constraint for every $j = 1, 2, \ldots, n$ and $k = 1, 2, \ldots, l$ is as follows. In a similar manner, using the same method to the demand and conveyance capacity constraints

$$\sum_{i=1}^{m}\sum_{k=1}^{l} x_{ijk} \leq E(F_{b_j}(w_{b_j})) + g_{\delta_j}\sqrt{V(F_{b_j}(w_{b_j}))} \tag{14}$$

$$\sum_{i=1}^{m}\sum_{j=1}^{m} x_{ijk} \leq E(F_{e_k}(w_{e_k})) - g_{\sigma_k}\sqrt{V(F_{e_k}(w_{e_k}))} \tag{15}$$

where, $E(F_{b_j}(w_{b_j}), E(F_{e_k}(w_{e_k})$ and $V(F_{b_j}(w_{b_j}), V(F_{e_k}(w_{e_k})$ denotes the mean and the variance of interpolating polynomial $F_{b_j}(w_{b_j})$ and $F_{e_k}(w_{e_k})$ respectively g_{δ_j} and g_{σ_k} denotes the value of standard normal variable. We compute the random interpolating polynomial's mean and variance as

$$\begin{aligned}\mathrm{E}(\mathrm{F}_{a_i}(w_{a_i})) &= E\{a_i^1 + (w_{a_i} - w_{a_i}^0)(a_i^2 - a_i^1) + (w_{a_i} - w_{a_i}^0)(w_{a_i} - w_{a_i}^1)\tfrac{a_i^3 - 2a_i^2 + a_i^1}{w_{a_i}^2 - w_{a_i}^0} \\ &\quad + \cdots + \sum_{t=1}^{s} \frac{a_i^t}{\substack{s-1 \\ t\neq p+1, p=0}}(w_{c_{ijk}}^{t-1} - w_{c_{ijk}}^{p})\} \\ &= \{E(a_i^1) + (w_{a_i} - w_{a_i}^0)(E(a_i^2) - E(a_i^1)) + (w_{a_i} - w_{a_i}^0)(w_{a_i} - w_{a_i}^1)\tfrac{E(a_i^3) - 2E(a_i^2) + E(a_i^1)}{w_{a_i}^2 - w_{a_i}^0} \\ &\quad + \ldots + \textstyle\sum_{t=1}^{s} \frac{E(a_i^t)}{\substack{s-1 \\ t\neq p+1, p=0}}(w_{c_{ijk}}^{t-1} - w_{c_{ijk}}^{p})\}\end{aligned} \tag{16}$$

$$\begin{aligned}\mathrm{V}(\mathrm{F}_{a_i}(w_{a_i})) &= V\{a_i^1 + (w_{a_i} - w_{a_i}^0)(a_i^2 - a_i^1) + (w_{a_i} - w_{a_i}^0)(w_{a_i} - w_{a_i}^1)\tfrac{a_i^3 - 2a_i^2 + a_i^1}{w_{a_i}^2 - w_{a_i}^0} \\ &\quad + \cdots + \sum_{t=1}^{s} \frac{a_i^t}{\substack{s-1 \\ t\neq p+1, p=0}}(w_{c_{ijk}}^{t-1} - w_{c_{ijk}}^{p})\} \\ &= \{V(a_i^1) + (w_{a_i} - w_{a_i}^0)(V(a_i^2) - V(a_i^1)) + (w_{a_i} - w_{a_i}^0)(w_{a_i} - w_{a_i}^1)\tfrac{V(a_i^3) - 2V(a_i^2) + V(a_i^1)}{w_{a_i}^2 - w_{a_i}^0} \\ &\quad + \ldots + \textstyle\sum_{t=1}^{s} \frac{V(a_i^t)}{\substack{s-1 \\ t\neq p+1, p=0}}(w_{c_{ijk}}^{t-1} - w_{c_{ijk}}^{p})\}\end{aligned} \tag{17}$$

The $F_{a_i}(w_{a_i})$ mean and variance are shown in equations (16) and (17). Equations (16) and (17) can also be used to calculate the mean and variance of the

interpolating polynomial for demand and conveyance capacity.

The deterministic model is implemented with chance constraints and Newton's Divided Difference Interpolation.

$$Min\ Z_r = \sum_{i=1}^{m}\sum_{j=1}^{n}\sum_{k=1}^{l} F_{ijk}(w_{ijk})x_{ijk}, \qquad r = 1, 2 \ldots, R$$

Subject to:

$$\sum_{j=1}^{n}\sum_{k=1}^{l} x_{ijk} \leq E(F_{a_i}(w_{a_i})) - g_{\theta_i}\sqrt{V(F_{a_i}(w_{a_i}))}$$

$$\sum_{i=1}^{m}\sum_{k=1}^{l} x_{ijk} \leq E(F_{b_j}(w_{b_j})) + g_{\delta_j}\sqrt{V(F_{b_j}(w_{b_j}))}$$

$$\sum_{i=1}^{m}\sum_{j=1}^{m} x_{ijk} \leq E(F_{e_k}(w_{e_k})) - g_{\sigma_k}\sqrt{V(F_{e_k}(w_{e_k}))}$$

$$x_{ijk} \geq 0, \forall\ i, j\ and\ k$$

The multi-choice solid stochastic multi-objective transportation problem (MCSS-MOTP) can be applied to a variety of real-world problems, such as:

- **Supply chain management:** The MCSS-MOTP can be used to optimize the transportation of goods and materials in a supply chain, where the cost coefficients are uncertain and the objective is to minimize the total transportation cost and satisfy the demand at each destination with a specified probability.
- **Project management:** The MCSS-MOTP can be used to optimize the allocation of resources in a project, where the cost coefficients are uncertain and the objective is to minimize the total cost and complete the project on time with a specified probability.
- **Financial planning:** The MCSS-MOTP can be used to optimize the allocation of funds in a financial portfolio, where the return on investment is uncertain and the objective is to maximize the expected return and minimize the risk with a specified probability.
- **Energy management:** The MCSS-MOTP can be used to optimize the generation and distribution of energy in a power grid, where the cost of energy is uncertain and the objective is to minimize the total cost and meet the demand at each node with a specified probability.

The MCSS-MOTP is a powerful tool that can be used to solve a variety of real-world problems. However, it is important to note that the problem may be

difficult to solve, especially if the number of sources, destinations, and probabilistic constraints are large.

Here are some of the challenges in solving the MCSS-MOTP:

- The problem may be computationally expensive to solve, especially if the number of sources, destinations, and probabilistic constraints are large.
- The problem may be non-convex, which means that there may be multiple local optima.
- The problem may be NP-hard, which means that it may not be possible to find an optimal solution in polynomial time.
- Despite these challenges, the MCSS-MOTP is a valuable tool that can be used to solve a variety of real-world problems.

6 Approaches to solve the MCSS-MOTP

6.1 First approach

In this we have used the weighted sum method to convert multiple objectives into a single objective. In which the multi-choice cost parameter is reduced to a single choice using Newton's divided difference method. The mathematical formulation is as follows:

$$Min\ Z = \sum_{r=1}^{R} d_r Z_r$$

Subject to:

$$\sum_{j=1}^{n}\sum_{k=1}^{l} x_{ijk} \leq E(F_{a_i}(w_{a_i})) - g_{\theta_i}\sqrt{V(F_{a_i}(w_{a_i}))}$$

$$\sum_{i=1}^{m}\sum_{k=1}^{l} x_{ijk} \leq E(F_{b_j}(w_{b_j})) + g_{\delta_j}\sqrt{V(F_{b_j}(w_{b_j}))}$$

$$\sum_{i=1}^{m}\sum_{j=1}^{m} x_{ijk} \leq E(F_{e_k}(w_{e_k})) - g_{\sigma_k}\sqrt{V(F_{e_k}(w_{e_k}))}$$

$$x_{ijk} \geq 0, \forall\ i, j\ and\ k$$

Where Z_r = individual objectives that converted into single choice using Newton's divided difference approach

6.2 Second approach

In this we have used the Joshi's method to convert multiple objectives into a single objective in which each multi choice objective converted into single choice using NDD approach. The mathematical formulation is as follows:

$$Min\ \mu' = \sum_{r=1}^{R} \mu(1 - d_r)$$

Subject to:

$$\sum_{i=1}^{m}\sum_{j=1}^{n}\sum_{k=1}^{l} F_{ijk}(w_{ijk})x_{ijk} \leq Z_r^* + \frac{\mu(1-d_r)}{Z_r^U - Z_r^L},\ r = 1, 2 \ldots, R$$

$$\sum_{j=1}^{n}\sum_{k=1}^{l} x_{ijk} \leq E(F_{a_i}(w_{a_i})) - g_{\theta_i}\sqrt{V(F_{a_i}(w_{a_i}))}$$

$$\sum_{i=1}^{m}\sum_{k=1}^{l} x_{ijk} \leq E(F_{b_j}(w_{b_j})) + g_{\delta_j}\sqrt{V(F_{b_j}(w_{b_j}))}$$

$$\sum_{i=1}^{m}\sum_{j=1}^{m} x_{ijk} \leq E(F_{e_k}(w_{e_k})) - g_{\sigma_k}\sqrt{V(F_{e_k}(w_{e_k}))}$$

$$x_{ijk} \geq 0, \forall\ i, j\ and\ k$$

Where Z_r^* = individual objectives that converted into single choice using Newton's divided difference approach

6.3 Third approach

Again, we convert multichoice into single choice using NDD approach and solved the converted problem using Nomani's method. The mathematical formulation is as follows:

$$Min\ \mu' = \sum_{r=1}^{R} \mu(1 - d_r)$$

Subject to:

$$\sum_{i=1}^{m}\sum_{j=1}^{n}\sum_{k=1}^{l} F_{ijk}(w_{ijk})x_{ijk} \leq Z_r^* + \mu(1-d_r),\ r = 1, 2 \ldots, R$$

$$\sum_{j=1}^{n}\sum_{k=1}^{l} x_{ijk} \leq E(F_{a_i}(w_{a_i})) - g_{\theta_i}\sqrt{V(F_{a_i}(w_{a_i}))}$$

$$\sum_{i=1}^{m}\sum_{k=1}^{l} x_{ijk} \leq E(F_{b_j}(w_{b_j})) + g_{\delta_j}\sqrt{V(F_{b_j}(w_{b_j}))}$$

$$\sum_{i=1}^{m}\sum_{j=1}^{m} x_{ijk} \leq E(F_{e_k}(w_{e_k})) - g_{\sigma_k}\sqrt{V(F_{e_k}(w_{e_k}))}$$

$$x_{ijk} \geq 0, \forall\ i, j\ and\ k$$

Where $Z_r^* =$ individual objectives that converted into single choice using Newton's divided difference approach

This introduces the need to rank these methods due to the variety of approaches available for handling multi-objective transportation problems. To address this, a tool is required to assist in ranking and selecting the most suitable method. It is at this point that the Technique for Order of Preference by Similarity to Ideal Solution (TOPSIS) [12] is useful. TOPSIS helps rank different methods based on their optimal solutions' performances. In this situation, the criteria are objective functions, and the alternatives are the best solutions. In essence, TOPSIS helps us determine which method is the most effective in terms of achieving optimal solutions for the problem at hand.

7 Numerical Example

Let's consider the attached MCSS-MOTP:

$$\text{Min } \mathrm{Z}_1 = c^1_{111}x_{111} + c^1_{121}x_{121} + c^1_{211}x_{211} + c^1_{221}x_{221} + c^1_{112}x_{112} + c^1_{122}x_{122} + c^1_{212}x_{212} + c^1_{222}x_{222}$$

$$Min\ Z_2 = c^2_{111}x_{111} + c^2_{121}x_{121} + c^2_{211}x_{211} + c^2_{221}x_{221} + c^2_{112}x_{112} + c^2_{122}x_{122} + c^2_{212}x_{212} + c^2_{222}x_{222}$$

Subject to:

Supply constraints

$$P\{\ x_{111} + x_{112} + x_{121} + x_{122} \leq (a^1_1, a^2_1, a^3_1)\} \geq 1 - \theta_1,$$

$$P\{\ x_{211} + x_{212} + x_{221} + x_{222} \leq (a^1_2, a^2_2, a^3_2)\} \geq 1 - \theta_2,$$

Demand constraints

$$P\{\ x_{111} + x_{112} + x_{211} + x_{212} \leq b^1_1\} \geq 1 - \delta_1,$$

$$P\{\ x_{121} + x_{122} + x_{221} + x_{222} \leq b^1_2\} \geq 1 - \delta_2,$$

Conveyance capacity constraints

$$P\{\ x_{111} + x_{121} + x_{211} + x_{221} \leq (e^1_1, e^2_1, e^3_1)\} \geq 1 - \sigma_1,$$

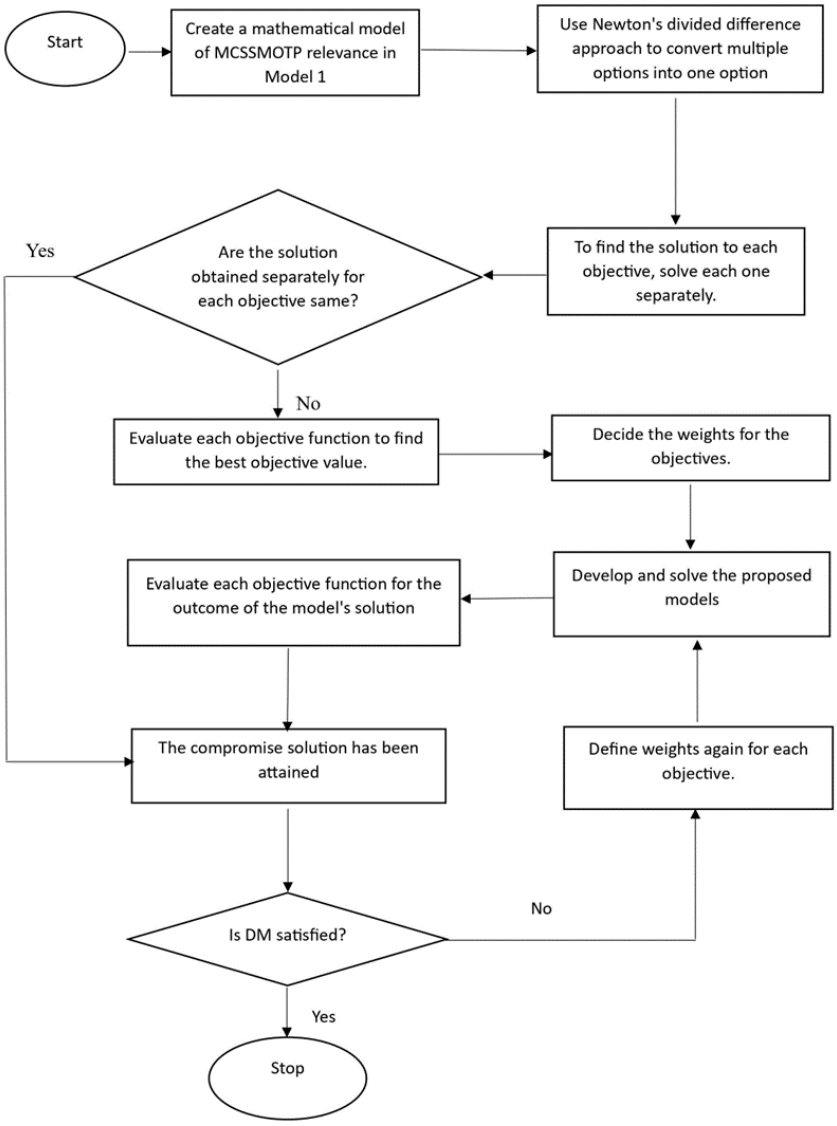

Figure 2: Flow chart for the proposed method

$$P\{\ x_{111} + x_{122} + x_{212} + x_{222} \leq (e_2^1, e_2^2, e_2^3)\} \geq 1 - \sigma_2,$$

$$x_{ijk} \geq 0, \forall\ i, j\ and\ k$$

where the multi-choice criteria are described as

Table 3: Transportation cost for first objective

		b_1	b_2
c_{ij1}^1	a_1	$15, 18, 20$	$15, 16, 18, 19$
	a_2	$16, 19, 22$	$25, 27, 28, 30$
c_{ij2}^1	a_1	$14, 17, 19, 22$	$12, 15, 19$
	a_2	$11, 18, 20$	$20, 21, 22, 25$

Table 4: Transportation cost for second objective

		b_1	b_2
c_{ij1}^2	a_1	$8, 10, 13$	$11, 13$
	a_2	$9, 12, 15$	$7, 9, 11, 14$
c_{ij2}^2	a_1	$5, 8, 9, 11$	$9, 11$
	a_2	$13, 17$	$11, 13, 14$

Table 5: Supply; mean, variance and significance level

RV	$E(a_i^1)$	$Var(a_i^1)$	$E(a_i^2)$	$Var(a_i^2)$	$E(a_i^3)$	$Var(a_i^3)$	**SL**
a_1	11.28	0.194	5.2	0.25	13.673	0.7712	0.89
a_2	10.1	0.17	5	0.24	13.647	0.489	0.97

RV^***=Random Variable**,SL^***=Significance Level**

Table 6: Demand; mean, variance and significance level

RV	$E(b_j^1)$	$Var(b_j^1)$	**SL**
b_1	10	3	0.15
b_2	9	2	0.2

Table 7:conveyance capacity; mean, variance and significance level

RV	$E(e_k^1)$	$Var(e_k^1)$	$E(e_k^2)$	$Var(e_k^2)$	$E(e_k^3)$	$Var(e_k^3)$	**SL**
e_1	11.28	0.18	6.2	0.24	13.07041	0.542	0.97
e_2	10.1	0.16	6	0.25	13.673	0.7412	0.96

$$\begin{aligned}\text{Min } \mathrm{Z}_1 = {} & [15 + 3w_{111} - 0.5w_{111}(w_{111} - 1)]x_{111} + [15 + w_{121} + 0.5w_{121} \\ & (w_{121} - 1) - \frac{1}{3}w_{121}(w_{121} - 1)(w_{121} - 2)]x_{121} + \\ & [16 + 3w_{211}]x_{211} + [25 + 2w_{221} - 0.5w_{221}(w_{221} - 1) \\ & + \frac{1}{3}w_{221}(w_{221} - 1)(w_{221} - 2)]x_{221} + [14 + 3w_{112} \\ & - 0.5w_{112}(w_{112} - 1) + \frac{1}{3}w_{112}(w_{112} - 1)(w_{112} - 2)]x_{112} + \\ & [12 + 3w_{122} - 0.5w_{122}(w_{122} - 1)]x_{122} + [11 + 7w_{212} \\ & - \frac{5}{2}w_{212}(w_{212} - 1)(w_{212} - 2)]x_{212} + [20 + w_{222} \\ & + \frac{1}{3}w_{222}(w_{222} - 1)(w_{222} - 2)]x_{222}\end{aligned}$$

$$\begin{aligned}\text{Min } \mathrm{Z}_2 = {} & [8 + 3v_{111} - 0.5v_{111}(v_{111} - 1)]x_{111} + [11 + 2v_{121}]x_{121} + \\ & [9 + 3v_{211}]x_{211} + [7 + 2v_{221} + \frac{1}{6}v_{221}(v_{221} - 1) \\ & (v_{221} - 2)]x_{221} + [5 + 3v_{112} - v_{112}(v_{112} - 1) \\ & + \frac{1}{2}v_{112}(v_{112} - 1) \\ & (v_{112} - 2)]x_{112} + [9 + 2v_{122}]x_{122} + \\ & [13 + 4v_{212}]x_{212} + [11 + 2v_{222} \\ & - \frac{1}{2}v_{222}(v_{222} - 1)(v_{222} - 2)]x_{222}\end{aligned}$$

Subject to:

Supply constraints

$$\begin{aligned}\mathrm{x}_{111} + x_{112} + x_{121} + x_{122} \leq {} & 11.28 - 6.08r_1 + 7.277r_1(r_1 - 1) \\ & + \phi^{-1}(0.89)\sqrt{(0.194 + 0.444r_1^2 + 0.491r_1^2(r_1 - 1)^2)}\end{aligned}$$

$$\begin{aligned}\mathrm{x}_{211} + x_{212} + x_{221} + x_{222} \leq {} & 10.1 - 5.1r_2 + 6.874r_2(r_2 - 1) \\ & + \phi^{-1}(0.97)\sqrt{(0.17 + 0.41r_2^2 + 0.404r_2^2(r_2 - 1)^2)}\end{aligned}$$

Demand constraints

$$x_{111} + x_{112} + x_{211} + x_{212} \geq 10 + \phi^{-1}(1 - 0.15)\sqrt{3}$$

$$x_{121} + x_{122} + x_{221} + x_{222} \geq 9 + \phi^{-1}(1 - 0.20)\sqrt{2}$$

Conveyance capacity constraints

$$\begin{aligned}\mathrm{x}_{111} + x_{121} + x_{211} + x_{221} \leq {} & 11.28 - 5.08r_3 + 5.9752r_3(r_3 - 1) + \\ & \phi^{-1}(0.97)\sqrt{(0.18 + 0.42r_3^2 + 0.4205r_3^2(r_3 - 1)^2)}\end{aligned}$$

$$\mathrm{x}_{112} + x_{122} + x_{212} + x_{222} \leq 10.1 - 4r_4 + 5.8865r_4(r_4 - 1) + \phi^{-1}(0.96)\sqrt{(0.16 + 0.41r_4^2 + 0.4753r_4^2(r_4 - 1)^2)}$$

$$0 \leq w_{111} \leq 2; 0 \leq w_{121} \leq 3; 0 \leq w_{211} \leq 2; 0 \leq w_{221} \leq 3;$$

$$0 \leq w_{112} \leq 3; 0 \leq w_{122} \leq 2; 0 \leq w_{212} \leq 2; 0 \leq w_{222} \leq 3;$$

$$0 \leq v_{111} \leq 2; 0 \leq v_{121} \leq 1; 0 \leq v_{211} \leq 2; 0 \leq v_{221} \leq 3;$$

$$0 \leq v_{112} \leq 3; 0 \leq v_{122} \leq 1; 0 \leq v_{212} \leq 1; 0 \leq v_{222} \leq 2;$$

$$0 \leq r_1 \leq 2; 0 \leq r_2 \leq 2; 0 \leq r_3 \leq 2; 0 \leq r_3 \leq 2, \quad s = 1, 2, 3, 4$$

$$x_{ijk} \geq 0, \forall\ i, j\ and\ k \qquad r_s, w_{ijk}, v_{ijk} \in Z^+$$

8 Results and Discussion

Using supply as a multi-choice random parameter, demands, and conveyance as random variables with Normal Distribution, the numerical examples demonstrate the multi-objective function in solid form with constraints. LINGO 18.0 software was used to generate the solutions.

Table 8: The solutions obtained for both the objectives separately, ignoring other objectives, are follows:

S.No.	$Z_1(IS)$	$Z_2(AIS)$	$Z_1(IS)$	$Z_2(AIS)$	X_1	X_2
1					$w_{111} = 1$	$v_{111} = 1$
2					$w_{121} = 0$	$v_{121} = 0$
3					$w_{211} = 0$	$v_{211} = 0$
4					$w_{221} = 0$	$v_{221} = 0$
5					$w_{112} = 0$	$v_{112} = 0$
6					$w_{122} = 0$	$v_{122} = 0$
7					$w_{212} = 0$	$v_{212} = 0$
8	287.6861	140.3208	455.6261	270.2812	$w_{222} = 0$	$v_{222} = 0$
9					$x_{111} = 0$	$x_{111} = 0$
10					$x_{121} = 6.1587$	$x_{121} = 0$
11					$x_{211} = 0$	$x_{211} = 0$
12					$x_{221} = 0$	$x_{221} = 11.6163$
13					$x_{112} = 0$	$x_{112} = 11.8013$
14					$x_{122} = 5.4576$	$x_{122} = 0$
15					$x_{212} = 11.8013$	$x_{212} = 0$
16					$x_{222} = 0$	$x_{222} = 0$

IS^***=Ideal Solution**, AIS^***= Anti-Ideal Solution**

Table 9: Comparison of proposed method

S.N.	W	$M1$	$M2$	$M3$	$R(M1)$	$R(M2)$	$R(M3)$
1	$n_1 = 0.1$	455.626	388.333	393.3888	0.4363	0.5563	0.5674
	$n_2 = 0.9$	140.321	155.073	455.626			
2	$n_1 = 0.2$	399.566	367.338	374.718	0.5436	0.6001	0.619
	$n_2 = 0.8$	148.945	166.524	399.566			
3	$n_1 = 0.3$	399.566	350.568	358.668	0.5436	0.6416	0.6621
	$n_2 = 0.7$	148.945	175.672	399.566			
4	$n_1 = 0.4$	319.222	336.863	344.723	0.7194	0.6762	0.6931
	$n_2 = 0.6$	192.769	183.147	319.222			
5	$n_1 = 0.5$	313.496	325.454	347.125	0.7185	0.6043	0.7123
	$n_2 = 0.5$	197.351	189.370	313.496			
6	$n_1 = 0.6$	313.496	322.961	321.683	0.7185	0.7169	0.6492
	$n_2 = 0.4$	197.351	210.589	313.496			
7	$n_1 = 0.7$	313.496	309.836	312.714	0. 7185	0.7156	0.6931
	$n_2 = 0.3$	197.351	207.108	313.496			
8	$n_1 = 0.8$	287.686	303.748	306.564	0.5637	0.6709	0.6528
	$n_2 = 0.2$	270.281	223.344	287.686			
9	$n_1 = 0.9$	288.786	296.569	298.516	0.5597	0.6206	0.6087
	$n_2 = 0.1$	271.581	243.632	288.786			
10	w.p.	313.496	305.454	347.125	0.7185	0.6043	0.707
		197.351	205.695	313.496			

W^***=Weights**, M^***=Method**, R^***=Ranking**, **w.p.*****=Without preference**

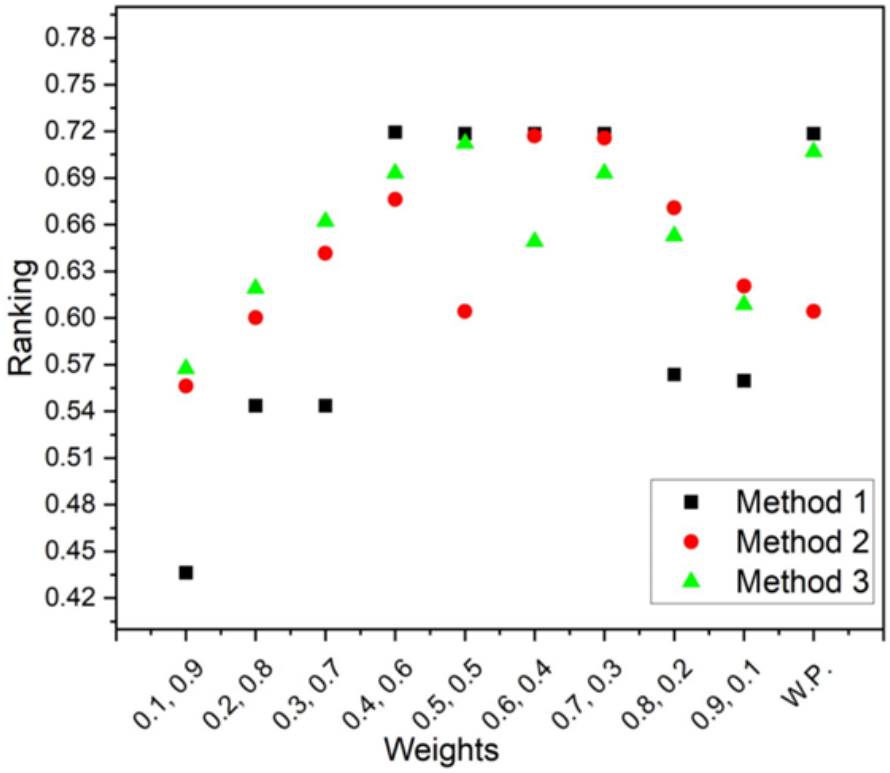

Figure 3: Graphical representation of a comparison of the consistency of the method 1,2 and 3.

A graph that shows the comparison between the method 1, 2 and 3. This graph is showing the rank. We can see that Method 3 is better than method 1 and 2. It's like a race, and our method is winning by being closer to what we want. The graph is like a storyteller that tells us method 3 is good at finding the right answers. Graph is 2 objective of solid stochastic transportation problem.

9 Conclusion

The MCSS-MOTP has been discussed in this research. Solid multi-choice parameters support the provided model's objective function. The transportation problem can be solved most effectively by combining three different ways (the stochastic approach, normal randomness, and Newton's divided difference approach). The constraints parameters are random multi-option parameters. Supply, demand, and conveyance are considered to be random variables with

a normal distribution. The deterministic constraints are obtained by applying the chance constrained programming to the probabilistic constraints. The multi-choice parameters were reduced to a single choice with the use of Newton's Divided Difference Interpolation, ensuring that the resulting solution would be ideal. LINGO 18.0 software are applied to solve the above MCSS-MOTP. In this you can work on MCSS-MOTP with fractional objective in future. In the real world, transportation problems are often characterized by uncertainty. For example, the demands at the destinations may be uncertain, or the cost of transportation may fluctuate due to changes in fuel prices. Stochastic programming is a programming approach that can be used to deal with uncertainty in transportation problems.

References

[1] Biswal-M.P. Acharya, S.(2009). Solving multi-choice linear programming problems by interpolating polynomials. *Math Comput Model*, 210(1):182—-188.

[2] Nomani-M.A. Ali I. Ahmed, A.(2017). A new approach for solving multi-objective transportation problems. *International journal of management science and engineering management*, 12(3):165–173.

[3] Gupta-S. Ali, I.A.A.(2018). Multi-choice multi-objective capacitated transportation problem-a case study of uncertain demand and supply. *J Stat Manag Syst*, 21(3):467–491.

[4] Sayed-M.A. El. Baky, I.A.(2023). Multi-choice fractional stochastic multi-objective transportation problem. *Soft Comput*, 27:11551–11567.

[5] Mahapatra-D.R. Roy S.K. Biswal, M.P.(2010). Stochastic based on multi-objective transportation problems involving normal randomness. *Adv Model Optim*, 12(2):205–223.

[6] Mahapatra-D.R. Roy S.K. Biswal, M.P.(2013). Multi-choice stochastic transportation problem involving extreme value distribution. *Appl. Math. Model*, 37(4):2230–2240.

[7] Pradhan-A. Biswal, M.P.(2017). Multi-choice probabilistic linear programming problem. *Opsearch*, 54(1):122–142.

[8] Roy-S.K. Mahapatra D.R. Biswal, M.P.(2012). Multi-choice stochastic transportation problem with exponential distribution. *J Uncertain Syst*, 6(3):200–213.

[9] Zhang-B. Peng J. Li S. Chen, L.(2016). Fixed charge solid transportation problem in uncertain environment and its algorithm. *Computers and Industrial Engineering*, 102:186–197.

[10] Mahapatra D.R.(2014). Multi-choice stochastic transportation problem involving weibull distribution. *Int J Optim Control Theor Appl*, 4(1):45–55.

[11] Schell E.D.(1955). Distribution of a product by several properties. in: Proceedings of the second symposium in linear programming. *DCS/Comptroller HQ, US Air Force, Washington, DC*, 2:615–642.

[12] Rizk-Allah R.M. Hassanien A.E. Elhoseny, M.(2018). A multi-objective transportation model under neutrosophic environment. *Computers and Electrical Engineering*, 69:705–719.

[13] Hitchcock F.(1941). Optimum utilization of the transportation system. *Econometrica*, 17:136–146.

[14] Agrawal-P. Ganesh, T.(2019). Solving multi-choice fractional stochastic transportation problem involving newton's divided difference interpolation. *In: Numerical Optimization in Engineering and Sciences Select Proceedings of NOIEAS, Springer*.

[15] Haley K.B.(1962). New methods in mathematical programming—the solid transportation problem. *Operations Research*, 10(4):448–463.

[16] Zadeh L.A.(1965). Information and control. *Fuzzy Sets*, 8(3):338–353.

[17] Das. A. Lee, G.M.(2021). A multi-objective stochastic solid transportation problem with the supply, demand, and conveyance capacity following the weibull distribution. *Mathematics*, 9:1757.

[18] Roy S.K. Mahapatra, D.R.(2014). Solving solid transportation problems with multi-choice cost and stochastic supply and demand. *Int J Strateg Decis Sci*, 5(3):1–26.

[19] Maity G. Roy, S.K.(2016). Solving a multi-objective transportation problem with nonlinear cost and multi-choice demand. *Int J Manag Sci Eng Manag*, 11(1):62–70.

[20] Sinha S.(2005). Mathematical programming: Theory and methods. *Elsevier, Amsterdam*.

[21] Joshi V.D. Agarwal K. Singh, J.(2022). Goal programming approach to solve linear transportation problems with multiple objectives. *J. Computational analysis and applications*, 31(1):127–139.

[22] Roy S.K.(2014). Multi-choice stochastic transportation problem involving weibull distribution. *International Journal of Operational Research*, 21(1):38–58.

[23] Roy S.K.(2015). Lagrange's interpolating polynomial approach to solve multi-choice transportation problem. *Int J Appl Comput Math*, 1(4):639–649.

[24] Roy S.K.(2016). Transportation problem with multi-choice cost and demand and stochastic supply. *J Oper Res Soc China*, 4:193–204.

[25] Healy W.C.(1964). Multiple choice programming: (a procedure for linear programming with zero one variables). *Oper Res*, 12(1):122–138.

On multi-valued nonexpansive mappings in UCBS

Kiran Dewangan[1], Laxmi Rathour[2,*],Vishnu Narayan Mishra[3] and Mohd Raiz[3]

[1]Department of Mathematics, Faculty of science, Government Dudhadhari Bajrang Girls Postgraduate Autonomous College, Raipur-492001, Chhattisgarh, India
[2]Department of Mathematics, Faculty of science, National Institute of Technology, Chaltlang, Aizawl-796012, Mizoram, India
[3]Department of Mathematics, Indira Gandhi National Tribal University, Lalpur, Amarkantak, Anuppur, Madhya Pradesh-484887, India
{dewangan.kiran@gmail.com, laxmirathour817@gmail.com, vnm@igntu.ac.in, mohdraizp@gmail.com}

Abstract

In this manuscript, we focus on the approximation of fixed points for multi-valued nonexpansive type mappings within uniformly convex Banach spaces. To achieve this goal, we utilize a three-step iteration scheme that was originally introduced by Ullah et al. Furthermore, we establish the rapid convergence properties of the Ullah et al. iteration scheme through the implementation of numerical examples using Matlab software.

2020 MSC. 47H09, 47H10
Keywords. nonexpansive mappings, fixed point, uniformly convex Banach spaces, Fejer monotone.

1 Introduction

In nonlinear analysis, fixed point theory has a great importance over last 90 years. In fact the technique of fixed point also have been used in different fields such as biology, physics, engineering, chemistry, game theory, economics, computer science etc.

Fixed point theorems are developed for both single-valued and multi-valuedd functions over different spaces. Banach contraction principle [2] is one of the pioneering

work in the field of fixed point theory and widely used to find out solution of different problems in the field of analysis.

There are lots of fixed point results available concerning single-valued nonexpansive mappings in the literature, while the study of the fixed points of multi-valued nonexpansive mappings are difficult. The multi-valued version of Banach contraction principle was given by Nadler [9] in 1969. Sastry and Babu [11] introduced multi-valued version of Mann [7] and Ishikawa [5] iteration and proved convergence theorems for nonexpansive mappings in Hilbert space. In 2016 Kim et al. [6] introduced multi-valued version of Thakur iteration [14] proved convergence results in uniformly convex Banach space and many more application are discussed on convergence ([17–19]).

The following three-step iteration scheme was introduced by Ullah et al. [15]-
Let $\mathcal{M}$ be a convex subset of a normed space B and $S : \mathcal{M} \to \mathcal{M}$ be a nonlinear mapping. For $w_1 \in \mathcal{M}$, the sequence $\{w_j\}$ in $\mathcal{M}$ is defined by

$$\begin{cases} t_j = (1-\alpha_j)w_j + \alpha_j S w_j, \\ z_j = S t_j, \\ w_{j+1} = S y_j, \ j \geq 1, \end{cases} \tag{1.1}$$

where $\{\alpha_j\}$ is a sequence in $(0, 1)$. Ullah proved that their iterative process converges faster than the iterative process given by Thakur [14].

The concept of Hausdorff metric, to approximate fixed points of multi-valued nonexpansive mapping was introduced by Markin [8] as follows:
Let $CB(\mathcal{M})$=collection of all non-empty closed bounded subset of $\mathcal{M}$ According to [6], a multi-valued mapping $S : \mathcal{M} \to CB(\mathcal{M})$ is said to be nonexpansive if

$$H(Sw, Sy) \leq ||w - y||,$$

for all $w, z \in \mathcal{M}$.

Following is the multi-valued version of Ullah iteration [16]. Let $\mathcal{M}$ be a non-empty subset which is closed convex of a UCBS B and $S : \mathcal{M} \to P(\mathcal{M})$ be a multi-valuedd function. For $w_1 \in \mathcal{M}$, the sequence $\{w_j\}$ in $\mathcal{M}$ is given by

$$\begin{cases} t_j = (1-\alpha_j)w_j + \alpha_j u_j, \\ z_j = w_j, \\ w_{j+1} = v_j, \ j \geq 1, \end{cases} \tag{1.2}$$

where $P_S : \mathcal{M} \to 2^{\mathcal{M}}$ be a multi-valued mapping, $u_j \in P_S(w_j)$, $v_j \in P_S(y_j)$, $w_j \in P_S(t_j)$, and $\{\alpha_j\} \in (0, 1)$.

In this study, we prove strong convergence of the iteration scheme given by (1.2), to approximate fixed points for the multi-valuedd nonexpansive functions in uniformly convex Banach space. For convinient,we denote uniformly convex Banach space by

UCBS. We also compare iteration scheme (1.2) with multi-valued version of some well known iteration schemes (refer [20]).

2 Preliminaries

Definition 2.1. Suppose non-empty subset $\mathcal{M}$ of a UCBS B and $S : \mathcal{M} \to 2^{\mathcal{M}}$ is a multi-valued functions. An element $w \in \mathcal{M}$ is known as fixed point of multi-valued functions S, if $w \in Sw$. Trough-out the literature, we represent the set of fixed points of S by $F(S)$.

Definition 2.2. [6] Suppose a non-empty $\mathcal{M}$ subset of a UCBS B. Then $\mathcal{M}$ is known as proximal if for each $w \in B$, there exists an element $y \in \mathcal{M}$, we have

$$||w - z|| = d(w, \mathcal{M}) = \inf\{||w - t|| : t \in \mathcal{M}\}.$$

Definition 2.3. [6] Suppose a non-empty $\mathcal{M}$ be subset of a UCBS B and $\{w_j\}$ in B is known as Fejer monotone subset $\mathcal{M}$, if

$$||w_{j+1} - p|| \leq ||w_j - q||,$$

for all $q \in \mathcal{M}$, $j \geq 1$.

Proposition 2.1. *[6] Suppose a non-empty M be subset of a UCBS B and $\{w_j\}$ is Fejer monotone sequence with respect to $\mathcal{M}$. Then, the followings are true:*

(a) $\{w_j\}$ is bounded.

(b) For each $w \in M$, $\{||w_j - w||\}$ converges.

Note that the concept of Condition (I) in Banach space was given by Dotson and Senter [13]. Given below are multi-valued version of Condition (I).

Definition 2.4. suppose $\mathcal{M}$be a non-empty subset of a UCBS B. A multi-valuedd nonexpansive function $S : j \to CB(\mathcal{M})$ holds Condition (I), if non-decreasing function $g : [0, \infty) \to [0, \infty)$ with $g(0) = 0$, $g(r) > 0$ for each $r \in (0, \infty)$ such that $||w - Sw|| \geq g(d(w, F(S)))$ for all $w \in M$.

Lemma 2.2. *[12] Suppose B be a UCBS and $\{\alpha_j\}$ is a sequence in $[\gamma, 1-\gamma]$ for some $\gamma \in (0, 1)$. Let $\{w_j\}$ and $\{z_j\} \in X$ then, $\limsup_{j\to\infty} ||w_j|| \leq q$, $\limsup_{j\to\infty} ||z_j|| \leq q$, and $\limsup_{j\to\infty} ||\alpha_j w_j + (1-\alpha_j)y_j|| = q$ for some $q \geq 0$. Then $\lim_{j\to\infty} ||w_j - z_j|| = 0$.*

Lemma 2.3. *[3] suppose $S : \mathcal{M} \to P(\mathcal{M})$ is a multi-valuedd function with $F(S) \neq \emptyset$ and let $P_S : \mathcal{M} \to 2^{\mathcal{M}}$ be a multi-valued function given by*

$$P_S(w) = \{z \in Sw : ||w - z|| = d(w, Sw)\}, w \in \mathcal{M}.$$

Then the following conclusion holds:

(a) P_S is multi-valuedd function from $\mathcal{M} \to P(\mathcal{M})$.

(b) $F(S) = F(P_S)$.

(c) $P_S(q) = \{q\}$, *for every* $q \in F(S)$.

(d) For each $w \in M$, $P_S(w)$ *and* Sw *is a compact because its a closed.*

(e) $d(w, Sw) = d(w, P_S(w))$ *for each* $w \in \mathcal{M}$.

3 Primary result

Lemma 3.1. *Considering* $\mathcal{M}$ *be a non-empty closed convex subset of a UCBS* B. *Let* $S : \mathcal{M} \to P(\mathcal{M})$ *be a multi-valuedd function such that* $F(S) \neq \emptyset$, *and* $P_S : \mathcal{M} \to 2^{\mathcal{M}}$ *be a multi-valuedd nonexpansive function. Let* $\{w_j\}$ *be a sequence in* $\mathcal{M}$ *given by (1.2), then* $\lim_{j\to\infty} ||w_j - t||$ *exists for all* $t \in F(S)$.

Proof. By our assumption, that $F(S) \neq \emptyset$, so suppose that $t \in F(S)$. Then, by Lemma 2.3, we have $t \in P_S(t) = \{t\}$. Also by Hausdorff metric, we have

$$H(P_S(w_j), P_S(t)) = \max\{\sup d(u_j, P_S(t)), \sup d(P_S(w_j), t)\},$$

where $d(u_j, P_S(t)) = \inf_{t\in P_S(t)} ||u_j - t||$.
By (1.2) we have,

$$\begin{aligned} ||t_j - t|| &= ||(1-\alpha_j)w_j + \alpha_j u_j - t|| \\ &\leq (1-\alpha_j)||w_j - t|| + \alpha_j||u_j - t|| \\ &\leq (1-\alpha_j)||w_j - t|| + \alpha_j H(P_S(w_j), P_S(t)) \\ &\leq (1-\alpha_j)||w_j - t|| + \alpha_j||w_j - t|| = ||w_j - t||, \end{aligned}$$

$$\begin{aligned} ||z_j - t|| &= ||w_j - t|| \\ &\leq H(P_S(t_j), P_S(t)) \\ &\leq ||t_j - t||, \end{aligned}$$

and

$$\begin{aligned} ||w_{j+1} - t|| &= ||v_j - t|| \\ &\leq H(P_S(z_j), P_S(t)) \\ &\leq ||z_j - t|| \\ &\leq ||w_j - t||. \end{aligned}$$

It follows that the sequence $\{w_j\}$ is a Fejer monotone with respect to $F(S)$. Hence from the Proposition 2.1, sequence $\{w_j\}$ is bounded and $\lim_{j\to\infty} ||w_j - t||$ exists for all $t \in F(S)$. □

Lemma 3.2. *Let $\mathcal{M}$ be a non-empty closed convex subset of a UCBS B. Let $S : \mathcal{M} \to P(M)$ be a multi-valued mapping such that $F(S) \neq \emptyset$, and $P_S : \mathcal{M} \to 2^{\mathcal{M}}$ be a multi-valued nonexpansive mapping. Let $\{w_j\}$ be a sequence in $\mathcal{M}$ defined by (1.2), then $\lim_{j\to\infty} d(w_j, Sw_j) = 0$.*

Proof. By Lemma 3.1, we have $\lim_{j\to\infty} ||w_j - t||$ exists for all $t \in F(S)$. Let $\lim_{j\to\infty} ||w_j - t|| = a$. If $a = 0$, then

$$\begin{aligned} d(w_j, Sw_j) &\leq ||w_j - u_j|| \\ &\leq ||w_j - t|| + ||t - u_j|| \\ &\leq ||w_j - t|| + H(P_S(w_j), P_S(t)) \\ &\leq 2||w_j - t|| \ \to \ 0 \ as \ j \to \infty. \end{aligned}$$

Let $a > 0$. Since $\lim_{j\to\infty} ||w_j - t|| = a$, we have $\limsup_{j\to\infty} ||w_j - t|| \leq a$. Also

$$||z_j - t|| \leq ||w_j - t|| \Rightarrow \limsup_{j\to\infty} ||z_j - t|| \leq a.$$

In addition to,

$$\begin{aligned} \limsup_{j\to\infty} ||u_j - t|| &\leq \limsup_{j\to\infty} H(P_S(w_j), P_S(t)) \\ &\leq \limsup_{j\to\infty} ||w_j - t|| \\ &\leq a. \end{aligned}$$

Also

$$\begin{aligned} \limsup_{j\to\infty} ||v_j - t|| &\leq \limsup_{j\to\infty} H(P_S(z_j), P_S(t)) \\ &\leq \limsup_{j\to\infty} ||z_j - t|| \\ &\leq a. \end{aligned}$$

Here, for each $\{\alpha_j\}$ in $[\gamma, 1-\gamma]$ for some $\gamma \in (0, 1)$, one has

$$\begin{aligned} \limsup_{j\to\infty} ||\alpha_j(w_j - t) + (1 - \alpha_j)(u_j - t)|| &\leq \alpha_j \limsup_{j\to\infty} ||w_j - t|| \\ &\quad + (1 - \alpha_j) \limsup_{j\to\infty} ||u_j - t|| \\ &\leq a. \end{aligned}$$

Hence, from Lemma 2.2, we have $\lim_{j\to\infty} ||(w_j - t) - (u_j - t)|| = 0$, i.e., $\lim_{j\to\infty} ||w_j - u_j|| = 0$.
Since

$$d(w_j, Sw_j) \leq ||w_j - u_j||,$$

we have

$$\lim_{j\to\infty} d(w_j, Sw_j) = 0.$$

□

Theorem 3.3. *Consider $\mathcal{M}$ is a non-empty closed convex subset of a UCBS X. Let $S : \mathcal{M} \to P(\mathcal{M})$ be a multi-valued mapping such that it satisfy Condition (I). Let $F(S) \neq \emptyset$, and $P_S : \mathcal{M} \to 2^{\mathcal{M}}$ be a multi-valued nonexpansive function. Then the sequence $\{w_j\}$ defined by (1.2), strongly converges to a fixed point of S.*

Proof. By Lemma 3.1, one has

$$||w_{j+1} - t|| \leq ||w_j - t||,$$

it gives that

$$d(w_{j+1}, F(S)) \leq d(w_j, F(S)).$$

This implies that $\lim_{j\to\infty} d(w_j, F(S))$ exists. Since S satisfy Condition (I) and by Lemma 3.2, we have $\lim_{j\to\infty} d(w_j, Sw_j) = 0$, we have $\lim_{j\to\infty} d(w_j, F(S)) = 0$.
Next we prove that $\{w_j\}$ is Cauchy sequence in M. As, we have $\lim_{j\to\infty} d(w_j, F(S)) = 0$ and $\epsilon > 0$, there is a constant j_0 for all $j \geq j_0$, one has

$$d(w_j, F(S)) < \frac{\epsilon}{4}.$$

In particular and must $p \in F(S)$ then we obtain

$$||w_{j_0} - p|| < \frac{\epsilon}{2}.$$

For $j, m \geq j_0$, we obtain

$$\begin{aligned} ||w_{j+m} - w_j|| &\leq ||w_{j+1} - p|| + ||p - w_j|| \\ &< \epsilon. \end{aligned}$$

It follows that $\{w_j\}$ is a Cauchy sequence in $\mathcal{M}$. Since $\mathcal{M}$ is closed subset of UCBS B, it must converges in $\mathcal{M}$ and $w \in M$ thus $\lim_{j\to\infty} ||w_j - w|| = 0$. Now

$$\begin{aligned} 0 \leq d(w, P_S(w)) &\leq ||w_j - w|| + d(w_j, P_S(w_j)) + H(P_S(w_j), P_S(w)) \\ &\leq ||w_j - w|| + ||w_j - u_j|| + ||w_j - w|| \to 0 \; as \; j \to \infty. \end{aligned}$$

So $d(w, P_S(w)) = 0$. By Lemma 2.2, $F(P_S)$ is closed, therefore $w \in F(P_S) = F(S)$. □

Theorem 3.4. *Consider $\mathcal{M}$ is a non-empty closed convex subset of a UCBS B and $S : \mathcal{M} \to P(\mathcal{M})$ be a multi-valuedd function with $F(S) \neq \emptyset$, and $P_S : \mathcal{M} \to 2^{\mathcal{M}}$ is a multi-valuedd nonexpansive function. Then, the sequence $\{w_j\}$ given by (1.2), strongly converges to a fixed point of S if and only in $\liminf_{j\to\infty} d(w_j, F(S)) = 0$.*

Proof. If $\liminf_{j\to\infty} d(w_j, F(S)) = 0$, then it is obvious that the sequence $\{w_j\}$ strongly converges to a fixed point of S.
For the conversation, suppose that $\liminf_{j\to\infty} d(w_j, F(S)) = 0$, then $\lim_{j\to\infty} d(w_j, F(S)) = 0$. Using similar argument of the proof as in Theorem 3.3, we obtain that $\{w_j\}$ is a Cauchy sequence in $\mathcal{M}$. Let $\lim_{j\to\infty} w_j = q$. Then

$$\begin{aligned} 0 \leq d(q, P_S(q)) &\leq ||w_j - q|| + d(w_j, P_S(w_j)) + H(P_S(w_j), P_S(q)) \\ &\leq ||w_j - q|| + ||w_j - u_j|| + ||w_j - q|| \to 0 \; as \; j \to \infty. \end{aligned}$$

It follows that $d(q, P_S(w)) = 0$. Since $F(P_S)$ is closed, therefore $q \in F(P_{S)} = F(S)$. □

4 Numerical example

Example 4.1. *Let $B = \mathbb{R}$ be a UCBS, with $||.||$ is produced by a metric d such that $d(w, y) = ||w - z||$, for all $w, y \in B$. Let $\mathcal{M} = [0, 1]$ be a non-empty subset of B. Let $S : \mathcal{M} \to P(\mathcal{M})$ defined by*

$$Sx = \begin{cases} [0, \frac{w+1}{2}], \ w \in [0, \frac{1}{2}), \\ \{0\}, \ w \in [\frac{1}{2}, 1). \end{cases}$$

Consider the following cases:

Case I: when $w \in [\frac{1}{2}, 1)$. Then $F(S) = \{0\}$ and from Lemma 2.3, we have $F(S) = \{0\} = F(P_S)$ and $P_S(0) = \{0\}$.

Case II: when $w \in [0, \frac{1}{2})$. Then $F(S) = [0, \frac{w+1}{2}]$. Now

$$\begin{aligned} P_S(w) &= \{z \in Sw : d(w, Sw) = ||z - w||\} \\ P_S(w) &= \{z \in Sw : ||z - w|| = d(w, [0, \frac{w+1}{2}])\} \\ &= \{z \in Sw : ||z - w|| = ||w - \frac{w+1}{2}||\} \\ &= \{z \in Sw : ||z - w|| = ||\frac{w-1}{2}||\} \\ &= \{z = \frac{w+1}{2}\} \end{aligned}$$

Therefore, we have $F(S) = F(P_S) = [0, \frac{w+1}{2}]$

Next, we show that a sequence $\{w_j\} \in \mathcal{M}$ given by (1.1) converges strongly to a point of $F(S)$.
Start with initial value $w_1 = \frac{1}{2}$ and choose $\alpha_k = \frac{2}{3}$, then we have

$$P_S(w_1) = \{\frac{w_1 + 1}{2}\} = \{\frac{3}{4}\}.$$

Choose $u_1 \in P_S(w_1)$, then $u_1 = \frac{3}{4}$. Now

$$\begin{aligned} z_1 &= (1 - \alpha_1)w_1 + \alpha_1 u_1 \\ &= \frac{1}{6} + \frac{1}{2} \\ &= \frac{2}{3}. \end{aligned}$$

$$P_S(t_1) = \{\frac{z_1 + 1}{2}\} = \frac{5}{6}.$$

Choose $w_1 \in P_S(t_1)$, then $w_1 = \frac{5}{6}$. Hence $z_1 = w_1 = \frac{5}{6}$. Choose $v_1 \in P_S(z_1) = \{\frac{z_1+1}{2}\} = \frac{11}{12}$.

Choose $w_2 = v_1 = \frac{11}{12}$, *then doing same procedure, we have* $u_2 = \frac{23}{24}$, $t_2 = \frac{17}{18}$, $z_2 = w_2 = \frac{35}{36}$ *and* $w_3 = v_2 = \frac{71}{72}$. *Continuing the process, we get that* $w_1 < 1$, $w_2 < 1$,...$w_n < 1, ...$ *Hence, we conclude that sequence* $\{w_k\} \in M$ *given by (1.2) converges strongly to a point of* $F(S)$.

Here we show the fastness of the iteration scheme (1.2) by comparing some well known iteration schemes with the help of some given below examples.

Example 4.2. *Let* $B = \mathbb{R}$ *convex Banach space which is uniformly, equipped with* $||.||$ *is produced by a metric* d *thus* $d(w, z) = ||w - z||$, *for all* $w, z \in B$. *Let* $M = [0, \infty)$ *be a non-empty subset of* B. *Let* $S : \mathcal{M} \to P(\mathcal{M})$ *defined by*

$$Sw = \begin{cases} \{0\},\ w \in [0, \frac{1}{100}) = A', \\ [0, \frac{w}{5}],\ w \in [\frac{1}{100}, \infty) - \{\frac{8}{7}\} = B', \\ [0, \frac{9}{10}],\ w \in \{\frac{8}{7}\} = C'. \end{cases}$$

We prove that S *is multi-valued nonexpansive functions. Consider the following cases*

Case I: when $w, z \in A'$ *and* $w, z \in C'$, *then it is clear that* $H(Sw, Sz) \leq ||w - z||$.

Case II: when $w, z \in B'$, *then*

$$\begin{aligned} H(Sw, Sz) &= H([0, \frac{w}{5}], [0, \frac{z}{5}]) \\ &= ||\frac{w}{5} - \frac{z}{5}|| \\ &= \frac{1}{5}||w - z|| < ||w - z||. \end{aligned}$$

Case III: when $w \in A'$ *and* $z = \frac{8}{7}$. *Then* $H(Sw, Sz) = H(\{0\}, [0, \frac{9}{10}]) = \frac{9}{10} < 1 = |w - z||$.

Case IV: when $w \in B'$ *and* $z = \frac{8}{7}$. *Then*

$$\begin{aligned} ||w - z|| = d(w, z) &= d(w, \frac{8}{7}) \\ &= ||w - \frac{8}{7}|| \\ &\leq ||w|| + \frac{8}{7}. \end{aligned}$$

and

$$\begin{aligned} H(Sw, Sy) &= H([0, \frac{w}{5}], [0, \frac{9}{10}]) \\ &= ||\frac{w}{5} - \frac{9}{10}|| \\ &\leq ||\frac{w}{5}|| + \frac{9}{10}. \end{aligned}$$

Clearly $H(Sw, Sy) \leq ||w - z||$.

Case V: when $w \in A^{'}$ *and* $z \in B^{'}$. *Then*

$$\begin{aligned} H(Sw, Sy) &= H(\{0\}, [0, \frac{z}{5}]) \\ &= ||\frac{z}{5}|| < ||z|| \\ &< ||w|| + ||z|| \\ &= ||w - z||. \end{aligned}$$

Hence, we conclude that S *is multi-valued nonexpansive mapping.*

Now with the help of Matlab software program, we compare iteration scheme (1.2) with multi-valued version of different iteration schemes given in [20].

Table 1: Strong convergence of multivalued version of Ullah (1.2), Abbas [1], Ishikawa [5], Noor [10], Picard S [4] and Thakur [6] iterations to the fixed point $x = 0$ of S in Example 4.2.

Iteration	Ullah	Thakur	Abbas	Noor	Ishikawa	Picard S
0	0.50000000	0.50000000	0.50000000	0.50000000	0.50000000	0.50000000
1	-0.01200000	-0.04400000	- 0.02800000	-0.58800000	-0.62000000	-0.09999911
2	0.00009600	0.00140800	0.00078400	0.32222400	0.34720000	-0.02000009
3	-0.00000026	-0.00002378	-0.00001417	-0.11466401	-0.12190578	0.00240000
4	0.00000000	0.00000024	0.00000018	0.03009930	0.03047644	-0.00005333
5	0.00000000	-0.00000000	-0.00000000	-0.00623946	-0.00580272	0.00000213
6	0.00000000	0.00000000	0.00000000	0.00106579	0.00087685	-0.00000017
7	0.00000000	0.00000000	-0.00000000	-0.00015444	-0.00010809	0.00000001
8	0.00000000	0.00000000	0.00000000	-0.00001939	0.00001108	-0.00000000

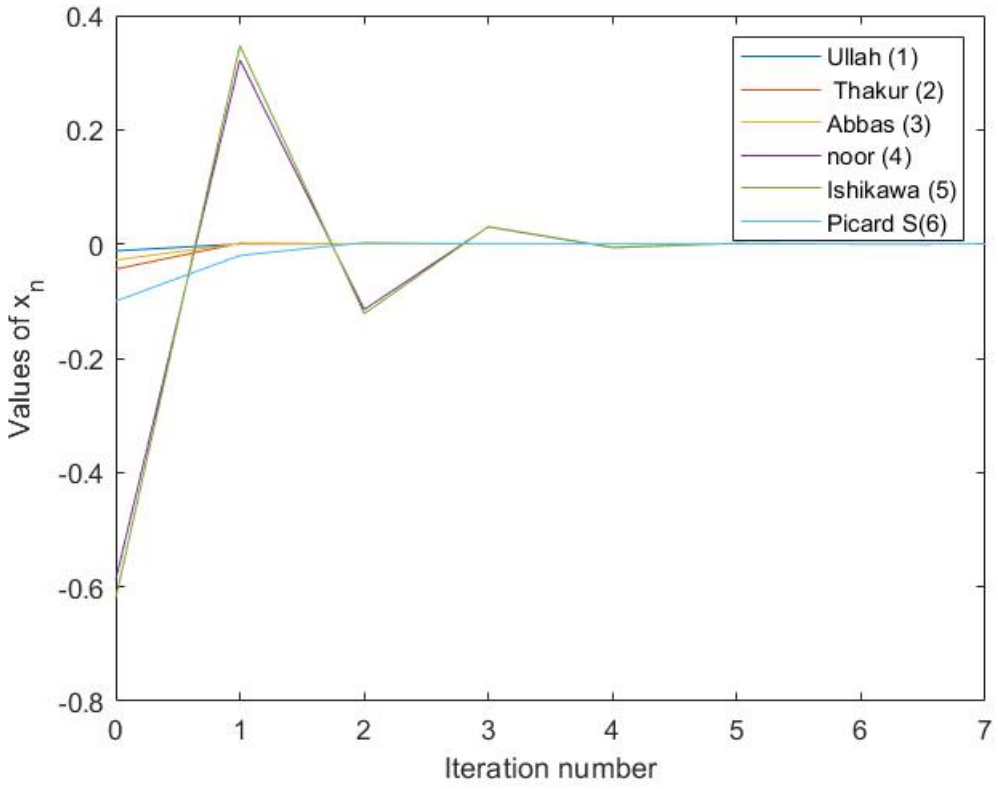

Figure 1. Behavior of Ullah iteration (magenta), Thakur iteration (carrot orange), Abbas iteration (yellow), Noor iteration (purple), Ishikawa iteration (green), Picard S iteration (cyan) to the fixed point $x = 0$ of the mapping S .

References

[1] Abbas M., Nazir T., A new faster iteration process applied to constrained minimization and feasibility problems. Math. Vesnik, 66 (2014), 223–234.

[2] Banach S., Sur les operations dans les ensembles abstaits et leau application aux eqautions untegrales, Fund. Math., 3 (1922), 133-181.

[3] Chang S.S., Agrawal R.P.,Wang L., Existence and convergence theorems of fixed points for multi-valued SCC, SKC, KSC, SCS and $C-$ type mappings in hyperbolic spaces, Fixed Point Theory and Appl., 2015:83 (2015), 1-17.

[4] Gursoy F., Karakaya V., A Picard S hybrid type iteration method for solving a differential equation with retarted argument, arXiv, arXiv:1403.2546 (2014), 1-16.

[5] Ishikawa S., Fixed points by new iteration method, Proc. Amer. Math. Soc., 149 (1974), 147-150.

[6] Kim J.K., Dashputre S., Lim W.H., Approximation of fixed points for multi-valued nonexpansive mappings in Banach space, Global j. pure Appl. Math., 12(6) (2016), 4901-4912.

[7] Mann W.R., Mean value methods in iterations, Proc. Amer. Math. Soc., 4 (1953), 506-510.

[8] Markin J.T., Continuous dependence of fixed point sets, Proc. Amer. Math. Soc., 38 (1973), 545-547.

[9] Nadler S.B., Multivalued contaction mappings, Pac. J. Math., 30 (1969), 475-488.

[10] Noor M.A., New approximation schemes for general variational inequalities, J. Math. Anal. Appl., 251 (2000), 217–229.

[11] Sastry K.P.R., Babu G.V.R., Convergence of Ishikawa iterates for a multi-valued mapping with a fixed point, Czechoslovak Math. J., 55 (2005), 817-826.

[12] Schu J., Weak and strong convergence of fixed point of asymptotically nonexpansive mappings, Bull. Aust. Math. Soc., 43(1) (1991), 153-159.

[13] Senter H.F., Dotson W.G., Approximating fixed points of nonexpansivemappings, Proc. Amer. Math. Soc., 44 (1974), 375–380.

[14] Thakur D., Thakur B.S., Postolache M., New iteration scheme for numerical reckoning fixed points of nonexpansive mappings, J. Inequal. Appl., 2014:328 (2014), 1-15.

[15] Ullah K., Arshad M., Numerical reckoning fixed points for Suzuki Generalized nonexpansive mappings via new iteration process, Filomat, 32(1) (2018), 187-196.

[16] Ullah K., Ullah M., Sen M. de la, Fixed Point Results on Multi-Valued Generalized $(\alpha, \beta)-$ Nonexpansive Mappings in Banach Spaces, Algorithms, 14(223) (2021), 2-17.

[17] Mohd R., Ruchi S. R., Vishnu N. M., α-Schurer-Durrmeyer operators and their approximation properties, Ann. Univ. Craiova Math. Comput. Sci. Ser. 50(2023), 189–204.

[18] Mohd R., Ruchi S. R., Vishnu N. M., Approximation on bivariate of Durrmeyer operators based on beta function, J. Anal. (2023):DOI: 10.1007/s41478-023-00639-7.

[19] Lakshmi N.M., Mohd R., Laxmi R., Vishnu N. M., Tauberian theorems for weighted means of double sequences in intuitionistic fuzzy normed spaces, Yugo. J. Oper. Research, 32(3), (2022), 377-388

[20] Ullah K., Ahmad J., and Khan A.R., On multi-valued version of M-iteration process, Asian-European Journal of Mathematics, 10:14 (2022), 1-13.

SOME NEW RESULTS ON FRACTIONAL INTEGRALS INVOLVING SRIVASTAVA POLYNOMIALS, (p,q)-EXTENDED HYPERGEOMETRIC FUNCTION AND M-SERIES

[1]Komal Prasad Sharma,[2]Alok Bhargava*and[3]Garima Agrawal

[1,2,3]Department of Mathematics and Statistics, Manipal University Jaipur, Jaipur, Rajasthan(India)

E-Mail: [1]keshav4maths@gmail.com,[2]alok.bhargava@jaipur.manipal.edu

E-Mail: [3]garima.agrawal@jaipur.manipal.edu

Abstract

Numerous prior publications on fractional calculus provide fascinating explanations of the theory and applications of fractional calculus operators throughout various mathematical analytic domains. In this paper, we introduce new fractional integral formulas using the Saigo-Maeda fractional integral operators and Appell's function F_3 along with the Srivastava polynomials, the (p,q)-extended Gauss hypergeometric function, and the M-Series. A few fascinating unusual cases of our main conclusions are also considered. This approach can be applied to explore a broad class of previously dispersed discoveries in the literature.

Key Words: (p, q)-Extended Gaussís hypergeometric function, Srivastava polynomials, (p, q)-Extended Beta function, S-Function, Generalized fractional integral operators.

AMS Subject Classification: Primary 33B15, 33C60, 26A33; Secondary 44A10, 33C05, 33C90.

1 Introduction

Over the past three decades, the field of fractional calculus has dealt with derivatives and integrals of arbitrary orders, and it has been applied to nearly every branch of science and engineering. Recently, a large number of scholars have investigated higher transcendent hypergeometric type special functions [10, 11, 28] and associated extensions, generalizations, and unifications of Euler's Beta function (refer [1], [2], [3], [7], [8], [9], [12], [13], [16], [19], [21], [24]). In particular, Chaudhry et al. [2, p. 20, Equation (1.7)] represented the extension of the Beta function as

$$B(x,y;p)=\int_0^1(\xi)^{x-1}(1-\xi)^{y-1}exp(\frac{-p}{\xi(1-\xi)})d\xi,\Re(p)>0 \tag{1.1}$$

where for $p=0$, $min(\Re(x),\Re(y))>0$

Chaudhry et al. [3] explored the relationships between the Beta function $B(\xi,\zeta;p)$, Error function, Whittaker function and Macdonald function (or modified Bessel function of the second kind). Moreover, the extended version of the Gaussian hypergeometric function was also derived by utilising (1.2) as -

$$F_p(a,b,c;\xi)=\sum_{n\geq 0}^{\infty}(a)_n\frac{B(b+n,c-b;p)}{B(b,c-b)}\frac{(\xi)^n}{n!} \tag{1.2}$$

$p>0$; for $p=0$, $|\xi|<1;\Re(c)>\Re(b)>0$

A recent expansion of $B(x,y;p)$ and $F_p(a,b,c;z)$ was presented by Choi et al. [4] in the following way

$$B(x,y;p,q)=\int_0^1(\xi)^{x-1}(1-\xi)^{y-1}exp(\frac{-p}{\xi}-\frac{q}{(1-\xi)})d\xi \tag{1.3}$$

provided $\min(\Re(p),\Re(q))\geq 0,\min(\Re(x),\Re(y))>0$

and

$$F_{p,q}(a,b;c;\xi)=\sum_{n\geq 0}^{\infty}(a)_n\frac{B(b+n,c-b;p,q)}{B(b,c-b)}\frac{\xi^n}{n!} \tag{1.4}$$

provided $p,q\geq 0$;for p=0, $|\xi|<1;\Re(c)>\Re(b)>0$

For further information on (1.3) and (1.4), see [23].

The goal of this inquiry is to comprehend the concept of the convolution of two analytical functions, generally known as the Hadamard product. A newly discovered function can be divided into two different functions. The Hadamard product series, in particular, defines a full function if a power series reflects an entire function. Let

$$f(z)=\sum_{n=0}^{\infty}a_n\xi^n,|\xi|<R_f\quad and\quad g(\xi)=\sum_{n=0}^{\infty}b_n\xi^n,|\xi|<R_g$$

Considering two given power series with, respectively, R_f and R_g as their radii of convergence. They produce a Hadamard product, which is a power series described by

$$(f*g)(\xi)=\sum_{n=0}^{\infty}a_nb_n\xi^n=(g*f)(\xi),|\xi|<R \tag{1.5}$$

where R is the radius of convergence

$$\frac{1}{R}=\lim_{n\to 0}sup(|a_nb_n|)^{\frac{1}{n}}\leq\lim_{n\to 0}sup(|a_n|)^{\frac{1}{n}}\lim_{n\to 0}sup(|b_n|)^{\frac{1}{n}}=\frac{1}{R_fR_g}$$

$$and\ so\ R>(R_fR_g)\ (see[15]).$$

Srivastava [22] defined polynomials of general class in the following way

$$S_w^u=\sum_{s=0}^{[\frac{w}{u}]}\frac{(-w)_{us}}{s!}A_{w,s}\,x^s,u\in\mathbb{N},s\in N_0 \tag{1.6}$$

Where $N_0 = \mathbb{N} \cup \{0\}$, and the coefficients $A_{w,s}$, $w,s \in N_0, w,s > 0$ are arbitrary constants either real or complex. The polynomial family $S_w^{\lceil}x]$ exhibits several well-known polynomials in addition to its distinct cases when the coefficient $A_{w,s}$. is suitably specialised.

Parmar and Purohit [14] recently explored certain formulae for fractional integral connected to Saigo operators, Furthermore, Choi et al. [4] stated the extended form of hypergeometric functions $F_{p,q}(\xi)$ [26]. In this work, we explored some novel fractional integral formulas involving (p,q)–extended Beta function, (p,q)–extended Gauss's hypergeometric function, the general class of polynomial, and M-Series developed employing generalized fractional integral operators.

2 Fractional Integral Approach

Fractional integral operators involving several special functions [29,30] have been extensively researched in numerous mathematical tools (see, [6]). We explore here the Saigo and Maeda generalized fractional integral operators involving Appell function $F_3(.)$[18] in the kernel.

The extended fractional integrals incorporating Appell's function [22] are stated as, Assuming, $\mu, \mu', \nu, \nu', \tau \in \mathbb{C}$ and $x > 0$, then

$$(I_{0,+}^{\mu,\mu',\nu,\nu',\tau} f)(x) = \frac{x^{-\mu}}{\Gamma(\tau)} \int_0^x (x-\xi)^{\tau-1} \xi^{-\mu'} F_3(\mu, \mu', \nu, \nu'; \tau; 1-\frac{\xi}{x}, 1-\frac{x}{\xi}) f(\xi) dt; \Re(\tau) > 0 \tag{2.1}$$

and

$$(I_{0,-}^{\mu,\mu',\nu,\nu',\tau} f)(x) = \frac{x^{-\mu}}{\Gamma(\tau)} \int_x^\infty (\xi-x)^{\tau-1} \xi^{-\mu} F_3(\mu, \mu', \nu, \nu'; \tau; 1-\frac{x}{\xi}, 1-\frac{\xi}{x}) f(\xi) dt; \Re(\tau) > 0 \tag{2.2}$$

We will first express a few image formulas related to (2.1) and (2.2), which are given in the lemma that follows.

Lemma 1

Let $\mu, \mu', \nu, \nu', \tau \in \mathbb{C}$ and $x > 0$, Then
(a) If $\Re(\varepsilon) > \max(0, \Re(\mu+\mu'+\nu'-\tau), \Re(\mu'-\nu'))$ and $\Re(\tau) > 0$

$$(I_{0,+}^{\mu,\mu',\nu,\nu',\tau} x^{\varepsilon-1})(x) = x^{\varepsilon-\mu-\mu'+\tau-1} \Gamma \left[\begin{matrix} \varepsilon, \varepsilon+\tau-\mu-\mu'-\nu, \varepsilon+\nu'-\mu' \\ \varepsilon+\nu', \varepsilon+\tau-\mu-\mu', \varepsilon+\tau-\mu'-\nu \end{matrix} \right] \tag{2.3}$$

(b) If $\Re(\varepsilon) < 1 + \min(\Re(-\nu), \Re(\mu+\mu'+\nu'-\tau), \Re(\mu'-\nu'))$ and $\Re(\tau) > 0$

$$(I_{0,-}^{\mu,\mu',\nu,\nu',\tau} x^{\varepsilon-1})(x) = x^{\varepsilon-\mu-\mu'+\tau-1} \Gamma \left[\begin{matrix} 1-\varepsilon-\nu, 1-\varepsilon+\mu+\mu', 1-\varepsilon-\tau+\mu+\nu' \\ 1-\varepsilon, 1-\varepsilon+\mu+\mu'+\nu'-\tau, 1-\varepsilon+\mu-\nu \end{matrix} \right] \tag{2.4}$$

The symbols occurring in (2.3) and (2.4) are presented as

$$\Gamma\left[\begin{array}{c} a_1,a_2,a_3 \\ a_4,a_5,a_6 \end{array}\right] = \frac{\Gamma(a_1)\Gamma(a_2)\Gamma(a_3)}{\Gamma(a_4)\Gamma(a_5)\Gamma(a_6)}$$

The composition formulas for generalized fractional integrals (2.3) and (2.4) now involve generalized Gauss hypergeometric type functions $F_{p,q}(a,b;c;\xi)$, and the general class of polynomials [25], M-Series[20] are given in Theorem 3.1 and 3.2.
The M-Series is defined as

$$M_{p',q'}^{\Im,\varepsilon} = \sum_{l=0}^{\infty} \frac{(\alpha_1)_l ... (\alpha_{p'})_l}{(\beta_1)_l ... (\beta_{q'})_l} \frac{1}{\Gamma(\Im l+\varepsilon)} \tag{2.5}$$

Here α_j, β_j and $(\alpha_j)_l, (\beta_j)_l$ are pochhammer symbols. the series is defined by (2.5), where neither a negative integer nor zero can be found in any of the denominator parameters β_j, $j = 1,2,\ldots q'$. If any parameter $\alpha_j < 0, j = 1,2,...,p'$, then the series converts to a polynomial in x. The series is convergent for all x when $q' \geq p'$, and $p' = q'+1, \mod x < 1$. The series is divergent when $p' \geq q'+1$.

3 Main Results

In this paper, two new results are developed via generalized fractional operators, which involve Srivastava Polynomials [25], (p,q) - extended Gaussís Hypergeometric function [17, 22] and M-Series [20]. Further, their consequences are also mentioned in the form of simpler functions as special cases of these results

Theorem 3.1

Let $\mu, \mu', \nu, \nu', \tau, \varepsilon \in \mathbb{C}$ be such that $min(\Re(p,q)) > 0, \Re(\tau) > 0$ and $\Re(\varepsilon+s) > max[0, \Re(\mu+\mu'+\nu-\tau), \Re(\mu'-\nu')]$ then for $x > 0$

$$\left(I_{0,+}^{\mu,\mu',\nu,\nu',\tau} \left[\xi^{\varepsilon-1} S_W^u(\sigma\xi) F_{p,q}\left[\begin{array}{c} a,b \\ c \end{array}; e\xi\right] M_{p',q'}^{\Im,\varepsilon}(\xi^{\lambda}\ ) \right] \right)(x)$$

$$= x^{\varepsilon+\lambda l-\mu-\mu'+\tau-1} \sum_{s=0}^{\left[\frac{w}{u}\right]} \frac{(-w)_{us}}{s!} A_{w,s}(\sigma x)^s \sum_{l=0}^{\infty} \frac{(\alpha_1)_l ... (\alpha_{p'})_l}{(\beta_1)_l ... (\beta_{q'})_l} \frac{1}{\Gamma(\Im l+\varepsilon)}$$

$$\times \frac{\Gamma(\varepsilon+\lambda l+s)\Gamma(\varepsilon+\lambda l+\tau-\mu-\mu'-\nu+s)\Gamma(\varepsilon+\lambda l+\nu'-\mu'+s)}{\Gamma(\varepsilon+\lambda l+\nu'+s)\Gamma(\varepsilon+\lambda l+\tau-\mu-\mu'+s)\Gamma(\varepsilon+\lambda l+\tau-\mu'-\nu+s)}$$

$$\times F_{p,q}\left[\begin{array}{c} a,b \\ c \end{array}; ex\right] *_4 F_3\left[\begin{array}{c} 1,\theta_1,\theta_2,\theta_3 \\ \theta_4,\theta_5,\theta_6 \end{array}; ex\right] \tag{3.1}$$

where

$$\begin{aligned}\theta_1 &= \varepsilon+\lambda l+s, \theta_2=\varepsilon+\lambda l+\tau-\mu-\mu'-\nu+s,\\ \theta_3 &= \varepsilon+\lambda l+\nu'-\mu'+s, \theta_4=\varepsilon+\lambda l+\tau-\mu-\mu'+s,\\ \theta_5 &= \varepsilon+\lambda l+\tau-\mu'-\nu+s, \theta_6=\varepsilon+\lambda l+\nu'+s\end{aligned}$$

and $'*'$ signifies the Hadamard product

Proof.
Applying (1.4) and (1.6) to (2.1) and changing the order of integration and summation, which is valid under the given conditions here, and using (2.3), we find the LHS of (3.1) (say L) as

$$L=\sum_{s=0}^{[\frac{w}{u}]}\sum_{n=0}^{\infty}\frac{(-w)_{us}}{s!}A_{w,s}(\sigma)^s(a)_n\sum_{l=0}^{\infty}\frac{(\alpha_1)_l...(\alpha'_p}{(\beta_1)_l...(\beta'_q)_l}\frac{1}{\Gamma(\Im l+\varepsilon)}\frac{B_{p,q}(b+n,c-b)}{B(b,c-b)}\frac{e^n}{n!}$$

$$\times\left(\ I_{0,+}^{\mu,\mu',\nu,\nu',\tau}(t)^{\varepsilon+n+\lambda l+s-1}\ \right)(x)$$

$$\begin{aligned}&= (x)^{\varepsilon+\lambda l-\mu-\mu'+\tau-1}\sum_{s=0}^{[\frac{w}{u}]}\sum_{n=0}^{\infty}\frac{(-w)_{us}}{s!}A_{w,s}(\sigma)^s(a)_n\sum_{l=0}^{\infty}\frac{(\alpha_1)_l...(\alpha_{p'})_l}{(\beta_1)_l...(\beta_{q'})_l}\frac{1}{\Gamma(\Im l+\varepsilon)}\frac{B_{p,q}(b+n,c-b)}{B(b,c-b)}\\ &\times\frac{\Gamma(\varepsilon+\lambda l+n+s)\Gamma(\varepsilon+\lambda l+n+\tau-\mu-\mu'-\nu+s)\Gamma(\varepsilon+\lambda l+n+\nu'-\mu'+s)}{\Gamma(\varepsilon+\lambda l+n+\nu'+s)\Gamma(\varepsilon+\lambda l+n+\tau-\mu-\mu'+s)\Gamma(\varepsilon+\lambda l+n+\tau-\mu'-\nu+s)}\frac{(ex)^n}{n!}\end{aligned}\tag{3.2}$$

Expressing the last summation in (3.2) in terms of the Hadamard product with the functions $F_{p,q}(.)$ mentioned in (1.4) and generalized hypergeometric function [22, 24], we obtain the RHS of (3.1).

Theorem 3.2

Let $\mu,\mu',\nu,\nu',\delta,\rho\in\mathbb{C}$ be such that $min(\Re(p),\Re(q))>0,\Re(\delta)>0$ and $\Re(\rho)<1+min[\Re(-v),\Re(\mu+\mu'-\delta),\Re(-\mu-\nu-\delta)]$ then for $x>0$

$$\left(\ I_{0,-}^{\mu,\mu',\nu,\nu',\tau}\left[\ \xi^{\varepsilon-1}S_W^u(\sigma\xi)F_{p,q}\left[\begin{matrix}a,b\\ c\end{matrix};\frac{e}{\xi}\right]M_{p',q'}^{\Im,\varepsilon}(\xi^{\lambda}\ \right]\ \right)(x)$$

$$=x^{\varepsilon+\lambda l-\mu-\mu'+\tau-1}\sum_{s=0}^{[\frac{w}{u}]}\frac{(-w)_{us}}{s!}A_{w,s}(\sigma,s)^s\sum_{l=0}^{\infty}\frac{(\alpha_1)_l...(\alpha_{p'})_l}{(\beta_1)_l...(\beta_{q'})_l}\frac{1}{\Gamma(\Im l+\varepsilon)}$$

$$\times\frac{\Gamma(1-\nu-\varepsilon-\lambda l-s)\Gamma(1+\mu+\nu'-\varepsilon-\lambda l-s)\Gamma(1+\mu+\nu'-\varepsilon-\lambda l-s)}{\Gamma(1-\varepsilon-\lambda l-s,)\Gamma(1+\mu+\mu'+\nu'-\tau-\varepsilon-\lambda l-s)\Gamma(1+\mu-\nu-\varepsilon-\lambda l-s)}$$

$$\times F_{p,q}\left[\begin{array}{c} a,b \\ c \end{array};\frac{e}{x}\right] *_4 F_3\left[\begin{array}{c} 1,\delta_1,\delta_2,\delta_3 \\ \delta_4,\delta_5,\delta_6 \end{array};\frac{e}{x}\right] \tag{3.3}$$

where

$$\begin{aligned}\delta_1 &= 1-\nu-\varepsilon-\lambda l-s, \delta_2 = 1+\mu+\nu'-\varepsilon-\lambda l-s,\\ \delta_3 &= 1+\mu+\nu'-\varepsilon-\lambda l-s, \delta_4 = 1-\varepsilon-\lambda l-s\\ \delta_5 &= 1+\mu+\mu'+\nu'-\tau-\varepsilon-\lambda l-s, \delta_6 = 1+\mu-\nu-\varepsilon-\lambda l-s\end{aligned}$$

and $'*'$ signifies the Hadamard product

Proof. Applying a similar argument as in the proof of Theorem 3.1 by using (1.4) and (1.6) to (2.2), and using (2.4), we obtain the RHS of (3.3).

4 Special Cases

(i) If we set $\mu'=\nu'=0, \nu=-\eta, \mu=\mu+\nu, \delta=\mu, \Re(\mu)>0$ in the operators (2.1) and (2.2), then we arrive at Saigo hypergeometric fractional integral operators [6]

$$\left(I_{0,+}^{\mu,\nu,\eta} f(\xi) \right)(x) = \frac{x^{-\mu-\nu}}{\Gamma(\mu)} \int_0^x (x-\xi)^{\mu-1} {}_2F_1\left(\mu+\nu, -\eta; \mu; (1-\tfrac{\xi}{x}) \right) f(\xi) d\xi \tag{4.1}$$

and

$$\left(I_{0,-}^{\mu,\nu,\eta} f(\xi) \right)(x) = \frac{x^{-\mu-\nu}}{\Gamma(\mu)} \int_x^\infty (\xi-x)^{\mu-1} {}_2F_1\left(\mu+\nu, -\eta; \mu; (1-\tfrac{x}{\xi}) \right) f(\xi) d\xi \tag{4.2}$$

Corollary 1. Let $\mu,\mu',\eta,\rho \in \mathbb{C}$ be such that $\min(\Re(p),\Re(q))>0, \Re(\mu)>0$ and $\Re(\rho)>\max[0,\Re(\nu-\eta)], x>0$

then the result (3.1) reduced as

$$\left(I_{0,+}^{\mu,\nu,\eta} \left[t^{\varepsilon-1} S_w^u(\sigma\xi) F_{p,q}\left[\begin{array}{c} a,b \\ c \end{array};e\xi\right] M_{p',q'}^{\Im,\varepsilon}(\xi^\lambda \right] \right)(x)$$

$$= x^{\varepsilon+\lambda l-\nu-1} \sum_{s=0}^{\left[\frac{w}{u}\right]} \frac{(-w)_{us}}{s!} A_{w,s}(\sigma x)^s \sum_{l=0}^{\infty} \frac{(\alpha_1)_l \ldots (\alpha_{p'})_l}{(\beta_1)_l \ldots (\beta_{q'})_l} \frac{1}{\Gamma(\Im l+\varepsilon)}$$

$$\times \frac{\Gamma(\varepsilon+\lambda l+s)\Gamma(\varepsilon+\lambda l-\nu+\eta+s)}{\Gamma(\varepsilon+\lambda l+\mu+\eta+s)\Gamma(\varepsilon+\lambda l-\nu+s)}$$

$$\times F_{p,q}\left[\begin{array}{c} a,b \\ c \end{array};ex\right] *_3 F_2\left[\begin{array}{c} 1,\varepsilon+\lambda l+s,\varepsilon+\lambda l-\nu+\eta+s \\ \varepsilon+\lambda l-\nu+s,\varepsilon+\lambda l+\mu+\eta+s \end{array};ex\right] \tag{4.3}$$

Corollary 2 Let $\mu,\nu,\eta,\rho \in \mathbb{C}$ be such that $\min(\Re(p),\Re(q)) > 0, \Re(\mu) > 0$ and $\Re(\rho) < 1+\min[\Re(\eta),\Re(\nu)]$ as

$$\left(I_{0,-}^{\mu,\nu,\eta} \left[\xi^{\varepsilon-1} S_W^u(\sigma\xi) F_{p,q}\left[\begin{matrix} a,b \\ c \end{matrix} ; \frac{e}{\xi} \right] M_{p',q'}^{\Im,\varepsilon}(\xi^\lambda \right] \right)(x)$$

$$= x^{\varepsilon+\lambda l-\nu-1} \sum_{s=0}^{\left[\frac{w}{u}\right]} \frac{(-w)_{us}}{s!} A_{w,s}(\sigma x)^s \sum_{l=0}^{\infty} \frac{(\alpha_1)_l \ldots (\alpha_{p'})_l}{(\beta_1)_l \ldots (\beta_{q'})_l} \frac{1}{\Gamma(\Im l+\varepsilon)}$$

$$\times \frac{\Gamma(1-\varepsilon-\lambda l+n+\nu-s)\Gamma(1-\varepsilon-\lambda l+\eta-s)}{\Gamma(1-\varepsilon-\lambda l-s)\Gamma(1-\varepsilon-\lambda l+\eta+\mu+\nu-s)}$$

$$\times F_{p,q}\left[\begin{matrix} a,b \\ c \end{matrix} ; \frac{e}{x} \right] *_3 F_2\left[\begin{matrix} 1, 1-\varepsilon-\lambda l+\nu-s, 1-\varepsilon-\lambda l+\eta-s \\ 1-\varepsilon-\lambda l-s, 1-\varepsilon-\lambda l+\eta+\mu+\nu-s \end{matrix} ; \frac{e}{x} \right] \tag{4.4}$$

(ii) The operator $I_{0,+}^{\mu,\nu,\eta}(.)$ contains both the Riemann-Liouville $I_{0-}^{\mu}(.)$ and the Erdélyi-Kober [5] $I_{\eta,\mu}^{+}(.)$ fractional integral operators which can be defined as

$$\left(I_{0,+}^{\mu} f(\xi) \right)(x) = \left(I_{0,+}^{\mu,-\mu,\eta} f(\xi) \right)(x) = \frac{1}{\Gamma(\mu)} \int_0^x (x-\xi)^{\mu-1} f(\xi) d\xi \tag{4.5}$$

and

$$\left(I_{\eta,\mu}^{+} f(\xi) \right)(x) = \left(I_{0,+}^{\mu,0,\eta} f(\xi) \right)(x) = \frac{(x)^{-\mu-\eta}}{\Gamma(\mu)} \int_0^x (x-\xi)^{\mu-1} (\xi)^n f(\xi) d\xi \tag{4.6}$$

Corollary 3. Let $\mu,\eta,\rho \in \mathbb{C}$ be such that $min(\Re(p),\Re(q)) > 0, \Re(\mu) > 0$ and $\Re(\rho+s) > \Re(-\eta), x > 0$

By using (4.6), the result (3.1) reduced as

$$\left(I_{\eta,\mu}^{+} \left[\xi^{\varepsilon-1} S_w^u(\sigma\xi) F_{p,q}\left[\begin{matrix} a,b \\ c \end{matrix} ; e\xi \right] M_{p',q'}^{\Im,\varepsilon}(\xi^\lambda \right] \right)(x)$$

$$= x^{\varepsilon+\lambda l-1} \sum_{s=0}^{\left[\frac{w}{u}\right]} \frac{(-w)_{us}}{s!} A_{w,s}(\sigma x)^s \sum_{l=0}^{\infty} \frac{(\alpha_1)_l \ldots (\alpha_{p'})_l}{(\beta_1)_l \ldots (\beta_{q'})_l} \frac{1}{\Gamma(\Im l+\varepsilon)}$$

$$\times \frac{\Gamma(\varepsilon+\lambda l+\eta+s)}{\Gamma(\varepsilon+\lambda l+\mu+\eta+s)} \times F_{p,q}\left[\begin{matrix} a,b \\ c \end{matrix} ; ex \right] *_2 F_1\left[\begin{matrix} 1, \varepsilon+\lambda l+\eta+s \\ \varepsilon+\lambda l+\mu+\eta+s, \end{matrix} ; ex \right] \tag{4.7}$$

(iii) It can be observed that the operator (4.2) unifies the Erdélyi-Kober fractional operators with the Weyl type as follows:

$$\left(I_{-}^{\mu} f(\xi) \right)(x) = \left(I_{-}^{\mu,-\mu,\eta} f(\xi) \right)(x) = \frac{1}{\Gamma(\mu)} \int_x^{\infty} (\xi - x)^{\mu-1} f(\xi) d\xi \tag{4.8}$$

and

$$\left(K_{\eta,\mu}^{-} f(\xi) \right)(x) = \left(I_{-}^{\mu,0,\eta} f(\xi) \right)(x) = \frac{(x)^{-\mu-\eta}}{\Gamma(\mu)} \int_x^{\infty} (\xi - x)^{\mu-1} (\xi)^{-\mu-\eta} f(\xi) d\xi \tag{4.9}$$

Corollary 4. Let $\mu, \eta, \rho \in \mathbb{C}$ be such that $min(\Re(p), \Re(q)) > 0, \Re(\mu) > 0$ and $\Re(\rho + s) < 1 + \Re(\eta), x > 0$ By using (4.9), the result (3.3) reduced as

$$\left(K_{\eta,\mu}^{-} \left[\xi^{\varepsilon-1} S_w^u(\sigma\xi) F_{p,q} \left[\begin{matrix} a,b \\ c \end{matrix} ; e\xi \right] M_{p',q'}^{\Im,\varepsilon}(\xi^{\lambda} \right] \right)(x)$$

$$= x^{\varepsilon+\lambda l-1} \sum_{s=0}^{\left[\frac{w}{u}\right]} \frac{(-w)_{us}}{s!} A_{w,s}(\sigma x)^s \sum_{l=0}^{\infty} \frac{(\alpha_1)_l \ldots (\alpha_{p'})_l}{(\beta_1)_l \ldots (\beta_{q'})_l} \frac{1}{\Gamma(\Im l + \varepsilon)}$$

$$\times \frac{\Gamma(\varepsilon + \lambda l + \eta + s)}{\Gamma(\varepsilon + \lambda l + \mu + \eta + s)} \times F_{p,q} \left[\begin{matrix} a,b \\ c \end{matrix} ; ex \right] *_2 F_1 \left[\begin{matrix} 1, \varepsilon + \lambda l + \eta + s \\ \varepsilon + \lambda l + \mu + \eta + s, \end{matrix} ; ex \right] \tag{4.10}$$

(iv) Additionally, on replacing ν by $-\mu$ in Corollary 1 and 2 and making use of the relations (4.5) and (4.8) give the other Riemann-Liouville and Weyl fractional integrals of the extended hypergeometric function in (1.4) are provided by the following corollaries

Corollary 5. Let $\mu, \rho \in \mathbb{C}$ be such that $min(\Re(p), \Re(q)) > 0, \Re(\mu) > 0$, $x > 0$ By using (4.5), the result (3.1) reduced as

$$\left(I_{0,+}^{\mu} \left[\xi^{\varepsilon-1} S_w^u(\sigma\xi) F_{p,q} \left[\begin{matrix} a,b \\ c \end{matrix} ; e\xi \right] M_{p',q'}^{\Im,\varepsilon}(\xi^{\lambda} \right] \right)(x)$$

$$= x^{\varepsilon+\lambda l+\mu-1} \sum_{s=0}^{\left[\frac{w}{u}\right]} \frac{(-w)_{us}}{s!} A_{w,s}(\sigma x)^s \sum_{l=0}^{\infty} \frac{(\alpha_1)_l \ldots (\alpha_{p'})_l}{(\beta_1)_l \ldots (\beta_{q'})_l} \frac{1}{\Gamma(\Im l + \varepsilon)}$$

$$\times \frac{\Gamma(\varepsilon + \lambda l + \mu + \eta + s)}{\Gamma(\varepsilon + \lambda l + \mu + s)} \times F_{p,q} \left[\begin{matrix} a,b \\ c \end{matrix} ; ex \right] *_2 F_1 \left[\begin{matrix} 1, \varepsilon + \lambda l + s \\ \varepsilon + \lambda l + \mu + s, \end{matrix} ; ex \right] \tag{4.11}$$

Corollary 6. Let $\mu, \rho \in \mathbb{C}$ be such that $min(\Re(p), \Re(q)) > 0, \Re(\mu) > 0$, $x > 0$ By using (4.8), the result (3.3) reduced as

$$\left(I_{-}^{\mu} \left[\xi^{\varepsilon-1} S_w^u(\sigma\xi) F_{p,q} \left[\begin{matrix} a,b \\ c \end{matrix} ; \frac{e}{\xi} \right] M_{p',q'}^{\Im,\varepsilon}(\xi^{\lambda} \right] \right)(x)$$

$$= x^{\varepsilon+\lambda l+\mu-1}\sum_{s=0}^{\left[\frac{w}{u}\right]}\frac{(-w)_{us}}{s!}A_{w,s}(\sigma x)^s\sum_{l=0}^{\infty}\frac{(\alpha_1)_l\ldots(\alpha_{p'})_l}{(\beta_1)_l\ldots(\beta_{q'})_l}\frac{1}{\Gamma(\Im l+\varepsilon)}$$

$$\times\frac{\Gamma(1-\varepsilon-\lambda l-\mu-s)\Gamma(1-\varepsilon-\lambda l+\eta-s)}{\Gamma(1-\varepsilon-\lambda l-s)\Gamma(1-\varepsilon-\lambda l-\eta-s)}$$

$$\times F_{p,q}\left[\begin{matrix}a,b\\c\end{matrix};\frac{e}{\xi}\right]*_3F_2\left[\begin{matrix}1,1-\varepsilon-\lambda l-\mu-s,1-\varepsilon-\lambda l+\eta-s\\1-\varepsilon-\lambda l-s,1-\varepsilon-\lambda l-\eta-s\end{matrix};\frac{e}{\xi}\right] \tag{4.12}$$

(v) If we emphasise in our conclusion that the general class of polynomials yields numerous well-known classical orthogonal polynomials as its particular cases when appropriate unique values are provided for the coefficient $A_{w,s}$.More specifically, if we set $w=0$, $A_{0,0}=1$ then $S_w^u=1$ in (3.1) and (3.3), we gain the fresh findings claimed in corollaries 7 and 8 as

Corollary 7. Let $\mu,\mu',\nu,\nu',\delta,\rho\in\mathbb{C}$ be such that $min(\Re(p),\Re(q))>0,\Re(\delta)>0$ and $\Re(\rho+s)>max[0,\Re(\mu+\mu'+\nu-\delta),\Re(\mu'-\nu')],x>0$
then the result (3.1) reduced as

$$\left(I_{0,+}^{\mu,\mu',\nu,\nu',\tau}\left[\xi^{\varepsilon-1}F_{p,q}\left[\begin{matrix}a,b\\c\end{matrix};e\xi\right]M_{p',q'}^{\Im,\varepsilon}(\xi^{\lambda})\right]\right)(x)$$

$$= x^{\varepsilon+\lambda l-\mu-\mu'+\tau-1}\sum_{l=0}^{\infty}\frac{(\alpha_1)_l\ldots(\alpha_{p'})_l}{(\beta_1)_l\ldots(\beta_{q'})_l}\frac{(\varepsilon')_{l\tau,k}}{\Gamma_k(\sigma l+\eta)}\frac{1}{l!}$$

$$\times\frac{\Gamma(\varepsilon+\lambda l)\Gamma(\varepsilon+\lambda l+\tau-\mu-\mu'-\nu)\Gamma(\varepsilon+\lambda l+\nu'-\mu')}{\Gamma(\varepsilon+\lambda l+\tau-\mu-\mu')\Gamma(\varepsilon+\lambda l+\tau-\mu'-\nu)\Gamma(\varepsilon+\lambda l+\nu')}$$

$$\times F_{p,q}\left[\begin{matrix}a,b\\c\end{matrix};ex\right]*_4F_3\left[\begin{matrix}1,\theta_7,\theta_8,\theta_9\\\theta_{10},\theta_{11},\theta_{12}\end{matrix};ex\right] \tag{4.13}$$

where
$\theta_7=\varepsilon+\lambda l,\theta_8=\varepsilon+\lambda l+\tau-\mu-\mu'-\nu,$
$\theta_9=\varepsilon+\lambda l+\nu'-\mu',\theta_{10}=\varepsilon+\lambda l+\tau-\mu-\mu',$
$\theta_{11}=\varepsilon+\lambda l+\tau-\mu'-\nu,\theta_{12}=\varepsilon+\lambda l+\nu'$

Corollary 8. Let $\mu,\mu',\nu,\nu',\delta,\rho\in\mathbb{C}$ be such that $min(\Re(p),\Re(q))>0,\Re(\delta)>0$ and $\Re(\rho)<1+min[\Re(-\nu),\Re(\mu+\mu'-\delta),\Re(\mu-\nu'-\delta)],x>0$ then the result (3.3) reduced as

$$\left(I_{-}^{\mu,\mu',\nu,\nu',\tau}\left[\xi^{\varepsilon-1}F_{p,q}\left[\begin{matrix}a,b\\c\end{matrix};\frac{e}{\xi}\right]M_{p',q'}^{\gamma,\zeta}(\xi^{\lambda})\right]\right)(x)$$

$$= x^{\varepsilon+\lambda l-\mu-\mu'+\tau-1}\sum_{l=0}^{\infty}\frac{(\alpha_1)_l\ldots(\alpha_{p'})_l}{(\beta_1)_l\ldots(\beta_{q'})_l}\frac{(\varepsilon')_{l\tau,k}}{\Gamma_k(\sigma l+\eta)}\frac{1}{l!}$$

$$\times \frac{\Gamma(1+\mu+\mu'-\tau-\varepsilon-\lambda l)\Gamma(1+\mu+\nu'-\tau-\varepsilon-\lambda l)\Gamma(1-\nu-\varepsilon-\lambda l)}{\Gamma(1-\varepsilon-\lambda l)\Gamma(1+\mu+\mu'+\nu'-\tau-\varepsilon-\lambda l)\Gamma(1+\mu-\nu-\varepsilon-\lambda l)}$$

$$\times F_{p,q}\left[\begin{matrix} a,b \\ c \end{matrix};\frac{e}{x}\right] *_4 F_3\left[\begin{matrix} 1,\theta_{13},\theta_{14},\theta_{15} \\ \theta_{16},\theta_{17},\theta_{18} \end{matrix};\frac{e}{x}\right] \tag{4.14}$$

where
$\theta_{13} = 1+\mu+\mu'-\tau-\varepsilon-\lambda l, \theta_{14} = 1+\mu+\nu'-\tau-\varepsilon-\lambda l,$
$\theta_{15} = 1-\nu-\varepsilon-\lambda l, \theta_{16} = 1-\varepsilon-\lambda l,$
$\theta_{17} = 1+\mu+\mu'+\nu'-\tau-\varepsilon-\lambda l, \theta_{18} = 1+\mu-\nu-\varepsilon-\lambda l$

(vi) Also, it is interesting to note that if we set $w = 0$, $A_{0,0} = 1$ and $S_W^u = 1$, the results obtained in Corollaries 1 to 6, yield corresponding results given due to Parmar and Purohit [14]. If we set $u = 2$ and $A_w, s = (-1)^s$, then the general class of polynomials become

$$S_w^u[x] \to x^{u/2} H_w\left(\frac{1}{2\sqrt{x}}\right)$$

$H_w(x)$ denotes the well known Hermite polynomials and are defined by

$$H_w(x) = \sum_{s=0}^{[u/2]} (-1)^s \frac{w}{(w-2s)!s!} (2x)^{w-2s}$$

Conclusion

Our findings are significant because of their broad applicability. Given the universality of Srivastava's polynomial and hypergeometric function, we can obtain multiple results comprising a fairly large variety of useful functions and their various special instances by specialising the various parameters. As a result, the main result described in this article would yield a very large number of results containing a wide range of simpler special functions happening in scientific and technological disciplines all at once. This study involves the establishment of two formulas involving specific special functions through the use of generalised fractional integral operators. Several novel and well-known results are produced as a result of their further ramifications, and it is projected that these results will have an impact on numerous applied science fields.

Conflict of Interests

None

References

[1] R. G. Buschman, H. M. Srivastava, The H function associated with a certain class of Feynman integrals, J. Phys. A Math. Gen. 23, 4707–4710 (1990).

[2] M. A. Chaudhry, A. Qadir, M. Rafique, and S. M. Zubair, Extension of Euler's Beta function, J. Comput. Appl. Math., 78, pp. 19-32, (1997).

[3] M. A. Chaudhry, A. Qadir, H. M. Srivastava, and R. B. Paris, Extended hypergeometric and confluent hypergeometric functions, Appl. Math. Comput., 159, pp. 589-602, (2004).

[4] J. Choi, A. K. Rathie, and R. K. Parmar, Extension of extended beta, hypergeometric and confluent hypergeometric functions, Honam Math. J., 36(2), pp. 339-367, (2014).

[5] A. Erde lyi, W. Magnus, F. Oberhettinger, and F. G Tricomi, Higher Transcendental Functions, Vol.1, McGraw-Hill, New York, (1953).

[6] A. A. Inayat-Hussain, New properties of hypergeometric series derivable from Feynman integrals, I transformation and reduction formulae. J. Phys. A. Math. Gen. 20, 4109–4117 (1987).

[7] A. A. Inayat-Hussain, New properties of hypergeometric series derivable from Feynman integrals, II a generalization of H-function. J. Phys. A. Math. Gen. 20, 4119–4128 (1987).

[8] A. A. Kilbas, H. M. Srivastava, and J. J. Trujillo, Theory and Applications of Fractional Differential Equations, North-Holland Mathematical Studies, 204, Elsevier (North-Holland) Science Publishers, Amsterdam, London and New York, (2006).

[9] D. M. Lee, A. K. Rathie, R. K. Parmar, and Y. S. Kim, Generalization of extended Beta function, hypergeometric and confluent hypergeometric functions, Honam Math. J., 33, pp. 187-206, (2011).

[10] A. M. Mathai and R. K. Saxena, Generalized Hypergeometric Functions with Applications in Statistics and Physical Sciences, Lecture Notes Series No. 348, Springer-Verlag, Berlin, New York. Heidelberg, Germany, (1973).

[11] A. M. Mathai, R. K. Saxena, and H. J. Haubold, The H-Functions, Theory and Applications, Springer, New York, (2010).

[12] R. K. Parmar, A new generalization of Gamma, Beta, hypergeometric and confluent hypergeometric functions, Matematiche (Catania), 69, pp. 33-52, (2013).

[13] R. K. Parmar, Some generating relations for generalized extended hypergeometric functions involving generalized fractional derivative operator, J. Concr. Appl. Math., 12, pp. 217-228, (2014).

[14] R. K. Parmar and S. D. Purohit, Certain integral transforms and fractional integral formulas for the extended hypergeometric functions, TWMS J. Appl. Engg. Math., 7(1), In press, (2017).

[15] T. Pohlen, The Hadamard Product and Universal Power Series, Dissertation, Universita t Trier, (2009).

[16] A. P. Prudnikov, Yu. A. Brychkov, and O. I. Marichev, Integrals and Series. Special Functions, Gordon and Breach, New York, Vol. 1-5, (1992).

[17] M. Saigo, A remark on integral operators involving the Gauss hypergeometric functions, Math. Rep. Kyushu Univ., 11, pp. 135-143, (1978).

[18] M. Saigo, and N. Maeda, More generalization of fractional calculus, Transform Methods and Special Function, Verna Bulgaria, pp. 386-400, (1996).

[19] K. P. Sharma, and A. Bhargava, A Note on Properties of Mittag-Leffler Function under Generalized Fractional Operators in International Journal of Mechanical engineering Vol. 7, No. 5 May, (2022).

[20] M. Sharma, and R. Jain, A Note on a Generalized M-Series as a Special Function of Fractional Calculus, Fractional Calculus and Applied Analysis, (2009).

[21] H. M. Srivastava, A contour integral involving Fox's H-function, Indian J. Math., 14, pp. 1-6, (1972).

[22] H. M. Srivastava, and P. W. Karlsson, Multiple Gaussian Hypergeometric Series, Halsted Press, (Ellis Horwood Limited, Chichester), John Wiley and Sons, New York, Chichester, Brisbane and Toronto, (1985).

[23] H. M. Srivastava, R. K. Parmar, and P. Chopra, A class of extended fractional derivative operators and associated generating relations involving hypergeometric functions, Axioms, 1, pp. 238- 258, (2012).

[24] H. M. Srivastava, and R. K. Saxena, Operators of fractional integration and their applications, Appl. Math. Comput., 118, pp. 1-52, (2001).

[25] D. L. Suthar and S. Aggarwal, Fractional integral formulas involving generalized hypergeometric functions and general class of multivariable polynomial, Int. Bull. Math. Res., 3(2), pp. 28-34, (2016).

[26] V. B. L. Chaurasia and V. Gill, New fractional calculus involving Srivastava's general class of multivariable polynomials and The H -function, 11(1),19-32,(2015).

[27] R. Sharna, J. Singh, D. Kumar, Y. Singh, Certain Unified Integrals Associated with Product of the General Class of Polynomials and Incomplete I-Functions, International Journal of Applied and Computational Mathematics, https://doi.org/10.1007/s40819-021-01181-5, 8, 7 (2022).

[28] S. Tyagi, M. Jain, J. Singh, Large Deflection of a Circular Plate with Incomplete Aleph Functions under Non-Uniform Load, International Journal of Applied and Computational Mathematics, 8, 267 (2022).

[29] V. B. L. Chaurasia and V. Gill, Integral Formulae for Certain Product of Special Function Generalized Fractional Calculus, Global Journal of Science Frontier Research, 13-20, 11(6), (2011).

[30] V. B. L. Chaurasia and V. K. Singhal, On Fractional Integration of Certain Products of Special Functions, International Journal of Modern Mathematical Sciences, Florida, USA, 137-151, 13(2) (2015).

Under Quasi Nonexpansive Mapping Generalization of Weak Convergence and Study of Fixed Point in Hilbert Space

Mohd Jamshed Ali[1], Richa Sharma[2], Virendra Singh Chouhan[3]

December 26, 2023

Abstract

This manuscript proposes a generalization of weak convergence and study of fixed point in a real Hilbert space for quasi-nonexpanding maps. In this work, we introduce a class of fixed points theorems for nonexpansive mapping and generalized form of nonexpansive mapping under the Hilbert space. In addition, we obtained under quasi nonexpansive mapping weak convergence with respect to Hilbert space by Mann's Type.

Key Words and Phrases: Hilbert space, quasi-nonexpansive mappings, weak convergence.
2010 AMS Subject Classification: 47H10, 47H09.

1

1 Introduction

A significant area of research in pure as well as applied mathematics is fixed point theory. The Fixed-Point Theory has many applications in various fields namely Approximation Theory, Integral Equations, Game Theory, Optimization, Economics, and several others [1]. How to solve nonlinear equations like $Tx = 0$ is one of the fundamental issues in mathematics. We can utilise iterative techniques like Newton methods and its variations to solve these problems. We must therefore employ approximation techniques because the zeros of a nonlinear equation cannot be stated in closed forms. Nowadays, we frequently employ iterative techniques to obtain a system's approximate solution. The

[1,3]Department of Mathematics and Statistics, Manipal University Jaipur, India
[1]Email- mohdjamshed007@gmail.com
Corresponding author: [3]Virendra Singh Chouhan
[2]Department of Mathematics, Chandigarh University, Mohali (Punjab)
Email-richa.tuknait@gmail.com
[3]Email-darbarvsingh@yahoo.com(Corresponding Author)

general Newton's method is frequently used approach. Recent advancements in the solution system have made it possible for us to reach iterative formulae by employing Taylor's polynomial, quadrature formulas, and other methods. One of the powerful and versatile solution technique for solving nonlinear equations is Fixed point iterative method [2]. Recently many fixed-point results have been discussed in different type of non-expansive mappings [3, 4].
Let H be any Hilbert space having convex closed subset of K which is non empty. Now define a continuous mapping S from convex subset K to convex subset K. A point $a \in K$ known as a fixed point of continuous mapping S if $S(a) = a$. Additionally, the $F(S)$ denotes the collection of all fixed points for S. A fixed point's existence theorems of single-valued nonexpansive mappings has been studied by a few authors [5]. A mapping $T : B \to B$ defined on space B if is known as nonexpansive mapping $\|T\mu - T\zeta\| \leq \|\mu - \zeta\|, \forall \mu, \zeta$ in space B. A general map $T : B \to B$ defined on space B is called quasi-nonexpansive mapping provided it has fixed point in space B and if $\vartheta \in B$ is fixed point of T, then $\|T\mu - \vartheta\| \leq \|\mu - \vartheta\|, \forall \mu \in B$. Thus every nonexpansive mapping becomes quasi-nonexpansive if it has a minimum one fixed point. A mapping $T : B \to B$ described as being generalised nonexpansive if $\forall \mu, \vartheta \in B$ and $m, n, o \geq 0$, the mapping T satisfy
$\|T\mu - T\vartheta\| \leq m\|\mu - \vartheta\| + n\{\|\mu - T\mu\| + \|\vartheta - T\vartheta\|\} + o\{\|\mu - T\vartheta\| + \|\vartheta - T\mu\|\}$
with $m + 2n + 2o \leq 1$ [6].
Let B be convex subset of X. For $\mu_j \in B$, define a sequence $\{\mu\}_{n=1}^{\infty}$ such that $\mu_{n+1} = (1 - \beta_n)\mu_n + \beta_n T\mu_n$, where $\{\beta_n\}_{n=1}^{\infty}$ is a sequence of positive number $\beta_n \in [a, b]$ for all $n \in \mathbb{N}$ and $0 < a < b < 1$. A mapping $T : B \to B$ is demiclosed with respect to $\omega \in X$ if for each sequence $\{\mu_n\} \subset B$ and each $\mu \in X$ it follows from $\mu_n \rightharpoonup \mu$ and $\lim T(\mu_n) = \omega$ that $\mu \in B$ and $T(\mu) = \omega$. The set of fixed point of T is denoted by the abbreviation $F(T)$ [7].

2 Preliminaries

Firstly we introduce some lemmas and definitions.
Definition 2.1 [7] Any Banach space X is called a Hilbert space if there exit a scalar product defined on space X such that the norm defined in space X is same as the norm defined by the relation $\tau = <\tau, \tau>^{1/2}$.
• Let l^2 be the set contains the elements of the form $\tau = (\tau_1, \tau_2, ...)$ such that

$$\|\tau\| = \sum_{i=1}^{\infty} |\tau_i^2|^{1/2} < \infty.$$

• The inner product space $(R^n, <.,.>)$ equipped with the induced norm given by

$$\|\tau\| = <\tau, \tau>^{1/2} = \left(\sum_{i=1}^{\infty} |\eta_i|^2\right)^{1/2} \text{ such that } (\eta_1, \eta_2, ...\eta_n) \in R^n$$

Definition 2.2 [6] Let H be any Hilbert space, mapping T defined on Hilbert space H is nonexpansive if

$$d(T\zeta, T\vartheta) \leq d(\zeta, \vartheta), \forall \zeta, \vartheta \in H$$

Definition 2.3 [6] Let H be any Hilbert space then the mapping T on Hilbert space H is quasi nonexpansive if

$$d(T\mu, \vartheta) \leq d(\mu, \vartheta), \forall \mu \in H, \forall \vartheta \in F(T)$$

such that mapping T has at least one fixed point.

Definition 2.4 [7] The Opial's condition is crucial for understanding the demi-closed Ness the nonlinear mappings principle as well as the geometry of spaces and sequence convergence. Any If Space X meets the requirement of the Opial, a sequence ζ_n defined on space X converges weakly to any $\zeta_0 \in X$ then

$$\lim_{n\to\infty} inf\|\zeta_n - \zeta_0\| < \lim_{n\to\infty} inf\|\zeta_n - \zeta\|, \forall \zeta \in X \; and \; \zeta \neq \zeta_0$$

Here if we replace the strict inequality $<$ by the inequality $\leq$ then, we obtain weak Opial's condition.

Definition 2.5 [5] Let $E \subseteq H$ where H is a Hilbert space and $T : E \to H$ is a map defined from E to Hilbert space H. Then the mapping T is demiclosed at any $s \in H$ if for any corresponding sequence $\zeta_n \in E$ the mapping T follow the condition as:

$$\zeta_n \to \beta \in E \; and \; T\zeta_n \to \vartheta \Rightarrow T\beta = \vartheta$$

An Opial's Condition defined on reflexive Banach space X such that E is a not empty space X closed convex subset containing a nonexpansive mapping $T : E \to X$ then $I - T$ is demi closed.

Lemma 2.6 [8] Assume a Hilbert space H such that $E \in H$ then $S : E \to CB(E)$ is called mapping of Condition (A) if

$$\|\mu - \vartheta\| = d(\mu, S\vartheta), \; for \; all \; \mu \in H \; and \; \vartheta \in F(s).$$

Lemma 2.7 [9] Let H be a real Hilbert space and $K \in H$ such that a quasi nonexpansive map from $S : H \to CB(H)$ with $F(S)$ *nonempty*. Then, $F(S)$ is said to be closed and if S fullfill above Condition (A), then $F(S)$ is said to be convex. The mapping S is said to hybrid if

$$3H(S\mu, S\omega)^2 \leq \|\mu - \omega\|^2 + d(\omega, S\mu)^2 + d(\mu, S\omega)^2, \forall \mu, \omega \in K$$

Lemma 2.8 [5] Let H be a Hilbert space such that $E \in H$ and $S : E \to E(E)$ is hybrid mapping. Assume ϑ_n be a sequence in mapping E such that $\vartheta_n \to \vartheta$ and $\lim_{n\to\infty} \|\vartheta_n - y_n\| = 0$ for sequence $y_n \in S\vartheta_n$. Then, $\vartheta \in S\vartheta$.

3 Quasi Nonexpansive Mapping with Respect to Hilbert Space

Lemma 3.1 Let X be a normed space with a convex subset C and mapping $T : C \to C$ defined on space C be a quasi-nonexpansive mapping. Suppose that $\{\zeta_n\}_{n=1}^{\infty}$ is a sequence such that $\zeta_1 \in C$. Then, the limit $\lim_{n\to\infty} \|\zeta_n - \zeta\|$ exists for each $\zeta \in F(T)$.

Proof: We have given that the mapping T is a quasi-nonexpansive mapping. Hence, we have

$$\begin{aligned} \|\zeta_{n+1} - \zeta\| &= \|(\alpha_n T\zeta_n + (1-\alpha_n)\zeta_n) - \zeta\| \\ &\leq \alpha_n \|T\zeta_n - \zeta\| + (1-\alpha_n)\|\zeta_n - \zeta\| = \|\zeta_n - \zeta\|, \end{aligned}$$

For each $\zeta \in F(T)$. Hence, the sequence $\{\|\zeta_n - \zeta\|\}_{n=1}^{\infty}$ is a bounded below and nonincreasing sequence, so from this we conclude that the limit $\lim_{n\to\infty} \|\zeta_n - \zeta\|$ exists for each $\zeta \in F(T)$.

Lemma 3.2 Let us consider a uniformly convex Hilbert space X, $0 < b < d < 1$, $\beta \geq 0$, $t_n \in [\, b, d]$ and $\{\zeta_n\}_{n=1}^{\infty}$ and $\{\vartheta_n\}_{n=1}^{\infty}$ are sequences defined on Hilbert space X such that

$$\limsup \|\zeta_n\| \leq \beta,\ \limsup \|\vartheta_n\| \leq \beta,\ and\ \lim_{n\to\infty} \|t_n\zeta_n + (1-t_n)\vartheta_n\| = \beta$$

then the $\lim_{n\to\infty} \|\zeta_n - \vartheta_n\| = 0$.

Lemma 3.3 Let us consider uniformly convex Hilbert space X with a convex subset C of X and $T : C \to C$ be a quasi-nonexpansive mapping. Assume that $\mu_1 \in C$ and $\{\mu_n\}_{n=1}^{\infty}$ is a sequence then the limit $\lim_{n\to\infty} \|\mu_n - T\mu_n\| = 0$.

Proof: Let μ be fixed point of quasi-nonexpansive mapping T. Now, we know that limit $d = \lim_{n\to\infty} \|\mu_n - \mu\| = 0$. is well-defined by Lemma 3.1 and $\lim_{n\to\infty} Sup\|T\mu_n - \mu\| \leq d$ Since, $\|T\mu_n - \mu\| \leq \|\mu_n - \mu\|$ for all natural numbers. Additionally, we know that

$$\lim_{n\to\infty} \|\alpha_n(T\mu_n - \mu) + (1-\alpha_n)(\mu_n - \mu)\| = \lim_{n\to\infty} \|\mu_{n+1} - \mu\| = d$$

So, from lemma 3.2 we conclude that $\lim_{n\to\infty} \|T\mu_n - \mu_n\| = 0$.

Theorem 3.4 Let us consider a uniformly convex Hilbert space X satisfying Opial's condition and C be a closed subset of Hilbert space X, and mapping $T : C \to C$ be a quasi-non-expansive mapping with $I - T$ demiclosed with respect to zero. Suppose that $\zeta_1 \in C$ Then the sequence $\{\zeta_n\}_{n=1}^{\infty}$ converges weakly to some fixed point of quasi-non-expansive mapping T.

Proof: Let us consider two weakly convergent subsequences $\{\zeta_{\emptyset_n}\}$ and $\{\zeta_{\psi_n}\}$ of sequence $\{\zeta_n\}$ which are weakly convergent to some points ζ and ϑ in C, respectively. Since $\lim_{n\to\infty} \|\zeta_n - T\zeta_n\| = 0$ by Lemma 3.3 and $I - T$ is demiclosed with respect to zero such that $T\zeta = \zeta$ and $T\vartheta = \vartheta$

Now, put $a = \lim_{n\to\infty} \|\zeta_n - \vartheta\|$ by lemma 3.1. Assume that $\zeta \neq \vartheta$ and consider the fact that $\zeta_{\emptyset_n} \rightharpoonup \zeta$ and $\zeta_{\psi_n} \rightharpoonup \vartheta$ then from the Opial's condition we get

$$a = \liminf \|\zeta_{\emptyset_n} - \zeta\| < \liminf \|\zeta_{\emptyset_n} - \vartheta\| = b,$$
$$b = \liminf \|\zeta_{\psi_n} - \vartheta\| < \liminf \|\zeta_{\psi_n} - \zeta\| = a,$$

Which is a contradiction. Hence $\zeta = \vartheta$.
This shows that the above sequence $\{\zeta_n\}_{n=1}^{\infty}$ has exactly one weak cluster point, from which we conclude that the sequence $\{\zeta_n\}_{n=1}^{\infty}$ converges weakly to some $\tau \in C$. On Repeating the above concept we conclude that $T\tau = \tau$. Hence, the sequence $\{\zeta_n\}_{n=1}^{\infty}$ converges weakly to some fixed point of T.

4 Generalized Quasi-Nonexpansive Mapping under Hilbert Space

A map $T : H \to H$ defined on Hilbert space H is said to be generalized quasi nonexpansive mapping if $\forall \mu, \vartheta \in C$ and $m, n, o \geq 0$, mapping T satisfies

$$\|T\mu - T\vartheta\| \leq m\|\mu - \vartheta\| + n\{\|\mu - T\mu\| + \|\vartheta - T\vartheta\|\} + o\{\|\mu - T\vartheta\| + \|\vartheta - T\mu\|\}$$

with $m + 2n + 2o \leq 1$.
Theorem 4.1 Let H be a uniformly convex Hilbert space with a bounded convex subset C of H. Mapping T be a generalized quasi nonexpansive mapping. Then, for any small $\epsilon \geq 0$ there exists a small $\delta(\epsilon) > 0$ will be such that for each pair of points ζ_0, ζ_1 in C with $\|T\zeta_n - \zeta_1\| \leq \delta(\epsilon)$, and for any point ζ lies on the line segment joining point ζ_0 to point ζ_1 with $\|T\zeta - \zeta\| \leq \epsilon$.
Proof: We have given that the point ζ lies on the line segment joining point ζ_1 to point ζ_2. Therefore,

$$\zeta = (1 - \lambda)\zeta_1 + \lambda\zeta_2,\ 0 \leq \lambda \leq 1.$$

Now, define $f = b + c$. Suppose $\|\zeta_1 - \zeta_2\| \leq \epsilon(1 - f)/4$. Then, for each ζ lies on the line segment joining the points ζ_0 to ζ_1,

$$\|\zeta - \zeta_1\| \leq \epsilon(1 - f)/4$$
$$\|T\zeta - \zeta\| \leq \|T\zeta - T\zeta_1\| + \|T\zeta_1 - \zeta_1\| + \|\zeta_1 - \zeta\|$$

therefore, we get

$$\begin{aligned}(1 - c)\|T\zeta - T\zeta_1\| &\leq \alpha\|\zeta - \zeta_1\| + b\{\|\zeta - T\zeta\| + \|\zeta_1 - T\zeta_1\|\} \\ &\quad + c\{\|\zeta - T\zeta_1\| + \|\zeta_1 - T\zeta\|\} - c\|T\zeta - T\zeta_1\| \\ &\leq \alpha\|\zeta - \zeta_1\| + b\{\|\zeta - T\zeta\| + \|\zeta_1 - T\zeta_1\|\} \\ &\quad + c\{\|\zeta - T\zeta_1\| + \|\zeta_1 - T\zeta_1\|\} \\ &\leq (a + c)\|\zeta - \zeta_1\| + b\|\zeta - T\zeta\| + (b + 2c)\|\zeta_1 - T\zeta_1\|\end{aligned}$$

hence,

$$\begin{aligned}\|T\zeta-\zeta\|&\leq\|T\zeta-T\zeta_1\|+\|T\zeta_1-\zeta_1\|+\|\zeta_1-\zeta\|\\&\leq\left(1+\frac{a+c}{1-c}\right)\|\zeta-\zeta_1\|+\frac{b}{1-c}\|\zeta-T\zeta\|\\&\quad+\left(1+\frac{b+2c}{1-c}\right)\|\zeta_1-T\zeta_1\|\end{aligned}$$

and

$$\|T\zeta-\zeta\|\leq\frac{1+a}{1-b-c}\|\zeta-\zeta_1\|+\frac{1+b+c}{1-b-c}\|\zeta_2-T\zeta_1\|\leq\frac{\epsilon}{2}+\frac{2}{1-f}\delta(\epsilon)\leq\epsilon$$

if $\delta(\epsilon)<(1-f)\epsilon/4$.
Therefore, we consider only that couple of points ζ_1,ζ_2 which satisfying the condition $\|\zeta_1-\zeta_2\|\geq(1-f)\epsilon/4$.
Let $d_0=diam(C)$. Then, for $\lambda<\epsilon\frac{1-f}{4d_0}$, $\|\zeta-\zeta_1\|=\lambda\|\zeta_2-\zeta_1\|<\epsilon(1-f)/4$ and by the argument, $\|T\zeta-\zeta\|<\epsilon$. Hence, we must consider only $\lambda\geq\frac{\epsilon(1-f)}{4d_0}$. If $1-\lambda<\epsilon(1-f)/4d_0$, then $\|\zeta-\zeta_2\|=(1-\lambda)\|\zeta_2-\zeta_1\|<(1-f)/4d_0$. And, applying the same argument with ζ_2 replacing ζ_1, again we get $\|T\zeta-\zeta\|<\epsilon$. Therefor we get

$$\lambda\in\left[\frac{\epsilon(1-f)}{4d_0}\right].$$

set $y=T\zeta$. Then

$$\|y-\zeta_1\|\leq\|T\zeta-T\zeta_2\|+\|T\zeta_1-\zeta_1\|$$

and

$$\begin{aligned}\|T\zeta-T\zeta_1\|\leq\alpha\|\zeta-\zeta_1\|+b[\|\zeta-\zeta_1\|+\|\zeta_1-T\zeta\|+\|\zeta_1-T\zeta_1\|]\\+c[\|\zeta-\zeta_1\|+\|\zeta_1-T\zeta_1\|+\|\zeta_1-T\zeta\|].\end{aligned}$$

thus,

$$(1-b-c)\|T\zeta-\zeta_1\|\leq(a+b+c)\|\zeta-\zeta_1\|+(1+b+c)\|\zeta_1-T\zeta_1\|,$$

and

$$\|T\zeta-\zeta_1\|\leq\|\zeta-\zeta_1\|+2(1-f)^{-1}\|\zeta_1-T\zeta_2\|\leq\lambda\|\zeta_1-\zeta_2\|+2\delta(\epsilon)/(1-f).$$

similarly,

$$\|T\zeta-\zeta_2\|\leq(1-\lambda)\|\zeta_1-\zeta_2\|+2\delta(\epsilon)/(1-f)$$

set

$$\begin{aligned}z_0&=\lambda^{-1}\|\zeta_1-\zeta_2\|^{-1}(y-\zeta_1),\\z_1&=(1-\lambda)^{-1}\|\zeta_1-\zeta_2\|^{-1}(\zeta_2-y).\end{aligned}$$

then

$$\|z_0\| \leq 1 + \frac{64 d_0 \delta(\epsilon)}{\epsilon^2 (1-f)^3}.$$

similarly

$$\|z_1\| \leq 1 + \frac{64 d_0 \delta(\epsilon)}{\epsilon^2 (1-f)^3}.$$

but we know that

$$\|\lambda z_0 + (1-\lambda) z_1\| = 1.$$

and H is a Uniformly convex Hilbert space. Hence, if we choose positive $\delta(\epsilon)$ as small as possible then, we have $\|z_0 - z_1\| < \epsilon/d_0$. Thus,

$$\|y - \zeta\| = \|((1-\lambda)(y-\zeta_1) - \lambda(\zeta - y) = \lambda(1-\lambda)\|\zeta_1 - \zeta_2\| \|z_0 - z_1\| < \epsilon)\|.$$

Hence, for any small $\epsilon > 0$ there exists a small $\delta(\epsilon) > 0$ such that for each pair of points ζ_0, ζ_1 in C with $\|T\zeta_n - \zeta_1\| \leq \delta(\epsilon)$, and for any point ζ lies on the line segment joining point ζ_1 to point ζ_2 with $\|T\zeta - \zeta\| \leq \epsilon$.

5 Weak Convergence of Quasi-Nonexpansive Mapping with Respect to Hilbert Space by Mann's Type

In 1953, Mann[11] created the standard Mann's iteration technique. Since Mann's iterative approach for creating fixed points for nonexpansive mapping has been thoroughly studied by other authors. The typical Mann's iterative procedure produces the sequence $\{\vartheta_n\}$ as follows:

$$\vartheta_1 = \vartheta \in K$$

$$\vartheta_{n+1} = (1 - \zeta_n)\vartheta_n + \zeta_n T\vartheta_n, \ \forall \ n \geq 1$$

Where $< \zeta_n >$ is a sequence lies in 0 to 1. Mann's Type weak convergence theorem for quasi-nonexpansive mapping.
For quasi-nonexpansive mapping in Hilbert space, we provide a weak convergence theorem of mann's kind [11] in this section. Before demonstrating this, we address several common findings, such as:
Lemma 5.1 Let T be quasi-nonexpansive map defined from closed convex subset C of Hilbert space H to C. Then, $I - T$ is demiclosed.
Proof: We have given that $T : C \to C$ be a quasi nonexpansive mapping defined on Hilbert space H. Then, for any real $\gamma, \delta \in R$ we have

$$\gamma\|T\zeta - T\vartheta\|^2 + (1-\gamma)\|\zeta - T\vartheta\|^2 \leq \delta\|T\zeta - \vartheta\|^2 + (1-\delta)\|\zeta - \vartheta\|^2 \qquad (5.1)$$

for all $\zeta, \vartheta \in C$.
Now, suppose $\zeta_n \rightharpoonup r$ and $\vartheta_n \rightharpoonup T\zeta_n \to 0$. Let us consider

$$\gamma\|T\zeta_n - Tr\|^2+(1-\gamma)\|\zeta_n - Tr\|^2\leq \delta\|T\zeta_n - r\|^2+(1-\delta)\|\zeta_n - r\|^2 \qquad (5.2)$$

from these inequalities, we have

$$\gamma\|T\zeta_n - \zeta_n + \zeta_n - Tr\|^2+(1-\gamma)\|\zeta_n - Tr\|^2\leq \delta\|T\zeta_n - \zeta_n + \zeta_n - r\|^2+(1-\delta)\|\zeta_n - r\|^2$$

and hence

$$\begin{aligned}&\gamma(\|T\zeta_n - \zeta_n\|^2+\|\zeta_n - Tr\|^2+2\langle T\zeta_n - \zeta_n,\ \zeta_n - Tr\rangle) + (1-\gamma)\|\zeta_n - Tr\|^2\\ &\leq \delta(\|T\zeta_n - \zeta_n\|^2+\|\zeta_n - r\|^2+2\langle T\zeta_n - \zeta_n,\ \zeta_n - Tr\rangle) + (1-\delta)\|\zeta_n - r\|^2\end{aligned}$$

now, we apply a Hilbert limit μ on both the sides of the above inequality, then we have

$$\begin{aligned}&\gamma\mu_n(\|T\zeta_n - \zeta_n\|^2+\|\zeta_n - Tr\|^2+2\langle T\zeta_n - \zeta_n,\ \zeta_n - Tr\rangle) + (1-\gamma)\mu_n\|\zeta_n - Tr\|^2\\ &\leq \delta\mu_n(\|T\zeta_n - \zeta_n\|^2+\|\zeta_n - r\|^2+2\langle T\zeta_n - \zeta_n,\ \zeta_n - Tr\rangle) + (1-\delta)\mu_n\|\zeta_n - r\|^2\end{aligned}$$

and hence

$$\gamma\mu_n\|\zeta_n - Tr\|^2+(1-\gamma)\mu_n\|\zeta_n - Tr\|^2\leq \delta\mu_n\|\zeta_n - r\|^2+(1-\delta)\mu_n\|\zeta_n - r\|^2$$

so, we have

$$\mu_n\|\zeta_n - Tr\|^2\leq \mu_n\|\zeta_n - r\|^2$$

since,

$$\mu_n\|\zeta_n - r\|^2+\mu_n\|\zeta_n - r + r - Tr\|^2\leq \mu_n\|\zeta_n - r\|^2$$

therefore, finally we get

$$\mu_n\|\zeta_n - r\|^2+\mu_n\|r - Tr\|^2+2\mu_n\langle\zeta_n - r,\ r - Tr\rangle \leq \mu_n\|\zeta_n - r\|^2$$

so, we from all these we get $\mu_n\|r - Tr\|^2\leq 0$ and $\|r - Tr\|^2\leq 0$. Which implies, $Tr = r$. Therefore, $I - T$ is demiclosed.

Theorem 5.2 Let T be quasi-nonexpansive map defined from closed convex subset C of Hilbert space H to C with at least one fixed point i.e. $F(T) = \{\rho \in C : T\rho = \rho\}$ and $F(T) \neq \emptyset$. Let G be a metric protection of Hilbert space H onto $F(T)$ and $\{x_n\}$ be a real number sequence lies between 0 and 1 such that $\lim\limits_{n\to\infty} \inf x_n(1 - x_n) > 0$. Let $\langle x_n\rangle$ generates a sequence $\langle\rho_n\rangle$ such that

$$\rho_{n+1} = x_n\rho_n + (1 - x_n)T\rho_n,\ n = 1,\ 2,\ 3\ldots..,\ \rho_1 = \rho \in C$$

then the sequence $\langle\rho_n\rangle$ converges weakly to a member ϑ of $F(T)$ such that $\vartheta = \lim\limits_{n\to\infty} G\rho_n$.

Proof: : Let $\zeta \in F(T)$ and T be a quasi-nonexpansive mapping defined on Hilbert space H. Then, we have

$$\|\rho_{n+1}-\zeta\|^2= \|x\rho_n+(1-x_n)T\rho_n-\zeta\|^2\leq x_n\|\rho_n-\zeta\|^2+(1-x_n)\|T\rho_n-\zeta\|^2$$

$$\leq x_n\|\rho_n-\zeta\|^2+(1-x_n)\|\rho_n-\zeta\|^2= \|\rho_n-\zeta\|^2$$

For all natural numbers. Hence, the limit $\lim_{n\to\infty}\|\rho_n-\zeta\|^2$ exists. So, we can say that the sequence $\{\rho_n\}$ is bounded.
we also have

$$\begin{aligned}\|\rho_{n+1}-\zeta\|^2&= \|x_n\rho_n+(1-x_n)T\rho_n-\zeta\|^2\\ &= x_n\|\rho_n-\zeta\|^2+(1-x_n)\|T\rho_n-\zeta\|^2-x_n(1-x_n)\|T\rho_n-\rho_n\|^2\\ &\leq x_n\|\rho_n-\zeta\|^2+(1-x_n)\|\rho_n-\zeta\|^2-x_n(1-x_n)\|T\rho_n-\rho_n\|^2\\ &= \|\rho_n-\zeta\|^2-x_n(1-x_n)\|T\rho_n-\rho_n\|^2\end{aligned}$$

so, we have

$$x_n(1-x_n)\|T\rho_n-\rho_n\|^2\leq \|\rho_n-\zeta\|^2-\|\rho_{n+1}-\zeta\|^2$$

since the limit $\lim_{n\to\infty}\|\rho_n-\zeta\|^2$ exists and $\lim\inf_{n\to\infty} x_n(1-x_n)>0$, we have $\|T\rho_n-\rho_n\|^2\to 0$. The above defined sequence $\{\rho_n\}$ is bounded. Hence, there exists a subsequence $\{\rho_{n_i}\}$ of sequence $\{\rho_n\}$ such that $\rho_{n_i}\to v$. By lemma 5.1, we obtained a fixed point $\vartheta\in F(T)$. Similarly, let us assume that $\{\rho_{n_i}\}$ and $\{\rho_{n_j}\}$ are the two sub sequences of sequence $\{\rho_n\}$ such that $\rho_{n_i}\to\vartheta_1 and \rho_{n_j}\to\vartheta_2$. Now, for proving the given theorem we must show that $\vartheta_1=\vartheta_2$. we know $\vartheta_1,\ \vartheta_2\in F(T)$ and hence, the limits $\lim_{n\to\infty}\|\rho_n-\vartheta_1\|^2$ and $\lim_{n\to\infty}\|\rho_n-\vartheta_2\|^2$ are exist.
now, Put

$$\alpha=\lim_{n\to\infty}(\|\rho_n-\vartheta_1\|^2-\|\rho_n-\vartheta_2\|^2),\ \textit{for all positive integers.}$$

$$\|\rho_n-\vartheta_1\|^2-\|\rho_n-\vartheta_2\|^2= 2\langle\rho_n,\ \vartheta_2-\vartheta_1\rangle+\|\vartheta_1\|^2-\|\vartheta_2\|^2$$

such that $\rho_{n_i}\rightharpoonup\vartheta_1$ *and* $\rho_{n_j}\rightharpoonup\vartheta_2$ then, we get

$$\alpha=2\langle\vartheta_2,\ \vartheta_2-\vartheta_1\rangle+\|\vartheta_1\|^2-\|\vartheta_2\|^2 \tag{5.3}$$

and

$$\alpha=2\langle\vartheta_2,\ \vartheta_2-\vartheta_1\rangle+\|\vartheta_1\|^2-\|\vartheta_2\|^2 \tag{5.4}$$

Now, by combining these two equations, we obtain $0=2\langle\vartheta_2-\vartheta_1,\ \vartheta_2-\vartheta_1\rangle$ and hence $\|\vartheta_2-\vartheta_1\|^2=0$. So, we get $\vartheta_2=\vartheta_1$. This implies that the sequence $\{\rho_n\}$ converges weakly to an fixed point ϑ of $F(T)$.

Since $\|\rho_{n+1} - \zeta\|^2 \leq \|\rho_n - \zeta\|$ for all $\zeta \in F(T)$ and $n \in N$ and we already see that the sequence $\{Gx_n\}$ firmly converges to a fixed point g of $F(T)$. From the property of g we have

$$\langle x_n - Gx_n,\ Gx_n - y\rangle \geq 0$$

for all fixed points $y \in F(T)$ and $n \in N$. Since the sequence ρ_n converges to ϑ and the sequence Gx_n converges to g. So, we can say that

$$\langle \vartheta - g,\ g - y\rangle \geq 0$$

for all $y \in F(T)$. Putting $y = \vartheta$, we get $g = \vartheta$. This means $\vartheta = \lim_{n\to\infty} G\rho_n$. Therefore, the sequence $\langle \rho_n \rangle$ converges weakly to a member ϑ of $F(T)$ such that $\vartheta = \lim_{n\to\infty} G\rho_n$.

Conclusion

This article's objective is to give a common approach for talking about the fixed point of generalized quasi-nonexpansive mapping and quasi-nonexpansive mapping with respect to Hilbert space. The research piece concludes by presenting a novel approach to examining the fixed-point theorems for quasi-nonexpansive mapping and its generalized form about Hilbert space.

References

[1] T. Suzuki, *Fixed point theorems and convergence theorems for some generalized nonexpansive mappings*, Journal of mathematical analysis and applications, 340 (2008) 1088-1095.

[2] R. Shukla, R. Panicket, *Some new fixed-point theorems for nonexpansive-type mapping in geodesic spaces*, Journal of Mathematical Analysis and ApplicationsOpen Mathematics, 20 (2022) 1246-1260.

[3] J. Yeoul, J. Jeong, *Weak convergence to a fixed point of the sequence of mann type iterates*, Journal of mathematical analysis and applications, 184 (1994) 75-81.

[4] T. Ibaraki, W. Takahashi, *Fixed point theorems for nonlinear mappings of non-expansive type in Banach spaces*, J. Nonlinear Convex Anal, 10 (2009) 21-32.

[5] W. Chaolamjiak, D. Yambangwai, H. A. Hammad, *Modified hybrid projection methods with SP iterations for quasi-nonexpansive multivalued mappings in Hilbert spaces*, B. Iran. Math. Soc., 47 (2021) 1399–1422.

[6] S. Iemoto, W. Takahashi, *Approximating fixed points of nonexpansive mappings and nonspreading mappings in a Hilbert space*, Nonlinear Anal., 71 (2009) 2082-2089.

[7] S. Itoh, W. Takahashi, *The common fixed-point theory of single-valued mappings and multi-valued mappings*, Pacific J. Math., 79 (1978) 493-508.

[8] F. Kohsaka, W. Takahashi, *Existence and approximation of fixed points of firmly nonexpansive-type mappings in Banach spaces*, SIAM. J. Optim., 19 (2008) 824-835.

[9] F. Kohsaka, W. Takahashi, *Fixed point theorems for a class of nonlinear mappings related to maximal monotone operators in Banach spaces*, Arch. Math., 91 (2008), 166-177.

[10] P. Cholamjiak, W. Cholamjiak, *Fixed point theorems for hybrid multivalued mappings in Hilbert spaces*, J. Fixed Point Theory Appl., 18 (2016) 673–688.

[11] I. Yildirim, M. Ozdemir, *A new iterative process for common fixed points of finite families of ¨ non-self-asymptotically non-expansive mappings*, Nonlinear Anal. -Theor., 71 (2009) 991–999.

[12] P. Sainuan *Rate of convergence of P-iteration and S-iteration for continuous functions on closed intervals*, Thai J. Math., 13 (2015) 449–457.

[13] J. Daengsaen, A. Khemphet, *On the rate of convergence of P-iteration, SP-iteration, and D-iteration methods for continuous nondecreasing functions on closed intervals*, Abstr. Appl. Anal., 2018 (2018) 7345401.

[14] T. Ibaraki, W. Takahashi, *Weak convergence theorem for new nonexpansive mappings in Banach spaces and its applications*, Taiwanese J. Math., 11 (2007) 929-944.

On the Certain Properties and Results of Incomplete Generalized Hypergeometric Functions with Matrix Argument

Rahul Sharma[1], Jagdev Singh[2,3,*], Devendra Kumar[4] and Yudhveer Singh[5]

January 8, 2024

[1]Department of Mathematics, University of Engineering and Management Jaipur-303807, Rajasthan, India
[2]Department of Mathematics, JECRC University, Jaipur-303905, Rajasthan, India
[3]Department of Computer Science and Mathematics, Lebanese American University, Beirut, Lebanon
[4]Department of Mathematics, University of Rajasthan, Jaipur-302004, Rajasthan, India
[5]Amity Institute of Information Technology, Amity University Rajasthan, Jaipur-303002, Rajasthan, India
*Corresponding author: jagdevsinghrathore@gmail.com

Abstract

This study aims to assess the generalized matrix transform (M-transform) of various incomplete types of special functions named generalized incomplete hypergeometric functions, incomplete H-functions, incomplete $\overline{H}$-functions, incomplete I-functions, all of which possess a matrix argument. The matrix argument in this case is a real symmetric positive definite matrix of size $k \times k$ having $\frac{k(k+1)}{2}$ variables. Here, we establish the special functions with a matrix argument by extending the existing special functions with a scalar argument. Both scalar and matrix arguments are significant in statistical distribution problems, particularly in scenarios where the null hypothesis is not assumed to be true. Additionally, we derived specific cases by extending the univariate cases.

Keywords: Generalized Incomplete Hypergeometric functions, Incomplete H-functions, Incomplete $\overline{H}$-functions, Incomplete I-functions, M-transform.

1 Introduction

Special functions with a matrix argument have demonstrated their significance since 1950 when Bochner [24] resolved a Lattice point problem utilizing the

Bessel function of matrix argument. Furthermore, Herz [11] established the hypergeometric function of matrix argument in terms of the hypergeometric function by utilizing the Laplace transform, which is an extension of the univariate Laplace transform presented in (Eq. 16, P. 219, [1]). This univariate Laplace transform and its inverse formula aid in defining the hypergeometric function ${}_pF_q$ for all p and q. However, the explicit expression of the hypergeometric function ${}_pF_q$ with a matrix argument remains undefined.
In 1955, Herz [11] derived the hypergeometric function with matrix argument by using the Laplace transform and inductive method starting from ${}_0F_0(A) = e^{tr(A)}$ and defined it by:

$$
\begin{aligned}
&{}_{p+1}F_q\left(a_1,\ldots,a_p,y;b_1,\ldots,b_q;-z^{-1}\right)|z|^{-y} \\
&\qquad = \frac{1}{\Gamma_k(y)}\int_{\Lambda>0} e^{-tr(\Lambda z)}{}_pF_q\left(a_1,\ldots,a_p;b_1,\ldots,b_q;-\Lambda\right)|\Lambda|^{y-\phi}d\Lambda, \quad (1)
\end{aligned}
$$

where, $\mathbb{R}(z) > 0, \phi = \frac{k+1}{2}, y = \phi - 1$ and

$$
\begin{aligned}
&{}_pF_{q+1}\left(a_1,\ldots,a_p,b_1,\ldots,b_q,y;-\Lambda\right)|\Lambda|^{y-\phi} = \Gamma_k(y)\frac{1}{(2\pi i)^{k(k+1)/2}}\times \\
&\int_{R(z)=X_0>0} e^{tr(\Lambda z)}{}_pF_q\left(a_1,\ldots,a_p;b_1,\ldots,b_q;-z^{-1}\right)|z|^{-y}dz, \quad \mathbb{R}(\Lambda) > 0. \quad (2)
\end{aligned}
$$

Further, Mathai [6, 8, 9] introduced the **generalized matrix transform (M-transform)** defined an integral over the $k\times k$ positive symmetric definite matrix A as follows:

$$
M(f) = \int_{A>0} |A|^{s-\frac{k+1}{2}} f(A)dA. \quad (3)
$$

This integral exists for $\mathbb{R}(s) > \frac{k+1}{2} - 1$, where $R(.)$ is the real part of $(.)$. For $f(A) = e^{-trA}$ the M-transform will be $M(f) = \Gamma_k(s)$ (real matrix-variate gamma function).
Real matrix-variate gamma function $\Gamma_k(s)$ is defined as follows:

$$
\Gamma_k(s) = \pi^{k(k-1)/4}\Gamma(s)\Gamma(s-\frac{1}{2})\Gamma(s-1)\ldots\Gamma(s-\frac{k-1}{2}), \quad \mathbb{R}(s) > \frac{k-1}{2}. \quad (4)
$$

The M-transform of the hypergeometric function of $k\times k$ real symmetric positive definite matrix argument by the integral

$$
\begin{aligned}
&\int_{Z>0} |Z|^{s-\frac{k+1}{2}}{}_pF_q\left(a_1,\ldots,a_p;b_1,\ldots,b_q;-Z\right)dZ \\
&\qquad = \frac{\prod_{j=1}^q \Gamma_k(b_j)\prod_{j=1}^p \Gamma_k(a_j-s)}{\prod_{j=1}^p \Gamma_k(a_j)\prod_{j=1}^q \Gamma_k(b_j-s)}\Gamma_k(s), \quad (5)
\end{aligned}
$$

provided the left-hand side integral exists and it is equal to the gamma products on the right-hand side.

Application of hypergeometric functions of matrix argument in the field of statistical distributions developed by Mathai [10].
Progressively, Mathai [7] figure out the Fox's H-function $H(Z)$ of $k \times k$ real symmetric positive definite matrix argument z satisfies the integral equation:

$$\int_{Z>0} |Z|^{s-\frac{k+1}{2}} H(Z)dZ = \frac{\prod_{j=1}^{m} \Gamma_k(b_j + B_j s) \prod_{j=1}^{n} \Gamma_k(\frac{k+1}{2} - a_j - A_j s)}{\prod_{j=m+1}^{q} \Gamma_k(\frac{k+1}{2} - b_j - B_j s) \prod_{j=n+1}^{p} \Gamma_k(a_j + A_j s)}, \quad (6)$$

whenever the left-hand side integral exists, it is equal to the gamma products on the right side and for more conditions (see [7]). Result (6) can transform to two known results:

1. By putting $k = 1$, matrix argument converts to scalar argument and
2. By putting A_j $(j = 1, \ldots, p) = B_j$ $(j = 1, \ldots, q) = 1$, Fox's H-function of matrix argument convert to Meijer's G-function of matrix argument detail literature available in [5].

Special functions with a matrix argument are employed to address fading issues in wireless communication. Several authors have explored the applications of special functions with scalar and matrix argument, including [3, 20, 16, 17, 28, 21, 26, 22, 29, 27].

2 Some Definitions and Preliminary Results

In this section, we discuss a few more elementary definitions and preliminary results which we use to derive main theorems.

2.1 Incomplete Gamma Functions

The incomplete gamma functions $\gamma(s, x)$ and $\Gamma(s, x)$ for $x = 1$ was introduced by Prym [13] in 1877. Systematically, the incomplete gamma functions $\gamma(s, x)$ and $\Gamma(s, x)$ defined by

$$\gamma(s, y) = \int_0^y t^{s-1} e^{-t} dt, \quad (\mathbb{R}(s) > 0;\ y \geq 0), \quad (7)$$

and

$$\Gamma(s, y) = \int_y^\infty t^{s-1} e^{-t} dt, \quad (y \geq 0;\ \mathbb{R}(s) > 0\ when\ y = 0), \quad (8)$$

respectively. The incomplete gamma functions holds the decomposition formula $\gamma(s, y) + \Gamma(s, y) = \Gamma(s)$, here $\Gamma(.)$ is the well known gamma function given by $\Gamma(s) = \int_0^\infty t^{s-1} e^{-t} dt$, $\mathbb{R}(s) > 0$.

2.2 Incomplete Pochhammer Symbols

In terms of incomplete gamma functions $\gamma(s,y)$ and $\Gamma(s,y)$ defined in (7) and (8) Srivastava et al. [14] introduced incomplete Pochhammer symbols $(\nu;x)_\lambda$ and $[\nu;x]_\lambda$ as follows:

$$(\nu;x)_\lambda = \frac{\gamma(\nu+\lambda,s)}{\Gamma(\nu)} \quad \text{and} \quad [\nu;x]_\lambda = \frac{\Gamma(\nu+\lambda,s)}{\Gamma(\nu)}, \tag{9}$$

here $\nu,\lambda \in \mathbb{C},\ x \geq 0$. These incomplete Pochhammer symbols $(\nu;x)_\lambda$ and $[\nu;x]_\lambda$ given in (9) holds the decomposition formula as:

$$(\nu;x)_\lambda + [\nu;x]_\lambda = (\nu)_\lambda \quad (\nu,\lambda \in \mathbb{C},\ x \geq 0)\,,$$

where well known Pochhammer symbol $(\nu)_\lambda = \frac{\Gamma(\nu+\lambda)}{\Gamma(\lambda)},\ \nu \in \mathbb{C}\backslash Z_0^-$.

2.3 Generalized Incomplete Hypergeometric Functions

The incomplete Pochhammer symbols are the backbone of the incomplete form of special functions defined in this section. For $(|arg(-z)| < \pi)$, Srivastava et al. [14] introduced generalized incomplete hypergeometric functions along with Mellin-Barnes integral in terms of incomplete Pochhammer symbols as follows:

$$\begin{aligned} {}_p\gamma_q\left[\begin{array}{l}(\alpha_1,x),\alpha_2,\ldots,\alpha_p;\\ \delta_1,\ldots,\delta_q;\end{array}\ z\right] &= \sum_{n=0}^{\infty}\frac{(\alpha_1;x)_n(\alpha_2)_n,\ldots,(\alpha_p)_n}{(\delta_1)_n,\ldots,(\delta_q)_n}\frac{z^n}{n!} \\ &= \frac{1}{2\pi i}\frac{\Gamma(\delta_1)\ldots\Gamma(\delta_q)}{\Gamma(\alpha_1)\ldots\Gamma(\alpha_p)}\int_L \frac{\gamma(\alpha_1+s,x)\Gamma(\alpha_2+s)\ldots\Gamma(\alpha_p+s)}{\Gamma(\delta_1+s)\ldots\Gamma(\delta_q+s)}\Gamma(-s)(-z)^s ds, \end{aligned} \tag{10}$$

and

$$\begin{aligned} {}_p\Gamma_q\left[\begin{array}{l}(\alpha_1,x),\alpha_2,\ldots,\alpha_p;\\ \delta_1,\ldots,\delta_q;\end{array}\ z\right] &= \sum_{n=0}^{\infty}\frac{[\alpha_1;x]_n(\alpha_2)_n,\ldots,(\alpha_p)_n}{(\delta_1)_n,\ldots,(\delta_q)_n}\frac{z^n}{n!} \\ &= \frac{1}{2\pi i}\frac{\Gamma(\delta_1)\ldots\Gamma(\delta_q)}{\Gamma(\alpha_1)\ldots\Gamma(\alpha_p)}\int_L \frac{\Gamma(\alpha_1+s,x)\Gamma(\alpha_2+s)\ldots\Gamma(\alpha_p+s)}{\Gamma(\delta_1+s)\ldots\Gamma(\delta_q+s)}\Gamma(-s)(-z)^s ds. \end{aligned} \tag{11}$$

Let $L = L_{(\sigma;\mp i\infty)}$ be a MellinBarnes-type contour from $\sigma - i\infty$ to $\sigma + i\infty$ $(\sigma \in \mathbb{R})$ with the usual indentations to separate one set of poles from the other set of poles of the integrand.
Further, we have the following decomposition formula in terms of the well-known generalized hypergeometric function ${}_pF_q$ $(p,q \in \mathbb{N})$ as follows:

$$\begin{aligned} {}_p\gamma_q\left[\begin{array}{l}(\alpha_1,x),\alpha_2,\ldots,\alpha_p;\\ \delta_1,\ldots,\delta_q;\end{array}\ z\right] + {}_p\Gamma_q\left[\begin{array}{l}(\alpha_1,x),\alpha_2,\ldots,\alpha_p;\\ \delta_1,\ldots,\delta_q;\end{array}\ z\right] \\ = {}_pF_q\left[\begin{array}{l}\alpha_1,\ldots,\alpha_p;\\ \delta_1,\ldots,\delta_q;\end{array}\ z\right]. \end{aligned}$$

2.4 Incomplete H-Functions

The incomplete H-functions introduced by Srivastava et al. [15] in terms of incomplete gamma functions $\gamma(s,y)$ and $\Gamma(s,y)$ as follows:

$$\gamma_{P,Q}^{M,N}(z)=\gamma_{P,Q}^{M,N}\left[z\,\middle|\,\begin{matrix}(\mathfrak{f}_1,\mathfrak{F}_1,t),(\mathfrak{f}_j,\mathfrak{F}_j)_{2,P}\\(\mathfrak{w}_j,\mathfrak{W}_j)_{1,Q}\end{matrix}\right]:=\frac{1}{2\pi i}\int_L\varphi(s,t)z^{-s}ds,\qquad(12)$$

where

$$\varphi(s,t)=\frac{\gamma(1-\mathfrak{f}_1-\mathfrak{F}_1s,t)\prod_{j=1}^{M}\Gamma(\mathfrak{w}_j+\mathfrak{W}_js)\prod_{j=2}^{N}\Gamma(1-\mathfrak{f}_j-\mathfrak{F}_js)}{\prod_{j=M+1}^{Q}\Gamma(1-\mathfrak{w}_j-\mathfrak{W}_js)\prod_{j=N+1}^{P}\Gamma(\mathfrak{f}_j+\mathfrak{F}_js)},\qquad(13)$$

and

$$\Gamma_{P,Q}^{M,N}(z)=\Gamma_{P,Q}^{M,N}\left[z\,\middle|\,\begin{matrix}(\mathfrak{f}_1,\mathfrak{F}_1,t),(\mathfrak{f}_j,\mathfrak{F}_j)_{2,P}\\(\mathfrak{w}_j,\mathfrak{W}_j)_{1,Q}\end{matrix}\right]:=\frac{1}{2\pi i}\int_L\phi(s,t)z^{-s}ds,\qquad(14)$$

where

$$\phi(s,t)=\frac{\Gamma(1-\mathfrak{f}_1-\mathfrak{F}_1s,t)\prod_{j=1}^{M}\Gamma(\mathfrak{w}_j+\mathfrak{W}_js)\prod_{j=2}^{N}\Gamma(1-\mathfrak{f}_j-\mathfrak{F}_js)}{\prod_{j=M+1}^{Q}\Gamma(1-\mathfrak{w}_j-\mathfrak{W}_js)\prod_{j=N+1}^{P}\Gamma(\mathfrak{f}_j+\mathfrak{F}_js)}.\qquad(15)$$

The incomplete H-functions $\gamma_{P,Q}^{M,N}(z)$ and $\Gamma_{P,Q}^{M,N}(z)$ are exist for all $t\geq 0$ and for more existing conditions (see [12], [15]).

2.5 Incomplete $\overline{H}$-Functions

The incomplete $\overline{H}$-functions $\overline{\gamma}_{P,Q}^{M,N}(z)$ and $\overline{\Gamma}_{P,Q}^{M,N}(z)$ introduced by Srivastava et al. [15] in terms of incomplete gamma functions $\gamma(s,y)$ and $\Gamma(s,y)$ as follows:

$$\overline{\gamma}_{P,Q}^{M,N}\left[z\,\middle|\,\begin{matrix}(\mathfrak{f}_1,\mathfrak{F}_1;\beta_1:t),(\mathfrak{f}_j,\mathfrak{F}_j;\beta_j)_{2,N},(\mathfrak{f}_j,\mathfrak{F}_j)_{N+1,P}\\(\mathfrak{w}_j,\mathfrak{W}_j)_{1,M},(\mathfrak{w}_j,\mathfrak{W}_j;\alpha_j)_{M+1,Q}\end{matrix}\right]:=\frac{1}{2\pi i}\int_L\overline{\varphi}(s,t)z^{-s}ds,\qquad(16)$$

where

$$\overline{\varphi}(s,t)=\frac{[\gamma(1-\mathfrak{f}_1-\mathfrak{F}_1s,t)]^{\beta_1}\prod_{j=1}^{M}\Gamma(\mathfrak{w}_j+\mathfrak{W}_js)\prod_{j=2}^{N}[\Gamma(1-\mathfrak{f}_j-\mathfrak{F}_js)]^{\beta_j}}{\prod_{j=M+1}^{Q}[\Gamma(1-\mathfrak{w}_j-\mathfrak{W}_js)]^{\alpha_j}\prod_{j=N+1}^{P}\Gamma(\mathfrak{f}_j+\mathfrak{F}_js)},\qquad(17)$$

and

$$\overline{\Gamma}_{P,Q}^{M,N}\left[z\,\middle|\,\begin{matrix}(\mathfrak{f}_1,\mathfrak{F}_1;\beta_1:t),(\mathfrak{f}_j,\mathfrak{F}_j;\beta_j)_{2,N},(\mathfrak{f}_j,\mathfrak{F}_j)_{N+1,P}\\(\mathfrak{w}_j,\mathfrak{W}_j)_{1,M},(\mathfrak{w}_j,\mathfrak{W}_j;\alpha_j)_{M+1,Q}\end{matrix}\right]:=\frac{1}{2\pi i}\int_L\overline{\phi}(s,t)z^{-s}ds,\qquad(18)$$

where

$$\overline{\phi}(s,t)=\frac{[\Gamma(1-\mathfrak{f}_1-\mathfrak{F}_1 s,t)]^{\beta_1}\prod_{j=1}^{M}\Gamma(\mathfrak{w}_j+\mathfrak{W}_j s)\prod_{j=2}^{N}[\Gamma(1-\mathfrak{f}_j-\mathfrak{F}_j s)]^{\beta_j}}{\prod_{j=M+1}^{Q}[\Gamma(1-\mathfrak{w}_j-\mathfrak{W}_j s)]^{\alpha_j}\prod_{j=N+1}^{P}\Gamma(\mathfrak{f}_j+\mathfrak{F}_j s)}. \tag{19}$$

The incomplete $\overline{H}$-functions $\overline{\gamma}_{P,Q}^{M,N}(z)$ and $\overline{\Gamma}_{P,Q}^{M,N}(z)$ for conditions (see [15]) are exist for all $t\geq 0$ and for more existing conditions (see, [15]).

2.6 Incomplete I-Functions

The incomplete I-functions ${}^{(\gamma)}I_{P_i.Q_i,R}^{M,N}(z)$ and ${}^{(\Gamma)}I_{P_i.Q_i,R}^{M,N}(z)$ introduced by Bansal et al. [18] in terms of incomplete gamma functions $\gamma(s,y)$ and $\Gamma(s,y)$ as follows:

$${}^{(\gamma)}I_{P_i.Q_i,R}^{M,N}\left[z\,\middle|\,\begin{matrix}(\mathfrak{f}_1,\mathfrak{F}_1,t),(\mathfrak{f}_j,\mathfrak{F}_j)_{2,N},(\mathfrak{f}_{ji},\mathfrak{F}_{ji})_{N+1,P_i}\\(\mathfrak{w}_j,\mathfrak{W}_j)_{1,M},(\mathfrak{w}_{ji},\mathfrak{W}_{ji})_{M+1,Q_i}\end{matrix}\right]:=\frac{1}{2\pi i}\int_L\varphi(s,t)z^{-s}ds, \tag{20}$$

where

$$\varphi(s,t)=\frac{\gamma(1-\mathfrak{f}_1-\mathfrak{F}_1 s,t)\prod_{j=1}^{M}\Gamma(\mathfrak{w}_j+\mathfrak{W}_j s)\prod_{j=2}^{N}\Gamma(1-\mathfrak{f}_j-\mathfrak{F}_j s)}{\sum_{i=1}^{R}\left[\prod_{j=M+1}^{Q_i}\Gamma(1-\mathfrak{w}_{ji}-\mathfrak{W}_{ji}s)\prod_{j=N+1}^{P_i}\Gamma(\mathfrak{f}_{ji}+\mathfrak{F}_{ji}s)\right]}, \tag{21}$$

and

$${}^{(\Gamma)}I_{P_i.Q_i,R}^{M,N}\left[z\,\middle|\,\begin{matrix}(\mathfrak{f}_1,\mathfrak{F}_1,t),(\mathfrak{f}_j,\mathfrak{F}_j)_{2,N},(\mathfrak{f}_{ji},\mathfrak{F}_{ji})_{N+1,P_i}\\(\mathfrak{w}_j,\mathfrak{W}_j)_{1,M},(\mathfrak{w}_{ji},\mathfrak{W}_{ji})_{M+1,Q_i}\end{matrix}\right]:=\frac{1}{2\pi i}\int_L\phi(s,t)z^{-s}ds, \tag{22}$$

where

$$\phi(s,t)=\frac{\Gamma(1-\mathfrak{f}_1-\mathfrak{F}_1 s,t)\prod_{j=1}^{M}\Gamma(\mathfrak{w}_j+\mathfrak{W}_j s)\prod_{j=2}^{N}\Gamma(1-\mathfrak{f}_j-\mathfrak{F}_j s)}{\sum_{i=1}^{R}\left[\prod_{j=M+1}^{Q_i}\Gamma(1-\mathfrak{w}_{ji}-\mathfrak{W}_{ji}s)\prod_{j=N+1}^{P_i}\Gamma(\mathfrak{f}_{ji}+\mathfrak{F}_{ji}s)\right]}. \tag{23}$$

The incomplete I-functions ${}^{(\gamma)}I_{P_i,Q_i,R}^{M,N}(z)$ and ${}^{(\Gamma)}I_{P_i,Q_i,R}^{M,N}(z)$ exists for all $t\geq 0$ and for existing conditions (see, [18, 21, 23]). We can easily define the decomposition formula of incomplete form of special functions.

2.7 Jacobians of Matrix Transformations

This section will present a few outcomes on the Jacobians of transformations that we require. For now, we will focus on the prerequisites for formulating the special functions with matrix argument. We define a real symmetric positive definite matrix X as $X=X'>0$ (where X' is the transpose of matrix X).

We use the notations $X \geq 0$ to represent a positive semi-definite matrix, $X < 0$ for a negative definite matrix, $X \leq 0$ for a negative semi-definite matrix, and indefinite matrices for all other matrices. The notations $\int_{X>0} f(X)dX$ and $\int_{X=0}^{I} g(X)dX$ represent the integration of $f(X)$ over all positive matrices $X = X' > 0$ and the integration of $g(X)$ over all matrices $I - X > 0$ that are positive definite. The symbol dX represents the differential element.
Let us now discuss some elementary results regarding the Jacobians of transformations. Let L be a symmetric matrix of order k. Then L involves $\frac{k(k+1)}{2}$ variables, and its differential element is defined as $dL = dl_{11} \dots dl_{1k}; dl_{22} \dots dl_{2k} \dots dl_{k-1k}; dl_{kk}$. In the case of an asymmetric (non-symmetric) matrix $L = [l]\, ij$ of order k, L involves k^2 variables, and its differential element dL is defined as $dl_{11} \dots dl_{1k}; dl_{21} \dots dl_{2k} \dots dl_{k1} \dots dl_{kk}$. Transformation of $L = [l]_{ij}$ to $M = [m]_{ij}$ here both are symmetric matrix of order k. Which implies that $\frac{k(k+1)}{2}$ variables of L transform to $\frac{k(k+1)}{2}$ variables of M. Here, we have a few results given in the previous literature.

1. If A and B are $k \times k$ symmetric and X is a $k \times k$ non singular then

$$A = XBX' \implies dA = |X|^{k+1} dB, \tag{24}$$

   where $|X|$ and X' represent the determinant and transpose of X.

2. If $L = [l]_{ij}$ is $k \times k$ symmetric and $M = [m]_{ij}$ is $k \times k$ lower triangular matrices respectively then

$$L = MM' \implies dL = \left[2^k \prod_{i=1}^{k} m_{ii}^{k+1-i} \right] dM. \tag{25}$$

Convolution Property: If M-transform of two symmetric functions $f_1(A)$ and $f_2(A)$ are $G_1(s)$ and $G_2(s)$ respectively, then M.transform of a function $f_3(A) = \int_{\Lambda>0} |\Lambda|^a f_1(A\Lambda) f_2(\Lambda) d\Lambda$ is defiend by

$$M(f_3) = G_1(s) G_2 \left(\frac{k+1}{2} + a - s \right). \tag{26}$$

From the (3) we observe that $M(f)$ is a function of s (univariate), although $f(\Lambda)$ is a multivariate we need not have uniqueness for $f(\Lambda)$.
Real matrix-variate Beta function $B_k(s_1, s_2)$ define as follows:

$$B_k(s_1, s_2) = \frac{\Gamma_k(s_1)\Gamma_k(s_2)}{\Gamma_k(s_1 + s_2)}, \quad \mathbb{R}(s_1) > \frac{k-1}{2}, \, \mathbb{R}(s_2) > \frac{k-1}{2}.$$

The integral representation of the Real Matrix-variate Beta function is defined as follows:

$$B_k(s_1, s_2) = \int_X |X|^{s_1 - \frac{k+1}{2}} |I - X|^{s_2 - \frac{k+1}{2}} dX, \tag{27}$$

here, $X > 0,\ 0 < X < I \implies I - X > 0$ and $\mathbb{R}(s_1) > \frac{k-1}{2},\ \mathbb{R}(s_2) > \frac{k-1}{2}$. Eigen values of X i.e. $\lambda_1, \lambda_2, \ldots, \lambda_k$ are in the interval of $(0, 1)$.
We can extend more univariate integrals to matrix cases by using convolution property (26) as follows:

1. Taking $a = \alpha - \frac{k+1}{2},\ f_1(A) = e^{-trA}$ and $f_2(A) = |I - A|^{\beta - \frac{k+1}{2}}$ in (26), we get

$$\int_0^I |A|^{\alpha - \frac{k+1}{2}} |I - A|^{\beta - \frac{k+1}{2}} e^{-tr\Lambda A} dA$$
$$= \frac{\Gamma_k(\alpha)\Gamma_k(\beta)}{\Gamma_k(\alpha + \beta)} {}_1F_1(\alpha; \alpha + \beta; -\Lambda), \quad \mathbb{R}(\alpha),\ \mathbb{R}(\beta) > \frac{k+1}{2} - 1. \quad (28)$$

2. Putting $a = \alpha - \frac{k+1}{2},\ f_1(A) = |I - A|^{-\beta}$ and $f_2(A) = |I - A|^{\gamma - \alpha - \frac{k+1}{2}}$ in (26), we get

$$\int_0^I |I - \Lambda A|^{-\beta} |\Lambda|^{\alpha - \frac{k+1}{2}} |I - \Lambda|^{\gamma - \alpha - \frac{k+1}{2}} d\Lambda = \frac{\Gamma_k(\alpha)\Gamma_k(\gamma - \alpha)}{\Gamma_k(\gamma)} \times$$
$${}_2F_1(\alpha, \beta; \gamma; A), \quad \mathbb{R}(\beta) > 0,\ \mathbb{R}(\alpha),\ \mathbb{R}(\gamma - \alpha) > \frac{k+1}{2} - 1. \quad (29)$$

3. Another extension of univariate integral to matrix case as follows:

$$\int_{\Lambda > 0} |\Lambda|^{\alpha - \frac{k+1}{2}} |I + A\Lambda|^{-\mu} d\Lambda$$
$$= \frac{\Gamma_k(\alpha)\Gamma_k(\mu - \alpha)}{\Gamma_k(\mu)} |A|^{-\alpha}, \quad A > 0,\ \mathbb{R}(\alpha),\ \mathbb{R}(\mu - \alpha) > \frac{k+1}{2} - 1. \quad (30)$$

Here, we substitute $V = A^{1/2}\Lambda A^{1/2}$. Then $dV = |A|^{\frac{k+1}{2}} d\Lambda$ in (30).

4. Further, set $U^{-1} = I + V$ i.e. $dV = |U|^{-(k+1)} dU$ and $0 < U < I$ then LHS of (30) can be written as $|A|^{-\alpha} \int_{V>0} |V|^{\alpha - \frac{k+1}{2}} |I + V|^{-\mu} dV$ and reduces to beta integral defined in (27) and on transforming $CV = A$ in (29), we get a new univariate integral as follows:

$$\int_0^C |I + ZA|^{-\mu} |A|^{\alpha - \frac{k+1}{2}} dA = \frac{\Gamma_k(\alpha)\Gamma_k(\frac{k+1}{2})}{\Gamma_k(\alpha + \frac{k+1}{2})} |C|^{\alpha} \times$$
$${}_2F_1(\alpha, \mu; \alpha + \frac{k+1}{2}; -ZC), \quad C > 0,\ \mathbb{R}(\alpha) > \frac{k+1}{2} - 1. \quad (31)$$

5. In (31), making the transformations $V = I + \Lambda,\ U = V^{-1}$ and then use ${}_2F_1(\alpha, \beta; \gamma; A) = |(I - A)|^{-\beta} {}_2F_1(\gamma - \alpha, \beta; \gamma; -A(I - A)^{-1})$. We have

$$\int_{\Lambda > 0} |\Lambda|^{\alpha - \frac{k+1}{2}} |I + \Lambda|^{\mu} |I + Z\Lambda|^{\nu} d\Lambda = \frac{\Gamma_k(\alpha)\Gamma_k(\nu + \mu - \alpha)}{\Gamma_k(-\nu - \mu)} \times$$
$${}_2F_1(-\nu, \alpha; -\nu - \mu; I - Z),\ -\mathbb{R}(\nu + \mu) > \mathbb{R}(\alpha) > \frac{k+1}{2} - 1. \quad (32)$$

6. Making the transformation $V = A^{-1/2}\Lambda A^{-1/2}$ in (28). We get

$$\int_0^Z |\Lambda|^{\alpha-\frac{k+1}{2}} e^{-trC\Lambda} d\Lambda = |Z|^{\alpha} \frac{\Gamma_k(\alpha)\Gamma_k(\frac{k+1}{2})}{\Gamma_k(\alpha+\frac{k+1}{2})} \times {}_1F_1(\alpha; \alpha+\frac{k+1}{2}; -ZC), \quad \mathbb{R}(\alpha) > \frac{k+1}{2} - 1. \quad (33)$$

It is important to note that **the incomplete gamma function** can be generalized using $C = I$ in (33). The incomplete gamma functions for univariate matrix cases can be written as:

$$\begin{aligned} &\gamma_k(\alpha, Z) = \int_{\Lambda=0}^{Z} |\Lambda|^{\alpha-\frac{k+1}{2}} e^{-tr\Lambda} d\Lambda, \\ &\text{and } \Gamma_k(\alpha, Z) = \int_{\Lambda>Z} |\Lambda|^{\alpha-\frac{k+1}{2}} e^{-tr\Lambda} d\Lambda = \Gamma_k(\alpha) - \gamma_k(\alpha, Z). \end{aligned} \quad (34)$$

For multivariate cases $\int_{\Lambda>Z} |\Lambda|^{\alpha-\frac{k+1}{2}} e^{-tr\Lambda} d\Lambda \neq \Gamma_k(\alpha) - \gamma_k(\alpha, Z)$ since $\int_A^B + \int_B^C \neq \int_A^C$ is not valid for all values of Z when Z is a matrix.
There are three approaches to deriving special functions of matrix argument:

1. Bochner [24] and Herz's [11] using Laplace approach,
2. James [2, 3] and Constantine's [4] develop zonal polynomial approach and
3. Mathai's [19, 7] generalized matrix transform (M-transform) method.

In this work, we use the M-transform method to derive the special functions of the matrix argument.

3 Main Results

In this section, we evaluate some results using the M-transform of various incomplete types of special functions like generalized incomplete hypergeometric functions, incomplete H-functions, incomplete $\overline{H}$-functions, incomplete I-functions.
Theorem 1: Let Z be a $k \times k$ real symmetric positive definite matrix with eigenvalues $\lambda_1 > \lambda_2 > \cdots > \lambda_k > 0$ and generalized incomplete hypergeometric functions ${}_p\gamma_q(Z)$ and ${}_p\Gamma_q(Z)$ are symmetric functions in the sense ${}_p\gamma_q(Z) = {}_p\gamma_q(lZl')$ and ${}_p\Gamma_q(Z) = {}_p\Gamma_q(lZl')$, $ll' = I$ for all orthogonal matrices. If s is an arbitrary parameter then consider the integral equations:

$$\int_{Z>0} |Z|^{s-\frac{k+1}{2}} {}_p\gamma_q \left[\begin{matrix} (\alpha_1, A), \alpha_2, \ldots, \alpha_p; \\ \delta_1, \ldots, \delta_q; \end{matrix} -Z \right] dZ = \frac{\prod_{j=1}^{q} \Gamma_k(\delta_j)}{\prod_{i=1}^{p} \Gamma_k(\alpha_i)} \frac{\gamma_k(\alpha_1 - s, A) \prod_{i=2}^{p} \Gamma_k(\alpha_i - s)}{\prod_{j=1}^{q} \Gamma_k(\delta_j - s)} \Gamma_k(s), \quad (35)$$

and

$$\int_{Z>0}|Z|^{s-\frac{k+1}{2}}{}_p\Gamma_q\left[\begin{array}{l}(\alpha_1,A),\alpha_2,\ldots,\alpha_p;\\ \delta_1,\ldots,\delta_q;\end{array}-Z\right]dZ$$
$$=\frac{\prod_{j=1}^q\Gamma_k(\delta_j)}{\prod_{i=1}^p\Gamma_k(\alpha_i)}\frac{\Gamma_k(\alpha_1-s,A)\prod_{i=2}^p\Gamma_k(\alpha_i-s)}{\prod_{j=1}^q\Gamma_k(\delta_j-s)}\Gamma_k(s),\quad(36)$$

provided these gamma products are defined.

Proof: Here Z is a $k\times k$ real symmetric positive definite matrix with eigenvalues $\lambda_1>\lambda_2>\cdots>\lambda_k>0$ and generalized incomplete hypergeometric functions ${}_p\gamma_q(Z)$ and ${}_p\Gamma_q(Z)$ are symmetric functions in the sense that ${}_p\gamma_q(Z)={}_p\gamma_q(lZl')$ and ${}_p\Gamma_q(Z)={}_p\Gamma_q(lZl'),\ ll'=I$ for all orthogonal matrices. In this case, we have $f(Z\Lambda)=f(\Lambda Z)=f(\Lambda^{1/2}Z\Lambda^{1/2})$ whenever $\Lambda^{1/2}$ is defined.
For the positive semi definite matrix Z there exists a lower triangular matrix T such that $Z=TT'$. Now transforming Z to T by using (25) as $dZ=\left[2^k\prod_{i=1}^k t_{ii}^{k+1-i}\right]dT$ and $|TT'|=\prod_{i=1}^k t_{ii}^2$. After substituting these values in the left-hand of (35) and (36), use (34) and after a bit of simplification, we get the desired result.

Theorem 2: This generalized incomplete hypergeometric functions with matrix argument hold the decomposition formula as follows:

$$\int_{Z>0}|Z|^{s-\frac{k+1}{2}}{}_p\gamma_q\left[\begin{array}{l}(\alpha_1,A),\alpha_2,\ldots,\alpha_p;\\ \delta_1,\ldots,\delta_q;\end{array}-Z\right]dZ$$
$$+\int_{Z>0}|Z|^{s-\frac{k+1}{2}}{}_p\Gamma_q\left[\begin{array}{l}(\alpha_1,A),\alpha_2,\ldots,\alpha_p;\\ \delta_1,\ldots,\delta_q;\end{array}-Z\right]dZ$$
$$=\int_{Z>0}|Z|^{s-\frac{k+1}{2}}{}_pF_q\left[\begin{array}{l}\alpha_1,\ldots,\alpha_p;\\ \delta_1,\ldots,\delta_q;\end{array}-Z\right]dZ.\quad(37)$$

Proof: We can write left hand side of (37) by using (35) and (36) as follows:

$$\frac{\prod_{j=1}^q\Gamma_k(\delta_j)}{\prod_{i=1}^p\Gamma_k(\alpha_i)}\frac{\gamma_k(\alpha_1-s,A)\prod_{i=2}^p\Gamma_k(\alpha_i-s)}{\prod_{j=1}^q\Gamma_k(\delta_j-s)}\Gamma_k(s)$$
$$+\frac{\prod_{j=1}^q\Gamma_k(\delta_j)}{\prod_{i=1}^p\Gamma_k(\alpha_i)}\frac{\Gamma_k(\alpha_1-s,A)\prod_{i=2}^p\Gamma_k(\alpha_i-s)}{\prod_{j=1}^q\Gamma_k(\delta_j-s)}\Gamma_k(s)$$
$$=\frac{\prod_{j=1}^q\Gamma_k(\delta_j)}{\prod_{i=1}^p\Gamma_k(\alpha_i)}\frac{\prod_{i=1}^p\Gamma_k(\alpha_i-s)}{\prod_{j=1}^q\Gamma_k(\delta_j-s)}\Gamma_k(s).\quad(38)$$

The right-hand side of (38) is the same as derived by Mathai (eq. 3.3, [6]).

Theorem 3: Let Z be a $k\times k$ real symmetric positive definite matrix with eigenvalues $\lambda_1>\lambda_2>\cdots>\lambda_k>0$ and the incomplete H-functions $\gamma_{P,Q}^{M,N}(Z)$

and $\Gamma_{P,Q}^{M,N}(Z)$ be a symmetric functions in the sense $\gamma_{P,Q}^{M,N}(Z)=\gamma_{P,Q}^{M,N}(lZl')$ and $\Gamma_{P,Q}^{M,N}(Z)=\Gamma_{P,Q}^{M,N}(lZl'),\ ll'=I$ for all orthogonal matrices. If s is an arbitrary parameter then consider the integral equations for incomplete H-functions as follows:

$$\int_{Z>0}|Z|^{s-\frac{k+1}{2}}\gamma_{P,Q}^{M,N}\left[Z\left|\begin{array}{l}(\mathfrak{f}_1,\mathfrak{F}_1,A),(\mathfrak{f}_j,\mathfrak{F}_j)_{2,P}\\(\mathfrak{w}_j,\mathfrak{W}_j)_{1,Q}\end{array}\right.\right]dZ$$
$$=\frac{\gamma_k(\frac{k+1}{2}-\mathfrak{f}_1-\mathfrak{F}_1s,A)\prod_{j=1}^{M}\Gamma_k(\mathfrak{w}_j+\mathfrak{W}_js)\prod_{j=2}^{N}\Gamma_k(\frac{k+1}{2}-\mathfrak{f}_j-\mathfrak{F}_js)}{\prod_{j=M+1}^{Q}\Gamma_k(\frac{k+1}{2}-\mathfrak{w}_j-\mathfrak{W}_js)\prod_{j=N+1}^{P}\Gamma_k(\mathfrak{f}_j+\mathfrak{F}_js)},\quad(39)$$

and

$$\int_{Z>0}|Z|^{s-\frac{k+1}{2}}\Gamma_{P,Q}^{M,N}\left[Z\left|\begin{array}{l}(\mathfrak{f}_1,\mathfrak{F}_1,A),(\mathfrak{f}_j,\mathfrak{F}_j)_{2,P}\\(\mathfrak{w}_j,\mathfrak{W}_j)_{1,Q}\end{array}\right.\right]dZ$$
$$=\frac{\Gamma_k(\frac{k+1}{2}-\mathfrak{f}_1-\mathfrak{F}_1s,A)\prod_{j=1}^{M}\Gamma_k(\mathfrak{w}_j+\mathfrak{W}_js)\prod_{j=2}^{N}\Gamma_k(\frac{k+1}{2}-\mathfrak{f}_j-\mathfrak{F}_js)}{\prod_{j=M+1}^{Q}\Gamma_k(\frac{k+1}{2}-\mathfrak{w}_j-\mathfrak{W}_js)\prod_{j=N+1}^{P}\Gamma_k(\mathfrak{f}_j+\mathfrak{F}_js)}.\quad(40)$$

provided these gamma products are defined.

Proof: Here Z is a $k\times k$ real symmetric positive definite matrix with eigenvalues $\lambda_1>\lambda_2>\cdots>\lambda_k>0$ and generalized incomplete hypergeometric functions ${}_p\gamma_q(Z)$ and ${}_p\Gamma_q(Z)$ are symmetric functions in the sense that ${}_p\gamma_q(Z)={}_p\gamma_q(lZl')$ and ${}_p\Gamma_q(Z)={}_p\Gamma_q(lZl'),\ ll'=I$ for all orthogonal matrices. In this case, we have $f(Z\Lambda)=f(\Lambda Z)=f(\Lambda^{1/2}Z\Lambda^{1/2})$ whenever $\Lambda^{1/2}$ is defined.
For the positive semi definite matrix Z there exists a lower triangular matrix T such that $Z=TT'$. Now transforming Z to T by using (25) as $dZ=\left[2^k\prod_{i=1}^{k}t_{ii}^{k+1-i}\right]dT$ and $|TT'|=\prod_{i=1}^{k}t_{ii}^2$. After substituting these values in the left-hand of (35) and (36), use (34) and after a bit of simplification, we get the desired result.

Theorem 4: The incomplete H-functions with matrix argument also hold the decomposition formula as follows:

$$\int_{Z>0}|Z|^{s-\frac{k+1}{2}}\gamma_{P,Q}^{M,N}\left[Z\left|\begin{array}{l}(\mathfrak{f}_1,\mathfrak{F}_1,A),(\mathfrak{f}_j,\mathfrak{F}_j)_{2,P}\\(\mathfrak{w}_j,\mathfrak{W}_j)_{1,Q}\end{array}\right.\right]dZ+$$
$$\int_{Z>0}|Z|^{s-\frac{k+1}{2}}\Gamma_{P,Q}^{M,N}\left[Z\left|\begin{array}{l}(\mathfrak{f}_1,\mathfrak{F}_1,A),(\mathfrak{f}_j,\mathfrak{F}_j)_{2,P}\\(\mathfrak{w}_j,\mathfrak{W}_j)_{1,Q}\end{array}\right.\right]dZ$$
$$=\int_{Z>0}|Z|^{s-\frac{k+1}{2}}H_{P,Q}^{M,N}\left[Z\left|\begin{array}{l}(\mathfrak{f}_j,\mathfrak{F}_j)_{1,P}\\(\mathfrak{w}_j,\mathfrak{W}_j)_{1,Q}\end{array}\right.\right]dZ.\quad(41)$$

Proof: We can write left hand side of (41) as

$$\frac{\gamma_k(\frac{k+1}{2}-\mathfrak{f}_1-\mathfrak{F}_1 s,A)\prod_{j=1}^{M}\Gamma_k(\mathfrak{w}_j+\mathfrak{W}_j s)\prod_{j=2}^{N}\Gamma_k(\frac{k+1}{2}-\mathfrak{f}_j-\mathfrak{F}_j s)}{\prod_{j=M+1}^{Q}\Gamma_k(\frac{k+1}{2}-\mathfrak{w}_j-\mathfrak{W}_j s)\prod_{j=N+1}^{P}\Gamma_k(\mathfrak{f}_j+\mathfrak{F}_j s)}+$$
$$\frac{\Gamma_k(\frac{k+1}{2}-\mathfrak{f}_1-\mathfrak{F}_1 s,A)\prod_{j=1}^{M}\Gamma_k(\mathfrak{w}_j+\mathfrak{W}_j s)\prod_{j=2}^{N}\Gamma_k(\frac{k+1}{2}-\mathfrak{f}_j-\mathfrak{F}_j s)}{\prod_{j=M+1}^{Q}\Gamma_k(\frac{k+1}{2}-\mathfrak{w}_j-\mathfrak{W}_j s)\prod_{j=N+1}^{P}\Gamma_k(\mathfrak{f}_j+\mathfrak{F}_j s)}$$
$$=\frac{\prod_{j=1}^{M}\Gamma_k(\mathfrak{w}_j+\mathfrak{W}_j s)\prod_{j=1}^{N}\Gamma_k(\frac{k+1}{2}-\mathfrak{f}_j-\mathfrak{F}_j s)}{\prod_{j=M+1}^{Q}\Gamma_k(\frac{k+1}{2}-\mathfrak{w}_j-\mathfrak{W}_j s)\prod_{j=N+1}^{P}\Gamma_k(\mathfrak{f}_j+\mathfrak{F}_j s)}. \quad (42)$$

The right-hand side of (42) is the same as derived by Mathai (eq. 3.1, [7]).

Corollary 1: Let Z be a $k\times k$ real symmetric positive definite matrix. Then by using the definition of incomplete H-function $\Gamma_{P,Q}^{M,N}(Z)$. We have

$$|Z|^{\omega}\Gamma_{P,Q}^{M,N}\left[Z\left|\begin{array}{l}(\mathfrak{f}_1,\mathfrak{F}_1,A),(\mathfrak{f}_j,\mathfrak{F}_j)_{2,P}\\(\mathfrak{w}_j,\mathfrak{W}_j)_{1,Q}\end{array}\right.\right]$$
$$=\Gamma_{P,Q}^{M,N}\left[Z\left|\begin{array}{l}(\mathfrak{f}_1+\omega\mathfrak{F}_1,\mathfrak{F}_1,A),(\mathfrak{f}_j+\omega\mathfrak{F}_j,\mathfrak{F}_j)_{2,P}\\(\mathfrak{w}_j+\omega\mathfrak{W}_j,\mathfrak{W}_j)_{1,Q}\end{array}\right.\right]. \quad (43)$$

Proof: By using a similar matrix argument, we can obtain property (43) if we substitute $s+\omega=\mathfrak{s};(\omega>0)$ and $ds=d\mathfrak{s}$. This will give us the desired result.

Corollary 2: Let Z be a $k\times k$ real symmetric positive definite matrix. Then by using the definition of incomplete H-function $\Gamma_{P,Q}^{M,N}(Z)$. We have the following result

$$\Gamma_{P,Q}^{M,N}\left[Z^{-1}\left|\begin{array}{l}(\mathfrak{f}_1,\mathfrak{F}_1,A),(\mathfrak{f}_j,\mathfrak{F}_j)_{2,P}\\(\mathfrak{w}_j,\mathfrak{W}_j)_{1,Q}\end{array}\right.\right]$$
$$=\Gamma_{Q,P}^{N,M}\left[Z\left|\begin{array}{l}(\frac{k+1}{2}-\mathfrak{w}_j,\mathfrak{W}_j)_{1,Q}\\(\frac{k+1}{2}-\mathfrak{f}_1,\mathfrak{F}_1,A),(\frac{k+1}{2}-\mathfrak{f}_j,\mathfrak{F}_j)_{2,P}\end{array}\right.\right]. \quad (44)$$

Proof: This result is obtained by using equation (40), and applying the transformation $L=Z^{-1}$ while noting that $dZ=|L|^{-(k+1)}dL$.

Theorem 5: Let Z be a $k\times k$ real symmetric positive definite matrix with eigenvalues $\lambda_1>\lambda_2>\cdots>\lambda_k>0$ and the incomplete $\overline{H}$-functions $\overline{\gamma}_{P,Q}^{M,N}(z)$ and $\overline{\Gamma}_{P,Q}^{M,N}(z)$ be a symmetric functions in the sense $\overline{\gamma}_{P,Q}^{M,N}(Z)=\overline{\gamma}_{P,Q}^{M,N}(lZl')$ and $\overline{\Gamma}_{P,Q}^{M,N}(Z)=\overline{\Gamma}_{P,Q}^{M,N}(lZl'),\ ll'=I$ for all orthogonal matrices. If s is an arbitrary

parameter then consider the integral equations:

$$\int_{Z>0}|Z|^{s-\frac{k+1}{2}}\overline{\gamma}_{P,Q}^{M,N}\left[Z\left|\begin{array}{l}(\mathfrak{f}_1,\mathfrak{F}_1;\beta_1:A),(\mathfrak{f}_j,\mathfrak{F}_j;\beta_j)_{2,N},(\mathfrak{f}_j,\mathfrak{F}_j)_{N+1,P}\\(\mathfrak{w}_j,\mathfrak{W}_j)_{1,M},(\mathfrak{w}_j,\mathfrak{W}_j;\alpha_j)_{M+1,Q}\end{array}\right.\right]dZ$$
$$=\frac{[\gamma_k(\frac{k+1}{2}-\mathfrak{f}_1-\mathfrak{F}_1s,A)]^{\beta_1}\prod_{j=1}^{M}\Gamma_k(\mathfrak{w}_j+\mathfrak{W}_js)\prod_{j=2}^{N}[\Gamma_k(\frac{k+1}{2}-\mathfrak{f}_j-\mathfrak{F}_js)]^{\beta_j}}{\prod_{j=M+1}^{Q}[\Gamma_k(\frac{k+1}{2}-\mathfrak{w}_j-\mathfrak{W}_js)]^{\alpha_j}\prod_{j=N+1}^{P}\Gamma_k(\mathfrak{f}_j+\mathfrak{F}_js)},\tag{45}$$

and

$$\int_{Z>0}|Z|^{s-\frac{k+1}{2}}\overline{\Gamma}_{P,Q}^{M,N}\left[Z\left|\begin{array}{l}(\mathfrak{f}_1,\mathfrak{F}_1;\beta_1:A),(\mathfrak{f}_j,\mathfrak{F}_j;\beta_j)_{2,N},(\mathfrak{f}_j,\mathfrak{F}_j)_{N+1,P}\\(\mathfrak{w}_j,\mathfrak{W}_j)_{1,M},(\mathfrak{w}_j,\mathfrak{W}_j;\alpha_j)_{M+1,Q}\end{array}\right.\right]dZ$$
$$=\frac{[\Gamma_k(\frac{k+1}{2}-\mathfrak{f}_1-\mathfrak{F}_1s,A)]^{\beta_1}\prod_{j=1}^{M}\Gamma_k(\mathfrak{w}_j+\mathfrak{W}_js)\prod_{j=2}^{N}[\Gamma_k(\frac{k+1}{2}-\mathfrak{f}_j-\mathfrak{F}_js)]^{\beta_j}}{\prod_{j=M+1}^{Q}[\Gamma_k(\frac{k+1}{2}-\mathfrak{w}_j-\mathfrak{W}_js)]^{\alpha_j}\prod_{j=N+1}^{P}\Gamma_k(\mathfrak{f}_j+\mathfrak{F}_js)}.\tag{46}$$

Proof: We can prove this Theorem by follow same steps as in Theorem 1.

Theorem 6: Let Z be a $k\times k$ real symmetric positive definite matrix with eigenvalues $\lambda_1>\lambda_2>\cdots>\lambda_k>0$ and the incomplete I-functions ${}^{(\gamma)}I_{P_i.Q_i,R}^{M,N}(z)$ and ${}^{(\Gamma)}I_{P_i.Q_i,R}^{M,N}(z)$ be a symmetric functions ${}^{(\gamma)}I_{P_i.Q_i,R}^{M,N}(z)={}^{(\gamma)}I_{P_i.Q_i,R}^{M,N}(z)(lZl')$ and ${}^{(\Gamma)}I_{P_i.Q_i,R}^{M,N}(z)={}^{(\Gamma)}I_{P_i.Q_i,R}^{M,N}(z)(lZl')$, $ll'=I$ for all orthogonal matrices. If s is an arbitrary parameter then consider the integral equations:

$$\int_{Z>0}|Z|^{s-\frac{k+1}{2}}{}^{(\gamma)}I_{P_i.Q_i,R}^{M,N}\left[z\left|\begin{array}{l}(\mathfrak{f}_1,\mathfrak{F}_1,A),(\mathfrak{f}_j,\mathfrak{F}_j)_{2,N},(\mathfrak{f}_{ji},\mathfrak{F}_{ji})_{N+1,P_i}\\(\mathfrak{w}_j,\mathfrak{W}_j)_{1,M},(\mathfrak{w}_{ji},\mathfrak{W}_{ji})_{M+1,Q_i}\end{array}\right.\right]$$
$$=\frac{\gamma_k(\frac{k+1}{2}-\mathfrak{f}_1-\mathfrak{F}_1s,A)\prod_{j=1}^{M}\Gamma_k(\mathfrak{w}_j+\mathfrak{W}_js)\prod_{j=2}^{N}\Gamma_k(\frac{k+1}{2}-\mathfrak{f}_j-\mathfrak{F}_js)}{\sum_{i=1}^{R}\left[\prod_{j=M+1}^{Q_i}\Gamma_k(\frac{k+1}{2}-\mathfrak{w}_{ji}-\mathfrak{W}_{ji}s)\prod_{j=N+1}^{P_i}\Gamma_k(\mathfrak{f}_{ji}+\mathfrak{F}_{ji}s)\right]},\tag{47}$$

and

$$\int_{Z>0}|Z|^{s-\frac{k+1}{2}}{}^{(\Gamma)}I_{P_i.Q_i,R}^{M,N}\left[z\left|\begin{array}{l}(\mathfrak{f}_1,\mathfrak{F}_1,A),(\mathfrak{f}_j,\mathfrak{F}_j)_{2,N},(\mathfrak{f}_{ji},\mathfrak{F}_{ji})_{N+1,P_i}\\(\mathfrak{w}_j,\mathfrak{W}_j)_{1,M},(\mathfrak{w}_{ji},\mathfrak{W}_{ji})_{M+1,Q_i}\end{array}\right.\right]$$
$$=\frac{\Gamma_k(\frac{k+1}{2}-\mathfrak{f}_1-\mathfrak{F}_1s,A)\prod_{j=1}^{M}\Gamma_k(\mathfrak{w}_j+\mathfrak{W}_js)\prod_{j=2}^{N}\Gamma_k(\frac{k+1}{2}-\mathfrak{f}_j-\mathfrak{F}_js)}{\sum_{i=1}^{R}\left[\prod_{j=M+1}^{Q_i}\Gamma_k(\frac{k+1}{2}-\mathfrak{w}_{ji}-\mathfrak{W}_{ji}s)\prod_{j=N+1}^{P_i}\Gamma_k(\mathfrak{f}_{ji}+\mathfrak{F}_{ji}s)\right]}.\tag{48}$$

Proof: We can prove this Theorem by follow same steps as in Theorem 1.

We can formulate two additional theorems for the decomposition formula of the incomplete $\overline{H}$-functions and the incomplete I-functions, similar to what we did in Theorems 2 and 4.

4 Particular Cases

This section delves into the analysis of specific cases that arise from our main findings. When considering a matrix argument Z (which is a real symmetric positive definite matrix of size $k \times k$), we can identify the following particular cases:

1. When $\mathfrak{F}_j = \mathfrak{W}_j = 1$, it is possible to demonstrate that the M-transform of incomplete H-functions, which have a matrix argument defined in (40), satisfy the M-transform of incomplete Meijer ${}^{(\Gamma)}G$-function (see [25]) with a matrix argument given by:

$$\begin{aligned}
&\int_{Z>0} |Z|^{s-\frac{k+1}{2}} \Gamma_{P,Q}^{M,N}\left[Z \,\middle|\, \begin{matrix}(\mathfrak{f}_1,1,A),(\mathfrak{f}_j,1)_{2,P}\\ (\mathfrak{w}_j,1)_{1,Q}\end{matrix}\right] dZ \\
&\qquad = \int_{Z>0} |Z|^{s-\frac{k+1}{2}} {}^{(\Gamma)}G_{P,Q}^{M,N}\left[Z \,\middle|\, \begin{matrix}(\mathfrak{f}_1,A),(\mathfrak{f}_j)_{2,P}\\ (\mathfrak{w}_j)_{1,Q}\end{matrix}\right] dz \\
&\qquad = \frac{\Gamma_k(1-\mathfrak{f}_1-s,A)\prod_{j=1}^{M}\Gamma_k(\mathfrak{w}_j+s)\prod_{j=2}^{N}\Gamma_k(1-\mathfrak{f}_j-s)}{\prod_{j=M+1}^{Q}\Gamma_k(1-\mathfrak{w}_j-s)\prod_{j=N+1}^{P}\Gamma_k(\mathfrak{f}_j+s)}. \quad (49)
\end{aligned}$$

2. When $M = 1$, $N = P$, and we replace Q with $Q+1$, we can obtain incomplete H-functions with matrix arguments (39) and (40) by appropriately choosing parameters. Specifically, we can set $Z = -Z$ and $\mathfrak{f}_j \to (1-\mathfrak{f}_j)$ for $j = 1,\ldots,P$, and $\mathfrak{w}_j \to (1-\mathfrak{w}_j)$ for $j = 1,\ldots,Q$. With these choices, the incomplete H-functions can be transformed into incomplete Fox-Wright functions with matrix arguments ${}_P\psi_Q{}^{(\gamma)}(Z)$ and ${}_P\psi_Q{}^{(\Gamma)}(Z)$, as follows:

$$\begin{aligned}
&\int_{Z>0} |Z|^{s-\frac{k+1}{2}} \gamma_{P,Q+1}^{1,P}\left[-Z \,\middle|\, \begin{matrix}(1-\mathfrak{f}_1,\mathfrak{F}_1,A),(1-\mathfrak{f}_j,\mathfrak{F}_j)_{2,P}\\ (0,1),(1-\mathfrak{w}_j,\mathfrak{W}_j)_{1,Q}\end{matrix}\right] dZ \\
&\qquad = \int_{Z>0} |Z|^{s-\frac{k+1}{2}} {}_P\psi_Q{}^{(\gamma)}\left[Z \,\middle|\, \begin{matrix}(\mathfrak{f}_1,\mathfrak{F}_1,A),(\mathfrak{f}_j,\mathfrak{F}_j)_{2,P}\\ (\mathfrak{w}_j,\mathfrak{W}_j)_{1,Q}\end{matrix}\right] dZ \\
&\qquad = \frac{\prod_{j=1}^{Q}\Gamma_k(\mathfrak{w}_j)}{\prod_{j=1}^{P}\Gamma_k(\mathfrak{f}_j)} \times \frac{\gamma_k(\mathfrak{f}_1-s,A)\prod_{j=2}^{P}\Gamma_k(\mathfrak{f}_j-s)}{\prod_{j=1}^{Q}\Gamma_k(\mathfrak{w}_j-s)}\Gamma_k(s), \quad (50)
\end{aligned}$$

and

$$\begin{aligned}
&\int_{Z>0} |Z|^{s-\frac{k+1}{2}} \Gamma_{P,Q+1}^{1,P}\left[-Z \,\middle|\, \begin{matrix}(1-\mathfrak{f}_1,\mathfrak{F}_1,A),(1-\mathfrak{f}_j,\mathfrak{F}_j)_{2,P}\\ (0,1),(1-\mathfrak{w}_j,\mathfrak{W}_j)_{1,Q}\end{matrix}\right] dZ \\
&\qquad = \int_{Z>0} |Z|^{s-\frac{k+1}{2}} {}_P\psi_Q{}^{(\Gamma)}\left[Z \,\middle|\, \begin{matrix}(\mathfrak{f}_1,\mathfrak{F}_1,A),(\mathfrak{f}_j,\mathfrak{F}_j)_{2,P}\\ (\mathfrak{w}_j,\mathfrak{W}_j)_{1,Q}\end{matrix}\right] dZ \\
&\qquad = \frac{\prod_{j=1}^{Q}\Gamma_k(\mathfrak{w}_j)}{\prod_{j=1}^{P}\Gamma_k(\mathfrak{f}_j)} \times \frac{\Gamma_k(\mathfrak{f}_1-s,A)\prod_{j=2}^{P}\Gamma_k(\mathfrak{f}_j-s)}{\prod_{j=1}^{Q}\Gamma_k(\mathfrak{w}_j-s)}\Gamma_k(s). \quad (51)
\end{aligned}$$

In this context, the M-transform of incomplete Fox-Wright functions with matrix argument (50) and (51) represent particular cases of the M-transform

of generalized incomplete hypergeometric functions (35) and (36), respectively (see [15]).

3. When $A = 0$, it is possible to demonstrate that the M-transform of incomplete H-functions with matrix argument defined in (40) satisfies the M-transform of H-functions with matrix argument given in (6).

4. When $A = 0$ and $\mathfrak{F}_j = \mathfrak{W}_j = 1$, it is possible to demonstrate that the M-transform of incomplete H-functions with matrix argument defined in (40) satisfies the M-transform of G-functions with matrix argument given in [5].

5. When $A = 0$, it is possible to demonstrate that the M-transform of generalized incomplete hypergeometric functions with matrix argument defined in (36) satisfies the M-transform of hypergeometric functions with matrix argument given in (5).

5 Conclusions

This study aims to establish the definition of special functions with a matrix argument of a symmetric matrix of size $k \times k$, which involves $k(k+1)/2$ variables. To achieve this, we utilized a generalized matrix transform technique to derive the definition of the special function of the matrix argument. Using Jacobians of transformations and substituting specific values into the derived definition, we can obtain various outcomes based on our findings.

References

[1] A. Erdelyi, W. Magnus, F. Oberhettinger, F. G. Tricomi, *Higher Transcendental Functions Vol. 1*, McGraw-Hill Book Co., Inc., New York, 1953.

[2] A. T. James, Zonal polynomials of the real positive definite symmetric matrices, *Annals of Mathematics*, 456-469, (1961).

[3] A. T. James, Special functions of matrix and single argument in statistics, *Theory and Application of Special Functions. Academic Press*, 497-520, (1975).

[4] A. G. Constantine, Some non-central distribution problems in multivariate analysis, *The Annals of Mathematical Statistics*, 34(4), 1270-1285, (1963).

[5] A. M. Mathai, R. K. Saxena, *Generalized hypergeometric functions with applications in statistics and physical sciences*, Springer, 348, 2006.

[6] A. M. Mathai, Some results on functions of matrix argument, *Mathematische Nachrichten*, 84(1), 171-177, (1978).

[7] A. M. Mathai, Foxs H-function with Matrix Argument, *Journal de Matematicae Estadistica*, 91-106, (1979).

[8] A. M. Mathai, Special functions of matrix arguments and statistical distributions, *Indian J. Pure Applied Math.*, 22(11), 887-903, (1989).

[9] A. M. Mathai, *Jacobians of matrix transformations and functions of matrix argument*, World Scientific, 1997.

[10] A. M. Mathai, A pathway to matrix-variate gamma and normal densities, *Linear Algebra and Its Applications*, 396, 317-328, (2005).

[11] C. S. Herz, Bessel functions of matrix argument, *Annals of Mathematics*, 474-523, (1955).

[12] C. Fox, The G and H functions as symmetrical Fourier kernels, *Transactions of the American Mathematical Society*, 98(3), 395-429, (1961).

[13] F. E. Prym, Zur Theorie der Gamma function, *J. Reine Angew. Math.*, 82, 165-172, (1877).

[14] H. M. Srivastava, M. A. Chaudhry, R. P. Agarwal, The incomplete Pochhammer symbols and their applications to hypergeometric and related functions, *Integral Transforms and Special Functions*, 23(9), 659-683, (2012).

[15] H. M. Srivastava, R. K. Saxena, R. K. Parmar, Some Families of the Incomplete H-Functions and the Incomplete $\overline{H}$-Functions and Associated Integral Transforms and Operators of Fractional Calculus with Applications, *Russian Journal of Mathematical Physics*, 25, 116-138, (2018).

[16] K. I. Gross, D. P. Richards, Special functions of matrix argument- I. Algebraic induction, zonal polynomials, and hypergeometric functions, *Transactions of the American Mathematical Society*, 301(2), 781-811, (1987).

[17] K. I. Gross, D. P. Richards, Total positivity, spherical series, and hypergeometric functions of matrix argument, *Journal of Approximation Theory*, 59(2), 224-246, (1989).

[18] M. K. Bansal, D. Kumar, On the integral operators pertaining to a family of incomplete I-functions, *AIMS-Math.*, 5, 12471259, (2020).

[19] R. J. Muirhead, Expressions for some hypergeometric functions of matrix argument with applications, *Journal of multivariate analysis*, 5(3), 283-293, (1975).

[20] R. D. Gupta, D. P. Richards, Hypergeometric functions of scalar matrix argument are expressible in terms of classical hypergeometric functions, *SIAM journal on mathematical analysis*, 16(4), 852-858, (1985).

[21] R. Sharma, J. Singh, D. Kumar, Y. Singh, Certain Unified Integrals Associated with Product of the General Class of Polynomials and Incomplete I-Functions, *Int. J. Appl. Comput. Math.*, 8(7), (2021).

[22] R. W. Butler, A. T. A. Wood, Laplace approximations for hypergeometric functions with Hermitian matrix argument, *Journal of Multivariate Analysis*, 192, 105087, (2022).

[23] R. Sharma, J. Singh, D. Kumar, Y. Singh, An Application of Incomplete I-Functions with Two Variables to Solve the Nonlinear Differential Equations Using S-Function, *Journal of Computational Analysis and Applications*, 31(1), 80-95, (2023).

[24] S. Bochner, W. T. Martin, Local Transformations with Fixed Points on Complex Spaces with Singularities, *Proceedings of the National Academy of Sciences*, 38(8), 726-732 (1952).

[25] S. Meena, S. Bhatter, K. Jangid, S. D. Purohit, Some expansion formulas for incomplete H and $\overline{H}$-functions involving Bessel functions, *Advances in Difference Equations*, 2020, 562, (2020).

[26] S. A. Deif, E. C. D. Oliveira, A system of Cauchy fractional differential equations and new properties of Mittag-Leffler functions with matrix argument, *Journal of Computational and Applied Mathematics*, 406, 113977, (2022).

[27] S. Momani, R. Sharma, J. Singh, Y. Singh, S. Hadid, Fractional Order Mathematical Modelling for Studying the Impact on the Emergence of Pollution and Biodiversity Pertaining to Incomplete Aleph Functions, *Progress in Fractional Differentiation and Applications*, 10(1), 15-22, (2024)

[28] Y. Chikuse, Properties of Hermite and Laguerre polynomials in matrix argument and their applications, *Linear algebra and its applications*, 176, 237-260, (1992).

[29] Y. Singh, R. Sharma, R. Maanju, Beer-Lamberts law as an application of incomplete Aleph (ℵ) functions, *AIP Conf. Proc.*, 2768 (1), 020038, (2023).

TABLE OF CONTENTS, JOURNAL OF COMPUTATIONAL ANALYSIS AND APPLICATIONS, VOL. 33, NO. 1, 2024